1964 LINEAR ACCELERATOR CONFERENCE

July 20-24, 1964

Midwestern Universities Research Association

LEGAL NOTICE

This report was prepared as an account of Government sponsored work. Neither the United States, nor the Commission, nor any person acting on behalf of the Commission:

A. Makes any warranty or representation, expressed or implied, with respect to the accuracy, completeness, or usefulness of the information contained in this report, or that the use of any information, apparatus, method, or process disclosed in this report may not infringe privately owned rights; or

B. Assumes any liabilities with respect to the use of, or for damages resulting from the use of any information, apparatus, method, or process disclosed in this report.

As used in the above, "person acting on behalf of the Commission" includes any employee or contractor of the Commission, or employee of such contractor, to the extent that such employee or contractor of the Commission, or employee of such contractor prepares, disseminates, or provides access to, any information pursuant to his employment or contract with the Commission, or his employment with such contractor.

Printed in USA. Price $9.42. Available from the

Clearinghouse for Federal Scientific and Technical Information
National Bureau of Standards, U. S. Department of Commerce
Springfield, Virginia

UC-28: Particle Accelerators and
High Voltage Machines
TID-4500 (37th Edition)
MURA REPORT 714

MINUTES

of the

1964 CONFERENCE

on

PROTON LINEAR ACCELERATORS

held at

MIDWESTERN UNIVERSITIES RESEARCH ASSOCIATION

July 20-24, 1964

CONFERENCE PLANNING COMMITTEE
AND BOARD OF EDITORS

F. E. Mills, Chairman
C. D. Curtis
D. A. Swenson
D. E. Young

Note by the Editors:

The task of compiling these minutes was greatly reduced by the splendid cooperation of the authors who for the most part supplied manuscripts of their talks. We are most appreciative of these efforts. The discussion was taken from tape recordings, and although an effort was made to identify the speaker and to correctly interpret their remarks, undoubtedly mistakes have been made. An effort was made in most cases to give the persons involved in the discussion a chance to edit their remarks, but to expedite the publication and prevent multiple exchanges of correspondence it was necessary to referee this procedure. It has not been feasible to submit to the authors the final versions of their papers or discussions.

Some of the papers included in these proceedings have also appeared as internal reports from the author's laboratories. These papers are included here for the sake of completeness and coherence.

The editors express their appreciation to all those who have labored over the arduous task of putting together these minutes. We especially appreciate the efforts of Miss Jean Luniak and Miss Rosemary Mulrooney for transcribing and typing the manuscripts, making arrangements, and helping in the correspondence; to Mr. Dave Gill for setting up the figures and assistance in proofreading; to Mr. Homer Clover who redrew figures where necessary; and to Mr. Dean Wilke for his conscientious job of duplication. The technical assistance of Mr. Henry Boatner, Mr. Ed Wille, and Dr. Phil Meads in recording the conference was especially commendable. The efforts of Dr. Charles Pruett, Mr. J. Laufenberg, and Mr. R. Fasking in making and reproducing slides greatly assisted in the presentation of the papers during the conference and in the reproduction of the figures in these minutes.

The Editors

TABLE OF CONTENTS

Introduction viii

List of Participants x

R. F. Accelerating Structures: The Cross-Bar Structure 1
A. Carne - Rutherford High Energy Laboratory

Coupled Resonator Model of Linear Accelerator Tanks 21
D. E. Nagle - Los Alamos Scientific Laboratory

800 MeV RF Structures 31
E. Knapp - Los Alamos Scientific Laboratory

Characteristics of Slotted Irises 60
S. Giordano - Brookhaven National Laboratory

Fabrication and Measuring Methods for Disk-Loaded Waveguides 75
T. Nishikawa - Brookhaven National Laboratory

The 500 MeV Linac Proposed as a New Injector for the AGS at the Brookhaven National Laboratory 84
G. W. Wheeler - Yale University and Brookhaven National Laboratory

The LASL Meson Factory 94
D. E. Nagle - Los Alamos Scientific Laboratory

Study for a Superconducting Multi-GeV Proton Linac 108
H. Schopper - Der Technischen Hochschule Karlsruhe, Germany

The New ZGS Injector Proposal 110
Rolland Perry - Argonne National Laboratory

Preliminary Design of a High Energy High Duty Cycle Proton Linear Accelerator 123
H. Leboutet, G. Guilbaud, Kervesic, Mangin, Tran - Compagnie Générale de Télégraphie Sans Fil

Progress Report on the Stanford Linear Accelerator Center 131
G. A. Loew - Stanford Linear Accelerator Center

A Green's Function Approach to the Calculation of Drift Tube Cavities 144
M. Rich and W. M. Visscher - Los Alamos Scientific Laboratory

Drift Tube Calculations 153
Harry C. Hoyt - Los Alamos Scientific Laboratory

The Saclay Design Study of Proton Linear Accelerators 162
M. Promé - Centre D'Etudes Nucleaires de Saclay

Drift Tube and Parameter Selection for Linear Accelerator Structures Below 150 MeV 177
D. E. Young - Midwestern Universities Research Association

Transverse Beam Blow-up in Standing Wave Linacs 186
R. L. Gluckstern - Yale University and Brookhaven National Laboratory

Dynamic Effects of Higher RF Harmonics 204
Frank J. Kriegler - Midwestern Universities Research Association

An Approach to the Study of Beam Loading for the Linear Accelerator 214
T. Nishikawa - Brookhaven National Laboratory

The CERN-PS Linac - Beam Loading and RF Studies 239
C. S. Taylor and Y. Dupuis - CERN

Model Measurements and Correction of Beam Loading Effects in Proton Linacs 252
S. Giordano - Brookhaven National Laboratory

Particle Motions and the Focusing System in Proton Linacs 266
S. Ohnuma - Yale University

Numerical Study of Particle Dynamics in a High-Energy Proton Linear Accelerator 283
M. Jakobson and W. M. Visscher - Los Alamos Scientific Laboratory

Constant Phase Velocity Acceleration Sections in a Proton Linac 301
J. Parain - Centre D'Etudes Nucleaires de Saclay

Focusing of an Alvarez Linac by Use of Magnetic Quadrupoles Oriented at 45° 309
D. T. Tran - Compagnie Générale de Télégraphie Sans Fil (Presented by M. G. Gilbaud)

Application of Calculated Fields to the Study of Particle Dynamics 328
D. A. Swenson - Midwestern Universities Research Association

Beam Dynamics Calculations for Alvarez-Type Linear Accelerators 341
Marvin Rich - Los Alamos Scientific Laboratory

Performance of the PS Linac 353
C. S. Taylor - CERN

Performance of the PLA 362
J. M. Dickson - Rutherford High Energy Laboratory

Beam Energy Measurements on the Rutherford Laboratory PLA 372
K. Batchelor, A. Carne, J. M. Dickson, D. J. Warner - Rutherford High Energy Laboratory

ZGS Injector Observations 384
Philip V. Livdahl - Argonne National Laboratory

Experiments on RF Field Patterns in the BNL Linac 398
J. T. Keane - Brookhaven National Laboratory

Automatic Control and Stabilization of the Orsay Linac 407
P. Brunet, L. Burnod and L. Lheritier - Ecole Normale Superieure - Orsay, France

Progress in High Intensity Ion Source and Accelerator Column Development 414
A. van Steenbergen - Brookhaven National Laboratory

Recent Developments in RF Proton Sources 430
H. Wroe - Rutherford High Energy Laboratory

Recent Measurements on the Duoplasmatron Source 447
L. W. Oleksiuk - Brookhaven National Laboratory

Ion Source and Column Performance at ORNL 456
G. G. Kelley and O. B. Morgan - Oak Ridge National Laboratory

The PLA Polarized Proton Source 465
J. M. Dickson - Rutherford High Energy Laboratory

Ion Source Work at ANL 470
D. H. Nordby - Argonne National Laboratory

An Extended RF Ion Source with Small Phase Space Emittance Area 474
Rolland Perry - Argonne National Laboratory

A New Approach to Preinjectors 480
H. Wroe - Rutherford High Energy Laboratory

Preaccelerator Column Design 487
C. D. Curtis and G. M. Lee - Midwestern Universities Research Association

Thoughts on Mode Distribution in RF Manifolds 497
F. Voelker - Lawrence Radiation Laboratory

RF Phase and Amplitude Control 505
Robert A. Jameson - Los Alamos Scientific Laboratory

Recharging Large Capacitor Banks 520
H. R. Shaylor - Brookhaven National Laboratory

Status Report on the Coaxitron Development Program 531
G. W. Wheeler - Yale University

A Possible Approach to the Initial Adjustment of a Long Linac 533
G. W. Wheeler and T. W. Ludlam - Yale University

RF Superconductivity Measurements 540
J. M. Dickson - Rutherford High Energy Laboratory

Deuteron Acceleration in the CLA (CERN Linear Accelerator) 545
Th. Sluyters - Brookhaven National Laboratory

The ANL Second Harmonic Buncher 555
W. Myers - Argonne National Laboratory

A Family of Improved Linac Bunchers 564
R. Beringer and R. L. Gluckstern - Brookhaven National Laboratory and Yale University

Nimrod Injector 602
N. D. West - Rutherford High Energy Laboratory (Presented by H. Wroe)

Informal Discussion of Sparking Phenomena 606
D. A. Swenson, Moderator - Midwestern Universities Research Association

Summary of Informal Session on Mechanical Engineering Aspects 616
John E. O'Meara - Midwestern Universities Research Association

Summary of Evening Session on Beam Loading Effects 622
J. E. Leiss - National Bureau of Standards

INTRODUCTION

The conference whose minutes are reported in this volume was the fourth in a series, previous conferences having been held in 1961 and 1962 at Brookhaven National Laboratory and in 1963 at Yale University. These conferences have been informal in nature, stressing primarily the progress made in the design of proton linear accelerators. This conference was sponsored by the Midwestern Universities Research Association and supported by the U. S. Atomic Energy Commission.

The interest in these conferences has grown appreciably, as evidenced by the increased participation and number of contributions. Starting from 20 participants and 17 contributions in 1961, we have reached a level of 96 participants and 54 contributions. The participants at this conference represented 24 institutions coming from seven different countries. Even with this size, it was possible to preserve informality and to allow speakers sufficient time to make their presentations and to hold adequate discussion. Fortunately, it was not necessary to turn away any worthy contribution or to hold concurrent sessions.

The conference was held at an especially opportune time for linac enthusiasts. In the U. S. there were three proposals for construction of linacs of energy 200 MeV or greater, these being the 500 MeV injector for the AGS at Brookhaven National Laboratory, the 200 MeV injector for the ZGS at Argonne National Laboratory, and the 800 MeV meson factory at Los Alamos Scientific Laboratory. On the foreign scene, there are plans for meson factories at Strasbourg and Karlsruhe, a new injector for the PS at CERN, and plans for an injector for a high energy AGS (Jupiter) at Saclay. Within the U. S., design studies of linacs have been closely coordinated under the auspices of the AEC by the Linac Coordination Committee. This conference gave the working members of the design teams a chance to interact freely.

The new linacs being designed require increased beam current and pulse length. This has spurred interest in beam loading phenomena and improved design of preinjectors. Much progress was reported at the conference in those areas but neither has yet arrived at a satisfactory state. For linacs whose energy is greater than 200 MeV the question of choice of rf structure remains unresolved although considerable progress has been reported. Renewed interest in the design of superconducting linacs was in evidence, particularly as reported from Karlsruhe.

We would like to take this opportunity to thank the many people, both MURA staff members and visitors, who helped make the conference run smoothly. We would particularly like to thank Lloyd Smith, Rolland Perry, Keith Symon, John O'Meara, Jim Leiss, George Wheeler, and John Blewett who assisted by serving as session chairmen.

F. E. Mills

LIST OF PARTICIPANTS

Argonne National Laboratory

Abraham, J.
Castor, R. W.
Goodrich, R. R.
Livdahl, P. V.
Martin, J. H.
Myers, W. W.
Nordby, D. H.
Perry, R.
Rihel, R. K.
Teng, L. C.

Atomic Energy of Canada Ltd., Chalk River, Canada

Schneider, H. R.

William M. Brobeck and Associates

Eukel, W.

Brookhaven National Laboratory

Blewett, J. P.
Keane, J. T.
Larson, R.
Oleksiuk, L.
Parzen, G.
Polk, I. J.
Shaylor, H. R.
Spiro, J.
Van Steenbergen, A.

Centre D'Etudes Nucleaires de Saclay

Parain, J.
Prome, M.

CERN

Lapostolle, P.
Sluyters, Th.
Taylor, C. S.

Compagnie Generale de Telegraphie Sans Fil, France

Guilbaud, G.
Jean, R.

Ecole Normale Superieure Orsay

Burnod, L.

Edgerton, Germeshausen and Grier, Inc.

Norris, N. J.

Eitel-McCullough, Inc.

Priest, D. H.

Institut de Recherches Nucleaires
Strasbourg, France

Armbruster, R.
Frick, G.
Gorodetzky, S.

Der Technischen Hochschule Karlsruhe

Schopper, H.

Lawrence Radiation Laboratory

Hubbard, E. L.
Lamb, W. A. S.
Smith, L.
Voelker, F.

Los Alamos Scientific Laboratory

Butler, H.
Hagerman, D. C.
Hart, V.
Hoyt, H. C.
Jameson, R. A.
Knapp, B.
Knapp, E.
Mueller, D. W.
Nagle, D.
Parker, J.
Potter, J.
Putnam, T. M.
Stokes, R. H.
Turner, T. F.
Visscher, W.
Worstell, H. G.

Midwestern Universities Research Association

Curtis, C. D.
Edwards, T.
Kriegler, F. J.
Meads, P. F.
Mills, F. E.
O'Meara, J. E.
Otte, R. A.
Owen, C. W.
Palmer, M.
Pruett, C. H.
Radmer, C. A.
Rowe, E. M.
Shea, M. F.
Snowdon, S. C.
Swenson, D. A.
Symon, K. R.
Young, D. E.

University of Minnesota

Featherstone, R. P.
Hendricks, R. H.

National Bureau of Standards

Leiss, J. E.

Oak Ridge National Laboratory

Kelley, G. G.
Martin, J. A.
Morgan, O. B.
Worsham, R. E.

Rutherford High Energy Laboratory

Carne, A.
Dickson, J. M.
Walkinshaw, W.
Wroe, H.

University of Southern California

Waddell, C. N.
White, E. I.

Stanford Linear Accelerator Center

Johnston, L. H.
Loew, G. A.

University of Tokyo

Nishikawa, T.

U. S. Atomic Energy Commission

McGee, R. P.
Reardon, P.
Wallenmeyer, W. A.

Yale University

Giordano, S.
Gluckstern, R. L.
Grand, P.
Ohnuma, S.
Wheeler, G. W.

R. F. ACCELERATING STRUCTURES: THE CROSS-BAR STRUCTURE

A. Carne
Rutherford High Energy Laboratory, Chilton, England

1. Introduction

Interest in the Cross-Bar Structure is now centred on the energy range 100-200 MeV. Here it is being considered as an alternative to the Alvarez structure for the 200 MeV, 200 Mc/s, Pre-Injector Linac for the CERN 300 GeV A. G. S. project (1). The Cross Bar structure offers several advantages over the Alvarez Guide: Comparable shunt impedance, wide bandwidth and high group velocity in π-mode operation, physical compactness and good mechanical tolerances. In this energy range, focusing is a structure design requirement (though no specific calculations have been done so far), so that drift tube diameter must be chosen on the familiar basis of focusing, and r.f. breakdown capability in conflict with shunt impedance.

It is the purpose of this paper to report on the theoretical work, practical measurements on $\beta = .4$, $\beta = .56$ models, corresponding to 85 and 200 MeV, and further work on the early 400 Mc/s Cross-Bar Structure described elsewhere (2).

2. Theoretical

The major theoretical work is being carried out by Georges Dôme at CERN, and some of the conclusions are presented here.

The formation of field patterns has been derived on a basis of rectangular or square guide (where the side of the square equals the liner diameter), and the fields computed as if the currents were carried on the centres of the bars. Shunt impedance and Q at π-mode have been found as functions of bar diameter d_s and β, by assuming losses in the current carrying bars and side walls only. Losses in drift tubes and the non (total) current carrying bars are not included. If L, D, d, have meanings given in figure 8, and if $k = \omega/c$, $\ell = (D-d)/2$, we have

$$Q = Q_o \left\{ 1 + \frac{8}{\pi} \log\left(\frac{2L}{Kd_s}\right) \beta \left(\frac{\pi d_s}{4L}\right) F + \left(\frac{\pi d_s}{4L}\right) \frac{16e^{-\pi D/L}}{1+2e^{-\pi D/L}} \right\}^{-1} \qquad \ldots \text{ i)}$$

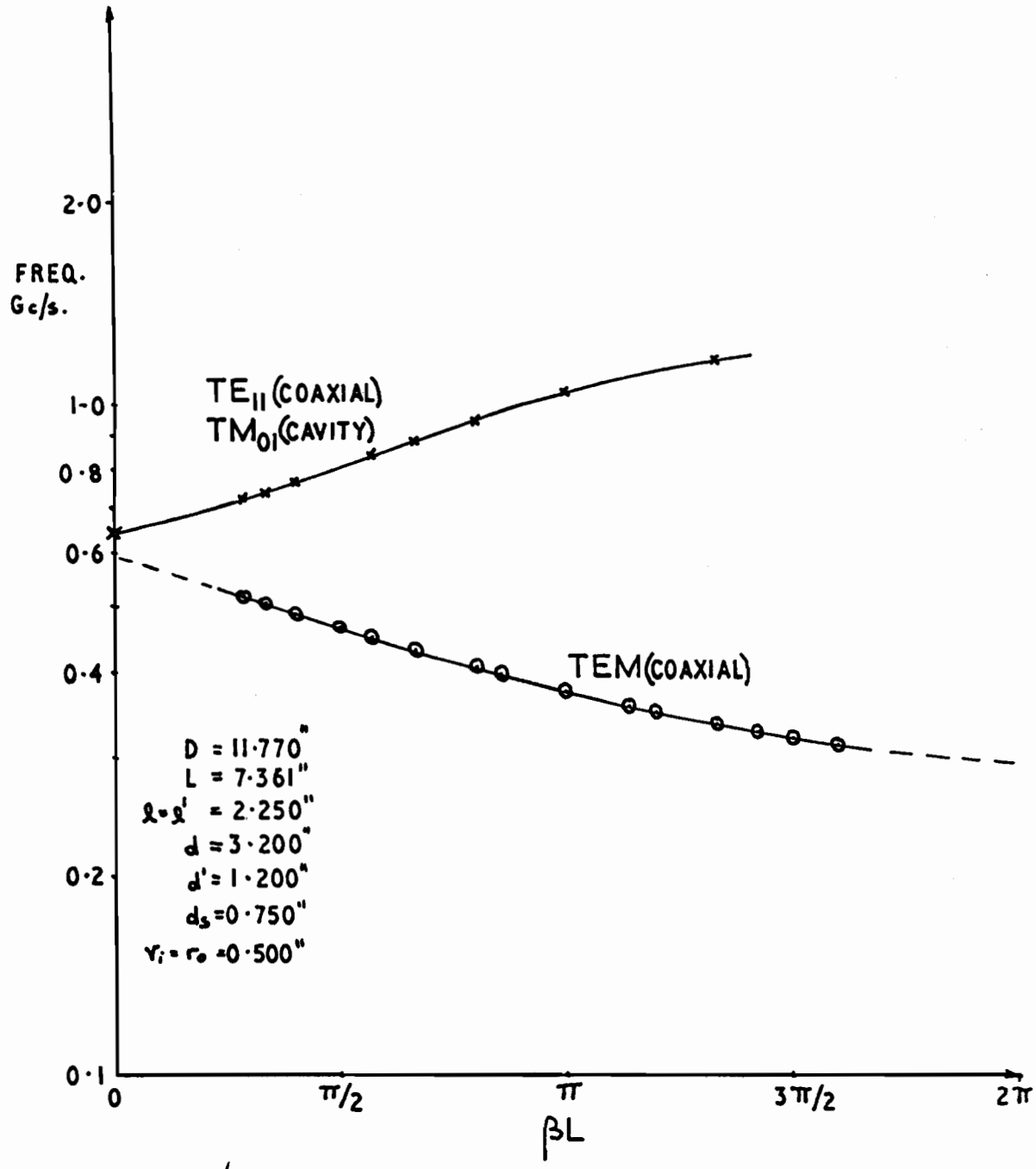

ω/β DIAGRAM FOR SYMMETRICAL CROSS-BAR

FIG. 1

where K is the complete elliptic integral: $K = \pi/2 \left(1 + 2e^{-\pi D/L} + \ldots\right)^2$;

$Q_o = \mathrm{Log}\left(\frac{2L}{Kd_s}\right) \frac{\pi d_s}{\lambda} \sqrt{\frac{\sigma}{\pi \epsilon f}}$ is the Q-value for losses on bars only ...

and $F = \pi/2 \left(k\ell + \sin k\ell \cos k\ell\right)^{-1} \geq 1$. Since D/L is usually >> 1,

$K \sim \pi/2$, and equation i) reduces to

$$Q \sim Q_o \left\{1 + \frac{8\beta}{\pi} \left(\frac{\pi d_s}{4L}\right) F \,\mathrm{Log}\left(\frac{4L}{\pi d_s}\right)\right\}^{-1} \qquad \ldots \text{iii)}$$

Equation iii) has been checked against the early 400 Mc/s model to give Q = 11, 200 against a measured 11, 900 (scaled from brass). This is very good agreement. Shunt impedance is given by:

$$\eta = \frac{QZ_o}{L} \frac{8M^2}{k\ell\,(1+\cot^2 k\ell) + \cot k\ell} = \frac{16}{\pi}\left(\frac{QZ_o}{L}\right)\left[M^2 F \sin^2 k\ell\right] \qquad \ldots \text{iv)}$$

where $Z_o = 60 \log\left(\frac{2L}{Kd_s}\right)$ is the characteristic impedance of a coaxial line, centre conductor d_s, (square) side L; and M is the transit time factor (the experimental approach to T. T. F. is given in section 4b). The variation of maximum shunt impedance with bar diameter and velocity is found by considering the maximum value of $(Q\,Z_o/L)$ with d_s and β. (The term inside the square bracket of eqn. iv) is proportional to (particle energy gain)^2/(stored energy), again discussed in section 4b). Considering only the second terms inside the bracket of eqn. i), we must maximise the function

$$\left(\frac{QZ_o}{L}\right) = \left(\frac{Q}{Q_o}\right)\frac{Q_oZ_o}{L} \quad \alpha \quad \frac{\pi d_s}{4L} \frac{\left[\mathrm{Log}\left(\frac{\pi d_s}{4L}\right) - 2\,\mathrm{Log}\left(1+2e^{-\pi D/L} + \ldots\right)\right]^2}{1 + \frac{8}{\pi} F\beta\left(\frac{\pi d_s}{4L}\right)\mathrm{Log}\left(\frac{4L}{\pi d_s}\right)}$$

A good approximation to the maximum is given when

$$\mathrm{Log}\left(\frac{4L}{\pi d_s}\right) = 1 + \xi + \sqrt{1 + 0.541\gamma}$$

where $\xi = 2 \log\left(1 + 2e^{-\pi D/L} + \ldots\right) = 2 \log\left[1 + 2e^{-\frac{\pi D}{D-d}\left(\frac{2k\ell}{\pi}\right)\frac{1}{\beta}}\right]$, and

$\gamma = \frac{8}{\pi} F\beta$. Since ξ and γ increase with β, η decreases (slowly)

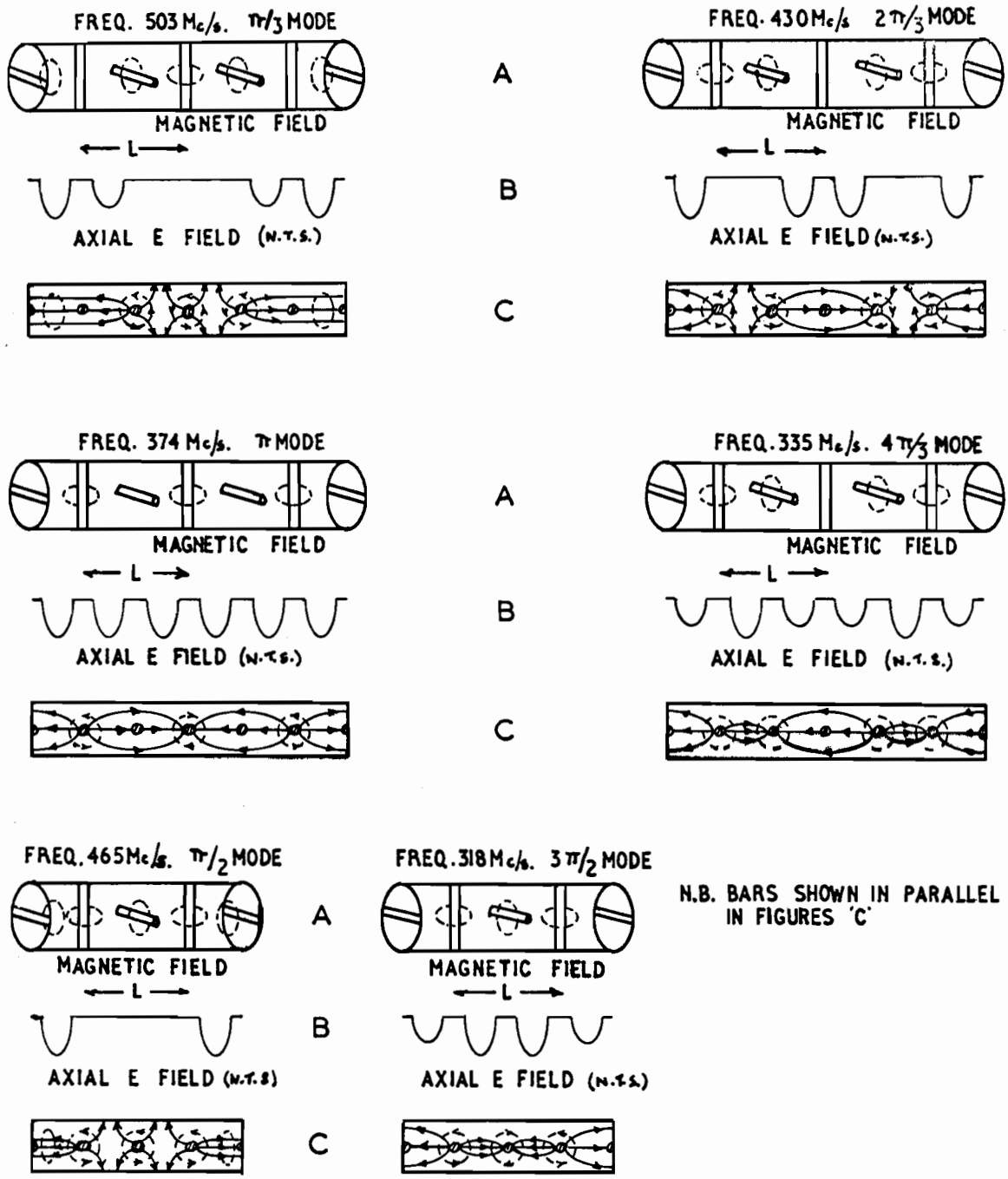

FIELD PATTERNS INSIDE CROSS-BAR STRUCTURE

FIG. 2

with β. If the optimum shunt impedance at $\beta = 0$ is given by unity, then we have for η and (L/d_s) opt:

β	(L/d_s) opt.	$\eta_{max.}$
0	5.8	1
.5	8.7	0.69
1	16.6	0.42

It is of interest to note that the bar need not be changed for $\beta = 0.5$ to 1.0. Over the energy range of interest (100-200 MeV), the fall of η max is 12%.

3. Field Patterns in the Cross-Bar Structure

Further measurements have been carried out on the early, symmetrical, 400 Mc/s model to determine field patterns in the various modes. This was done by axial field perturbation, and by magnetic loops through holes in the liner. The results are summarized in figures 1 and 2. In addition to the two $\omega - \beta$ branches shown in figure 1, there were many other resonances, all of them very much smaller than those plotted (of the order 30 db down) and may be H-modes, cable resonances, or harmonic resonances from the signal generator used.

The upper branch of the $\omega - \beta$ curve is obtained when the guide behaves as coupled coaxial resonators in the TE_{11} mode, giving rise to the TM_{01} mode along the guide. In this mode the magnetic field lines are purely circumferential, but distorted into oval, rather than circular, loops. Note also that for the TE_{11} mode (coax.) or TM_{01} guide, the zero mode can exist as the boundary conditions at the end plates can be satisfied. (The zero mode point in Figure 9, reference 2, is in fact the zero mode point for the upper branch). This mode has a forward fundamental, and is similar to the fundamental mode for the Alvarez structure. That this is so can be seen by linking together a series of coaxial resonators in the TE_{11} mode. Distorting the outside diameters to give a cylindrical waveguide with partitions reduces both 0 and π mode frequencies. Note the current flow is in opposite directions, 0-mode, and in the same direction in π-mode on either side of a partition. Cutting slots in the outside edges of the partitions in the direction perpendicular to the plane of the bars, does not affect the current lines in 0-mode, but shortens them in π-mode, i.e. causes the π-mode frequency to increase. The same effect can be seen by considering the capacitive effect of the slots. Putting in drift tubes loads down the two frequencies by roughly the same amount.

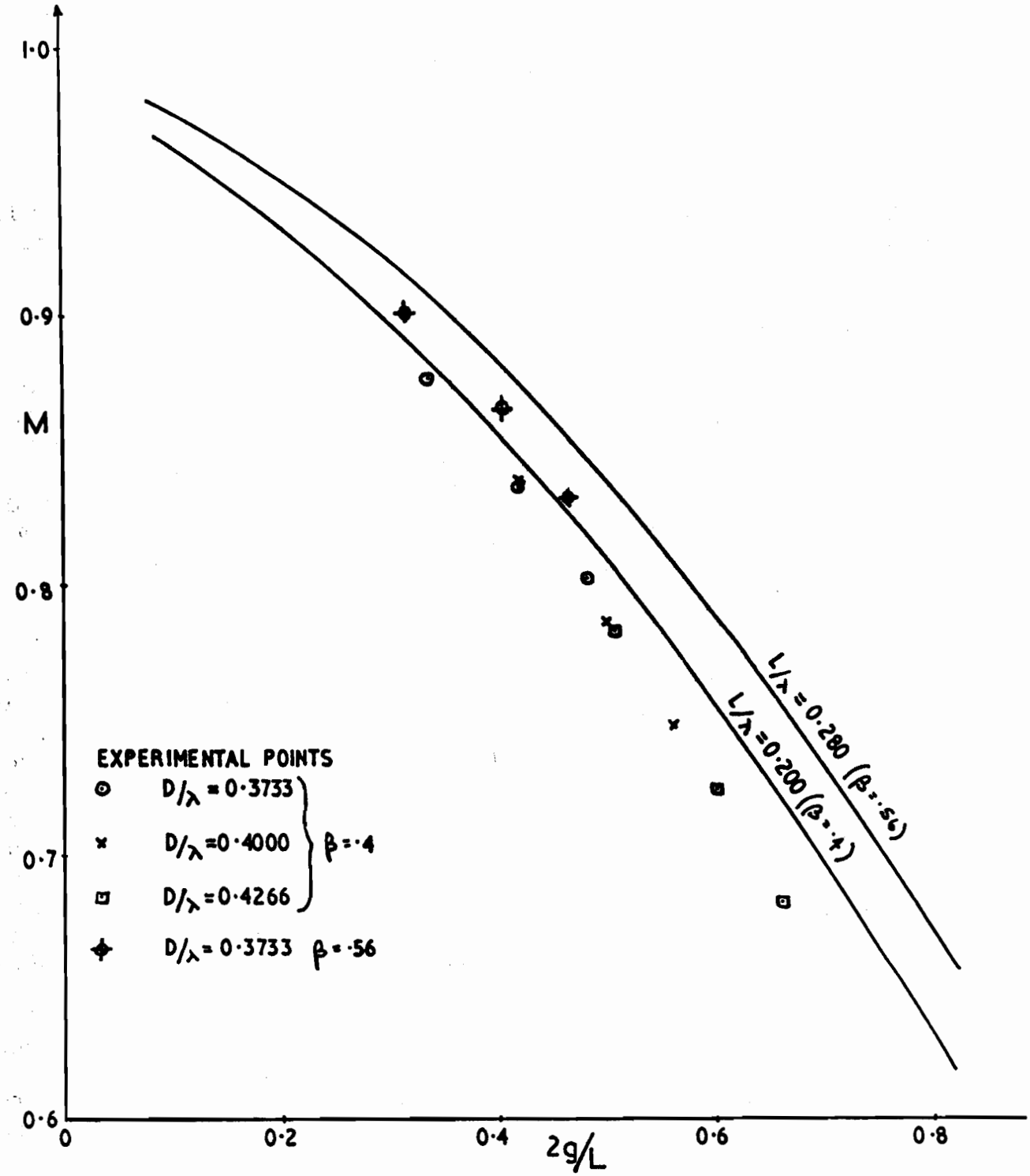

TRANSIT TIME vs. 2g/L IN CROSS BAR MODELS

FIG. 3

The "Cross-Bar Mode" is the lower branch in the $\omega - \beta$ diagram, and has been previously (2) described in terms of coupled coaxial resonators in the TEM (fundamental) mode*. (It should be remarked that this synthesis of modes in terms of partitioned coaxial resonators, rather than by starting with cylindrical guide with thin partitions, is preferable since it does allow for the effect of the finite thickness of the structure components). As such it is not possible to terminate the structure in 0 or 2π (i.e. when all the bars act as coaxial resonators) modes. On the 4 whole section model used with terminations in half bars, in π-mode the magnetic field was seen to exist in loops round one set of bars, and none at all in the second set containing the terminations. Figure 2 shows the magnetic field patterns, and the axial field plots (N. T. S.) in some of the modes measured in the model. It can be seen that for modes $\theta < \pi$, circumferential as well as coaxial H fields can exist. How much the circumferential components of H fields depend on the terminations than perhaps on some hybrid coaxial mode is not clear at present. Further measurements on the model with flat-plate terminations are to be done to clarify this (and, more important to enable us to find the characteristics of the structure with one set of bars removed). For modes $2\pi > \theta \geq \pi$ H-lines coaxial with the bars only were found. In this short symmetrical model no degeneracy was seen (but not surprisingly). A long 30-cell model, without drift tubes, with bars whose diameters are in the ratio 2:1, has been made to study the π-mode region, but there are no results to report as yet. Although there is a physical asymmetry in a long structure, it should be possible to have a continuous $\omega - \beta$ curve at π mode and hence a high group velocity. For small gaps with resulting uniform E fields, asymmetries in the drift tube lengths will have only a second order effect on capacitance, referred to one set of drift tubes or the other. Equalizing the bar diameters (or nearly so) to give the same π-mode resonant frequencies has only a small effect on the shunt impedance. Fine tuning can be obtained by use of tuners in the neighbourhood of one set of bars.

---

*NB. In Yale Conference Report P121, figure 9A '0'-mode, ALL E-lines should go from bars to liner, and not only alternate bars as drawn.

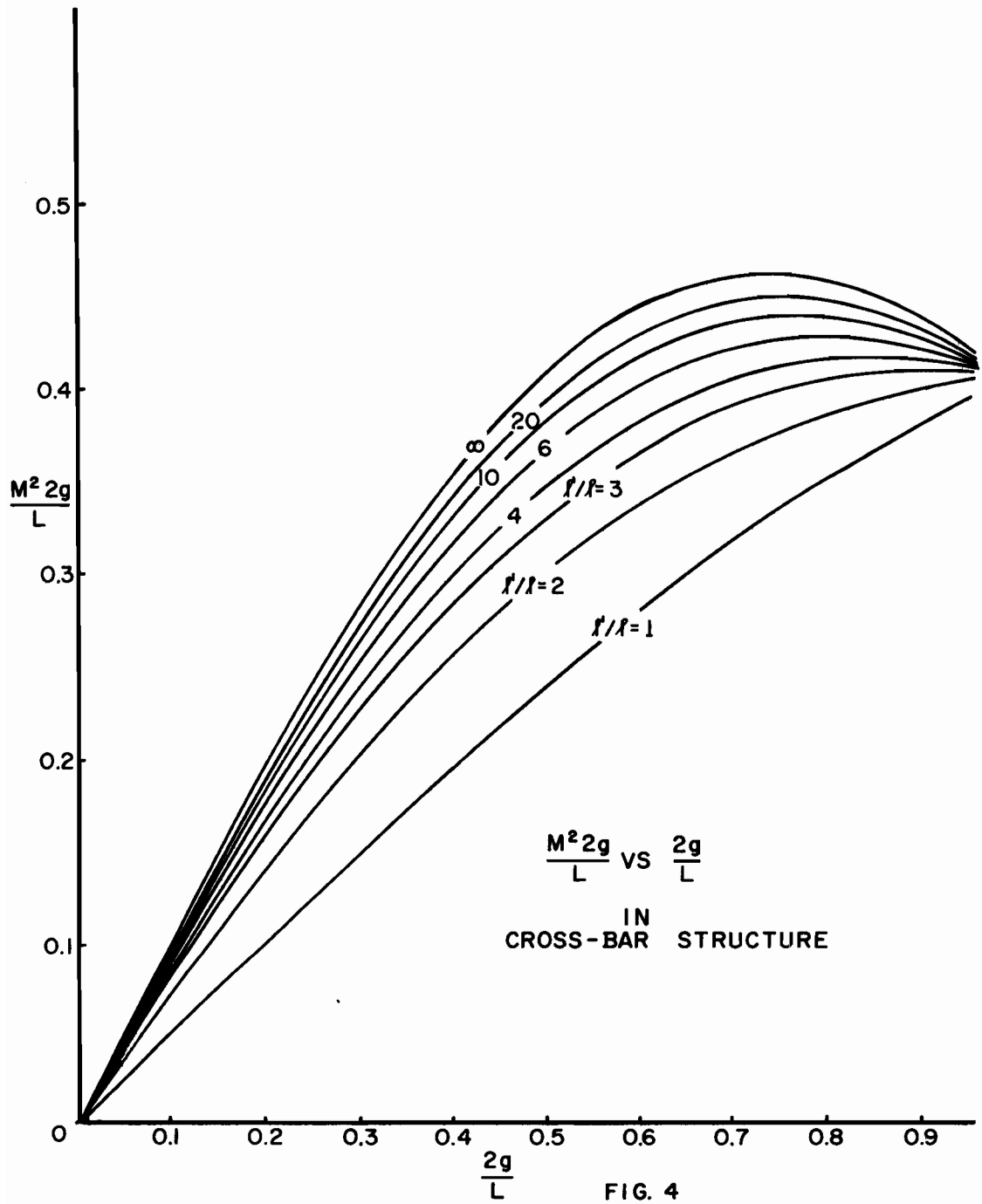
0.5
0.4
0.3
0.2
0.1
0
$\frac{M^2 2g}{L}$
0.1
0.2
0.3
0.4
0.5
0.6
0.7
0.8
0.9
$\frac{2g}{L}$
∞
20
10
6
4
$l'/l = 3$
$l'/l = 2$
$l'/l = 1$
$\frac{M^2 2g}{L}$ VS $\frac{2g}{L}$
IN
CROSS-BAR STRUCTURE

FIG. 4

4. Quarter-Scale Models for CERN 200 MeV Linac

Two 800 Mc/s (1+2 (1/2)) cell models have been made, for velocities β = .4 (~ 85 MeV) and β = .56 (~ 200 MeV). The two sets of drift tubes are of different lengths but constant diameters d/λ = 0.0868, corresponding to d = 5.125 inches, full scale, to enable them to house quadrupoles; drift tube bores d'/λ = 0.0233, as the value taken for the stage 1 design for the Alvarez structure. In each model, 3 different diameters for the current carrying bars (corresponding to L/d_s = 6, 8, 10) and 3 values of liner diameter (D/λ = 0.373, 0.4, 0.427, i.e. 14, 15, 16 cm at 800 Mc/s) were used. For a given liner diameter, for each diameter bar, the length of the 'large' drift tubes was adjusted to give a π -mode resonant frequency within 2 Mc/s of 800 Mc/s, and the η /Q measured. The liner was then bored out and the measurements repeated. The same sets of drift tubes and bars could be used, since boring out the liner increases the cavity inductance, and reducing the lengths of drift tubes (i.e. increasing gap lengths) reduces the capacitance and restores the resonant frequency. Bandwidths, defined here by $(f_{2\pi} - f_o)/f_\pi$ cannot be measured directly for the reasons given previously, but extrapolation from the modes measured give values of the order of 100%.

Further aspects of these models are discussed under separate headings..

(a) R.F. Breakdown

As yet there is no detailed information on the field distribution across the drift tubes, so that r.f. breakdown capabilities are not known. To this end, high power measurements are to be carried out in the near future. However, rough estimates on performance can be obtained from data given by Wilkins (3) for re-entrant cavities. Treating each half-cell as a separate cavity, for which T.T.F. (measured) and E_o (the mean gap field, assumed uniform) are known, then for the drift tubes for the given diameter and profiles given by r_o/λ = 0.0127, r_1/λ = 0.0062, (i.e. the same as the Rutherford Lab. or CERN 50 MeV Linacs), values of E_s/E_o in the range 1.2 - 1.5 for β = .4 - .56 can be expected, and for $E_s \not> 14.7$ Mv/m (Kilpatrick's Criterion at 200 Mc/s) acceleration rates of the order 4 MeV/m could be achieved. Alternatively, and subject to the practical requirements of quadrupole focusing, smaller drift tube diameters could be used with a lower acceleration rate, with an improvement in shunt impedance. (Maximum shunt impedance requires that d/L and ℓ/d be as small as possible for a given (g/d), where the terms have the meanings given in figure 8).

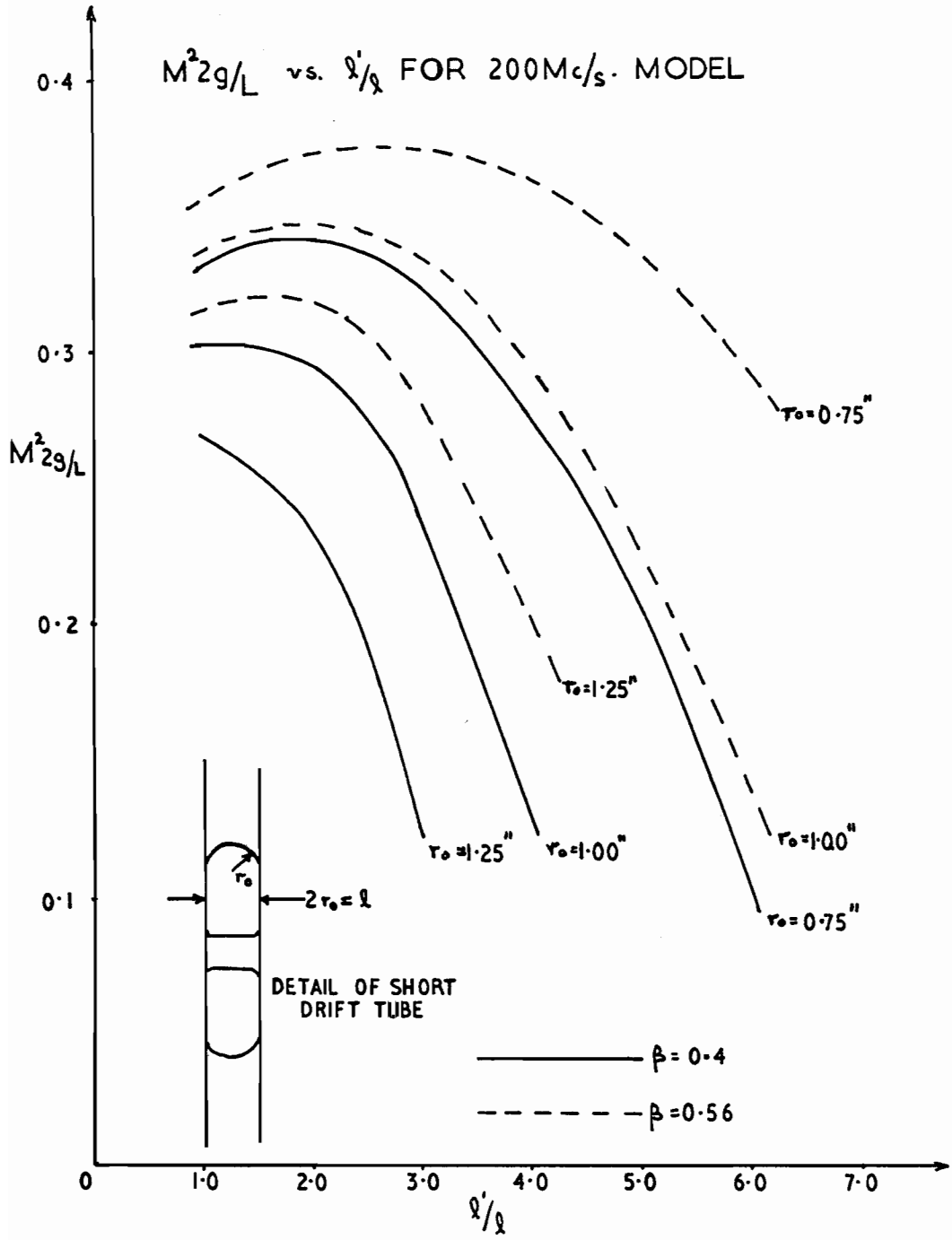
M²2g/L vs. ℓ'/ℓ FOR 200Mc/s. MODEL
0·4
0·3
0·2
0·1
M²2g/L
0
1·0
2·0
3·0
4·0
5·0
6·0
7·0
ℓ'/ℓ
r₀=0·75"
r₀=1·25"
r₀=1·25"
r₀=1·00"
r₀=1·00"
r₀=0·75"
r₀
2r₀=ℓ
DETAIL OF SHORT DRIFT TUBE
β=0·4
β=0·56

FIG. 5

(b) Transit Time Factor, and η/Q

It was clear from the measurements on the early 400 Mc/s model that although the shunt impedance was high, so too was the content of higher order space harmonics. Since these contribute only to the losses, and not to acceleration, the Cross-Bar Structure is from this point of view still somewhat inefficient. By changing the lengths of drift tubes, but keeping the gap lengths constant so that the effect on resonant frequency is only second order, a change in harmonic content can be obtained. The π -mode wave form is given in the sketch, where

ℓ is the length of the small drift tube
ℓ' is the length of the large drift tube
L, periodic length, $= \ell+\ell'+2g$;
$\beta_o L = \pi$ for π -mode

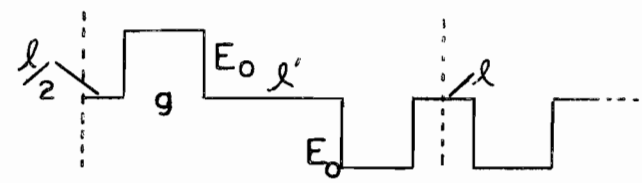

The field is assumed uniform in the region of the gaps (a fair assumption providing the gaps are small), and zero inside the drift tubes ℓ, ℓ'. The amplitude of the nth harmonic is given by

$$(\text{T. T. F.})_n = \int_0^L E(z)\cos\beta_n z \, dz \Big/ \int_0^L E(z)\, dz$$

$$= \frac{\sin\left(\frac{\beta_n g}{2}\right)}{\frac{\beta_n g}{2}} \sin\left(\frac{\beta_n L}{2}\right) \sin \frac{\beta_n}{2}\left(g+\ell'\right) ,$$

and for the fundamental, the T. T. F. is

$$M = \sin\frac{\pi g}{2L} \sin\frac{\pi}{2L}(g+\ell') \Big/ \pi g/2L \quad .$$

Clearly the smaller the gap, the larger the T. T. F. (practically obtainable by use of small diameter drift tubes), and the smaller the drift tube ℓ,

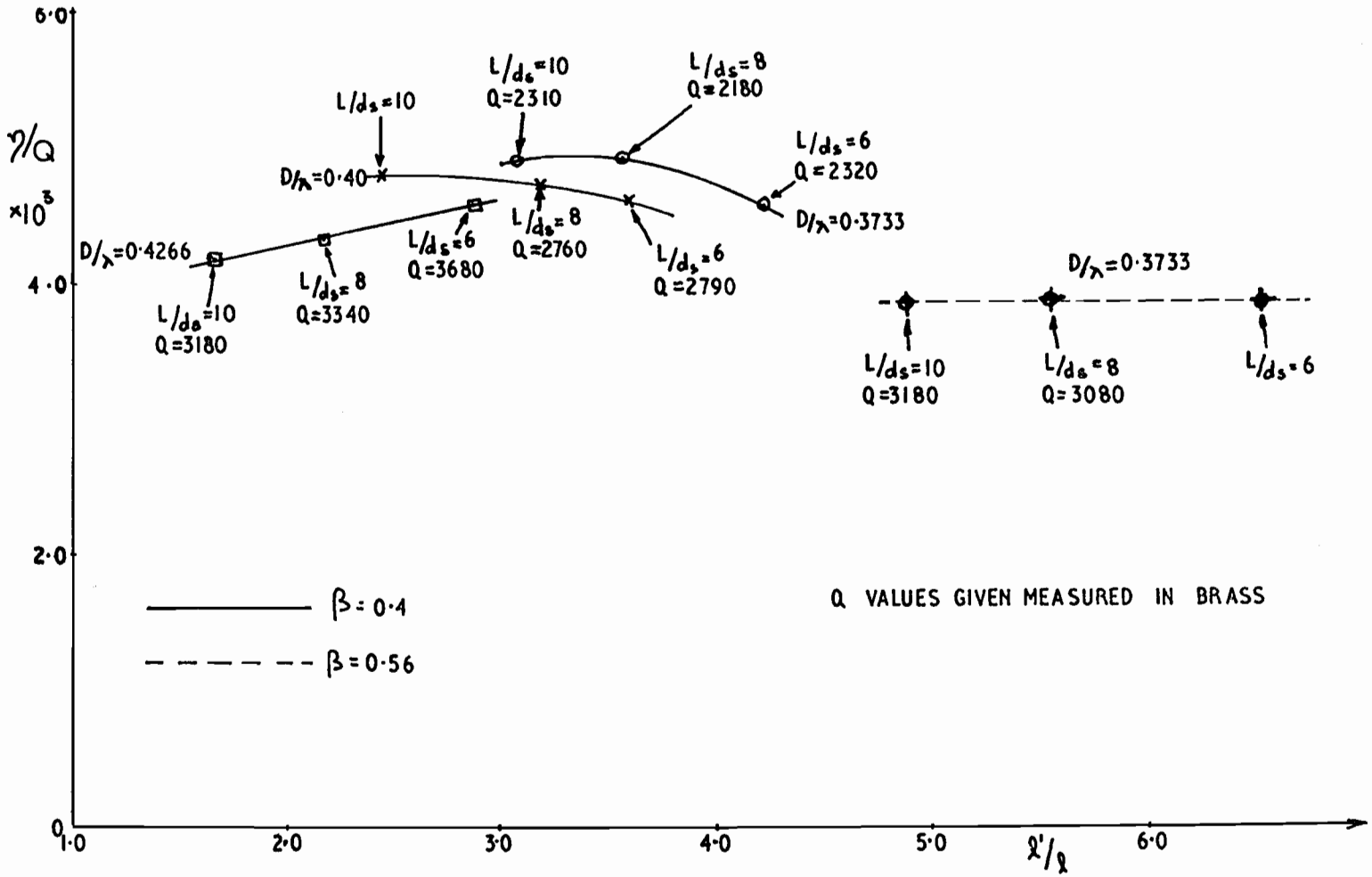

MEASURED VALUES OF η/Q vs. ℓ'/ℓ FOR CROSS-BAR MODEL AT 800Mc/s

FIG. 6

the greater the T. T. F.. Curves of T. T. F. to include the drift tubes geometries of the two models are given in figure 3, and compared with measured values: agreement is good for small gaps, $\sim 3/4\%$, but for larger gaps the error is larger, $\sim 5\text{-}1/2\%$, as to be expected since the gap field becomes non-uniform (but more like $1/r$ variation from the large drift tubes, as for a coaxial field).

The optimum efficiency for the structure is when the ratio (Energy gain per unit length)^2/(Stored energy per unit length) is a maximum, i.e. the stored energy needed to produce a required accelerating field in a minimum. This ratio is proportional to η/Q, and for small gaps, proportional to $M^2(2g/L)$. Curves of $M^2(2g/L)$ against $(2g/L)$ for values of ℓ'/ℓ are plotted in figure 4. For most values of ℓ'/ℓ the optimum ratios are for $(2g/L) \sim 0.7\text{-}0.8$. Note that the maximum value is for $\ell'/\ell = \infty$, i.e. when there are no small drift tubes, and $(2g/L) = 0.74$, but since field lines exist round these bars and drift tubes in the $(\pi, 2\pi)$ region, doing this removes some capacitive loading, with a consequent reduction in bandwidth. For ℓ'/ℓ 3-4 there is little variation in $M^2(2g/L)$ with $(2g/L)$ in the range 0.6-0.8. For a given small drift tube length ℓ (as used in both models where ℓ = stem diam. = 2 x outer profile radius, equal to 1-1/2 inches at 200 Mc/s) $M^2(2g/L)$ is given in figure 5, where the optimum values are for $\ell'/\ell \sim 2$, $\beta = .4$; $\ell'/\ell \sim 3$, $\beta = .56$.

For a given liner diameter, for each value of bar diameter, the large drift tubes were machined to give the correct frequency, and the (η/Q) value was measured, according to the formula

$$\eta/Q = A \left(\int_0^L E(z) \cos \beta_n z \, dz\right)^2 / \omega \epsilon L, \quad \beta_n = \beta_0 = \pi/L$$

where ϵ is the stored energy, and A = 2 for T. W. operation, = 1 for S. W. (e.g. π). (Results given previously (2) were in fact for T. W. operation, so that π-mode values should be reduced by a factor 2). Results obtained so far are given in figure 6, and scaled to 200 Mc/s ($\eta/Q \propto 1/\lambda$), in table 1 below. Values of η/Q are between 2 (at $\beta = .4$) and 3 ($\beta = .56$) times greater than corresponding values for the Alvarez structure (1). That there is a change of shape in the sets of points ($\beta = .4$) is in agreement with figure 5, where for D = 14, 15 cm (model) all points are to one side of the peak, but for D = 16 cm. includes the peak.

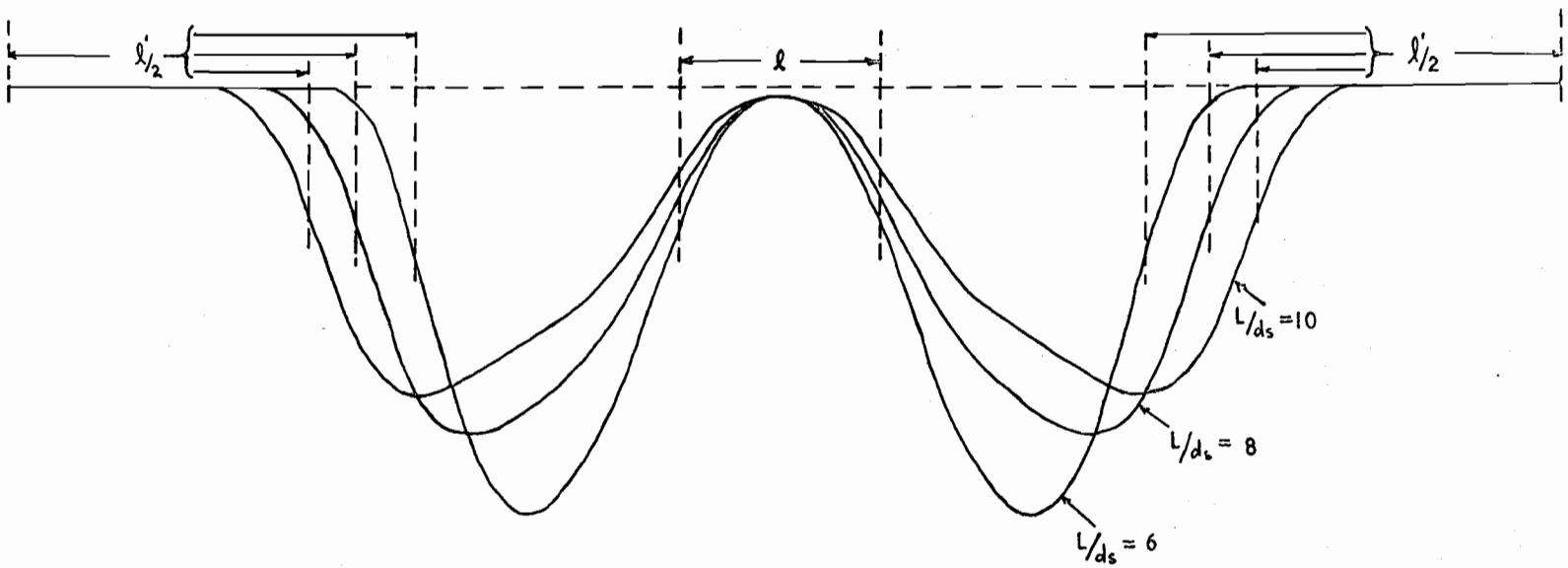

FIG. 7 PLOT OF $\Delta f \propto |E|^2$ AT $\beta = 0{\cdot}4$ ($D = 14$ cm)

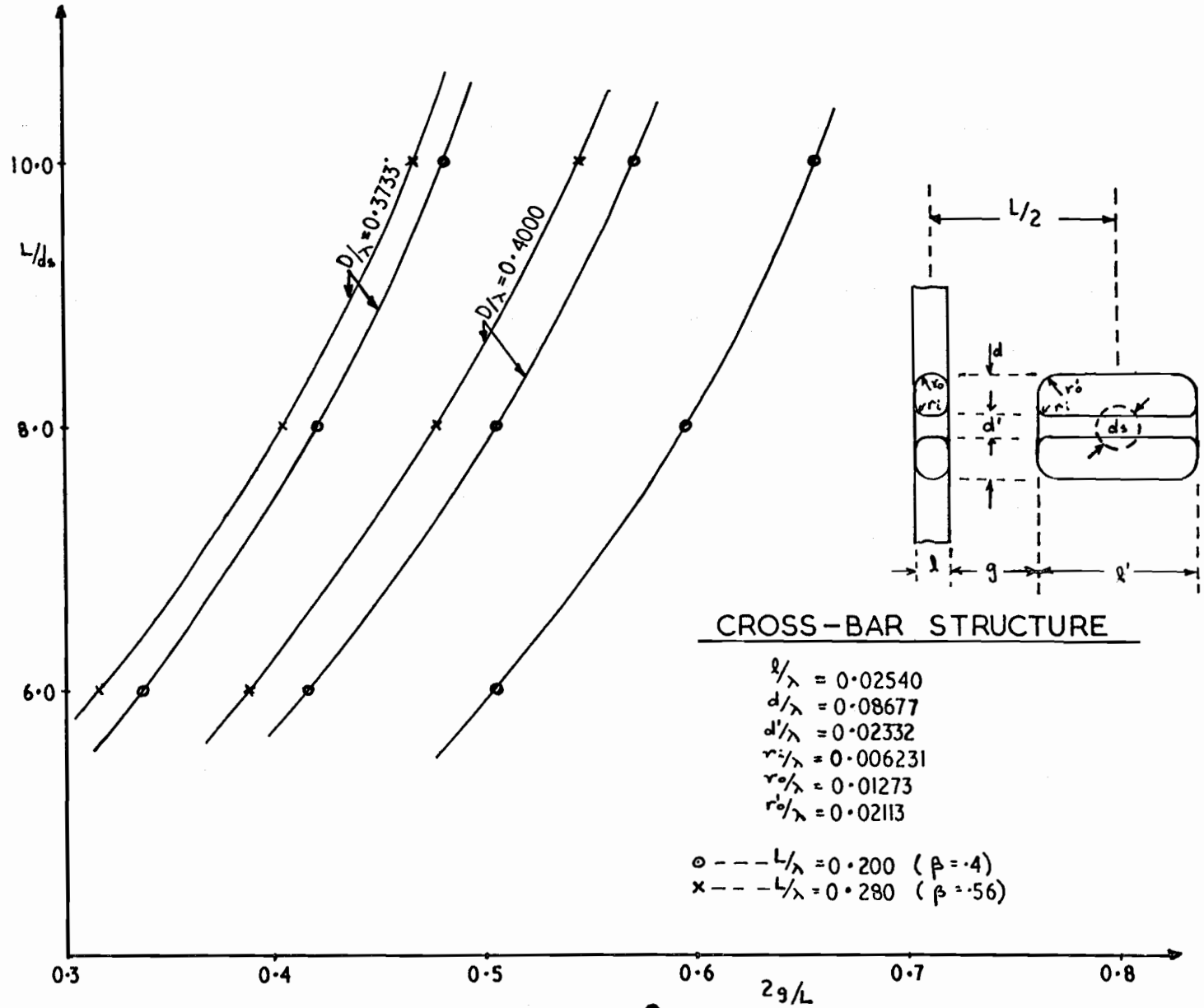
10·0
8·0
6·0
L/ds
D/λ = 0·3733
D/λ = 0·4000
0·3
0·4
0·5
0·6
0·7
0·8
2g/L
L/2
d
d'
ds
g
ℓ
ℓ'
CROSS-BAR STRUCTURE
ℓ/λ = 0·02540
d/λ = 0·08677
d'/λ = 0·02332
ri/λ = 0·006231
ro/λ = 0·01273
r'o/λ = 0·02113
o - - - L/λ = 0·200 (β = ·4)
x - - - L/λ = 0·280 (β = ·56)

FIG. 8

TABLE 1

800 Mc/s CROSS BAR MODEL MEASUREMENTS

$\beta = 0.4$ $\ell = 0.375''$

D (cm)	L/d_s	2g/L	ℓ'/ℓ	M	M(cal)	η/Q	Q (Brass)	η/Q (Scaled to 200 Mc/s)	η/Q th. 800 Mc/s
14	6	0.337	4.219	0.8757	0.8845	4.55×10^3	2,320	1.14×10^3	4.50×10^3
14	8	0.421	3.560	0.8371	0.8472	4.91×10^3	2,180	1.23×10^3	4.72×10^3
14	10	0.482	3.080	0.8026	0.8178	4.87×10^3	2,130	1.22×10^3	4.83×10^3
15	6	0.417	3.592	0.8390	0.8486	4.58×10^3	2,790	1.15×10^3	
15	8	0.501	2.931	0.7866	0.8080	4.68×10^3	2,760	1.18×10^3	
15	10	0.561	2.453	0.7481	0.7764	4.78×10^3	-	1.20×10^3	
16	6	0.507	2.880	0.7821	0.8050	4.55×10^3	3,680	1.14×10^3	
16	8	0.597	2.176	0.7246	0.7565	4.30×10^3	3,340	1.07×10^3	
16	10	0.661	1.666	0.6816	0.7195	4.16×10^3	3,180	1.04×10^3	
$\beta = 0.56$	$\ell = 0.375$								
14	6	0.317	6.533	0.9008	0.9155	3.83×10^3	-	0.96×10^3	
14	8	0.405	5.560	0.8652	0.8808	3.86×10^3	3,080	0.97×10^3	
14	10	0.466	4.885	0.8315	0.8537	3.82×10^3	3,180	0.96×10^3	
15	6	0.388	5.747				3,610		
15	8	0.479	4.739				3,630		
15	10	0.543	4.035				3,290		

Of particular interest is the set of perturbation curves shown in figure 7, for the β = .4, D = 14 cm model. The distorting effect on gap field of increasing gap length can be seen. Comparison of the L/d_s = 6 and 10 curves shows that for L/d_s = 6, η/Q is 7% greater and the peak total E-field 18% LESS than for L/d_s = 10. Generally as the gap increases (i.e. ℓ' gets smaller), the peak total E-field decreases, but not necessarily (η/Q).

Q values on the models are also included in figure 6 and the table, showing generally that as the volume of the cavity is increased (increasing D for a given L, or vice versa) Q increases, and for a given model, Q increases more rapidly than (η/Q) decreases with D. For a given D and L, Q decreases slowly with increasing L/d_s. The actual Q values are low due to the multiplicity of dry (demountable) joints: in particular the joints of the current carrying bars with liner used indium rings in grooves in the liner. (Since these joints will carry a heavy current in high power conditions, their quality becomes a major problem). The final 800 Mc/s model will have soldered joints to give a more representative Q-value. Scaled to 200 Mc/s and copper, the model values become of the order 12-14000. At least a doubling of this value is hoped for in the high power structure with good joints.

(c) Dimensional Tolerances

As already stated, for given D, d_s the large drift tubes ℓ' were machined to give the correct frequency. A summary of dimensions for constant frequency in the models is given in figure 8. From the data obtained we deduce the following tolerances per thousandth inch

	β = .4	200 Mc/s	β = .56
D	7 kc/s		7.3 kc/s
bar d_s	25 kc/s		21 kc/s
ℓ' (or total gap)	11 kc/s		8.75 kc/s

These tolerances are generally very similar to the Alvarez structure at 200 Mc/s and can be seen to get easier with increasing energy.

5. Conclusions

Model measurements show the Cross-Bar Structure to have (η/Q) values between 2 and 3 times greater than the Alvarez Structure in the range 100-200 MeV. Providing the theoretical Q-values can be achieved - and this requires attention to r.f. joints, particularly between the current carrying bars and line - then the Cross-Bar Structure should have shunt impedances

(200 Mc/s, $\phi_s = 0$) of the order 25-20 M Ω/m between 80-100 and 200 MeV. These values are comparable with the Alvarez structure at 80-100 MeV, and certainly better at 200 MeV. (At much higher energies ($\beta \sim 1$), the shunt impedance would be of the order 30%-50% less than the values quoted (i.e. $\sim$ 25 M Ω/m at v = 0, 800 Mc/s).) Further enhancement of these figures can be achieved by increasing D and reducing d, ℓ to obtain ratios nearer (2 g/L) $\sim$. 7, (ℓ'/ℓ) $\sim$ 3 - 4, giving optimum values for M^2 (2 g/L). Reduction of ℓ, d now depends on requirements for focusing, and r.f. breakdown capabilities. Future work will include high power model measurements to assess the r.f. voltage breakdown performance, and to check the design of r.f. joints.

Further advantages of the Cross-Bar Structure are its physical size (where the liner diameter is now of the order 60 cm, compared with the $\sim$80 cm Alvarez guide at β = .4), its mechanical tolerances (certainly no worse than the Alvarez guide), and its high group velocity v_g. If the structure is symmetrical, then at π-mode $v_g \neq 0$ (and on the early 400 Mc/s model v_g = 0.193 c); if the structure is asymmetric (as is required by transit time considerations above), a continuous $\omega - \beta$ curve at π-mode is still possible by selective tuning. Again, future work will include a study of the region around π-mode to determine the magnitude of mode splitting in an asymmetric structure and the effects of correction.

6. Acknowledgments

The author would like to express his thanks to Dr. George Dôme of CERN for making freely available his theory of the Cross-Bar Structure, and for much stimulating discussion, and Mr. Normal Fewell who carried out the experimental measurements.

NAGLE: Did you say your practical value for shunt impedance was 20 megohms per meter?

CARNE: Yes, 20 megohms per meter at 200 MeV and 200 Mc is a value that we expect to achieve. This includes all losses.

KNAPP: How did you scale that result?

CARNE: Taking the Q values that we have in the 800 Mc model, Q's of around 3000 to 3500, and scale from brass to copper, and from 800 to 200 Mc, we get Q's of about 14,000. Experience suggests that we can increase this value by a factor 1-1/2, by making the models with better joints. An important point about these model measurements is that the cavities were demountable in many ways in order to change the outside

diameter, stem diameter and drift tube length. In particular, the cross section of the joint of a current-carrying bar with the liner is shown in the sketch. Contact was made by compressing indium rings in grooves in the body of the liner. (Three grooves were cut: one for each of the three liner diameters, D, used). It was hoped that this system would give good rf contact, but, in fact, it turned out to be rather poor. This is similar to the experience that we also had on the original 400 Mc/s model (described at the Yale Conference). There we had dry joints, and the Q's were poor. As we increased the number of cells, instead of the Q increasing as expected, we found it actually went down due to the increase in number of joints. We have really to make good soldered rf joints to get good Q values.

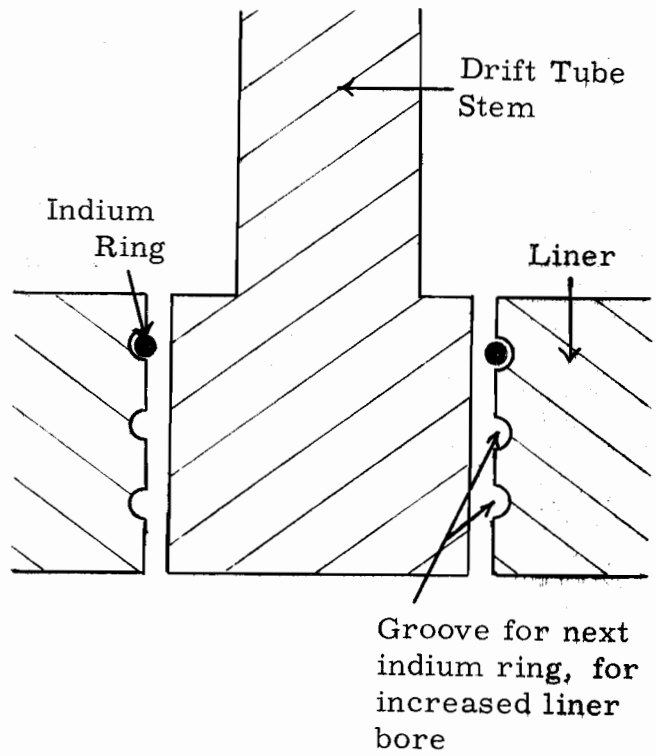

HUBBARD: How many cells are there in your model?

CARNE: On the 800 Mc models we have one full cell and two half cells for doing the R/Q measurements. We are not taking end plate losses into account for the Q values, it not being necessary in the cross-bar structure.

GIORDANO: As you increased the drift tube diameter, you found an increase in shunt impedance and a decrease in field intensity. Was this decrease in field intensity on the axis? And were there any other regions where the field was higher?

CARNE: That I don't know. The actual plot you saw was just that of an axial field perturbation.

References

(1) "Design of a High Current 200 MeV Proton Linear Accelerator".

A Carne, K. Batchelor, NIRL/R/55 March 1964, and Yale Linac Conference Report, p 404, October 1963.

(2) "Structures for High Energy Proton Linear Accelerators". A Carne.

International Conference, Dubna, August 1963; also Yale Conference, October 1963.

(3) "Design Notes on Resonators for P.L.A.'s" J. J. Wilkins. AERE GP/R 1613, 1955.

COUPLED RESONATOR MODEL OF LINEAR ACCELERATOR TANKS*

D. E. Nagle
Los Alamos Scientific Laboratory, University of California
Los Alamos, New Mexico

I. Introduction

This paper will review the coupled resonator model of the linear accelerator resonant tanks, in the form in which we have applied it for understanding our experimental results, both with the computers and with experimental models. The present form of the model has grown out of discussions with Ed Knapp, Bruce Knapp, and others. The steady state results will be discussed by E. Knapp in the following paper. R. Jameson in a talk to be given later in the week will discuss his theory and measurements of the transient behavior of the tanks and the design of a servo control system for rf amplitude and phase. In his talk you will see that many purely algebraic properties connected with the symmetry of the system are common to the transient and to the steady state theory.

The dispersion relations for the simple and for the doubly periodic ring or chain of coupled oscillators are familiar results of lattice vibration theory; see, for example, Brillouin's book.[1]

Some results are perhaps novel, particularly those concerned with phase shifts, effects of perturbations, and locking phenomena. Also, the discussion of the relation between ring and chain has been used extensively in our work.

Although pictorially we often refer to the familiar lumped circuits, which suggests a severe limitation on generality, this is only a convenience. The important equations refer to the resonant frequencies, their widths, amplitudes, and phases, and to the strength of coupling, quantities which at these frequencies are directly or indirectly easily measurable. The approach is useful so long as it is possible to describe the behavior using separated modes of a single cavity as they develop into bands of the coupled system. (We always refer to a tank as a chain of coupled cavities.) The agreement with measurement, as you will see in the following paper, is remarkably good.

Figure 1 illustrates the correspondence between coupled cavities, coupled circuits, and a linear lattice. The correspondence between

*Work performed under the auspices of the U. S. Atomic Energy Commission.

circuits and cavities is direct as shown if we talk in terms of the amplitude and resonant frequency, a single mode of oscillation of the single cavity, and the coupling strength of this mode to the next cavity. Of course, k can be given in terms of overlap integrals of field quantities. The analogy with the linear lattice with next-nearest-neighbor coupling is familiar. For most of the talk we consider only a single cavity mode at a time; this describes most of the experimental data.

II. Circuit Equations

The circuit equations are $n = 1 \ldots . 2N$

$$\epsilon_n = (2 j \omega L + R + \frac{1}{j \omega C} i_n + j k \omega L (i_{n-1} + i_{n+1}) \tag{1}$$

$$\frac{\epsilon_n}{2 j \omega L} \equiv I_n \cong (1 - \frac{\omega_o^2}{\omega^2}) i_n + \frac{k}{2} (i_{n-1} + i_{n+1}) \tag{2}$$

$$\text{where } \omega_o^{-2} = 2 L C (1 + \frac{1}{j Q}); \; Q = \frac{2 \omega L}{R} . \tag{3}$$

There are 2 N solutions to homogeneous equations ($I_n = 0$) of the form

$$i_n^{(q)} \cong \text{const. } x \; e^{2\pi j \frac{qn}{2N}} \tag{4}$$

(q is the mode number, n is the circuit number). Provided that

$$0 = (1 - \frac{\omega_o^2}{\omega_q^2}) e^{\frac{2\pi j q n}{2N}} + \frac{k}{2} (e^{\frac{2\pi j q [n-1]}{2N}} + e^{\frac{2\pi j q [n+1]}{2N}})$$

as may be seen by substituting (4) into (2), or

$$\omega_o^{-2} - \omega_q^{-2} + k \, \omega_o^{-2} \cos \frac{\pi q}{N} = 0 . \tag{5}$$

This is the dispersion relation for the simple ring of 2 N circuits, or for the lattice with periodic boundary conditions. It is plotted as Fig. 2.

$\pi q/N = \varphi$ is the mode phase shift per cell; e.g., $q = N$ is called the π-mode.

III. Matrix Form at Circuit Equations

We had

$$(\omega_o^{-2} - \omega^{-2}) i_n + \frac{k}{2} \omega_o^{-2} (i_{n-1} + i_{n+1}) = \omega_o^{-2} I_n .$$

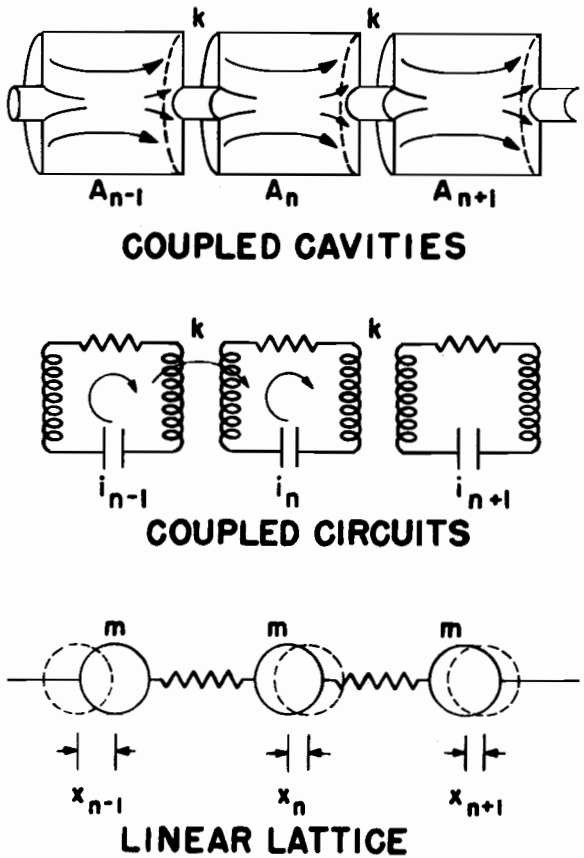

LINEAR MODEL OF COUPLED CAVITIES

FIG. 1

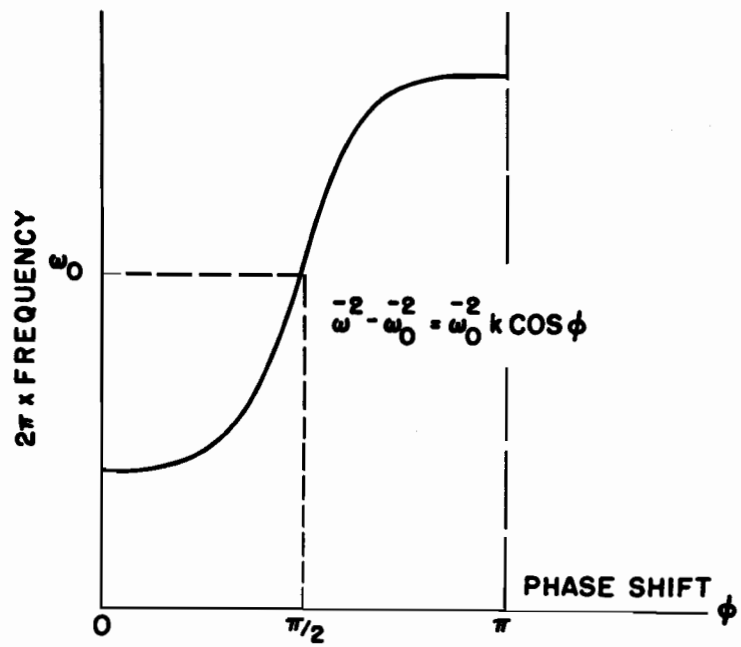

DISPERSION CURVE FOR SIMPLE CHAIN

FIG. 2

$$\text{Let } \vec{i} = \begin{pmatrix} i_1 \\ \cdot \\ \cdot \\ \cdot \\ \cdot \\ i_N \end{pmatrix} \qquad \vec{I} = \begin{pmatrix} I_1 \\ \cdot \\ \cdot \\ \cdot \\ \cdot \\ I_n \end{pmatrix}$$

$$\Omega = \begin{bmatrix} 1 & \frac{k}{2} & 0 & 0 & & \frac{k}{2} \\ \frac{k}{2} & 1 & \frac{k}{2} & 0 & & 0 \\ 0 & \frac{k}{2} & 1 & \frac{k}{2} & 0 & 0 \\ & & & & & \\ \frac{k}{2} & 0 & & 0 & \frac{k}{2} & 1 \end{bmatrix} \qquad \text{(ring)} \tag{6}$$

Circuit equations are

$$\omega_o^{-2}\, \Omega\, \vec{i} - \omega^{-2}\, \vec{i} = \omega_o^{-2}\, \vec{I}. \tag{7}$$

The normal modes $\vec{i}^q$ are the eigenvectors of the homogeneous problem, and the resonant frequencies of the modes are the eigenvalues.

Solution to inhomogeneous problem $I_s = 1 \times \omega_o^2$ is the Green's Function

$$G(r, s) = \sum_{\substack{\text{all} \\ \text{modes}}} \frac{\varphi^q(r)\, \varphi^q(s)\, w(q)}{\omega_q^{-2} - \omega^{-2}}$$

$w(q) = 1/2 \qquad q = 0 \text{ or } N$

$w(q) = 1 \qquad q = 1, 2, \cdots, (N - 1)$

i.e., this is the response of the tank at the rth cavity to unit drive at cavity number s.

IV. Relation Between Travelling Waves in a Ring and Standing Waves in a Tank

Figure 3 illustrates the relation between travelling waves on a ring and standing waves in a tank. The circumference of the circle is divided into 2 N equal segments, representing 2 N cavities connected in a ring. The travelling wave solutions, eq. (4), satisfy the periodic boundary condition $i_{2N+1} = i_1$. They represent waves travelling counterclockwise around the ring. Now imagine the ring bisected by the line cutting cavities number 2 N and number N in half, fold the figure along this line and straighten out the half circle to get a line segment. Number the line so that

$$\begin{array}{lcl} 2\,N & \longrightarrow & 0 \\ 1 & \longrightarrow & 1 \\ 2\,N - 1 & \longrightarrow & 1 \\ 2 & \longrightarrow & 2 \\ 2\,N - 2 & \longrightarrow & 2 \\ & \text{etc.} & \end{array}$$

The line represents the tank, with caviites of 1/2 length at each end. The solutions (eq. (4)) map into

$$(i_p^q + i_p^{q*}) = \frac{1 \cos}{\sqrt{N/2}} \frac{\pi p q}{N} . \tag{8}$$

The running wave solutions (4) satisfy

$$\sum_{p=1}^{2N} i_p^{q*} i_p^r = \delta_{2N} (r - q) \tag{4'}$$

where $\delta_{2N}(x) = 1 \quad x = 0, \quad 2N, \quad 4N \cdots$

$\qquad\qquad\qquad = 0 \quad$ otherwise,

and the standing wave solutions satisfy

$$2 \sum_{p=o}^{N} w_p \cos \frac{\pi p q}{N} \cos \frac{\pi r p}{N} = \delta_{2N} (r - q) + \delta_{2N} (r + q) \tag{4''}$$

where $\begin{cases} w_p = 1 & p = 1 \cdots N - 1 \\ \quad\;\; = 1/2 & p = 0 \text{ or } N . \end{cases}$

For the chain the circuit matrix is

$$\Omega = \begin{bmatrix} 1 & k & 0 & \cdot & \cdot & 0 \\ \frac{k}{2} & 1 & \frac{k}{2} & 0 & \cdot & 0 \\ 0 & \frac{k}{2} & 1 & \frac{k}{2} & \cdot & 0 \\ \cdot & & & & & \\ 0 & 0 & \cdot & \cdot & k & 1 \end{bmatrix} . \qquad (6')$$

V. Deviations from the Floquet Law

$$\varphi = \pi q/N .$$

In the presence of losses in the cavities, the above wave functions (8) are not exact. For example, in the π-mode, the first-order correction requires

$$\varphi_n = \frac{\pi q}{N} + \Delta\varphi_n \text{ where}$$

$$\Delta\varphi_{n+1} - 2\Delta\varphi_n + \Delta\varphi_{n-1} = \frac{2}{k Q \pi} .$$

This is plotted in Fig. 4. With the drive in the center, the cell-to-cell phase shift is a maximum in the center and decreases linearly. For $k = 0.1$, $Q = 20,000$ and a tank of 65 cells, the center-to-end phase shift is 28°. By cutting the cavities halfway between beam loaded and unloaded, the over-all change in phase shift would be 2.8°. Visscher's program shows 10° is quite all right.

VI. Perturbation Theory

We can use the ordinary first-order perturbation theory to calculate the effect of deviations in cavity geometry:

Unperturbed Circuit Equation

$$\omega_o^{-2} \Omega \vec{i} = \omega^{-2} \vec{i} . \qquad (7')$$

Now perturb resonant frequencies of cavities

$$\omega_o^{-2} (\Omega + \delta\Omega)(\vec{i} + \delta\vec{i}) = (\omega^{-2} + \delta\omega^{-2})(\vec{i} + \delta\vec{i}) ;$$

define

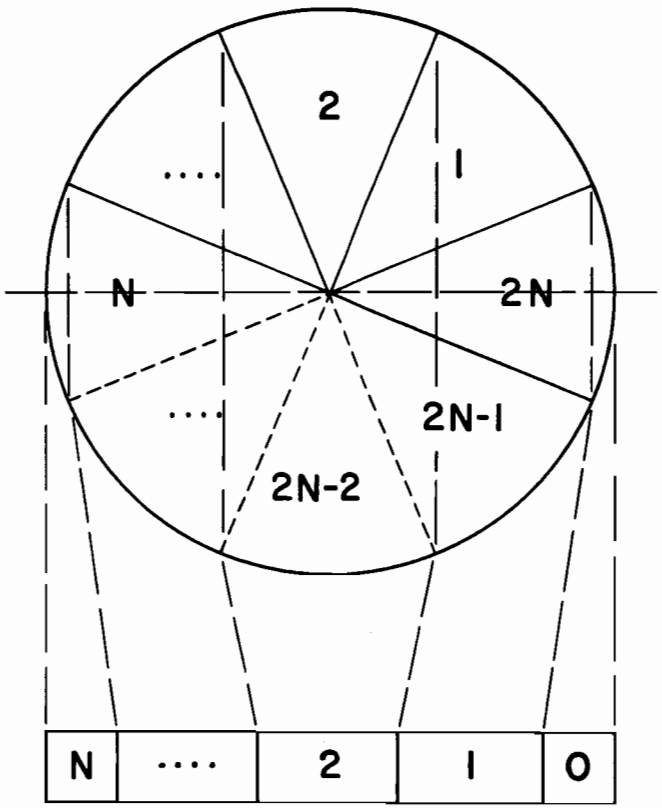

MAPPING OF THE RING
ONTO THE CHAIN
FIG. 3

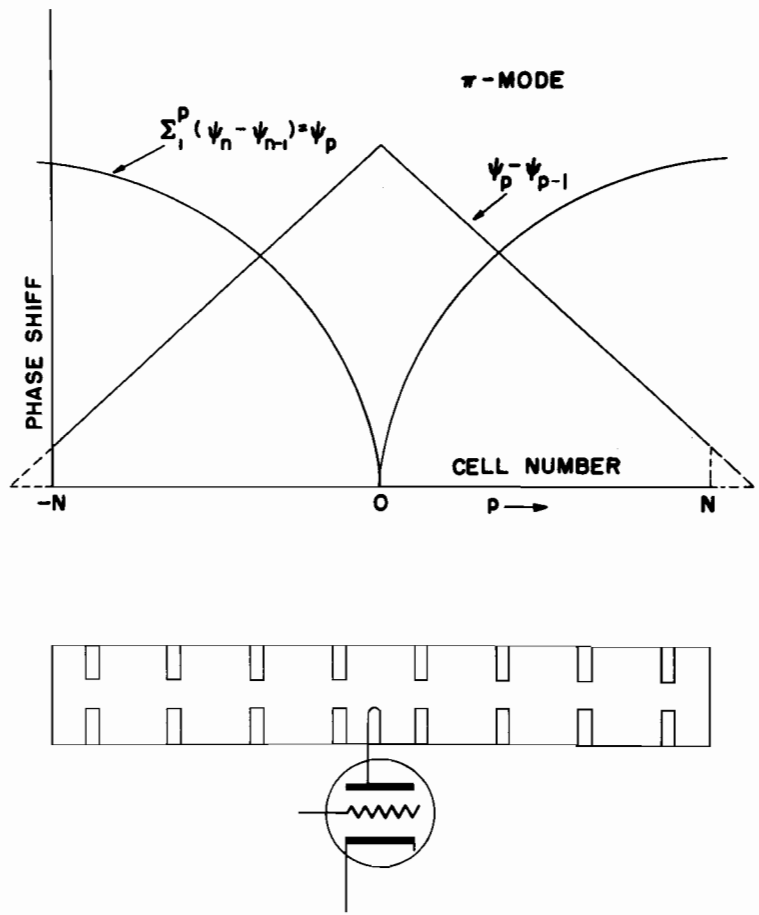

FIG. 4

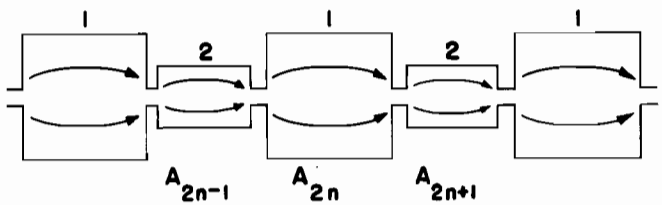

CAVITIES OF TWO KINDS

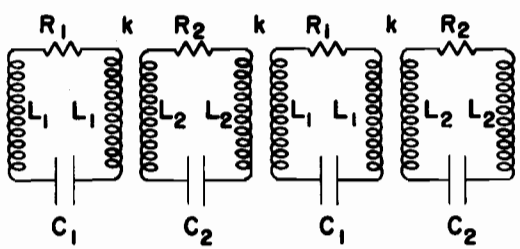

CIRCUITS OF TWO KINDS

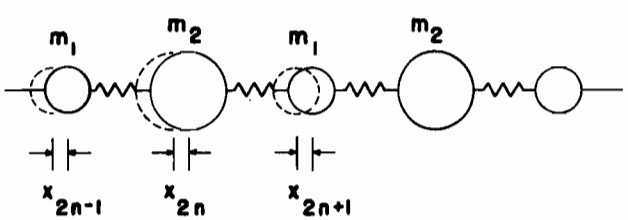

DIATOMIC LINEAR LATTICE

Fig. 5

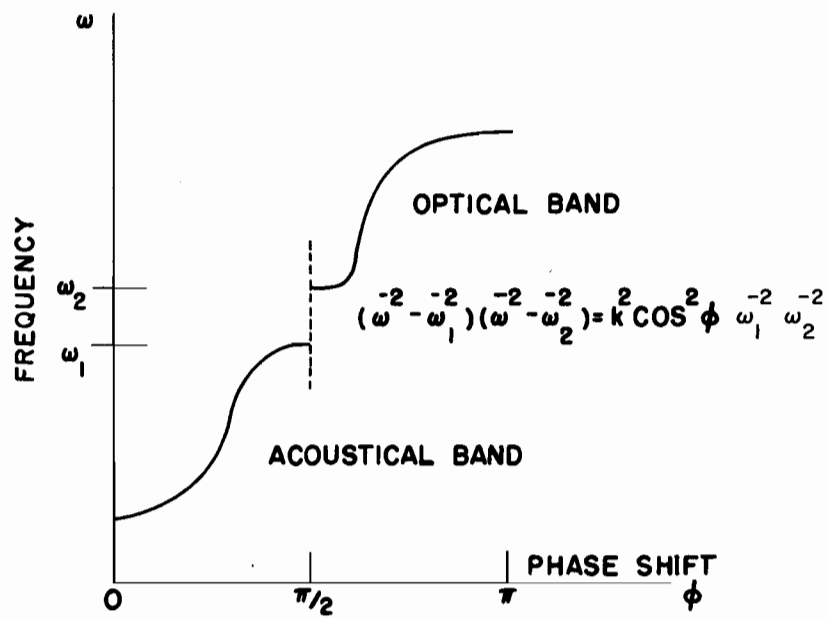

DISPERSION RELATION FOR CAVITIES OF TWO KINDS

Fig. 6

$$\omega_n^{-2} = \omega_o^{-2} (1 + \epsilon_n) .$$

First-Order Solutions

$$\delta\omega_\ell^{-2} = \omega_\ell^{-2} \left(\frac{1}{N} \sum_{o}^{N} \epsilon_n\right) \tag{9}$$

$$\delta \vec{i}^{\ell} = \sum_r \frac{\vec{i}^{\ell+r} \tilde{\epsilon}_r \left\{ - 1 + \frac{k}{2} \left(\cos \frac{2\pi Q}{N} - \cos \frac{2\pi r}{N}\right)\right\}}{k \left(\cos \frac{2\pi\ell}{N} - \cos \frac{2\pi r}{N}\right)} \tag{10}$$

where $\tilde{\epsilon}_r$ is the rth Fourier Transform of the error. This is written for a ring, but the application to the line is straightforward. One sees k must be kept large.

VII. Circuits of Two Kinds

Many of the structures of interest, cloverleaf, crossbar, side coupled iris, loop coupled iris, etc., are of doubly resonant character. The cavities useful mode resonates at frequency ω_1, say, and the coupling region itself resonates at frequency ω_2. Thus in the cloverleaf the slots themselves have a resonance at the frequency ω_2. We may represent approximately the actual behavior by a very simple model, namely of circuits of two kinds, as shown in Fig. 5. The equations now become

$$\begin{aligned} (\omega_1^{-2} - \omega^{-2}) i_{2n} + \frac{k}{2} \omega_1^{-1} \omega_2^{-1} (i_{2n-1} + i_{2n+1}) &= I_{2n} \omega_1^{-2} ; \\ (\omega_2^{-2} - \omega^{-2}) i_{2n+1} + \frac{k}{2} \omega_1^{-1} \omega_2^{-1} (i_{2n} + i_{2n+2}) &= I_{2n+1} \omega_2^{-2} . \end{aligned} \tag{11}$$

There are solutions to $\vec{I} = 0$ of the form

$$\begin{aligned} i_{2n} &= i_2 e^{2nj\varphi} \\ i_{2n+1} &= i_1 e^{(2n+1)j\varphi} , \end{aligned} \tag{12}$$

if

$$(\omega_1^{-2} - \omega^{-2})(\omega_2^{-2} - \omega^{-2}) = k^2 \omega_1^{-2} \omega_2^{-2} \cos^2\varphi . \tag{13}$$

This is the dispersion relation for the ring or chain of such resonators. It is shown in Fig. 6. It has two branches, known in lattice dynamics as the acoustical and optical branches.

There is a forbidden band of frequencies between the two branches. For $\omega_1 < \omega_2$ the lower $\pi/2$ mode corresponds to excitation of the main cavities +, -, +, -, $\cdots$, and zero energy in the coupling cells. This mode is called the π-mode if we use the simple model. The upper $\frac{\pi}{2}$ mode (energy in the coupling cells and none in the cavities) is missing for $\omega_1 < \omega_2$ because of the boundary conditions at the ends. The top of the acoustical band $\omega = \omega_1$, $\varphi = \pi/2$ turns out to be a useful operating point, as will be explained in the following paper. The fit of the measured points to this very simple model is remarkably close.

REFERENCES

1. L. Brillouin, Wave Propagation in Periodic Structures, Dover, New York (1953).

800 MEV RF STRUCTURES*

E. Knapp
Los Alamos Scientific Laboratory, University of California
Los Alamos, New Mexico

I would first like to say that the people who have been working on this are Bruce Knapp, Bill Shlaer, Jim Potter and myself. This report is certainly that of a joint effort.

For the successful construction of a high energy proton linear accelerator, an rf structure which provides an electromagnetic wave traveling with the velocity of the accelerating proton, which is insensitive to beam level in the accelerator, is easily monitored and controlled by the driving amplifier, and which has a minimum of power loss in its walls is necessary. It appears that a chain of cavities operating as a resonant structure, whose lengths are adjusted to provide the changing phase velocity required for the acceleration, best fulfills the above requirements. Due to the resonant cavity nature of the system, the axial dependence of the amplitude of the accelerating wave is not cirtically dependent on beam level as it would be in a traveling wave accelerator. It also has been possible to obtain structures which have good shunt impedances in a resonant mode and thus fulfill the efficiency requirement mentioned above.

Many structures which may be operated in π-mode have been proposed as accelerator elements. Among the possibilities are 1) an iris-loaded structure such as is used in a traveling wave application in the Stanford linear electron accelerators, 2) a crossed-bar structure suggested by Walkinshaw at Harwell and investigated by A. Carne there, 3) the cloverleaf structure discussed by Chodorow and Craig and investigated by A. Carne at Harwell, 4) a basket-weave structure such as has been suggested by Chodorow and Craig, 5) alternatively a set of loop-coupled pill-box cavities as have been discussed by the Harwell group, 6) modifications of many of the traveling wave amplifier tube structures, such as slow wave helices, which have been used successfully in that application. Structures which basically operate in the $\pi/2$ mode (resonant coupling, are also considered in this paper. Some work has been done on structures with resonant coupling loops by the Harwell group. A series of measurements on model cavities of the above types has been undertaken in order to choose a structure for use in the proposed linear accelerator meson facility at Los Alamos. In the following we will discuss in detail

*Work performed under the auspices of the U. S. Atomic Energy Commission.

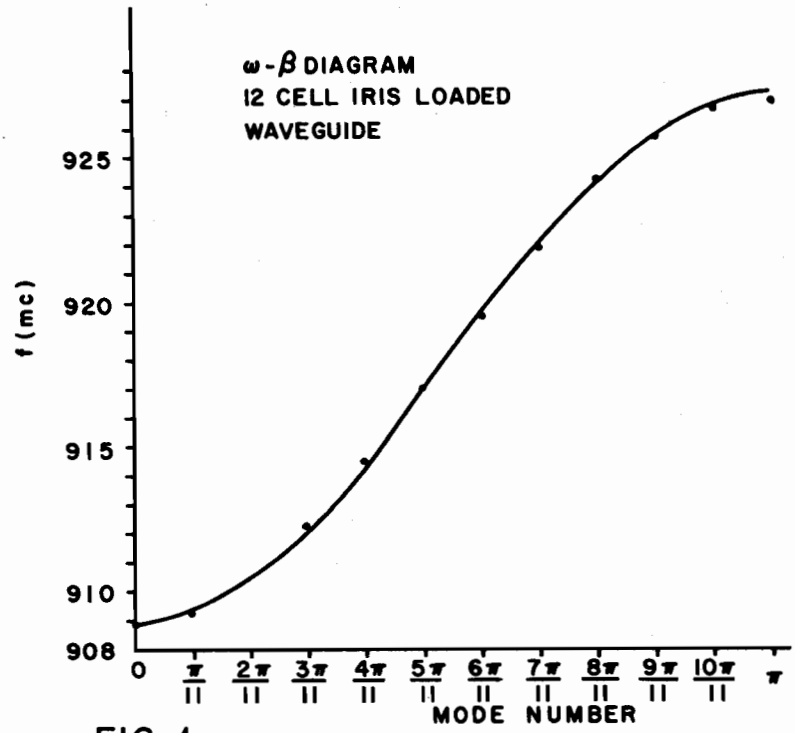
ω-β DIAGRAM
12 CELL IRIS LOADED
WAVEGUIDE
f (mc)
925
920
915
910
908
0
π/11
2π/11
3π/11
4π/11
5π/11
6π/11
7π/11
8π/11
9π/11
10π/11
π
MODE NUMBER

FIG. 1

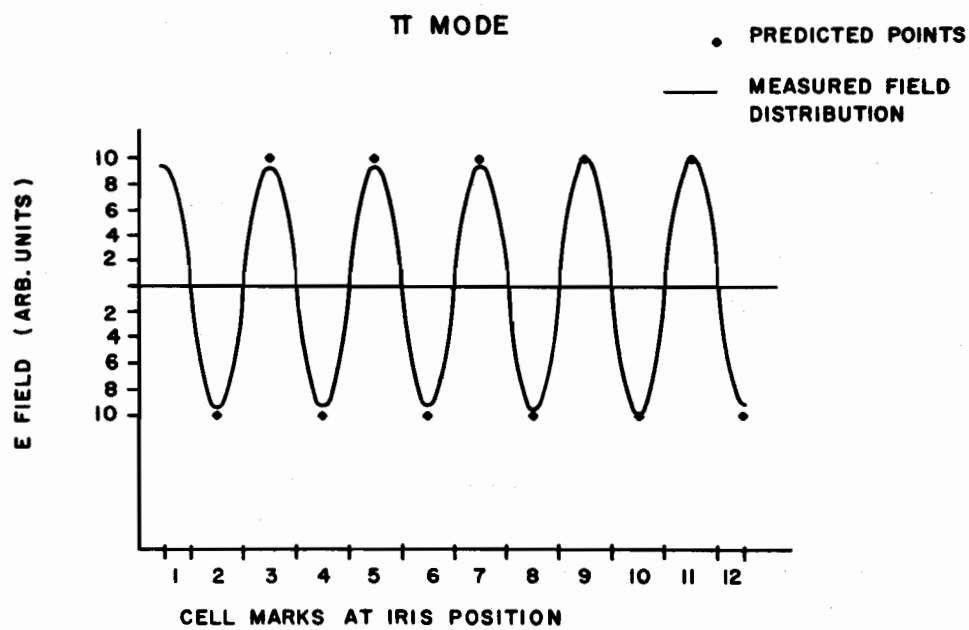
π MODE
PREDICTED POINTS
MEASURED FIELD DISTRIBUTION
E FIELD (ARB. UNITS)
10
8
6
4
2
2
4
6
8
10
1 2 3 4 5 6 7 8 9 10 11 12
CELL MARKS AT IRIS POSITION

FIG. 2

the cloverleaf structure mentioned above, and a possible $\pi/2$ mode configuration which exhibits good shunt impedance.

Electrical Properties of N Coupled Cavities

The electrical properties of n magnetically coupled lumped constant resonant circuits may be taken as a guide to the properties of n coupled cavities, with the appropriate identification of properties of the circuits to characteristics of the cavities. Such an analysis has been carried out and has been described in the previous paper. If there are N cells or cavities coupled together with a mutual inductance $M = k L$ where L is the self-inductance in each loop of the equivalent circuit, then there will be N resonant frequencies for the circuit as a whole, distributed in frequency as

$$1 - \frac{\omega_o^2}{\omega^2} + k \cos \phi = 0 \tag{1}$$

where ω_o = individual cell frequency. The circulating currents in the individual loops have amplitudes

$$i_n = \cos \frac{\pi q n}{N} ,$$

where n is the cell number and q the mode number. In π mode for a lossless case (q = N) all currents are equal, there is a π phase change from cell to cell, and the separation of the $\frac{(N-1)}{N}\pi$ mode from the π mode is

$$\frac{\Delta\omega}{\omega_o} = \frac{k \pi^2}{4 N^2}$$

for $k << 1$. Cleraly the coupling from cell to cell must be made as great as possible in order to keep good mode separation. If there are losses in the individual circuits, the phase change from cell to cell is no longer π, but $\pi - \Delta\phi$ where

$$\phi_{n, n+1} = \frac{2 (1 - k)}{k Q} \left(n + \frac{1}{2} \right)$$

or the phase shift across n cells is

$$\phi_{o, n} = \frac{(1 - k)}{k Q} n^2 \tag{3}$$

where n = 0 is the cell furthest from the drive and the numbering is toward the cell into which energy is introduced. In order to keep the phase velocity of the accelerating wave correct, $\Delta\phi$ must not change appreciably with beam level, which means k must be as high as possible. Finally, in order to be able to effectively tune or flatten the tank, the theory also indicates k must be as large as possible. First-order perturbation theory indicates that the amplitude error associated with a frequency error distribution

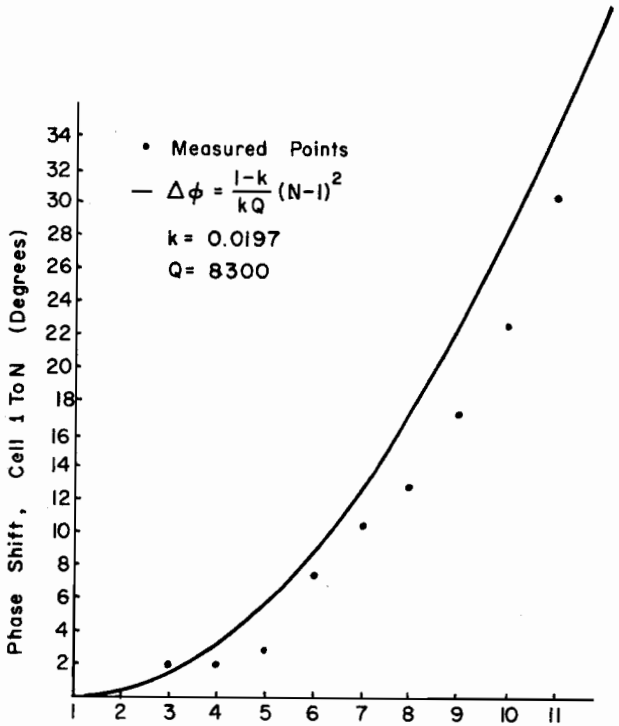

FIG. 3 Cell Number

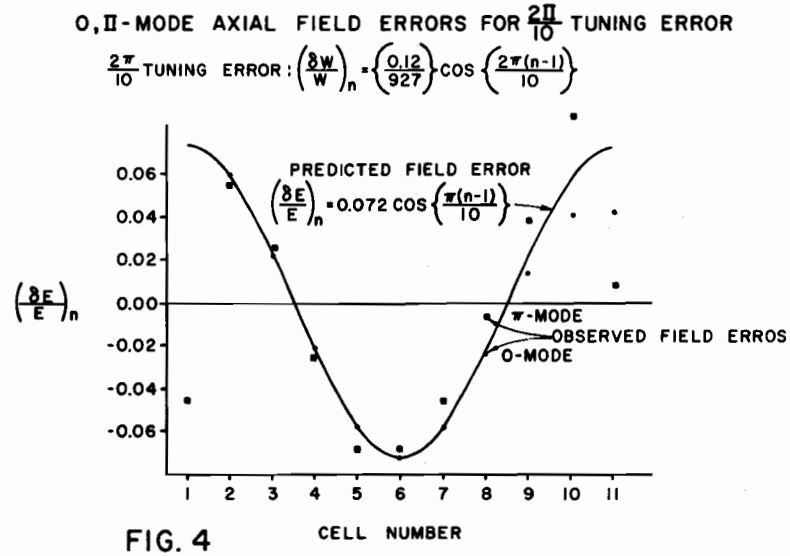

FIG. 4

$$\tilde{\epsilon}_r = \frac{2\,W(r)}{N} \sum_{p=0}^{N} W(p)\ \epsilon_p \cos\frac{\pi p r}{N} \tag{4}$$

where $W(p) = \frac{1}{2}$, $p = 0, N$

$W(p) = 1$, $p \neq 0, N$

$$\epsilon_p = \left(\frac{\omega_{op}^2 - \omega_o^2}{\omega_o^2} \right)_{p^{th}\ \text{cell}}$$

is

$$\delta i_n^q = \sum_{r=1}^{N} \tilde{\epsilon}_r \frac{1}{2} \left\{ \frac{W(q-r)}{W(r)}\ a_r \cos\frac{\pi(q+r)n}{N} + \frac{W(q+r)}{W(r)}\ a_{-r} \cos\frac{\pi(q-r)n}{N} \right\} \tag{5}$$

where $a_r = \left\{ \left(\frac{\omega_o}{\omega_{q+r}} \right)^2 - \left(\frac{\omega_o}{\omega_q} \right)^2 \right\}^{-1}$.

For a π mode

$$\frac{\delta I_n^N}{I_n^N} = \frac{1}{k} + \sum_{r=1}^{N} \tilde{\epsilon}_r \frac{\cos\frac{\pi r n}{N}}{1 - \cos\frac{\pi r}{N}} \tag{6}$$

and for $\pi/2$ mode we have

$$\frac{\delta I_n^{n/2}}{I_o^{N/2}} = -\frac{1}{k} \sum_{r=1}^{N} \tilde{\epsilon}_r \frac{W(N/2 - r)}{\sin\frac{\pi r}{N}} \sin\frac{\pi n}{2} \sin\frac{\pi r n}{N}, \tag{7}$$

These relationships have been verified for a 12-cell iris-loaded cavity to better than 5% accuracy. Here k is identified with the bandwidth of the structure

$$k = \frac{\omega_{(\pi)} - \omega_{(o)}}{\omega_{AVE}}$$

as would be indicated by Eq. (1). The current in Eq. (2) has been experimentally identified with the electric field at the center of individual cells.

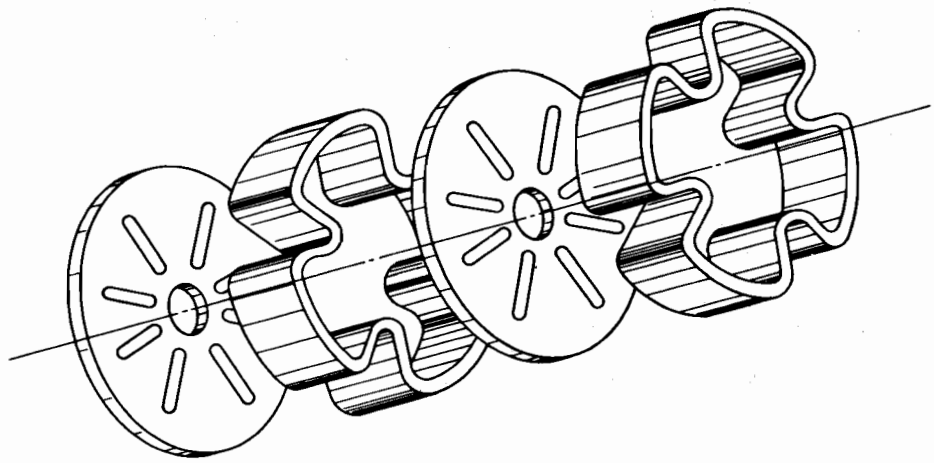

800 MEGACYCLE
CLOVERLEAF COMPONENTS

FIG. 5

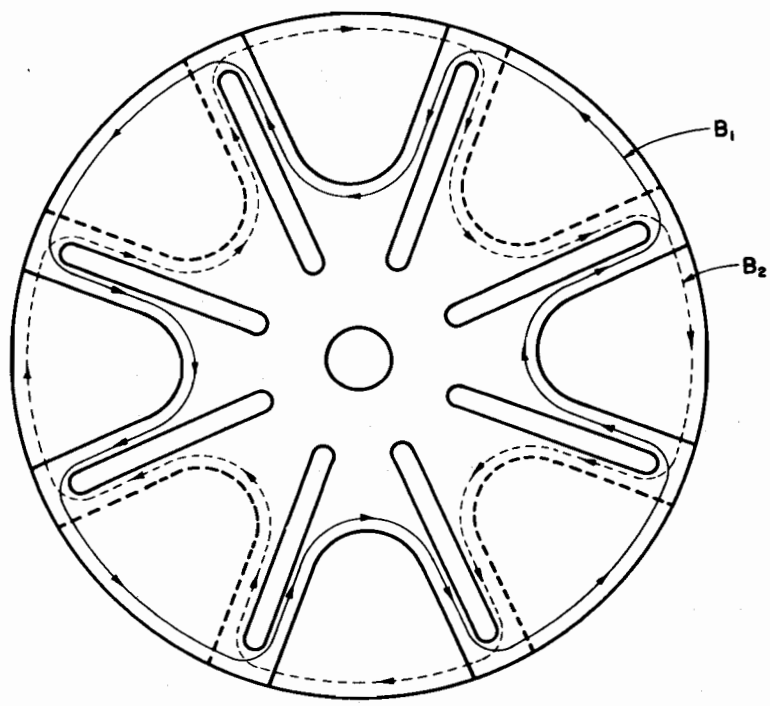

FIG. 6

Figure 1 shows the dispersion curve for a 12-cell iris-loaded waveguide resonator, compared to the predicted curve for k = 0.0197. Figure 2 shows the predicted center cell amplitudes vs measured field distributions for the π mode in the structure. Figure 3 shows the measured phase shift vs predicted phase shift for Q = 8300. Figure 4 shows a comparison of the measured and predicted ampltiude distributions for programmed tuning errors in the cavities.

The above theory suffices for an iris-loaded waveguide. However, in many instances the coupling mechanism itself may have resonances near the cavity resonant frequency. For this reason we have considered a chain of coupled resonators as before, but now alternating with frequencies ω_1 and ω_2, as also described in the previous paper. We then find a dispersion relation

$$\left(\omega^2 - \omega_1^2\right)\left(\omega^2 - \omega_2^2\right) = \omega^4 K^2 \cos^2 \phi \qquad (8)$$

where now ϕ is the phase change from cell to slot, say, and K is identified with the coupling of slot to cell. K may be identified with the full passband width if $\omega_1 = \omega_2$. The dispersion curve for a structure of this type displays a stop band as discussed in the previous paper. While the behavior of a chain of circuits such as this is somewhat more complex for the general case, an effective coupling constant k_{eff} may be defined to allow use of the single resonant frequency theory of phase shifts near the $\pi/2$ mode of the multiply resonant structures. This coupling constant may be defined by making a Taylor expansion of the dispersion curve near the $\pi/2$ mode for the multiply-periodic circuit and matching this to a symmetric dispersion curve as obtained in the theory for a chain of resonant cavities with a single resonant frequency. Carrying this out we find that

$$k = \frac{K^2}{2(P-1) + K^2} \qquad (9)$$

where $P = \omega_1^2 / \omega_2^2$.

The validity of this approximation has been investigated for the phase shift problem with computer runs and on experimental models and agrees very well with the observed results. For the perturbation theory, agreement with experiment seems excellent also.

In general, we find k's considerably bigger than the measured bandwidth, which would intuitively be the case since the dispersion curves are quite asymmetric. We shall refer to these expressions often as we describe the experimental results obtained.

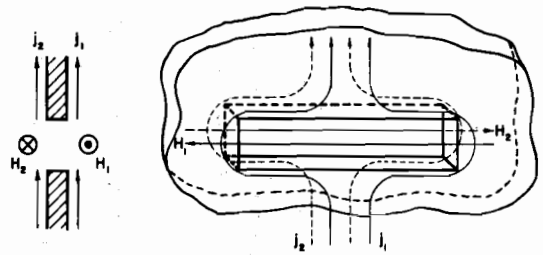

MAGNETIC FIELD OPPOSITE
ON EACH SIDE OF SLOT

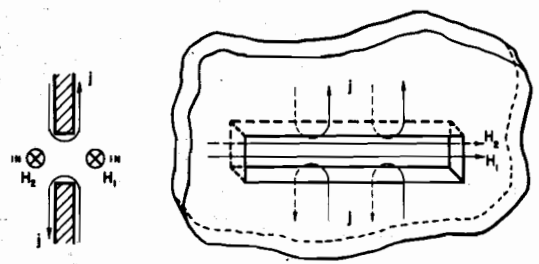

MAGNETIC FIELD IN SAME DIRECTION
ON EACH SIDE OF SLOT

FIG. 7

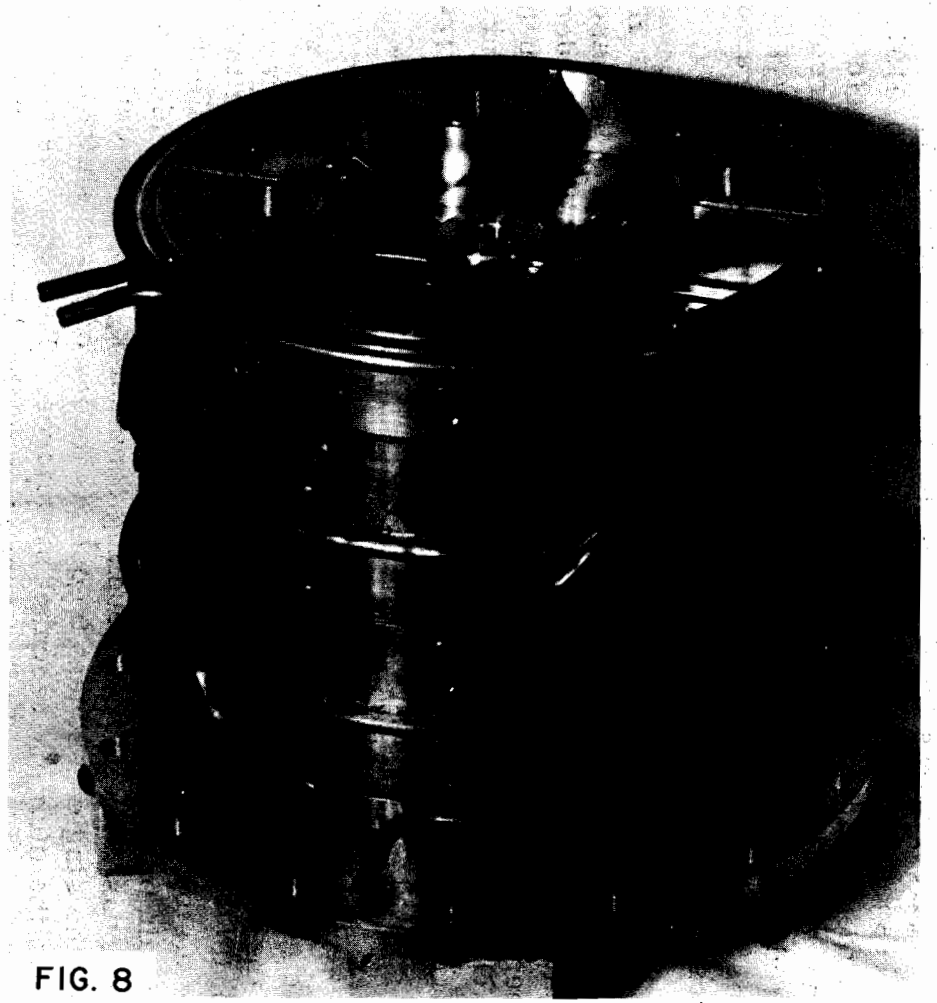

FIG. 8

Accelerator Efficiency

The efficiency of a resonant cavity as a particle accelerating device may be measured by considering the power required to provide a given acceleration; it is usually expressed in terms of the effective shunt impedance

$$ZT^2 = \frac{(\text{energy gain/meter})^2}{\text{power dissipated/meter}} = \frac{\text{ohms}}{\text{meter}}$$

where the energy gain is taken for a particle located in the center of the accelerating gap at peak electric field.

$$ZT^2 = \frac{\left(\int E\,(z,t)\,dz\right)^2}{P\,L} \tag{10}$$

where P = power dissipated in cavity, L = cavity length, and the integral is taken with the particle at the center of the cell at peak field.

The two most important criteria to be met by a π mode accelerating structure are that it have a large bandwidth (large k), and that the shunt impedance ZT^2 be as great as possible. In addition to these two criteria, it is reasonable also to expect the structure to develop no large electric fields in the mechanism used for coupling from cell to cell and not to present unsurmountable alignment or fabrication problems.

Structures Considered

Most of the mentioned type structures have been at least given a cursory examination with models using reasonable geometrical parameters. However, we have defined our principal investigation to two structures which look most promising to us, the cloverleaf π-mode structure and a version of a $\pi/2$ mode structure. Other laboratories are investigating most of the other structures more thoroughly than we could, so we will not comment on our results with these structures at this time.

CLOVERLEAF STRUCTURE

Historically the cloverleaf structure was invented for a traveling wave tube application by Chodorow and Craig and has been used commercially (Varian Assoc.) as an active element in a high power S-band traveling wave tube (types VA 125, VA 126, VA 145). Tube type VA 145 amplifies to 7 MW peak over an 8% bandwidth near 3 kMc. Other commercial tubes may be available of which we are not aware.

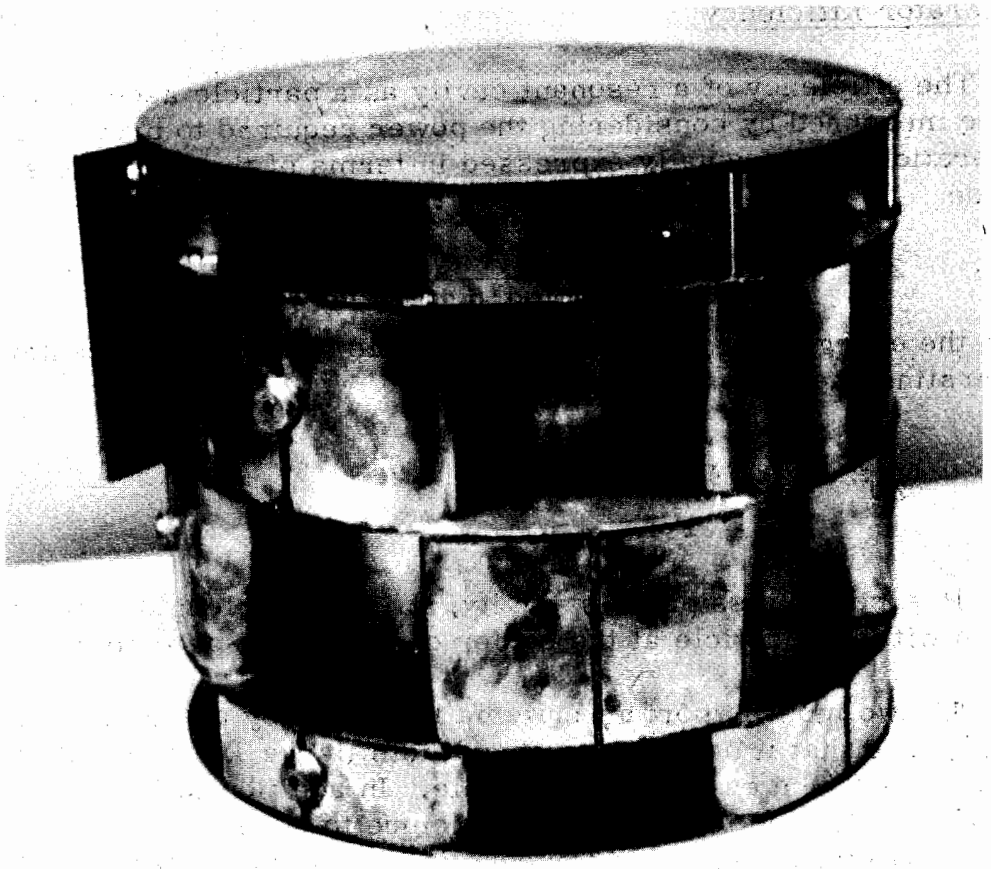

FIG. 9

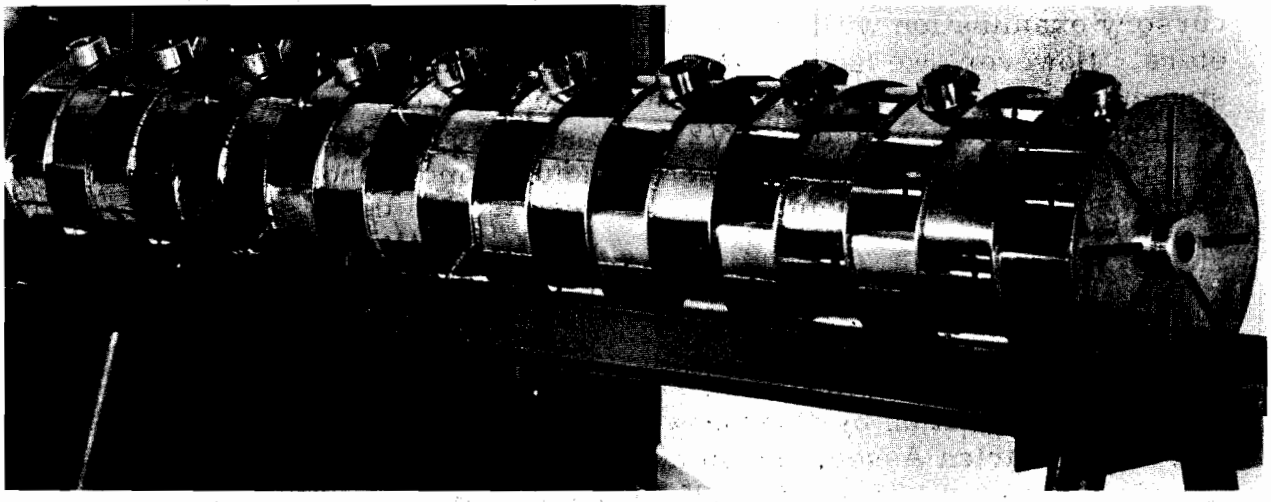

FIG. 10

Alan Carne from the Rutherford Laboratory has reported some studies on this structure as a possible element for a proton linear accelerator (Dubna Conference), and it was these measurements which drew our attention to this structure. As far as we know, no other measurements have been made for proton accelerator application of this structure.

Figure 5 shows an exploded view of the cloverleaf chain as envisioned by Chodorow and Craig. The periodicity operation in the cloverleaf is a translation by a cell length L and a rotation by 45°, as is indicated in more detail in Fig. 6.

Electromagnetically, the cloverleaf operates qualitatively as follows: Radial magnetic field lines are produced in the TM_{010} mode of a cylinder by deformations or noses in the walls of a cylindrical cavity at 90° intervals around its circumference. These radial fields may then be used to efficiently couple energy from one cell of the cloverleaf to the next by placing slots along these field lines. Eight slots are radially placed at 45° intervals straddling the noses protruding into the volume. On the other side of the septum we may have a 45° rotation of the cavity (forward wave structure) or 0° rotation of the structure (backward wave structure). For use as a standing wave accelerator structure, it is immaterial whether the structure is forward or backward wave. However, slot field levels and effective coupling strengths are important, and these are both favorable in the forward wave configuration for π-mode operation. In π mode with 45° rotation of the noses the radial fields are in the same direction on both sides of the slot. Figure 7 illustrates the current configurations near the slots in the cloverleaf for the zero mode (magnetic field opposite across slot) and π mode (magnetic field in same direction on each side of slot) in the forward wave configuration. The wall currents are clearly strongly perturbed in the zero mode and virtually unperturbed in the π mode, indicating a lowering of the zero mode frequency relative to that of the π mode (forward wave structure), and indicating that in π mode very little electric field will be developed across the slot. Energy transfer may be considered as a current interchange through the slot with almost no perturbation of the cavity mode fields in the process. The advantages we see in the cloverleaf as a standing wave accelerator structure are:

1. Coupling not dependent on beam aperture configuration.
2. Strong coupling available in π mode standing wave operation.
3. No strong electric fields present in coupling mechanisms.
4. Excellent shunt impedance possible, especially with capacitive loading in the cavities.

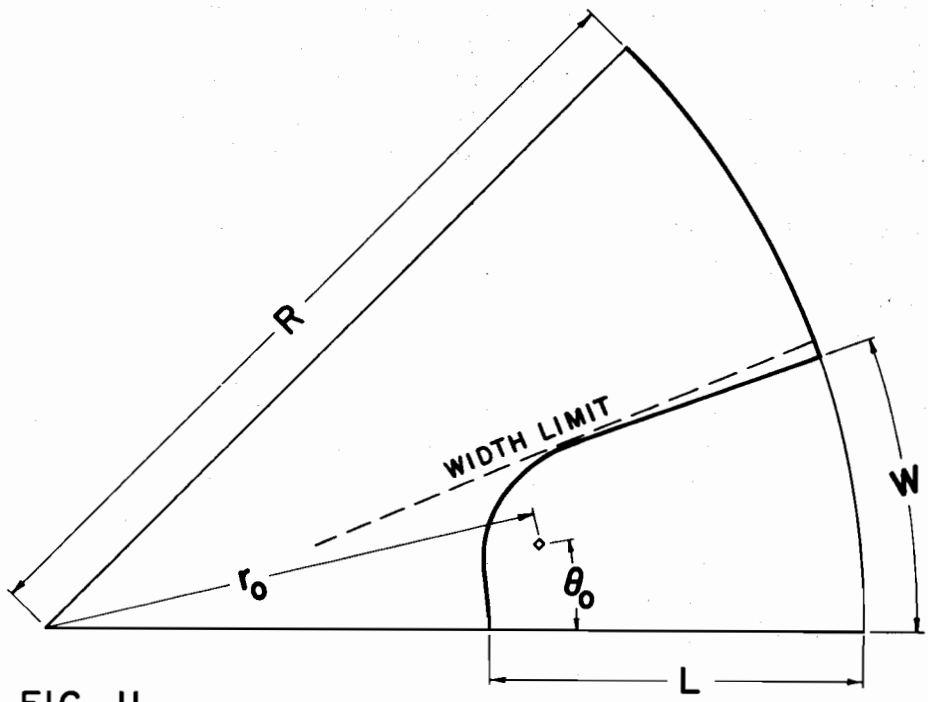
R
WIDTH LIMIT
W
r_o
θ_o
L

FIG. 11

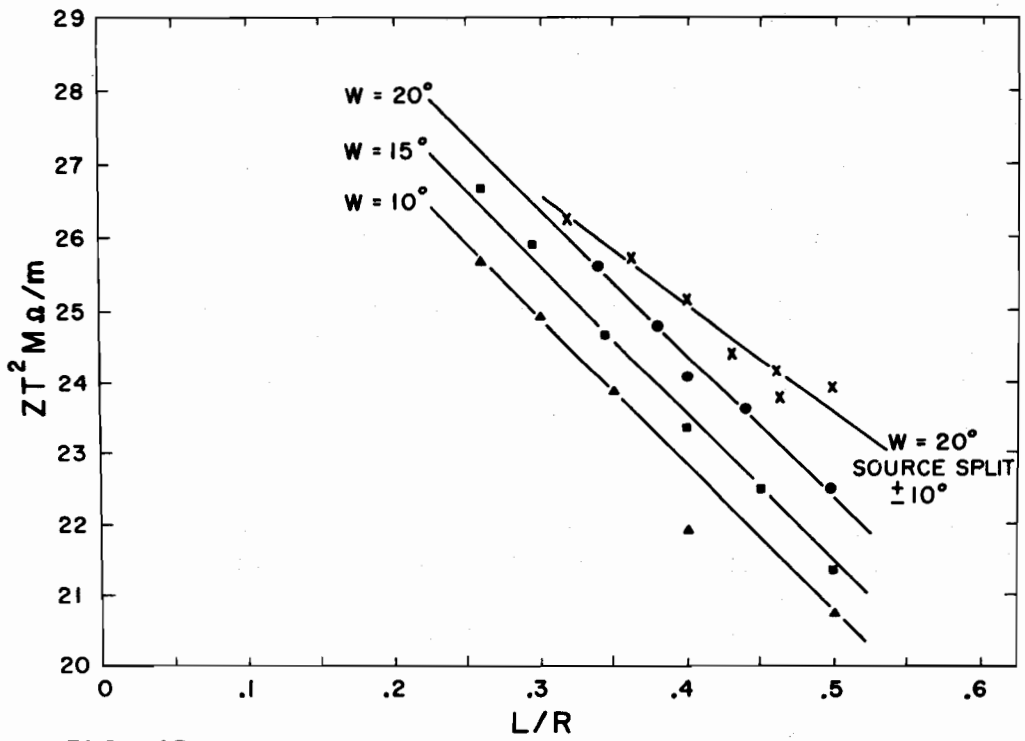
W = 20°
W = 15°
W = 10°
W = 20°
SOURCE SPLIT
± 10°
$ZT^2 M\Omega/m$
L/R
29
28
27
26
25
24
23
22
21
20
0
.1
.2
.3
.4
.5
.6

FIG. 12

In order to investigate the properties of the cloverleaf more fully, we have constructed several models and measured their properties. Figure 8 shows a photograph of a demountable carefully machined model on which most of the optimizing studies have been done. This model allows the septum configuration to be changed at will, allowing studies of slot dimensions, beam hole size and configuration, and so on to be made. This model does not allow changes to be made in nose dimension. Also this model, because of its demountable joints, does not allow reliable Q measurements to be made; however, Z/Q measurements are quite reliable.

In order to make reliable Q measurements, several models were made up of two cells and two half cells (similar to the demountable configuration) in which all joints were brazed. These were manufactured by pressing 1/16-inch copper sheet in quadrants to form the cloverleaf walls, and heli-arc brazing the parts together with Sil-Fos solder. Using this same technique several single cell cloverleaf cavities were constructed also. Figure 9 shows a representative cavity of this type.

Figure 10 shows a 21-cell tank made by the same technique as above. This tank has been designed rather conservatively and has been used so far to check out the results of the shorter model studies and the predictions of the coupled circuit theory.

OPTIMIZATION OF NOSE SHAPE

Bill Shlaer at this laboratory has developed a computational program that allows calculation of electric and magnetic fields in a resonator similar to the cloverleaf. The fields in these resonators are generated by line currents oscillating at 800 Mc and located symmetrically in quadrants of a metal cylinder. The fields are assumed z-independent. In many respects this calculation is similar to that done by R. Gluckstern for drift tube and iris structures. Figure 11 shows the configuration of line currents (shown at position r_o and θ_o in an octant). The resultant fields may be varied by varying the cylinder radius and source radius. For certain ranges of these parameters, there is a zero of the electric field along which a new boundary may be drawn that will separate the currents from the rest of the cylinder. This remainder is resonant at 800 Mc with the same field distribution and may have the shape of a cloverleaf. These calculations do not include slots, beam holes, or any z-asymmetries. However, they do allow optimization of lobe shape for a given lobe penetration. Figure 12 shows shunt impedances calculated vs nose penetration L/R with nose width as a parameter. One family of flat-nosed lobes is included. It appears that for minimum losses, flat-nosed lobes are to be preferred with maximum width possible. These

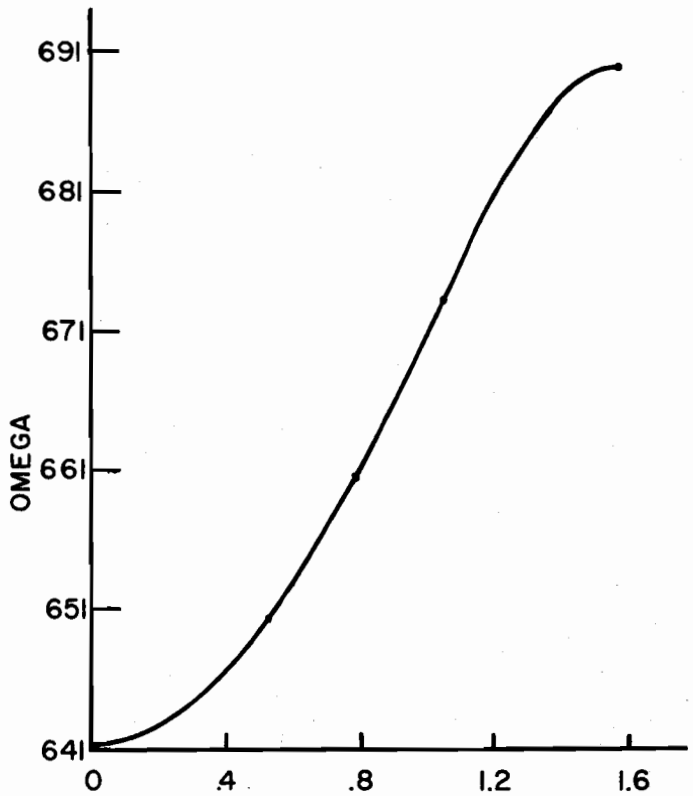
691
681
671
661
651
641
OMEGA
0
.4
.8
1.2
1.6
RADIANS

FIG. 13

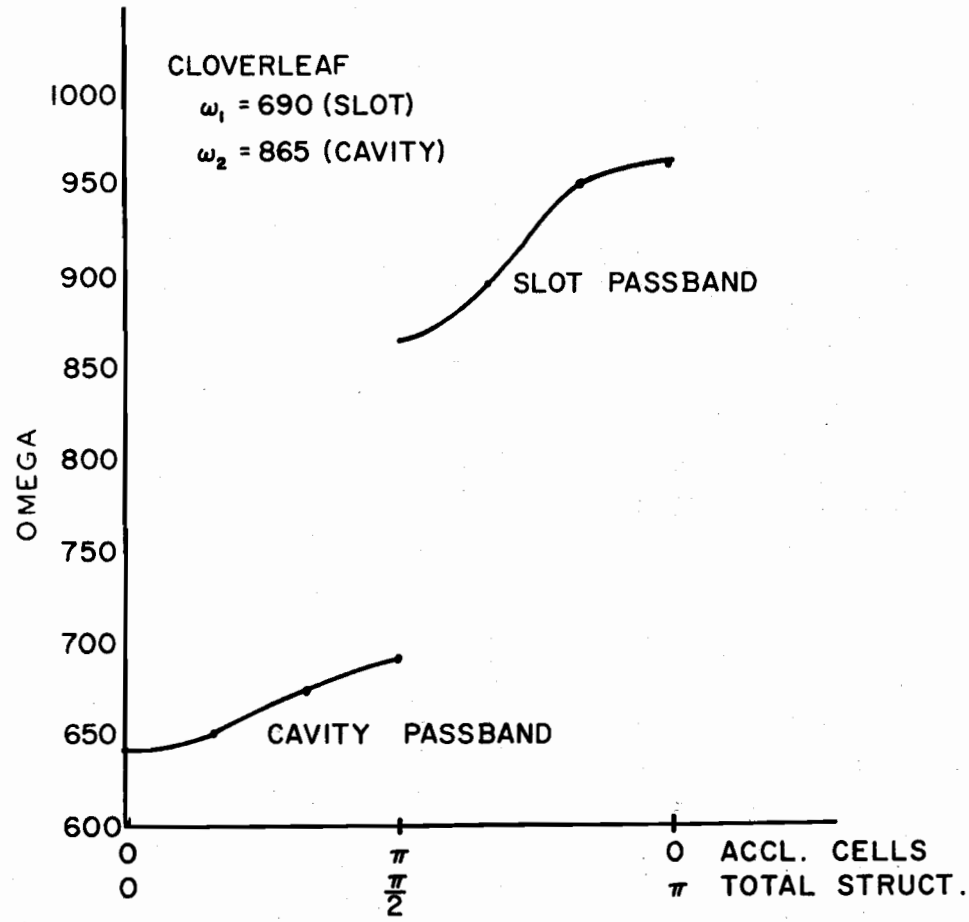
CLOVERLEAF
ω_1 = 690 (SLOT)
ω_2 = 865 (CAVITY)
1000
950
900
850
800
750
700
650
600
OMEGA
SLOT PASSBAND
CAVITY PASSBAND
0
0
π
$\frac{\pi}{2}$
0 ACCL. CELLS
π TOTAL STRUCT.
MODE

FIG. 14

calculations have been checked at two points with single cell cloverleaf cavities, and the quantities measured agree with calculated values quite well.

COUPLING STUDIES

The coupled circuit theory has been used extensively to analyze the behavior of the cloverleaf as far as its dispersion curve, tuning sensitivity, phase shifts and other electrical behaviors are concerned. It should be clear that the coupled circuits of two kinds with frequencies ω_1 and ω_2 certainly approximate the cloverleaf, with frequencies ω_1 associated with the cavities and ω_2 associated with the slots. Figure 13 shows a dispersion curve fitted to five data points taken from the demountable cloverleaf model. In this case, the cavity was capacitively loaded so that π mode frequency was 690 Mc/sec. This is a five-point fit to a three-parameter function (ω_1, ω_2, K); the maximum deviation of any point from the fitted curve is 28 kc which is only a little larger than measurement accuracy (full Q width at 3 db = 50 kc). We would thus say the theory fits the performance of this cloverleaf model exceedingly well. Many other model configurations have been fit and almost all agree this well with the theory. The upper branch of the passband may also be observed, and although the fit is no longer as good if these data points are included, indications are that the theory does adequately describe the observations. Fits with deviations to about 1 Mc are observed for this procedure. The presence of higher cavity modes not orthogonal to the slot mode, which couples the cavities in the TM_{010} mode, can effectively change the position of the upper branch somewhat. Figure 14 shows a fit of this type. In this case, the data are the same as in Fig. 13, but the slot mode points have been included. If ω_{cavity} is greater than ω_{slot}, the relative positions of the passbands are reversed and the structure becomes a backward wave device. Figure 15 illustrates this.

The important parameter as far as coupling is concerned is the effective bandwidth k_{eff} defined previously. As was mentioned this parameter enters strongly in the mode separation, phase shifts, and flattening sensitivity of the structure. Figure 16 shows a plot of k_{eff} vs slot length and width for the demountable cloverleaf, this time with no capacitive loading. The π mode frequency is 840 Mc. This curve is derived from the dispersion curve data points by fitting these points to the theoretical expressions to obtain K, ω_1 and ω_2, and then calculating k_{eff} from these parameters. It is found that the parameter K, yielding the coupling from slot to cavity, is virtually independent of slot configuration. This might be expected since the slot is very tightly coupled to the cavity fields, almost independent of its dimensions. With this information, it is clear from the figure that the effective coupling

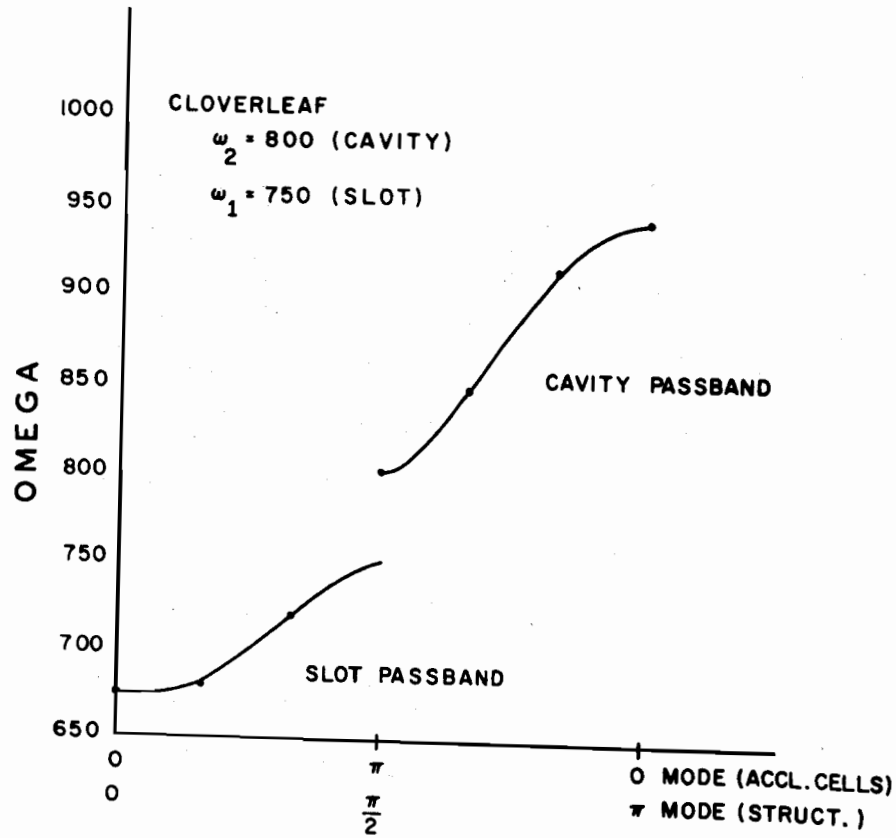
CLOVERLEAF
ω_2 = 800 (CAVITY)
ω_1 = 750 (SLOT)
OMEGA
1000
950
900
850
800
750
700
650
CAVITY PASSBAND
SLOT PASSBAND
0
0
π
$\frac{\pi}{2}$
0 MODE (ACCL. CELLS)
π MODE (STRUCT.)

FIG. 15

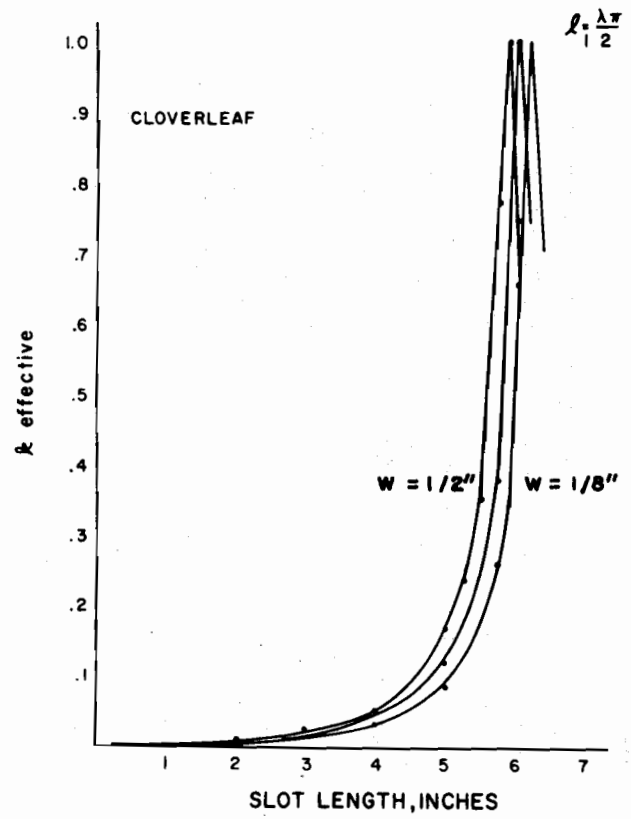
$\ell = \frac{\lambda\pi}{12}$
CLOVERLEAF
k effective
1.0
.9
.8
.7
.6
.5
.4
.3
.2
.1
W = 1/2"
W = 1/8"
1
2
3
4
5
6
7
SLOT LENGTH, INCHES

FIG. 16

depends almost entirely on the resonant frequency of the slot. The dependence on width appears only as a change in resonant frequency with length (the effective length of the slot being somewhat longer than the actual length, the wider the slot the longer the effective length). At the slot length where the cavity frequency and the slot frequency are equal $k_{eff} = 1$, there are no phase shifts down the system, and the structure behaves as a $\pi/2$ mode structure as far as flattening and stability are concerned. It might be noted at this juncture that at resonance the slots should not have any appreciable electric field present, for a $\pi/2$ mode structure stores no energy in alternate cells in standing wave operation. For slot lengths giving resonant frequencies higher than the cavity frequency, very reasonable effective coupling constants may be obtained. Computer studies indicate very loose tolerance requirements are necessary on slot dimensions in order to get satisfactory performance. Even at resonance, variations of several megacycles in slot resonant frequency (like 0.025" in slot length) should have virtually no effect on performance.

As the accelerating cells get shorter, we should expect K to increase, yielding somewhat higher k_{eff} for the same slot length at lower energies.

Optimization of Shunt Impedance

The equation for shunt impedance may be written

$$ZT^2 = \frac{\left(\int E(z,t)\,dz\right)^2}{P\,L} = \frac{\left(n\int_0^{\ell} E(z)\sin\frac{\pi z}{\ell}\,dz\right)^2 Q}{\omega U\, n\ell}$$

where $Q = \frac{\omega U}{P}$, U = total stored energy in cavity, ℓ = cell length, L = cavity length, $n\ell = L$. The quantity ZT^2/Q may be evaluated using standard perturbation techniques (1). For a spherical metallic bead of radius r_o on the axis of a cavity of the type considered,

$$\frac{ZT^2}{Q} = \frac{\left(\int \left(\frac{\Delta f}{f}\right)^{1/2} \sin\frac{\pi z}{\ell}\,dz\right)^2 n}{\epsilon_o\,\pi\, r_o^3\,\omega} \tag{11}$$

where $\frac{\Delta f}{f}$ = fractional resonant frequency shift produced at position z. It should be noted that this quantity is dependent upon geometrical factors only; losses in the cavity walls do not enter the expression. From a practical point of view, this means that errors in the values of ZT^2/Q

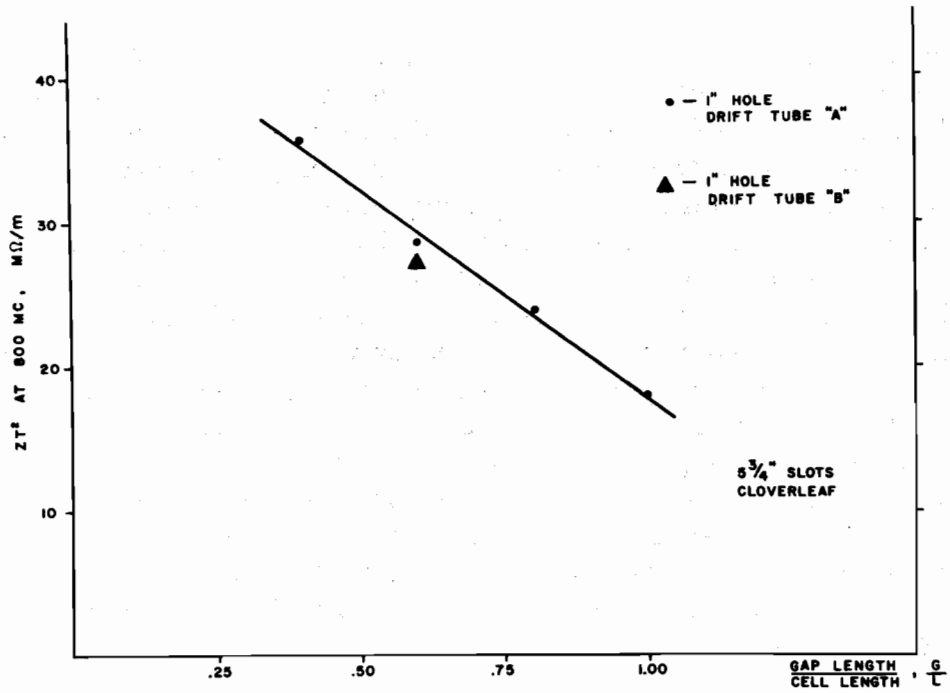

VARIATION OF SHUNT IMPEDANCE WITH DRIFT TUBE PARAMETERS

FIG. 17

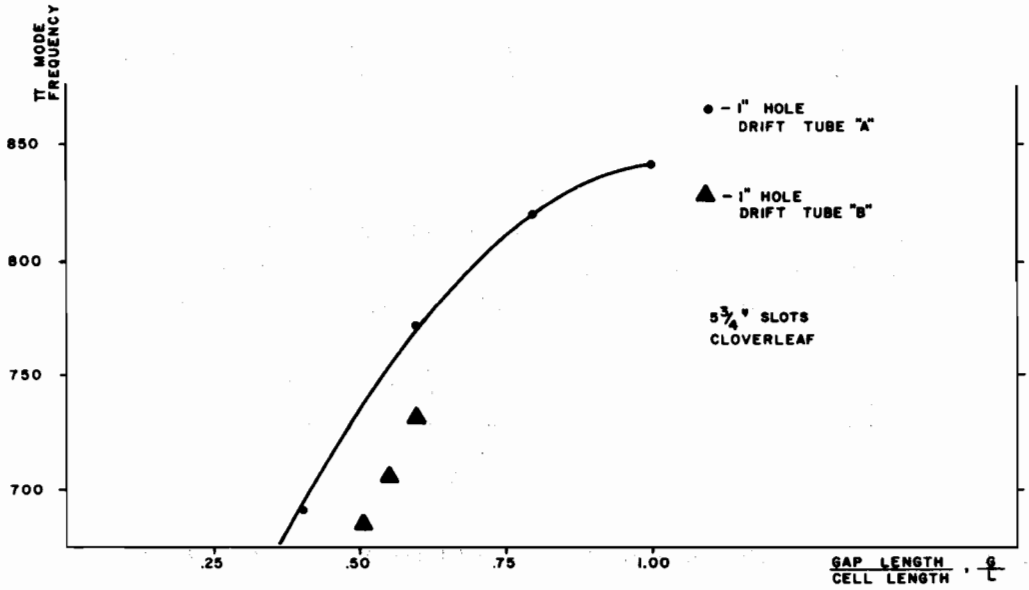

VARIATION OF π MODE FREQUENCY WITH DRIFT TUBE PARAMETERS

FIG. 18

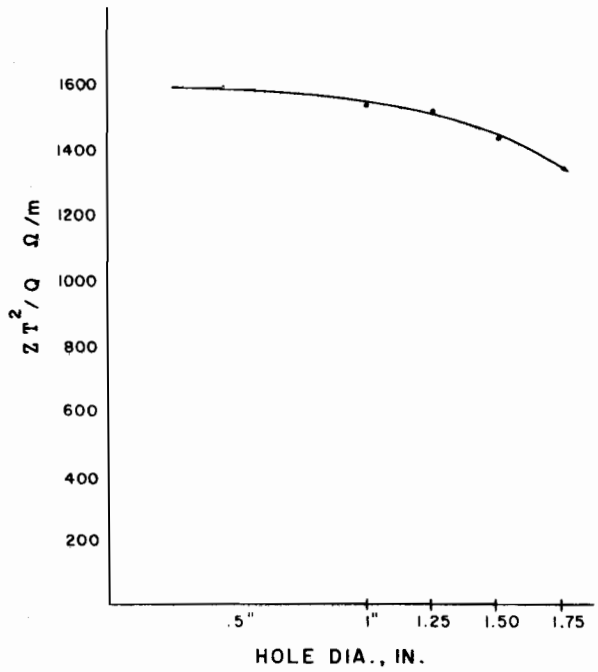
1600
1400
1200
1000
800
600
400
200
ZT^2/Q Ω/m
.5"
1"
1.25
1.50
1.75
HOLE DIA., IN.

FIG. 19

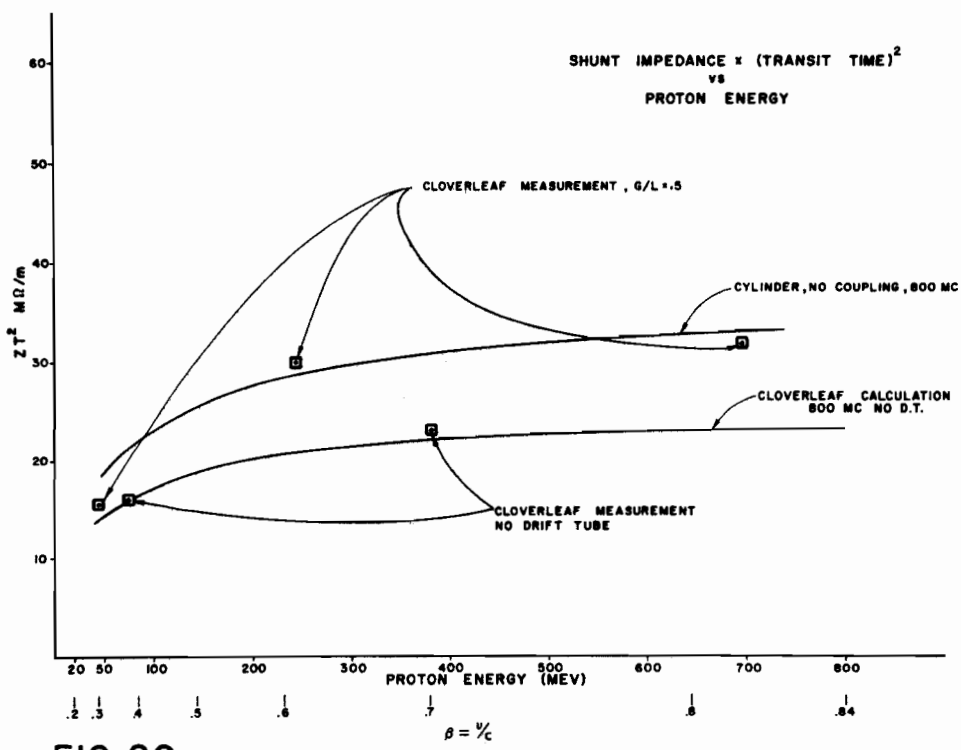
SHUNT IMPEDANCE x (TRANSIT TIME)^2
VS
PROTON ENERGY
CLOVERLEAF MEASUREMENT, G/L = .5
CYLINDER, NO COUPLING, 800 MC
CLOVERLEAF CALCULATION
800 MC NO D.T.
CLOVERLEAF MEASUREMENT
NO DRIFT TUBE
ZT^2 MΩ/m
60
50
40
30
20
10
20
50
100
200
300
400
500
600
700
800
PROTON ENERGY (MEV)
.2
.3
.4
.5
.6
.7
.8
.84
$\beta = v/c$

FIG. 20

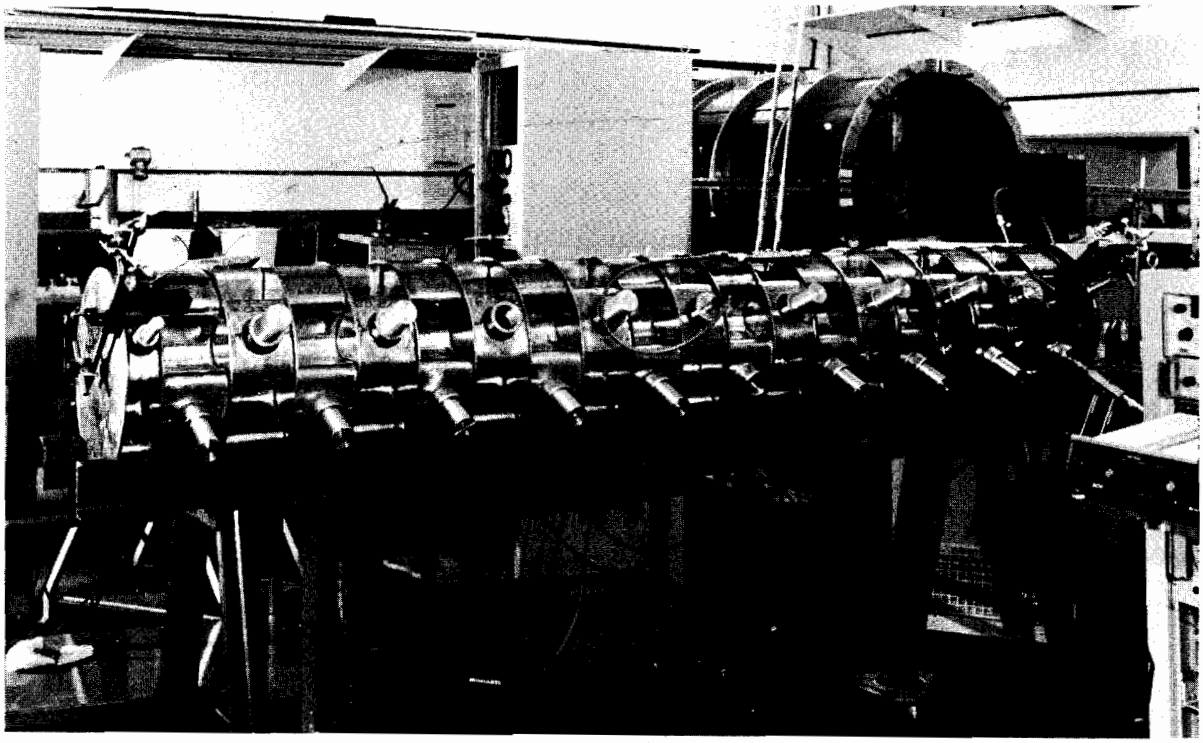

FIG. 21

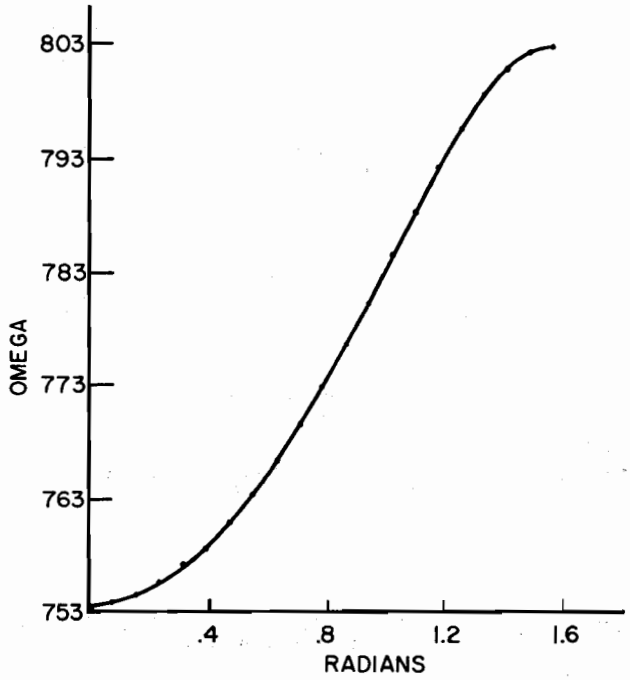

FIG. 22 21 Cell Air Model Cloverleaf Axial Field Flat To 1 Per Cent

obtained with demountable models are not dependent to any great extent upon the quality of the current joints attainable, and a relatively great trust may be placed in values obtained in somewhat crude models. However, to determine the effective shunt impedance accurately, an accurate determination of Q as well as ZT^2/Q is necessary. This is not a trivial problem, for the Q of a cavity depends very critically on the quality of the current joints in that cavity. Great pains have been taken to make high quality current joints in the demountable models tested, and even then variations on the order of 10% may be observed from one assembly to the next for identical configurations. In general, we can say that the values of ZT^2 quoted are lower than those realizable in cavities with all brazed joints, perhaps as much as 10% low. Q has been measured by measuring the power transmitted through a cavity as a function of frequency. With a highly undercoupled situation (small coupling loops) the frequency width of the half power points yields Q directly.

$$\left(\frac{\Delta f}{f}\right)_{1/2\ \text{power}} = \frac{1}{Q}$$

Other methods have been used, but this is the simplest and is accurate enough for the measurements we wish to make.

Variation of Shunt Impedance with Drift Tube Parameters

A reasonable way to increase the shunt impedance of the cloverleaf structure is to add drift tubes to the center of the septum walls in order to increase the transit time factor T^2 and to concentrate the stored energy in the cavity near the axis, effectively increasing Z/Q as well as T^2. Measurements have been made on the demountable model for two different shaped drift tubes. Figure 17 shows the variation of shunt impedance observed with g/ℓ (the ratio of gap length to cell length) for a 1" beam aperture. These results have been scaled to 800 Mc. Figure 18 shows the variation of π mode frequency. Figure 19 shows the variation of shunt impedance with hole size for $g/\ell = 0.6$. It is apparent that a large improvement in shunt impedance may be produced with the addition of drift tubes to the structure.

Several models with formed walls and all brazed construction have been fabricated to get reliable values of Q and ZT^2 for geometries which might be considered as elements in an accelerator. These models show Q's within 5% of theoretical for geometries where calculations are available.

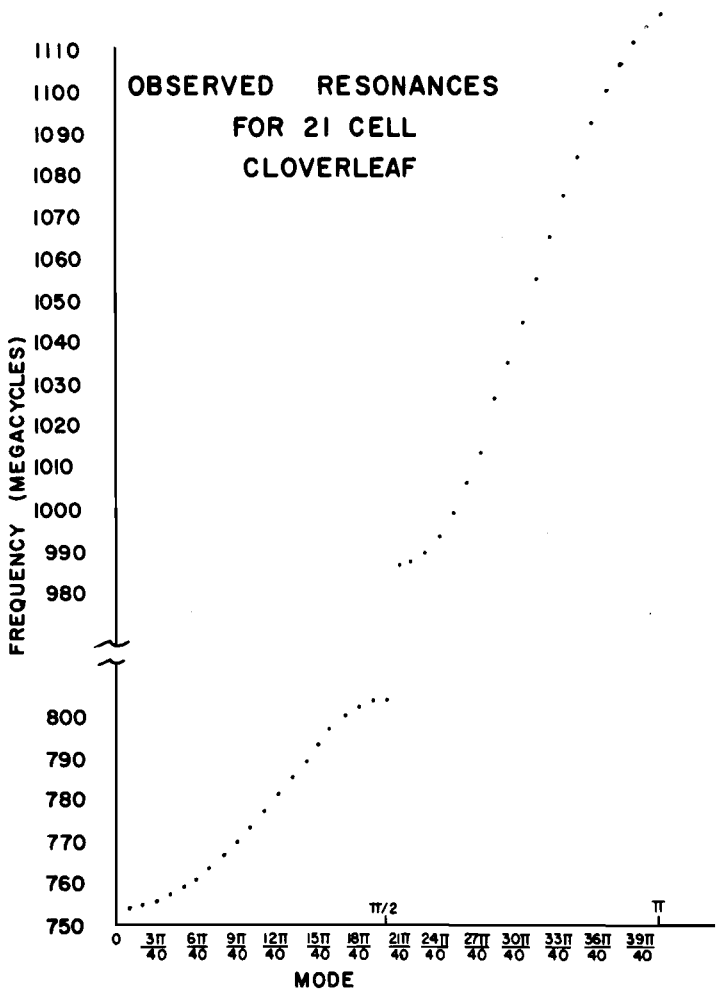
OBSERVED RESONANCES
FOR 21 CELL
CLOVERLEAF
FREQUENCY (MEGACYCLES)
1110
1100
1090
1080
1070
1060
1050
1040
1030
1020
1010
1000
990
980
800
790
780
770
760
750
0
3π/40
6π/40
9π/40
12π/40
15π/40
18π/40
π/2
21π/40
24π/40
27π/40
30π/40
33π/40
36π/40
39π/40
π
MODE

FIG. 23

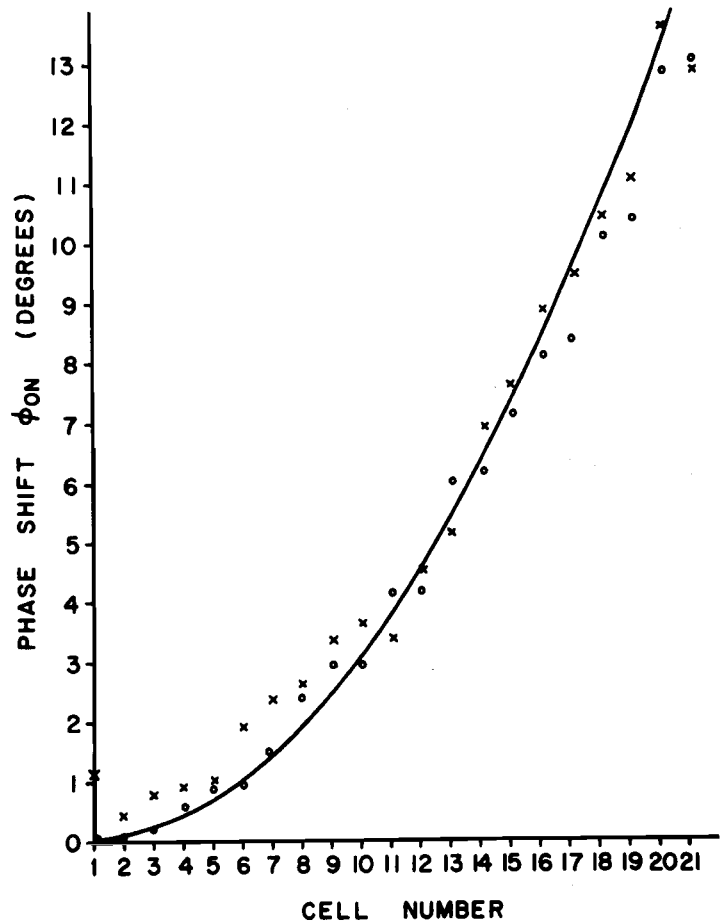
PHASE SHIFT ϕ_{ON} (DEGREES)
0
1
2
3
4
5
6
7
8
9
10
11
12
13
1 2 3 4 5 6 7 8 9 10 11 12 13 14 15 16 17 18 19 20 21
CELL NUMBER

FIG. 24

A conservative set of parameters which we have investigated is:

g/ℓ	=	0.5
ω_{slot}	=	980 Mc (scaled from 840)
W_{π}	=	805 Mc/sec (scaled from 690)
k_{eff}	=	0.1042
L_{nose}/R	=	0.505
Hole size	=	1.25"
ZT^2	=	17 MΩ/m at β = 0.30 29 MΩ/m at β = 0.61 32 MΩ/m at β = 0.81

Figure 20 shows these data points plotted vs energy.

Higher values of shunt impedance could be obtained for various changes in the parameters above. It appears that decreasing g/ℓ will increase ZT^2 even more. Peak fields will set the limit for this change, and since no sparking measurements have yet been made, we do not feel justified in pushing this parameter. From dielectric bead measurements, we calculate peak fields on the drift tube surfaces of about 5 MV/m for 1 MV/m acceleration rate in the g/ℓ = 0.5 cavity at β = 0.6. This is certainly conservative. Flattening the ends of the noses will add a few per cent to the shunt impedance, but it is not felt worthwhile at this time.

21-Cell Prototype Model

Using approximately the above parameters (β = 0.68), a 21-cell cavity has been constructed using the bent sheet metal technique with brazed joints. Figure 21 shows this model set up in our laboratory. The dispersion curve for this model is shown in Fig. 22. This was taken after the tank was flattened to about 1% in E. All points on this curve fit the calculated curve to better than 300 kc, the average error being about 75 kc. Figure 23 shows this dispersion curve with both passbands indicated. Analysis of these data gives an effective coupling k = 0.94, ω_1 = 803, and ω_2 = 934 Mc/sec.

The power flow phase shift has been measured in this model with the tank driven at one end (equivalent to a 40-cell tank driven in the middle). Figure 24 shows the measured values of phase shift along with the theoretical value given by

$$\Delta\phi_{n,o} = \frac{1 - k_{eff}}{k_{eff}\, Q} \quad n^2$$

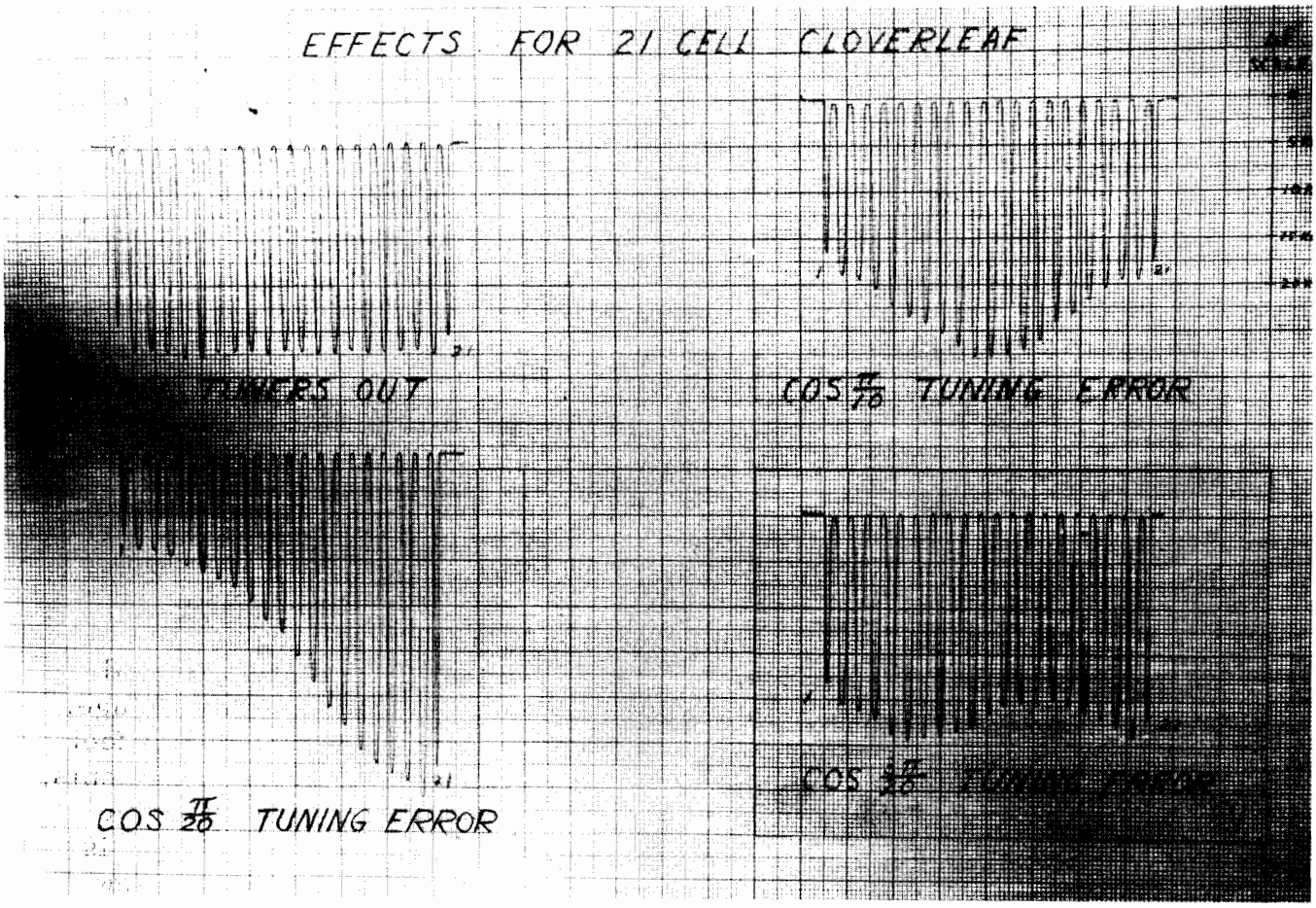
EFFECTS FOR 21 CELL CLOVERLEAF
COS π/20 TUNING ERROR

FIG. 25

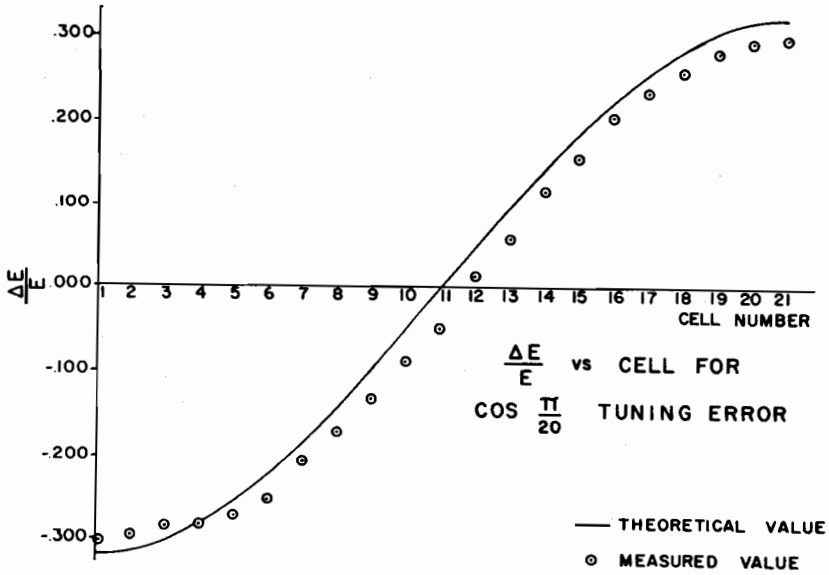
.300
.200
.100
ΔE/E .000
-.100
-.200
-.300
1 2 3 4 5 6 7 8 9 10 11 12 13 14 15 16 17 18 19 20 21
CELL NUMBER
ΔE/E vs CELL FOR
COS π/20 TUNING ERROR
THEORETICAL VALUE
MEASURED VALUE

FIG. 26

where n is the number of cells downstream (away from the power source) from the cell in question.

The agreement between our theoretical expressions and the model measurements seems quite good.

For a π mode structure with effective coupling k we have the perturbation expression

$$\frac{\delta I_n^N}{I_n^N} = \frac{1}{k_{eff}} \sum_{r=1}^{N} \tilde{\epsilon}_r \frac{\cos \frac{\pi r n}{N}}{1 - \cos \frac{\pi r}{N}} .$$

If we introduce a tuning error $\frac{\delta \omega_n}{\omega_o} = a \cos \frac{\pi n p}{N}$ into our tank, we may check the predictions of the perturbation theory with the observed changes in field level in the tank. We have done this for p = 1, 2, and 3. Figure 25 shows the data for these measurements. A bead was pulled along the cavity axis at a constant rate, and the resonant frequency of the cavity scaled on a fast scaler. Frequency differences were recorded using a digital-to-analog converter; they were plotted directly by a x-y plotter, providing the records shown in the figure. The amplitude error induced may then be compared to the predictions of the perturbation theory. Figures 26, 27 and 28 show the comparison between the theoretical curves and the experimental points measured. Agreement seems quite good. From experience gained in flattening this prototype it appears that wall deformation will be adequate for tuning; no tuners should be required. Shunt impedance measurements indicate the same values quoted above for the shorter models.

Resonant Coupled Structures

Dunn, Sable and Thompson at Harwell were perhaps the first to point out some of the advantages of operating a structure with resonant coupling. The equivalent circuit theory used here allows even more advantages to be seen in the use of structures of this type. A resonant coupled π mode structure may be considered as a $\pi/2$ mode structure with cells of type 1 and 2 operating at the same resonant frequencies. Some properties of $\pi/2$ mode operation are

1. Every other cell (in this case the resonant coupling element) has no stored energy associated with it other than that required to transmit power to make up losses. This can be seen directly from the eigenfunctions of the chain

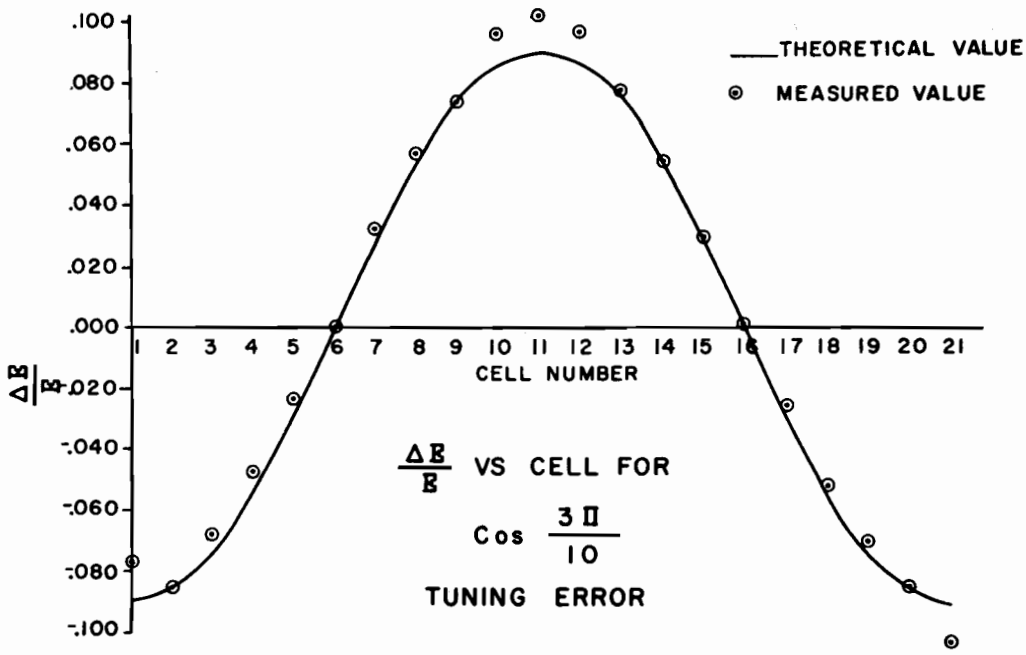
.100
.080
.060
.040
.020
.000
-.020
-.040
-.060
-.080
-.100
ΔE/E
1 2 3 4 5 6 7 8 9 10 11 12 13 14 15 16 17 18 19 20 21
CELL NUMBER
THEORETICAL VALUE
MEASURED VALUE
ΔE/E VS CELL FOR
Cos 3Π/10
TUNING ERROR

FIG. 27

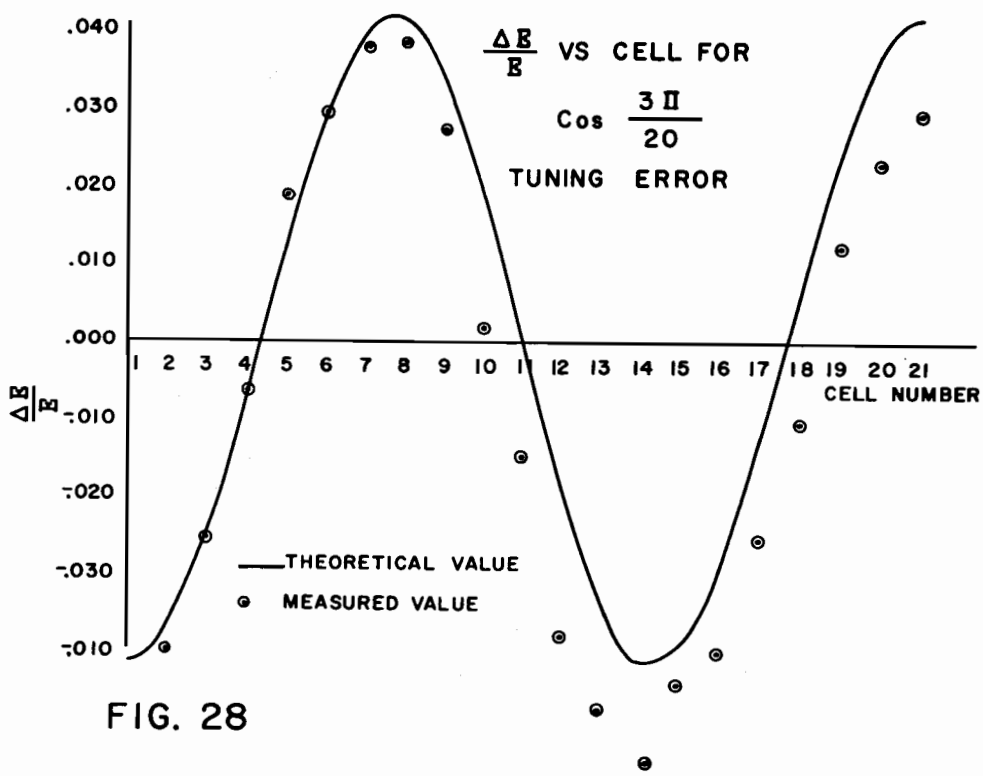
.040
.030
.020
.010
.000
-.010
-.020
-.030
-.010
ΔE/E
1 2 3 4 5 6 7 8 9 10 11 12 13 14 15 16 17 18 19 20 21
CELL NUMBER
ΔE/E VS CELL FOR
Cos 3Π/20
TUNING ERROR
THEORETICAL VALUE
MEASURED VALUE

FIG. 28

$$i_n^{N/2} = \cos \frac{\pi}{2} n .$$

Thus one should not have to worry about sparking in coupling elements, losses in coupling elements, etc.

2. The phase of all accelerating cells is locked at π, any variations occurring only through second-order effects in frequency errors. This may be seen by considering the circuit equation

$$X_{n+2} = -X_n + \frac{2}{k} \left(- \frac{2\,\Delta\omega_{n+1}}{\omega} + \frac{i\,\omega_n}{\omega\,Q}\right) X_{n+1} ; \qquad (12)$$

if cell n + 1 is a coupling cell, its amplitude is small (point 1) and imaginary (for power flow). The phase shift is then the product of two numbers which are small, $\frac{\Delta\omega_n}{\omega}$ and X_{n+1}. For no errors, we see no phase shift.

3. The amplitude of the fields in the accelerating cells is independent of frequency errors in any cells in first-order theory. Second-order effects do occur but only for very large amplitude errors. This may also be seen from Eq. (12), amplitude variations being the quotient X_{n+1}/Qk which is very small indeed. If X_{n+1} has a real component (due to other frequency errors in accelerating cells), then some amplitude variation may take place due to coupling cell mistunings, but the sensitivity is very low.

4. From Eq. (12), if X_{n+2}, X_n are coupling cell amplitudes and X_{n+1} an accelerating cell amplitude, we see that as $\Delta\omega_{n+1}$ goes through zero we should see a minimum in the coupling cell field X_n. This provides an exceedingly easy way to tune a structure of this type, for now one can choose a frequency, and successfully tune coupling cell fields to minima by changing accelerating cell tuners, working from a point furthest from the drive point toward the drive. It can thus be tuned, one cell at a time, to any predetermined frequency.

5. Since operation is now at the center of the passband where the slope is steepest, mode separation is maximum, and considerably narrower bandwidth may be tolerated for satisfactory performance.

6. This allows us to separate the shunt impedance problem from the coupling problem to some extent and may allow better shunt impedance optimizations.

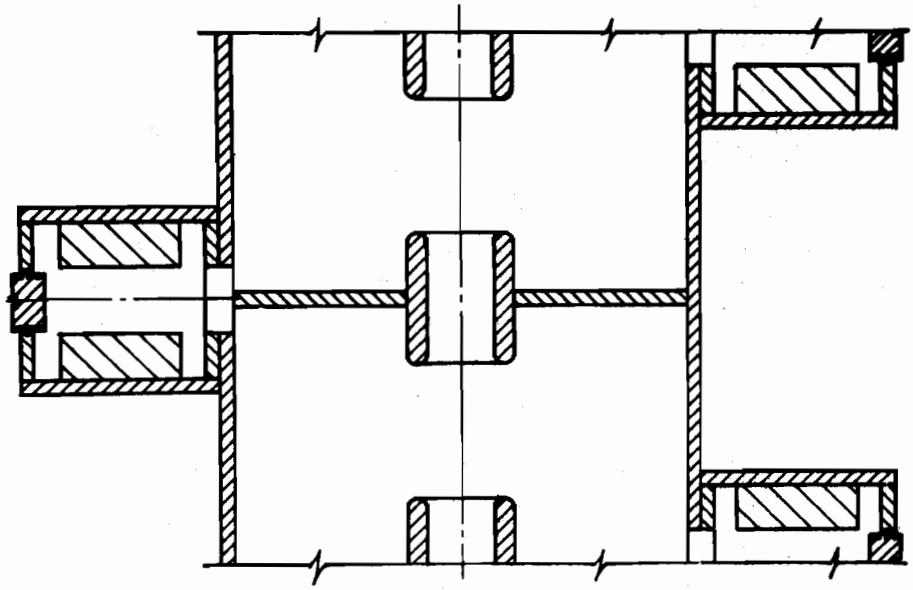

FIG. 29

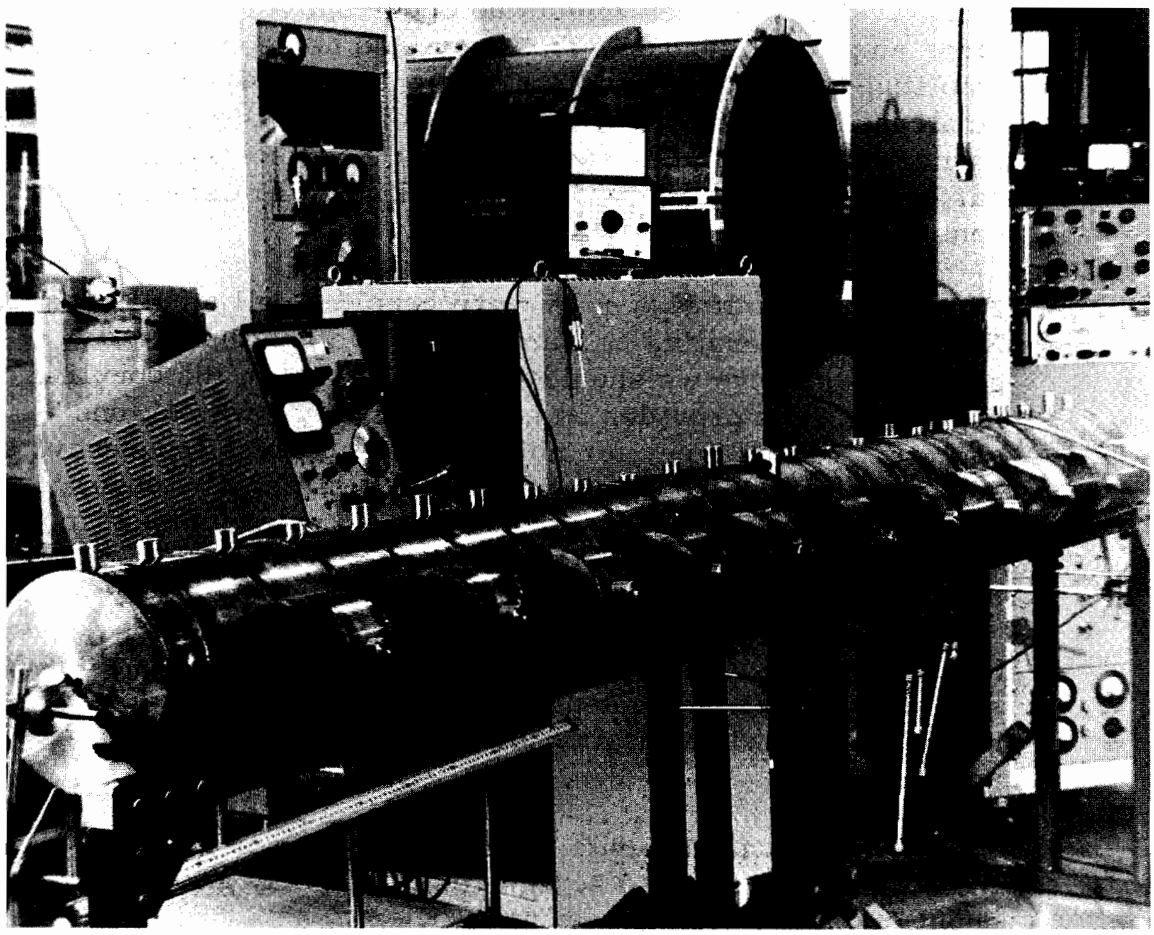

FIG. 30

We have built two models with resonant coupling devices and quite narrow bandwidths to investigate these properties. Figure 29 shows two accelerating cavities coupled by a side cavity which is resonant at the same frequency as the accelerating cavities. A slot cut in the mutual side walls of the cavities provides energy transfer from accelerating cell to coupling cell, etc. Since the coupling cell stores no energy in $\pi/2$ mode, its Q does not contribute to the shunt impedance values obtained, and thus this cavity may be made without too much regard to the Q obtained. We thus may heavily load the side cavity to make it small without affecting the shunt impedance appreciably. Since the slot which couples energy may be made quite small, one is free to modify the accelerating cavity at will in order to increase its shunt impedance. We have not tried to do this as yet. Figure 30 shows a photograph of a 24-cell model of a structure of this type. Shorter models have also been constructed of this configuration. After tuning up by the method described in point 4 above, a very reasonable dispersion curve is obtained near the $\pi/2$ mode with 1" x 2" slots. The structure shows a 20 Mc bandwidth at 810 Mc with 500 kc mode separation on either side of the $\pi/2$ mode. Near the zero and π modes, the Q curves overlap so badly no data are available.

In the limited time available before this meeting, we have seen no deviations from the predictions of the theory. When just tuned up, the tank was flat to $\sim \pm 5\%$ in E, and we have not been able to change this with any reasonable tuning arrangement. Since construction of this tank was quite crude, we might expect geometrical errors to account for this. Measurement of field levels in coupling cells indicates negligible energy stored in them. No phase shift can be detected between one end and the other of the model. Detailed measurements and comparison with theory are under way and should be completed shortly. Shunt impedance values of 30 MΩ/m at $\beta = 0.7$ have been obtained with the models.

In closing I would like to note that the cloverleaf can also be run resonantly coupled. No field should develop in the slot for, as we have noted, alternate cells store no energy in the $\pi/2$ mode operation. This would make a structure which should be extremely stable.

Development work is continuing on these structures. We also hope to check sparking levels in a short cloverleaf cavity with 100 kw of pulsed rf at 805 Mc/sec soon.

CARNE: What was the Q of your 21-cell model?

KNAPP: The Q is about 16,500.

CHARACTERISTICS OF SLOTTED IRISES

S. Giordano
Brookhaven National Laboratory

Some preliminary measurements of slotted iris structures are reported in the minutes of the Conference on Proton Linear Accelerators at Yale University, October 21-25, 1963, p. 153.

Although the above measurements were made with sheet metal irises, the results were sufficiently encouraging to warrant further investigation.

Before embarking on a full-scale modeling program, it was decided that some additional measurements would be useful. The purpose of these measurements was, first, to measure such parameters as shunt impedance, bandwidth, etc., and, second, to gain some experience in setting up a full-scale modeling program.

The measurements to be discussed in this paper were made on a limited number of available cavities. With the limited amount of data available, some interpolation and extrapolation of the data was necessary.

A slotted iris model was constructed as shown in Fig. 1. Measurements were made with two different bore hole diameters of D = 1.625" and D = 2.1", four different drift tube lengths of ℓ = 1.0", ℓ = 1.5", ℓ = 2.0" and ℓ = 2.5", and two different cell lengths of L = 4.0" and L = 6.0". All measurements were made in the "π" mode.

Figures 2 and 3 are plots of frequency vs β for various drift tube lengths. Figures 4 and 5 are plots of shunt impedance vs β for various drift tube lengths. In all of the above plots, straight lines were used to join the measured data points. (Results generally obtained on various structures in the range of β = 0.5 to β = 0.8 show that the variation of frequency and shunt impedance do not vary appreciably from a straight line.) In Figures 2, 3, 4, and 5, we see that the actual measured points are grouped around β = 0.5 and β = 0.8, so that the conclusions, which will be drawn in the neighborhood of these values of β, should have about the same accuracy as the measured data.

From Figs. 4 and 5, by drawing lines at constant β's of 0.5, 0.6, 0.7, and 0.8, it is now possible to draw curves of shunt impedance vs drift tube length for constant β as shown on Fig. 6 for a bore hole of 1.625" and Fig. 7 for a bore hole of 2.1". In Fig. 7, the region between the drift tube lengths of 2.0" to 2.5" may be in error by as much as 10% due to the lack of data points in this region. A comparison of Figs. 6 and 7 reveals some interesting features. There is a considerable change

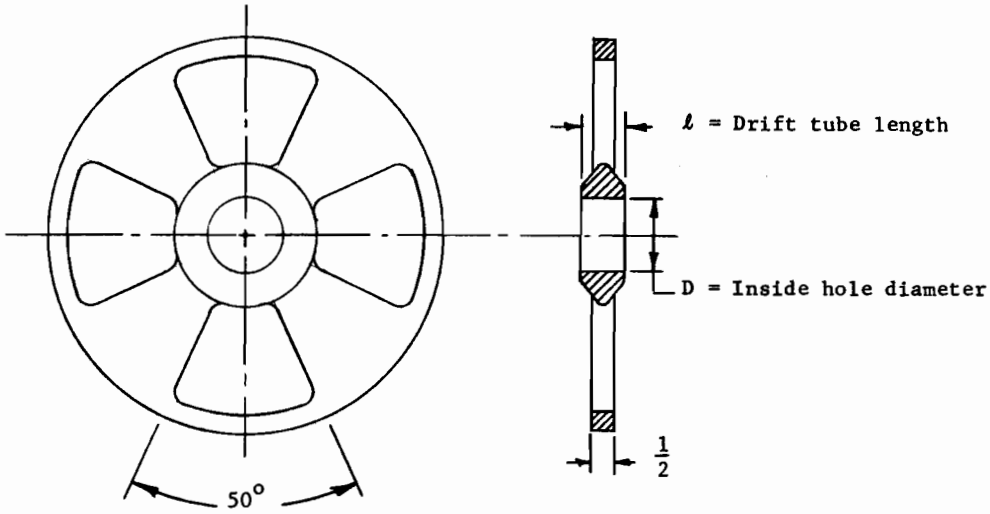

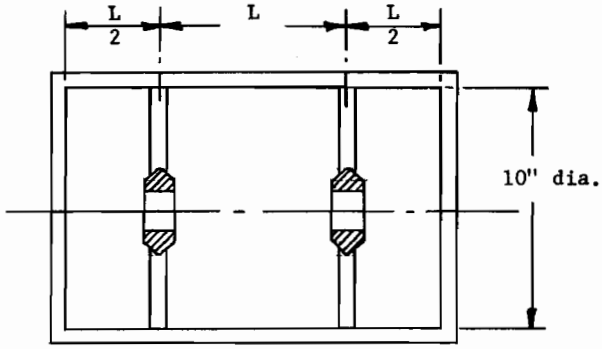

Fig. 1

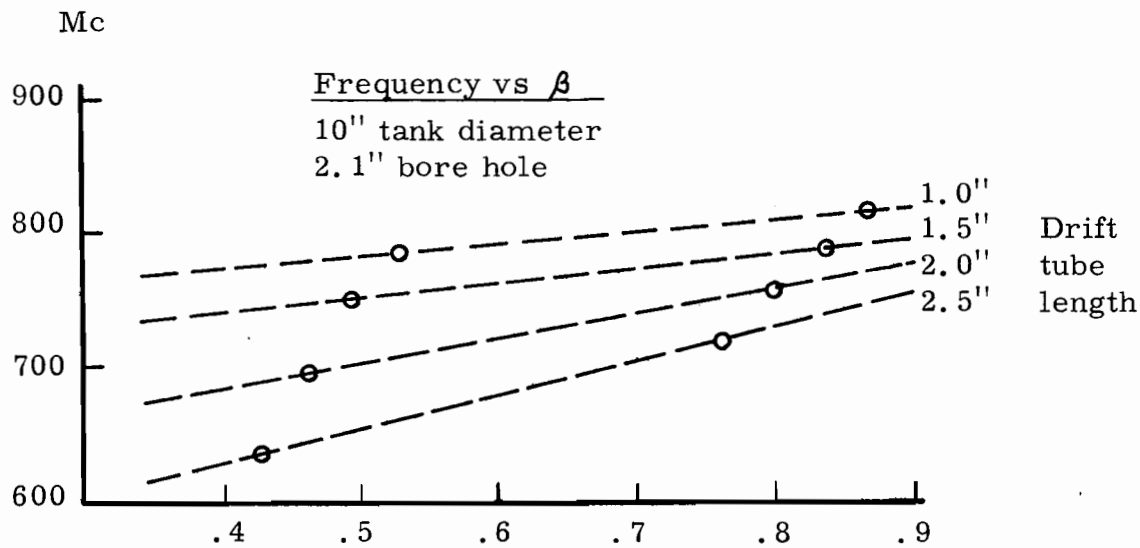
Mc
Frequency vs β
10" tank diameter
2.1" bore hole
900
800
700
600
.4
.5
.6
.7
.8
.9
1.0"
1.5"
2.0"
2.5"
Drift
tube
length

Fig. 2

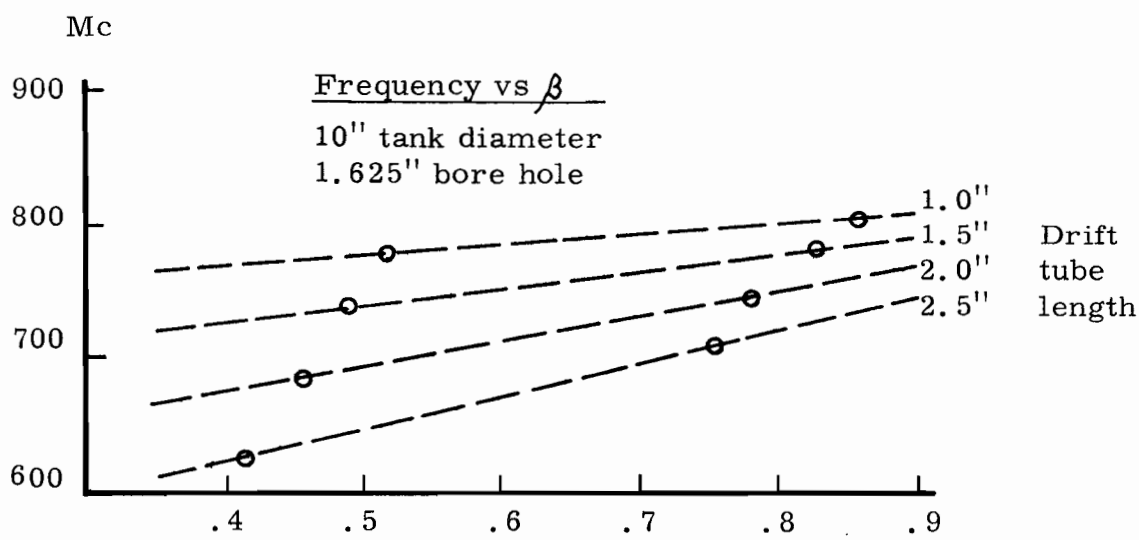
Mc
Frequency vs β
10" tank diameter
1.625" bore hole
900
800
700
600
.4
.5
.6
.7
.8
.9
1.0"
1.5"
2.0"
2.5"
Drift
tube
length

Fig. 3

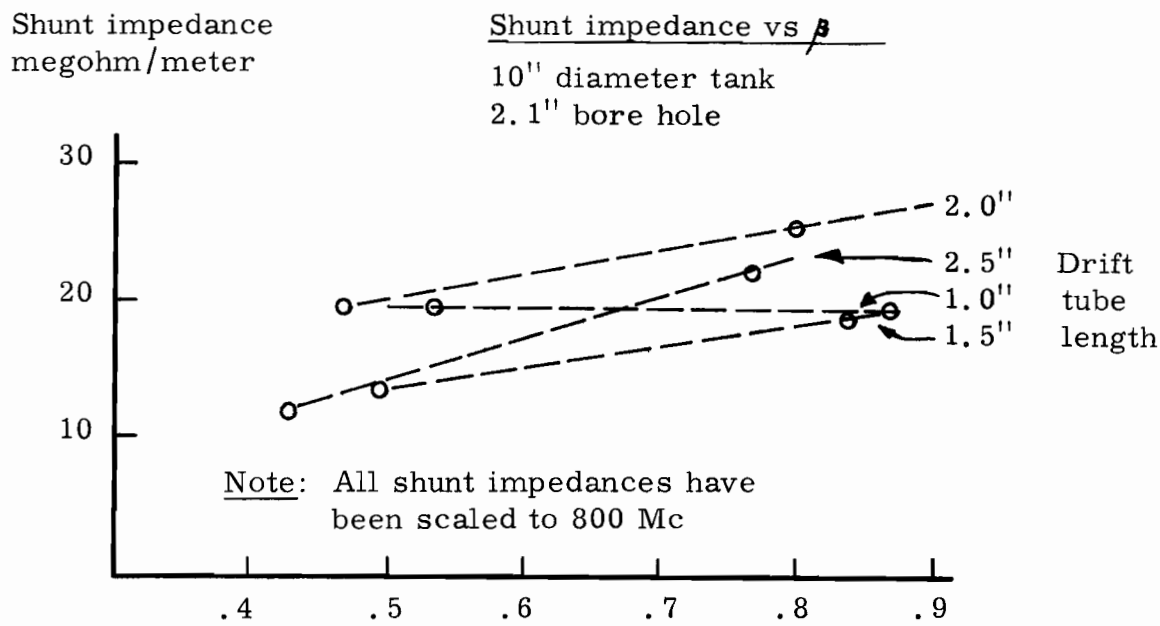
Shunt impedance
megohm/meter
Shunt impedance vs β
10" diameter tank
2.1" bore hole
30
20
10
2.0"
2.5"
1.0"
1.5"
Drift
tube
length
Note: All shunt impedances have
been scaled to 800 Mc
.4
.5
.6
.7
.8
.9

Fig. 4

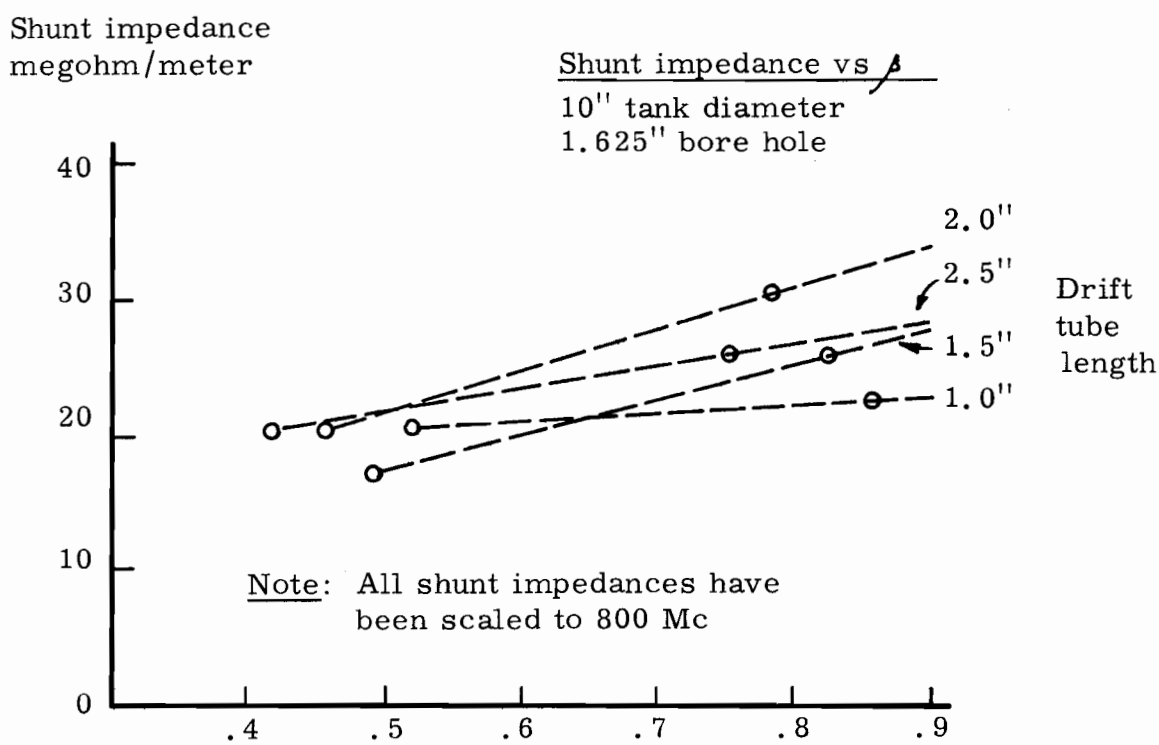
Shunt impedance
megohm/meter
Shunt impedance vs β
10" tank diameter
1.625" bore hole
40
30
20
10
0
2.0"
2.5"
1.5"
1.0"
Drift
tube
length
Note: All shunt impedances have
been scaled to 800 Mc
.4
.5
.6
.7
.8
.9

Fig. 5

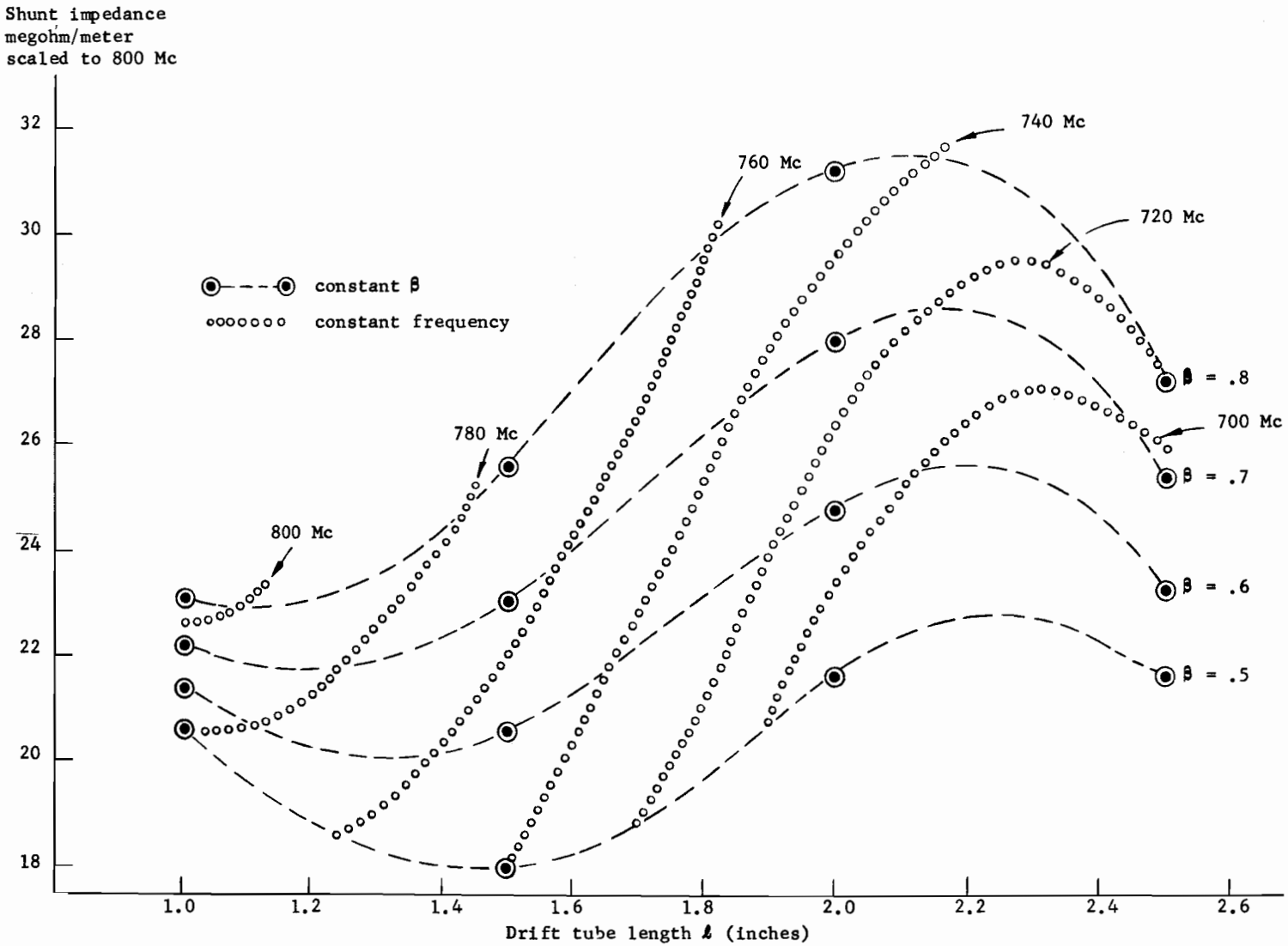

Fig. 6 Shunt impedance vs drift tube length for 50° slotted iris (1.625" bore hole) (curves of constant frequency and β)

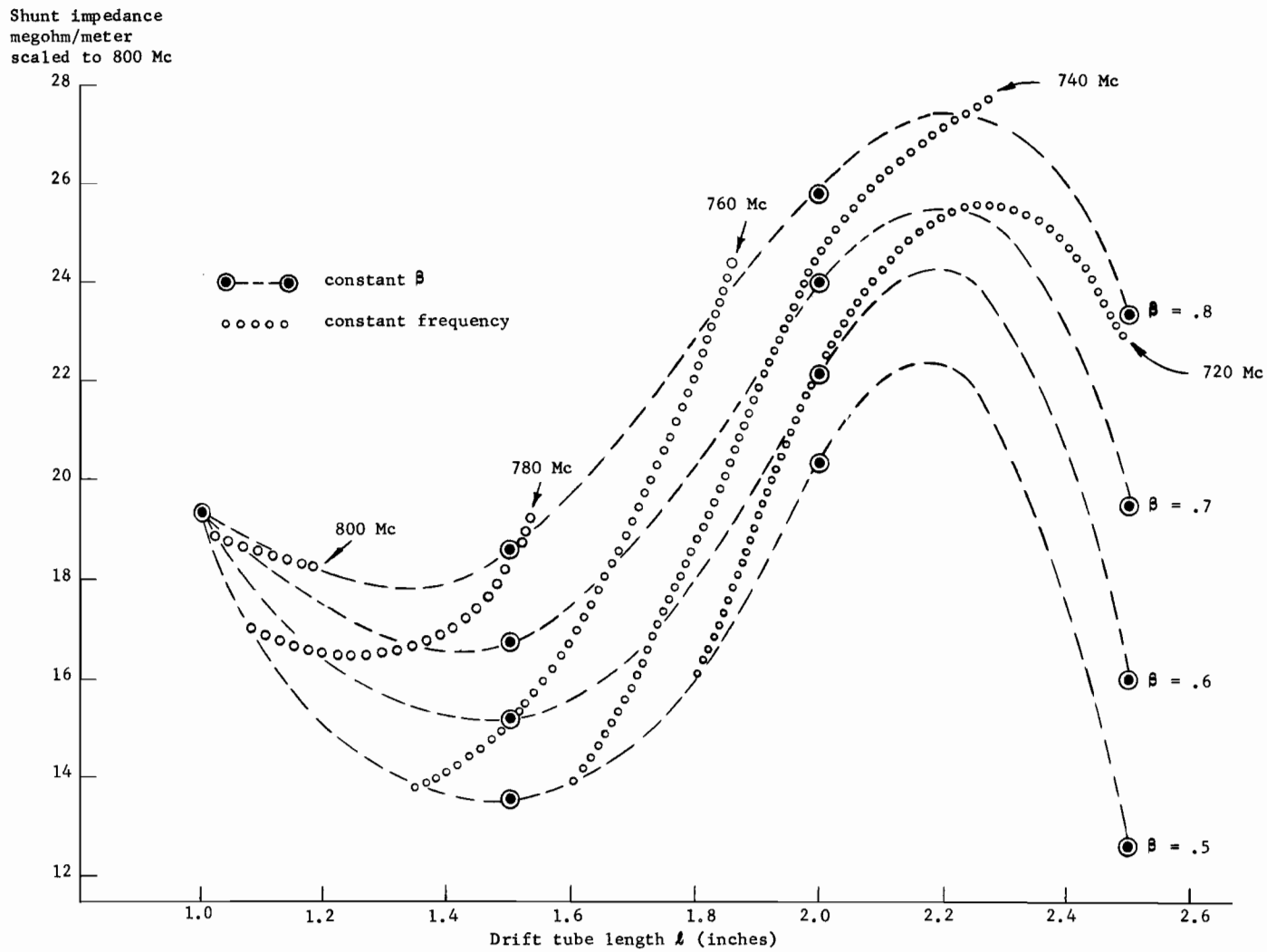

Fig. 7 Shunt impedance vs drift tube length for 50° slotted iris (2.1" bore hole) (curves of constant frequency and β)

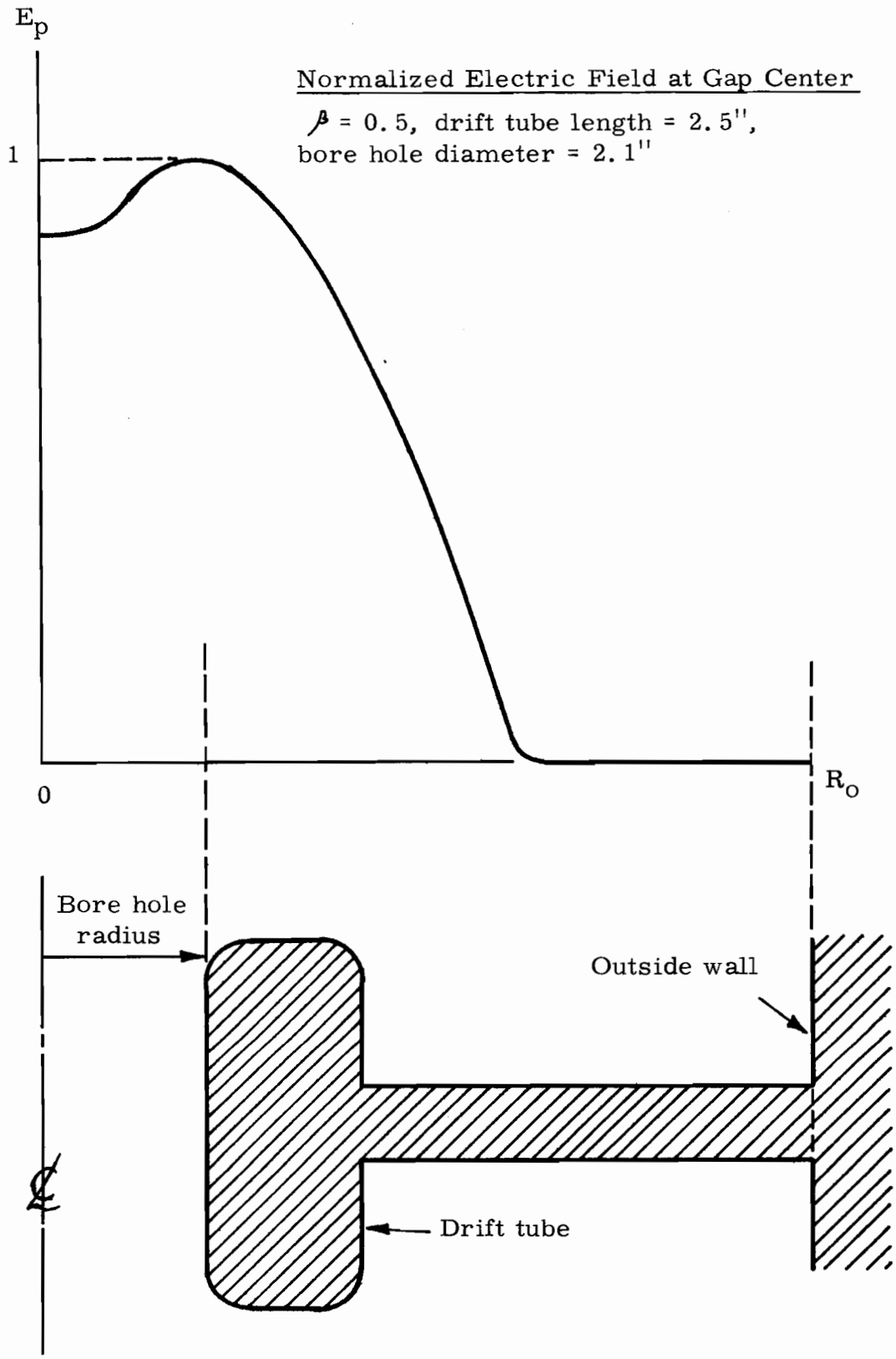
E_p
Normalized Electric Field at Gap Center
β = 0.5, drift tube length = 2.5",
bore hole diameter = 2.1"
1
0
R_o
Bore hole radius
Outside wall
Drift tube
℄

Fig. 8

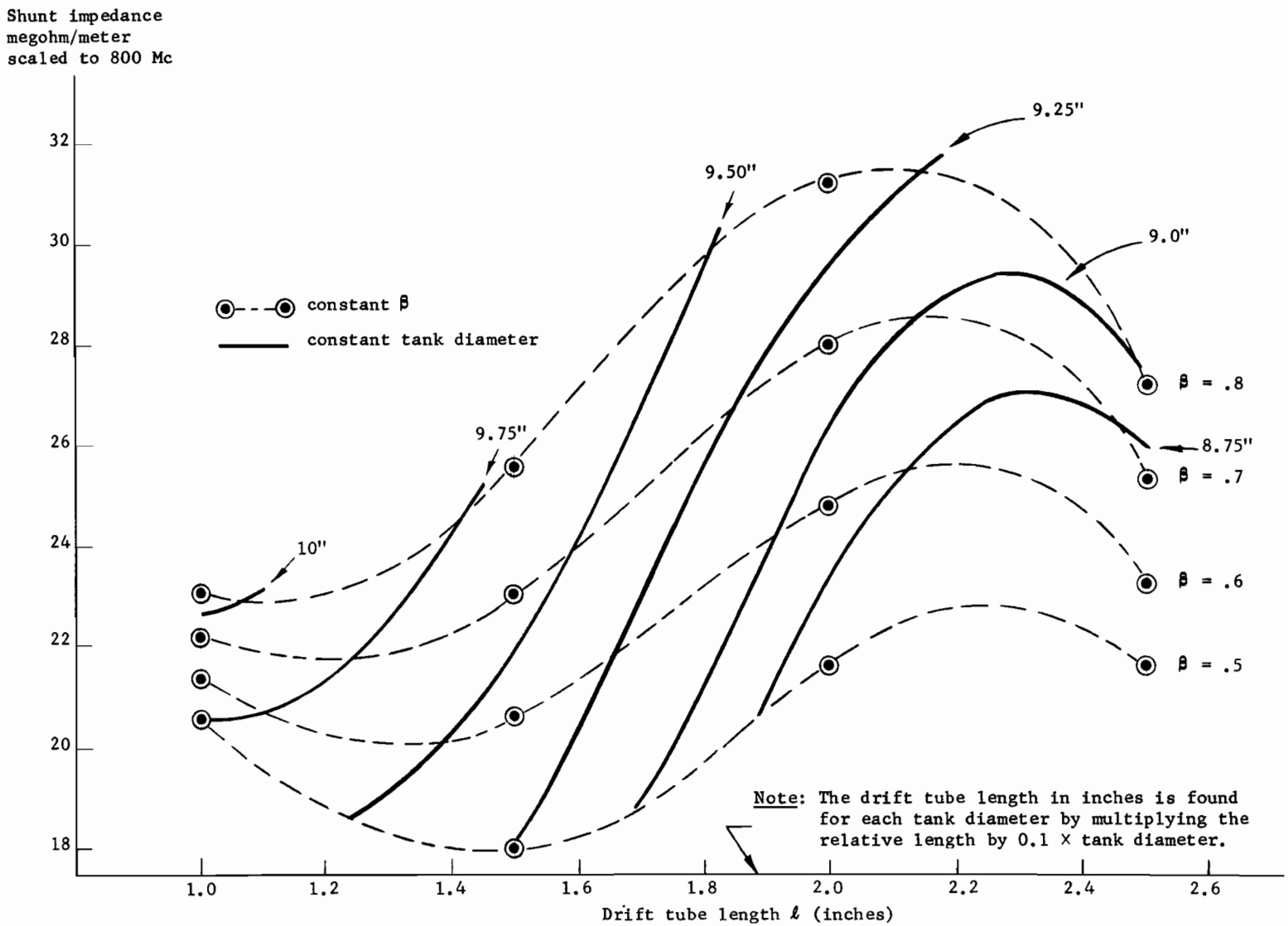

Fig. 9 Shunt impedance vs. drift tube length for 50° slotted iris (bore hole corresponding to 10" tank is 1.625") (curves of constant tank diameter and constant β) at 800 Mc

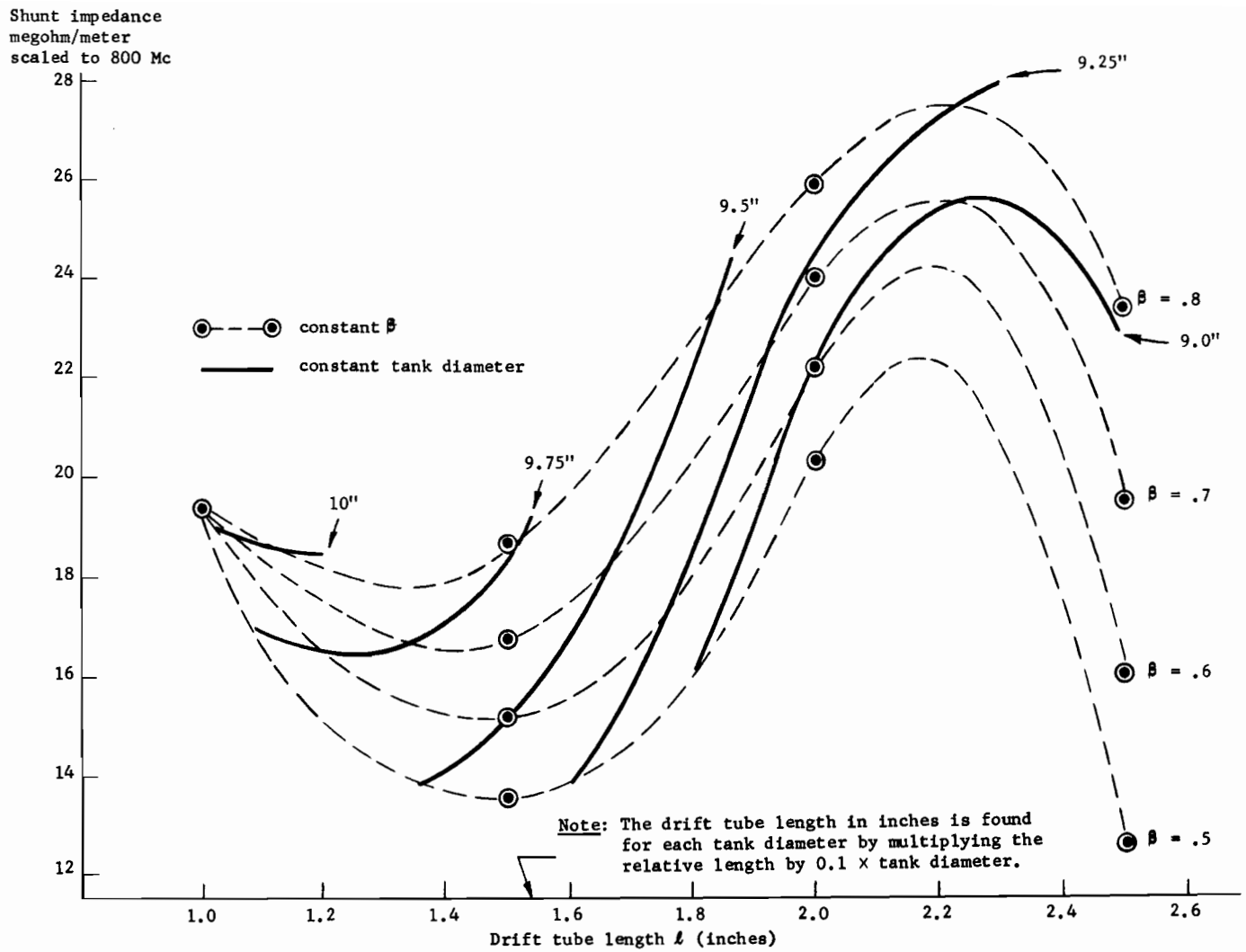

Fig. 10 Shunt impedance vs. drift tube length for 50° slotted iris (bore hole corresponding to 10" tank is 2.1") (curves of constant tank diameter and constant β) at 800 Mc

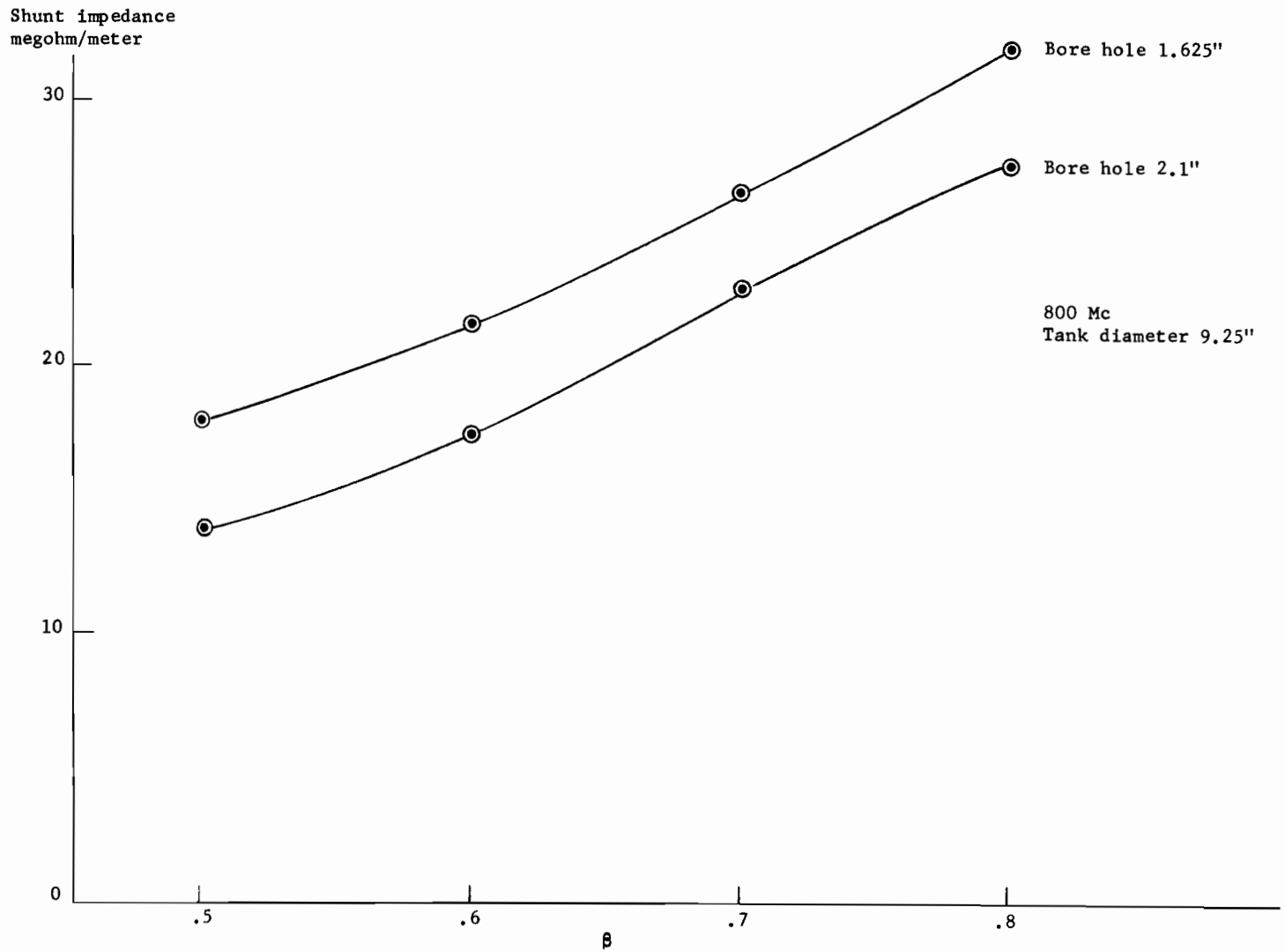

Fig. 11 Shunt impedance vs β for 50° slotted iris

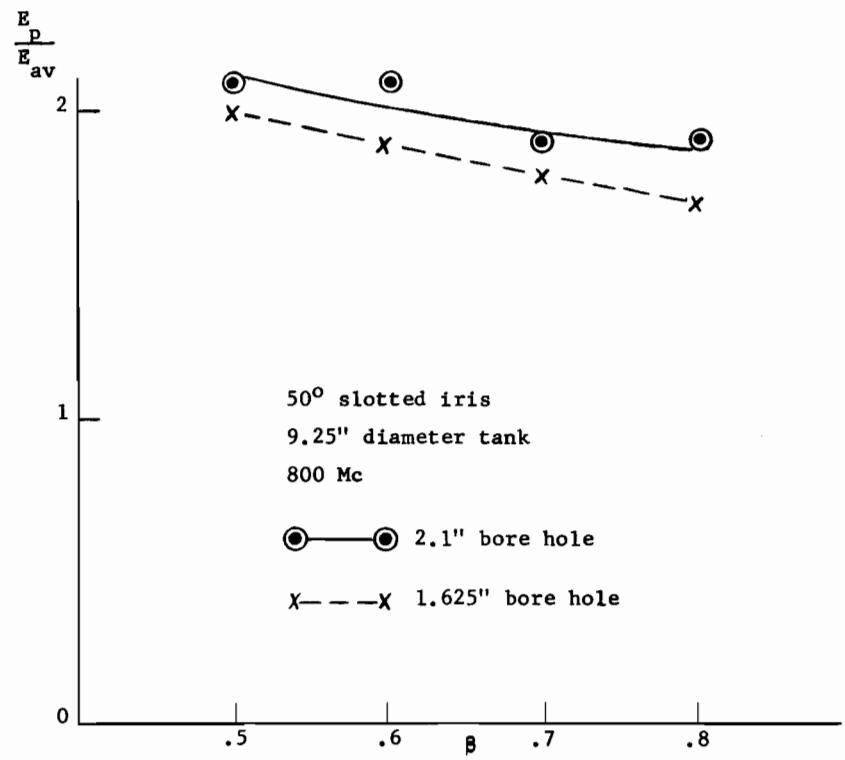

Fig. 12 Ratio of peak field to average field vs β for the 50° slotted iris

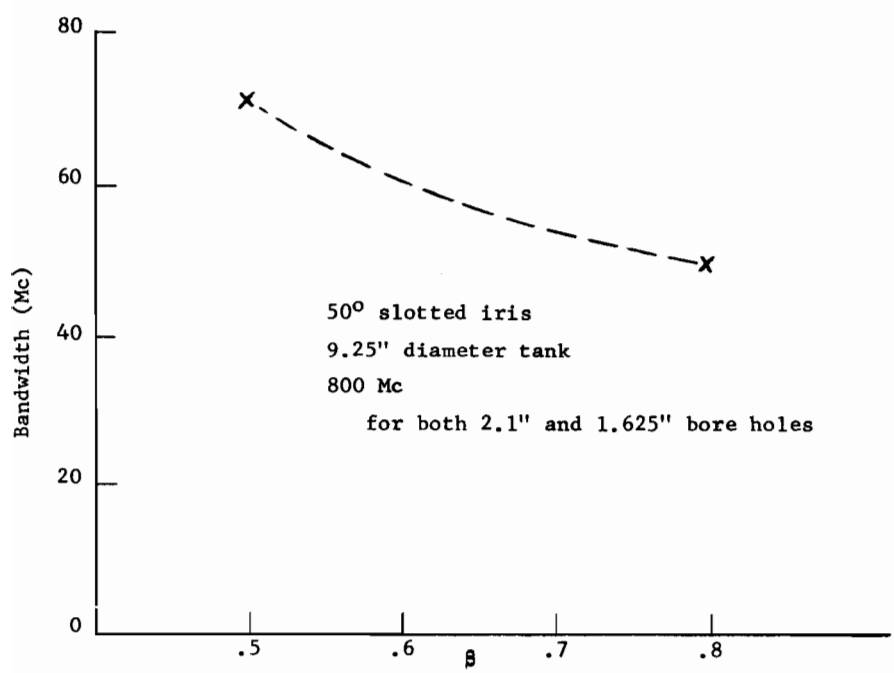

Fig. 13 Bandwidth vs β for the 50° slotted iris

in shunt impedance between the 1.625" bore hole and the 2.1" bore hole. Another interesting point is the rapid fall-off of shunt impedance with longer drift tubes. At $\beta = 0.5$ and a drift tube length of 2.5", we see that, with increasing drift tube length, fall-off of shunt impedance for the 1.625" bore hole is small as compared to the 2.1" bore hole. One reason for fall of shunt impedance can be seen in Fig. 8, which is a radial plot of the electric field at the center of a cell and shows a dip of 11% in the electric field on the axis for the larger bore hole.

From Figs. 2 and 3, by drawing lines of constant frequency at 800 Mc, 780 Mc, 760 Mc, 720 Mc, and 700 Mc, and by interpolating between the various drift tube lengths at β's of 0.5, 0.6, 0.7, and 0.8, we may sketch in the contours of constant frequency in Figs. 6 and 7. The data in Figs. 6 and 7 were made on a 10" diameter tank. It is interesting to note that the constant frequency contours in Figs. 6 and 7 can be made to represent constant tank diameters at some other frequency. If, for example, we select 800 Mc/sec as an operating frequency, and if we scale the dimensions of the original 10" diameter tank (used for the measurements in Figs. 6 and 7) by $\frac{780}{800}$, we get a tank whose diameter is 9.75", and the constant frequency contours of 780 Mc in Figs. 6 and 7 become constant tank diameter contours of 9.75" at an operating frequency of 800 Mc. We may now draw Figs. 9 and 10, noting that the drift tube length is scaled proportionately.

If an operating frequency of 800 Mc is selected, we see that a tank diameter of 9.25" would be a good choice. If one is willing to change tank diameters, some over-all improvement in the average shunt impedance can be gained. Figure 11 shows the shunt impedance as a function of β for a 9.25" diameter tank at 800 Mc. There may be as much as a $\pm$ 15% error in shunt impedance due to the original measurements of "$\bar{Q}$".

It can be shown that

$$\frac{E_p}{E_{av}} = \frac{1}{f} \sqrt{\left(\frac{L\,N}{2\,\pi^2\,\epsilon_o\,r_o^3}\right) \times \left(\frac{Q\,\Delta f}{R_s}\right)},$$

where E_p is the peak electric field at the center of a cavity, E_{av} is the average electric field as seen by a synchronous particle, f is the operating frequency, L is the length of the cavity in meters, r_o is the radius in meters of a small metal sphere placed at the center of the cavity, Δf is the frequency perturbation due to the metal sphere placed at the center of the cavity, and N is the number of cells. Figure 12 is a plot of

E_p/E_{av} scaled to a 9.25" diameter tank. Figure 13 is a plot of bandwidth vs β at 800 Mc/sec.

From the results of the above measurements, a new series of test cavities is being built, having a tank diameter of 9.25". Measurements will be made on four sets of irises with slots, subtending angles of 35°, 40°, 45°, and 50°, as shown in Fig. 1.

JOHNSTON: Was this a zero-mode structure?

GIORDANO: No, all these measurements were made in the π mode. It should be pointed out that the shaped iris cavity is a forward wave structure, and the slotted iris cavity is a backward wave structure.

CARNE: You gave us shunt impedance measurements at 800 Mc. What were the η/Q and the Q values?

GIORDANO: The Q values, as I recall, were around 14,000 at $\beta \cong 0.5$ and about 16,000 at $\beta \cong 0.9$.

NAGLE: What were the actual measurement frequencies? As I recall, they were about 700 Mc?

GIORDANO: For these particular measurements, the tank diameter was kept constant, and the only thing I varied was the drift tube length. The measured data points ran from about 625 Mc up to about 825 Mc.

NAGLE: Over what frequencies were the extrapolations made?

GIORDANO: In extrapolating from a 10-inch diameter tank to a 9-1/4 inch diameter tank, my actual frequency extrapolation was from 740 Mc to 800 Mc.

NAGLE: Were these models constructed with spring-ring contacts?

GIORDANO: Yes.

HUBBARD: I wanted to say that at Berkeley we have made some preliminary measurements on an 800 Mc slotted iris structure similar to one described by Giordano. I will put the numbers on the board:

β	R_{sh}
0.38	27 M Ω/meter
0.77	39 M Ω /meter

These values of R_{sh} are based on measured values of Q.

NAGLE: Does that have a transit time factor in it?

HUBBARD: Yes, I would also like to point out that our measured Q's are almost the same as yours. We did a fair amount of optimizing of the slot shape, but very little optimizing of the drift tubes.

GIORDANO: What was the bore hole size?

HUBBARD: That was for a 1.5-inch diameter hole.

GIORDANO: There should be very little difference in comparing the shunt impedance for your 1.5-inch diameter bore hole and my 1.625-inch diameter bore hole. I selected 50° slots and optimized the shunt impedance by varying the drift tube lengths. You (Hubbard) selected a fixed drift tube length and varied the slot angle to optimize the shunt impedance. Both our results are in good agreement.

LOEW: Do you know what happens if you alternate the angles of the slots of the cavities, like the colverleaf?

GIORDANO: Very little. Actually for the particular model I have, which is terminated in half cells, the irises have to be alternated in pairs with the exception of the first and last iris. This is necessary to match the boundary conditions at the ends. I was hoping to change the shape of the dispersion curve, but found there was very little change.

LOEW: It remains backward?

GIORDANO: Yes.

HAGERMAN: Did you ever look for any azimuthal asymmetries in this? Since you seem to be taking the energy density stored on the axis by varying the slot width, you might wonder whether these things are azimuthally symmetric.

GIORDANO: Perturbation measurements of the azimuthal field were made. These measurements were made at $\beta \approx 0.5$, slot angles of 35° and 50°, with a drift tube length of one inch. The field was measured at the center of a cell at a radius approximately 0.75 inch. I could not detect any appreciable azimuthal asymmetries.

LOEW: I just wanted to mention something that might be useful to some of these studies. There was a man by the name of Mike Allen who wrote

his Ph. D. thesis on something very similar for a traveling wave tube a few years ago (he was a student of Chodorow), and he has a lot of curves put into it.

LEISS: Could you please tell me roughly what is the magnitude of the transit time correction in either one of the two cases described?

HUBBARD: About 85%.

LEISS: So about 15% is in other modes?

GIORDANO: The actual measurement of shunt impedance was made by the perturbation method, and numerically integrated.

LEISS: I'm asking for reasons of beam loading.

GIORDANO: Well, you actually have to compare the shape of the field here to the average field.

FABRICATION AND MEASURING METHODS FOR DISK-LOADED WAVEGUIDES

T. Nishikawa*
Brookhaven National Laboratory

I. Introduction

During the past ten years, extensive studies on electron linacs have been carried out in Japan. About ten machines, which were constructed by the universities or by Japanese manufacturers, are working well for various purposes. The author wishes to report on the new methods developed recently in that country to fabricate disk-loaded guides and to measure their performance precisely. This work was carried out by the group of the University of Tokyo and by the staffs of the Mitsubishi Heavy Industries, Inc. and the Toshiba Electric Company.

II. New Methods for Fabricating Guides with High Accuracies

Disk-loaded guides used in electron linacs are usually made either by a brazing or an electroforming method. These two methods were also tried in Japan and led to fairly good results in obtaining accurate guides.[1] However, in the former method, one needs to tune each cell after its fabrication unless one is extremely careful during the brazing process, while the usual electroforming method is expensive because of time consuming and troublesome procedures during fabrication. A new method has now been developed which is a combination of the strong points of these two and which eliminates those difficulties.[2]

In order to achieve and to maintain high accuracy throughout the fabrication process, copper disks and cylinders are machined separately and assembled by jigs. The outer surface of the assembled body is then electroplated to form a complete structure (Fig. 1). This method is considerably simpler than the brazing or electroforming technique previously used and eliminates a number of undesirable effects such as: 1) high temperature due to brazing, which results in dimensional distortion, and 2) use of aluminum spacers and the necessity for removing them by etching. Typical values of machining errors obtained are shown in Fig. 2. It should be stated that the resonant frequency of each cell is strongly dependent on the shaping of the cross section of the disk holes since the field strength should be strongest at that point. A rough

---

*On leave from the Department of Physics, University of Tokyo.

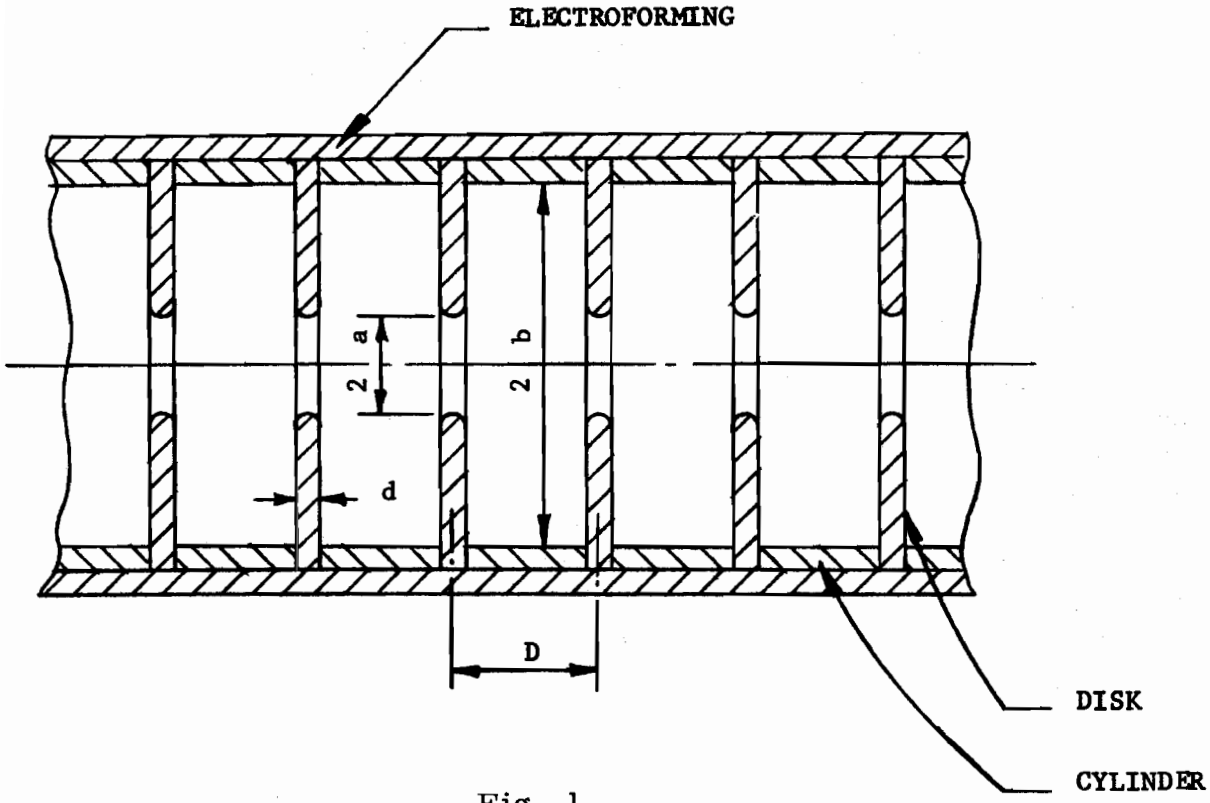

Fig. 1

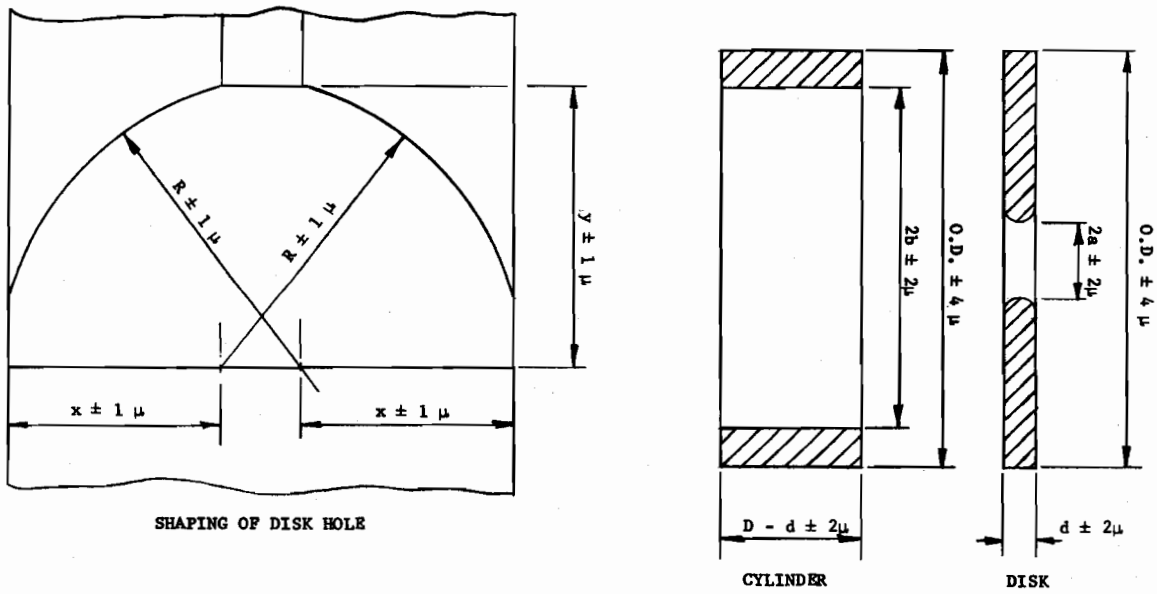

MATERIAL OFHC 99.99%

SURFACE ROUGHNESS 0.3 μ OR LESS

Fig. 2

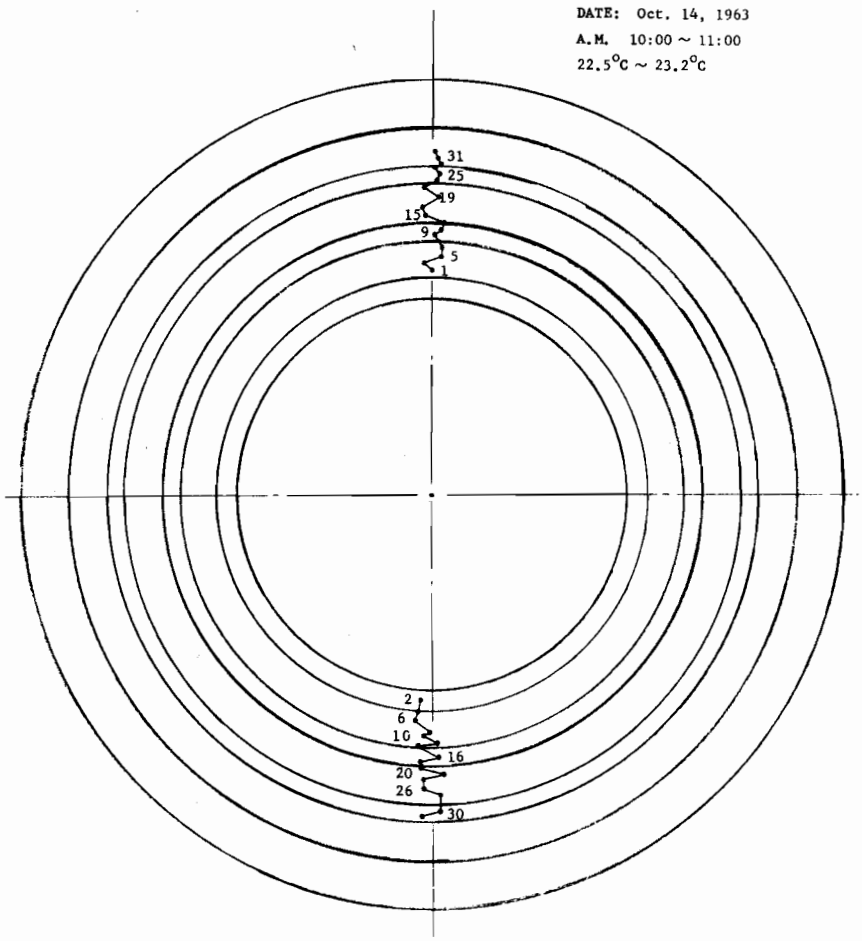
DATE: Oct. 14, 1963
A.M. 10:00 ~ 11:00
22.5°C ~ 23.2°C
31
25
19
15
9
5
1
2
6
10
16
20
26
30

Fig. 3

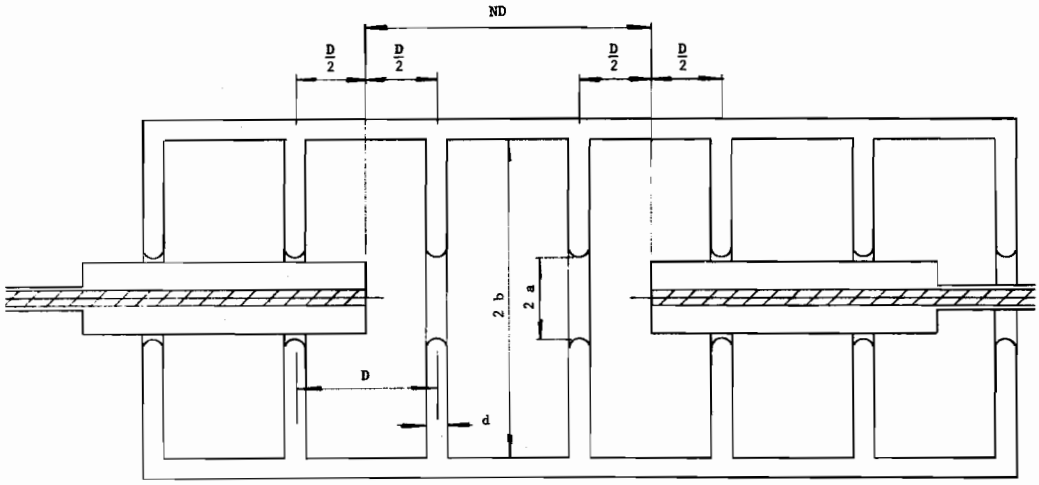
ND
D/2
D/2
D/2
D/2
2 b
2 a
D
d

Fig. 4

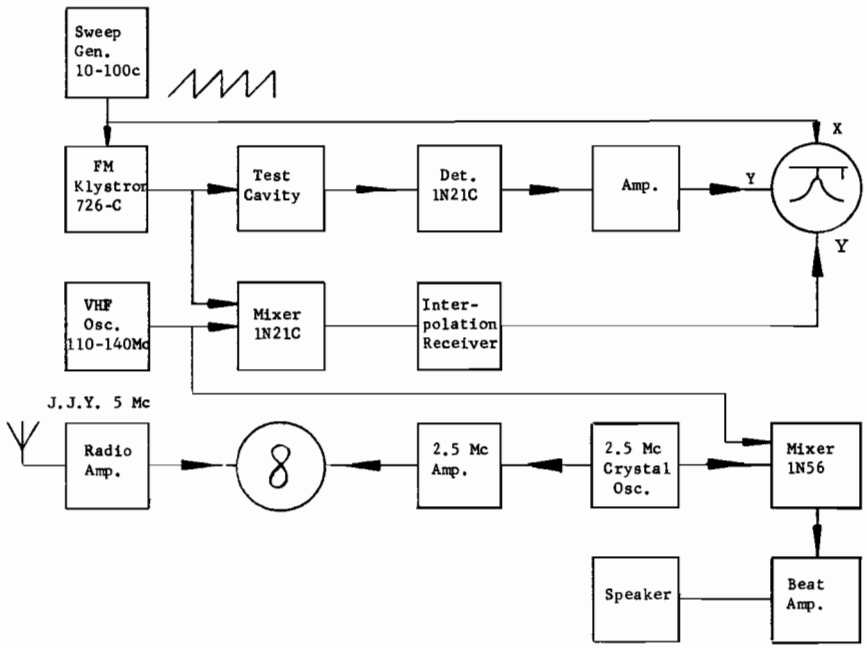
Sweep Gen. 10-100c
FM Klystron 726-C
Test Cavity
Det. 1N21C
Amp.
X
Y
Y
VHF Osc. 110-140Mc
Mixer 1N21C
Inter-polation Receiver
J.J.Y. 5 Mc
Radio Amp.
8
2.5 Mc Amp.
2.5 Mc Crystal Osc.
Mixer 1N56
Speaker
Beat Amp.

Fig. 5

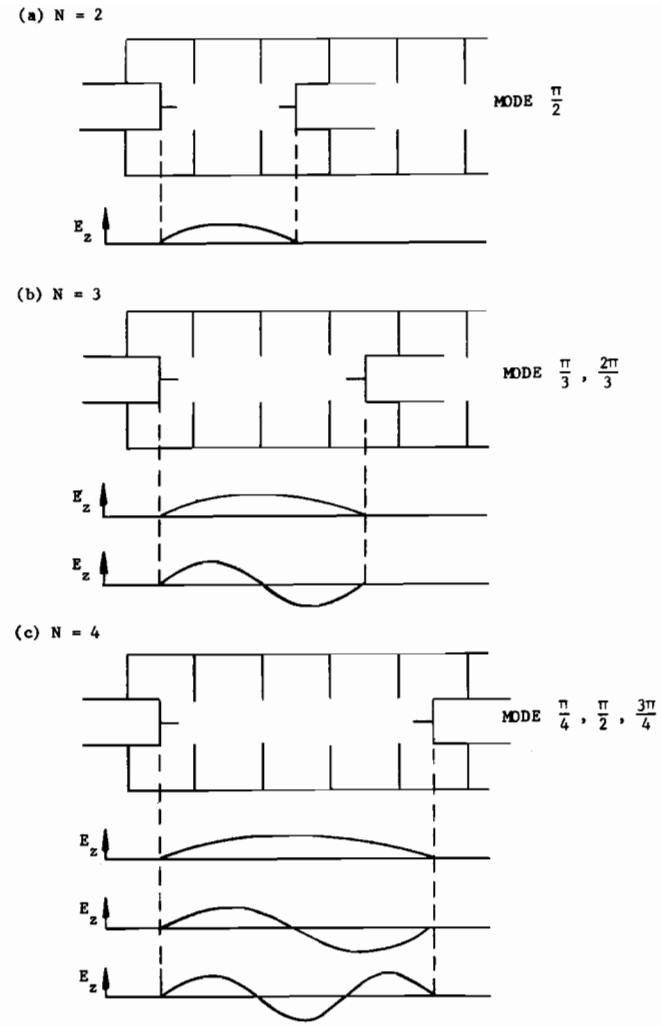
(a) N = 2
MODE $\frac{\pi}{2}$
E_z
(b) N = 3
MODE $\frac{\pi}{3}$, $\frac{2\pi}{3}$
E_z
E_z
(c) N = 4
MODE $\frac{\pi}{4}$, $\frac{\pi}{2}$, $\frac{3\pi}{4}$
E_z
E_z
E_z

Fig. 6

estimate, using a perturbation calculation, shows that an accuracy of about one micron is necessary in order to keep the frequency error to less than 10^{-5}. Also the surface roughness of the finished disks is held to 0.3 microns to get high Q values.* Good rf contact between disks and cylinders is assured by a knife-edge contact with appropriate pressures leading to Q values as high as 13,000 for the S-band $2\pi/3$ mode guide.** The vacuum seal of the guide is obtained by electroforming ; the gases escaping from a fabricated guide were measured to be about 2×10^{-8} $\ell\mu$/sec/cm^2. Figure 3 shows the results of a nodal-shift phase measurement for a one-meter section, giving an error of less than 2.5 degrees when plotted on a Smith chart, which is certainly the order of the experimental error in such a measuring method.

III. New Method for Measuring Performance of Guides

A simple new method for measuring the resonant frequency and the Q value of each cell has been developed.[3] A metallic plunger with an antenna probe is inserted from each end of the guide. Their positions are adjusted to be set at the center of a cell or at the center of a disk hole so as to make the distance between the two ND (D is the cell length and N is an integer) (Fig. 4). Such a position can easily be found by a slight shift from the correct position, as shown in Fig. 7, and the following description. The radio-frequency power is fed into one of the antennas and detected by the other. The radio-frequency power is frequency modulated by a sawtooth wave, and the resonance behavior is measured by comparison with a wavemeter. A block diagram of the typical electronic device used is shown in Fig. 5.

In the usual nodal-shift method with a metal plunger and a standing-wave detector, the axial electric field can take a maximum at the plunger surface. In the present method such a mode is detuned by the antenna probes, and only the mode having a zero field at the plunger surface should be excited, as shown in Fig. 6. If one moves the plunger position, the detected amplitude and the frequency of the resonance vary as shown in Fig. 7, giving the correct position of the plunger with a minimum detected power. In the nodal-shift method, the error in the measurements is caused by mismatching at the input coupler of the guide. Such an error

---

*Precise optical and matching techniques to measure and control the disk-hole shaping and the surface roughness are described also in Reference 1.

**Combined with the field measurement, the corresponding shunt impedance obtained is 59 MΩ/m.

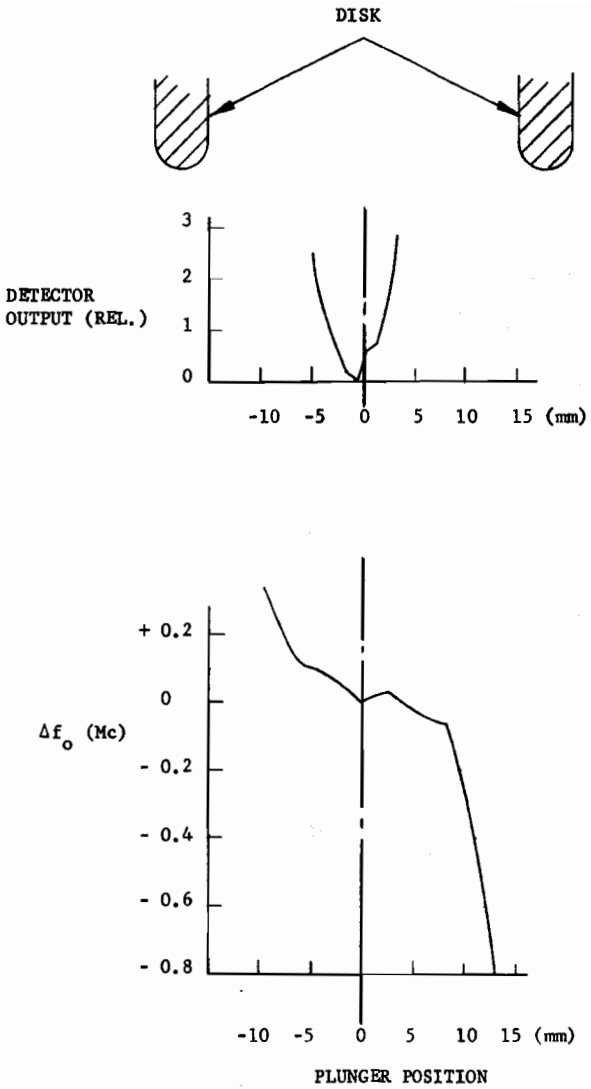
DISK
DETECTOR OUTPUT (REL.)
3
2
1
0
-10 -5 0 5 10 15 (mm)
Δf_o (Mc)
+ 0.2
0
- 0.2
- 0.4
- 0.6
- 0.8
-10 -5 0 5 10 15 (mm)
PLUNGER POSITION

Fig. 7

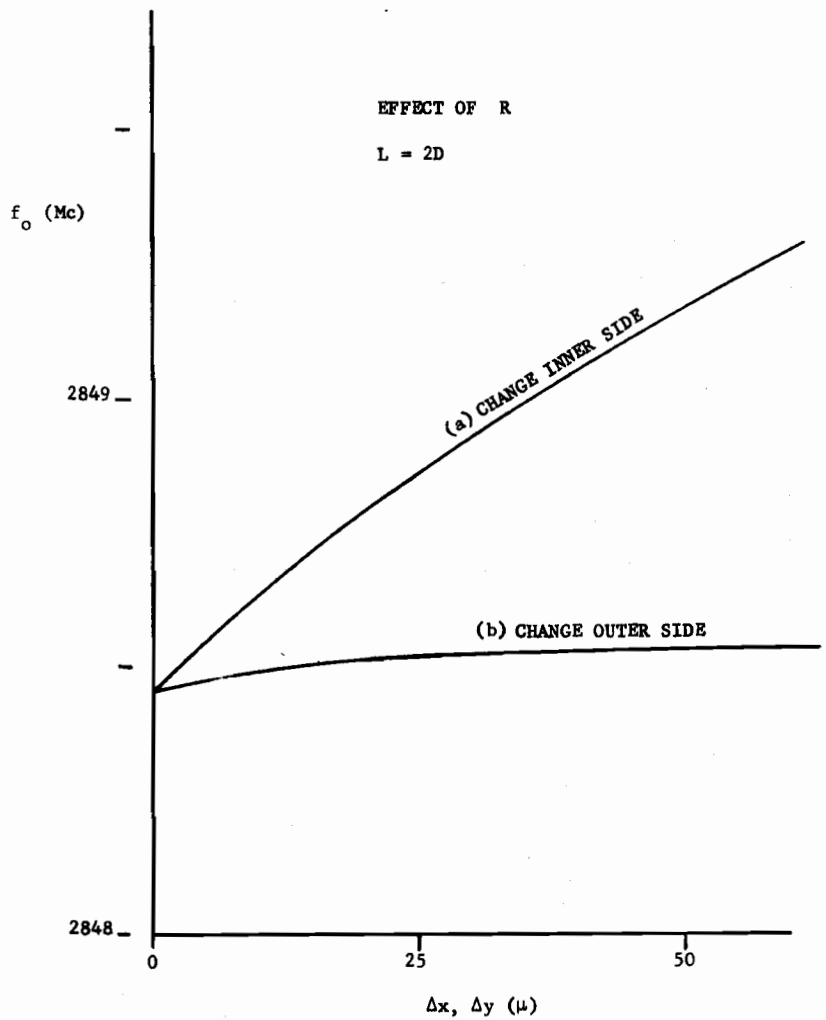
EFFECT OF R
L = 2D
f_o (Mc)
2849
2848
(a) CHANGE INNER SIDE
(b) CHANGE OUTER SIDE
0
25
50
Δx, Δy (μ)

Fig. 8

is eliminated in the present method, where the length of the antenna loops affects the frequency measurements. By an extrapolation of the results obtained for various antenna lengths, this measuring error can also be corrected.

IV. Some Typical Results of Performance Measurements

The resonant frequency of each cell fabricated by the new method is found by the above measuring method to be within $\pm$ 25 kc of the desired frequency (S-band, $2\pi/3$ mode). The corresponding phase error for a one-meter section should be 0.1° or 2×10^{-3} rad.* Some other interesting results follow:

1. The effect of hole shaping

A disk having an unsymmetrically shaped hole was used to examine the effect of hole shaping. It had a correct dimension on one half-side of the cross section and an incorrect dimension on the other side. The resonant frequency of a $\pi/2$ mode cell was measured with this disk. The disk was turned over, and measurements were done for both cases: (i) the incorrect side is inwards to the measuring cell (Fig. 8, curve a), and (ii) it is outwards (Fig. 8, curve b). The result indicates a frequency shift in case (i) but not in case (ii). Since, with the present measuring method, microwave energies are stored mainly in the inner cell and not in the half outer cells, the result obtained is quite understandable and means that we can inspect the performance of each cell separately by successive measurements. This assures also that one can make Q measurements without effects of end walls.

2. Tuning of each cell

If we had observed a big frequency error in one of the cells, we could easily make a correction by a tuning operation, observing the frequency of that cell. Some typical examples of tuning are shown in Fig. 9 where a small portion of the wall is pushed down in the usual manner, and the resonant frequency is corrected by a trial-and-error method. Also the aging effect of the deformed wall was examined over several days as shown in the right-hand side of Fig. 9.

3. Measurement of field distribution

One can also obtain the field distribution of a cavity by measuring the resonant frequency when the boundary is perturbed. An example of

*At the present stage, a guide having the total length of 3 m can be made with a similar performance.

TUNING BY PRESSURE METHOD

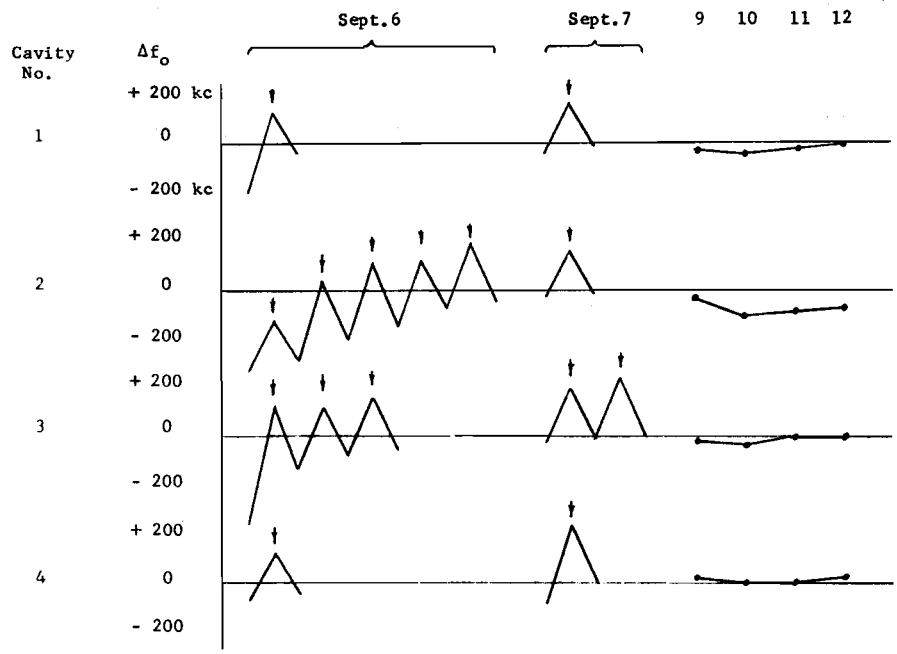

Fig. 9

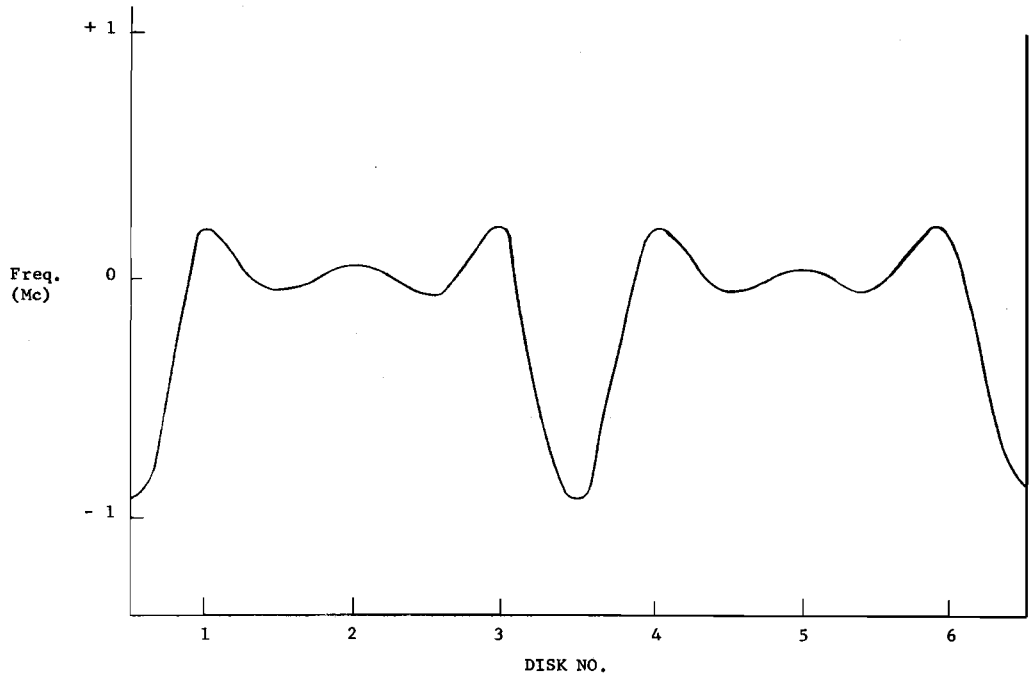

Fig. 10

the $\pi/2$ mode, in which a small teflon bead is slid down along the axis, is shown in Fig. 10.

LOEW: Do you plan to use this method and tune afterwards also, or do you plan to use only one method?

NISHIKAWA: We usually do not use the tuning, but if we have made an error, we can adjust it easily.

LOEW: Was the number 10^{-2}, for the total phase shift per cavity, expressed in radians?

NISHIKAWA: Yes, radians.

REFERENCES

1. J. Tanaka, "The Construction and Test Operation of INS Linear Electron Accelerator", J. Phys. Soc. Japan 16, 2081 (1961); J. Tanaka, T. Nishikawa, A. Miyahara et al., "On Electroforming of Disk-Loaded Waveguide for Linear Accelerators", Appl. Phys. in Japan 31, 146 (1962); J. Tanaka, T. Nishikawa, A. Miyahara, and K. Kobayashi, "Microwave Measurements on Disk-Loaded Waveguide for Electron Linear Accelerators", Internal Report of the Institute for Nuclear Study, University of Tokyo (March 1961, in Japanese).

2. "Mitsubishi Linear Accelerator Tube Manufactured by Electroforming Method with Copper Spacer", (July, 1964), issued by Mitsubishi Heavy Industries, Ltd., Nagoya, Japan.

3. T. Okada, N. Shigemura and K. Takeuchi, "A Measuring Method of Frequencies of Accelerator Guides", Report on the Meeting of the Physical Society of Japan (April 1964).

THE 500 MEV LINAC PROPOSED AS A NEW INJECTOR FOR THE AGS AT THE BROOKHAVEN NATIONAL LABORATORY

G. W. Wheeler
Yale University and Brookhaven National Laboratory

The Brookhaven National Laboratory has proposed a conversion program* to increase the intensity of the AGS to about 2×10^{13} protons per second. A major feature of this program is a new linac injector to replace the present 50 MeV machine. This paper will describe the general features of the new linac. The work presented here represents the efforts of a large group of people from BNL and Yale.

The principal characteristics of the linac are shown in Table I. The initial design goal is for 50 mA of peak current at 500 MeV. However, it is important that the linac ultimately be capable of 100 mA peak current. Consequently, the accelerator is designed for a 100 mA beam and all of the necessary power equipment and other features are included. At full energy, the energy spread will be about 0.3% and the area in transverse will be about $5\pi \times 10^{-4}$ cm-rad. Both of these figures include the effects of the estimated errors in alignment and adjustment of the accelerator.

A maximum of approximately 10 pps will be needed for injection into the AGS when it is being operated at reduced output energy. The design pulse rate for the linac is set at 30 pps which increases the cost by about 1%. This means that there can be at least 20 pps of 500 MeV protons available for use as an independent research facility should this prove desirable. Although the duty cycle of such a facility would be low, it would still have an average current capability between 200 and 500 μamp at 500 MeV which is adequate for the copious production of stopped mesons.

The preinjector will be a 750 kV Cockcroft-Walton generator. Existing proton linacs have used injection energies between 500 keV and 4 MeV. A lower limit is imposed by several considerations once the frequency of the drift tube linac is set. 1) The quadrupole field strength requirement increases and the cell length decreases as the injection energy is lowered, resulting in difficulty in installing the quadrupoles in the drift tubes. 2) As the drift tube gap decreases, the radial transit factor decreases, resulting in a worse radial distribution of field in the

---

*A Proposal for Increasing the Intensity of the Alternating Gradient Synchrotron at the Brookhaven National Laboratory, May, 1964, BNL 7956.

TABLE I

Principal Characteristics of the Proton Linac

1. Beam Energy

   (a) Maximum energy: 503 MeV.
   (b) Energy variable in steps of 5-6 MeV from 187 MeV to 503 MeV.
   (c) Energy spread at full energy: approximately $\pm$ 0.3% or or $\pm$ 1500 keV.

2. Beam Intensity

   (a) Average current: 0.3 mA or 2×10^{15} protons/sec.
   (b) Peak pulse current: 50 mA (eventually 100 mA).
   (c) Pulse length and rate: 200 μ sec, 30 pps.
   (d) Beam duty cycle: 0.6%.
   (e) The rf microstructure of the beam will consist of 0.2 nsec pulses separated by 5 nsec.
   (f) Average beam power: 150 kW.
   (g) Beam quality, area in transverse phase space, $5 \pi \times 10^{-4}$ cm-rad at 500 MeV.

3. Physical Characteristics

   (a) Total length: 1200 feet.
   (b) Total peak rf power: 77 MW (at 50 mA beam current).
   (c) Preinjector: 750 kV Cockcroft-Walton generator.
   (d) Drift tube accelerator: 0.75 to 187 MeV at 201.25 Mc/sec. One cavity $\sim$ 8 m long followed by six cavities each $\sim$ 21 m long.
   (e) Loaded waveguide accelerator: 187 to 503 MeV at 805 Mc/sec: 54 cavities each 3 m long, 54 rf amplifiers.
   (f) Transverse focusing by magnetic quadrupoles.

gap which in turn can adversely affect the quality of the beam. 3) At lower injection energies, space-charge blow-up of the beam will be more serious in the space between the preinjector and the linac. The upper limit on the injection energy is set by the dc generator. The maximum voltage for an air-insulated set is about 1.25 MV and about 12 MV for a pressurized machine. Furthermore, as the injection energy is increased, the amount of phase oscillation damping is decreased which could lead to serious difficulty at the transition in structures. For a linac frequency of 200 Mc/sec, there is little to be gained by going above 750 keV, at which energy the technology is well developed.

It is planned to install two completely independent preinjector systems with a switching magnet in the drift space so that either may be used to inject into the linac. The duplication of the preinjector is necessary to insure high reliability of the linac and also will provide facilities for a polarized ion source and for ion source development.

In order to achieve accelerated beams of 50 mA and eventually 100 mA from the linac, the ion source must be capable of delivering 200 and 400 mA, respectively, with sufficiently small emittances. The present choice is a modified duoplasmatron which should be capable of 200 mA output with a minimum of development. At present, no source is clearly capable of delivering 400 mA with a sufficiently small emittance to be injectable into the linac. Thus considerable design and development will be needed on the source before the linac can deliver 100 mA.

A buncher will be used to increase the capture efficiency and particularly to concentrate the particles near the synchronous phase. This latter function is particularly important because particles which are near the boundaries of the stable region at injection may be lost at higher energies, contributing to activation of the structure or at best will emerge from the linac with poor quality and hence be of little use. Several new designs for high efficiency bunchers are now being developed, and one of these will be used.

The drift tube section of the linac will operate at 201.25 Mc/sec and will accelerate the beam to 187 MeV. The general parameters of the drift tube section are shown in Table II. The possibility of operating the drift tube section at 400 Mc/sec has been considered but abandoned for the following reasons. A pressurized preinjector at about 3 MeV would be required which would greatly complicate the preinjector design. Even at this injection energy, the design of the first cavity of the linac would be very difficult. Furthermore, the loss of damping between 750 keV and 3 MeV would be serious. However, if the new high efficiency bunchers are successful, it may prove desirable to change from 200 Mc/sec

TABLE II

General Parameters of the Drift Tube Section

Input energy (MeV)	0.75	
Output energy (MeV)	187	
Energy gain (MeV)	186	
Peak beam current (mA)	50	(100)*
Beam duty cycle (%)	0.6	
Beam pulse length (μsec)	200	
Pulse repetition rate (pps)	30	
Rf pulse length (μsec)	400	
Rf duty cycle (%)	1.2	
Operating frequency (Mc/sec)	201.25	
Wavelength (cm)	148.97	
Number of cavities	7	
Peak excitation power (MW)	13.3	
Peak beam power (MW)	9.3	(18.7)
Total peak rf power (MW)	22.6	(32)
Average excitation power (kW)	160	
Average beam power (kW)	56	(112)
Total average power (kW)	271	(384)
Total length of cavities (m)	133.7	
Total intercavity drift space (m)	5.3	
Buncher space (m)	7	
Transition drift space (m)	10	
Total length (m)	156	

*Numbers in parentheses are for a peak beam current of 100 mA.

to 400 Mc/sec at an energy near 20 MeV which could lead to a reduction in the cost of the linac.

There will be seven independent cavities containing a total of 261 drift tubes. The cavities will be of conventional copper-clad steel construction. The first cavity will be about 8 m long and will operate at a reduced gradient (about 5 MV/m) to avoid the sparking problems which have been encountered at the low energy end of some linacs. The design of this cavity is intended primarily to assure good shaping of the beam in both transverse and longitudinal phase space. A very short drift space will be used between the first and second cavities. About 30 cm is the maximum allowable distance because of the debunching of the beam. It is planned to make the vacuum envelope continuous for the two cavities. The details of the drift tube cavities are given in Table III.

The second through seventh cavities will use shaped drift tubes, and the cost will be minimized with respect to shunt impedance and the sparking limit. It is expected that the MURA method of calculating cylindrical drift tubes will be used. The length of each cavity is so chosen that the peak power required per cavity will be about 5 Mw at 100 mA of beam current which will match the capability of one power amplifier. The lengths will vary from about 24 to 19 m which is short enough to assure reasonable ease in flattening the cavities.

The drift spaces between these cavities will be about 1 m long, and matching triplets may be required in the drift space, depending on the final choice of focusing arrangement. The details of the focusing system and of the particle motion will be treated in another paper.

The final rf amplifier stages will use the RCA 7835 triode which should be capable of delivering 5 MW peak power output in this service. Thus, there will be six final stages. The power to drive these six stages and the power for the first cavity will be obtained from another 7835 stage with power splitters and phase shifters in each drive line. Each 7835 will have its own hard tube modulator and power supply.

The vacuum system, cooling and other support systems will be generally conventional. Ion pumps will be used throughout. The rough tuning of each cavity to resonance will be accomplished by temperature control.

Following the drift tube section, there will be a drift space between 5 and 10 m long before the beam enters the loaded waveguide section. Because of the debunching of the beam, it is desirable to keep this distance as short as possible, but there is a considerable amount of equipment to be

TABLE III

Summary of Drift-Tube Tables

Cavity No.	1	2	3	4	5	6	7
β_{in}	0.040	0.140	0.294	0.383	0.443	0.487	0.522
β_{out}	0.140	0.294	0.383	0.443	0.487	0.522	0.552
Energy in (Mev)	0.75	9.33	43.34	77.35	108.07	135.79	162.01
Energy out (Mev)	9.33	43.34	77.35	108.07	135.79	162.01	187.09
Energy gain (Mev)	8.58	34.01	34.01	30.72	27.72	26.22	25.08
E_{gap} (Mv/m)	5.0	8.0	12.0	12.0	12.0	12.0	12.0
Range of R_s (MΩ/m)	41.0	50.0	56/40	40/31	31/25	25/21	21/18
Excitation power (Mw)	0.38	1.69	1.67	2.06	2.26	2.50	2.70
Beam power[1] (Mw)	0.43 (0.86)	1.70 (3.40)	1.70 (3.40)	1.54 (3.07)	1.38 (2.77)	1.31 (2.62)	1.26 (2.51)
Total power (Mw)	0.81 (1.24)	3.39 (5.09)	3.37 (5.07)	3.60 (5.13)	3.64 (5.03)	3.81 (5.12)	3.96 (5.21)
Accumulated power (Mw)	0.81 (1.24)	4.20 (6.33)	7.57 (11.40)	11.17 (16.53)	14.81 (21.56)	18.62 (26.68)	22.58 (31.89)
Cavity length (m)	7.78	21.81	23.66	21.51	20.06	19.53	19.19
Cavity diameter (cm)	94.8	95.0	89.4	87.9	86.4	84.9	84.0
Range of D.T. diameter (cm)	17.6	23.9/16.5	11.74/14.4	14.4/16.4	16.6/18.3	18.6/20.0	20.1/21.4
Range of D.T. length (cm)	4.65/13.9	16.3/32.9	33.7/38.0	38.6/41.0	41.8/43.3	44.1/45.2	45.7/46.6
Range of gap (cm)	1.50/6.97	4.93/10.9	10.1/18.7	18.3/24.7	24.2/30.0	28.4/32.4	32.1/35.5
Range of g/L ($\times 10^3$)	247/332	234/248	230/329	321/375	366/401	392/417	413/432
$\Delta W/L$ (Mev/m)	1.10	1.55	1.44	1.43	1.38	1.34	1.31
$\Delta W/P_{excit.}$ (Mev/Mw)	22.5	20.1	20.4	14.9	12.2	10.5	9.4
Bore diameter (cm)	2.0	2.0 & 2.5	3.0	3.5	4.0	4.5	4.5
No. of unit cells	59	67	47	35	29	26	24
Accum. No. of full D.T.[2]	58	124	170	204	232	257	280
Drift space length[3] (m)	7.0 + 0.3	1.0	1.0	1.0	1.0	1.0	10.0
Accumulated length[3] (m)	15.1	37.9	62.6	85.1	106.1	126.7	155.8
No. of quadrupole magnets	58	66	15	9	6	5	4
No. of magnets between cavities[4]	6 + 0	3	3	3	3	3	12
Accumulated No. of magnets[4]	64	133	151	163	172	180	196

(1) Numbers in parentheses are for a peak beam current of 100 ma.

(2) There are N_{cell}-1 full D.T.'s in each cavity plus 2 half D.T.'s

(3) The buncher space preceding Cavity No. 1 is 7.0 m and the space between Cavities No. 1 and No. 2 is 0.3 m. The accumulated length is measured from the start of the buncher space to the end of the transition section following Cavity No. 7.

(4) There are two triplet lenses in the buncher space, none between Cavities No. 1 and No. 2, one lens each between Cavities No. 2 - No. 7, and three lenses in the transition section.

installed in this space. There will be one or more quadrupole triplets for matching the beam emittance from the drift tube section into the transverse acceptance of the waveguide section. It seems clear that the analysis of the beam from the drift tube section can best be done here rather than drifting the low energy beam through the entire waveguide section. Consequently, a deflecting magnet must also be installed in the drift space. Complete beam analysis equipment and a small beam stop will be provided.

The choice of frequency for the loaded waveguide section is based primarily on the longitudinal dynamics of the particles at the transition. Extensive numerical calculations have been made and lead to the conclusion that 800 Mc/sec is the highest frequency which can be used safely when the drift tube section is operated at 200 Mc/sec. In the ideal case, it would be possible to transfer the beam from a 200 Mc/sec to a 1200 Mc/sec accelerator section at about 200 MeV, without loss of beam from the phase stable region. However, when the effects of improper adjustments and a reasonable safety factor are included, it becomes clear that 800 Mc/sec is a reasonable figure.

The conventional iris-loaded waveguide is clearly a usable structure in the standing wave mode for the acceleration of protons. However, better structures have been developed, as discussed in another paper. The slotted iris structure has been chosen for the high energy section of this linac because it gives the best compromise between bandwidth, shunt impedance, ease of fabrication and other factors. The operating frequency will be 805 Mc/sec, and there will be 54 independent standing wave cavities which will accelerate the beam from 187 to 503 MeV. The general parameters of the waveguide section are given in Table IV.

The cost minimization procedure has been applied to the design and results in a rather low acceleration rate which increases from 1.67 MeV/m to 2.06 MeV/m. This leads to a maximum value of E_0 of about 4.1 MV/m so that the peak fields on the surfaces should not exceed 10 MV/m which should be well below the sparking limit. Each cavity will be about 3 m or 8.5 λ long so that flattening should present no problem. The number of unit cells per cavity will vary from 30 to 22. The excitation power per cavity will be about 0.7 MW, and the total power per cavity at 100 mA will be about 1.25 MW. The energy gain per cavity varies from 5.1 to 6.4 MeV.

Each cavity will be powered by a single amplifier tube so that power splitting at high power levels will not be needed. The final amplifier tubes will be type RCA A15191 negative grid triode coaxitrons. It is believed that klystrons are not suitable for this application. Drive power for the 54 final amplifiers will be supplied by seven A15191's, each capable of driving eight finals through the appropriate power splitting networks.

TABLE IV

General Parameters of the Waveguide Section

Input energy (MeV)	187	
Output energy (MeV)	503	
Energy gain (MeV)	316	
Peak beam current (mA)	50	(100)*
Beam duty cycle (%)	0.6	
Beam pulse length (μsec)	200	
Pulse repetition rate (pps)	30	
Rf pulse length (μ sec)	250	
Rf duty cycle (%)	0.75	
Operating frequency (Mc/sec)	805.00	
Wavelength (cm)	37.241	
Number of cavities	54	
Peak excitation power (MW)	38.4	
Peak beam power (MW)	15.8	(31.6)
Total peak rf power (MW)	54.2	(70)
Average excitation power (kW)	288	
Average beam power (kW)	95	(190)
Total average power (kW)	406	(525)
Total length of cavities (m)	165	
Total intercavity drift space (m)	34	
Drift space at end of accelerator (m)	6	
Total length (m)	205	

*Numbers in parentheses are for a peak beam current of 100 mA.

These seven drivers in turn will be driven by an intermediate power amplifier employing a single A15191. Thus, there will be 62 A15191's and a single low level drive chain. Each tube will have a separate hard tube plate modulator in order to allow individual control of the field amplitube in each cavity. Phase control between cavities will be accomplished by servo-controlled phase shifters in the drive lines to the final amplifiers. By including only the final amplifier in the servo-loop, the number of elements introducing phase noise is minimized.

The frequency of the accelerator is set by a highly stabilized 805 Mc/sec oscillator, and all of the cavities are tuned to this frequency. For the drift tube section, a 201 Mc/sec oscillator is phased locked by a signal taken from the first 805 Mc/sec cavity.

The cavities will be assembled in subsections consisting of two cavities separated by a 30 cm drift space which will be used as the vacuum pumping connection. The subsections are connected by a 1 m long drift space. Transverse focusing will be accomplished by quadrupole doublets placed in each 1 m drift space.

The vacuum system will employ ion pumps throughout and will operate at a pressure below 10^{-6} Torr. The cooling system and other accelerator support equipment will be generally conventional. Because the coaxitrons are fixed tuned and have no mechanical adjustments, they will be placed directly alongside the waveguide to minimize the length of waveguide. The accelerator will be located in a shielded tunnel, separated from the support equipment by a wall which varies from about 2 to 11 feet thick.

More detailed discussion of the design of this linac is included in several other papers presented at this Conference and in the Brookhaven Proposal BNL 7956.

WROE: I would like to know why you have so much more injected current than accelerated current. It seems to me that one should be able to accelerate more than half of the current from the injector.

VAN STEENBERGEN: In the conventional bunchers which are in use now, the effective capture in the linac is less than 50%. One wishes to operate the buncher to achieve good beam quality rather than for maximum capture. Hence, it seems that 400 mA from a source is not too much to assure 100 mA of accelerated beam at the end of the linac.

WHEELER: I think it is necessary to stress the importance of beam quality in these high intensity, high energy linacs. One must not lose many particles at energies above the neutron production threshold, so that particular care must be taken when the beam is transferred from the drift tube linac to the waveguide section at about 200 MeV. We have made estimates of the radiation background and activation of the accelerator. These will be very severe if more than about 0.1% of the beam is lost. Beam quality is also most important in an injector linac in order to assure good capture by the synchrotron.

CARNE: Why do you set a field strength of 10 MV/m at 800 Mc/sec?

WHEELER: That is an estimate (see text of paper). The cost minimization procedure indicates an average acceleration rate of about 1.75 MeV/m, and from this it is estimated that the peak surface fields should not exceed 10 MV/m. I think that this figure is conservatively below the sparking limit.

WROE: Are there any parts of the preinjectors which are more unreliable than the others?

WHEELER: Particularly at these high currents, the source itself is the biggest problem. However, since the source is in the high voltage terminal, you must shut off the Cockcroft-Walton set in order to get at the source. Hence, in order to allow rapid change over to a new source, two complete preinjectors are required. These can be switched by simply changing a magnet in the buncher space. The amount of money involved is small compared to the improved operating efficiency of the linac.

THE LASL MESON FACTORY*

D. E. Nagle
Los Alamos Scientific Laboratory, University of California
Los Alamos, New Mexico

The LASL accelerator group has been engaged for the past two years in the design of a high current, medium energy (800 MeV) proton linac and associated experimental areas and equipment. A complete facility is planned, comprising experimental areas, office building, branch shops, data-handling equipment, high level radiochemistry laboratories, etc. It would have supporting it the libraries, computers, and other services presently available at Los Alamos. This facility would become a major tool for the program of research by physicists and chemists into the structure of the nucleus. The facility would be used by qualified scientists at LASL and throughout the country, with a natural emphasis on faculty and students from the Rocky Mountain and Southwest universities. It would be the only accelerator above the low energy range between the West Coast on the one hand and Chicago on the other.

Although nuclear physics is a relatively mature science, qualitative improvements in the tools of research are still giving rise to qualitative changes in our understanding of nuclear structure. We are confident that this will be true of this instrument as well.

The characteristics which make the linac especially valuable for this application are:

1) Completely extracted proton beam
2) Variable energy
3) Small radial and angular spread of the beam
4) Small energy spread of the beam
5) Complete rf debunching possible, i.e., 100% micro duty factor
6) Possibility of extending the energy range
7) Ease of servicing accelerator components
8) High rf efficiency
9) Low activation of the machine by lost beam.

Table I gives the basic parameters of the machine as a research tool.

Tables II and III give the characteristics of some of the secondary beams as calculated by A. McGuire and H. Butler.

---

*Work performed under the auspices of the U. S. Atomic Energy Commission.

A method of complete debunching of the microstructure has been studied by W. Visscher and will be discussed later in the week. It seems quite practical. This gives the linac an overall duty factor of six per cent which compares favorably with most circular machines.

Table IV shows the principal parameters of the machine. The injector is a conventional 750-keV Cockcroft-Walton with von Ardenne source and accelerating tube, followed by a prebuncher. The first 175 MeV of the linac is the Alvarez type operating at 201.25 Mc. The present design layout of this part of the machine is given in Table V.

H. Hoyt and W. Visscher will discuss the LASL programs that do the same type of calculations. LASL is, of course, participating in the effort to see if joint designs can result in savings in hardware costs for the several linacs now proposed in this country.

Table V gives the present 200-Mc design. Figure 1 shows the acceptance fish corresponding to this design, calculated by M. Rich.

As you have heard this morning, one of the very interesting features of the last year's work has been the rapid development of new structures for the 800-Mc part of the linac. As E. Knapp said, the cloverleaf structure offers a factor of two or more improvement in shunt impedance and a factor of 10 or more in coupling over the center-coupled iris at this frequency. The other electrical properties, e.g., field patterns, higher cell modes, and tank behavior are now understood in great detail as a result of a very satisfactory agreement between theory and measurements.

The fabrication problem appears to be tractable. We regard the cloverleaf, therefore, as a practical solution to the problem of finding a better 800-Mc structure. The present design of the 800-Mc linac is based on the cloverleaf, although the side-coupled structure is an attractive alternative.

Table VI shows the basic 800-Mc layout. Forty-five (45) power amplifiers, each driving two resonant π-mode tanks of 40 cells each, are used to get to 793 MeV. The phase velocity is constant in each tank. The final amplifier tubes, RCA A15191 coaxitrons, have a design power of 1.25 MW. We have rated them at 1.0 at the tanks, including beam loading.

The problem of the phase and amplitude control of the tank voltages is an interesting and important one. Bob Jameson will discuss one system for doing this.

The choice of transition energy is a compromise between considerations of power economy and beam dynamics. Power economy considerations would argue for a transition at less than 140 MeV. However, the cost is not very sensitive to a 30 MeV change. With 40 cells per section, the computer runs predict a resonance between the radial and phase oscillation at about 130 MeV. Above 130 MeV, the curves for radial and phase oscillation diverge quite rapidly as shown in Fig. 2. The problem of fitting in focus magnets is much easier at the higher energy. Finally, the additional phase damping helps the 800-Mc fish to digest the 200-Mc fish. All of these considerations together point to 175 Mev as a suitable transition energy.

The remaining part of the talk is to show you some slides which illustrate the artist's conception of the physical appearance of the accelerator and the buildings. They are Figs. 3 through 8. Figures 9 through 11 show the 800-Mc test stand and development models of the 200-Mc and 800-Mc structures.

TABLE I

Research Characteristics of the LASL Linac

1. Average proton beam 1 mA.
2. Extraction efficiency 100%.
3. Micro duty factor can be 100% from 200-700 MeV.
4. Macro duty factor 6%.
5. Energy variable 300-800 MeV, with possibility of extending energy later.
6. Radial emittance $\cong \pi$ mr-cm.
7. Energy spread $\cong$ 0.3% (rms, with errors).
8. 800-MeV phase width, if not debunched = $\pm 15^{\circ}$.
9. Beam loading 26%.

TABLE II

Pion Beam Intensities

Conditions: 1 mA Proton Beam - 800 MeV
6 gm/cm^2 Target
3×10^{-3} Steradian Pion Channel Acceptance
$\Delta p/p$ = 0.04 - Momentum Acceptance of Pion Channel
Channel Length = 40 Ft. (Minimum $\Delta p/p$ of Channel = 0.007)

Pion Energy MeV	Positive Pion Intensity	Negative Pion Intensity
100	2.5×10^8/sec	4×10^7/sec
200	1.6×10^9/sec	2.8×10^8/sec
300	2.2×10^9/sec	3.1×10^8/sec
400	1.7×10^9/sec	2.8×10^8/sec
500	1.0×10^9/sec	1.6×10^8/sec

TABLE III

Muon Beam Intensities

Conditions: 1 mA - 800 MeV Proton Beam
30 gm/cm^2 Target
$\Omega = 10^{-2}$ Steradian = Acceptance of Pion Matching Channel
X_1 = 45 Ft. = Length of Pion Matching Channel
$\Delta p/p)_\pi$ = Momentum Acceptance of Pion Channel = 0.10
$\Delta p/p)_\mu$ = Momentum Interval of Muons Considered = 0.10
F = Probability of Muon Remaining in Channel = 0.2 for 50 Ft. Channel
= 0.1 for 100 Ft. Channel

Pion Energy MeV	Positive Pion Beam at μ Channel in	Muon Energy	Positive Muon Beam Intensity		Negative Muon Beam Intensity	
			50 Ft. Channel	100 Ft. Channel	50 Ft. Channel	100 Ft. Channel
100	9×10^9/sec	70 MeV	2×10^7/sec	--	3×10^6/sec	--
200	6×10^{10}/sec	175 MeV	2×10^9/sec	--	3×10^8/sec	--
300	8.5×10^{10}/sec	265 MeV	2×10^9/sec	1.3×10^9/sec	3×10^8/sec	2×10^8/sec
400	7×10^{10}/sec	360 MeV	1.3×10^9/sec	1.0×10^9/sec	2×10^8/sec	1.6×10^8/sec
500	5.5×10^{10}/sec	435 MeV	8.8×10^8/sec	6.9×10^8/sec	1.4×10^8/sec	1.1×10^7/sec

TABLE IV

Machine Characteristics

Proton Energy	792 million electron volts
External Average Beam Current	1000 microamperes
Length of Beam Channel	2330 feet
Radiofrequency	201.25 Mcps below 176 MeV 805.0 Mcps above 176 MeV
Total Peak Rf Power	62 MW
Total Average Rf Power	3.8 MW
Macroscopic Duty Factor	6.0 %
Injection Energy	750 keV
Total Facility Power	33 MW
Average Beam Loading	26 %

TABLE V

200-Mc Linac Design

MURA Shape Drift Tubes

Tank	1	2	3	4	5
E in	0.75	10.76	60.50	103.1	142.2
E out	10.76	60.50	103.1	142.2	176.5
ΔE	10.01	49.74	42.6	39.1	34.3
L	9.01	30.25	29.62	30.53	30.15
$\Delta E/L$	1.11 MeV/m	1.64	1.44	1.28	1.14
Z_p	30	29	19	15	12
P_{cu}	0.47 MW	2.84	3.20	3.34	3.25
P_B	0.20	0.995	0.85	0.78	0.685
P_T	0.67	3.84	4.05	4.12	3.92
Cavity D	94 cm	90	88	86	84
DT D's	18	16-14	16	16	16
Hole d	2	2.5	3	3.5	4
R_c	2	4	4	4	4
Range G/L	.2-.3	.19-.33	.35-.42	.40-.44	.43-.46
No. Unit Cells	64	81	51	44	39
Drift Space	30.5 cm	61	61	61	
No. Quads	64	41	26	22	20
Quad Power	32 kW	16	10	8.8	8.0
Quad Cooling(B)	30 gpm	16	10	9	8
Final Power amp	2:4616's	RCA 7835	RCA 7835	RCA 7835	RCA 7835

TABLE VI

805-Mc Accelerator Summary

Section Number	1 to 90
Input Energy (MeV)	176.5
Accelerator Section Length (meters)	4.0741 to 6.2960
Quad Length $4\beta\lambda/2$ (meters)	0.4096 to 0.6302
Drift Length $4\beta\lambda/2 + 0.4$ (meters)	0.8096 to 1.0302
Accumulated Length (meters)	575.3462
Structure Power (MW)	0.387 to 0.350
Beam Power (MW)	0.113 to 0.150
$\Delta w/L$ (MeV/m)	1.389 to 1.192
Final Energy (MeV)	792.0

JOHNSTON: Did you say that in a given cavity you do change the length of the cell as beta increases?

NAGLE: No, we do not; we keep it constant until the next cavity.

JOHNSTON: Doesn't this shake the phase oscillations too badly for each proton?

NAGLE: No.

OHNUMA: I should like to ask about your choice of the final energy. You mentioned that this machine will be primarily for nuclear physics. What would be the particular advantage of getting 800 MeV instead of say 500 MeV?

NAGLE: Well, there is certainly no precise energy that you must reach. The difference between an accelerator that runs at 500 MeV and one that runs at 800 MeV is primarily in the range of high energy pion and muon beams that are available, and the range of high energy nucleon beams that are available. If you go to 500 MeV, you will not have many pions above 190 MeV because there's just not much phase space available. If you go to 800 MeV, you could have 300-350 MeV pions.

SYMON: I think it is a little amusing that the figure 800 MeV first arose because that was the natural dynamical limit for AVF cyclotrons. When we first discovered this, we were a little unhappy because it seemed one would like to go higher to get over the strange particle thresholds. We looked very hard to try to find reasons to justify building a machine at 800 MeV. Now I guess the tables are turned and the AVF cyclotrons are no longer so attractive. But this particular energy seems to be attractive still.

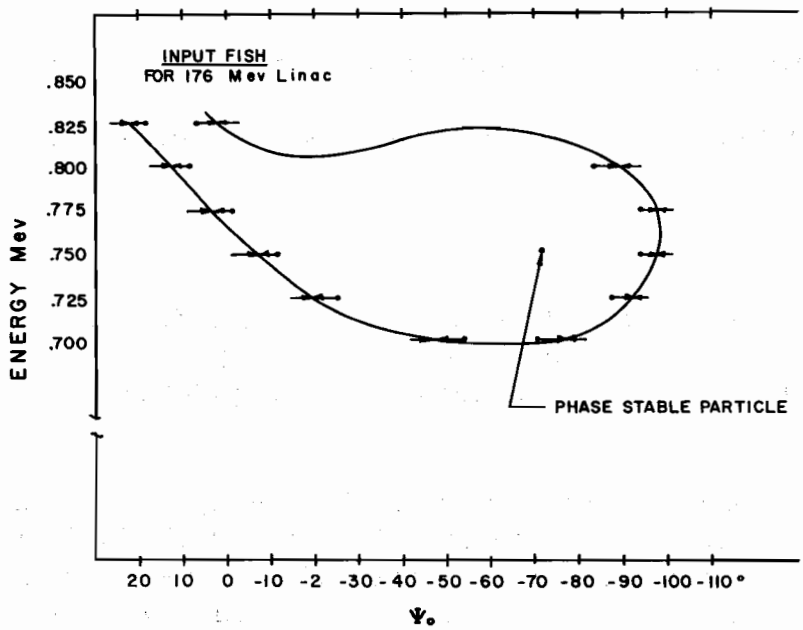
INPUT FISH
FOR 176 Mev Linac
ENERGY Mev
.850
.825
.800
.775
.750
.725
.700
PHASE STABLE PARTICLE
20 10 0 -10 -2 -30 -40 -50 -60 -70 -80 -90 -100 -110°
Ψ₀

Fig. I

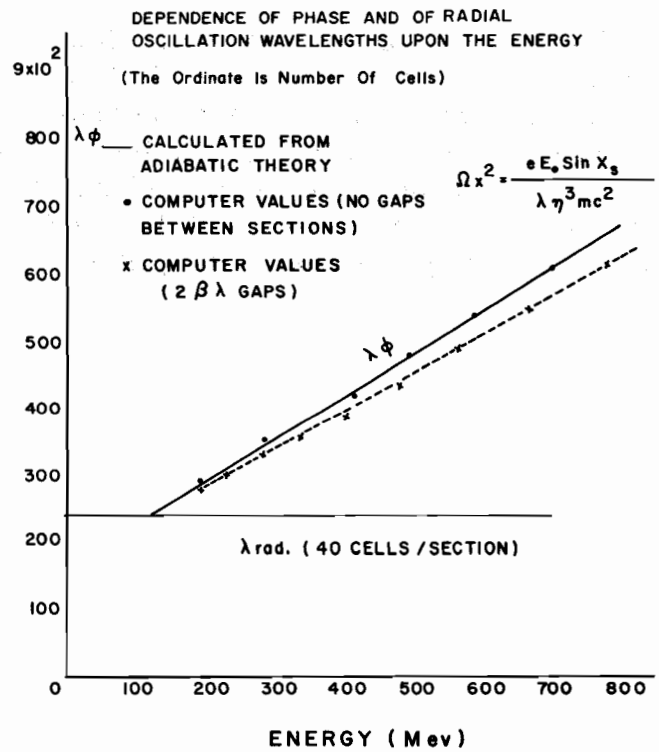
DEPENDENCE OF PHASE AND OF RADIAL
OSCILLATION WAVELENGTHS UPON THE ENERGY
(The Ordinate Is Number Of Cells)
9x10²
800
700
600
500
400
300
200
100
0
λφ CALCULATED FROM
ADIABATIC THEORY
• COMPUTER VALUES (NO GAPS
BETWEEN SECTIONS)
x COMPUTER VALUES
(2 β λ GAPS)
Ωx² = eE₀ Sin X_s / λ η³ mc²
λφ
λ rad. (40 CELLS / SECTION)
100 200 300 400 500 600 700 800
ENERGY (Mev)

Fig. 2

MESON FACILITY SITE LAYOUT

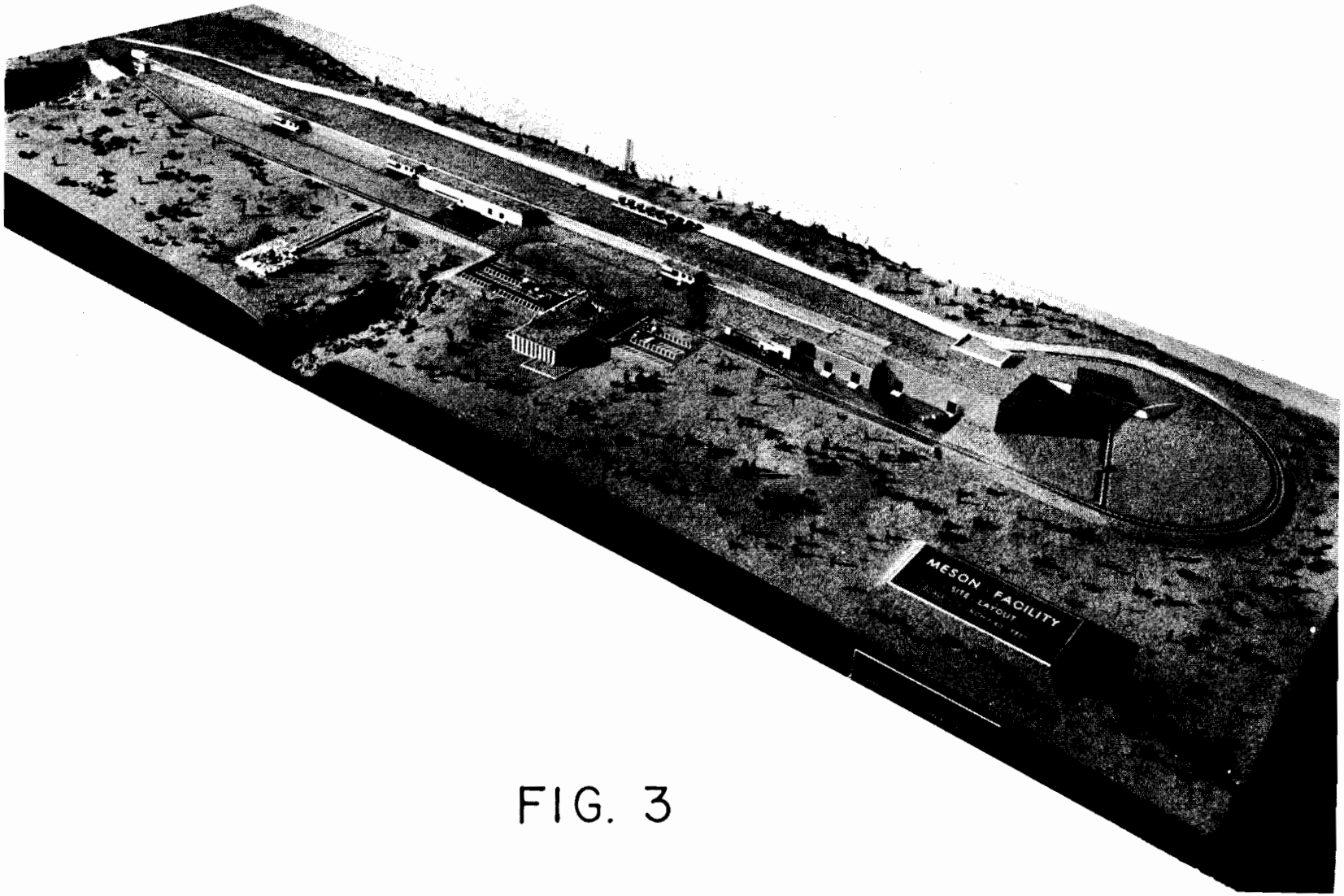

FIG. 3

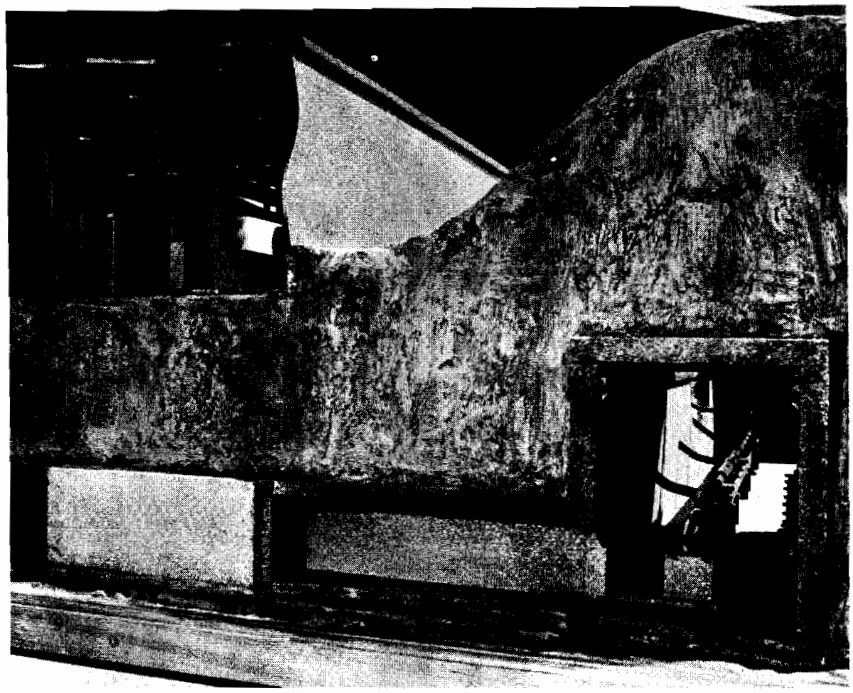

Fig. 4 ACCESS CORRIDOR AND ACCELERATOR CHANNEL

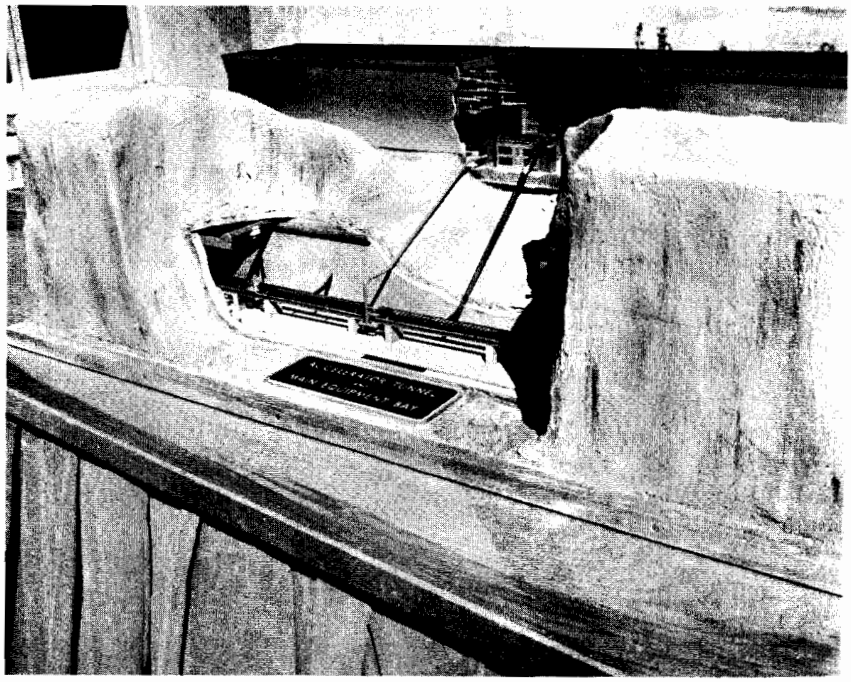

Fig. 5 ACCELERATOR CHANNEL AND MAIN EQUIPMENT AISLE

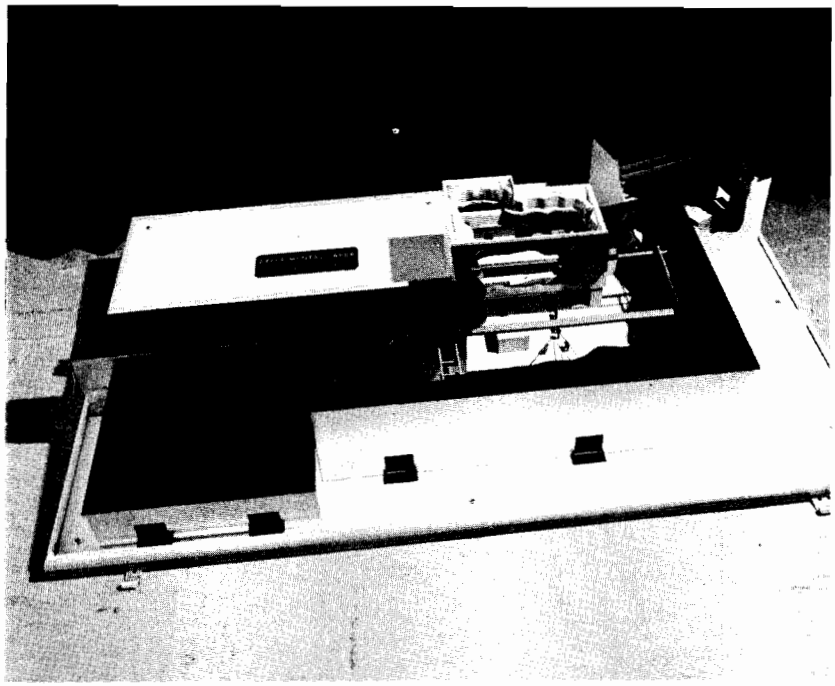

Fig. 6 EXPERIMENTAL AREA LAYOUT

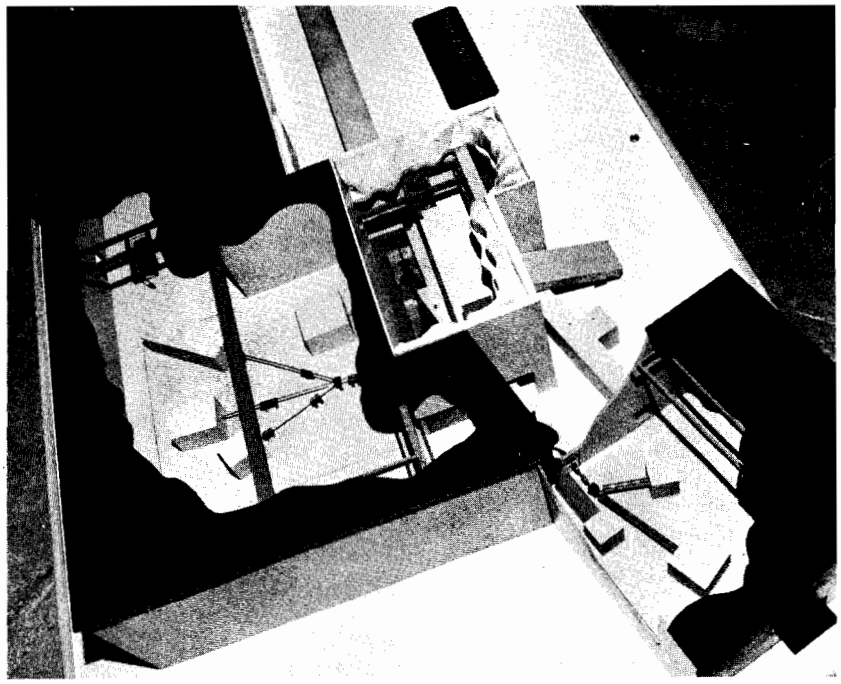

Fig. 7 EXPERIMENTAL AREA SHOWING TARGET ROOM PION AND MUON BEAMS

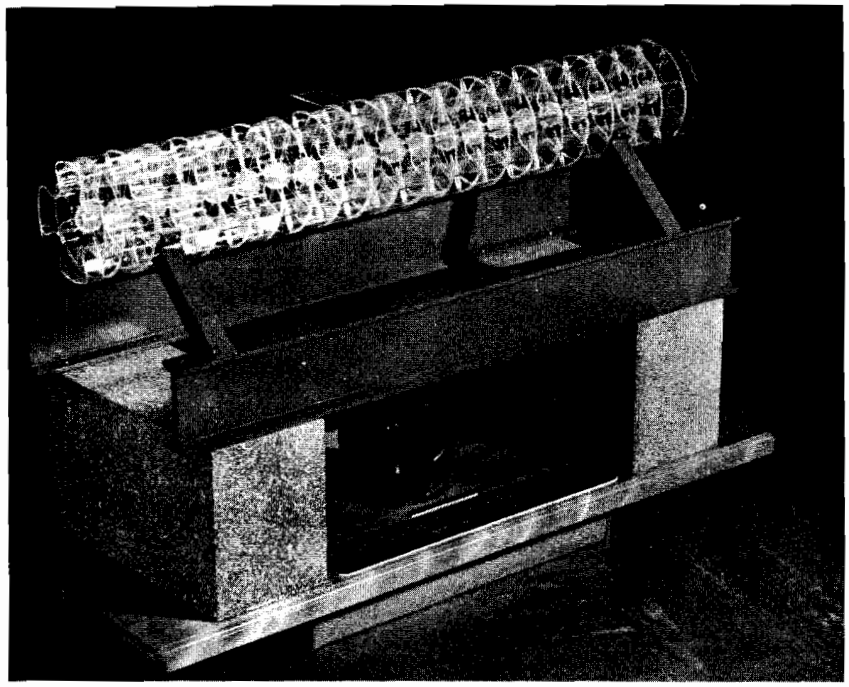

Fig. 8 PLASTIC MODEL OF WAVEGUIDE CLOVERLEAF TANK

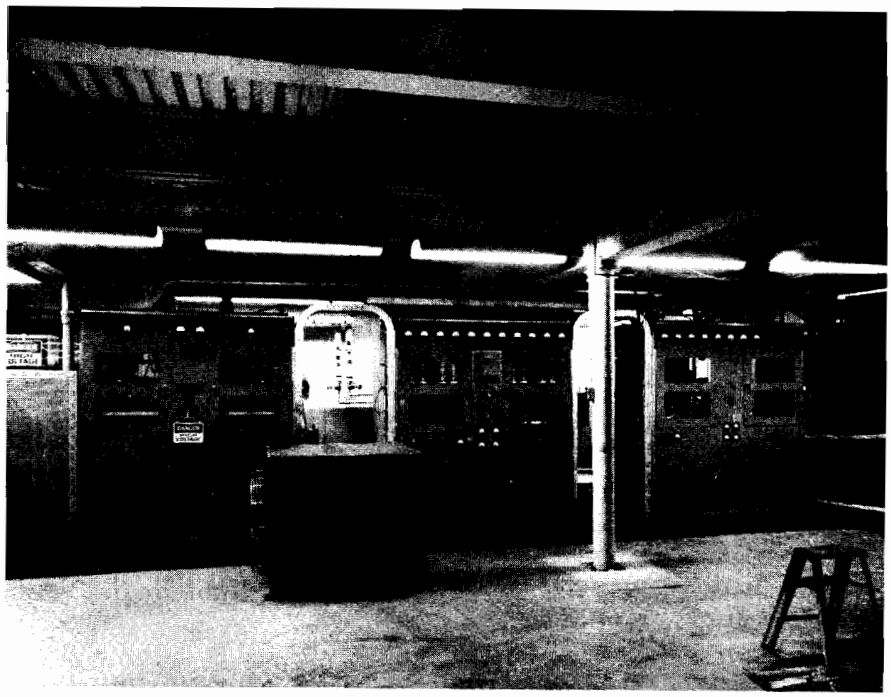

Fig. 9 800-Mc HIGH POWER TEST STAND

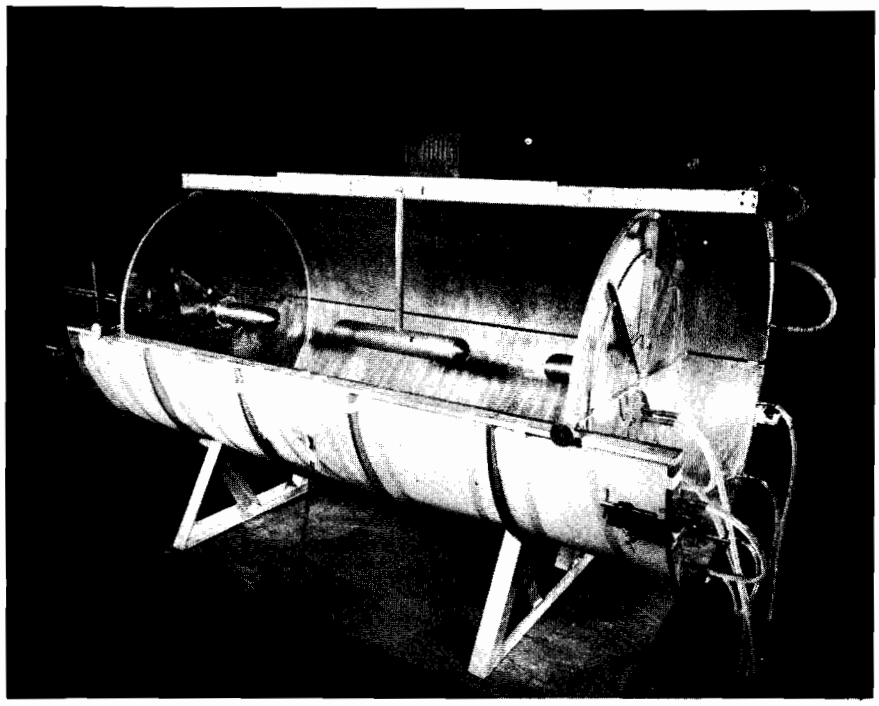

Fig. 10 ALVAREZ SECTION EXPERIMENTAL MODEL

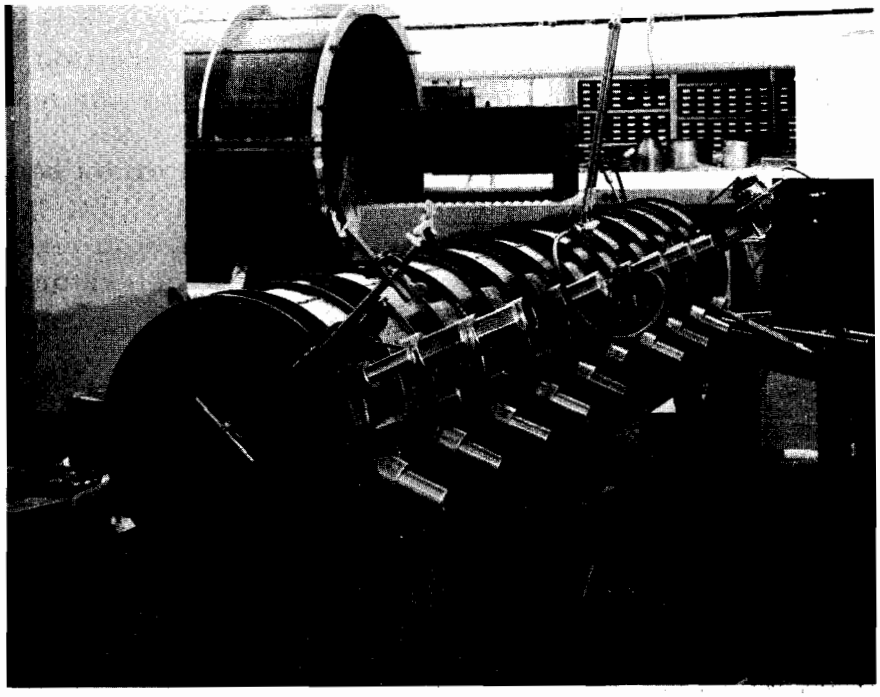

Fig. 11 CLOVERLEAF EXPERIMENTAL MODEL

STUDY FOR A SUPERCONDUCTING MULTI-GEV PROTON LINAC

H. Schopper
Karlsruhe, Germany

A study group has been established which will investigate the problems connected with a high energy superconducting linac. This type of accelerator has been selected for various reasons, the three most important of which are:

1. The experience with synchrocyclotrons has shown that for many experiments high currents are useful only if combined with a high duty cycle.

2. The technology of a superconducting accelerator is interesting in itself.

3. If a proton accelerator is built in Germany, it should be of an advanced type and it should permit the production of strange particles.

The advantages offered by a superconducting linac seem to be so attractive that we think it worthwhile to make an effort to overcome the great difficulties and to take into account the unavoidable delay in the construction.

The study group will investigate the physical and technological problems of superconducting cavities at 1200 Mc. In addition, various accelerating structures will be studied at room temperature and 400 Mc.

Since experimental data for the production cross sections of secondary particle beams are very scarce between 1 and 10 GeV, calculations based on the statistical model are being performed in order to provide a basis for the final choice of the energy of the accelerator. It is hoped that a definite proposal can be worked out within 1 or 2 years.

In order to give an impression of the implications of such a project, a few very tentative figures may be quoted. A major advantage of a superconducting linac lies in the fact that,because of the small rf losses and the good vacuum high gradients can be used,resulting in a large energy gain/m. Values of about 5 MeV/m seem possible. For a disc-loaded structure this implies maximum magnetic fields of about 200 gauss compared to the critical field of 500 gauss for Pb and 1400 gauss for Nb.

Adopting an energy of 3 GeV, the accelerator length would then be only about 600 m. For a frequency of 400 Mc, and scaling the improvement factors q obtained at Stanford for Pb at 2800 Mc to this frequency, one expects $q \simeq 40{,}000$ or perhaps even more if other superconductors are used. With an average shunt impedance of 20 M Ω/m (which seems conservative, considering the new structures discussed at this conference), one calculates a power loss for lead of P = 40 kW which has to be cooled away at liquid He-temperature.

The refrigeration system able to achieve this will require an input power of about 20 MW and is estimated to cost approximately 6 M$. Since the saving on the rf system is much higher, it is to be expected that a superconducting linac will not be more expensive than an ordinary linac with the same energy but a much lower duty cycle.

NAGLE: What current do you expect to get?

SCHOPPER: The current will be limited mainly by the shielding and the power the target can stand. Most of the rf power will go into the beam, of course. Assuming a current of 100 μA, the beam power would be 300 kW compared to the power loss of 40 kW.

MARTIN, J. H.: Do these figures push you uncomfortably high in rf magnetic field strengths?

SCHOPPER: No, it depends on the structure of course. If we assume the ordinary iris-loaded structure, then the maximum field that you get is 260 G compared to the critical field for lead of 500 G, and 1400 G for Miobium. I forgot to mention that in calculating the power, I assumed an average shunt impedance of 20 MΩ/m, which I think is on the safe side.

WORSHAM: Have you looked at the problem of how you would build the cryostat?

SCHOPPER: We haven't made any detailed studies. This will be one of the tasks of the study group.

DICKSON: Have you done any rf measurements yet on superconducting surfaces?

SCHOPPER: Not yet, but we hope to start in about two months.

GUILBAUD: The rf magnetic field you mentioned is related to the 40 kW energy loss?

SCHOPPER: Yes, the field is proportional to the energy gain per meter which in turn is related to the energy loss.

THE NEW ZGS INJECTOR PROPOSAL

Rolland Perry
Argonne National Laboratory

The history of accelerators shows that as each one becomes operational and as new experiments are designed, there is an ever increasing demand for higher beam intensity or higher energy, or both. The ZGS is no exception to this rule. Consequently, we are presently considering an improvement program for the ZGS which includes (a) a new 200 MeV, high intensity injector system, (b) remodeling of the ZGS rf system to accommodate larger beams, (c) rebuilding of the ZGS inner vacuum chambers to withstand full atmospheric pressure and to eliminate the likelihood of radiation damage, and (d) provisions for remote handling of targetry and other highly radioactive components in the ZGS.

I shall discuss only the proposed injector system.

In the early planning of the Zero Gradient Synchrotron (ZGS), it was conservatively estimated that a 50 MeV linac could be expected to inject into the ZGS a proton beam of about 5 mA with pulse lengths of about 200μsec. This would give about 6×10^{12} protons per pulse; and assuming a capture efficiency of 50% for the ZGS, the latter should then be able to accelerate about 3×10^{12} protons per pulse to full energy. As this was nearly two orders of magnitude higher than the achievements of any then existing proton synchrotron, it was expected that the ZGS would be in a very favorable position with respect to beam intensity for some time after its completion.

When the parameters for the ZGS were finalized, the space-charge limit was determined to be about 2.6×10^{13} protons per pulse after bunching for a 50 MeV injected beam.[1] To reach this level would require an injected beam of 50 mA from the linac. Up to the present time the 50 MeV linac has injected 17 mA into the ZGS. Presumably, with careful adjustment of all parameters, 50 mA might be achieved with the rf power available. This will bring the injected beam approximately to the space-charge limit of the ZGS.

Consideration of how it might be possible to increase the output of the ZGS beyond the inherent existing space-charge limit led to the realization that increase of the injection energy would push the space-charge limit to a higher level and thus permit acceleration of a larger number of particles per pulse. Furthermore, increasing the energy of the injected beam will reduce its angular divergence and thus permit injecting through a

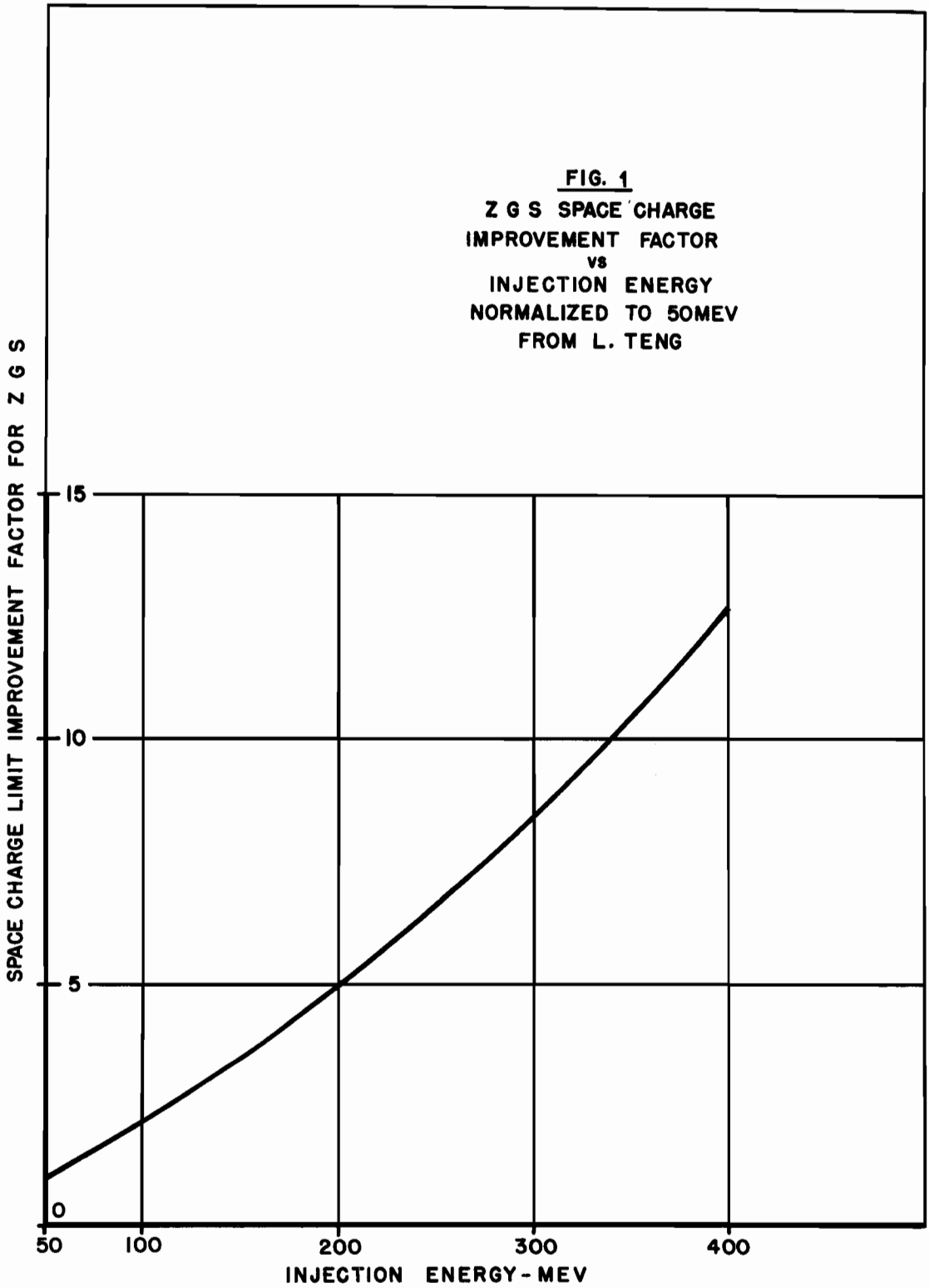
FIG. 1
Z G S SPACE CHARGE
IMPROVEMENT FACTOR
VS
INJECTION ENERGY
NORMALIZED TO 50MEV
FROM L. TENG
SPACE CHARGE LIMIT IMPROVEMENT FACTOR FOR Z G S
15
10
5
0
50
100
200
300
400
INJECTION ENERGY - MEV

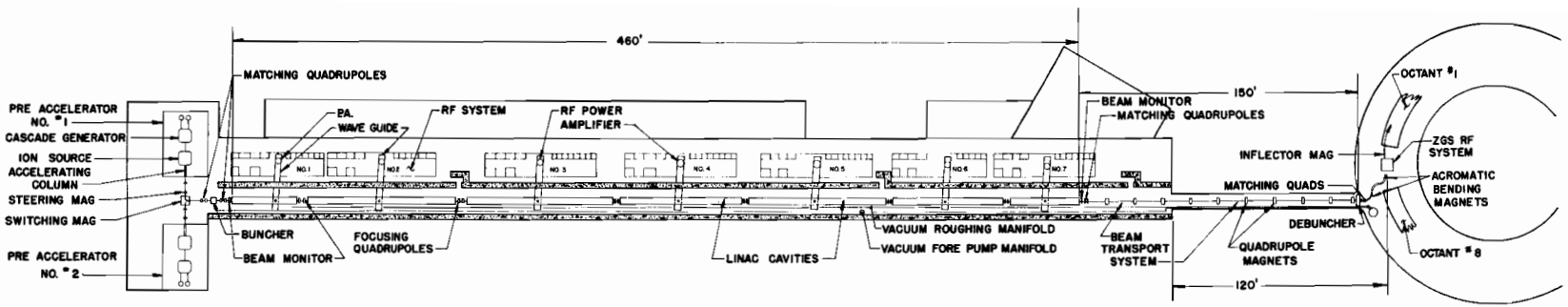

FIG. 2
200 MeV INJECTOR SYSTEM FOR THE
ZERO GRADIENT SYNCHROTRON

smaller aperture into the ZGS, with the consequence that, by decreasing the rate of rise of the ZGS guide field, the injection time can be increased to about 400 μ sec.

The space-charge limit of the ZGS at injection increases with injection energy somewhat more rapidly than linearly, as shown in Fig. 1 up to 400 MeV.

However, as the intensity of an accelerator rises, shielding requirements also increase. The safe limit of intensity for the ZGS basic shielding is believed to be about 10^{14} particles per pulse, which imposes a practical upper limit on injection energy.

Choosing an injection energy of 200 MeV provides an increase in the ZGS space-charge limit by a factor of five above the limit at 50 MeV, which would just about match the limit of the basic shielding.

The proposed injector system is comprised of the following major components shown in Fig. 2.

A 750 keV preaccelerator, including an ion source and ion focusing and accelerating elements.

A beam transport system and beam analysis system for the 750 keV ion beam.

An ion buncher for phase bunching of the ion beam.

A 200 MeV linear accelerator, comprised of seven or eight separate cavities, each driven by a high-powered rf amplifier and all properly phased together and locked to a common rf oscillator.

A beam analyzing and beam transport system for the 200 MeV proton beam.

A set of achromatic deflecting magnets to conduct the proton beam into the Zero Gradient Synchrotron and place it on its proper orbit.

It is planned to inject the 200 MeV beam into the ZGS at the No. 1 straight section but along a beam line which will permit building and testing the new system completely, except for the beam transport and debuncher portion, before disturbing the existing system. It is expected that a period of three years will be required for construction and testing and about six months for installation of the connecting equipment and modifications to the ZGS equipment.

Two complete preaccelerators are planned in order to reduce the probability of down time of the ZGS facility due to ion source or other preaccelerator problems. The beam switching magnet will permit use of either preaccelerator beam for injection. At the same time the beam from the other preaccelerator could be deflected in the opposite direction for beam analysis, etc.

The parameters selected for the preaccelerator are as follows:

Beam energy	750 keV $\pm$ 0.1%
Peak proton beam current	200 mA
Beam pulse duration	400 - 800 μsec.
Pulse repetition rate	5 - 10 per sec.
Beam emittance	10 π - 17 π cm-mr.

An ion source development program is presently under way, including investigation of the Russian plasma expansion cup idea. Also, in cooperation with MURA personnel, plans are being made for testing short accelerating column designs, with the hope of attaining improved beam quality by use of rapid acceleration in a controlled field configuration.

The beam from the preaccelerator will be focused through the apertures of a multiple-harmonic buncher by a set of quadrupole magnets and will be matched into the first cavity of the linac by another set of quadrupole lenses. Beam pulse transformers, Faraday cups, and beam-defining slits will be placed appropriately along the beam path to permit amplitude and beam quality measurements ahead of the linac. An electrostatic deflection type fast beam chopper will also be placed ahead of the linac.

Because the linac is to serve the ZGS with high efficiency, the parameters chosen should be such as to meet all the minimum requirements without imposing stress on any components. The following parameters are based on this basic philosophy.

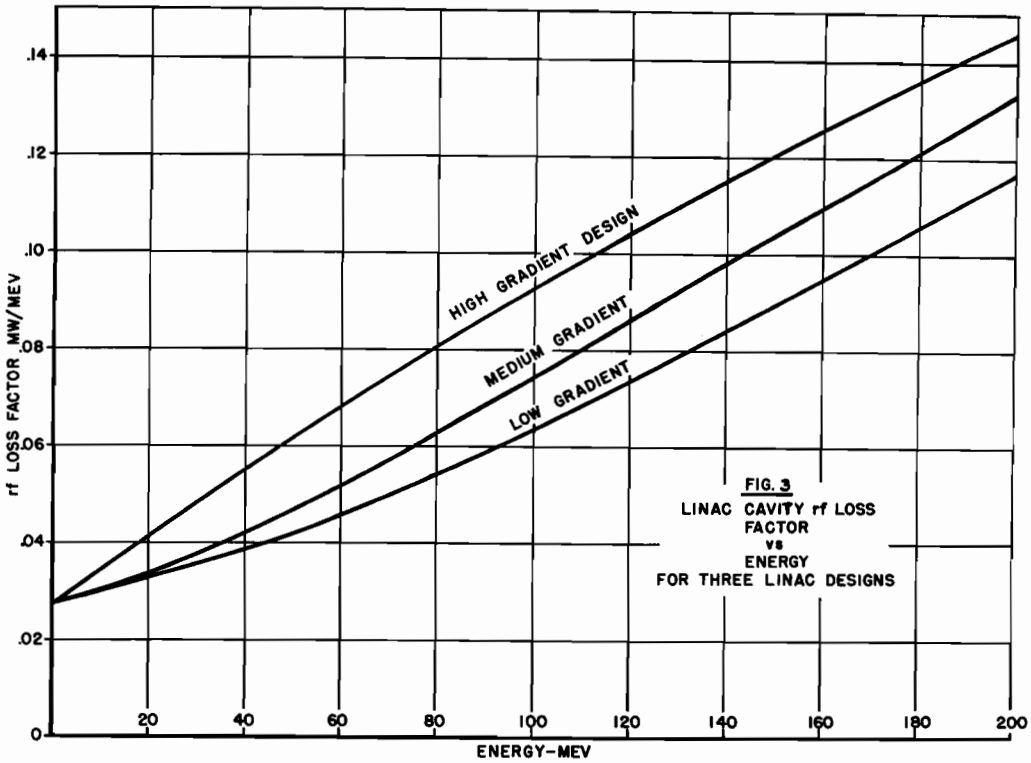

FIG. 3
LINAC CAVITY rf LOSS FACTOR vs ENERGY FOR THREE LINAC DESIGNS

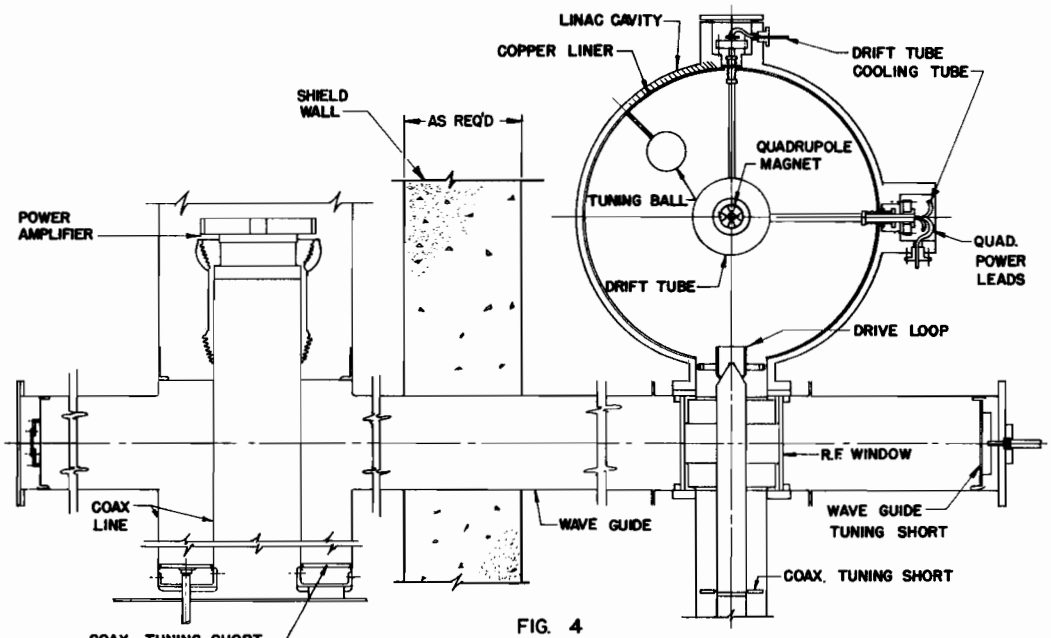

FIG. 4
CROSS SECTION OF LINAC CAVITY

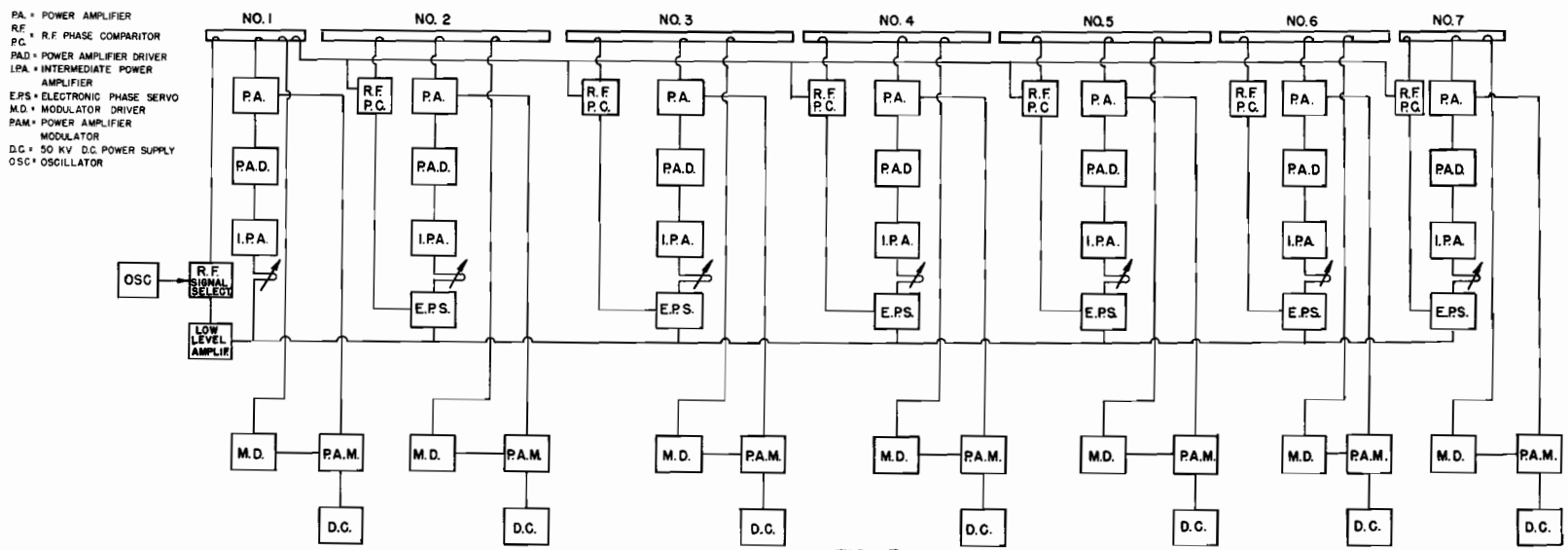

FIG. 5

BLOCK DIAGRAM OF THE R.F. SYSTEM FOR THE 200 MeV LINAC

Linac Parameters

Item	Value
Number of Cavities	7 - 8
Input Energy	750 keV
Final Energy	200 MeV
Input Current (protons)	150 mA
Output Current	100 mA
Transverse Phase Acceptance	17π cm-mr
Output Beam Emittance	4.6π cm-mr
Repetition Rate	5 per sec
Beam Pulse Length	400 - 500 μsec
RF Pulse Length	1000 μ sec
RF Duty Factor	0.5%
RF Losses in Cavities	17 MW
RF Power for Beam Acceleration	16 MW
Temperature Stability	$< \pm 0.25^{\circ}$ C

The linac will be comprised of seven[2] separate cavities, each powered by a single rf amplifier capable of at least 5 MW peak rf power. The parameters of each cavity will be so chosen as to give the most efficient division of rf power, P_n, between cavity losses and beam power at the design beam current, I. The incremental energy gain, ΔW_n, for the nth cavity when this condition is satisfied is given by

$$\Delta W_n = \frac{P_n}{L_n + I} \quad \text{(MeV)}$$

where $L_n \equiv$ average rf losses/MeV in the nth cavity.

The rf loss factor, L_n, is a function of drift tube and cavity geometry. For a given cell it increases with drift tube diameter. It also increases with energy since drift tube lengths must increase with energy. It is also proportional to the square of the mean rf gradient, E_o, in the cavity. Figure 3 shows the general behavior of this factor as a function of energy for three different 200 MeV linac designs computed by MURA personnel who are cooperating with ANL in the design of the linac.

The linac cavities will be much like the present 50 MeV cavity. A cross section through the cavity and drive line is shown in Fig. 4. RF power from a power amplifier is coupled via a coax transition into a rectangular wave guide. At the linac end of the wave guide, power is

coupled through a cylindrical ceramic window into a short coaxial line which is terminated by a coupling loop at the linac cavity. The loop penetration is adjustable, and irises in the wave guide, together with tuning shorts at the ends of both wave guide and coax lines, permit impedance matching.

Drift tubes will be of the cylindrical type, which MURA people have computed, because of the simplicity of this design and the resultant economy of fabrication. However, the drift tubes for the first cavity may be of the Christofilos type, used in the existing injector, because the computer program is not yet capable of giving reliable results below 20 MeV. A dc quadrupole magnet will be installed in each drift tube although they may not all be necessary at the high energy end.

The type of tuner has not been established although ball tuners similar to those in the existing linac are being considered. It is believed from our experience in setting up the field distribution in the 50 MeV linac that a tuner in each cell may be very desirable, and this is presently being planned. For slow servo tuning of an entire cavity, an eccentric bar running along the cavity wall offers an interesting possibility.

Each of the cavities of the linac must be driven at the same rf frequency, and each must have the proper phase and amplitude. Because of the relatively large beam loading expected and the variation of cavity shunt impedance with energy, amplitude control must be either preprogrammed or servo controlled. Phasing also will require fast servo control.

The rf system is shown in block diagram form in Fig. 5. Each of the amplifier chains will be identical in operational requirements, and each will be separately controllable. The following table lists the specific requirements of the system.

Performance Specifications for the 200 MeV Linac RF System

Item	Value
Operating Frequency	201.25 Mc/sec
Pulse Length, Variable to	700 - 1000 μsec
Pulse Repetition Rate, Variable to	0.5 - 5 per sec
RF Duty Factor	0.035% - 0.5%
Number of Power Amplifiers	7 - 8
Peak RF Power per Amplifer	5 MW
Total Peak RF Power	33 - 37 MW

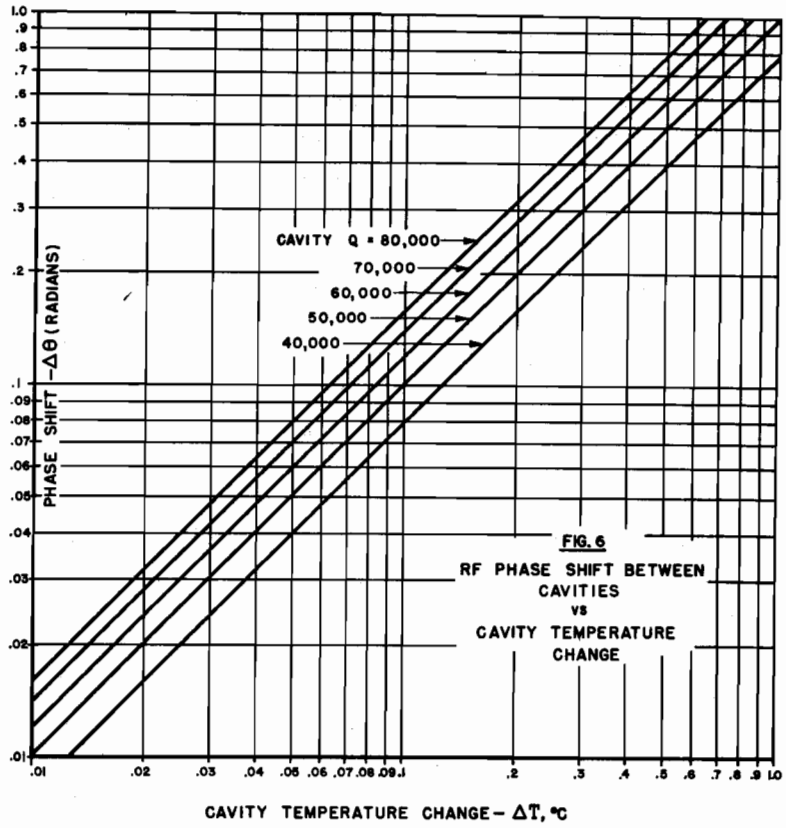

FIG. 6
RF PHASE SHIFT BETWEEN CAVITIES vs CAVITY TEMPERATURE CHANGE

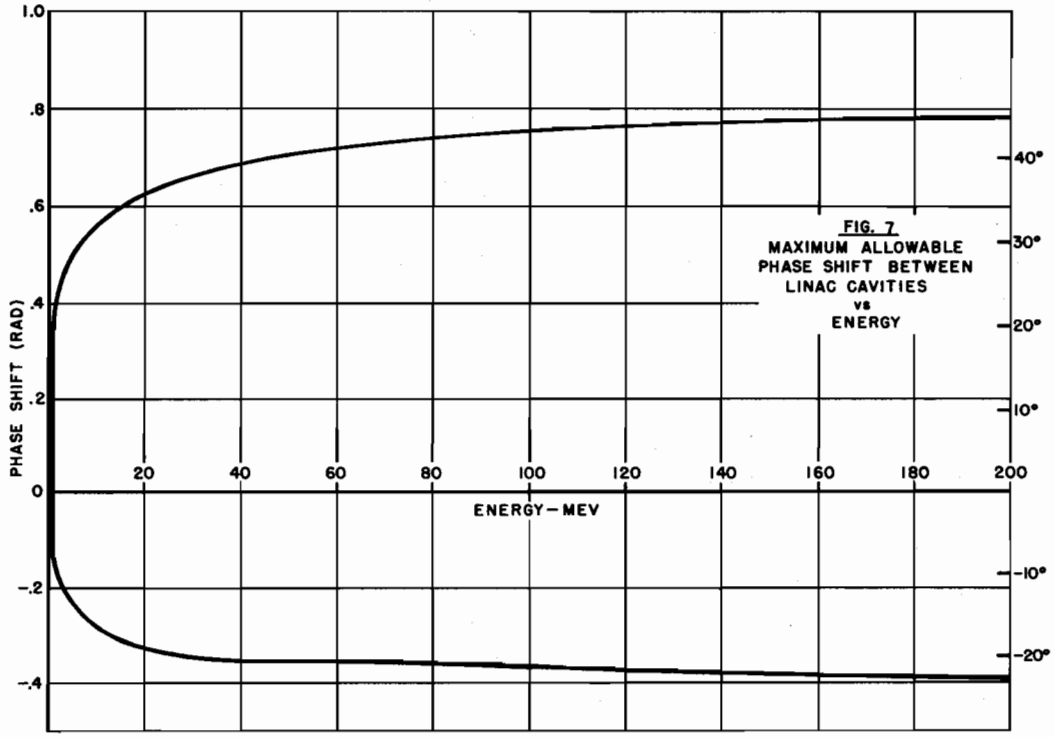

FIG. 7
MAXIMUM ALLOWABLE PHASE SHIFT BETWEEN LINAC CAVITIES vs ENERGY

The rf system, shown in Fig. 5, will consist of seven rf power amplifiers (PA's), one for each of the linac cavities. Each PA will use a single RCA 7835 super-power triode rated at 5 MW peak power and will be driven by an amplifier chain, capable of supplying approximately 160 kW peak drive power. The amplifier chains will be excited by a single low level oscillator-amplifier system so that all final amplifiers will be driven at a single frequency and at controllable relative phase, maintained by fast servo systems at the low level amplifier stages. This arrangement will permit independent testing of each of the rf amplifier systems and of the cavity it drives. It will also preclude interaction between one PA system and any other. Thus, from the standpoint of tune up and trouble diagnosis, this system will be most versatile. By eliminating interactions at the high power levels, it will be more reliable than with high level coupling.

A separate amplifier chain will drive the buncher and debuncher in order to avoid the effect of beam loading interactions on the amplitude and phase of these cavities.

It is proposed in the new system to use the same scheme that is presently in use on the 50 MeV linac in maintaining frequency stability; i.e., the rf system will be driven from an oscillator until the rf level in the linac cavity reaches approximately the accelerating gradient. At this time, a signal from No. 1 cavity will be gated on in place of the oscillator so that the No. 1 cavity will thereafter be driven at its resonant frequency. All other cavities would be driven at this same frequency, and all would, of course, require very good thermal stability in order to resonate at or near the same frequency, as $\frac{\Delta f}{f} = -\alpha \Delta T$, where α is the coefficient of thermal expansion for the cavity metal.

A further consequence of cavity temperature change is the phase shift resulting from driving a cavity at a frequency different from resonance. The magnitude of this phase shift is proportional to the Q of the cavity, i.e.,

$$\theta \simeq -2 Q \alpha \Delta T .$$

Figure 6 shows the magnitude of the phase shift as a function of temperature for a few values of Q.

Taking into account the phase damping that can be expected, one can set an upper limit to the magnitude of phase shift between cavities that can be tolerated without loss of particles. As the phase damping is proportional to $\beta^{-3/4}$ one finds that the maximum allowable phase shift varies with energy, as shown in Fig. 7.

This in conjunction with Fig. 6 indicates that cavity temperature stability must be good to $\pm 0.25^{\circ}$ C in order not to spill particles from the phase bucket in successive cavities. Considering energy spread and other factors, the thermal stability must be very much better than this.

The shape of the curves in Fig. 7 suggests that, since there is still considerable phase damping after the 10 MeV region, it would be desirable to design the first cavity of the linac for 20 MeV or even higher energy. In the ANL case, since we propose to use identical amplifier systems for each of the linac cavities, it will be advantageous to design the first cavity for 20 MeV or more in order to reserve more rf power for the remaining cavities. These are the two main reasons for designing the first cavity for 20 MeV rather than 10 MeV.

SYMON: I didn't see why this diagram that you have here really shows what the tolerance is on the phase shift. If you had one single phase shift that occurs, then I can see that this diagram is relevant, but if you suddenly jump the rf phase, then the packet moves over to where you have shown. If that situation lasts for on the order of a phase oscillation, you have smeared the packet around the boundary so that you no longer can tolerate another jump in phase. The packet is now equal to the full bucket size.

PERRY: Yes, what I showed on the curve was the maximum phase shift.

SYMON: Yes, but it would seem to me that what you are really interested in is a series of small phase errors from tank to tank, which occur at intervals that are short compared to a phase oscillation. Then I don't see that the diagram that you have drawn is relevant.

PERRY: In the case of which you are speaking, it is true, it is not relevant. I was looking only at the maximum phase shift allowable due to frequency shift or temperature change between the first and any successive cavity without loss of particles. This essentially places a maximum tolerance on frequency control or cavity temperature stability. The maximum allowable temperature variation of any cavity would be $\pm 0.25^{\circ}$C just to prevent particle spill, and in order to keep the phase spread, and thus the energy spread, to a minimum the temperature stability would have to be very much better than that.

REFERENCES

1. Expected Beam Intensities of the FFAG and ZGS Accelerators, Report to the Atomic Energy Commission of the Ad Hoc Committee, July 31, 1963.

2. Young, D. E. and Austin, B., "Design Study of 200 MeV Injector for ZGS," MURA Technical Note TN-469, April 7, 1964.

PRELIMINARY DESIGN OF A HIGH ENERGY HIGH DUTY CYCLE PROTON LINEAR ACCELERATOR

H. Leboutet, G. Guilbaud, Kervesic, Mangin, Tran
CSF - Compagnie Générale de Télégraphie Sans Fil - France

(Presented by G. Guilbaud)

One of the applications of proton linacs considered these days is the production of intense π meson beams. Roughly, this will be best achieved by use of protons of energies higher than 500 MeV. A high average current, of several hundred microamperes is desired, together with as high a duty cycle as possible.

The advantages of the linear accelerator for this application have been discussed at great length in many publications. The main one is extraction of the total beam current and the related absence of any induced radioactivity in the machine. Another is energy variation.

The Institut de Recherches Nucléaires of Strasbourg is planning to build such a meson factory and we have been attempting to evaluate the technical and financial implications of such a project. Work started about a year ago and this paper describes the present status of it.

Desired Performance

The performance we have been asked to take as an objective are the following: energy higher than 500 MeV, up to 800 MeV, average current: 200 μA, to be increased to 1 mA after some time of operation; duty cycle: 5%, this being essentially defined by the present state of the art for microwave tubes. These objectives are very similar to those of other projects and the following arguments are also the same. In short, the 200 Mc/s Alvarez structure cannot be used efficiently after some 150 or 200 MeV. One needs to look for other structures at higher frequencies, which implies a frequency jump at some point.

Our preliminary design has been guided by the following:

(a) Try and use a low voltage injector, to avoid pressurization.
(b) Limit the frequency jump to a minimum.
(c) Make the project as a whole as cheap as possible.

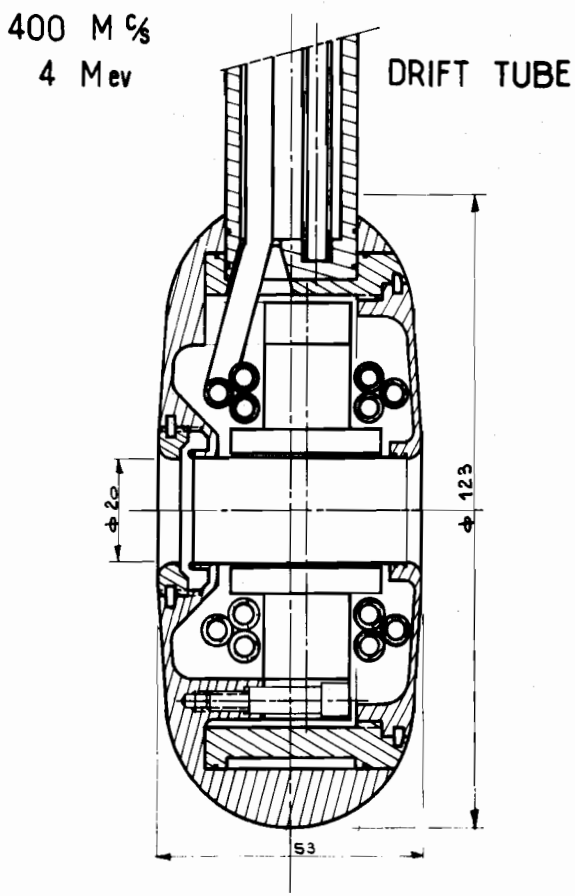

Fig. 1

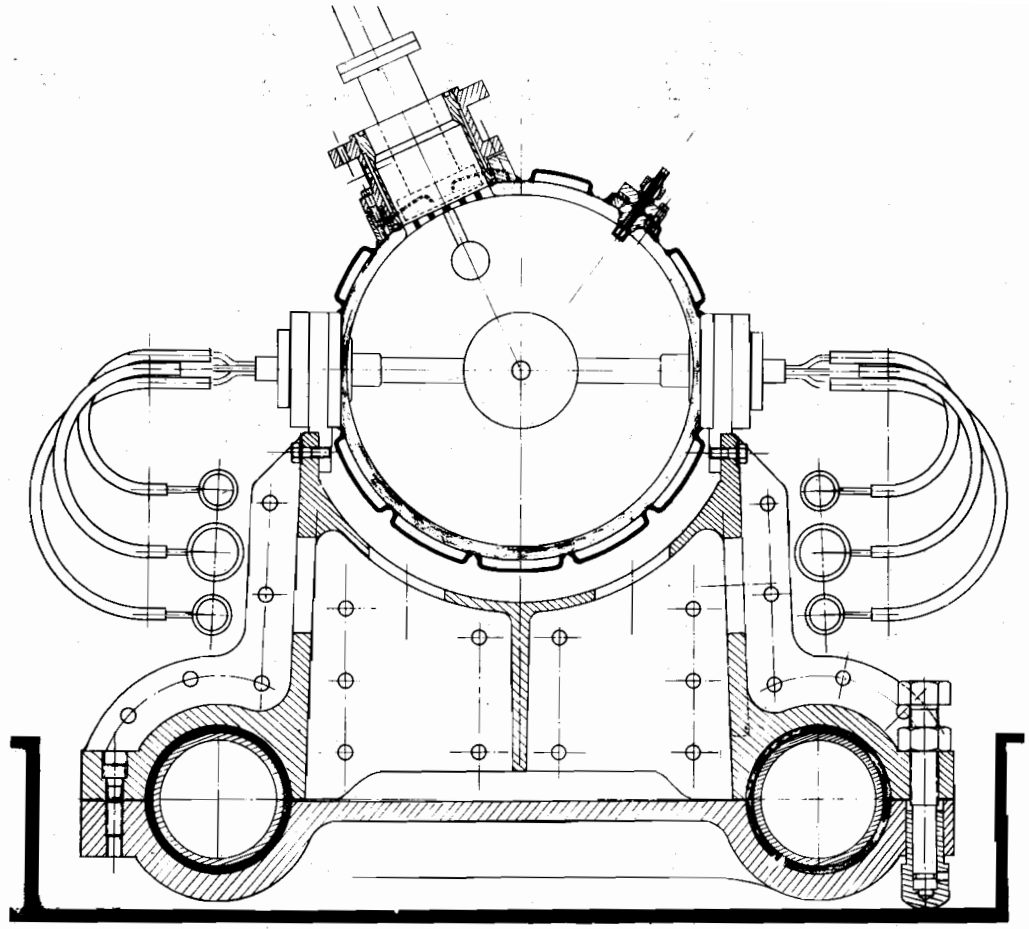

Fig. 2

Choice of the Accelerating Structures and Frequencies

A number of arguments make it desirable to operate at frequencies as high as possible at low energy: Shunt impedance is higher, the jump to the higher frequency will be smaller, and the filling time of cavities will be reduced, resulting in shorter pulses for the rf.

However, a number of practical reasons oppose this. The main one is the necessity to house, in the drift tubes, quadrupoles of a sufficient strength to compensate the rf defocusing effects.

Having looked into this with some detail, it appears that operation at 400 Mc/s at the low energy end of the machine is possible. Two possibilities have been considered.

(a) One is to inject 3 to 4 MeV protons. The general dimensions of the drift tube are then given by Fig. 1. The outer diameter is a little over 12 cm. The length is 5.3 cm. A model quadrupole is being built for magnetic testing. These figures, of course, are indicative. These lead to the general dimensions of the Alvarez structure, as shown on Fig. 2. It can be seen that the diameter of the cavity is of the order of 40 cm at most. The drift tube supports are shown here in alternate horizontal positions. This may not be final. One must position all parts so as to have enough perimeter for the water cooling which will have to be very efficient since dissipation will be of the order of 10 kW/m.

Models of 400 Mc/s Alvarez are being tested for shunt impedance requirements.

From the technological point of view, we are investigating the possibility of using an electrolytic copper tubing, supplied by a European firm who claims very good conductivity. The water pipes could be provided in the thickness of the copper, and the design of Fig. 2 could be greatly simplified.

Figure 3 shows the general structure of a tank and its support. The electrolytic tubing comes in 8 m lengths and, of course, tolerances being those of the mandril, a very precise tank can be obtained, avoiding the use of correcting bars.

(b) Another possibility is to operate on the $2\beta\lambda$ mode, at reduced rf electric field. At 500 kV/m, one is led to inject 750 kV protons into a 400 Mc/s Alvarez structure. These values correspond to the same quadrupole strength and drift tube size as before, so that Figs. 1, 2, and 3 give approximately the dimensions of a first cavity which could be used

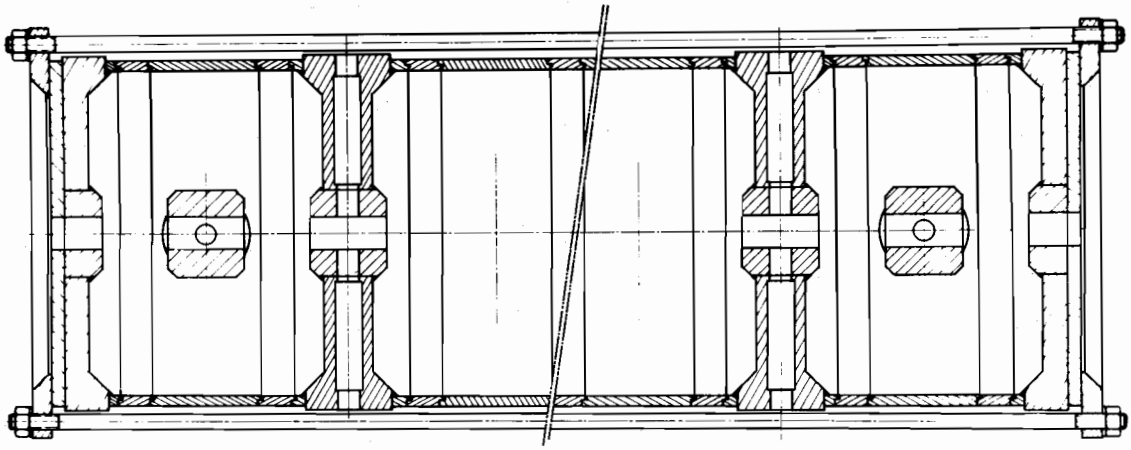

Fig. 3 400 Mc/s CROSS BAR EXPERIMENTAL MODEL

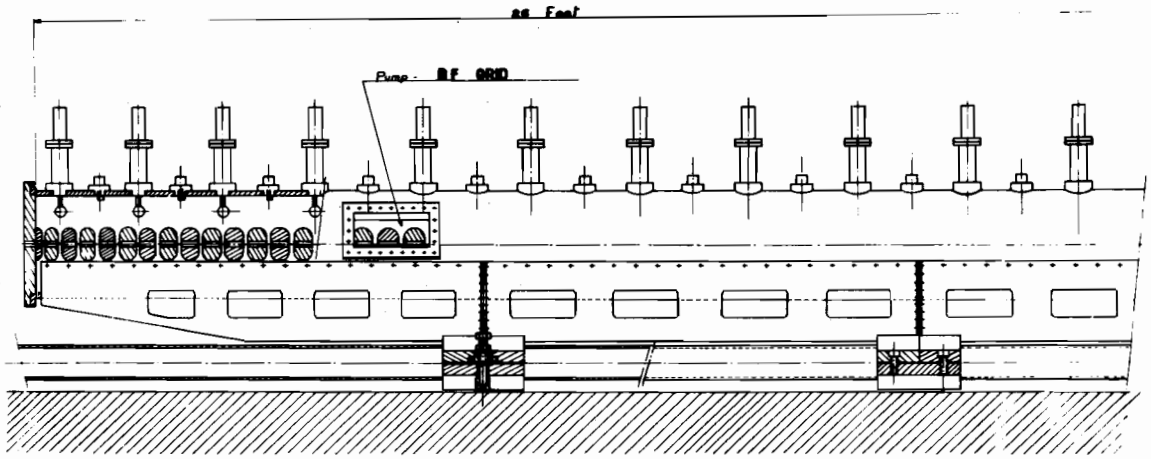

Fig. 4 400 Mc/s ALVAREZ CAVITY

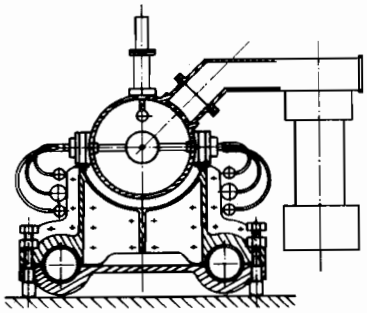

to take the protons from 0.750 to 4 MeV, where they would enter an ordinary $\beta\lambda$ Alvarez structure at 1.8 to 2 MV/m.

This low injection voltage is very attractive. Of course, it involves taking some precautions. The main one is to reduce the drift tube inner hole diameter, to limit transverse field variation effects. According to $\frac{2\pi A}{\gamma^2\beta\lambda} \leq 1$, the hole should not exceed 1 cm in diameter. Since the peak current will be of the order of 10 A, this should not be a difficulty.

The 400 Mc/s Alvarez structure should be used for the first 100 MeV. After this, a number of other structures might prove useful, and we are presently investigating two main types.

(a) The first is the general class of bar structures. A model is presently being built according to the drawing of Fig. 4. The model will allow making measurements on X bar structure, on the interdigital structure, by suppressing half bars, and a number of intermediate ones, by varying the angle from one cell to the next. Measurement may be underway presently and results are expected in September or October.

(b) The second class is that of iris loaded structures. Our electron linear accelerator work has been done with the $\pi/2$ disc-loaded circular waveguide. Since a passband may be desirable here, variations of this guide should be used. We are investigating the one that was previously examined for backward wave oscillations at CSF; we call it the diabolo line. The discs are cut by two very wide slots, about 120° wide, and the remaining sectors are not aligned from one cell to the next, but at an angle, which gives wide band characteristics. This circuit is about half way between the cross bar and the disc-loaded waveguide. Measurements made last fall with very low values of β are now extended to the region of β_s corresponding to 100 MeV. Such structures should be used after some 100 or 200 MeV, at an 800 or 1200 Mc/s frequency. The choice of the step energy will depend very much on the results of shunt impedance measurement. In any event, after 100 MeV, focusing can be made by magnetic doublets or triplets between short sections, of 4 to 5 m, so that the structure can be chosen without taking in account any focusing inside it.

Before turning to the general design of the machine, we should like to point out that beam-loading effects will bear heavily on the choice of the accelerating structure. We have just started an analysis of these, to understand them and determine their amplitude and ways of correcting them. It is our feeling that resonant π modes should be avoided because they lead to very large field amplitude variations and also to very large phase shifts along the structure, causing great difficulty during the beam-loading

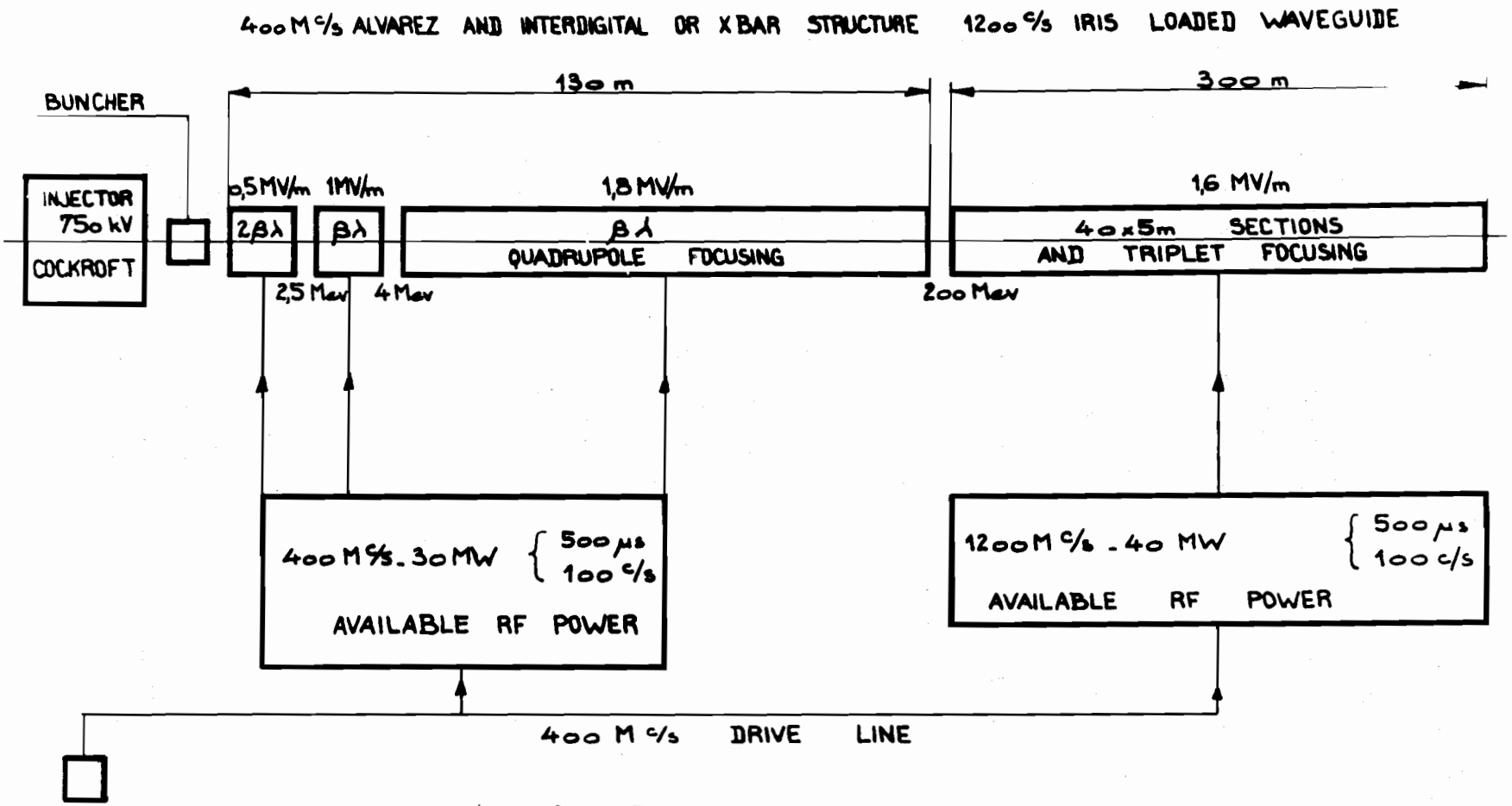
400 M c/s ALVAREZ AND INTERDIGITAL OR X BAR STRUCTURE
1200 c/s IRIS LOADED WAVEGUIDE
130 m
300 m
BUNCHER
INJECTOR
750 kV
COCKROFT
0,5 MV/m
1 MV/m
1,8 MV/m
1,6 MV/m
2βλ
βλ
βλ
QUADRUPOLE FOCUSING
40 x 5m SECTIONS
AND TRIPLET FOCUSING
2,5 Mev
4 Mev
200 Mev
400 M c/s . 30 MW
500 μs
100 c/s
AVAILABLE RF POWER
1200 M c/s . 40 MW
500 μs
100 c/s
AVAILABLE RF POWER
400 M c/s DRIVE LINE

Fig. 5

transients. We would greatly favor the use of short travelling wave sections, where these effects will remain very small, at the cost of some complication in the use of residual power at the end of the sections. This subject will be studied in the next year; it may prove to be the most important criterion in the choice of the design.

General Design

As can be understood from above, we have not yet determined our exact choice for the circuit to be used at high energies. However, if we assume that the effective shunt impedance will average to 25 M Ω /m along the machine, one can fairly well determine its composition, including length, rf power, and later, the cost.

Figure 5 shows our present design, for the following performances:

500 MeV
4 ma peak accelerated current
5% duty cycle

Since the filling time at 400 Mc/s will be some 50 to 70 μs, 500 μs beam pulses can be used, which is very good for the higher frequency power tube.

First, we use a 750 kV Cockcroft, capable of 20 ma at 5% duty cycle. It is followed by a buncher, including beam transfer lenses. Next comes a 2 $\beta\lambda$-400 Mc/s – 0.5 MV/m cavity, either up to 4 MeV, or only to 2.5 MeV. In the latter case, a short section on the $\beta\lambda$ mode but at reduced electric field takes the protons from 2.5 to 4 MeV. After that, we have assumed that 400 Mc/s structures are used up to 200 MeV and 1200 Mc/s structures afterwards. The step energy is not determined. We have taken it to be 200 MeV here. The rf power has been estimated on the basis of an average shunt impedance of 25 M Ω /m and available evaluation of beam-loading effects. The length and rf power have been chosen by economical arguments: the product of rf losses and accelerator length is a constant, and consequently cost goes up with length for the waveguide and building and goes down with length for the rf power. The result is shown on Fig. 5. The breakdown of this over-all design in units has not been determined yet. At 400 Mc/s and up, good klystrons can be made, and some U. S. firms are already producing them. Units of 300 kW to 5 MW would lead to the lowest cost. However, these would feed about 20 m of accelerating structure each, and, according to what is known of beam-loading effects, this power would then have to broken down to feed several shorter sections. In that respect, the rf pool idea proposed by Berkeley is a very attractive solution.

Summary

As can be seen, the past year has been used to determine the main problems to be solved for the construction of such a machine and to lay the general design. The year to come will be used essentially to measure new structures and choose which one offers the best compromise at each energy, to get a good understanding of beam-loading effects, and to make as close a cost evaluation as possible, by going into detailed mechanical and electrical design.

HUBBARD: With respect to your drawing on the board, do you think there is any advantage in skewing the angles at other than 90°?

GUILBAUD: Well, I think varying this angle will give you different pass bands and we will have to play with that.

HUBBARD: You do not have any obvious advantage in mind then?

GUILBAUD: This line was done at a time when we were working on wide-band tubes and were looking for wide pass bands and certain slopes for tuning of oscillators. Measurements made last fall do not show any great dependence of shunt impedance on this angle, but only of pass band, which may be of definite interest.

PROGRESS REPORT ON THE STANFORD LINEAR ACCELERATOR CENTER*

G. A. Loew
Stanford Linear Accelerator Center

A. Introduction

This report describes some of the highlights of the present state of construction of the Stanford 20 GeV Linear Accelerator. Comprehensive descriptions, statistics and specifications of the two-mile linear electron accelerator have been given on numerous other occasions[1] and will not be included here. By the nature of progress in our construction schedule, hopefully a substantial fraction of the information and pictures given in this report will soon become obsolete.

B. Building Construction

Figure 1 shows a cross section of the accelerator layout. Two buildings are seen. The lower one, underground, called the accelerator housing, contains the accelerator structure proper, supported by a 24-inch aluminum girder which also provides the optical alignment vacuum pipe to be used to align the two-mile machine. Three jacks are used to adjust the position of each 40-foot girder in the transverse plane. The upper building, called the klystron gallery, is separated from the accelerator housing by 25 feet of earth shielding. The gallery contains all the equipment necessary to power the accelerator and includes the klystrons, their associated microwave equipment, the modulators, vacuum equipment, utilities and over-all instrumentation. In Stage I of the construction program, there will be 240 klystrons with their individual modulators, each feeding four 10-foot long accelerator sections. The vertical tube connecting the two buildings, shown in the picture, is one of the waveguide runs which feeds two accelerator sections. Extra modulators in the gallery are shown to illustrate the configuration foreseen for Stage II when there will be one klystron per accelerator section, hence 960 klystrons and modulators. Plans for this expansion are not firm at this date.

Initial excavations on the SLAC site for the housing started in December, 1962. The construction of the accelerator housing began in June, 1963. Figure 2 shows the concrete slab and the beginning of the

---

*Work supported by the U. S. Atomic Energy Commission.

accelerator housing construction. Figure 3 shows the same building after completion of the concrete housing, on July 3, 1964. The first parts of the water-cooling system installation can be seen. The Klystron Gallery construction was started in November, 1963 and Fig. 4 illustrates the first few hundred feet of construction of that building. Figure 5 shows the inside of the klystron gallery with some installed utilities as well as the klystron supporting frame structure.

C. Accelerator Structure

Figure 6 illustrates some of the slow-wave structures investigated three or four years ago to optimize the accelerator structure of the two-mile machine in terms of shunt impedance, pumping speed and ease of construction. This figure is included here only because of the renewed interest in more complex accelerator structures for high energy proton accelerators, such as the cross-bar structure, the slotted-disk structure and the cloverleaf structure. It should be restated here that for a phase velocity equal to the velocity of light, the highest shunt impedance was obtained with the simple disk-loaded structure operating in the $\frac{2\pi}{3}$ mode. Although a higher vacuum pumping speed could be obtained with the so-called ventilated structure, it was not adopted because of the difficulties in maintaining tolerances on the ventilating holes.

The specific design of the disk-loaded waveguide accelerator structure has been described in detail elsewhere.[2] The accelerator sections using the constant-gradient design are presently under fabrication at SLAC at the rate of about two sections per day. Figure 7 shows the layout of the waveguide circuitry, from the 24 MW klystron through a window, a vacuum pumpout, a waveguide valve, a 3-db coupler, the waveguide feeds, two additional couplers, the input to the accelerator sections, the accelerator sections themselves and the output loads. The configuration of the waveguide as it is shown in the lower part of this figure has recently been modified because the need was found to feed the accelerator sections alternately from right and left. This alternation, called "operation flip flop", was found necessary because it was not possible to cancel entirely the asymmetry in the longitudinal electric field present in the first and last cavities of each section. Microwave measurements showed that both an amplitude asymmetry in the field as well as a phase shift of this field exist across the cavity in the transverse plane. Since the net effect of this residual amplitude and phase asymmetry is to create a transverse force on the electron beam, it was believed safer to alternate coupler inputs. The final result of "operation flip flop" was the building of sections such as the one shown in Fig. 8 with input and output couplers on the same side. However, the mode of coupling into successive sections is to follow

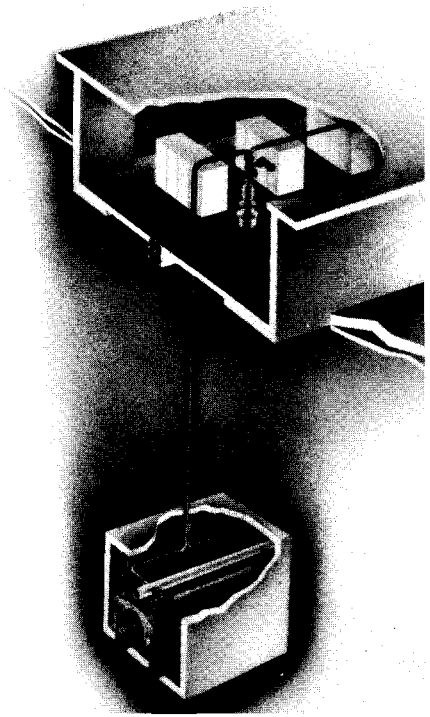

Fig. 1 Cross-sectional layout of klystron gallery (top) and accelerator housing (bottom).

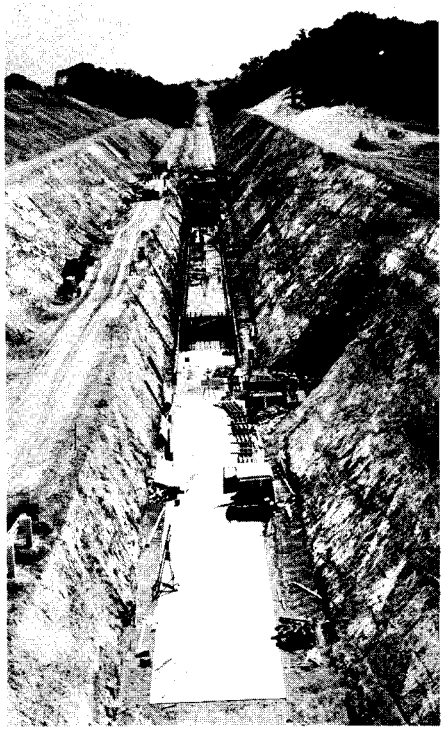

Fig. 2 Beginning of accelerator housing construction.

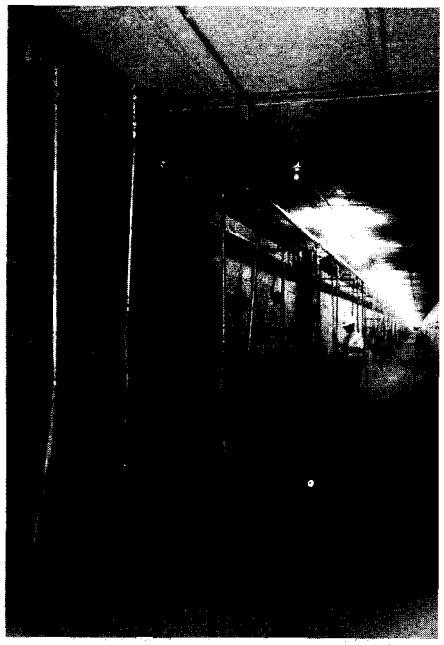

Fig. 3 Inside of accelerator housing shortly after completion.

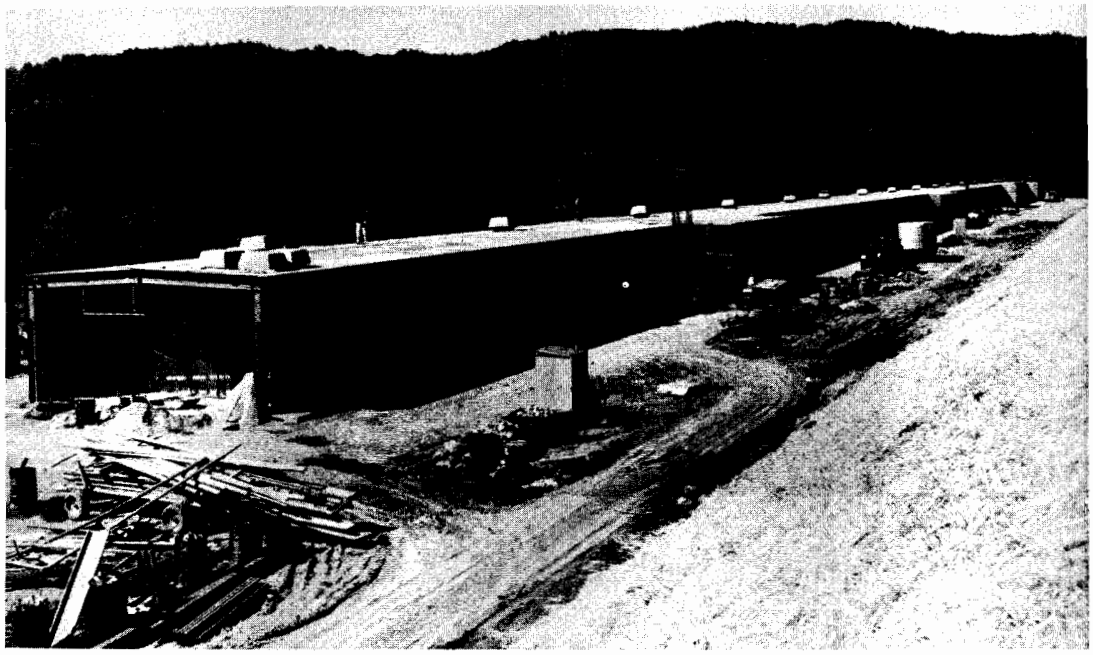

Fig. 4 Beginning of klystron gallery construction.

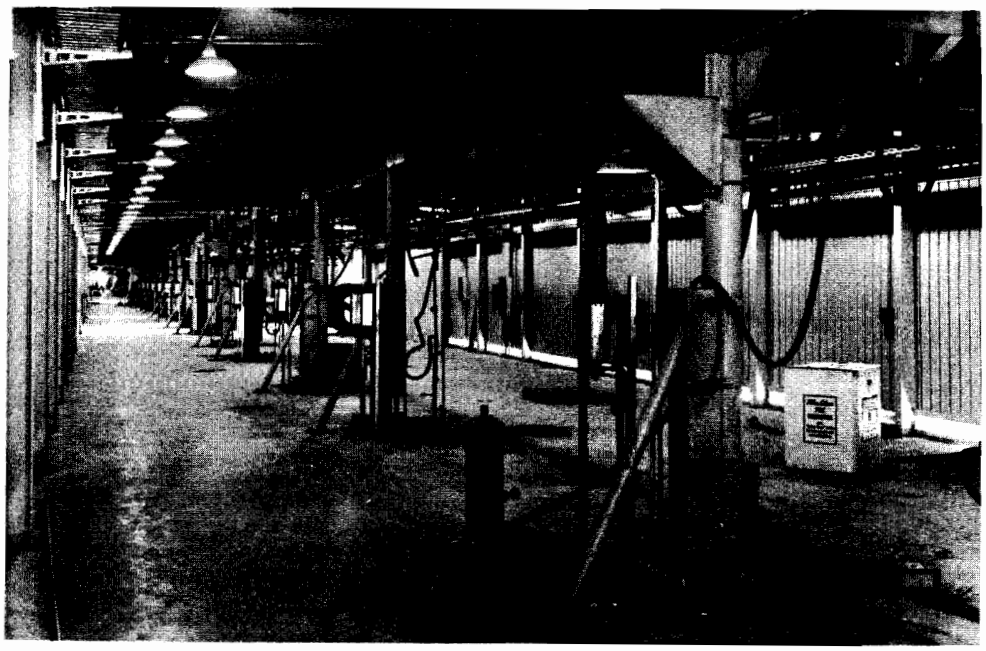

Fig. 5 Inside of first sector of klystron gallery showing utilities and klystron frame supporting structures.

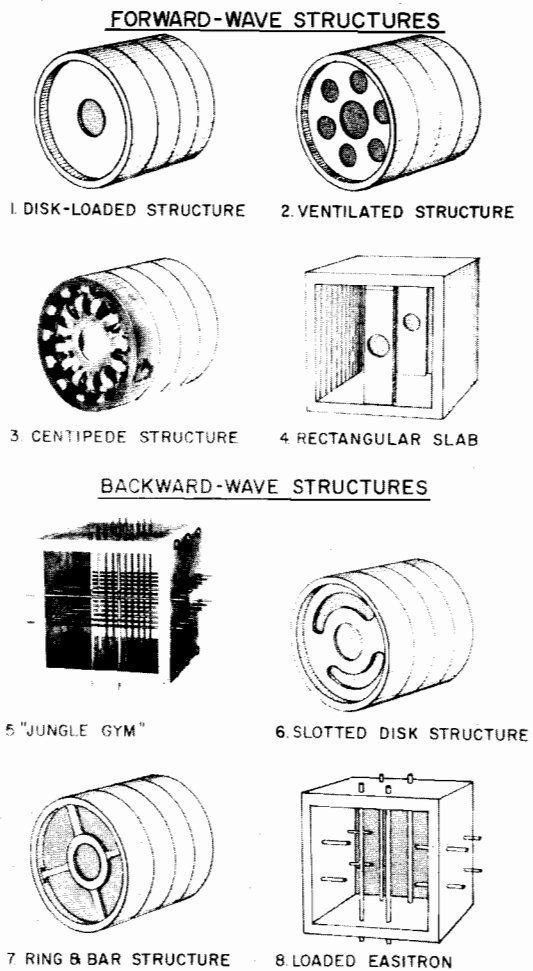

Fig. 6 Museum of forward- and backward-wave structures originally examined for use in the SLAC accelerator for $v_p = c$.

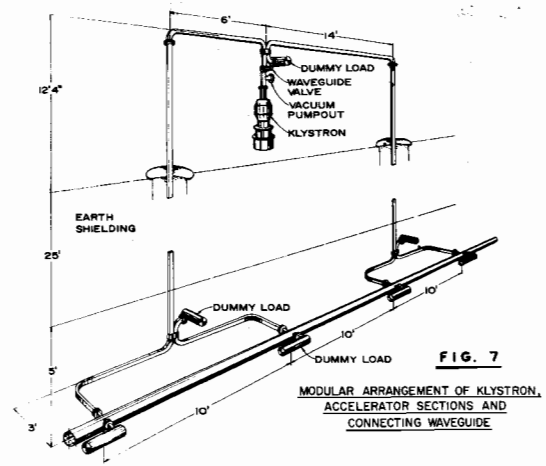

FIG. 7

MODULAR ARRANGEMENT OF KLYSTRON, ACCELERATOR SECTIONS AND CONNECTING WAVEGUIDE

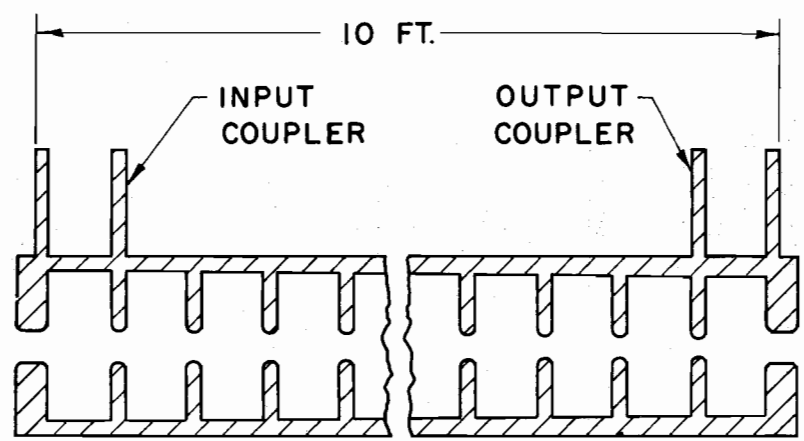

Fig. 8 Constant-gradient accelerator section.

the pattern right-left-right-left, followed by left-right-left-right. This is accomplished by rotating successive sections by 180 degrees. By this method, transverse deflections should cancel out. Over an 80-foot length, then, the beam should be back on axis and parallel to it without any increase in transverse phase space.

D. Drive and Phasing Systems

Figure 9 illustrates the microwave drive system from the master oscillator to the high-power klystrons. One main booster amplifier at 476 Mc/sec fed by a master oscillator powers the entire two-mile length of the drive system by means of a 3-1/8" coaxial line. Each of the 30 sectors into which the machine is divided obtains its rf power from a coupler in the main drive line. The frequency of the rf power is then multiplied by 6 by means of a varactor multiplier. The resulting 2856 Mc/sec rf power is then amplified by means of a sub-booster klystron to 60 kW of pulsed output power. Another coaxial line (1-5/8" diameter) feeds this rf power to each of the eight klystrons in a sector. The phase and amplitude of this signal is controlled by means of an isolator, a phase shifter, and an attenuator. A special protection attenuator is incorporated which automatically removes the rf drive power to the 24-MW klystron every time a major gas burst or modulator failure temporarily disables the klystron. The protection attenuator subsequently slowly restores this drive power to its former level, thereby preventing full output rf power from striking the klystron window instantaneously. As has been reported earlier, this procedure should prevent the frequency fractures and punctures of windows experienced in the Stanford Mark III accelerator.

Figure 10 illustrates the principle upon which the operation of the automatic phasing system for klystrons is based. It is known that when a klystron is correctly phased, the phase of the klystron output signal in the accelerator, E_W, is 180 degrees out of phase with the signal induced by the electron beam, E_e. Hence, maximum energy transfer is obtained from the klystron output wave to the electron beam, resulting in the resultant vector, E_R. On the other hand, if E_e is not 180 degrees out of phase with E_W, less than the maximum energy transfer takes place and one obtains a rotated resultant vector E_R as shown in the lower part of Fig. 10. This principle is used as follows. The klystron pulse is momentarily delayed in time, thereby allowing E_e to be compared in phase with a reference signal obtained from the drive line. A so-called "calibrating" phase shifter is used to null the output of a phase bridge under this condition. E_W is then compared with the reference signal and caused to be 180 degrees out of phase with E_e by means of the same phase bridge. This bridge consists of a magic T and is followed by a

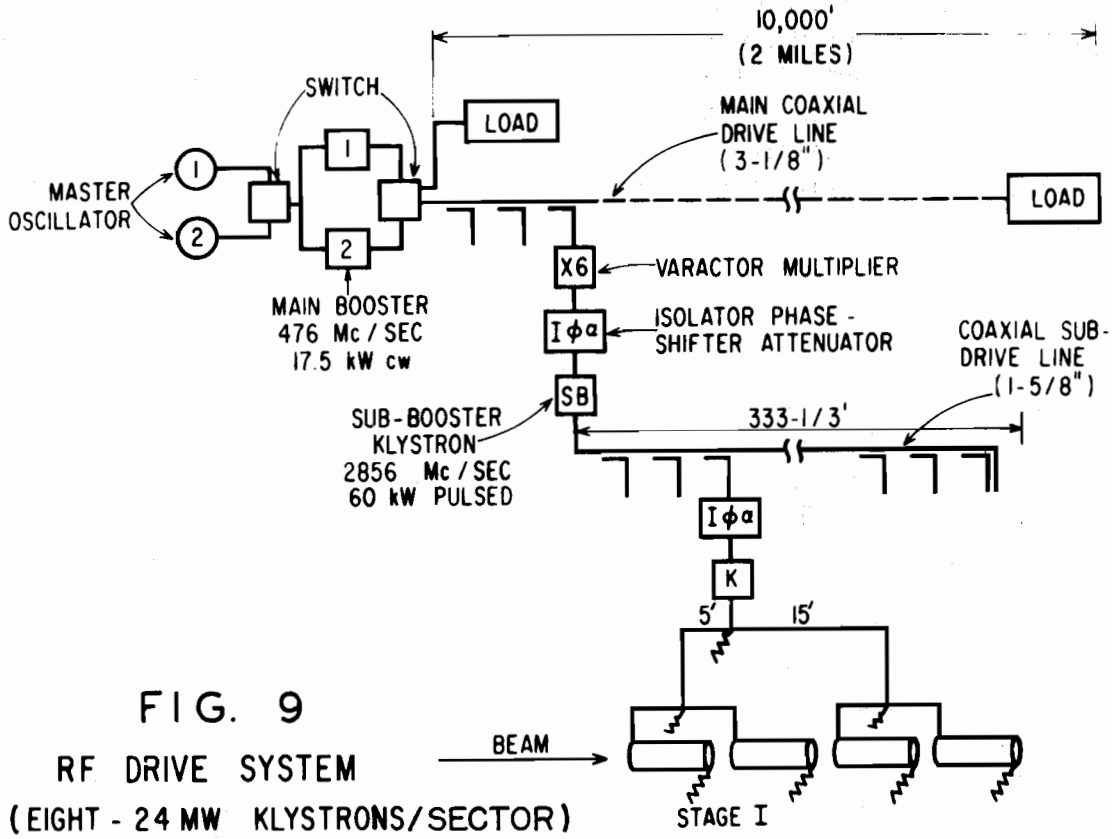

FIG. 9

RF DRIVE SYSTEM

(EIGHT - 24 MW KLYSTRONS/SECTOR)

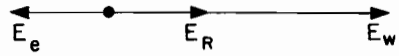

ORIENTATION OF FIELD VECTORS
WHEN PHASING IS CORRECT

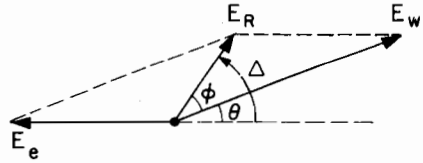

ORIENTATION OF FIELD VECTORS
WHEN PHASING IS INCORRECT

Fig. 10 Principle of automatic phasing system for klystrons using beam induction technique.

pair of linear thermionic diodes, a gated voltmeter, a phase wobbler and two servo amplifiers. These feed into the two windings of an ac motor which controls the rotation of the klystron phase shifter until a null is obtained. An automatic programmer causes all klystrons in a sector to be sequentially and automatically phased according to this technique. The operation should take no longer than one minute per sector.

E. Injection System

Figure 11 shows the main elements of the electron beam injection system to be used at the input to the accelerator. Briefly, this system will consist of a gridded gun, a prebuncher fed with approximately 1 kW of peak rf power and followed by a drift space, a constant velocity buncher (v_p = 0.75 c) and finally a standard accelerator section (v_p = c). The bunching process which results from this setup is illustrated in the lower part of the figure. An experimental injection system is presently being tested at SLAC and the various parameters including rf power levels, gun modulator settings, and magnetic focusing currents are being studied. It has been found by means of an rf deflector used as a bunch analyzer illustrated in Fig. 12 that 5 degree bunches can be obtained with this system. The structure used for the rf deflector is the same as that proposed for rf separators.[3] By varying the setting of the calibrated variable phase shifter which controls the phase to the input of the deflector, it is possible to study the charge density inside the electron bunch.

F. Beam Guidance

At the end of every sector, i.e. at 30 points along the machine, there will be a special drift space containing special devices to locate and to guide the electron beam. This drift space will include a set of quadrupole triplets, a set of two steering dipoles, a set of beam position monitors, a toroid to measure beam current, an insertable beam profile monitor, a beam scraper to protect the accelerator and to localize the radiation, and two vacuum valves enabling the operator to isolate one sector from the next. The principle of the microwave beam position monitors is illustrated in Fig. 13. The pickup cavity which is shown here as a structure similar to the beam deflector structure shown in Fig. 12, will, in fact, consist simply of a single cavity operating in the TM_{120} mode. Two such cavities will be used, one for x and the other for y position. Depending on whether the beam is up or down, left or right, the phase of the rf induced signal will flip by 180 degrees. This induced signal will be compared with a phase reference signal induced in a third cavity and compared by means of a magic T and two linear detector diodes. The information obtained from each of these drift spaces

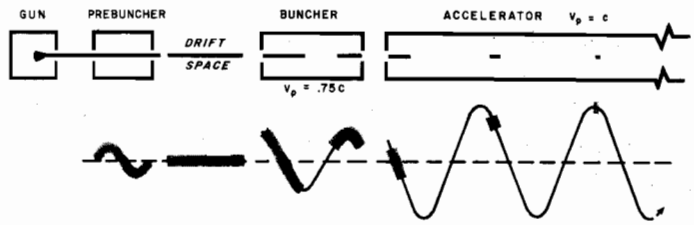

Fig. 11 Progressive bunching of electron beam.

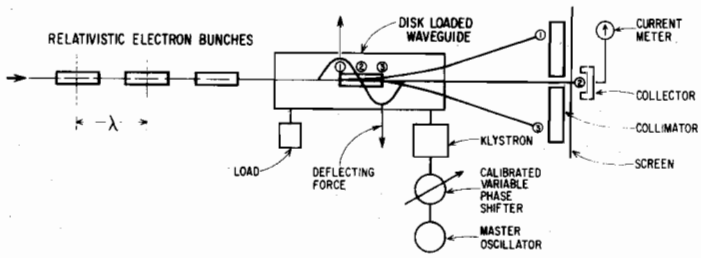

FIG. 12 DEFLECTOR-BUNCH ANALYZER

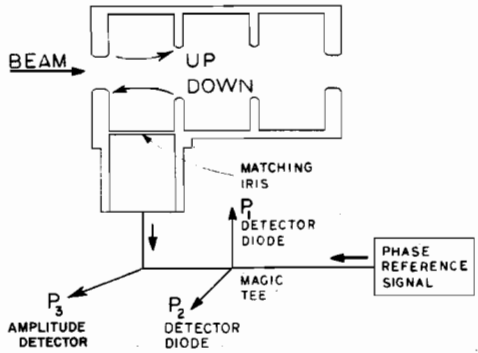

Fig. 13 Beam position monitor using TM_{11} mode structure and magic tee for phase comparison. For example, a maximum for P_1 indicates that the beam is up, a maximum for P_2 that the beam is down. The amplitude of P_3 indicates the distance from the axis.

will be sent to the Central Control Building by means of a base-band telemetry system and an FM system. There this information will be displayed on a set of oscilloscopes, allowing the operator to take corrective action by means of the remotely controllable steering dipoles and quadrupoles.

G. Support and Alignment

Figure 14 shows an expanded view of the support and alignment system. The three jacks which control the position of the beginning of each 40-foot support girder, are shown together with the accelerator tube and a retractable Fresnel lens mounted inside the girder. This Fresnel lens is part of the optical alignment system which will consist of three basic elements: (1) a laser mounted at the injector end of the accelerator, (2) 300 of these retractable lenses consisting of square copper and nickel plated targets perforated with an appropriate Fresnel pattern, and (3) at the end of the accelerator, a light intensity scanner and detector to determine the position of the image center. By determining the coordinates of successive spot centers formed by inserting successive lenses in the light path, it will be possible to measure the misalignment of each lens and hence of each corresponding girder. Corrective action can be taken accordingly. Because the focal length of the Fresnel lenses must change as a function of their position along the two-mile length, the hole pattern must change gradually from lens to lens. A special computer program has been used to determine the pattern pertaining to each lens position and a punched tape has been derived to control the ruling machine used to fabricate each target. Experiments with sample targets have already been conducted in an abandoned railway tunnel, not far from San Francisco, and it has been shown that over a 1,000-foot distance, displacements of a target of the order of 0.001 inch can be resolved.

H. Beam Switchyard

Figure 15 shows the layout of the array of magnets following the two-mile length of the machine which will be capable of switching the beam into the various experimental areas such as End Station A (for electron scattering experiments), and End Station B (for secondary beams, bubble chambers, etc.). A straight ahead beam is also provided. Before entering the beam switchyard, the beam will be steered onto and through an adjustable collimator. Electron energy of the deflected beams is measured in the switchyard by means of several momentum spectrometers.

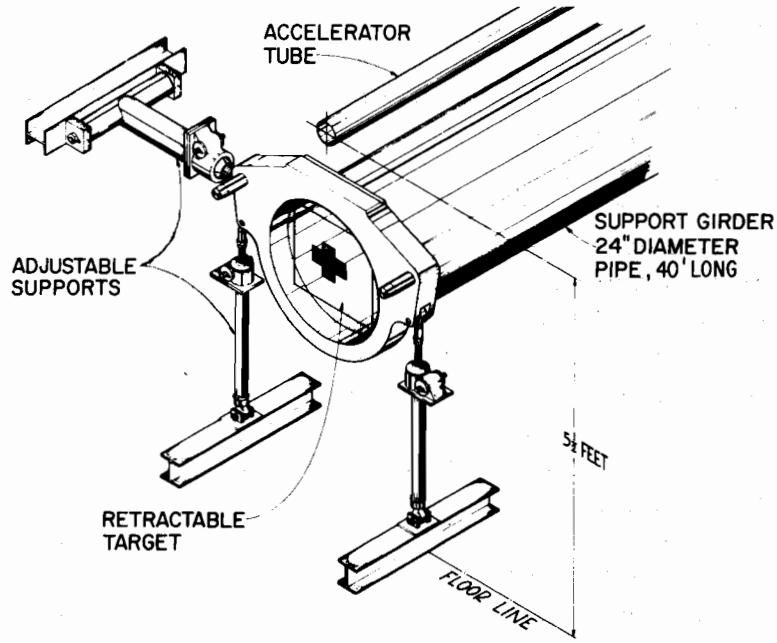

FIG. 14 SUPPORT AND ALIGNMENT SYSTEM

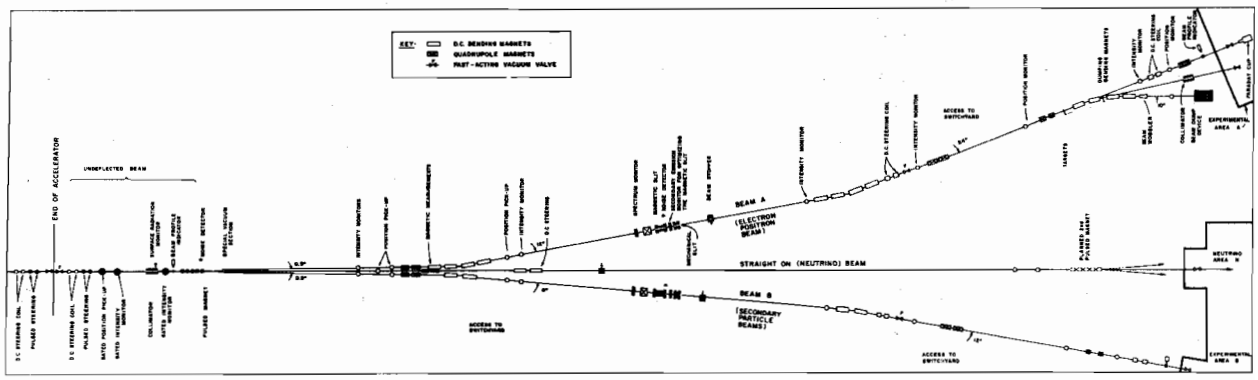

Fig. 15 Beam switchyard layout.

I. Instrumentation and Control

All essential instrumentation and control information will be available at the Central Control Building to be constructed close to the end of the machine. Several systems are being engineered and procured to permit monitoring and control of the accelerator, the switchyard, and some of the essential beam parameters in the experimental areas. These instrumentation and control systems include an "on-off" type status monitoring system based on the time-sharing multiplexing principle, an analog system to transmit information concerning certain analog signals available at each sector, a base-band telemetry system to transmit beam position and intensity information, a more accurate FM system to transmit accurate electron beam charge information and a remote control system consisting of a relay tree enabling the central control operator to actuate a number of devices along the machine, such as trigger delays, steering and quadrupole currents, gain controls, automatic phasing, etc. Because of the complexity of this instrumentation and control system and the difficulties foreseen in operating the accelerator with interlaced beams of different energies accelerated by different complements of klystrons on a pulse-to-pulse basis, it is now being contemplated to acquire at least one small computer to take over some of the control functions and many of the data logging functions which a human operator would not be able to perform. The first computer will be used to set up the magnet currents required in the beam switchyard for beams of specific energies. The next step may be to design a computer system capable of automatically controlling the beam guidance system along the two-mile length. Studies of these computer systems are presently beginning and will develop further in the near future.

J. Conclusion

While it outlines some of the highlights of the present construction status at SLAC, this report is by no means complete and several systems such as the modulators, the vacuum system, the cooling-water system, the variable voltage substations, and others have not even been touched upon. It is believed that the information on these systems can either be found in other SLAC reports or will be forthcoming at future conferences.

YOUNG: Can you tell us briefly what the situation is concerning klystron procurement and delivery.

LOEW: We are making klystrons at Stanford. In addition, we have two contracts, one with RCA and one with Sperry. We are now receiving tubes

from these suppliers which are meeting the specifications. To protect the project we have just signed two more study contracts, one with Eimac and one with Litton. These companies will make something like six tubes each in the next year with an incentive plan so that they will receive more for each additional megawatt output.

REFERENCES

1. W. K. H. Panofsky, et al., "Linear Electron Accelerator Progress at Stanford University", Proceedings of 1961 International Conference On High Energy Accelerators, Brookhaven; pp. 79-118; and W. K. H. Panofsky, "Progress Report on the Stanford Two-Mile Linear Accelerator", Proceedings of 1963 International Conference On High Energy Accelerators, Dubna; pp. 407-418.

2. A. L. Eldredge, G. A. Loew, and R. B. Neal, "Design and Fabrication of the Accelerating Structure for the Stanford Two-Mile Accelerator", SLAC Report No. 7, Stanford Linear Accelerator Center, Stanford University, Stanford California (November 1962).

3. O. A. Altenmueller, R. R. Larsen, and G. A. Loew, "Investitagions of Traveling Wave Separators for the Stanford Two-Mile Accelerator", SLAC Report No. 17, Stanford Linear Accelerator Center, Stanford University, Stanford, California (August 1963).

A GREEN'S FUNCTION APPROACH TO THE CALCULATION OF DRIFT TUBE CAVITIES*

M. Rich and W. M. Visscher
University of California, Los Alamos Scientific Laboratory
Los Alamos, New Mexico

I. Introduction

We report here on a calculation similar in spirit and method to that of Gluckstern[1] with some simplification and some generalization. Briefly, our method is to first use the symmetries of the drift tube calculation problem to reduce Maxwell's equations to a single one, which we solve by use of a cylindrical Green's function.[2] The Green's function gives directly and exactly the fields inside a cylindrical conductor for a prescribed dipole disc (or tube) source with sinusoidal time dependence of arbitrary frequency. By integrating this Green's function over a source distribution, we can in principle (and, with enough patience, in practice) obtain an exact solution for the fields due to an arbitrary internal current distribution. We have chosen a particular form for the internal current distribution, with which we hope to be able to mock up a variety of drift tube shapes.

Given a current distribution, the fields can be obtained exactly. If the fields have a mode on the transverse plane which bisects the current distribution, then one can start at that point to construct a surface which is everywhere normal to the electric vector. If this surface is found to stay outside of the current distribution, then the fields would be unchanged if the surface were made of a perfect conductor. If the conductor has a reasonable shape, we have designed a drift tube and can easily obtain the shunt impedance and transit time factor by numerical integration.

II. Equations

We define, in cylindrical coordinates

$$r\, B_\theta\,(r, z, t) = e^{i\omega t}\, F\,(r, z)\,. \tag{1}$$

Then for a current

$$\vec{j}\,(r, z, t) = e^{i\omega t}\,\vec{j}\,(r, z)\,, \tag{2}$$

Maxwell's equations reduce to

$$r\,\frac{\partial}{\partial r}\frac{1}{r}\frac{\partial F}{\partial r} + \frac{\partial^2 F}{\partial z^2} + \frac{\omega^2}{c^2}\,F = \mu_o\, r\left(\frac{\partial j_z}{\partial r} - \frac{\partial j_r}{\partial z}\right) \tag{3}$$

*Work performed under the auspices of the U. S. Atomic Energy Commission.

in MKS units. The Green's function for Eq. (3) satisfies

$$(\mathcal{L} + \lambda^2)\, G\,(r, z;\, r', z') = r\, \delta\,(r - r')\, \delta\,(z - z') \tag{4}$$

with

$$\begin{aligned} \mathcal{L} &= r \frac{\partial}{\partial r} \frac{1}{r} \frac{\partial}{\partial r} + \frac{\partial^2}{\partial z^2} \,. \\ \lambda^2 &= \omega^2/c^2 \,. \end{aligned} \tag{5}$$

Upon defining χ_k as a complete set of eigenfunctions of

$$\mathcal{L}\, \chi_k = -k^2 \chi_k \,, \tag{6}$$

G can be formally written down as

$$G\,(r, z;\, r', z') = \sum_k \frac{\chi_k\,(r, z)\quad \chi_k^\dagger\,(r', z')}{\lambda^2 - k^2} \,, \tag{7}$$

which is verifiable by inspection of Eqs. (4) and (6) if the normalization of χ_k is such that

$$\int_o^R \frac{dr}{r} \int_o^L dz\; \chi^\dagger_{k'}\,(r, z)\; \chi_k\,(r, z) = \delta_{kk'} \,, \tag{8}$$

where R and L are the cavity radius and half length respectively (see Fig. 1). A complete set of χ_k's satisfying Eqs. (6) and (8) and the boundary conditions imposed by the physics of the problem, namely

$$\begin{aligned} \chi \Big|_{r=0} &= 0 \\ \frac{\partial \chi}{\partial r}\Big|_{r=R} &= 0 \\ \frac{\partial \chi}{\partial z}\Big|_{z=0,\,L} &= 0 \end{aligned} \tag{9}$$

is the two-parameter set

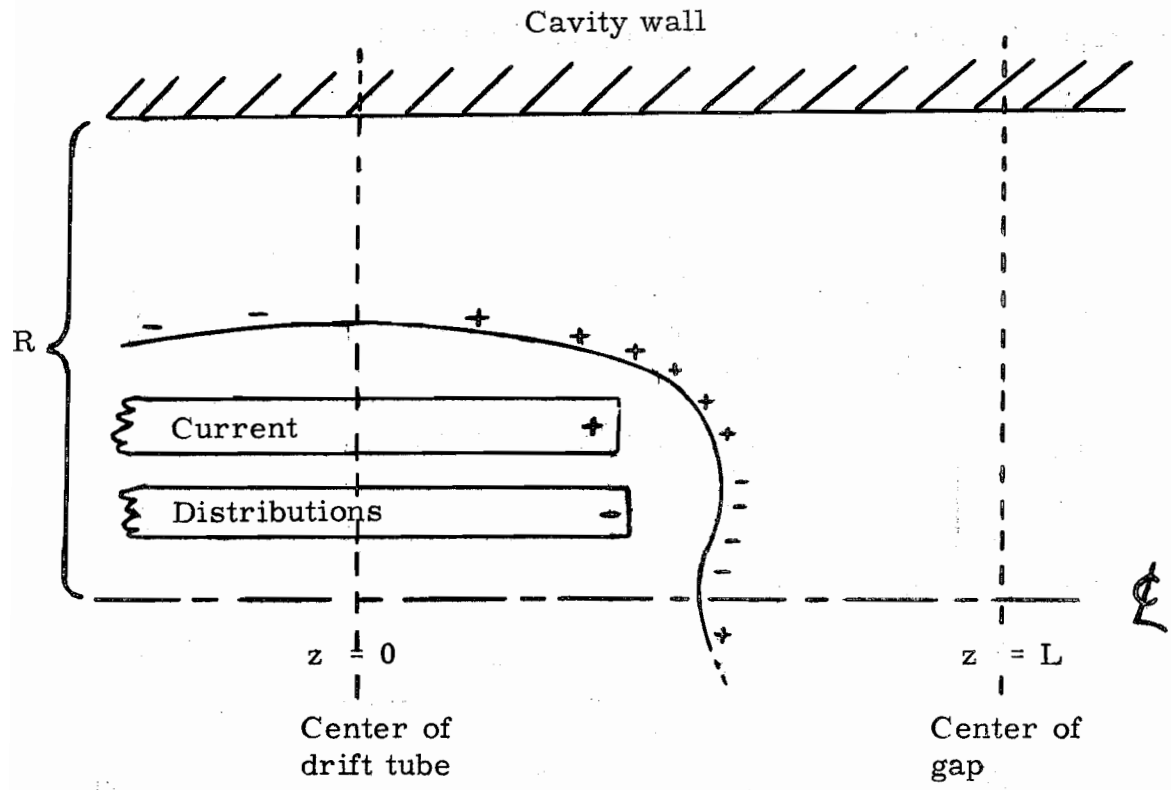

Fig. 1 Unit cell quadrant

$$\chi_{m,n} = \sqrt{\frac{2-\delta_{m,0}}{L}} \cos\frac{m\pi z}{L} \frac{\sqrt{2}}{\rho_n |J_1(\rho_n)|} \rho_n \frac{r}{R} J_1\left(\rho_n \frac{r}{R}\right), \quad (10)$$

where m runs over all the non-negative integers and ρ_n is the nth root of J_0.

Equation (7) is therefore a double sum, over n and m. Either, but not both, of them can be summed in closed form. One of the sums must be left for the computer to do numerically. The choice is made on the basis of speed of convergence; the more slowly converging sum always being done first, analytically. The relevant results are

$$\sum_n \frac{2\,rr'}{R^2 J_1^2(\rho_n)} \frac{J_1(\rho_n r/R)\, J_1(\rho_n r'/R)}{\kappa^2 - (\rho_n/R)^2} = \frac{\pi\, rr'}{2} J_1(\kappa r_<) \left[N_1(\kappa r_>) - J_1(\kappa r_>) \frac{N_0(\kappa R)}{J_0(\kappa R)}\right], \quad (11)$$

or, if $\kappa^2 = -\kappa'^2$ is negative,

$$\sum_n = -rr' I_1(\kappa' r_<)\left[I_1(\kappa' r_>)\frac{K_0(\kappa' R)}{I_0(\kappa' R)} + K_1(\kappa' r_>)\right], \quad (12)$$

where $r_>$ is the greater of r and r' and $r_<$ the lesser of the two. If one wishes to do the sum over m analytically, it is

$$\sum^{\infty} \frac{2-\delta_{m,0}}{L} \frac{\cos\frac{m\pi z}{L}\cos\frac{m\pi z'}{L}}{\beta^2 + \left(\frac{m\pi}{2}\right)^2} = \frac{\cosh\beta(z_> - L)\cosh\beta z_<}{\beta\sinh\beta L}. \quad (13)$$

The solution $F(r,z)$ of Eq. (3) is found from the Green's function according to

$$F(r,z) = \mu_0 \int_0^R dr' \int_0^L dz'\, G(r,z;r',z')\left(\frac{\partial j_z(r'z')}{\partial r'} - \frac{\partial j_r(r',z')}{\partial z'}\right). \quad (14)$$

Here we must specify the form of $\vec{j}$. We stipulate that only j_z differs from zero, and that it has the form

$$j_z(r'z') = \frac{1}{\mu_0}\sum_\mu j_\mu \cos k_\mu z'\, \theta(r' - a_\mu)\,\theta(b_\mu - r')\,\theta(y_\mu - z') \quad (15)$$

where θ is the unit step function $\theta(x) = \frac{1}{2}(1 + \frac{x}{|x|})$. Since the derivative of θ is a δ function, the integral over r' in Eq. (14) can be performed by inspection, and the integral over z' is elementary. The task remaining is then to perform either the n or m sum and the μ sum (which we have never yet taken to have more than two terms).

III. Calculations

A Fortran code for the IBM 7094 has been written to calculate drift tube shapes using Eq. (14) for F. The input consists of the parameters of Eq. (15) describing the current distribution, the frequency, the cavity radius, the proton energy (length of the cavity), the surface resistivity of the structural material, and a number to provide a convergence criterion for the Bessel function sums. Since the metallic boundary condition for Maxwell's equations specifies that the normal derivative of F vanish at the surface

$$\frac{\partial F}{\partial n} = 0, \tag{16}$$

and since at $z = 0$ the surface of the drift tube is parallel to the axis, F must satisfy

$$\frac{\partial F}{\partial r} = 0 \tag{17}$$

at the point r_d where the metal cuts the median plane. The code searches r at $z = 0$ for a point satisfying Eq. (17); if one is found, it then integrates Eq. (16) to find the surface along which one can put a metallic drift tube without altering the fields. The method used to integrate Eq. (16) is the same as that used by Gluckstern; briefly, it approximates the curve of the surface by a series of circular arcs of constant chord. By reducing the chord length one can increase the accuracy indefinitely; we find 1/2 cm to be usually adequate.

The transit time factor is formed by a Simpson's rule integration of the E field along the axis

$$T = - \frac{\int_0^L \left(\frac{1}{r}\frac{\partial F}{\partial r}\right)_{0,z} \cos\frac{\pi z}{L}\, dz}{\int_0^L \left(\frac{1}{r}\frac{\partial F}{\partial r}\right)_{0,z} dz} . \tag{18}$$

The shunt impedance is found by a Simpson's rule integration of B^2 over the metal surfaces of the drift tube and the outer cylinder:

$$ZT^2 = \frac{(\text{numerator of Eq. (18)})^2}{L\,\omega^2\,\epsilon^2\,\pi\,R_s \int \frac{F^2}{r}\, d\ell} , \tag{19}$$

where $R_s = 3.6 \times 10^{-3}$ ohms for copper at 200 Mc, $\epsilon^{-1} = 36\pi \times 10^9$, and the integral is a line integral over all the metal surfaces in a quarter cell as shown in Fig. 1.

Other output available from this code includes the maximum electric field on the drift tube, the electric fields everywhere in the cavity, and the fraction of the total power dissipation which occurs on the drift tube.

IV. Results

The form of Eq. (15) allows the construction of distributed charge distributions for excitation of a cavity. Except for comparisons with some cases of Gluckstern,[1] the problems which have been run with the present code were done with two charge distributions of opposite sign running parallel to the cavity axis, the lower one usually carrying less charge than the upper. This choice was made with the hope that it would more nearly approximate the charge configuration which must be produced in the metallic surface of a real drift tube, as illustrated by the + and - signs in Fig. 1, in order to result in an interior shielded region. In this we have only been partially successful. Axial indentations in the drift tubes can be accomplished with such dipole charge distributions and the axial fields interior to the drift tubes can be made approximately zero, but the electric fields near the end of the charge distribution and close to the axis vary rapidly in such a way that formation of a true hole seems impossible. Presumably a more complicated charge distribution would produce a drift tube with an axial hole.

No exhaustive study of drift tube shapes has been made with the present code. Some problems have been run at 10, 50, 100, and 150 MeV in an effort to obtain relatively cylindrical drift tubes with reasonable values of $Z\,T^2$, G/L, and radius. Because of the large number of parameters involved with these distributed "dipole" charge distributions and the restriction to reasonable shapes, optimization of the drift tubes becomes very difficult.

Running times with 0.5 centimeter integration stop and a maximum of sixty sum terms are about three minutes per problem. These use a single sinusoidal form for the Z-dependence of each of two distributions. The phase of the cosine function at the end of the distribution was kept the same for both in each case. For similar drift tube sizes and shapes in the neighborhood of what appeared to be optimum, ZT^2 values were not overly sensitive to changes in the parameters of the charge configurations, as would be expected. Relative to an arbitrary configuration in this neighborhood, increasing the cavity radius decreases the drift tube radius, generally with a resultant increase in ZT^2. An increase of the length of the charge distribution would decrease the drift tube radius while slightly increasing its length. As the phase of the sinusoidal charge distributions were made to approach 90°, distributing the charge more uniformly, the drift tube radius would in general increase, reducing ZT^2. Finally, making the magnitude of the charge on the lower distribution approach that of the upper tended to result in a reduction of the drift tube radius and the formation of an indentation at its front, the beginnings of a hole.

Figures 2, 3, 4, and 5 show some typical results for drift tube shapes and axial electric fields within the gap for energies of 10, 50, 100, and 150 MeV, respectively. Pertinent data with respect to cavity radius, g/L, T, ZT^2, etc., are contained in the figures. These results are consistent with those of Gluckstern[1] and with MURA MESSYMESH calculations,[3] although there seems to be a tendency to obtain lower ZT^2 values than do the latter.

In conclusion, we would like to emphasize that the material presented here is very preliminary. It is hoped that as more detailed parameter studies are made and more "realistic" charge distributions used, a closer approach to drift tube optimization will be achieved.

YOUNG: I have two questions. The first is: How much effort have you put into making a drift tube hole and are you going to devote more attention to this? The second is: Have you checked your program against the results of other programs?

VISSCHER: To the first question: We have made an effort to achieve a drift tube hole. I don't think that it is practical for us because we have so many parameters to change to optimize the drift tube shape. By adding one or more current distributions close to the point where the drift tube contour intersects the axis when these currents are not present, we can get a deep depression in the nose of the drift tube, but not a real hole.

As far as our agreement with other calculations that have been done, we have tried to reproduce some of Gluckstern's single-charge drift tube shapes. We were able to do that all right with the agreement in shunt impedance to within a couple of percent. The difference may be due to the fact that we didn't quite duplicate his shape. We can't really duplicate the shapes calculated by the MURA MESSYMESH program but our results are in general agreement considering this fact.

REFERENCES

1. R. L. Gluckstern, Proceedings of the International Conference on Accelerators, Brookhaven National Laboratory, 1961.

2. P. M. Morse and H. Feshbach, Methods of Theoretical Physics, McGraw-Hill Publishing Company, 1953.

3. See, for example, MURA reports 622 and 642.

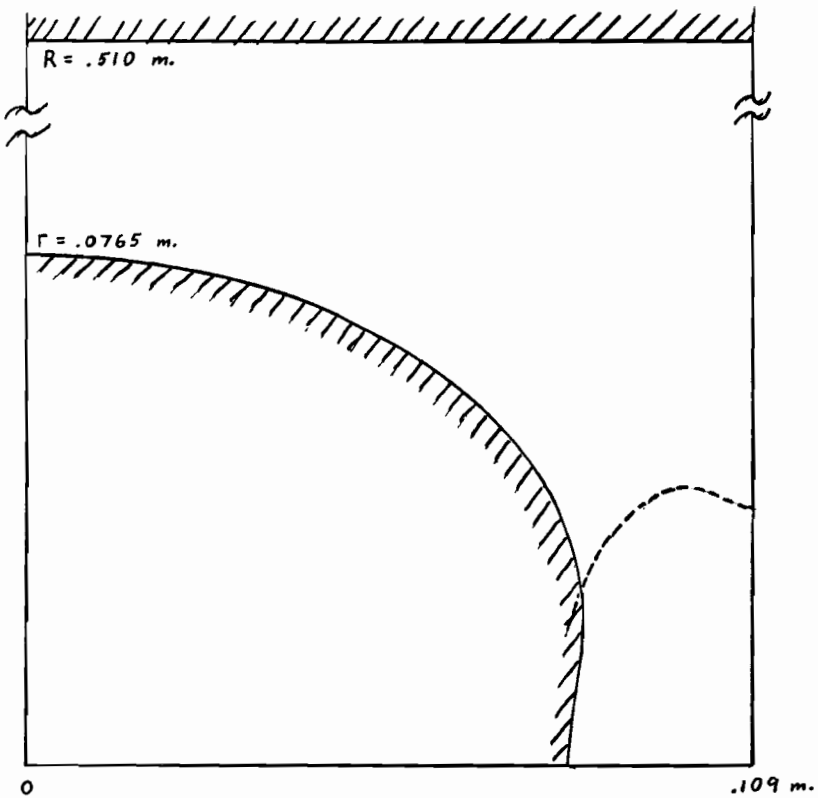

$g/L = .226$

$T = .908$

$ZT^2 = 78.1\ M\Omega/m$

$E_{max} = 1.26$

$f = .195$

Fig. 2: Example of a 10 Mev drift tube shape and axial E field. E_{max} is the maximum field on the drift tube in units of the field at the center of the gap; f is the fraction of the total RF power dissipated on the drift tube.

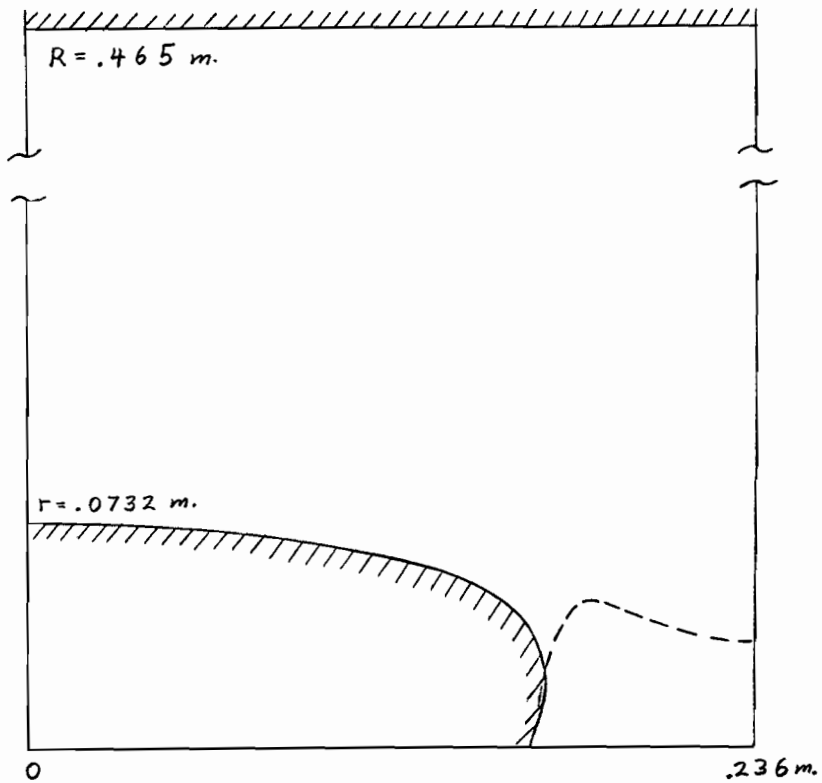

$g/L = .285$

$T = .849$

$ZT^2 = 53.3\ M\Omega/m.$

$E_{max} = 2.26$

$f = .398$

Fig. 3: Example of a 50 Mev drift tube shape and axial E field.

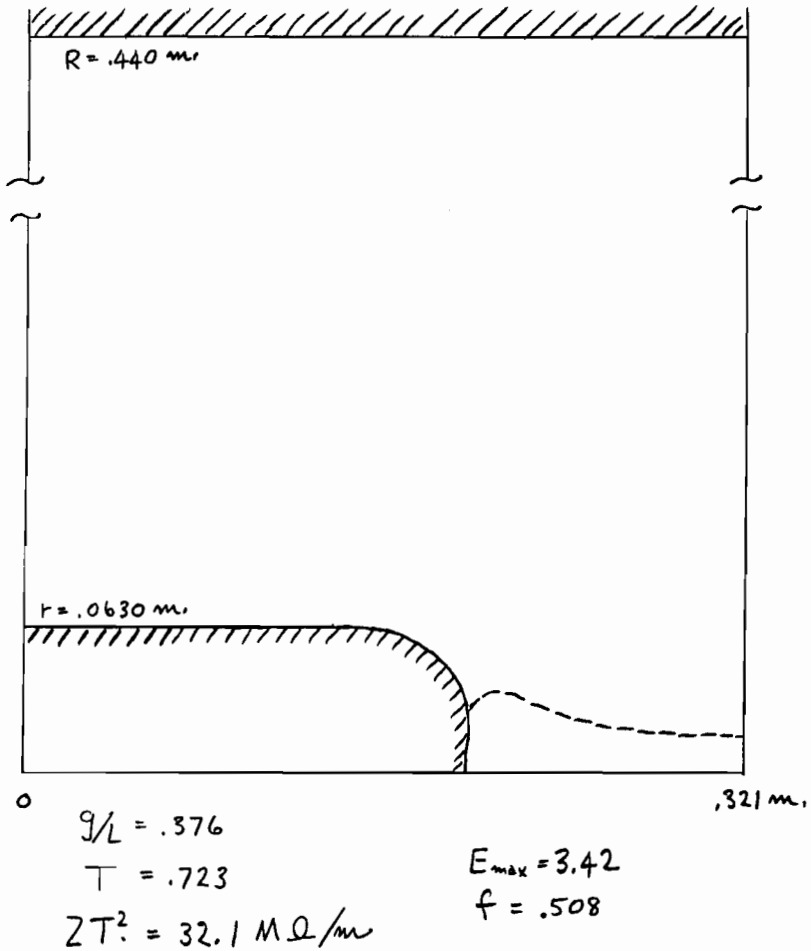

Fig. 4: Example of a 100 Mev drift tube shape and axial E field.

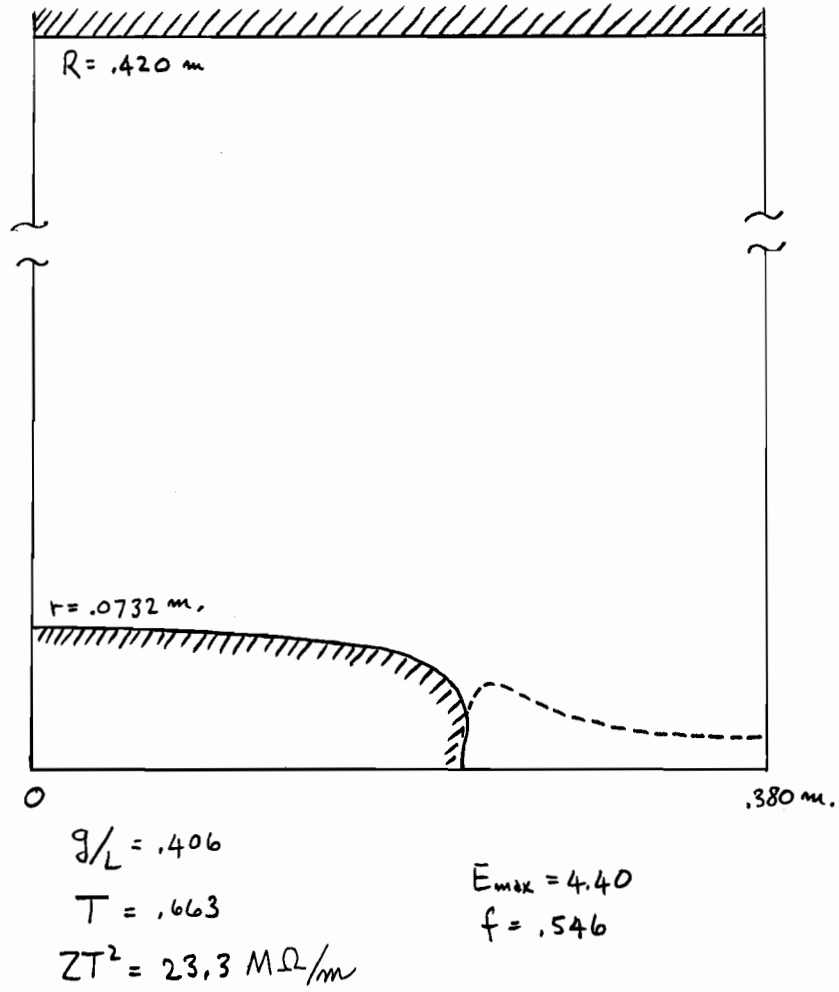

Fig. 5: Example of a 150 Mev drift tube shape and axial E field.

DRIFT TUBE CALCULATIONS*

Harry C. Hoyt
Los Alamos Scientific Laboratory, University of California
Los Alamos, New Mexico

I would like to talk about the mesh calculation that we are trying to set up at Los Alamos for the calculation of resonant cavities. I know quite a number of you have heard about these mesh calculations before, and I hope that you will bear with me as I go through some of the more elementary details. Our calculation divides the resonant cavity into a mesh containing a finite number of points, and then uses a finite difference scheme for computing the values for the magnetic field strength at the points in the mesh. Once we know the magnetic field we can compute other quantities of interest, such as the frequency, shunt impedance, transit time factor, and so on. The voltage is also computed, but is used to determine the normalizing factor needed to get rid of an arbitrary constant which multiplies all the values for the magnetic field strength.

My reasons for wanting to do this mesh calculation are two in number: First, I wanted to learn how to do this type of calculation, and second, there seemed to be a need for a mesh calculation which could be used for a cavity having any arbitrary boundary shape. Consequently our mesh calculation has been set up to allow any boundary shape; in this respect it is different from those calculations which have been done previously. The freedom that we might gain from having a calculation in which we can easily draw in new boundaries will allow us to actually do some comparisons between a lot of strange ideas which are not easily adaptable to other methods of calculation. Also, the mesh calculation is readily adaptable to parameter studies if one has a man who has the time to look at several million numbers.

A resonant cavity which can be handled by our mesh calculation has symmetry with respect to an axis, that is, such a cavity is a figure of revolution. Because of the symmetry, the calculation is carried out for points in a plane which contains the axis, and we have a two-dimensional problem. The calculation may cover either the entire cavity or, if the two halves of the cavity are identical, only half of the cavity. Figure 1 shows the sections used for half-cavity and full-cavity calculations. In Fig. 1 the holes in the drift tubes have not been shown; the calculation, however, can treat the holes.

---

*Work performed under the auspices of the U. S. Atomic Energy Commission.

The mesh used in a given calculation is chosen so that there are an integral number of spaces along the axis, or z-direction. The mesh interval is the same in the radial direction or r-direction, as in the z-direction; that is, we have a square mesh. The outer surface of the cavity does not have to coincide with a mesh line. Figure 2a shows how a mesh might look for a half-cavity calculation. The curved lines show a drift tube and a curved outer wall. The principal difference between MURA's MESSYMESH code and the Los Alamos program is in the way in which we treat the boundary. Since we decided to allow for any boundary shape, we abandoned the idea of doing our calculating on the actual boundary. Instead we compute at points on a zig-zag approximation to the actual boundary. Figure 2b illustrates different ways of determining a zig-zag boundary. The curved line represents an actual boundary, say a metallic surface. One can draw a zig-zag boundary which is the closest approximation to the actual boundary, or one can draw a zig-zag boundary either completely inside the actual boundary or completely outside the actual boundary. How one chooses which zig-zag boundary to use can depend on the type of difference equations one decides to use for the boundary points. Other considerations also may indicate a preference for a particular way of drawing the zig-zag boundary. Hopefully we will be able to choose the zig-zag boundary and the difference equations for the boundary points so that we will get the greatest accuracy for the boundary equations.

We have decided to use the zig-zag boundary which lies completely outside the actual boundary. One of the original reasons for this choice was that it allowed us to choose a set of boundary point equations with nice mathematical properties; however, we have since abandoned that particular set of boundary point equations. Another reason for choosing the zig-zag boundary outside the actual boundary is that we can find field values on the actual boundary by interpolation, rather than by extrapolation. In setting up our difference equations for the boundary points, we do insist that the boundary conditions are satisfied on the actual boundary. Thus, although the mathematical properties of our set of difference equations are not ideal, the physics is correct. Figure 2a shows how the zig-zag boundary would be drawn for the configuration shown.

The partial differential equation for our problem is given below. In

$$\frac{\partial^2 F}{\partial r^2} - \frac{1}{r}\frac{\partial F}{\partial r} + \frac{\partial^2 F}{\partial z^2} + \lambda^2 F = 0 \qquad (1)$$

equation (1), $F = r H_\theta$ and $\lambda^2 = \omega^2/c^2$, where H_θ is the only component of the magnetic field present. Equation (1) is the equation which remains after the time dependence has been removed from the wave equation. The boundary conditions are

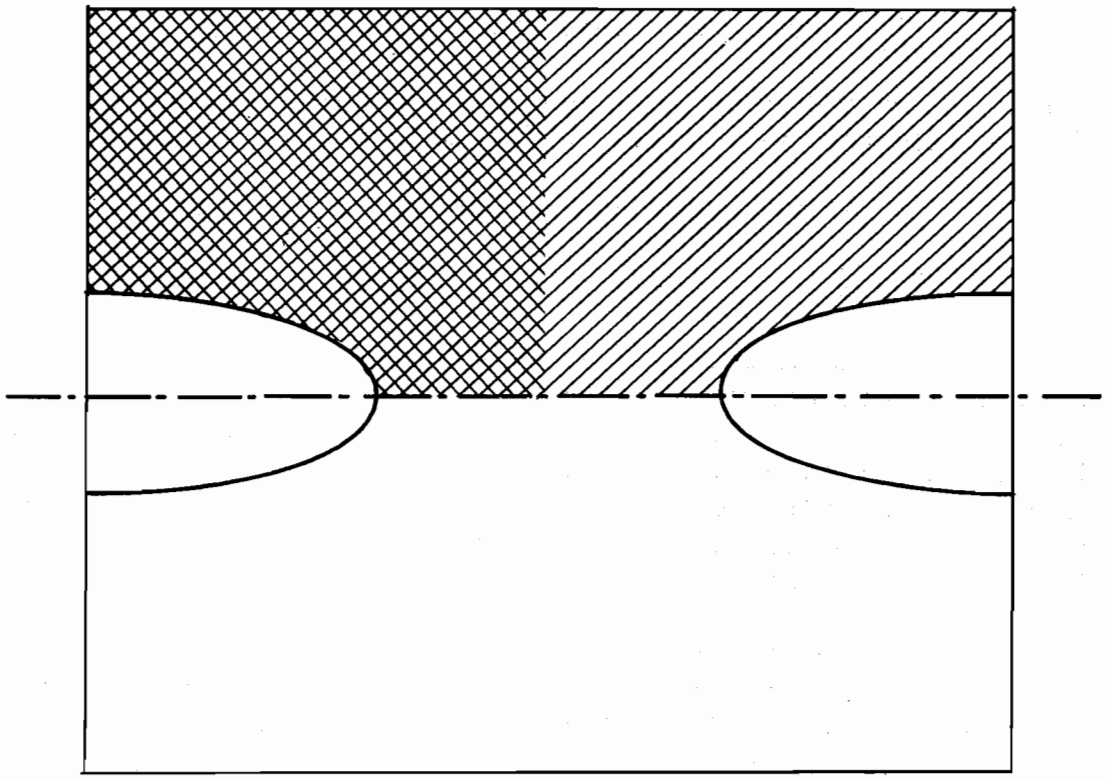

Drift tube Cavity (holes not shown)

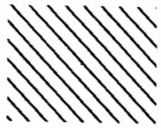

Section used for Half-cavity calculation

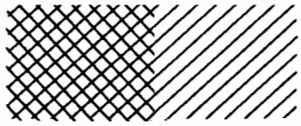

Section used for Full-cavity calculation

Figure 1.

$$F = 0 \quad \text{on the axis, and}$$
$$\frac{\partial F}{\partial n} = 0 \quad \text{on the remainder of the boundary.} \tag{2}$$

$\frac{\partial F}{\partial n}$ is the derivative of F normal to the boundary. These conditions are equivalent to the following conditions on the electric field:

$$E_r = 0 \quad \text{on the axis, and}$$
$$\vec{n} \times \vec{E} = 0 \quad \text{on the remainder of the boundary.} \tag{3}$$

Equations (3) say that there can be no radial component of the electric field on the axis because of symmetry, and that on the remainder of the boundary the electric field must be perpendicular to the boundary either because of the presence of a conducting surface or because of symmetry. The second condition of (2) is called a Neumann condition, and it is the difficulty in treating this condition numerically which is a major problem in a mesh calculation of this type.

Our method for getting the difference equations is somewhat different from that used by others, at least insofar as the interior points of the mesh are concerned. Our original intention was to obtain a set of difference equations which would have a positive definite matrix, since this would assure convergence to a solution. To get such a set of equations, one uses a variational principle. Consider the following integral:

$$I = \frac{1}{2} \iint \frac{1}{r^2} \left[\left(\frac{\partial F}{\partial r} \right)^2 + \left(\frac{\partial F}{\partial z} \right)^2 - \lambda^2 F^2 \right] r \, dr dz \, . \tag{4}$$

If we take the variation of (4) and require it to be equal to zero, i.e.,

$$\delta I = 0 \, , \tag{5}$$

we find that the condition for (5) to be satisfied is that the differential equation (1) be satisfied. Equation (5) says that the integral (4) will be either a maximum or a minimum. Substitution from Maxwell's equations into (4) shows that

$$I \propto \int (\epsilon E^2 + \mu H^2) \, dV \, , \tag{6}$$

that is, I is proportional to the energy in the cavity. Equation (5) then requires that the energy be a minimum. The procedure for obtaining the

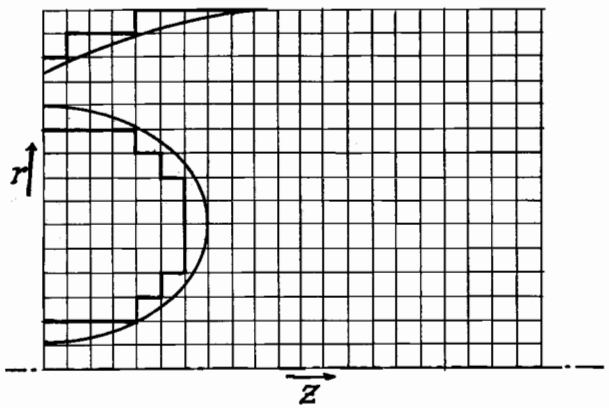

(a) Actual and Zig-Zag Boundaries for Mesh Calculation

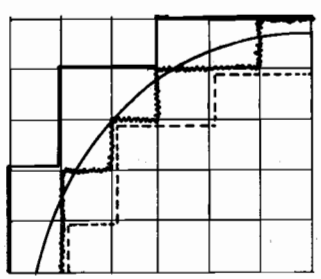

(b) Ways of Drawing Zig-Zag Boundary
Closest approximation
Inside
Outside

Figure 2.

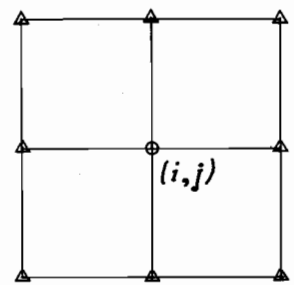

(a) Points used in 9-point difference equation for interior point (i,j)

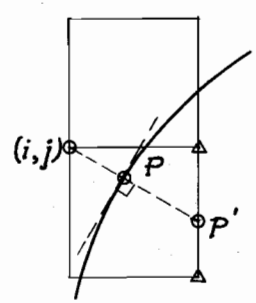

(b) Points used for difference equation for one type of boundary point.

Figure 3

difference equations is to substitute our difference approximations in (5) rather than in the differential equation (1). We then perform the process of taking the variation of I and setting it equal to zero. The result gives us our difference equations, both for interior points and for points on the zig-zag boundary. However, the difference equations for the points on the zig-zag boundary say that the normal derivative of F on the zig-zag boundary--not the actual boundary--is zero. Because we want the condition to apply on the actual boundary, we have substituted a new set of equations for the boundary points.

Figure 3 shows the points which are involved in the resulting difference equations. For the interior points we have a 9-point difference equation. In Fig. 3a, we wish to compute a value of F for the point (i, j), where i and j are integers giving the location of the point. The illustration shows the other points which are referred to in the difference equation. Figure 3b shows an example of how the equation for a boundary point can be obtained. We wish to compute the value of F at point (i, j). However, the boundary point equation must say that $\frac{\partial F}{\partial n} = 0$ on the actual boundary at P, the intersection of the actual boundary with the normal to the boundary which passes through (i, j). The first approximation satisfying the boundary condition is to say that F at (i, j) equals F at point P'. The value of F at P' is found by interpolation from the values at the adjacent mesh points. Figure 3b shows what points will be referred to in the difference equation.

Once we have a complete set of difference equations for the mesh, we would like to compute the F values for the mesh points. We also would like to compute the lowest eigenvalue for the system of equations; this will give us the frequency of the cavity. The eigenvalue, λ^2, is computed from equation (7). This

$$\lambda^2 = \frac{\iint \frac{1}{r^2}\left[\left(\frac{\partial F}{\partial r}\right)^2 + \left(\frac{\partial F}{\partial z}\right)^2\right] r\, dr\, dz}{\iint \frac{1}{r^2} F^2\, r\, dr\, dz} \tag{7}$$

equation can be shown to give the eigenvalue we want by taking

$$\delta \lambda^2 = 0 . \tag{8}$$

Again we can find that the condition (8) for an extremum is that the differential equation (1) be satisfied.

The input data required to describe the boundary have been chosen as follows: For each point where the actual boundary crosses a line of

the mesh, three numbers are given. These three numbers are the coordinates, r and z, of the point and the slope m of the actual boundary at that point. Any given problem may require several thousand input numbers to describe the boundary, but the data handling problem can be reduced considerably by considering each problem as a modification of a previous problem. Then the input for the previous problem can be used, together with the necessary information which shows the changes from the previous problem. In addition to data describing the boundary, we must provide input, or guessed, values for the F's at the mesh points and the eigenvalue λ^2. Once you have a backlog of problems, the values for the solution of one problem can be used as the input for the next one. One cannot start a problem without this "mesh loading" of F's because F = 0 everywhere is a solution to the differential equation, and the program would get nowhere.

The calculational procedure used is point-by-point relaxation. This allows us to compute a new value for F at a given point on the basis of the values at adjacent points, regardless of whether they are new or old values. We proceed through the mesh systematically, starting at the bottom where r = 0 and going from left to right. When we finish one row, we go to the next row above and repeat the process. When we finish computing the F values, we compute a new value for λ^2 using equation (7). Then the process is repeated. The result is a kind of double iteration: you iterate with a given value for λ^2 until the F values settle down, then you calculate a new λ^2. Finally when both the F's and λ^2 have settled down, you can declare that the solution has converged. Once the F's and λ^2 have been computed, we can calculate Q, shunt impedance, transit time factor, and so on.

The status of our program is as follows: We have completed programming and check-out on the input program and the parts computing the F's and the eigenvalue, and we are in the process of programming the calculations for Q, Z, transit time factor, and so on. We have done some checking out on problems. Our first check-out problem was a spherical cavity, for which we have an analytic solution; this problem works very well. The F values for points in the interior (and some distance from the boundaries) agree with the analytic solution to 0.1 or 0.2 percent. Near the axis, F values seem to be within 2 percent, and near the outside boundary they are within 3 or 4 percent. Better values might be obtained by running the problem longer. Boundary point equations, however, do not have the same degree of accuracy as the equation for interior points, and some of the error near the boundary may be a more or less permanent feature. We are now trying to run a drift tube problem for a 50 MeV cavity. This is a problem which has been computed by

Bill Visscher and Marvin Rich using the methods described in the previous paper.

A word about the computer time involved might be in order. A problem with a 100 x 100 mesh, or 10,000 points, will take about 8 minutes on the IBM 7094 if we make reasonable guesses for the initial values of the F's and λ^2. By "reasonable guess", I mean that these values should be within 10 percent of the final values. As I mentioned before, this is not too difficult, since each problem is a slight variation from a previous problem. The calculation currently can handle a mesh having up to 40,000 points; this means mesh spacing of a few millimeters for the drift tube cavities we are now interested in. Our current estimate of the time required to complete the program is two to three months. If we are successful, perhaps we can answer some of the questions which have been the subject of many arguments.

EDWARDS: Do you use the technique of overrelaxation? We find here at MURA that it speeds up the convergence immensely.

HOYT: I set the calculation up in such a way that we can use overrelaxation. I found that on the spherical problem overrelaxation was not as fast as using a relaxation factor of one. One gets the answer in half to two-thirds the time required when a larger value for the relaxation factor is used. I also checked to see what theoretical estimates one can make for the relaxation factor, and found to my surprise that the estimate is very nearly one. The relaxation factor depends on the frequency of the cavity, so this might not be true for frequencies other than 200 Mc.

GLUCKSTERN: Didn't the numbers you gave as estimates of the accuracies of interior points also apply to the electric field on the axis?

HOYT: I don't know about this yet. We have not computed any electric field values on the axis yet. The procedure we plan to follow is this: One can compute the voltage across the cavity using Faraday's Law, which should be more accurate than obtaining it by computing the electric field on the axis. We would then also, using the best curve fitting methods, try to compute the electric field on the axis, integrate along the axis to get the voltage, and compare with the Faraday's Law value to estimate the accuracy. I feel this estimate is necessary, because E_z on the axis must be used in the calculation for the transit time factor, and we should know all we can about the accuracy. I might explain to those of you who are not familiar with the problem that E_z is proportional to $\frac{1}{r}\frac{\partial F}{\partial r}$, and so when r approaches zero, E_z is given by $\frac{\partial^2 F}{\partial r^2}$. Determining second derivatives

with accuracy is very difficult in numerical calculations. One must do some curve fitting, or use some other approximate methods. We are going to reflect into the axis for two or three points out and then do a curve fit which will give F as a function of r for fixed z. We will differentiate this to obtain E_z on the axis. With the spherical problem and some of Bill Visscher's problems, we should be able to determine the accuracy.

EDWARDS: We have done much the same thing in calculating the axial E field. We find that the difference between the two methods is of the order of 4 to 5 percent, if my memory is correct.

HOYT: I have a feeling that most of the errors which I have mentioned here, like the ones near the conducting surfaces and those near the axis, may well turn out to be systematic errors. If it can be established that they are systematic errors, and if someone can furnish good measurements, then we can correct for them. Then the errors would not be serious when we compare and evaluate different types of structures.

THE SACLAY DESIGN STUDY OF PROTON LINEAR ACCELERATORS

M. Promé
C. E. N. -Saclay

I. Introduction

A team* from Saclay has been dealing with proton linacs for about two years. The purpose is to design, with the collaboration of the Compagnie Générale de Télégraphie sans Fil (C. S. F.),** a 200 MeV linac capable of injecting a 100 milliamp beam into a future synchrotron.

Another purpose of these studies is to design a 20 MeV linac to replace the 3.6 MeV Van de Graaf injector of Saturne. In this case the required beam is about 20 milliamp.

The purpose of this talk is to present some information about the studies undertaken in connection with these projects: theoretical work, models, design of the preinjector, and a general survey of the 200 MeV project in its present form.

II. Theoretical Studies

Theoretical studies have proceeded in two different ways. On the one hand, a computation program for individual cells is being written at Saclay. This program will be similar to the MESSYMESH program of MURA. It will give the values of the resonance frequency, Q factor, shunt impedance, and will allow one to choose accurate dimensions for the linac.

On the other hand, studies have been made to find out if there is any interest in choosing a variable accelerating rate along the linac, from the point of view of an easy trapping of particles by the accelerating process. For instance, a small accelerating rate at the input end of the linac, and gradually increased over a few MeV up to a final value, increases the useful acceptance area for the axial motion. We are now investigating whether this does not implicate a growth in the energy spread of the beam at the exit of the linac.

---

* This team consists of MM. M. Gouttefangeas, M. Promé, G. Rastoix, under the direction of M. Levy-Mandel, and to whom M. P. Lapostolle (CERN) gave a lot of fruitful ideas.

**MM. F. Girard, G. Guilbaud, R. Jean, H. Leboutet, Tran Duc Tien.

Computations have been performed for particles on the axis with a simple program. It will be determined later whether such a variable accelerating rate damages the radial acceptance or not. This will be done by using a program taking into account the six phase coordinates, similar to the PARMILA program of MURA.

III. Experimental Program

The purpose of the experimental program undertaken at Saclay is to get some experience in the field of proton linac cavities.

A two-cell model at 50 MeV has been built and some experiments have already been performed. The 150 kW required to set the rf field to its nominal value inside this model are supplied by a 10 kW C.S.F. television transmitter. C.S.F. has reached the 150 kW level easily by improving the power tube anode insulation, and by adding a 200 μs, one pulse per second modulator.

It is planned to build a 3 m long model at 750 keV. Profiting from the experience acquired with the first model, this one will be closer to the final design.

Experiments performed or planned with these models involve measurements of the Q factor, measurements of the fields and determination of shunt impedance by the perturbation method, and the behavior of the cavity at full power.

IV. Preinjector*

A 750 keV injection energy has been chosen for the linac. The preinjector, a Cockcroft-type machine, offers the possibility of being pressurized. Such an injector has the advantage of being small, 2.5 m long and 2 m in diameter. With such technology, one can avoid setting the classical storage capacitor between the high voltage electrode and earth. Such a capacitor can be damaged when a breakdown occurs. This capacitor is replaced by a pulsed liner, which permits balancing the voltage decrease during the 200 milliamp pulsed beam. Such a liner already exists on the Van de Graaff injector of Saturne, with the different purpose of producing $\frac{dV}{dt} > 0$, and works in a satisfactory manner. The pulse to be applied to the liner will be supplied by a beam intensity transformer, and will be monitored by the beam itself.

The preinjector voltage will be controlled by a continuous beam of about 50 microamp. This beam, which is deflected by an electrostatic

*Preinjector design has been performed by MM. R. Vienet and J. Faure.

device at the exit of the preinjector, passes through a regulation slit which provides a control signal. This signal feeds back on the one hand to the Cockcroft (slow regulation), and on the other hand to the liner (fast regulation).

The behavior of the beam at the exit of the ion source remains to be checked experimentally. However, the focusing device has been computed for a 200 milliamp beam. Calculations have proceeded far enough to take into account the aberrations. In this scheme the beam is accelerated quickly up to 200 keV; the focusing process operates at this level. The whole column, between the ion source and zero potential, is 80 cm long. Moreover, there is a cross-over at about 50 cm after the exit of the preinjector tube. This will make the adjustment and tuning of the beam easier (Fig. 1).

It is estimated that the time spent to reach the ion source with such a pressurized device will be increased by about half an hour with respect to a nonpressurized device. It is planned to have at one's disposal two similar preinjectors, the time spent to switch from one to the other will be five minutes. Of course, one can repair the first one while the second one is running.

V. Design of the 200 MeV Linac

Cavities

The structure considered in this project is the conventional one, with drift tubes. Copper-clad technology, which seems to be cheaper than the separate vacuum tank solution, has been chosen. Elementary sections would be 3 m long.

It has been shown after some difficulty that it would be possible to manufacture copper-clad linac cavities in Europe; copper being either an American OFHC copper from "American Metal", or a European one, such as the BE58 copper, from Norddeutsche Affinerie, Hambourg, whose qualities are close to the OFHC one. The German Company, Phoenix Rheinrohr, will be able to perform the cladding by hot lamination without brazing compound. Rolling and welding operations could be made either by the same company with an accuracy of $\pm$ 5 mm on the diameter, so that it would be necessary to inlay copper at the ends of each section in order to machine an accurate circle, or in France by "Les Chantiers Navals de La Ciotat", in which case tolerances would be $\pm$ 8/10 mm on the diameter, thanks to encircling rings left afterwards on the cavities. In the latter case, it would be unnecessary to inlay copper at the end of the sections.

The mechanical tolerances are important from the point of view of the joining of two sections, not from the point of view of having cavities tuned exactly to the chosen frequency of 200 Mc/s. The coarse tuning will be made with auxiliary rods similar to Brookhaven. The fine tuning of the local frequency will be obtained by means of classical ball tuners which will also be used for setting the accelerating field law chosen along the cavity.

The accelerating structure will be about 125 m long. The temperature control system has been designed so that the linac temperature will be within 0.1° C along the machine, whatever the operating conditions.

Rf Power Supply

In the present design we are considering a short first cavity of 6 m maximum length and 4 to 6 cavities 20 to 30 m long (Figs. 2 and 3), each cavity being fed by a power tube. This choice results from the power available in one tube. Power estimations have been based on the shunt impedance values published by MURA. A conservative interpretation leads one to predict 65 kW/m at the input end of the linac and 130 kW/m at the output end, with a linear decrease. Calculations made on beam loading have shown that these figures have to be overvalued by about 55% during the beam acceleration process. A good security coefficient will be obtained by providing an rf power pulse of 5 MW maximum for each cavity during 200 μs for the filling up of the cavities, and 10 MW maximum during 20 μs to balance the beam loading. Either the well known RCA 7835 tube or the RCA 4617 tube will be used. The latter tube, which requires lower plate voltage, should lead to a simpler modulator (Fig. 4). The modulator is of the hard tube type and is more easily operated than a delay line when it is a question of nonrectangular pulses. The RCA 7835 tube leads to the design of a modulator with two sets of capacitors and a switching system from one to the other. The RCA 4617 tube allows the use of a single set of capacitors, with a hard tube grid controlled system.

It must be pointed out that according to the results of the experiments being performed on the PS linac at Geneva one will perhaps find it preferable to feed each cavity with two tubes, the first one working during 220 μs, the second one during 20 μs. This should lead to simpler modulators because each tube would have a quasi-rectangular pulse. Moreover, cheaper tubes than the RCA tubes previously mentioned could be employed if need be by dividing the accelerator into a large number of cavities. Another advantage would be to set free a new parameter, the rf phase angle between the two tubes.

Radial Focusing

Radial stability will be insured by magnetic quadrupoles in the ++-- pattern (Fig. 5). Quadrupoles will be fed by dc current; the first 20 could be made with 5-turn windings of a hollow 6 x 6 mm wire, with a 4 mm diameter hole for water cooling. Maximum current density will be then about 27 amp/mm^2. The other quadrupoles will be made with ordinary conductor windings and will be molded in plastified araldite. They will be cooled by a water jacket. Induction on the pole faces nowhere exceeds 6250 gauss (Figs. 6, 7, 8 and 9).

Vacuum System

Primary pumping will be in two steps: 20 minutes to reach 10 Torr starting from atmospheric pressure (the required pumping speed is 325 m^3/hr for a 30 m long cavity), then one hour to reach 10^{-4} Torr (the required pumping speed is then 600 m^3/hr). In the present state of this project, secondary pumping will be turned on at 10^{-4} Torr; later, it may be thought preferable to turn on the secondary pumping at a lower pressure. 1000 l/s VacIon pumps will be used for the secondary pumping. We are considering providing one pump every 3 m along the linac (Fig. 10).

Alignment

The method being considered is the following one: cavities lay on a main girder by means of wheels dependent on an adjusting system; each 3 m long section is machined at its ends in order to define its axis; the drift tubes are aligned along this axis. The sections are joined together to form a 20 or 30 m long cavity. A slight rectification of the drift tube position is sufficient to balance the lack of parallelism of the end faces of each section. Outside references allow checking the slow displacements of the drift tubes following a possible distortion of the main concrete girder. Stem attachment devices have been designed so that it is possible to correct the drift tube positions without opening the cavities (Fig. 11).

Planning

The planning has been conceived in order to keep in line with the building time of the synchrotron (Fig. 12). The critical path appears to be linked to the quadrupole studies, machining and controls; it is therefore planned to carry out special studies on this feature. From another point of view, copper-clad cavity models will be tested in conditions as close as possible to the operating conditions of a particle accelerator.

OHNUMA: I would like to ask about your choice of quadrupole magnet strength. I noticed that the magnet strength reduces very drastically as the energy increases. Are you always taking the optimum point at each energy? The solid line comes down rather rapidly and I don't believe those are optimum points.

PROMÉ: With reference to Fig. 5, one can choose lines inside the stability limits such that the beam keeps a constant size. These lines fall rather quickly and starting from the input point, you can choose such a line for the operating line so that the size of the beam does not increase. It is perhaps not the best, but is at least feasible.

OHNUMA: How far do the nonsynchronous particles penetrate into the unstable region?

PROMÉ: Not far and this is only at the beginning of the machine. Very quickly the nonsynchronous particles enter the stable area. Of course, this has to be checked with a computer program using the six coordinates.

FEATHERSTONE: I was interested in your reference to the possibility of using large power tubes of less cost than the RCA tubes that you have also considered. Is there anything concrete that you can say about this matter at this time?

PROMÉ: There is nothing new, to my knowledge, about these tubes.

FEATHERSTONE: F. T. H. has not done something interesting we should know about?

PROMÉ: Perhaps Colin Taylor will say something about this.

TAYLOR: I will give some information about this during my talk.

FEATHERSTONE: You referred to using a variable rate of acceleration at the injection end to improve capture. Would this be used in conjunction with conventional bunching or to the exclusion of an ordinary buncher?

PROMÉ: This does not exclude a buncher.

FEATHERSTONE: Would one inject a continuous stream of protons?

PROMÉ: No, you would need a buncher as well.

FEATHERSTONE: Do you have an estimate of the efficiency of capture that you should obtain with the combination of buncher and variable acceleration rate?

PROMÉ: I am afraid that I cannot give a number because we have not finished the calculation. However, we saw that we gained something.

CURTIS: You mentioned the use of a liner in your preinjector Van de Graaff. How much of a voltage droop do you have to correct for when you are drawing 200 milliamps?

LAPOSTOLLE: I think it was a few 10's of kilovolts. It depends on the capacity of the machine.

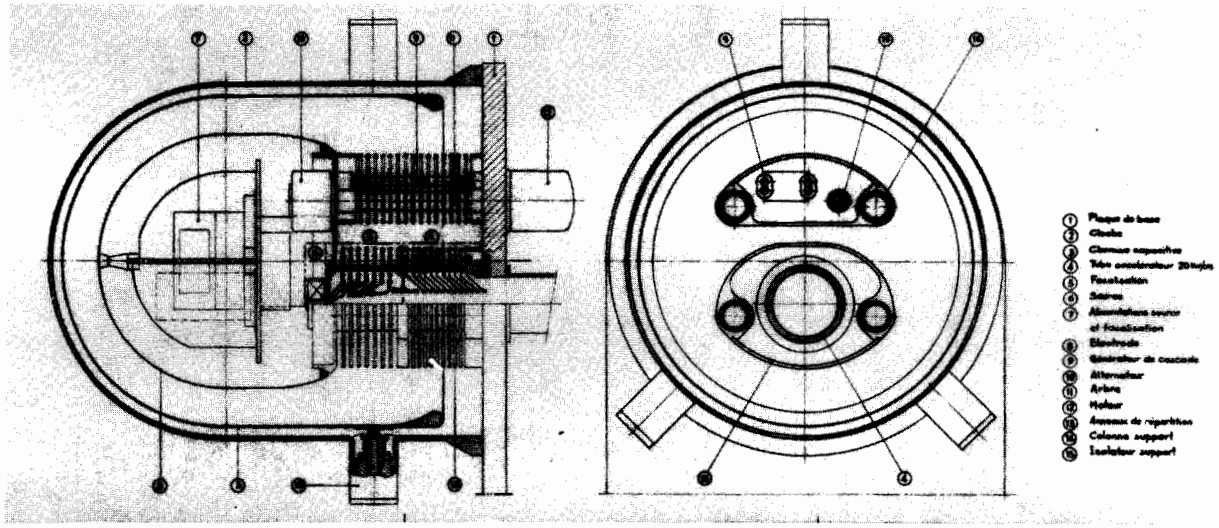

FIG. 1

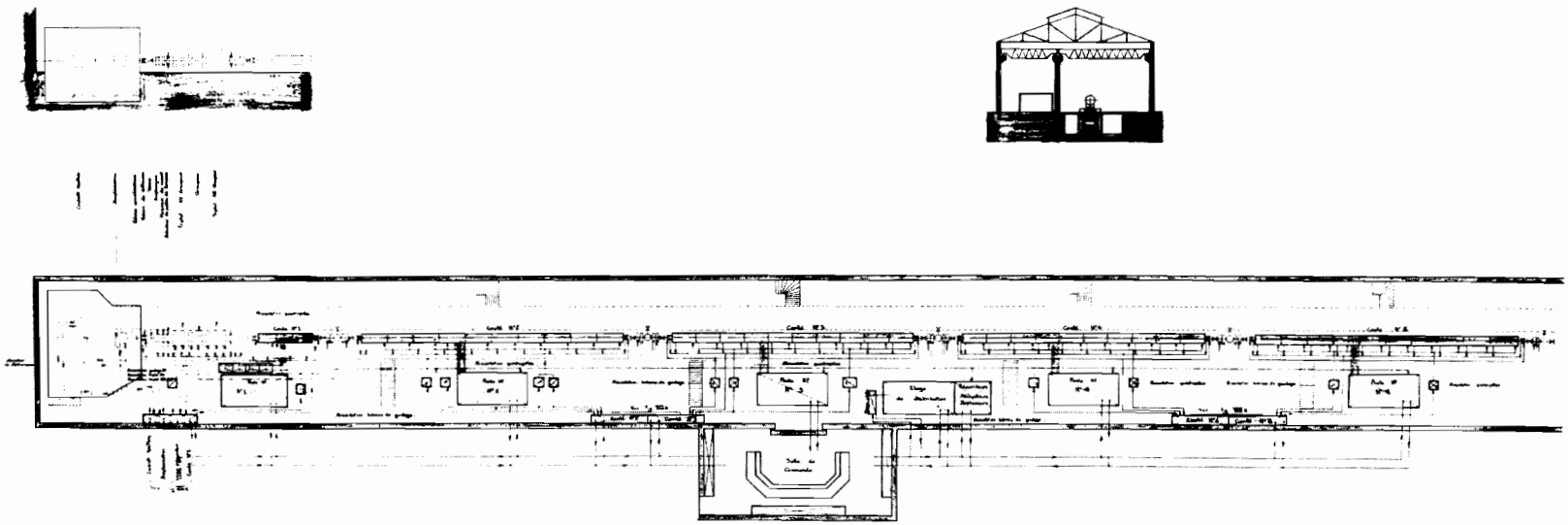

FIG. 2

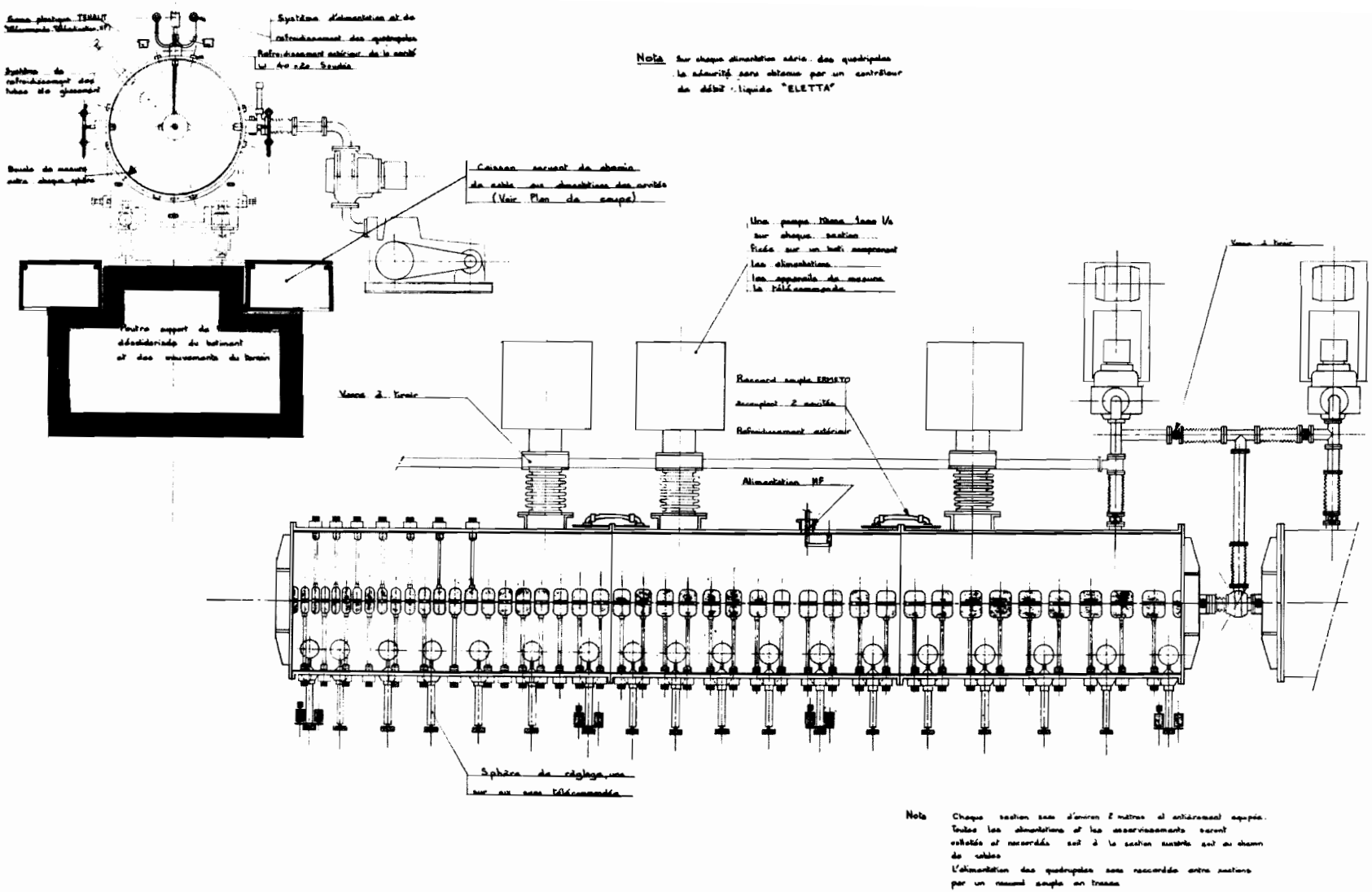
Système d'alimentation et de refroidissement des quadrupoles
Refroidissement extérieur de la cavité
Système de refroidissement des tubes de glissement
Sonde de mesure entre chaque sphère
Caisson servant de chemin de cable aux alimentations des cavités (Voir Plan de coupe)
Une pompe 10mm 1000 l/s sur chaque section
Fixée sur un bati supportant
Les alimentations
Les appareils de mesure
La télécommande
Vérins à levier
Vérins à levier
Raccord souple ERMETO
Accouplant 2 cavités
Refroidissement extérieur
Alimentation HF
Sphère de réglage, une sur six sans télécommande
Nota
Sur chaque alimentation série des quadripoles la sécurité sera obtenue par un contrôleur de débit liquide "ELETTA"
Nota
Chaque section sera d'environ 2 mètres et entièrement equipée.
Toutes les alimentations et les asservissements seront collétés et raccordés soit à la section suivante soit au chemin de cables
L'alimentation des quadripoles sera raccordée entre sections par un raccord souple en tresse

FIG. 3

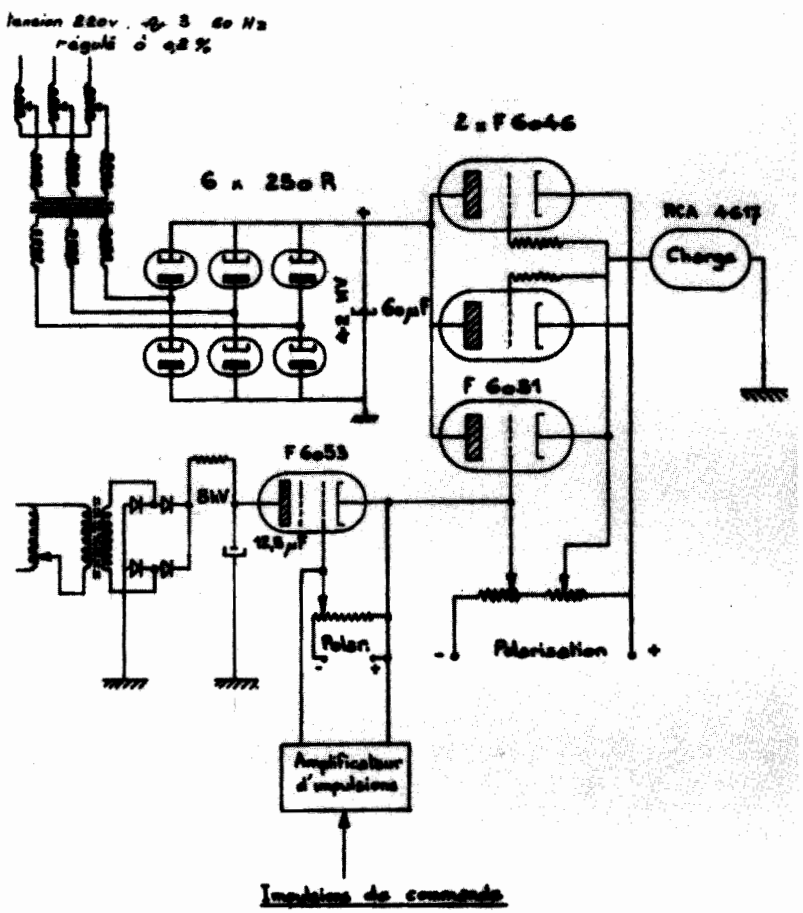

FIG. 4 Schéma du modulateur pour tube RCA 4617

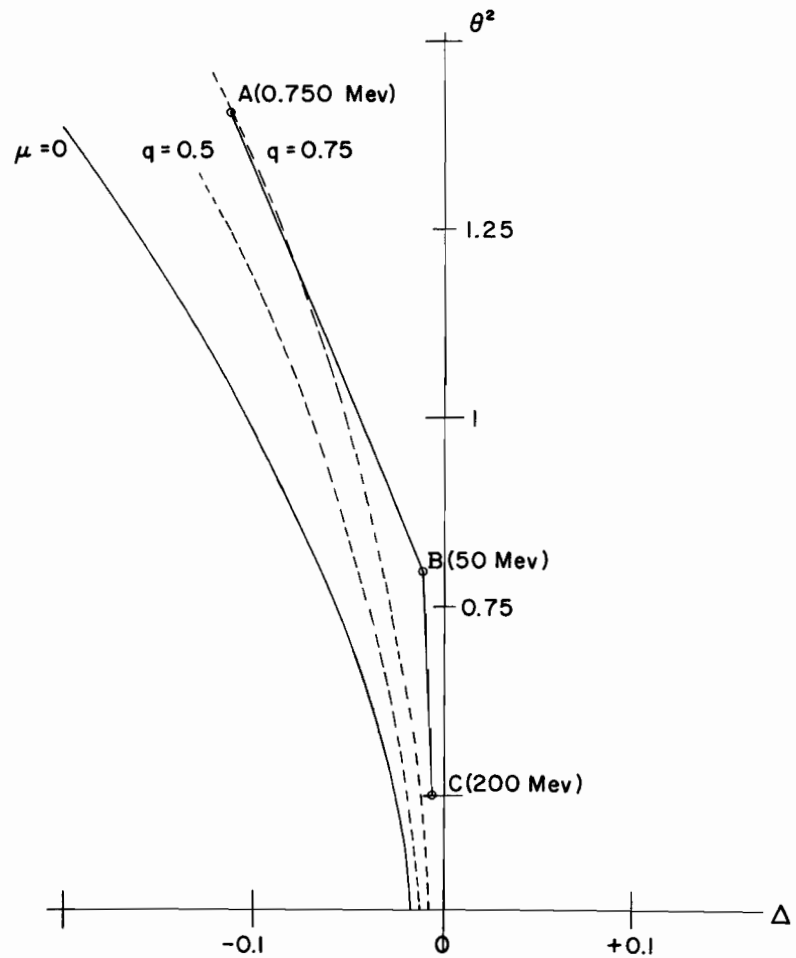

FIG. 5 DIAGRAMME DE STABILITÉ
ABC points de fonctionnement

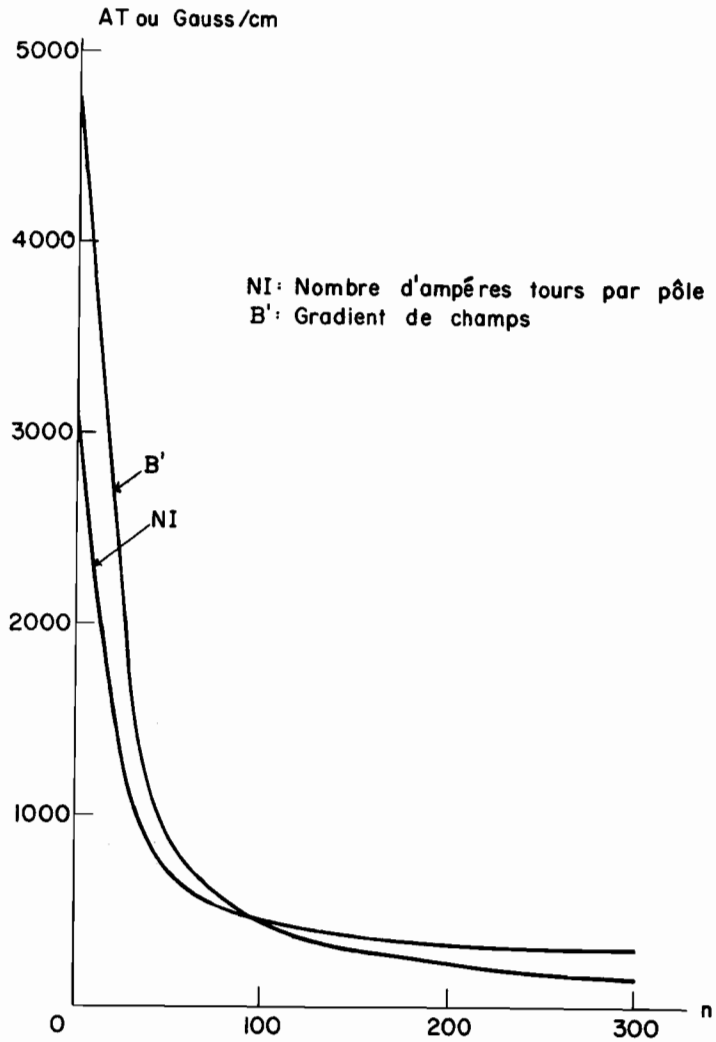

FIG. 6 Nombre d'ampéres tours par pôle et gradient de champ

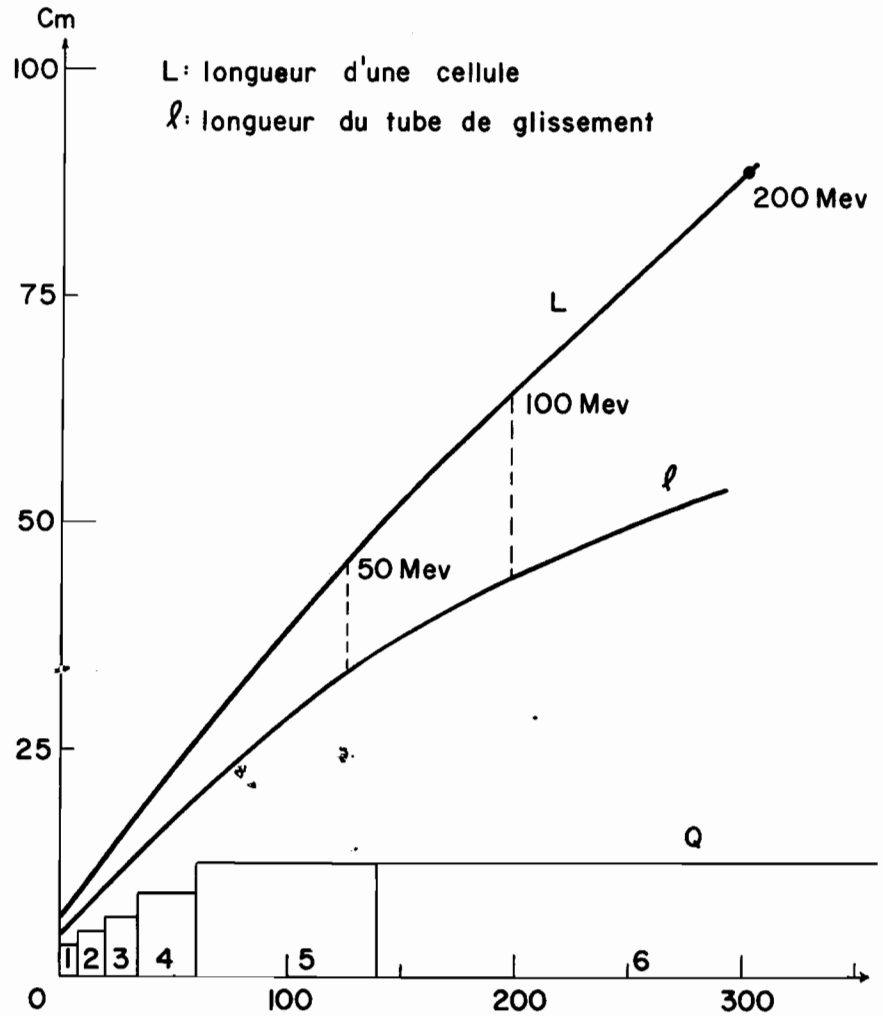

FIG. 7 Caracteristiques dimensionnelles de l'accelerateur

Type de section	Type I		Type II		Type III	Type IV
Type de bobine	Type 1	Type 2	Type 3	Type 4	Type 5	Type 6
Numéro de quadrupole	1 à 10	11 à 20	21 à 34	35 à 40	41 à 140	141 à 285
Type de Fil	creux $6x6mm^2$ $\phi 4mm$	creux $6x6mm^2$ $\phi 4mm$	plein $1x4mm^2$	plein $1x4mm^2$	plein $1x4mm^2$	plein $1x4mm^2$
Nombre de tours	5	5	80	80	60	40
Epaissaur. acier	3cm	4,5cm	6,5cm	9cm	13cm	13cm
Resistance 4 bob. en seria			0,420 Ω	0,52 Ω	0,368 Ω	0,224 Ω
Densité de courant	$\leqslant$ 27 A/mm^2	$\leqslant$ 15 A/mm^2	$\leqslant$ 5 A/mm^2	$\leqslant$ 3 A/mm^2	$\leqslant$ 2 A/mm^2	$\leqslant$ 2 A/mm^2
tension oux bornes			5 à 7,5 v	$\sim$ 6 v	2,5 à 5 v	$\sim$ 2 v

PARAMETRES DES QUADRUPOLES

Fig. 8

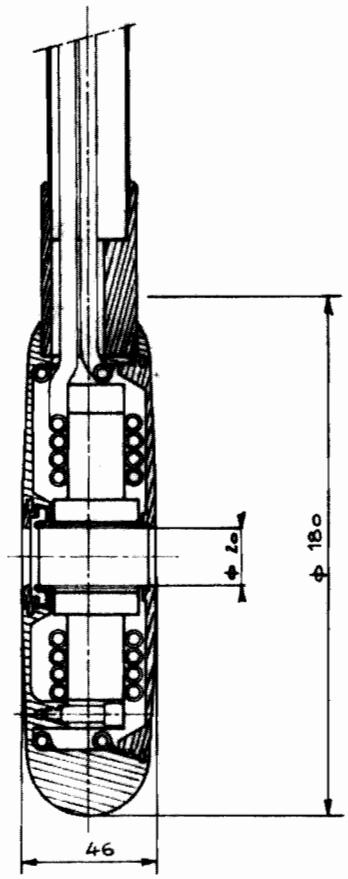

FIG. 9

PROJET JUPITER
Premier tube de glissement

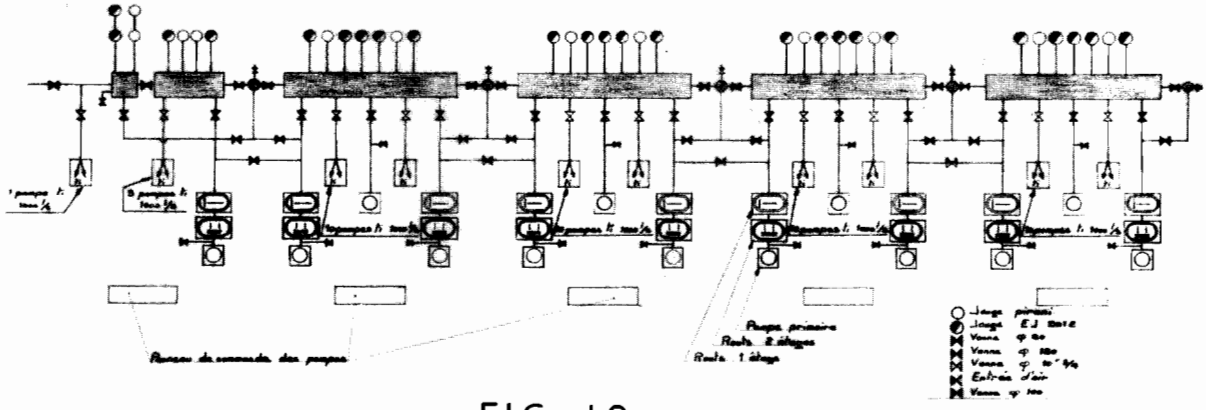

FIG. 10

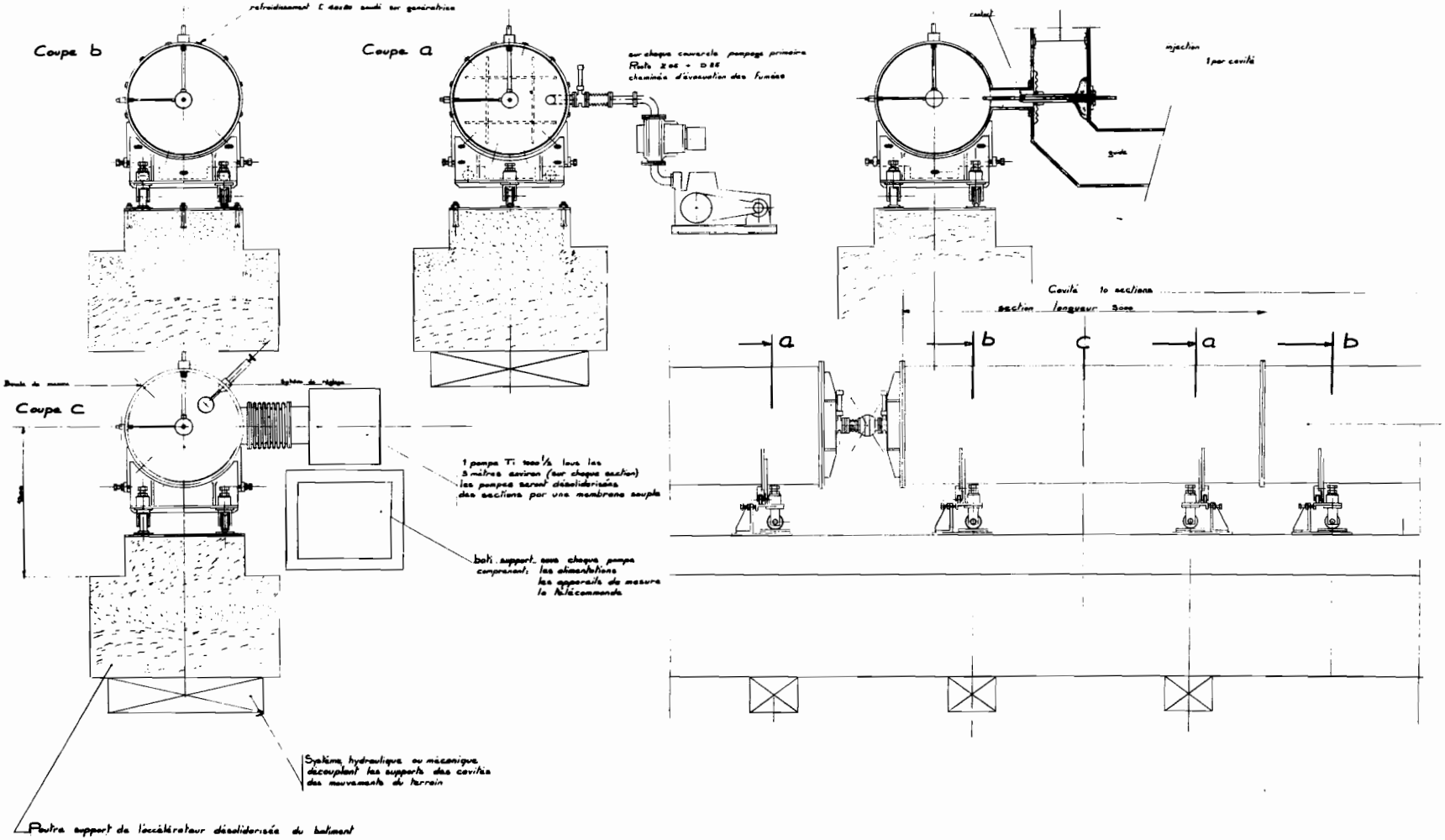
Coupe b
Coupe a
Coupe c
a
b
c
a
b
sur chaque couvercle pompage primaire
cheminée d'évacuation des fumées
cadre
injection
1 par cavité
Cavité 10 sections
section longueur
1 pompe
3 mètres environ (sur chaque section)
les pompes seront désolidarisées
des sections par une membrane souple
bâti support sous chaque pompe
comprenant: les alimentations
les appareils de mesure
la télécommande
Système hydraulique ou mécanique
découplant les supports des cavités
des mouvements du terrain
Poutre support de l'accélérateur désolidarisée du bâtiment

FIG. 11

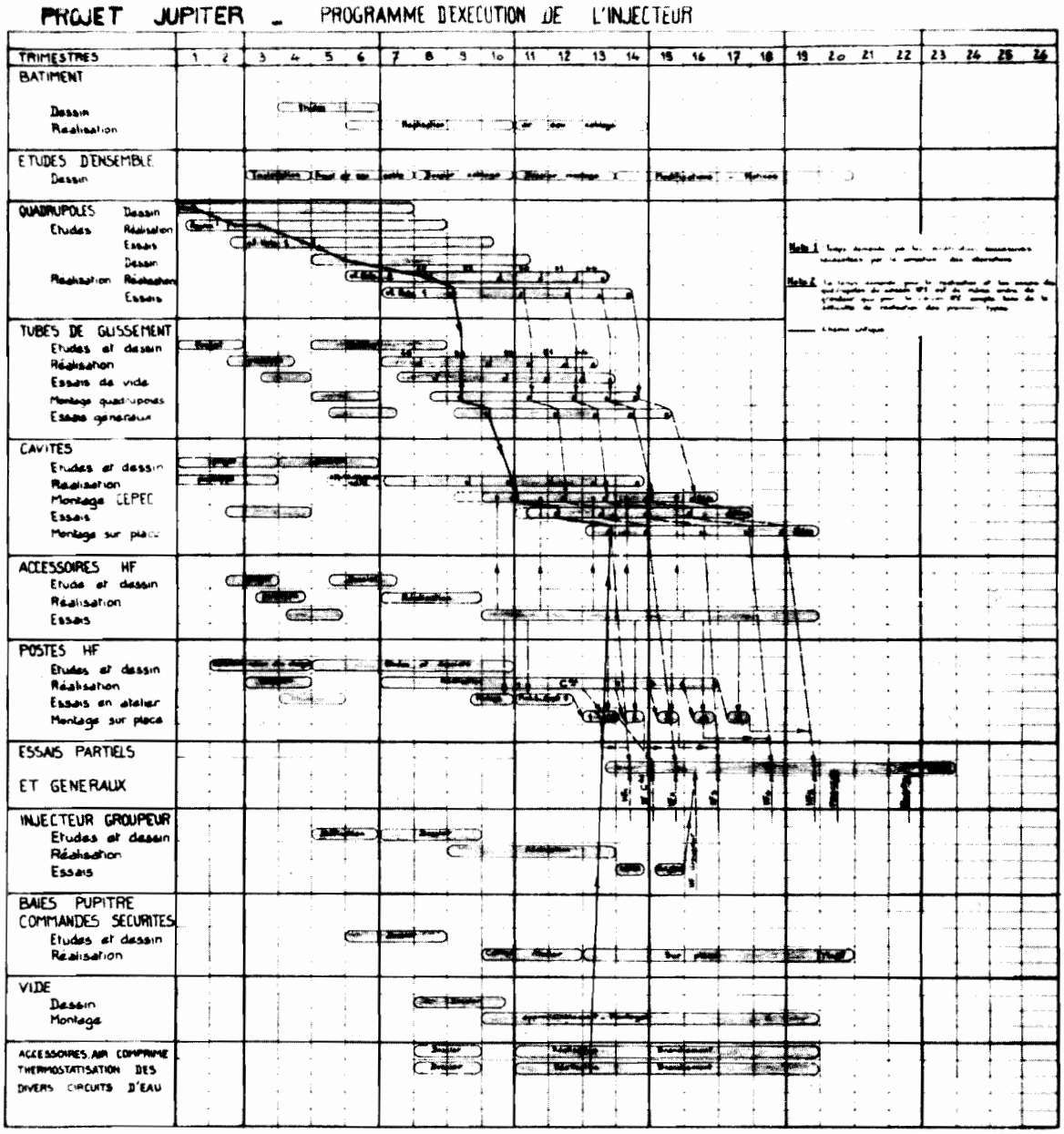
PROJET JUPITER - PROGRAMME D'EXECUTION DE L'INJECTEUR
TRIMESTRES
1 2 3 4 5 6 7 8 9 10 11 12 13 14 15 16 17 18 19 20 21 22 23 24 25 26
BATIMENT
Dessin
Réalisation
ETUDES D'ENSEMBLE
Dessin
QUADRUPOLES
Etudes
Dessin
Réalisation
Essais
Dessin
Réalisation
Réalisation
Essais
TUBES DE GLISSEMENT
Etudes et dessin
Réalisation
Essais de vide
Montage quadrupoles
Essais généraux
CAVITES
Etudes et dessin
Réalisation
Montage CEPEC
Essais
Montage sur place
ACCESSOIRES HF
Etudes et dessin
Réalisation
Essais
POSTES HF
Etudes et dessin
Réalisation
Essais en atelier
Montage sur place
ESSAIS PARTIELS
ET GENERAUX
INJECTEUR GROUPEUR
Etudes et dessin
Réalisation
Essais
BAIES PUPITRE
COMMANDES SECURITES
Etudes et dessin
Réalisation
VIDE
Dessin
Montage
ACCESSOIRES AIR COMPRIME
THERMOSTATISATION DES
DIVERS CIRCUITS D'EAU

FIG. 12

DRIFT TUBE AND PARAMETER SELECTION FOR LINEAR ACCELERATOR STRUCTURES BELOW 150 MEV

D. E. Young
Midwestern Universities Research Association

With three linac proposals being submitted to the USAEC this year, the question has arisen whether money could be saved by cooperation between the different groups. Savings could be realized in research and design, engineering, and in procuring similar items in greater quantities. Since each of these linacs have different basic design parameters such as the duty factor, beam current, energy, etc., the question arises whether a common design is really feasible. Certainly below 200 MeV where a drift tube loaded Alvarez structure is proposed there are many similarities. However, if one looks at the basic parameters which are to be met by each and tries to fit a common design to these parameters, one soon realizes that this is not possible. Wheeler has looked at this problem in detail[1] and concludes that if LASL agrees to derate their power supply so as to require an additional power module for the extra tank needed, which is the same as having the capability of accelerating a larger current but not doing so, and which of course would raise the cost of their proposal, then a common design is possible. If all three linacs were built, the saving in the common design might more than offset the added cost to LASL. I do not want to get too involved in this question. Rather I would like to point out that it is still possible to meet the basic parameters of each laboratory without adding greatly to fabrication costs if decisions can be reached on drift tube and tank structures which are fabricated of similar modules.

In order to reach agreement between the different laboratories on drift tube shapes, a committee was formed whose purpose was to try to enumerate the problem areas in adopting a particular drift tube shape and to try to expedite work in these areas. This committee made certain recommendations which I shall relate and work is proceeding in other areas. Since the committee was formed, its activities have been extended to a selection of parameters for the 200 Mc portion of the linac. If agreement can be reached, then savings should be realized in design and in larger volume purchases of similar components.

So far, the following recommendations have been made by the drift tube subcommittee:

1. Since sparking is mostly confined to the first gaps in operating linacs, it is desirable to design a short first section which can

be operated at reduced gradients. At 750 keV an average gap field of 8 MV/m or less should prevent excessive sparking for conventional shaped drift tubes. Above 10 MeV an average gap field of 12 to 13 MV/m is considered conservative.

2. An operating frequency of 201.25 Mc should allow design requirements to be met and give minimum interference with existing FCC allotted bands.

3. A drift tube hole of 2 cm has been achieved in the first drift tube at 0.75 MeV with a dc quadrupole and without unduly affecting the radial transit time factor. A linear increase from this size up to 4 cm at 200 MeV is recommended.

4. Satisfactory dc quadrupoles for drift tubes have been built and could be used in future design without major modifications.

5. A single drift tube stem is adequate even though a large diameter is required to accommodate four cooling leads.

6. The current computer programs for the calculation of drift tube shapes are sufficiently accurate so that extensive modelling is unnecessary.

7. Cylindrical shaped drift tubes at the higher energies can be chosen which are not far from an optimum shape and which, in addition, can be more easily fabricated.

In order to choose a drift tube shape, it is necessary to arrive at figures concerning the cost of rf power, the cost per unit length of the linac, the diameter of drift tubes which allow quadrupoles and adequate cooling, the maximum value of the accelerating rf gradients, the operating costs of the linac, as well as many other interacting requirements. In the months ahead many of these items will be better evaluated. To attempt to optimize the rf structure, including drift tube shape, clearly requires these considerations to be adequately assessed. However, even with the present knowledge it is instructive to understand the way these parameters affect the structure.

The total cost for building and operating a linac in terms of the power and length may be written as:

$$C = C_f + C_p P + C_{op} P t + C_L L + C_{oL} L t$$

where:

C_f = fixed costs
C_p = power costs per unit of power
C_{op} = power operating cost per unit of power per unit time
C_L = length costs per unit length
C_{oL} = length operating cost per unit length per unit time

A great deal of effort is being expended on an evaluation of the cost coefficients at the present time. The operating cost coefficients are difficult to assess, but after some searching through records of laboratories with operating linacs, we have found that if one takes $t = 10$ years, a possible lifetime of such a linac, then (within the error of determining these coefficients):

$$C_p \approx C_{op}\, t$$
$$C_L \approx C_{oL}\, t \ .$$

Now rewriting the formula in such a way as to give prominance to the factors which influence the structure

$$\frac{C - C_f}{2} = C_p P + C_L L$$

with the power P per energy gain ΔW given by

$$\frac{P}{\Delta W} = \frac{E_o T}{Z T^2 \cos\varphi}$$

and the length L per energy gain by

$$\frac{L}{\Delta W} = \frac{1}{E_o T \cos\varphi}$$

where E_o is the average peak axial accelerating field, T the longitudinal transit time factor, and φ the stable phase angle. In practice the power has to be increased, (a) to allow for losses on drift tube stems, tuners, and end plates as well as additional losses accounting for a lower Q value than the calculated value , and (b) reserve power to take care of beam loading. The power will be increased by a factor k to take care of the former, and a term $C_p I_B \Delta W$ added to allow for a beam I_B. With these considerations, the cost formula becomes:

$$\frac{C - C_f}{2} = \frac{C_p k E_o T \Delta W}{Z T^2 \cos\varphi} + C_p I_B \Delta W + C_L \frac{\Delta W}{E_o T \cos\varphi}$$

or

$$\frac{1}{\Delta W}\left[\frac{C - C_f}{2}\right] - C_p I_B = C_p\left[\frac{k E_o T}{ZT^2 \cos\varphi}\right] + C_L\left[\frac{1}{E_o T \cos\varphi}\right]$$

where the terms on the right are related to the choice of geometry. For any particular description of the geometry which specifes a value for Z and T, a cost can be calculated. The lowest cost will correspond to the largest value of Z and T. However, this alone does not allow one to choose a geometry that will allow the desired accelerating gradient to be achieved without excessive sparking. An accelerating gradient which will minimize this cost equation can be determined and is given by

$$E_o = \left[\frac{Z\, C_L}{k\, C_p}\right]^{1/2} .$$

This value of E_o is shown plotted in Fig. 1 as a function of Z. For any description of the geometry which gives a value of the shunt impedance Z, the value of E_o can be determined which gives a cost minimum. However before this information can be used in linac design, it is necessary to know what gradient can be maintained without problems due to sparking. Attempts are now being made to set safe sparking limits by accumulating data on operating linacs and by experimental measurements on a sparking cavity at this laboratory. Some preliminary results on the sparking cavity will be mentioned later. In the absence of a suitable explanation of sparking, one can use a value for the maximum field on the surface, such as the Kilpatrick criteria.[2] The MURA field computational program, MESSYMESH, can calculate the maximum value of the field on the surface of a drift tube. Actually what is calculated is a factor α, where

$$\alpha = \frac{E_{max}\ \text{(on surface)}}{E_o} .$$

For some peak value on the surface, the value E_o can be calculated for the geometry considered. This value of E_o may be less than the optimum value of E_o obtained from the cost function for that particular geometry. If this is so, then to go to the optimum value would clearly cause maximum fields in excess of the chosen peak value on the surface and a danger of sparking. However, if it turns out that this value is greater than the optimum E_o, then sparking is not a problem because power is too expensive to go to the sparking level anyhow.

Using the MURA field computational program, we have investigated nearly 2000 different geometries for cylindrical shaped drift tubes. A

large number of runs have been done at energies of 50, 100, 150, and 200 MeV. When these runs are evaluated using the cost formula, it is possible to choose an optimum set of parameters that describe the geometry. This optimizing procedure using a specified value of the maximum field on the surface was described at the Yale Linac Conference.[3] If each run is plotted on the Z, E_0 diagram with the value Z corresponding to the geometry and the value E_0 calculated on the basis of an upper limit for the maximum field on the surface, one can observe the importance of the sparking restriction. At 50 MeV the cluster of points lie to the left of the curve of optimum gradient; at 100 MeV the cluster of points lie closer to the curve; and as the energy increases, the cluster moves closer to the curve. At 50 MeV, clearly money can be saved by raising the gradient to more nearly approach the optimum. At the higher energies where the value of Z is lower, it is not as definite and depends on the diameter of the drift tube which may be specified from engineering considerations.

Any practical drift tube must allow space for quadrupoles and cooling. This places an additional restriction on the diameter of a drift tube. Our studies indicate that a diameter of 15 or 16 cm is necessary especially for a high duty factor linac at energies of about 200 MeV. The latest popular cost data indicate that this diameter is a departure from the cost minimum and that it is unwise from sparking considerations to raise the accelerating gradient to the optimum value. However, it should be pointed out that the cost minima are rather flat so that the departure from the minimum may not be a great penalty. When one considers raising the gradient to reduce cost, one must also consider the limitation on the power amplifier tube. A shorter linac with a greater multiplicity of tanks and power amplifier tubes, phasing systems, and poorer reliability may not be a suitable way to save money.

When the specifications of the 200 Mc linacs at the three laboratories are considered, it is found possible to arrive at a design which uses many similar components. In particular, it is possible to maintain a constant drift tube diameter from 50 or 60 MeV upwards. Thus cylindrical drift tubes could be fabricated out of stock material with similar end caps. Quadrupoles might also be alike. The tank diameters can be similar, although of different lengths. By mass procurement of these similar components or pieces overall cost reductions can be realized when two or more linacs are constructed simultaneously without the necessity of requiring a departure from the basic design parameters.

To gather more information on the sparking restriction we have fabricated a one unit-cell cavity, with movable end plates so that geometry from 5 MeV to 150 MeV can be investigated under full power conditions.

This cavity is driven by an RCA 2515E (2041) power amplifer capable of approximately 300 kW at pulse lengths of about 500 μsec and about 30 pulses per second, and at a frequency of 200 Mc. Our initial operation was at 50 MeV with a drift tube diameter of 16 cm, 3 cm hole, and 4 cm curvature on the outer corner (the cavity diameter is 79 cm). At the present time we have operated up to 125 kW in the cavity. This power level corresponds to an average accelerating gradient (E_o) of 2.7 MV/m, an average gap field of 10 MV/m, or a peak field on the surface of 16 MV/m. At this level there was not a single spark detected, it was just a matter of running the power up. We are now trying to get more power out of the power supply to go to a level where we can see a few sparks. However, the next step will be to go to 5 MeV where sparks should occur at a lower power level. Here hopefully we can study the phenomena.

WHEELER: This type of expression for cost, which both Don and I have used, leaves out a very important consideration especially for the injectors, that is, there is nothing in the equation which says anything about the reliability of the accelerator. The constant k, which comes from experience, can be used to contribute to the reliability and one should consider very seriously keeping k a fairly large number. Experience with most of the proton linacs to date certainly shows that they have been underpowered. By increasing k one can design for lots of reserve power and this of course will greatly improve the reliability. The other matter is the choice of E_o with respect to sparking limit. In the MURA sparking cavity I am told that the x-ray background at the 125 kW level is rising very rapidly and I would predict that, at 16 MV/m on the surface, you are very close to the sparking limit. We have observed in the heavy ion machine that the x-ray background rises very steeply just before the sparking level is reached. So again in terms of reliability for the machine, one should be very conservative in keeping the value of the maximum field safely below the sparking limit. These two factors are very important in terms of achieving highly reliable machines.

LEISS: People have been using cost formulas for years and have systematically left out what is really in many projects the biggest cost of all, that is the project salaries. Have you thought how to integrate some of this into guessing what is the best to do? This would be particularly advantageous, although difficult, if examining the desirability of a common design.

YOUNG: The rules are becoming clearer now on how you estimate cost, even the salary costs. MURA has a technical note on their experience on

cost estimation and other people have discussed these things with the AEC to see how salaries should be integrated into the total project cost. This has not been put into the cost formula used here; this is a bigger operation research project than has been undertaken so far.

HUBBARD: As Wheeler pointed out, when you get somewhere near the sparking limit, you get a large amount of x-rays out of the machine which you must shield against. If you just lower the gradient slightly, the x-rays go down rapidly. Have you given any consideration to the amount of shielding necessary if you operate close to the sparking limit or have you put this into the cost formula?

YOUNG: We have not put the cost of shielding into the cost formula as a function of the gradient, only the cost of shielding as a part of the building costs which is part of the length costs. We intend, however, to make some measurements on the sparking cavity of the radiation background as a function of the voltage across the gap. We would like to get some good values for these quantities.

FEATHERSTONE: For the benefit of those of you who have not been paying close attention to the argument about sparking, I would just like to say a couple of words that I think should be repeated again and again. Mr. Kilpatrick wrote his "criterion", as it is so often referred to, in an attempt to integrate a great deal of data from many different sources and to account for it in an approximate way. I do not believe that he himself has ever given it the degree of authority that one would think it had by listening to the use of "Kilpatrick's criterion." Second, it was not intended as a working upper limit, but rather as a threshold level below which no sparking at all is expected to occur. Third, at 200 Mc a great many of the terms of his equation drop out and one arrives at something which is related only to the maximum field strength at the surface of the electrode. I think there is an accumulating body of evidence which indicates this is not adequate to account for the sparking we have observed in practical machines. I am very glad to hear Don say that they are going to try the spark cavity down in the equivalent of the 5 MeV energy region. What was the equivalent energy range of the present drift tube size?

YOUNG: 50 MeV.

FEATHERSTONE: The experience with the Brookhaven and Argonne linacs suggests strongly that something different is going on at the low energy end of the machine where there seem to be lower gradients and more sparking than at the high energy end. I don't think the gradient alone is enough to account for what we see. Of course, everybody knows

that sparking is affected by surface conditions and vacuum quality, but we presume that the surface conditions and vacuum conditions are pretty uniform from end to end.

REFERENCES

1. G. W. Wheeler, "The Unified Drift Tube Linac", Yale University Internal Report, G.W. 16 (June 3, 1964).

2. W. D. Kilpatrick, "A Criterion for Vacuum Sparking Designed to Include Both RF and DC", UCRL-2321 (1953).

3. D. E. Young, "Drift Tube Structures", Minutes of the Conference on Proton Linear Accelerators at Yale University (1963).

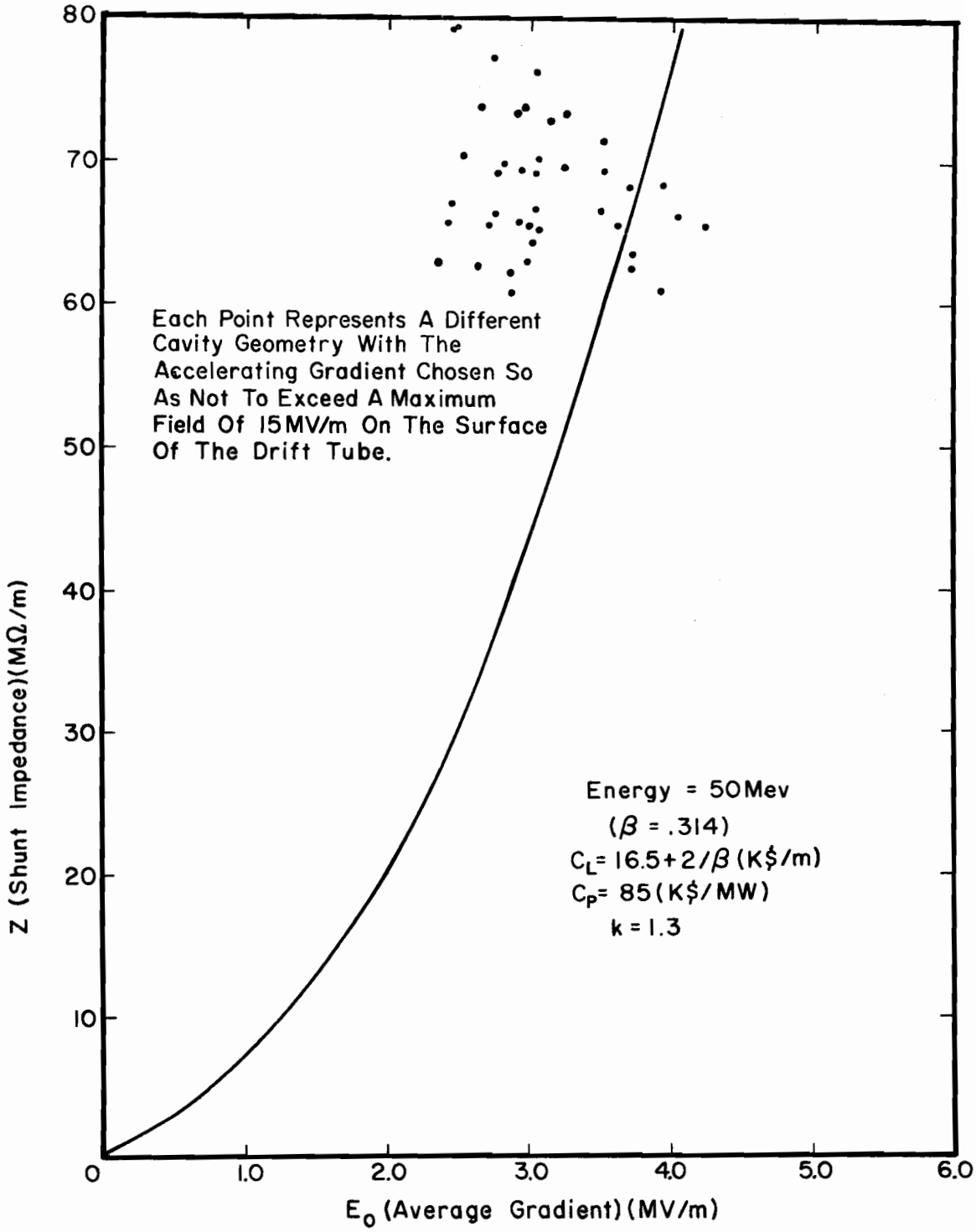

OPTIMUM ACCELERATING GRADIENT AS A FUNCTION OF SHUNT IMPEDANCE AT 50 MEV

Fig. 1

TRANSVERSE BEAM BLOW-UP IN STANDING WAVE LINACS

R. L. Gluckstern
Yale University and Brookhaven National Laboratory

I. Introduction

The phenomenon of beam blow-up in traveling wave electron linear accelerators[1] has caused concern as one has attempted to increase the beam current and pulse length. Among the explanations of the observed phenomenon is one presented by Wilson[2] in analogy with the theory of backward wave oscillators for accelerating-type fields. This explanation suggests that means exist to reduce the serious consequences of the blow-up by modifying the synchronism of the beam and backward wave deflecting mode. The effect discussed by Wilson takes place for bunched or unbunched beams.

A similar concern has been expressed by Leiss and Schrack[3] who point out that a bunched beam may have a harmonic which resonates with that component of the deflecting mode traveling with the beam velocity. For conventional iris-loaded guides, the deflecting mode frequency band is approximately 50% above that for the accelerating mode. If the beam bunching is, for example, at the 4th subharmonic of the accelerating mode (as it is at present for the AGS improvement program), then the 6th harmonic of the beam will be approximately resonant with the deflecting mode. This phenomenon clearly depends on the details of the mode spectrum for different values of β and can probably be influenced by transverse focusing and by perturbation of the deflecting modes where necessary.

The present work is an attempt to formulate the two corresponding effects for the case of a standing wave accelerator (proton linac in the case of the AGS improvement program). We will not treat here the additional serious effect of beam loading on the accelerating mode. (In this case the steady state effect can presumably be compensated for by adjusting the power source to supply additional power at high beam currents; the transient effect will require beam injection while the fields are rising in an appropriate way.)

II. Cavity Fields

We shall consider an iris-loaded guide of length $L = NL_o$, where L_o is the cell length, as shown in Fig. 1. The deflections will be assumed to be confined to the x - z plane, where z is taken as the longitudinal direction. In this plane the jth normalized standing wave

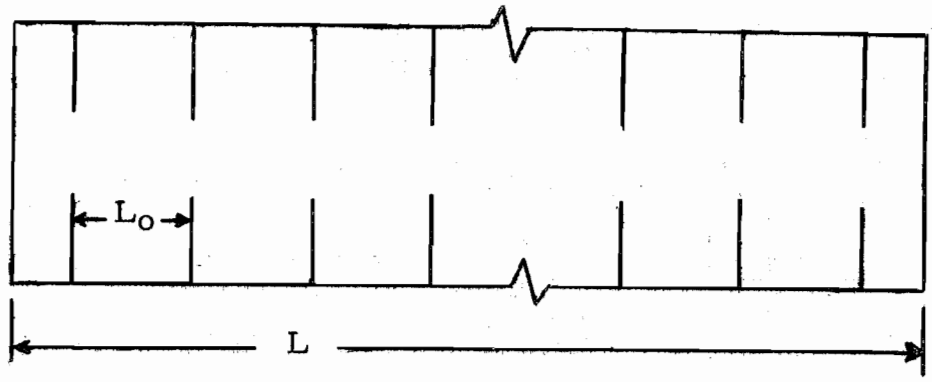

Fig. 1

deflecting mode can be written, because of Floquet's theorem, as

$$E_x^j\,(x, o, z) = \sum_{n=o}^{N-1} P_{jn}\,(x) \sin k_{jn} z\,,$$

$$H_y^j\,(x, o, z) = \sum Q_{jn}\,(x) \cos k_{jn} z\,, \qquad (2.1)$$

$$E_z^j\,(x, o, z) = \sum R_{jn}\,(x) \cos k_{jn} z\,,$$

where

$$k_{jn} = k_j + 2\,n\,\pi/L_o\,, \qquad k_j = j\,\pi/L\,. \qquad (2.2)$$

If we define the space harmonic of concern as that for $n = 0$, the important components of the fields in the vicinity of the axis may be written as

$$E_x^j \simeq P_j \sin k_j z$$

$$H_y^j \simeq Q_j \cos k_j z \qquad (2.3)$$

$$E_z^j \simeq x\,R_j \cos k_j z\,.$$

The fields are normalized such that

$$\nabla \times \vec{E}^j = (\omega_j/c)\,\vec{H}^j\,, \qquad \nabla \times \vec{H}^j = (\omega_j/c)\,\vec{E}^j\,,$$
$$\int dv\, \vec{E}^i \cdot \vec{E}^j = \int dv\, \vec{H}^i \cdot \vec{H}^j = \delta_{ij}\,, \tag{2.4}$$

and the actual fields are written in terms of the normalized fields as

$$\vec{E} = \sum_j C_j(t)\, E^j(\vec{x})\,, \qquad \vec{H} = \sum_j D_j(t)\, H^j(\vec{x})\,, \tag{2.5}$$

where C_j and D_j are related in the absence of beam by

$$D_j = (\epsilon c/\omega_j)\,\dot{C}_j\,, \qquad C_j = -(\mu c/\omega_j)\,\dot{D}_j\,. \tag{2.6}$$

Relations can be obtained between P_j, Q_j, R_j via Maxwell's equations. One must, however, take into account the component H_z in obtaining these relations, since the modes are not purely TE or TM, but are hybrid modes.[4] Let us write:

$$Q_j = F_j R_j\,, \qquad P_j = K_j R_j\,. \tag{2.7}$$

In the presence of a current pulse of the form

$$\vec{J}(\vec{x}, t) = \int_{-\infty}^{\infty} \vec{j}(\vec{x}, \omega)\, e^{i\omega t}\, d\omega \tag{2.8}$$

it can be shown that $C_j(t)$ satisfies a differential equation whose solution can be written in the form

$$C_j(t) = \frac{-i}{\epsilon}\int d\omega\, \frac{\omega e^{i\omega t}}{\omega^2 - \omega_j^2} \int \vec{j}(\vec{x}, \omega)\cdot E^j(\vec{x})\, dv\,. \tag{2.9}$$

The poles are moved into the upper half ω-plane because of losses. Assuming the losses to be small, one can write for late times (after the beam pulse has passed through the cavity)

$$C_j(t) = -(\pi/\epsilon)\left[e^{i\omega_j t}\int \vec{j}(\vec{x}, \omega_j)\cdot \vec{E}^j\, dv + c.c.\right]$$
$$\equiv -(\epsilon c)^{-1} D_j \cos(\omega_j t + \phi_j)$$
$$D_j(t) = -\pi c\left[i\, e^{i\omega_j t}\int \vec{j}(\vec{x}, \omega_j)\cdot \vec{E}^j\, dv + c.c.\right] \tag{2.10}$$
$$\equiv D_j \sin(\omega_j t + \phi_j)\,.$$

In the presence of losses these fields will decay at the rate

$$e^{-\frac{\omega_j}{2Q_j} t} . \tag{2.11}$$

The transverse angular impulse given to a particle entering the cavity at $t = t_m$ in the presence of deflecting fields can be calculated in the approximation that the trajectory is along the longitudinal axis. One then has

$$\Delta \theta_x = (e/pv) \int_0^L dz \left[E_x - \mu v H_y\right]_{t = t_m + z/v}$$

$$= (e/\epsilon pc) \sum_j \omega_j^{-1} \int_0^L dz\, R_j \cos k_j z\, D_j \sin(\omega_j z/v + \psi_j) , \tag{2.12}$$

where

$$\psi_j = \omega_j t_m + \phi_j . \tag{2.13}$$

Since one is interested only in those modes for which k_j and ω_j/v are almost equal (phase velocity of deflecting mode approximately the same as beam velocity), one may write

$$\Delta \theta_x \cong (eL/\epsilon pc) \sum_j (\omega_j \alpha_j)^{-1} D_j R_j \sin(\alpha_j/2) \sin(\psi_j - \alpha_j/2) , \tag{2.14}$$

where

$$\alpha_j \equiv (k_j - \omega_j/v) L \tag{2.15}$$

is the slip of beam relative to the wave in its transit through the cavity. If one adds angular impulses due to all effects, the beam will be lost when

$$\Lambda_x \Delta \theta_x \sim 2 \pi a , \tag{2.16}$$

where Λ_x is the wavelength of the transverse oscillation and a is the bore radius.

The remaining quantity needed for our analysis is $\vec{j}(\omega)$. Assuming a single bunch of spatial dependence f (z) (symmetric about z = 0

for convenience) whose center follows the trajectory $z = vt$, $x = x(t)$, one has

$$\vec{J}(\vec{x}, t) = I_o \Delta t\, \delta\left[x - x(t)\right]\, \delta(y)\, f\left[z - v(t - t_m)\right] \left[\vec{i}\,\dot{x}(t) + \vec{k}\, v\right]$$

where $\Delta t = 2\pi / \omega_o$ is the separation of beam bunches and I_o is the average current. Writing

$$f(u) = \frac{1}{2\pi v} \int d\omega\; e^{-i\frac{\omega}{v}u}\, g(\omega), \quad g(\omega) = \int_{-\infty}^{\infty} du\; e^{i\frac{\omega}{v}u}\, f(u) \tag{2.17}$$

one finds, for narrow bunches,

$$\vec{j}(\vec{x}, \omega) = \frac{I_o}{\omega_o}\, g(\omega)\, \delta\left[x - x(t_m + z/v)\right]\, \delta(y)\left[\vec{i}\,\dot{x}(t_m + z/v)/v + \vec{k}\right] e^{-i\omega t_m - i\omega z/v} \tag{2.18}$$

The normalization is such that for a delta function bunch $g(\omega) = 1$; that is, $g(\omega)$ is the relative harmonic content of the beam pulse. The relevant integral in (2.10) is therefore

$$\int \vec{j}(\vec{x}, \omega_j) \cdot \vec{E}^j\, dv =$$

$$(I_o/\omega_o v)\, g(\omega_j)\, e^{-i\omega_j z/v} \left[\dot{x}(t_m + z/v)\, E_x^j(x(t_m + z/v), 0, z) + \right.$$
$$\left. + v\, E_z^j(x(t_m + z/v), 0, z)\right] \tag{2.19}$$

In the limit of small transverse displacements, one then finds from (2.3), (2.7):

$$\int \vec{j}(\vec{x}, \omega_j) \cdot \vec{E}^j\, dv =$$

$$(I_o/\omega_o)\, g(\omega_j)\, e^{-i\omega_j t_m}\, R_j \int_o^L dz\, e^{-i\omega_j z/v} \left[K_j(\dot{x}/v) \sin k_j z + \right.$$
$$\left. + x \cos k_j z\right] \simeq (I_o/2\omega_o)\, g(\omega_j)\, e^{-i\omega_j t_m}\, R_j \int_o^L dz\, e^{i\alpha_j z/L}$$
$$\left[x(z) - K_j\, i x'(z)\right] . \tag{2.20}$$

III. Nonresonant Beam Blow-up

If one considers that the beam has transverse displacement and velocity unaffected by the cavity fields in calculating the contribution to (2.20), then the contribution of successive bunches will depend on their relative phase, and build-up will be serious only if there is a resonance between a beam pulse harmonic and a defelcting mode. This phenomenon is treated in Section IV. If no resonance exists, one must consider the effect of the field itself on the trajectory in order to get a significant contribution to (2.20). This is the effect considered by Wilson, and the one we shall treat in Section III for a standing wave linac.

In order to evaluate (2.20), we must find the trajectory of that particle entering the cavity which is oscillating with fields

$$\begin{aligned} C_j(t) &= -(\epsilon c)^{-1} D_j \cos(\omega_j t + \phi_j) \\ D_j(t) &= D_j \sin(\omega_j t + \phi_j), \end{aligned} \tag{3.1}$$

at the time t_m. According to (2.12) one has

$$\Delta\theta_x = x'(z) = (e/pv)\int_0^z dz \left[E_x - \mu v H_y\right]_{t = t_m + z/v} . \tag{3.2}$$

Keeping only those wave components traveling at approximately the same velocity as the particle, one finds

$$x'(z) \simeq -\sum_k (e/\epsilon p c \omega_k)\left\{\left[D_k(t_m + z/v) E_x^k\right]_0^z - \int_0^z dz\, D_k(t_m + z/v)(\partial E_z^k/\partial x)\right\}$$

$$\simeq (e/2\epsilon pc)\sum_k (D_k R_k/\omega_k)(L/\alpha_k - K_k)\left[\cos(\alpha_k z/L - \psi_k) - \cos\psi_k\right], \tag{3.3}$$

$$x(z) = (e/2\epsilon pc)\sum_k (D_k R_k/\omega_k)(L/\alpha_k - K_k)(L/\alpha_k)\left[\sin(\alpha_k z/L - \psi_k) + \sin\psi_k - (\alpha_k z/L)\cos\psi_k\right], \tag{3.4}$$

where

$$\psi_k = \omega_k t_m + \phi_k . \tag{3.5}$$

The nonresonant character of the values of t_m implies that only the $e^{i\psi_k}$ component of (3.3) and (3.4) is needed with the factor $e^{-i\omega_j t_m}$ in (2.20). In this approximation one has

$$\int \vec{j}\cdot\vec{E}^j\,dv = (e\,I_o/8\omega_o\epsilon\,pc)\,g(\omega_j)\sum_k e^{i(\omega_k-\omega_j)t_m+i\phi_k}(D_kR_jR_k/\omega_k)(L/\alpha_k - K_k)$$

$$\times\int_o^L dz\,e^{i\alpha_j z/L}\left[(L/\alpha_k)(i\,e^{-i\alpha_k z/L} - i - \alpha_k z/L) - K_j\,i\,(e^{-i\alpha_k z/L} - 1)\right]$$

$$\equiv \sum_k M_{jk}\,e^{im_{jk}}\,e^{i(\omega_k-\omega_j)t_m}\,D_k\,e^{i\phi_k}, \qquad (3.6)$$

where M_{jk} and m_{jk} are the amplitude and phase of all the factors not appearing explicitly in the last form of (3.6). From (2.10), the pulse entering at t_m contributes an increment to the field already present, which is given, including the decay of the field already present, by

$$\Delta D_j(t) \cong 2\pi c \sum_k D_k M_{jk} \sin\left[\omega_j t + (\omega_k - \omega_j)t_m + \phi_k + m_{jk}\right]$$

$$- (\omega_j \Delta t/2\,Q_j)\,D_j \sin(\omega_j t + \phi_j)\,. \qquad (3.7)$$

This is our result. It is, of course, dependent on the mode spectrum (ω_j vs j), the timing of the pulses* (t_m), the slip (α_j vs j), and all the other nonexponential factors appearing in M_{jk}. Particularly in cases of low group velocity (ω_k close to ω_j), one should proceed directly from (3.7) on a numerical basis.

We shall try to reduce (3.7) analytically by making further assumptions. In particular we shall assume a steady state solution for which the contributions for $k \neq j$ in (3.7) average to zero. In this case

$$\Delta D_j(t) = 2\pi c\,M_{jj}\,D_j \sin(\omega_j t + \phi_j + m_{jj}) - (\pi\omega_j/\omega_o Q_j)\,D_j \sin(\omega_j t + \phi)\,, \qquad (3.8)$$

---

*We have already assumed that the pulses are nonresonant and have ignored the term in $(\omega_k + \omega_j)\,t_m$. If they are resonant, the present considerations are modified by a factor of order 2.

which is equivalent to the relations

$$\frac{\Delta D_j}{D_j} = 2\pi c M_{jj} \cos m_{jj} - \frac{\pi \omega_j}{\omega_o Q_j} \tag{3.9}$$

and

$$\Delta \phi_j = -2\pi c M_{jj} \sin m_{jj} . \tag{3.10}$$

From (3.6), one finds

$$M_{jj} \cos m_{jj} = (e I_o/8 \omega_o \epsilon pc)\, g(\omega_j)\, (R_j^2/\omega_j)(L/\alpha - K)\, L$$

$$\times \operatorname{Re} \int_0^1 dx \left[i (L/\alpha - K)(1 - e^{i\alpha x}) - \alpha x e^{i\alpha x} L/\alpha \right]$$

$$= (e I_o/4 \omega_o \epsilon pc)\, g(\omega_j)\, (R_j^2/\omega_j)(L/\alpha - K)\, L/\alpha \left[L/\alpha\, (1 - \cos\alpha - \tfrac{\alpha}{2} \sin\alpha) - \right.$$

$$\left. - K (1 - \cos\alpha)/2 \right] . \tag{3.11}$$

In the approximation of small coupling holes it can be shown that

$$\frac{L}{\alpha} \gg K . \tag{3.12}$$

Equation (3.11) then becomes

$$M_{jj} \cos m_{jj} = (e I_o/2\pi^3 \omega_o \epsilon pc)\, g(\omega_j)(R_j^2/\omega_j)\, L^3\, g_2(\alpha_j) \tag{3.13}$$

where

$$g_2(\alpha) = \frac{1 - \cos\alpha - (\alpha/2)\sin\alpha}{2(\alpha/\pi)^3} \tag{3.14}$$

is the same function as that defined by Wilson, and has a maximum value of 1.04 when $\alpha = 2.65$.

The "starting current" for the beam blow-up is therefore given by the vanishing of (3.9), that is for

$$e I_o = \frac{\pi^3 \epsilon\, p\, \omega_j^2}{g_2\, g\, L^3\, R_j^2\, Q_j} . \tag{3.15}$$

The quantity $Q_j R_j^2$ is related to the ratio of the square of the electric field gradient along the axis to the power loss and therefore has the general form of a shunt resistance per unit length for the deflecting mode. Specifically, if one defines r_ℓ as

$$r_\ell = \frac{\left[(c/\omega_j)\int_0^L dz\,(\partial E_z^j/\partial x)\cos k_j z\right]^2}{L \times \text{Power Loss}}, \tag{3.16}$$

and notes that Q_j may be written as

$$Q_j = \frac{(\omega_j \epsilon/2)\int |\vec{E}^j|^2\, dv}{\text{Power Loss}} = (\omega_j \epsilon/2\ \text{Power Loss}) \tag{3.17}$$

one has

$$\frac{r_\ell}{Q_j} = L R_j^2 (c/\omega_j)^3 Z_o/2, \tag{3.18}$$

where

$$Z_o = \sqrt{\mu/\epsilon} = 377 \text{ ohms}. \tag{3.19}$$

This leads finally to

$$e I_o = \frac{\pi^3 Mc^2 (c/\omega_j)\beta\gamma}{2 g_2 g r_\ell L^2}. \tag{3.20}$$

As an illustration of the order of magnitude of (3.20), we shall apply it to the first iris cavity in the proposed new AGS injector where we use the following parameters:

$$\begin{aligned} Mc^2 &= 940 \text{ Mev} \\ 2\pi c/\omega_j &= 0.25 \text{ m} \\ \beta &= 0.6 \\ \gamma &= 1.25 \\ g_2 &\sim g \sim 1 \\ L &\sim 3 \text{ m} \\ r_\ell &\sim 20 \text{ megohms/m} \end{aligned} \tag{3.21}$$

leading to

$$I_o \simeq 2 \text{ amp}. \tag{3.22}$$

Several comments should be made at this time:

1) The value of r_ℓ has been chosen typical of accelerating modes. It will probably be considerably smaller since the square of a transit time factor should be included to correspond to the particular space harmonic used. This will lead to an even higher "starting current."*

2) Resonance between the deflecting mode and the beam bunch frequency will lead to a reduction of order of a factor 2 in (3.20) and (3.22).

3) If the current is higher than the limit in (3.20), the build-up time can be estimated from (3.9) with an assumption for the order of magnitude of the "noise" in the cavity. The result will be of the form

$$T_B = \frac{\text{Const.}}{I_o - I_{o,\,\text{starting}}} . \tag{3.23}$$

4) Although the present calculation is for a standing wave linac, the form of Wilson's result for a traveling wave linac can be obtained by going to the limit of large L in (3.6). The sum over k becomes an integral over k and a sum over beam pulses (m) leads to

$$\sum_m e^{i(\omega_k - \omega_j)m\Delta t} = 2\pi\, \delta\left[(\omega_k - \omega_j)\ \Delta t\right]$$

$$\cong \left(\frac{d\pi}{dk}\right)^{-1} \frac{\omega_o L}{\pi}\ \delta(k - j) = \frac{\omega_o L}{\pi v_g}\ \delta(k - j) . \tag{3.24}$$

The factor M_{jj} in (3.6) must then be multiplied by the factor $(\omega_o L/\pi v_g)$ and the self-consistent condition $\Delta D/D = 1$ leads to (3.20) multiplied by the factor $v_g Q_j/\omega_j L$. This factor, which is the ratio of the decay time to the filling time, is not surprising when one goes from a standing to a traveling wave linac. The net result for the starting current is an expression of the form

$$e\, I_o^{T.W.} \sim \frac{Mc^2 \beta\gamma (v_g/c)\ (c/\omega)^2}{g_2\, g\, L^3} \left(\frac{Q}{r_\ell}\right) , \tag{3.25}$$

which is identical in its dependence on the parameters with Wilson's result.

*An estimate of r_ℓ has been made for a model of independent cells. This leads to $r_\ell \sim 1$ megohm/m and gives a starting current of 40 amp. See Appendix.

5) The contributions from $k \neq j$ in (3.7) may not be negligible, as indicated by the traveling wave result. However, the factor M_{jk} has a structure which confines contributions to the vicinity $\alpha_j \sim \alpha_k \sim \pi$. An estimate of the effect of the term

$$(\omega_k - \omega_j)\, t_m \tag{3.26}$$

for an adjacent mode can be made by taking t_m to be the build-up time, which is assumed to be of the same order as the decay time, i.e.,

$$t_m \sim Q/\omega_j \,. \tag{3.27}$$

For this choice

$$(\omega_k - \omega_j)\, t_m \sim v_g\, Q_j/\omega_j\, L \,. \tag{3.28}$$

The contributions will therefore be confined to the mode $k = j$ or will extend to the neighboring modes according to whether the parameter in (3.28) is greater than or less than 1. If it were not for the factor M_{jk}, one would then multiply (3.20) by the factor $v_g\, Q/\omega_j\, L$ as we did in (3.25) for the traveling wave case.

6) Proper numerical investigation of this phenomenon should be performed starting with (3.7), with an appropriate deflecting mode spectrum.

7) Motion in the y direction has been neglected. If this is taken into account, the cavity oscillations may be induced with rotating polarization. This can, of course, be prevented by destroying the azimuthal symmetry.

IV. Resonant Beam Blow-up

The other possible serious effect previously mentioned occurs if one of the harmonics of the beam frequency resonates with one of the deflecting modes. In this case the transverse motion of the bunches induces cavity fields which may then build up from successive pulses. Since the build-up leads to deflections, this phenomenon involves not only the transverse focusing system, but the entire transverse history of the beam in preceding cavities.

According to (2.20), the mth beam bunch, traversing a cavity with average transverse displacement and angle given by x_m and x'_m, gives a contribution to the current of

$$\int \vec{j}(\vec{x}, \omega_j) \cdot \vec{E}^j \, dv =$$

$$= (I_o \, g/2\omega_o) \, R_j \, (L/\alpha) \, e^{-i\omega_j t_m} (x_m - K_j \, ix'_m)(e^{i\alpha} - 1) \, . \quad (4.1)$$

The contribution to the field is therefore

$$\Delta D_j \, (t) = (\pi c \, I_o \, g \, L \, R_j \, g_3/\omega_o) \, \mathrm{Re} \left\{ e^{i\omega_j (t - t_m) + i\alpha/2} (x_m - K_j \, ix'_m) \right\} \, . \quad (4.2)$$

The factor $g_3 = \frac{\sin(\alpha/2)}{\alpha/2}$ indicates that the effect is appreciable only for those deflecting modes with phase velocities close to the beam velocity. The factor $e^{-i\omega_j t_m}$ indicates that the contributions of successive bunches will be out of phase unless

$$\omega_j \, \Delta t/2\pi = \omega_j/\omega_o \simeq s \, , \quad (4.3)$$

that is, unless the ratio of deflecting mode frequency to beam frequency is close to an integer.

The angular deflection due to the presence of deflecting modes is given by (2.14). If one also includes the effects of the focusing forces, the coupled set of equations (2.14) and (4.2) allow one to follow the progress of the effect from cavity to cavity and from pulse to pulse numerically. [The effect treated in Section III may even be included by adding (3.8) to (4.2).] It is clear that in this case the effect depends even more sensitively on the deflecting mode spectrum.

An order of magnitude estimate of the effect can be made in the steady state condition (constant values of x_m, x'_m from pulse to pulse) by including the field decay due to losses. The field after the entrance of the nth bunch is then

$$D_j \, (t) = (\pi c \, I_o \, g \, L \, R_j \, g_3/\omega_o) \, \mathrm{Re} \left\{ e^{i\omega_j (t - t_n) + i\alpha/2} (x - K_j \, ix') \sum_{m=o}^{\infty} e^{2\pi m \left[i(\omega_j/\omega_o - s) - (\omega_j/2\omega_o Q_j) \right]} \right\}$$

$$\simeq (c \, I_o \, g \, L \, R_j \, g_3/2\omega_o) \, \mathrm{Re} \left\{ \frac{e^{i\omega_j (t - t_n) + i\alpha/2} (x - K_j \, ix')}{(\omega_j/2\omega_o Q_j) - i(\omega_j/\omega_o - s)} \right\} . \quad (4.4)$$

Since Q_j will normally be much larger than $\left|\omega_j/\omega_o - s\right|$, (4.4) can be reduced to

$$D_j(t) \simeq (\pi c I_o g L R_j g_3)\left[\frac{K_j x' \cos \chi_j - x \sin \chi_j}{\omega_j - s\,\omega_o}\right], \qquad (4.5)$$

where

$$\chi_j = \omega_j (t - t_n) + \alpha/2 . \qquad (4.6)$$

The deflection of the nth bunch in this field is given by (2.14). The $\cos \chi_j$ term in (4.5) corresponds to $\psi_j = \alpha_j/2 + \pi/2$ in (2.13), while the $\sin \chi_j$ term corresponds to $\psi_j = \alpha_j/2$. One therefore has, using (3.18),

$$\Delta x' \simeq x' \sum_j (e \pi I_o g g_3^2 L/p)(r_\ell/Q_j)/(\omega_j - s\,\omega_o) K_j (\omega_j/c)^2 . \qquad (4.7)$$

The increase in transverse amplitude due to this angular deflection is

$$\Delta A_x \simeq \sum_j \frac{\Lambda_x e I_o g g_3^2 L \omega_j r_\ell K_j (\omega_j/c)}{2 Mc^2 \beta \gamma Q_j (\omega_j - s\,\omega_o)} . \qquad (4.8)$$

For the independent cell model used before, and the AGS improvement program parameters, including I_o = 100 mA, one finds (see Appendix)

$$\Delta A_x \sim \frac{3 \times 10^{-7}}{(1 - \frac{s\,\omega_o}{\omega_j})} \text{ meters} . \qquad (4.9)$$

Thus, for a resonance accurate to 10^{-3}, the increase in transverse amplitude from this cavity is $\sim$ 0.03 cm. Since it is unlikely that this resonance will persist to an accuracy of 10^{-3} for several cavities, the effect appears not to be serious. If it should turn out that the resonance is more serious in one of the cavities, a perturbation of the deflecting modes of order 10^{-3} can undoubtedly be readily provided for.

In summary, therefore, it appears that the transverse motion of the beam can lead to a build-up of the deflecting mode if there is a resonance between the beam and deflecting mode frequencies. A rough estimate of the effect indicates that it is small, but numerical estimates

using (3.8), (4.2) and (2.14) are desirable. For these and other reasons it is recommended that both the accelerating and deflecting mode spectrum be measured carefully at several values of β.

We have of course neglected the variation of cell geometry within a cavity. This should reduce the effects discussed in this paper even further.

V. Summary

We have calculated the build-up of deflecting modes due to two separate causes. The first (Section III) is the nonresonant effect that comes from the deflection of the beam by the transverse fields already present. These deflections induce further transverse fields which have a component in phase with the original field. The appropriate equation governing the behavior of a bunched beam due to this effect is (3.7), with M_{jk} and m_{jk} defined in (3.6). For an approximate treatment of the steady state behavior, (3.20) is relevant. A further approximate calculation of r_ℓ is contained in the Appendix, and the corresponding current limit is given in (A-12).

The second effect treated (Section IV) is the resonant build-up of the deflecting modes due to the transverse oscillations of the beam. The average displacement and angle of a beam bunch with respect to the longitudinal cavity axis induces a transverse field. Successive bunches can build up this field if there is a resonance between the transverse mode and one of the harmonics of the beam. The appropriate equations governing the build-up of these coupled "displacement-field" oscillations are (4.2) and (2.14). For an approximate treatment of the steady state behavior, (4.5), (4.7) and (4.8) are relevant. A further approximate calculation of r_ℓ/Q_j is contained in the Appendix, and the corresponding limit is given in (A-10).

Numerical computation of the combination of the above two effects can also be performed. For this purpose the field increment per pulse is the sum of (3.8) and (4.2).

It is clear that both effects limit the contributions to those modes which slip no more than 180° behind the beam. In addition, the second effect is significant only if the resonance exists. For these reasons it is important to measure the mode spectrum for the cavities accurately for both the accelerating and deflecting bands at several values of β.

Estimates of the magnitudes of the two effects discussed have been made for the AGS improvement program parameters. Although these

are extremely crude, the values obtained are not at all serious and should not prove troublesome.

We have not treated the case of two transverse dimensions, nor have we considered the effects of the induced fields on the bunching of the beam pulses. Moreover, we have treated each cavity as having a constant value of v and a uniform cell geometry. These effects will hopefully not be serious. Besides, one always has the possibility of perturbing the transverse modes to modify transverse effects. We have also not considered the possibility of longitudinal beam blow-up.

VI. Acknowledgements

It is a pleasure to acknowledge several helpful conversations with Dr. T. Nishikawa of the University of Tokyo, and with Dr. W. Walkinshaw of the Rutherford Laboratory.

APPENDIX

We shall estimate r_ℓ and Q for the deflecting modes under the assumption that the cells are approximately uncoupled. In this case the fields in the mth cell are TM_{110} of the form

$$E_z^j = A_m^j \, J_1 (p_{11} \, r/b) \cos \theta$$

$$H_\varphi^j = A_m^j \, J_1' (p_{11} \, r/b) \cos \theta \qquad \text{(A-1)}$$

$$H_r^j = A_m \frac{J_1 (p_{11} \, r/b)}{p_{11} \, r/b} \sin \theta ,$$

where

$$A_m^j = A_o^j \cos (m \, k_j \, L_o) , \qquad b = p_{11} \, c/\omega_j , \qquad \text{(A-2)}$$

and p_{11} is the first zero of J_1. The Fourier decomposition of E_z^j can be shown to be

$$E_z^j = J_1 (p_{11} \, r/b) \cos \theta \, A_o^j \sum_{n=o}^{N-1} \frac{\sin k_{jn} \, L_o}{k_{jn} \, L_o} \cos k_{jn} \, z, \qquad \text{(A-3)}$$

where k_{jn} is given by (2.2). The relevant deflecting mode (n = 0) in the vicinity of the axis is therefore given by

$$E_z^j = x \, (p_{11} \, A_o^j \, g_1/2 \, b) \cos k_j \, z . \qquad \text{(A-4)}$$

Comparison with (2.3) indicates that

$$R_j = \omega_j \, A_o^j \, g_1/2 \, c , \qquad \text{(A-5)}$$

where

$$g_1 = \frac{\sin k_j \, L_o}{k_j \, L_o} . \qquad \text{(A-6)}$$

The quantity A_o^j is obtained from the normalization condition (2.4). It can be shown to be

$$A_o^{j2} = \left[4 \, \omega_j^2 / \pi L \, p_{11}^2 \, c^2 \, J_o^2 (p_{11}) \right] \simeq \left[2 \, \omega_j^2 / L \, p_{11} \, c^2 \right] . \qquad \text{(A-7)}$$

From (3.18) one has

$$\frac{r_\ell}{Q_j} = L R_j^2 (c/\omega_j)^3 Z_o/2 \simeq \frac{Z_o g_1^2 (\omega_j/c)}{4 p_{11}} . \qquad \text{(A-8)}$$

For small holes one can show that

$$K \omega/c \sim (p_{11}^2/4\beta)(a/b)^2 \qquad \text{(A-9)}$$

where a is the hole radius. Equation (4.8) can then be written as

$$\Delta A_x \simeq \sum_j \frac{\Lambda_x e I_o Z_o L g g_1^2 g_3^2 (\omega_j/c) p_{11} a^2}{32 Mc^2 (1 - s \omega_o/\omega_j) \beta^2 \gamma b^2} . \qquad \text{(A-10)}$$

In order to obtain r_ℓ or Q_j independently, one must calculate the power loss. This is obtained from the square of the tangential magnetic field on both the guide and cell walls, and turns out to be

$$r_\ell \simeq \left(\frac{Z_o}{\delta}\right)\left(\frac{g_1^2}{8}\right)\left(\frac{L_o}{L_o + b}\right) , \quad Q_j^{-1} = \frac{2\,\delta(\omega_j/c)}{p_{11}}\left(\frac{L_o + b}{L_o}\right) \qquad \text{(A-11)}$$

where δ is the skin depth. Equation (3.20) then becomes

$$e I_o = \left(\frac{4\pi^3}{g g_1^2 g_2}\right)\left[\frac{\delta\beta\gamma Mc^2 (c/\omega_j)}{Z_o L^2}\right]\left(\frac{L_o + b}{L_o}\right) . \qquad \text{(A-12)}$$

LEISS: Does not the resonant beam blow-up always contribute in a serious way?

GLUCKSTERN: It does in the sense that the nonaxial component of the beam current can be increased by the response of the cavity. However, this depends on a resonance between the transverse mode and a multiple of the beam frequency. In addition the presence of transverse forces may modify the build-up.

E. KNAPP: Isn't the value of shunt impedance used (20 Megohms/meter) high?

GLUCKSTERN: Yes. As a first conservative calculation I took a value comparable with the accelerating mode. However, for the transverse one should take the appropriate space harmonic with a phase velocity equal to that of the particle. In this case the "starting" current is increased by a factor of order 10.

WALKINSHAW: Shouldn't one include other field components for the transverse modes?

GLUCKSTERN: Yes. Although the only components which do not vanish in the x-z plane are the ones used, the relation between these components depend on the other components--in particular, on $\partial H_z / \partial y$. This has only been taken into account approximately in the present calculation.

LEISS: Isn't it true that both effects (resonant and nonresonant beam blow-up) are present together and are part of the same effect?

GLUCKSTERN: I do not believe the two effects are the same, but both effects should be taken together in any proper calculation.

LEISS: Aren't there important resonant effects in your calculation of nonresonant beam blow-up?

GLUCKSTERN: I don't believe that these modify the results by more than a factor 2.

REFERENCES

1. M. C. Crowley-Milling et al., Nature 191, 483 (1961).

2. P. B. Wilson, HEPL Report No. 297, Stanford.

3. J. E. Leiss and R. A. Schrack, "Transient and Beam-Loading Phenomena in Linear Electron Accelerators", NBS Internal Report, October 30, 1962.

4. See, for example, H. Hahn, Rev. Sci. Instr. 34, 1094 (1963).

DYNAMIC EFFECTS OF HIGHER RF HARMONICS

Frank J. Kriegler
Midwestern Universities Research Association

The acceleration process of a bunch of charged particles can be significantly altered when the passage of one bunch of particles through an accelerating gap of an rf cavity removes a significant fraction of the energy stored in the cavity. In a linear accelerator the ratio of energy removed by one bunch passing through one cell to the energy stored in one cell is of the order of 10^{-4}. However, in a circular accelerator this ratio may approach a value of 0.2.[1] The purpose of this paper is to investigate the particle dynamics for cases in which a high proportion of the energy is removed from the cavity by one bunch of particles. Clearly, this effect is extremely small in linear accelerators but the method of solution is of general interest.

In order to study the dynamics of beam-cavity interactions, we need a suitable representation of the beam induced voltage across the accelerating gap of the cavity. We may consider the cavity as a lumped RLC circuit upon which a sinusoidal voltage is impressed. The capacitor of this circuit may be thought of as representing the accelerating gap of an rf cavity. This representation is shown in Fig. 1a. Consider a charged particle repetitively passing through the capacitor thereby inducing a voltage change, $\Delta V = e/C$, on the capacitor, C. The distorted voltage waveform on the capacitor is shown in Fig. 1b. It must be noted that the particle may not pass through the capacitor at exactly the same phase in every period of the applied voltage, but rather at a slowly varying phase, which corresponds to the synchrotron oscillations of the particles. However, if the damping time for the circuit transients is less than the phase oscillation period of the particles, i.e., if

$$Q < \frac{f_{rev}}{f_{\text{phase osc.}}} , \qquad (1)$$

the transient amplitude behaves adiabatically.[2] Transients are not appreciably excited by the particles. We need, therefore, consider only steady-state response of the cavity to the particle current. This steady-state solution can be obtained by Fourier analysis of the beam current and the voltage waveform on the capacitor. A suitable expression for the voltage waveform shown in Fig. 1b is

$$V(t) = V_o (1 + k f_o t) \sin (2\pi f_o t + \theta_p) \quad \text{for } 0 \leq f_o t \leq 1 . \qquad (2)$$

By Fourier analyzing the voltage waveform of Eq. (2) the higher harmonics can be obtained. It may be shown that a convenient representation of the higher harmonics can be approximated by the following expression,

$$\frac{1}{2\pi} \sum_{n=2}^{\infty} V_n e^{j2n\pi f_o t} \approx \Delta V (0.5 - f_o t) \cos (2\pi f_o t)$$

$$0 \leq f_o t \leq 1 . \tag{3}$$

Thus, a particle (equivalently, a delta function pulse of current) passing through a narrow accelerating gap (a delta function gap) produces a distorted voltage waveform which may be Fourier analyzed. The usefulness of this for particle dynamics is now presented.

The beam current in a periodic accelerating structure may be Fourier analyzed:

$$I(\theta, t) = \sum_n a_n e^{in(\theta - \omega_o t)} = \sum_n a_n e^{in\theta'} , \quad \theta' = \theta - \omega_o t \tag{4}$$

where ω_o is the circular frequency of the rf source, θ is the angular coordinate relative to the synchronous particle, and the coefficients a_n are slowly varying. Each Fourier component of the beam excites fields in the cavity. The longitudinal electric field may be written as

$$E_z(\theta, t) = \sum_n \sum_\ell b_{n\ell} a_n e^{i(\ell\theta - n\omega_o t)} . \tag{5}$$

The terms for which $n \neq \ell$ are traveling waves which slip by the particles, causing the fields to vary rapidly at any particle position. We, therefore, neglect them as is customary in studying rf acceleration problems. The terms for which $n = \ell$ give a synchronous induced field

$$E_s(\theta, t) = \sum_n b_{nn} a_n e^{in(\theta - \omega_o t)} \tag{6}$$

or in the rotating coordinate system

$$E_s(\theta') = \sum_n b_{nn} a_n e^{in\theta'} . \tag{7}$$

In Eqs. (4) and (7) the a_n are given by

$$a_n = \frac{1}{2\pi} \int_0^{2\pi} I(\theta') e^{-in\theta'} d\theta' . \tag{8}$$

Substituting Eq. (8) into (7) and rearranging terms gives

$$E_s(\theta') = \int_o^{2\pi} I(\theta'') K(\theta' - \theta'') d\theta'' \tag{9}$$

where

$$K(\theta) = \frac{1}{2\pi} \sum_n b_{nn} e^{in\theta} . \tag{10}$$

Equation (9) has the same form as a space-charge field, except that the kernel, Eq. (10), has a different spatial dependence determined by the cavity geometry. It is possible to calculate a kernel for specific cavity geometries. A MURA computer program[3] exists that calculates a kernel for axially symmetric cavities of the types shown in Fig. 2. However, to see the meaning of the kernel more clearly and to illustrate the principles involved, the cavity is taken as the lumped RLC circuit considered previously. The capacitance represents a narrow gap located at $\theta = 0$, so that

$$E(\theta, t) = \frac{\delta(\theta) V(t)}{R} \tag{11}$$

where $V(t)$ is the gap voltage and R is the orbit radius. This delta function representation allows us to write immediately the $b_{n\ell}$ of Eq. (5) as

$$b_{n\ell} = \frac{V_n}{2\pi R} \tag{12}$$

where V_n is the voltage induced by a unit current at each harmonic frequency $n\omega_o$. The kernel can then be written as

$$K(\theta) = \frac{1}{2\pi} \sum_n \frac{V_n}{2\pi R} e^{in\theta} . \tag{13}$$

Thus the voltage waveform expression derived for the lumped RLC circuit may now be used in the subsequent calculations. Substituting Eq. (3) into Eq. (13) yields

$$K(\theta) = \frac{V}{2\pi R}\left(0.5 - \frac{\theta}{2\pi}\right)\cos\theta . \tag{14}$$

Figure 3 shows a plot of this kernel and a plot of a kernel obtained for a typical ferrite-loaded accelerator cavity having a narrow gap. The fundamental frequency component induced by the beam is not included in Eq. (14). The magnitude of the fundamental would depend upon a number of considerations such as Q of the cavity, internal impedance of the rf source and feedback loops. However, in this paper the results presented are based on the assumption that the fundamental is kept constant by some mechanism.

As was pointed out above, the kernel function generated by a particle passing an accelerating gap is similar to a space-charge force. Previous investigations[4, 5] have been made concerning the effects of space-charge forces on the rf acceleration process. Thus, the same techniques may be used to investigate effects of higher harmonics.

One result of these space-charge investigations is a MURA computer program[5] which integrates the equations of motion for a particle under the influence of a combined rf and space-charge field. A particle whose energy is sufficiently different from transition energy is governed by the following equations,

$$\dot{\theta} = f\frac{df}{dE}W \tag{15}$$

$$\dot{W} = -\dot{W}_s + e V_o \sin\theta + 2\pi e R\,\xi(\theta, t) , \tag{16}$$

where θ measures angles in a coordinate system rotating with the beam, $\dot{W}_s$ is related to the energy gain per turn of the synchronous particle, $\dot{W}$ is the energy gain of a particle relative to the synchronous particle, and V_o is the accelerating voltage on the gap. The electric field $\xi(\theta, t)$ is the beam-cavity interaction field. The term containing the frequency change with energy, $f\frac{df}{dE}$, can be taken as a constant (for example, + 1 for particles below transition and - 1 for cases above transition). The basic approach to the problem is to specify as many as 10,000 pairs of initial conditions (particles), θ, $\dot{W}$. The field $\xi(\theta, t)$ is computed by convolution (Eq. (9)) of the kernel function with the particle density at the beginning of each time-step. The integration is then performed by a linear integration of Eqs. (15) and (16). For example, Eq. (15) is written as

$$\theta\,(t + \Delta t) = \theta\,(t) \pm W\,(t)\ \Delta t\,, \tag{17}$$

and similarly for Eq. (16). It must be emphasized that since 10,000 or less particles are carried in the computation, the charge of these particles is greater than the electronic charge, e. The magnitude of charge on these "macroparticles" is determined by scaling the constant, $V = \Delta Q/C$, in the kernel function (Eq. (14)).

The numerical results obtained using this computer program are presented by Figs. 4 to 9. Figure 4 shows a phase plot in which no higher harmonic beam-cavity interaction takes place. This figure is shown merely to provide a reference figure for the form of the computer results as the rf capture process takes place. The initial conditions are a band of 1935 macroparticles spread uniformly in energy and phase, as shown in the top diagrams. The middle diagrams are an intermediate result of the computation. The bottom diagrams are the final buckets. The three diagrams on the right are for particles below transition, while the diagrams on the left are for particles above transition. The number of particles captured is 503 from the initial 1935. Figure 5 shows the effect of higher harmonic beam interaction. The magnitude of the kernel is based on an equivalent circuit in which the capacitance is 8 pf, the rf accelerating voltage is 2×10^4 volts, and a bucket contains 10^{13} particles. Thus, if all the particles passed through the capacitor at the same instant, the voltage change would be 2×10^5 volts. The constant, ΔV, in the kernel function (Eq. (14)) is $\Delta V = 2 \times 10^5/1935 = 103$. For this case, the initial conditions were the same as the unperturbed case shown in Fig. 4. In Fig. 5 the bucket boundary for the unperturbed case is outlined for comparison. Below transition the higher harmonic beam interaction reduces the number of particles captured from 510 to 205, while above transition the number of particles captured increases to 670. Figure 6 shows the distorted voltage waveform on the accelerating gap for the above case for particles below transition; Fig. 7 is the voltage waveform above transition. Figure 8 displays a severe case above transition for which the parameters are the same except that the bucket contains 6×10^{13} protons (the kernel is six times larger). The voltage waveform of this case is shown in Fig. 9.

The computer time required to run one case was from one to one and one-half hours on an IBM 704 computer. The running time varies approximately linearly with the number of macroparticles used.

ACKNOWLEDGEMENTS

I would like to express appreciation to Professor K. R. Symon and E. M. Rowe for helpful suggestions and comments. I would like to thank Dr. R. A. Dory for valuable help in providing his computer program.

SWENSON: Does Fig. 8 correspond to above or below transition?

KRIEGLER: This case is above transition.

SWENSON: In this terminology are all linacs essentially below transition?

KRIEGLER: Yes, and above transition the particles get a larger energy "kick" and take longer to come back again. This analysis would not hold too well with respect to linear accelerators. I assume that the particle comes back again and sees its effect, although I suppose if you stretch your imagination you could say that if one particle goes through, it starts to excite these higher harmonics and the next one will feel essentially the same effect, although it is a different particle. I have assumed up to now that the fundamental stays constant; there is a feedback mechanism which increases power into the cavity as the beam requires and keeps the fundamental constant. We could put in some kind of transfer function associated with a feedback loop. This would be done for a particular structure; here I have just tried to present general results.

J. H. MARTIN: You spoke of a feedback loop involving amplitude. Do you have any consideration for that involving phase?

KRIEGLER: I guess we were talking about including this. There is another consideration, the magnitude and phase of the fundamental would vary considerably if you're off resonance. Results could be obtained for all these considerations; however, it seems desirable to perform computer experiments of that type only for a specific accelerating system.

REFERENCES

1. E. M. Rowe, MURA Technical Note TN-471 (unpublished, 1964).

2. K. R. Symon, private communication.

3. F. J. Kriegler, F. E. Mills, and J. Van Bladel, Jour. Appl. Phys., Vol. 35, No. 6, pp. 1721-1726, June 1964.

4. C. E. Nielsen and A. M. Sessler, MURA Report No. 480 (unpublished, 1959).

5. R. A. Dory, MURA Report No. 654 (unpublished, 1962).

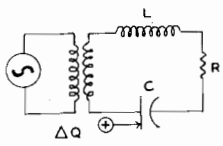

(a) EQUIVALENT CIRCUIT FOR ACCELERATOR CAVITY

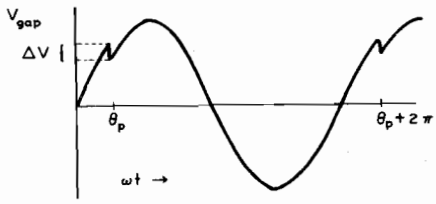

(b) VOLTAGE WAVEFORM ON ACCELERATING GAP (CAPACITOR)

FIG. 1

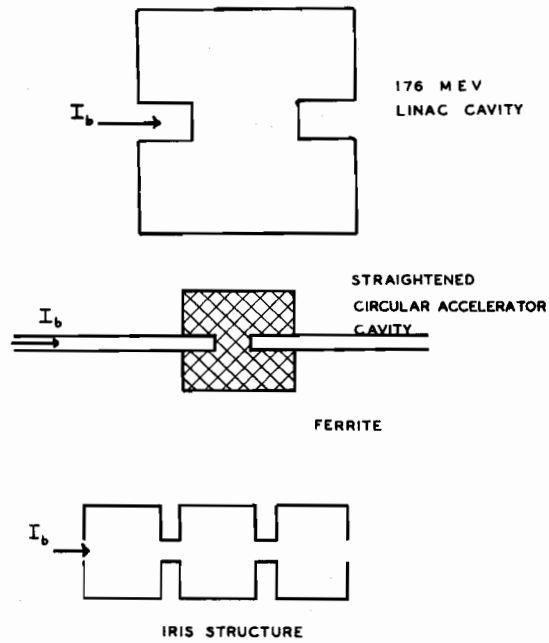

FIG. 2 AXIALLY SYMMETRIC ACCELERATOR CAVITIES

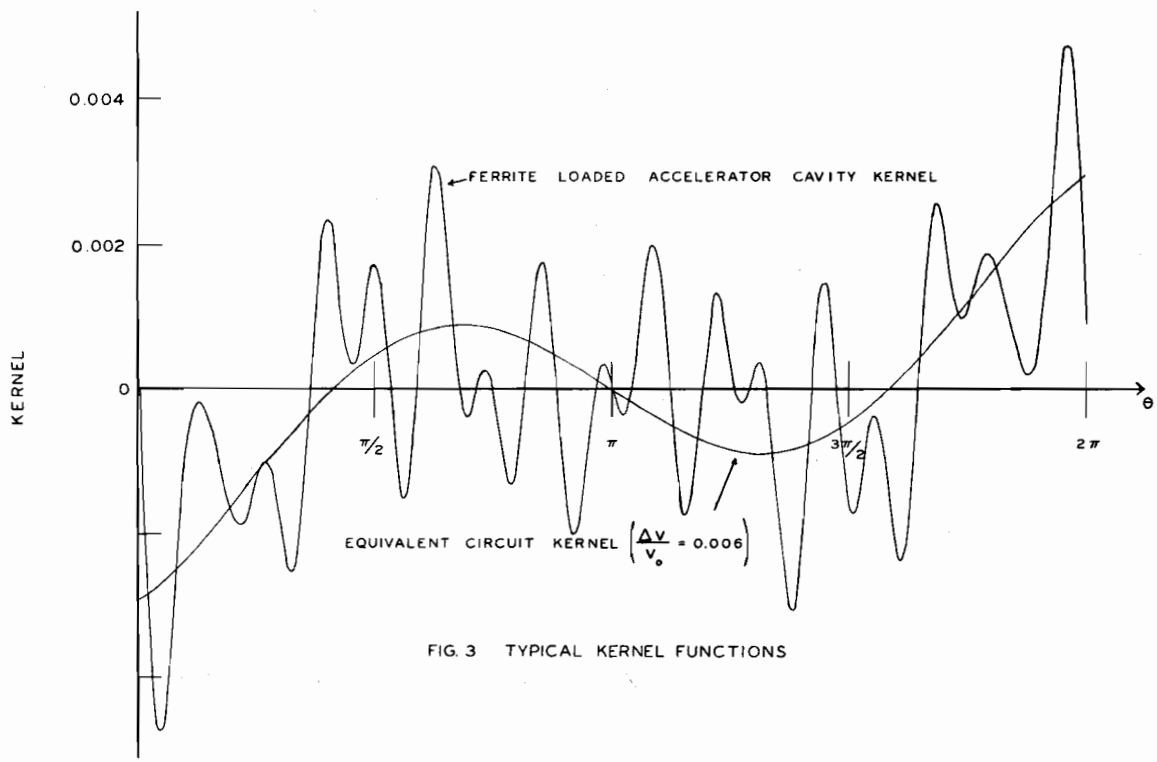

FIG. 3 TYPICAL KERNEL FUNCTIONS

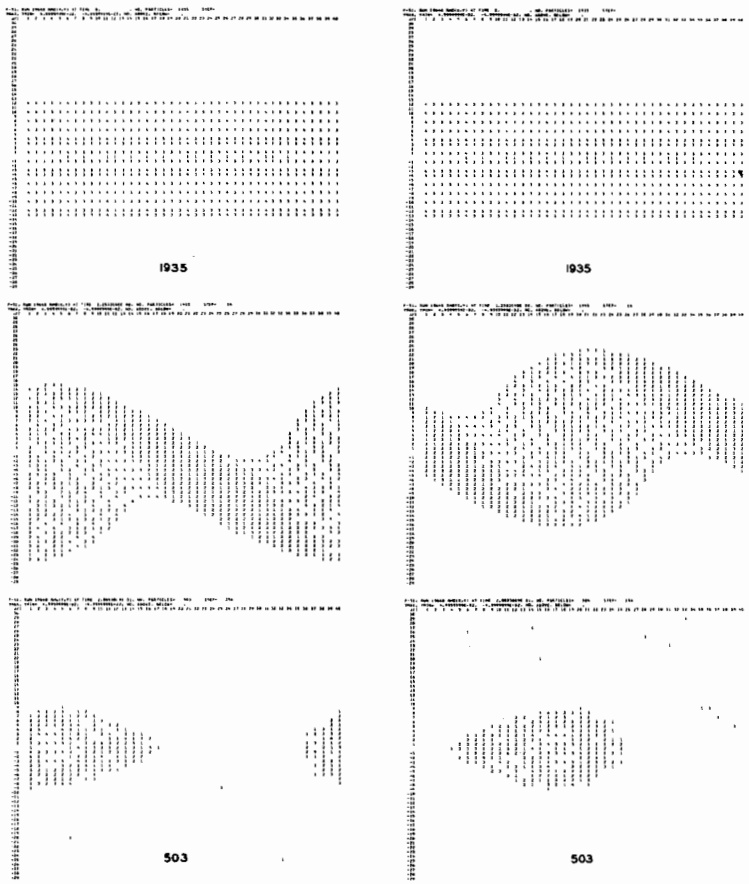

(a) BELOW TRANSITION (b) ABOVE TRANSITION

FIG. 4 PHASE PLOT FOR NO BEAM CAVITY INTERACTIONS

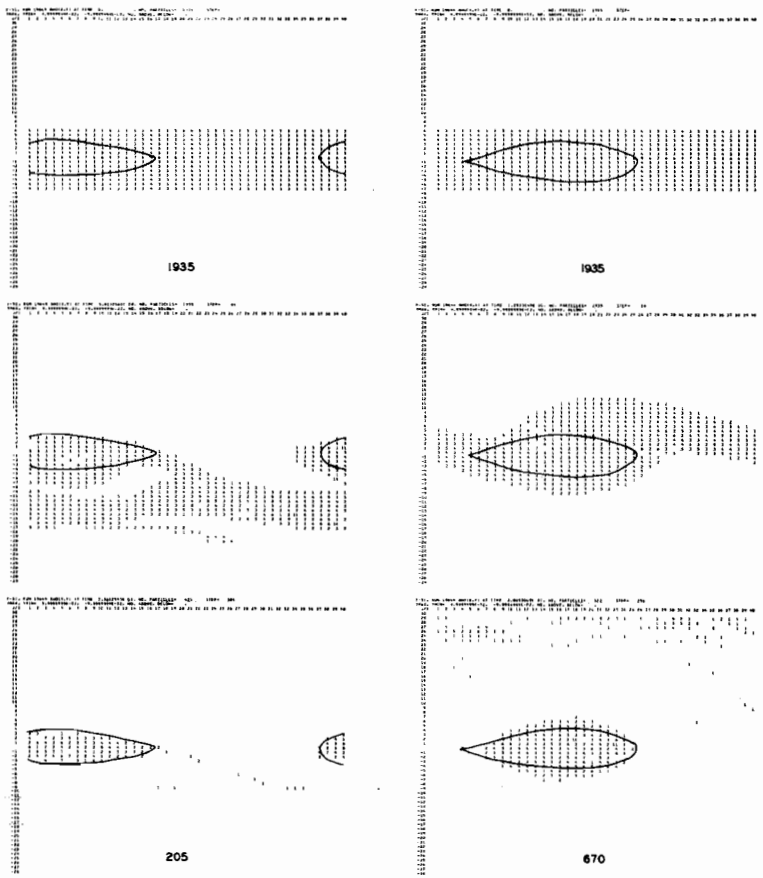

(a) BELOW TRANSITION (b) ABOVE TRANSITION

FIG. 5 PHASE PLOT FOR HIGHER HARMONIC BEAM CAVITY INTERACTIONS ($N = 10^{13}$ PARTICLES)

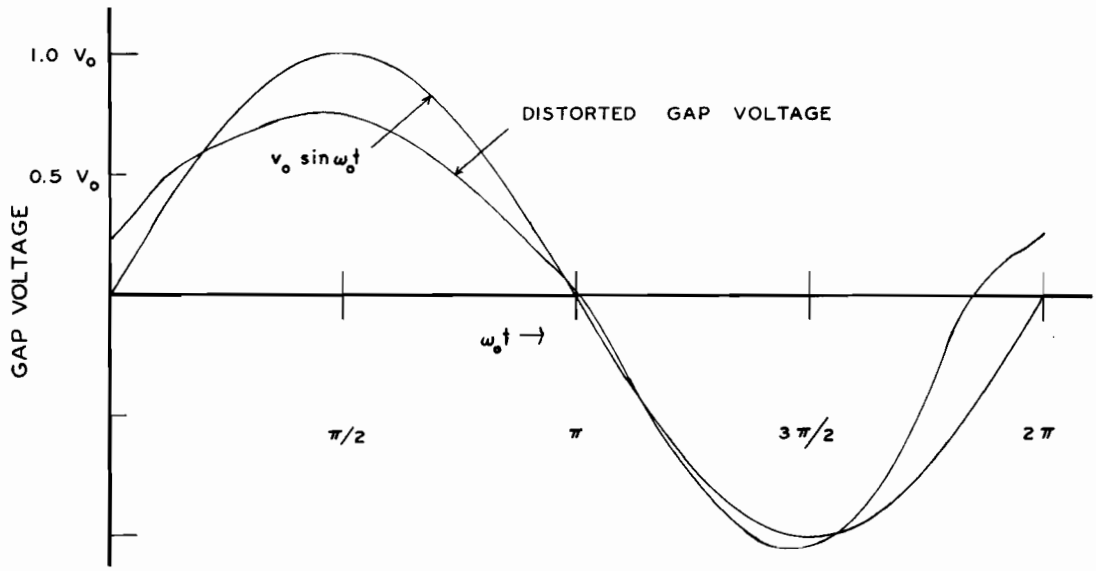

FIG. 6 VOLTAGE WAVEFORM ON ACCELERATOR GAP BELOW TRANSITION FOR 10^{13} PROTONS AND C_{gap} = 8 PF

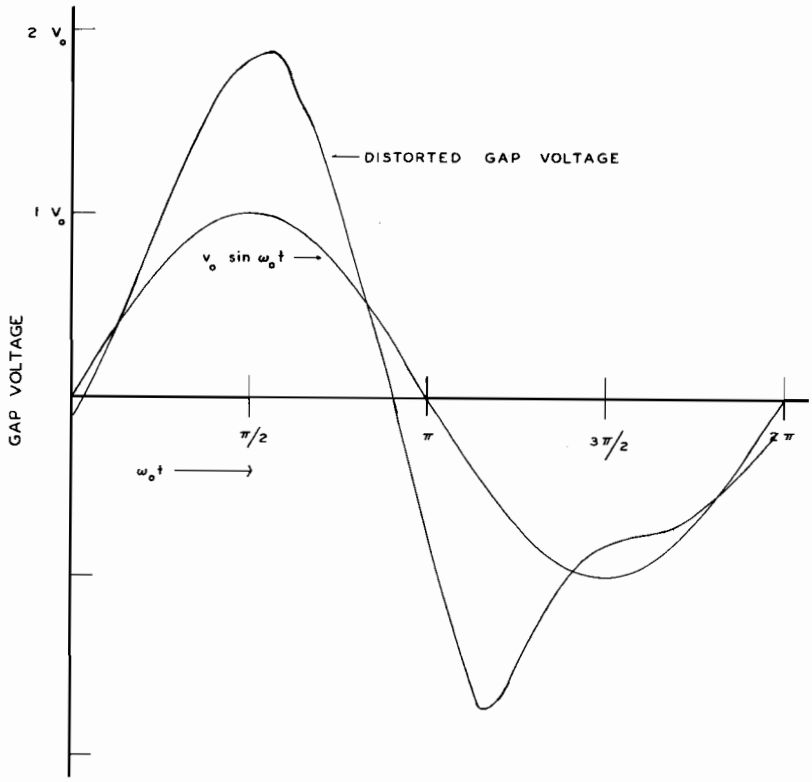

FIG. 7 VOLTAGE WAVEFORM ON ACCELERATOR GAP ABOVE TRANSITION FOR 10^{13} PROTONS AND C_{gap} = 8 PF

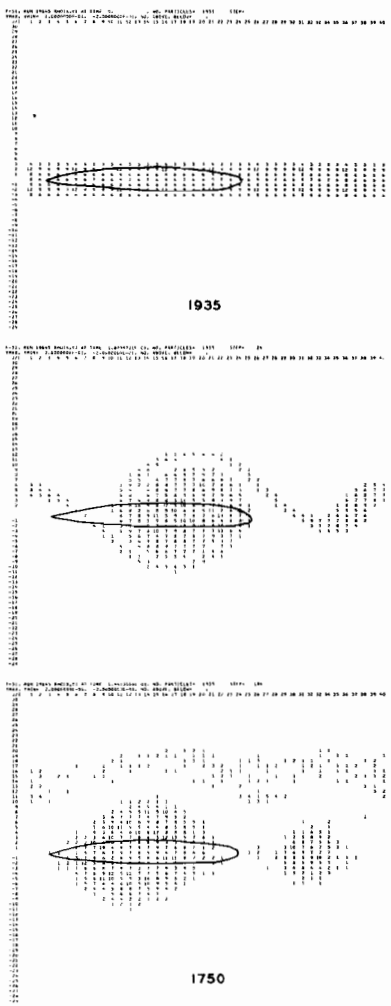

FIG. 8 PHASE PLOT FOR HIGHER HARMONIC BEAM CAVITY INTERACTION ($N = 6 \times 10^{13}$ PARTICLES)

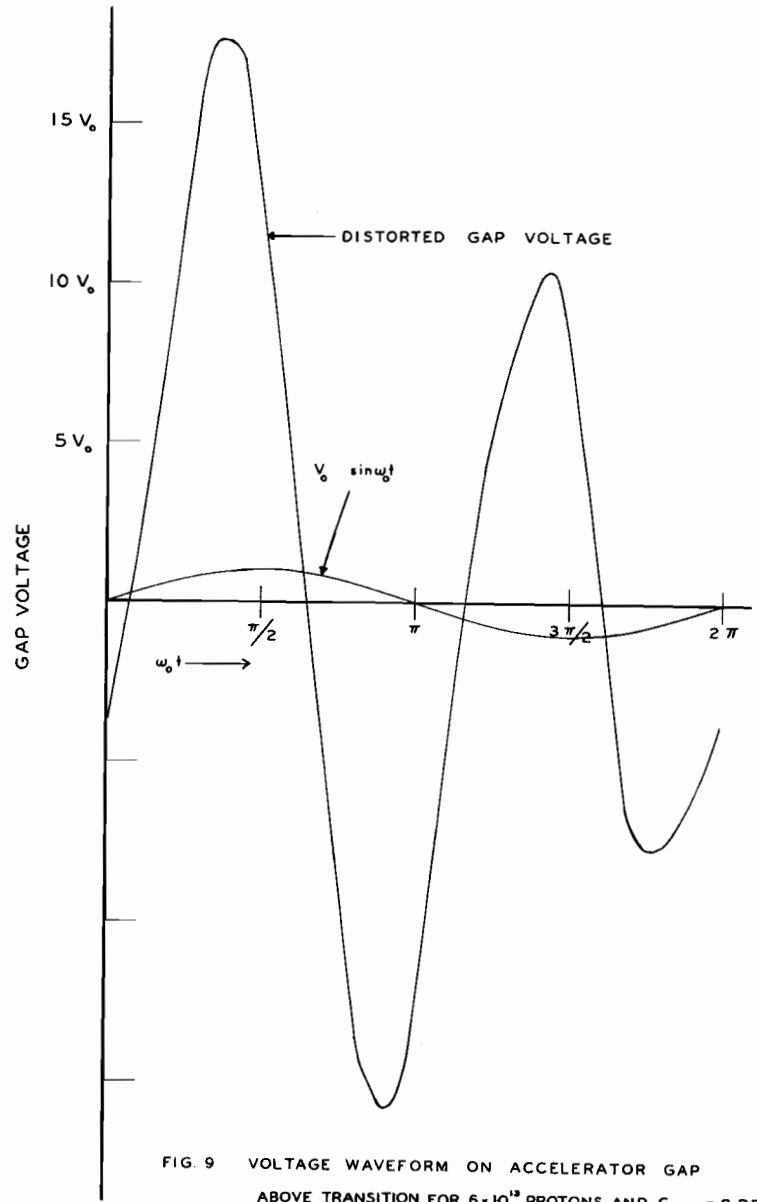

FIG. 9 VOLTAGE WAVEFORM ON ACCELERATOR GAP ABOVE TRANSITION FOR 6×10^{13} PROTONS AND $C_{gap} = 8$ PF

AN APPROACH TO THE STUDY OF BEAM LOADING FOR THE LINEAR ACCELERATOR

T. Nishikawa*
Brookhaven National Laboratory

1. Introduction

Most studies on the effects of beam loading in linear accelerators have been made using the power relations or the equivalent circuit analogies. On the other hand, the field equation for cavities and the equation of motion for the charged particles will give a more complete picture of this effect, especially when the accelerator is a standing wave type. This study was made for the iris-loaded structure being considered by the Brookhaven-Yale proton linac project.[1] The method is similar to the theories developed for microwave electronic devices, particularly traveling wave tubes, and the purpose is to give a brief physical picture but not exact numerical calculations.

2. Principle and Assumptions

According to Slater's well known theory for resonant cavities,[2] the solution of Maxwell's equations is expanded in terms of a summation over certain normal modes, which possess orthogonality properties. Any vector field can be broken into new fields, one of which is solenoidal and the other is irrotational and, so far as the wave propagation is considered, the space-charge effect can be separated for the first approximation. The effect of the beam current on the cavity field which is operated near the nth mode is quite generally expressed by**

$$-\frac{1}{\epsilon\,\omega_{no}}\frac{\int \vec{J}\vec{F}_n{}^* dv}{\int \vec{E}\vec{F}_n{}^* dv} = j\left(\frac{\omega}{\omega_n} - \frac{\omega_n}{\omega}\right) + \frac{1}{Q_n} \quad . \tag{1}$$

$\vec{J}$ is the current density, $\vec{E}$ the field, and $\vec{F}_n$ is the solenoidal normal mode field. $\vec{F}_n$ is obtained by solving Maxwell's equations when there is no current in the cavity and the walls are either short-circuited or open-circuited. ω_{no} is the resonant angular frequency of the nth mode and ω_n is that of the case when the effect of wall losses is taken into account. Rigorously $\omega_{no} \neq \omega_n$, but one can safely use ω_n instead of ω_{no} if the unloaded

---

* On leave from the Department of Physics, University of Tokyo.

** This equation is slightly modified from Slater's and immediately derived from the wave equation for the vector potential, and is quite general for the relativistic case. See Ref. 9 and its reference.

Q, Q_{on}, is sufficiently high. The total Q value of the cavity without beam, Q_n, is expressed by

$$\frac{1}{Q_n} = \frac{1}{Q_{on}} + \sum_i \frac{g_i}{Q_{ext,\ n,\ i}} , \tag{2}$$

where $Q_{ext,\ n,\ i}$ is the external Q to the ith output and g_i is the real part of the reduced admittance of the ith guide. If we study a standing wave type accelerator such as those operating in the π-mode, one section having N cells can be considered as a closed cavity of $Q_n = Q_{on}$. For simplicity throughout this paper a uniform cell structure in each cavity will be assumed, while an actual π-mode cavity would have nonuniform structure as discussed in the Appendix. The actual field, $\vec{E}$, is also assumed to vary as $e^{j\omega t}$ with the operating frequency ω, and the integration is performed over the cavity volume.

The effect of beam loading in a linac can be estimated from the left-hand side of (1); its imaginary part gives the shift of the resonant frequency or the detuning effect and the real part gives the further power loss or the beam Q-value.

3. Effect of Tightly Bunched Beam (Light-loading)

The assumption throughout this paper is that a tightly bunched beam interacts with the field propagating along the cavity axis. The beam is also assumed to be confined to a region having a small diameter about this axis (z axis).

In the first step, we neglect the field induced by the beam and the reaction of the field on the beam. This approximation will be valid when the loading is sufficiently small or in a transient stage when the induced field has not yet built up.

In terms of the field equation the stored energy for the nth mode may be written as

$$W_n = \frac{1}{2} \epsilon \int \vec{E}\vec{F}_n^{\,*} dv \int \vec{E}^* \vec{F}_n dv . \tag{3}$$

This equation may also be written in terms of circuit parameters as

$$\omega_n W_n = Q_{on} R \quad L = \frac{Q_{on} E_{no}^2 L}{r_{sn}} \quad , \tag{4}$$

where R is the wall loss per unit length, L the cavity length, E_{no} the axial-field amplitude (peak value of the field strength) of the nth harmonic field, and $r_{sn} = E_{no}^2/R$ the shunt impedance for the nth mode field. Substituting (3) and (4) into (1), we obtain

$$-\int \vec{J}\vec{F}_n^* dv \int \vec{E}^* \vec{F}_n dv = \frac{2Q_{on}}{r_{sn}} E_{no}^2 L \left[j\left(\frac{\omega}{\omega_n} - \frac{\omega_n}{\omega}\right) + \frac{1}{Q_n}\right] \tag{5}$$

Now the beam is assumed to be bunched in a wave having the propagation exponent $j(\omega' t - k' z)$ with a bunch width $\delta\phi$ at a center phase ϕ_o. The current density of such beam is analyzed in a Fourier series as

$$J = J_o + \mathrm{Re} \sum_{\nu=1}^{\infty} 4J_o \frac{\sin \frac{\nu \delta\phi}{2}}{\nu \delta\phi} e^{j\nu(\omega' t - k' z + \phi_o)} \tag{6}$$

where J_o is the mean density during one pulse of the linac operation. When $\nu \delta\phi << 1$, the ν component is

$$J_\nu \doteq 2J_o \,\mathrm{Re}\, e^{j\nu(\omega' t - k' z + \phi_o)} \tag{6'}$$

So far as a steady state solution is considered, only the term of $\omega_b = \nu\omega' \approx \omega_n$* should be important in the estimation of integral $\int \vec{J}\vec{F}_n^* dv$. Taking $k_b = \nu k'$ and $\phi_b = \nu \phi_o$, it becomes

---

* ν is four for the proton linac planned by Brookhaven.

$$\int \vec{J}\vec{F}_n^{\,*} dv = -2jI_o F_{no} e^{j\phi_b} \left\{ \frac{1}{k_n + k_b} \left[1 - e^{-j(k_n+k_b)L} \right] \right. \tag{7}$$

$$\left. + \frac{1}{k_n - k_b} \left[1 - e^{-j(k_n - k_b)L} \right] \right\},$$

where I_o is the mean current, F_{no} is the axial-field amplitude of the nth normal mode field which is given by $2F_{no} \cos k_n z$ in the standing wave case. For a π -mode, $k_n L = \pi N$ with the total number of cells, N, so that $k_n L >> 1$. In such a case, one can easily see that the right hand side of (7) is dominant for $|k_n - k_b| \approx 0$, or for the synchronized wave which hereafter is designated by n. It also should be pointed out that from here on only the synchronized primary mode will be considered, and the effects of all other modes have been neglected. Taking $|k_n - k_b| L << 1$, we get from (7),

$$\int \vec{J}\vec{F}_n^{\,*} dv \approx 2I_o F_{no} L e^{j\phi_b} . \tag{8}$$

Combining (5) and (8),

$$I_o e^{j\phi_{bn}} = - \frac{Q_{on}}{r_{sn}} E_{no} \left[j \left(\frac{\omega}{\omega_n} - \frac{\omega_n}{\omega} \right) + \frac{1}{Q_n} \right], \tag{9}$$

where we used a relation, $\vec{E} = \sum \vec{F}_n \int \vec{E}\vec{F}_n^{\,*} dv = \sum \vec{E}_n$ for the nth harmonic field $\vec{E}_n$; and ϕ_{bn} is the relative phase of the beam bunch to the nth harmonic field. Then we have the frequency shift, $\Delta\omega_n = \omega - \omega_n$, and the beam Q-value, Q_{bn}, as

$$\frac{2\,\Delta\omega_n}{\omega_n} = -\frac{r_{sn}}{Q_{on}}\,\frac{I_o}{E_{no}}\,\sin\phi_{bn} \tag{10a}$$

$$\frac{1}{Q_{bn}} = \frac{r_{sn}\,I_o}{Q_{on}\,E_{no}}\,\cos\phi_{bn}\,, \tag{10b}$$

where the total Q-value is expressed by $\frac{1}{Q_{tn}} = \frac{1}{Q_n} + \frac{1}{Q_{bn}}$.

4. Effect of Induced Field due to Beam Loading

If the beam loading increases, the field induced by the beam increases and becomes an appreciable part of the field, so that it should not be neglected. The actual field in a cavity can be divided into two parts; one is excited by the external source, $\vec{E}_e$, and the other is induced by the beam, $\vec{E}_b$. The total field is given by

$$\vec{E}_t = \vec{E}_e + \vec{E}_b \tag{11}$$

The induced field is also given by the use of (1), which is the so-called circuit equation in the present paper. The nth harmonic field of E_b is

$$\vec{E}_{bn} = \vec{F}_n \int \vec{E}_b\,\vec{F}_n^{\,*}dv \tag{12}$$

and its axial component will be given by

$$\dot{E}_{bno} = F_{no} \int \vec{E}_b\,\vec{F}_n^{\,*}dv \tag{12'}$$

where $\dot{E}_{bno}$ is the complex amplitude including the phase. The axial-field amplitude of the nth normal mode, F_{no}, which is, of course, a real number, is obtained from (3) and (4), where $\vec{E}$ is taken by $\vec{F}_n$. Since $W_n = \frac{\epsilon}{2}$ for the normal mode,

$$F_{no} = \sqrt{\frac{\epsilon}{2} \frac{r_{sn}\ \omega_n}{Q_{on}\ L}} \ . \tag{13}$$

The value of integral in (12') is given as

$$\int \vec{E}_b\ \vec{F}_n{}^* dv = - \frac{\int \vec{J}\vec{F}_n{}^* dv}{\epsilon\, \omega_n \left[j \left(\frac{\omega_b}{\omega_n} - \frac{\omega_n}{\omega_b} \right) + \frac{1}{Q_n} \right]}$$

$$= - \sqrt{\frac{r_{sn} L}{2 Q_{on} \epsilon\, \omega_n}} \ \frac{2 I_o\, e^{j\phi_b}}{\left[j \left(\frac{\omega_n}{\omega_n} - \frac{\omega_n}{\omega_b} \right) + \frac{1}{Q_n} \right]} \tag{14}$$

from (1) and (8). Substituting (13) and (14) into (12')

$$\dot{E}_{bno} = - \frac{r_{sn}}{Q_{on}} \ \frac{I_o\, e^{j\phi_b}}{\left[j \left(\frac{\omega_b}{\omega_n} - \frac{\omega_n}{\omega_b} \right) + \frac{1}{Q_n} \right]} \ , \tag{15}$$

just corresponding to (9).

In order to discuss the effect of induced field, we must consider the relation between ω_b and ω_n. The normal mode frequency, ω_n, is the proper frequency of the free oscillation of the cavity and is just the operating resonant frequency, ω_o, when beam is not present. If the beam comes in, the dynamic resonant frequency will move due to the reactive component of the load and differ from ω_n, the amount of this shift being given by (10a) in the first approximation. We can make a readjustment of the tuning of the cavity to resonate at the frequency ω_o, in order to keep the synchronous condition for the beam and the wave

velocities. In such a case, the normal mode frequency is moved in turn by the tuning process and is no longer equal to ω_o. Because of the phase oscillation in the preceding part of the accelerator, the beam will be bunched to the wave of ω_o rather than that of ω_n, or $\omega_b \approx \omega_o \neq \omega_n$. Howevever, as we can see from (10a) and (10b), if $|\phi_b| << 1$ or $Q_b >> Q_{on}$, we may put $|\omega_b - \omega_n| << \omega_n/Q_n$, and we have the expression

$$\dot{E}_{bno} = -\frac{Q_n}{Q_{on}} r_{sn} I_o e^{j\phi_b} \equiv - E_{bno} e^{j\phi_b}, \tag{15'}$$

where E_{bno} is the real amplitude or the peak strength of the induced field. The induced field is out of phase with that of the beam bunch and proportional to the shunt impedance.[3] In the present-designed accelerator, $\phi_b = \frac{\pi}{6}$ and $Q_b \gtrsim 2\, Q_{on}$, so that the approximation of (15') would be correct.

Superposing the induced field to the external field and repeating the process in paragraph 3, we have the following results as,

$$\frac{2\Delta W_n}{\omega_n} = -\frac{r_{sn}}{Q_{on}} \frac{I_o E_{eno} \sin \phi_{bn}}{E_{eno}^2 + E_{bno}^2 - 2E_{eno} E_{bno} \cos \phi_{bn}}$$

$$= -\frac{1}{Q_n} \frac{B_n \sin \phi_{bn}}{1 + B_n^2 - 2B_n \cos \phi_{bn}} \tag{16a}$$

$$\frac{1}{Q_b} = \frac{r_{sn}}{Q_{on}} \frac{I_o (E_{eno} \cos \phi_{bn} - E_{bno})}{E_{eno}^2 + E_{bno}^2 - 2E_{eno} E_{bno} \cos \phi_{bn}}$$

$$= \frac{1}{Q_n} \frac{B_n \cos \phi_{bn} - B_n^2}{1 + B_n^2 - 2 B_n \cos \phi_{bn}} \tag{16b}$$

instead of (10a) and (10b), with the beam loading parameter,

$$B_n = \frac{E_{bno}}{E_{eno}} = \frac{Q_n}{Q_{on}} \frac{r_{sn} I_o}{E_{eno}} , \tag{17}$$

E_{eno} being the nth harmonic amplitude of external field. If we take r_{sn} as 20 $M\Omega/m$, I_o as 0.1 A (the maximum design value), E_{eno} as 4 MeV/m and $Q_n = Q_{on}$, we find $B_n = 0.5$, leading to $\Delta\omega_n / \omega_n = 1.5 \times 10^{-5}$ (~ 10 kc for an 800 Mc accelerator) and $Q_{bn} = 4 \times 10^4$ for $Q_{on} = 2 \times 10^4$ and $\phi_{bn} = \pi/6$.

5. Self-Consistent Field

Up to the preceding section, the reaction of the field on the charged particles is neglected. In order to find the complete picture, we must solve the self-consistent field taking into account the induced current. The self-consistent field is the solution of the combination of the circuit equation and the equation of motion (electronic equation), this method has been extensively developed in studies of traveling wave tubes.[4] In contrast to the usual TWT theory, the following points should be considered:

a. The injected beam is already tightly bunched and the induced field is important. Also some of the nonlinear behavior should be considered.

b. The motion of the charged particle is relativistic.

c. The circuit is used for standing waves and not for traveling waves.

For the tightly bunched beam, the so-called small-signal theory should not be valid. In a small-signal theory, the velocity, v, and the linear charge density, ρ, of particles are expressed as

$$v = v_o + v_1 e^{j(\omega_b t - k_b z)}$$

$$|v_1| << v_o$$

$$\rho = \rho_o + \rho_1 e^{j(\omega_b t - k_b z)}$$

$$\rho_1 << \rho_o$$

The condition for v will still be valid in the present case, but the condition for ρ is violated since $\rho_1 \sim \rho_o$. Such a case is called a moderately large signal case,[5] and since the beam impedance is still high compared with the circuit impedance, the coupling between the wave and the beam should not be so strong. This is seen through estimation of the dimensionless coupling parameter, C, defined by Pierce,[4] the cube root of the ratio of circuit impedance to the beam impedance. As will soon be shown, C is of the order of 10^{-2} for the present case or of the same order as in the usual TWT. The weak coupling nonlinear theories for the TWT have been presented by Nordsiek and others,[6] and some numerical results are also available. Unfortunately, because of the different working conditions, these numerical results cannot be used for the present case.

On the other hand, by comparison of these numerical results with the results from the simple small-signal theory, Pierce pointed out that, if the beam is overbunched, the effect of nonlinearity can be estimated, at least qualitatively and almost quantitatively, from the results of the small-signal linear theory by setting the amplitude of the varying current equal to $2I_o$.[7] In order to obtain the physical picture, we examine the self-consistent field in this manner.

The circuit equation is again equation (1), and we make some modifications in order to express it in terms of the propagation constants. Then, corresponding to (9),

$$\dot{E}_{no} = - \frac{\omega_n r_{sn}}{2Q_{on} v_{ge}} \frac{\Gamma_n}{\left[(\Gamma_n^2 - \Gamma^2) + \alpha \Gamma_n\right]} \dot{i}_1 \tag{18}$$

where $\dot{E}_{no}$ and $\dot{i}$ are the complex amplitudes of field and current, having time and z-dependence as $\exp(j\omega t - \Gamma z)$. Taking the phase velocities, v_{pn} and v_p, for the case without and with the beam respectively, $\Gamma_n = j\,\omega/v_{pn}$ and $\Gamma = j\,\omega/v_p \left(\approx j\,\omega_n/v_{pn}\right)$. The effective group velocity, v_{ge}, is defined as

$$- j\, v_{ge} \equiv \frac{\omega - \omega_n}{\Gamma_n - \Gamma}, \tag{19}$$

and the attenuation constant α is

$$\alpha \equiv \frac{\omega_n}{v_{ge} Q_{on}} . \tag{20}$$

Equation (18) has the same form as given by Pierce for TWT theory and the solutions for both forward and backward waves.

The equation of motion for the changed particle is expressed by

$$\dot{i}_1 = \frac{e}{m_\ell} \frac{I_o}{v_o^2} \frac{\Gamma_b}{(\Gamma_b - \Gamma)^2} \dot{E}_{no} \tag{21}$$

where $\Gamma_b = jk_b = j\omega/v_o$. This is also derived in the similar manner as in TWT theory,[2,4] provided the relativistic effect is taken into the longitudinal phase motion by taking the longitudinal mass $m_\ell = m_o (1 - v_o^2/c^2)^{-3/2}$. To derive this equation the standing wave is divided into forward and backward waves, and is assumed to interact with the beam only through the forward wave due to the phase synchronism condition.*

Combining (18) and (21), the self-consistent field is obtained. Taking $\Gamma_b = \Gamma_n$ (or $v_o = v_{pn}$), the solution for the forward wave is given by

$$\delta^2 \left(\delta + \frac{\alpha}{2} \right) = C^3 k_b^3 , \tag{22}$$

where $\delta = \Gamma_b - \Gamma$ and the coupling parameter C is given by

$$C^3 = \left(\frac{e}{4m_\ell} \frac{r_{sn} I_o}{v_{ge} \omega Q_{on}} \right) . \tag{23}$$

---

* The particular situation of the π-mode, which is pointed out by Leiss, can be taken into the calculation of shunt impedance, which will be twice that which was calculated for the forward wave only (J. E. Leiss, Minutes of the Conference on Proton Linear Accelerators at Yale University, October 21-25, 1963, p. 74).

The following values of parameters: $\omega = 2\pi \times 800$ Mc/sec, $r_{sn} = 20\ M\Omega/m$, $Q_{on} = 2 \times 10^4$, $v_{ge} = 4 \times 10^5$ m/sec, $I_o = 0.1$ A, and the proton kinetic energy = 200 MeV, are taken leading to $C = 1.1 \times 10^{-2}$. The estimate of v_{ge} is difficult especially for a π-mode cavity. As is discussed in the Appendix, the group velocity will vary along the guide to keep the field distribution uniform in an actual cavity. However, assuming the uniform cell structure as is in the present approximation, we may use its average value $\langle v_g \rangle = \omega L/2\, Q_{on}$. This is about 3.7×10^5 m/sec for L = 3 m.

Now the two limiting cases will be considered; one is $\alpha << Ck_b$ and the other is $\alpha >> Ck_b$. As is shown later, the present case is the latter, while such effects as beam blow-up would occur in the former.

(1) Case 1, $\alpha << Ck_b$

As in the TWT theory, we have three roots of (22) for the forward wave. They are

$$\delta_1 = \frac{1}{2}\left(\sqrt{3} - j\right) Ck_b \tag{24a}$$

$$\delta_2 = \frac{1}{2}\left(-\sqrt{3} - j\right) Ck_b \tag{24b}$$

$$\delta_3 = j\, Ck_b \tag{24c}$$

which correspond to the increasing, decreasing, and unattenuated waves, respectively. We have also another solution for the backward wave which is given by

$$\Gamma_4 = -\Gamma_b - \delta_4 \tag{24d}$$

and

$$\delta_4 \doteq \frac{\alpha}{2} - j\frac{C^3 k_b}{4} \quad . \tag{24d'}$$

Since $C \ll 1$, we must take into account α for the δ_4 and may neglect the second term on the right-hand side.

These four waves should be superposed with the proper boundary condition. A finite beam current $I_1(0)$ at the input ($z = 0$) is considered and the standing wave conditions at the input and the output are taken as follows, at $z = 0$ assuming $|\delta_i| \ll k_b$,

$$\dot{E}_1(0) + \dot{E}_2(0) + \dot{E}_3(0) = \dot{E}_4(0) + \dot{E}_e(0) \tag{25a}$$

$$\frac{\dot{E}_1(0)}{\delta_1^2} + \frac{\dot{E}_2(0)}{\delta_2^2} + \frac{\dot{E}_3(0)}{\delta_3^2} = -jK\dot{I}_1(0) \tag{25b}$$

$$\frac{\dot{E}_1(0)}{\delta_1} + \frac{\dot{E}_2(0)}{\delta_2} + \frac{\dot{E}_3(0)}{\delta_3} = 0 \quad , \tag{25c}$$

and at $z = L$

$$\dot{E}_1(0)e^{\delta_1 L} + \dot{E}_2(0)e^{\delta_2 L} + \dot{E}_3(0)e^{\delta_3 L} = \dot{E}_4(0)e^{(2jk_b + \delta_4)L} \tag{25d}$$

where suffixes n and o for E are omitted for simplicity. The suffix i (= 1, 2, 3 and 4) of $\dot{E}_i$ corresponds to the above four solutions of δ_i and zero in parenthesis means $z = 0$. The constant K is given by

$$K = \frac{m_\ell v_o^2}{e\, k_b I_o} \tag{26}$$

from (21), and the third condition (25c) comes from the assumption of $v_1(0) = 0$. The solutions for $\dot{E}_i$ are given by

$$\dot{E}_i(0) = (-1)^{i+1} \frac{\dot{E}e(0)\,\Delta_{i1} + jK\dot{I}_1(0)\,\Delta_{i2}}{\Delta}, \tag{27}$$

where

$$\Delta = \begin{vmatrix} 1 & 1 & 1 & -1 \\ \frac{1}{\delta_1^2} & \frac{1}{\delta_2^2} & \frac{1}{\delta_3^2} & 0 \\ \frac{1}{\delta_1} & \frac{1}{\delta_2} & \frac{1}{\delta_3} & 0 \\ e^{\delta_1 L} & e^{\delta_2 L} & e^{\delta_3 L} & -e^{(2jk_b+\delta_4)L} \end{vmatrix} \tag{28}$$

and $\Delta_{i,j}$ is the subdeterminant of the ith column and the jth row. Taking δ_4 as $\alpha/2$,

$$\dot{E}_1(0) = \frac{\dot{E}_e(0) - jK\dot{I}_1(0)\,\delta_1^2 \left[1 - e^{-(2jk_b+\frac{\alpha}{2})L}\,\frac{\delta_2 e^{\delta_2 L} - \delta_3 e^{\delta_3 L}}{\delta_2 - \delta_3}\right]}{3 - e^{-(2jk_b+\frac{\alpha}{2})L}\left(e^{\delta_1 L} + e^{\delta_2 L} + e^{\delta_3 L}\right)} \tag{29a}$$

The components $\dot{E}_2(0)$ and $\dot{E}_3(0)$ are found by interchanging subscripts and the component $\dot{E}_4(0)$ is

$$\dot{E}_4(0) = \frac{e^{-(2jk_b + \frac{\alpha}{2})L}\left(\dot{E}_1^0 e^{\delta_1 L} + \dot{E}_2^0 e^{\delta_2 L} + \dot{E}_3^0 e^{\delta_3 L}\right)}{3 - e^{-(2jk_b + \frac{\alpha}{2})L}\left(e^{\delta_1 L} + e^{\delta_2 L} + e^{\delta_3 L}\right)} , \tag{29b}$$

where

$$\dot{E}_i^0 = \dot{E}_e(0) - jK\dot{I}_1(0)\,\delta_i^2 . \tag{30}$$

Terms having the form proportional to $jK\dot{I}_1(0)\delta_i^2$ give the induced field.

(2) Case 2, $\alpha >> Ck_b$

In this case the corresponding four roots of δ are

$$\delta_1 \doteq \frac{1}{\sqrt{2}}(1 - j)\,Dk_b \tag{31a}$$

$$\delta_2 \doteq -\frac{\alpha}{2} \tag{31b}$$

$$\delta_3 \doteq -\frac{1}{\sqrt{2}}(1 - j)\,Dk_b \tag{31c}$$

$$\delta_4 \doteq \frac{\alpha}{2} \tag{31d}$$

assuming $\alpha << k_b$. The modified coupling parameter D is

$$D = \sqrt{\frac{2\,Ck_b}{\alpha}}\,C. \tag{32}$$

General solutions are also obtained from (27) and (28), while, in the first approximation, they are

$$\dot{E}_1(0) \doteq \frac{\frac{\delta_1}{\alpha}\, e^{\frac{\alpha}{2}L}}{2\sinh\frac{\alpha}{2}L}\,\dot{E}_e(0) - \frac{jK\,\delta_1^{\,2}}{2}\,\dot{I}_1(0) \tag{33a}$$

$$\dot{E}_2(0) \doteq \frac{e^{\frac{\alpha}{2}L}}{2\sinh\frac{\alpha}{2}L}\,\dot{E}_e(0) + \left(\frac{e^{\frac{\alpha}{2}L} - \cosh\delta_1 L}{\sinh\frac{\alpha L}{2}}\right)\frac{jK\,\delta_1^{\,2}}{2}\,\dot{I}_1(0) \tag{33b}$$

$$\dot{E}_3(0) \doteq -\frac{\frac{\delta_1}{\alpha}\, e^{\frac{\alpha}{2}L}}{2\sinh\frac{\alpha}{2}L}\,\dot{E}_e(0) - \frac{jK\delta_1^{\,2}}{2}\,\dot{I}_1(0) \tag{33c}$$

$$\dot{E}_4(0) \doteq \frac{e^{-\frac{\alpha}{2}L}}{2\sinh\frac{\alpha}{2}L}\,\dot{E}_e(0) + \left(\frac{e^{-\frac{\alpha}{2}L} - \cosh\delta_1 L}{\sinh\frac{\alpha L}{2}}\right)\frac{jK\,\delta_1^{\,2}}{2}\,\dot{I}_1(0)\,, \tag{33d}$$

where we have assumed the resonance condition $2k_bL = 2\pi \times$ integer. When the phase shift due to the beam is sufficiently small as is expected in the present design, this assumption will not change the results. In the actual accelerator, α will also vary as z increases, for v_g varies. As

we have used the average value of $\langle v_g \rangle$ $(= \omega_n L/2\, Q_{on})$ for the uniform-cell assumption, one may use the corresponding $\alpha = \omega_n / \langle v_g \rangle Q_{on} = 2/L$. This value of α is about ten times larger than the parameter Ck_b for L = 3 m so that we can easily see, from numerical checks, that the above expressions (33a) ~ (33d) should be sufficiently close to exact calculated values. Using (20), (23), (26), (31a) and (32), the induced field given by the summation of the second terms in E_i's is found to be expressed as

$$\dot{E}_b = - f(z)\, r_{sn}\, \mathring{I}_1(0) \quad , \tag{34}$$

where f(z) is a function of z taking almost real-positive values. Using the above stated values for α , C and other parameters, f(z) is estimated to be about 0.27 at z = o and 0.73 at z = L. It is interesting to compare these values with that given by (15'), taking $I_1(0) = 2I_o$. Since the coupling effect between the beam and the field was neglected, f(z) was constant and equal to 0.5 in the preceding section. Taking into account the coupling interaction in a lossy guide, the induced field increases as z increases. This is because the assumed interaction is one-directional or the beam interacts only with the forward wave.

6. Discussion of the Beam Blow-up Effect

In a linear accelerator, which is heavily loaded by the coupling interaction between the beam and the wave, the so-called beam blow-up effect would occur as in electron linacs and traveling wave tubes. The beam blow-up effect in electron linacs is caused by the excitation of a deflecting mode HEM having a backward group velocity. Theoretical studies have been done by a method similar to the theory of backward wave tube oscillators leading to good agreement with experiments.[8, 9] Of course, a similar mechanism is possible in high energy proton linacs; however, if we use the π-mode structure, the excitation of the deflecting mode is only possible at its space-harmonics having a forward group velocity. Therefore, the wave excitation of a backward wave tube type cannot occur in this case. The regenerative wave excitation will only occur through the standing wave type interaction, or the feedback due to the backward phase velocity wave, when the loss at the walls has been compensated by the wave amplification due to the beam. Furthermore, the effective shunt impedance to excite such a space-harmonic wave should be much smaller than that for the fundamental wave, therefore one can expect that the starting current for the beam blow-up due to this mode should be relatively high in the present case. This problem has been

treated by Gluckstern who obtained a starting current as high as 40 A for the Brookhaven linac.[10]

On the other hand, in a standing wave linac, the regenerative interaction due to feedback through the backward phase velocity wave would also occur at the other modes having high shunt impedances, for example, at fundamental harmonics of TM modes. Similar phenomena have often been observed as an internal feedback oscillation in TWT's with low loss structures and may be referred to as longitudinal beam blow-up.

Since the beam blow-up effect could start even from a small signal such as the noise field, the small-signal theory would be applicable except for nonlinear effects as a coherent interaction due to the tightly bunched beam. The starting current will be sufficiently high to compensate losses, so that the Case 1 of $k_n C \gg \alpha$ (still $C < 1$) is probable rather than Case 2. After a numerical calculation in TWT theory including losses,[4] even when $k_n C/\alpha \sim 1$, the solution for δ_i, given by the Case 1 approximation, are still close to the exact calculations.

Then, the starting current for a longitudinal beam blow-up is examined as follows:

First, because of the relatively large value of Ck_bL, simultaneous tuning for the three forward waves cannot be made; i.e. wave 3 will be completely detuned when waves 1 and 2 have been adjusted to resonate the cavity so as to make the wave-beam interaction. Second, the decreasing wave 2 will have high attenuation so that terms of $e^{\delta_2 L}$ can be neglected. Thus, the beam blow-up effect will occur when the denominators in (29a) and (29b) become zero if we consider only the amplification due to wave 1, or

$$3 - e^{\frac{\alpha}{2} L} e^{\mathrm{Re}(\delta_1 L)} = 0 \tag{35}$$

Taking $\alpha = \frac{2}{L}$, we have $\sqrt{3}/2\, Ck_bL = 2.10$, and the starting current is given by using (23) as

$$I_{os} = 57.0 \frac{m_\ell v_o^2 v_{ge} Q_{on}}{e r_{sn} \omega k_b L^3} \tag{36}$$

$$\doteq 28.5 \frac{m_\ell v_o^2}{e r_{sn} k_b L^2}$$

If we use $v_o = 0.5\,c$, $L = 3$m, $\omega = 2\pi \times 800$ Mc, and $r_{sn} = 20$ MΩ/m, we obtain about 5.5 A for the starting current for the TM_{01} mode.* This current is considerably smaller than that estimated for the deflecting mode,[10] though it is sufficiently high compared with the present design. The build-up time, T_b, for this effect is also given by using (19) as

$$T_b = \frac{1}{\mathrm{Re}\, j(\omega - \omega_n)} \approx \frac{1}{\mathrm{Re}(v_{ge}\delta_1)} \approx \frac{Q_{on}}{\omega} \sim 4\ \mu\mathrm{sec}\ .$$

Certainly, a similar longitudinal blow-up having a lower starting current may be expected for the excitation of other modes as TM_{01n} $(n > 0)$ rather than TM_{010}. Also, there may be another mechanism of blow-up as a resonant or a coherent interaction suggested by Leiss,[11] which should be a quite nonlinear phenomenon and beyond this study; however, it might be strongly dependent on circuit conditions as discussed by Gluckstern.[10]

At any rate, before such a beam blow-up would appear, one can assume that the actual accelerator should become a decelerator as a TWT amplifier. In the first approximation, the critical current is given by (16b) when the value of Q_b becomes negative. Using (17) and taking the values of parameters used in the paragraph four, one will find about 0.2 A for the critical value. Although this value increases as the field strength due to the external source increases, the actual limiting current of a high energy proton linac will be determined by such a condition.

The author wishes to offer his sincere thanks to Dr. J. P. Blewett for his stimulating interest in this work and for the hospitality of the

---

* At the MURA Linac Conference, we had neglected the effect of the wall loss in (35) and obtained a much smaller value.

Brookhaven National Laboratory. It is a great pleasure to acknowledge the invaluable information about his experimental studies and the helpful discussion of Mr. S. Giordano, who contributed especially to the analysis in the Appendix. The author also thanks Dr. R. L. Gluckstern and Dr. H. Hirakawa for their useful discussions.

APPENDIX

Wave Propagation in a π-Mode Accelerator

As is well known, in the ideal π-mode section, we have essentially zero group velocity from the dispersion curve. On the other hand, in the actual guide with losses, to maintain the field distribution constant along the guide, we need continuous power flow from the external source to the guide, or a finite group velocity in the steady state. Such a condition is only fulfilled with phase shifts and shifts of resonant frequencies which are different for each cell in one section. This has been examined and verified experimentally by Giordano who obtained the dependence of these shifts on cell numbers and Q_o values[12] (Fig. 1 and Fig. 2). We have considered such effects from a simple power relation and a dispersion-equation, giving an idea of the group velocity in the π-mode.*

The energy flow along the guide is denoted by S(z) (J/sec) and the equation of continuity for the energy flow can be written as

$$\frac{\partial U}{\partial t} + \frac{\partial S}{\partial z} + R = 0 \qquad \text{(A-1)}$$

with the linear density of stored energy U(z) (J/m) and the loss per unit length R(z) (J/sec, m). In the steady state the time derivative is zero so that the first term of (A-1) is eliminated. The energy flow S is expressed quite generally by using the group velocity, v_g, which is also a function of z in the present case, by[13]

$$S(z) = v_g(z)\ U(z) \qquad \text{(A-2)}$$

Using this expression, (A-1) becomes

$$v_g(z) \frac{\partial U(z)}{\partial z} + \frac{\partial v_g(z)}{\partial z} U(z) = - R(z) \qquad \text{(A-3)}$$

As is shown in paragraph 2, the peak axial field $E_o(z)$ is related to U(z) through the shunt impedance and the Q-value by means of

---

* A somewhat similar analysis had been done by Nagle and Knapp using an equivalent circuit model (D. E. Nagle and E. A. Knapp, Minutes of the Conference on P. L. A. at Yale University, Oct. 1963, p. 171, E. A. Knapp, LASL Tech Memo P-11/EAK-3, Oct. 1963, unpublished).

$$\frac{E_o^{\,2}(z)}{R(z)} = r_s \qquad \text{and} \qquad \frac{\omega\, U(z)}{R(z)} = Q_o \quad . \tag{A-4}$$

Thus, so far as we consider the nearly uniform structure of cells, the constant field-distribution (i. e. E(z) is constant) corresponds to constant loss and stored energy density (i. e. both R(z) and U(z) are constant). Using the second expression of (A-4), (A-3) becomes

$$\frac{\partial\, v_g(z)}{\partial z} = -\frac{\omega}{Q_o} \quad . \tag{A-5}$$

By integration,

$$v_g(z) = -\frac{\omega}{Q_o}\ (z + \text{const.}) \ .$$

If the power is fed from z = o (single feed), it could be assumed to be completely reflected at the end-wall, or $v_g = 0$ at z = L. Then,

$$v_g(z) = \frac{\omega}{Q_o}\ (L - z) \tag{A-6}$$

Now, we assume a simple dispersion equation between the frequency and the propagation constant k like

$$\omega \doteq \omega_o - \frac{\delta\omega}{2} \cos k\, L_o \ , \tag{A-7}$$

taking the center frequency of the passband, ω_o, the bandwidth, $\delta\omega$, and the unit cell length, L_o. The group velocity is calculated from

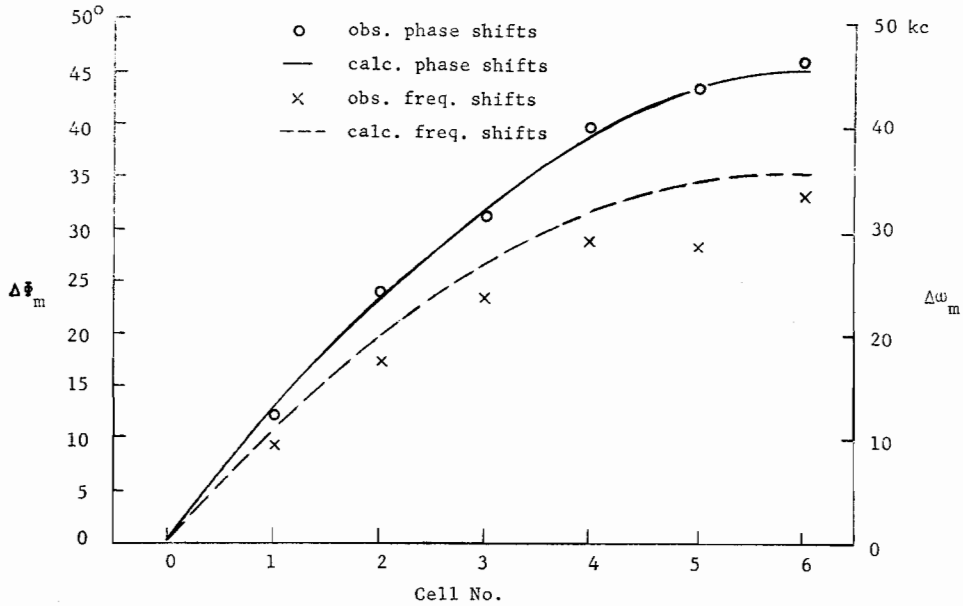

Fig. 1

Dependence of Phase and Frequency Shifts on Cell Numbers

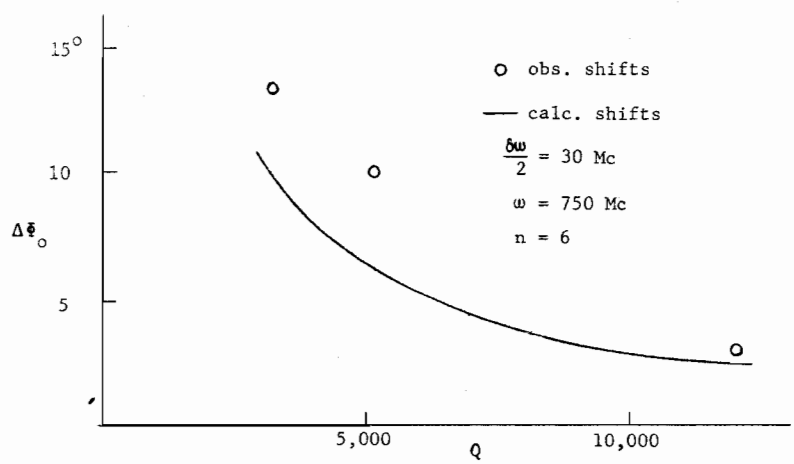

Fig. 2

Dependence of the Total Phase Shift on Q-Value (Experimental Condition is Different from Fig. 1)

this equation as,

$$v_g = \frac{d\omega}{dk} = \frac{\delta\omega L_o}{2} \sin kL_o \tag{A-8}$$

Combining (A-4) and (A-6), the necessary phase shift for the mth cell in a π-mode guide is

$$\Delta \phi_m = \Delta (kL_o)_m = \frac{2v_g}{\delta\omega L_o} = \frac{2}{Q_o} \frac{\omega}{\delta\omega} (N-m) , \tag{A-9}$$

where z is replaced by mL_o considering end half-cells (m = 0, 1, 2, ... N for an N-cell section). The phase shifts are accumulated and the total shift is given by

$$\Delta \Phi_o = \sum_{m=o}^{N} \Delta\phi_m = \frac{\omega}{Q_o \delta\omega} N(N+1) \tag{A-10}$$

The observed phase shift is the accumulated phase shift at the center of each cell. Referring to the first cell (m = o), they are

$$\Delta \Phi_m = \Delta \Phi_o - \sum_{n=m}^{N} \Delta \phi_n = \frac{\omega}{Q_o \delta\omega} m(2N - m + 1) . \tag{A-11}$$

Corresponding frequency shifts are also obtained by a Taylor expansion of (A-7) around the π-mode propagation constant, or

$$\omega'_\pi \doteq \omega_\pi + \frac{1}{2} \left(\frac{d^2\omega}{dk^2} \right) (\Delta\phi)^2 . \tag{A-12}$$

Taking $\Delta\omega_m = \omega'_{\pi m} - \omega_\pi$, we have

$$\Delta\omega_m = \frac{1}{4}\delta\omega\ (\Delta\phi_m)^2 = \frac{\omega^2}{Q_{on}^2}\ \frac{1}{\delta\omega}\ (N - m)^2 \ . \qquad \text{(A-13)}$$

One can compare these formulae with the experiments. Taking $\omega = 2\pi$ x 880 Mc, $\delta\omega = 2\pi$ x 2.7 Mc, $Q_o = 1.7 \times 10^4$,* and N = 6, the total phase shift and the maximum frequency shift calculated are 46° and 36 kc, respectively. Corresponding experimental values are 47° and 34 kc which are surprisingly close to the calculated values. Also their dependence on cell-numbers gives good agreement between calculations and experiments as shown in Fig. 1, and Fig. 2 gives results of another experiment showing the $1/Q_o$ dependence of the total phase shift, which is also expected by the above analysis, while the calculated absolute values are about 30% smaller than observed, probably because of the very wide band structure.

Now, we have an idea of the group velocity, which varies along the guide. In the present approximation of this article, which is based on a uniform-cell structure, we have no reason to use velocity other than its average value of $\langle v_g \rangle = \omega L/2Q_o$. This velocity also corresponds to the value obtained by the well known dispersion-relation between the phase change and the frequency change of a resonant circuit, in which we consider the whole π-mode section as one cavity.** In a transient phenomenon such as a pulse build-up, one may find another velocity for v_{ge}, which is the velocity of beats between the π-mode and other modes excited by disturbances. The slowest velocity is the velocity of the beat between the fundamental and the next modes, and should be most important. Fortunately, this slowest beat velocity is also of the same order and slightly slower than the above average group velocity in the steady state, in the present designed accelerator.

---

* Observed Q_o-value is 1.5×10^4, whereas a slightly high value is used by taking into account the effect of end-walls.

** The dispersion relation is $\Delta\Psi = -\frac{\Delta\omega}{2\omega_o} Q_o$, and considering

$$\frac{\Delta\lambda_g}{\lambda_g} = \frac{\Delta\Psi}{\pi N}\ , \quad v_g = \frac{\Delta\omega}{\Delta k} = \frac{\omega_o}{Q}\ \frac{L}{2}\ .$$

REFERENCES

1. A Proposal for Increasing the Intensity of the Alternating-Gradient Synchrotron at the Brookhaven National Laboratory, BNL 7956, (May 1964).

2. J.C. Slater, Microwave Electronics, (Van Nostrand, 1950), Chap. IV.

3. A.J. Lichtenberg, Rev. Sci. Instr. 33, 395, (1962), J.E. Leiss, NBS Int. Rept. (1958, unpublished).

4. J.R. Pierce, Traveling Wave Tubes, (Van Nostrand, 1950).

5. L. Brillouin, J. App. Phys. 20, 1196 (1949).

6. A. Nordsieck, Proc. IRE 41, 630 (1953), P.K. Tien, et al., Bell System Tech. J. 35, 349 (1956).

7. J.R. Pierce, ibid, Chap. XII.

8. P.B. Wilson, HELPL Rept. No. 297, (June 1963) Stanford University.

9. H. Hirakawa, Jap. J. App. Phys. 3, 27 (1964).

10. R.L. Gluckstern, AADD-38 (July, 1964) Brookhaven National Laboratory Internal Report.

11. J.E. Leiss, ibid and NBS Int. Rept. (Oct. 1962, unpublished).

12. S. Giordano, private communications. The author expresses his thanks for permission to quote here some of the unpublished experimental results.

13. J.C. Slater, ibid, Chap. III and App.

THE CERN-PS LINAC - BEAM LOADING AND RF STUDIES

C. S. Taylor and Y. Dupuis
CERN

ABSTRACT

The CERN-PS linac is at present accelerating currents of the order of 60 mA and partial compensation of the beam loading is being provided by "bumps" on the rf pulses. The evolution of this type of compensation is described and the results of energy spread and emittance measurements with and without compensation are presented.

An alternative method of supplying beam power from a supplementary power source is considered and preliminary tests are described.

Measurements of the phasing between tanks and the velocity of propagation of fields along the walls of the cavities are also reported.

I. INTRODUCTION

Beam loading in the accelerating cavities first became detectable in the rf envelopes with beam currents around 15 mA, and in 1961 attempts were made to compensate the fall in field during the beam pulse by moving the beam to the rising edge of the tank field and increasing the level. At that period, however, there was a 20 μs jitter in the initial rise of field in the 10 MeV tank, attributed to multipactor effect, and this jitter resulted in wide variation in accelerating field level and consequently in linac beam quality and PS intensity. The increased level also encouraged sparking although that could have been overcome by shortening the rf pulse.

Efforts were then directed towards supplying more power to the cavities during the beam pulse with the beam restored to its normal position near the end of the rf build-up.

II. EVOLUTION OF PRESENT METHOD OF COMPENSATION

In July 1962, attempts were made to increase the plate voltage of the TH 470 power amplifiers at the moment of beam injection. It was found that, with some sacrifice of pulse length, we could produce a useful "bump" on the anode pulse by increasing the terminal capacitor of the modulator delay line as shown in Fig. 1.

This method was applied first to the modulator of the three final amplifiers (see Fig. 8 for a general schematic of the rf system), and then extended to the drive modulator, both to increase the tank bumps and to suppress the over-voltages which appeared as a result of pulse length disparities.

The next step was to decrease the cathode bias voltage simultaneously with the anode bump by firing a hydrogen thyratron connected in parallel with part of the cathode resistor (Fig. 2). Careful adjustment of this combination of anode voltage and cathode current bumps led to the present situation, where a beam of 30-35 mA can be fully compensated in each of the three tanks.

It has been found convenient to assess these effects by displaying the time derivative of the tank field rather than the field itself. Both signals are shown in Fig. 3. Knowing the beam current we can immediately calibrate our signal and derive the percentage compensation for any given rf adjustment.

III. BEAM QUALITY WITH PRESENT METHOD

For the case of a beam pulse short by comparison with the cavity time constant, it can be shown by approximate solution[1] that the beam produces a change of accelerating field

$$\frac{\Delta V}{V_o} = -\frac{P_b}{2\,W_o}\,t$$

where P_b is the instantaneous power delivered to the beam and W_o is the cavity stored energy at $t = 0$, and a change of phase

$$\Delta\varphi = -\frac{P_b \tan\varphi_s}{2\,W_o}\,t$$

where φ_s is the synchronous phase angle.

Since this phase term is roughly the same for each of the three tanks (about 2.5^o for 50 mA), the original phase relations between the tanks will be preserved during the passage of beam, although not necessarily between the last tank and the debuncher.

The more significant effect of field change we should expect to be equivalent to a change of synchronous phase angle during the pulse and in our case on uncompensated 50 mA should produce an 8% change in $\cos\varphi_s$, for example from $\varphi_s = 30^o$ to $\varphi_s = 21^o$, and detectable changes in energy spread and emittance.

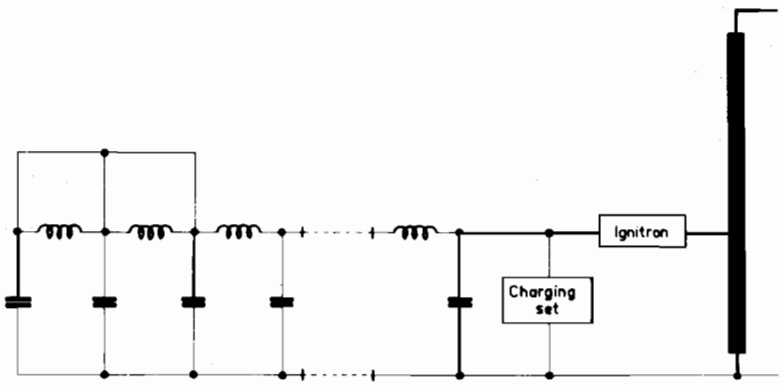

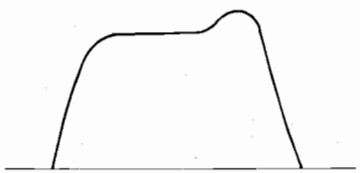

Resulting anode pulse

Fig. 1

Modified delay - line

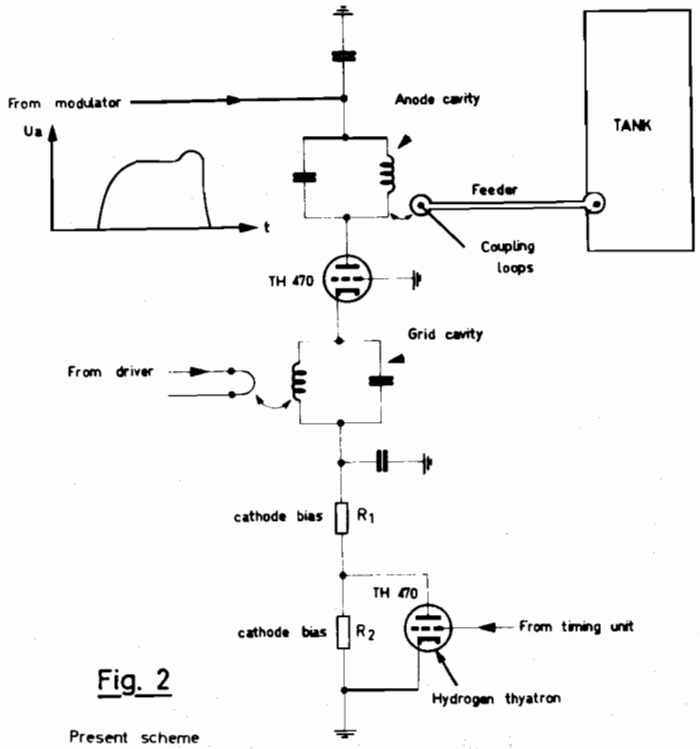

Fig. 2

Present scheme

Accelerating voltage : V

Fig. 3

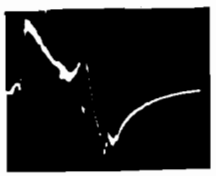

derivative : $\frac{dV}{dt}$

In Fig. 4a we see the measured energy spectra for an uncompensated 55 mA beam and for a beam compensated to an average value of 50% in the three tanks, with and without debuncher. It is evident that the debuncher is doing all the real work but that changes during the pulse are reduced by the compensation. The uncompensated beam is in fact not very satisfactory since particles are lost at the end of the pulse in the linear accelerator itself, the end of the pulse being only one-half the height at the beginning.

The experimental arrangement comprised a 0.5 mm object slit, approximately unity magnification, a 1 mm resolving slit equivalent to $\pm$ 30 kV, and about 6 mA of total beam current, with this reduced current passing through the debuncher. This resolution is not adequate for small energy spreads and the energy spread may be less than that measured. However, from the point of view of what the synchrotron actually sees with 60 mA, this error may be countered by the deterioration of the energy spread due to the reactive beam loading in the debuncher which we estimate to change the phase by some 10° and to add 80 kV to the energy spread.

In Figs. 4b and 4b' we see the emittance plots for the same condition of no compensation and 50% compensation. The horizontal plane (emittance Y) appears to be subjected to a clockwise rotation with time whereas this effect in the vertical plane (emittance Z) is much less marked. The distorted envelope for the end of the pulse in "emittance Y without compensation" probably indicates aperture limitations in the linear accelerator.

Care was taken during these measurements to keep the rf field constant in the middle of the pulse. However, the emittances with and without compensation in the middle of the pulse are not identical and this requires further investigation.

IV. SUPPLEMENTARY POWER SOURCE

In order to drive a 50 mA beam through the 30-50 MeV tank, we need 1 MW of rf power, and since this tank dissipates 1.5 MW, the total instantaneous power requirements are already beyond the capacity of our 2 MW amplifiers. If, however, we separate the functions of feeding losses and feeding beam power , we should be able to approach 100 mA beam currents with our present amplifiers.

Our present proposal is to drive the tank up to operating level by means of the existing delay line modulator, and then to supply the beam power by means of a second coupling loop and power amplifier for the

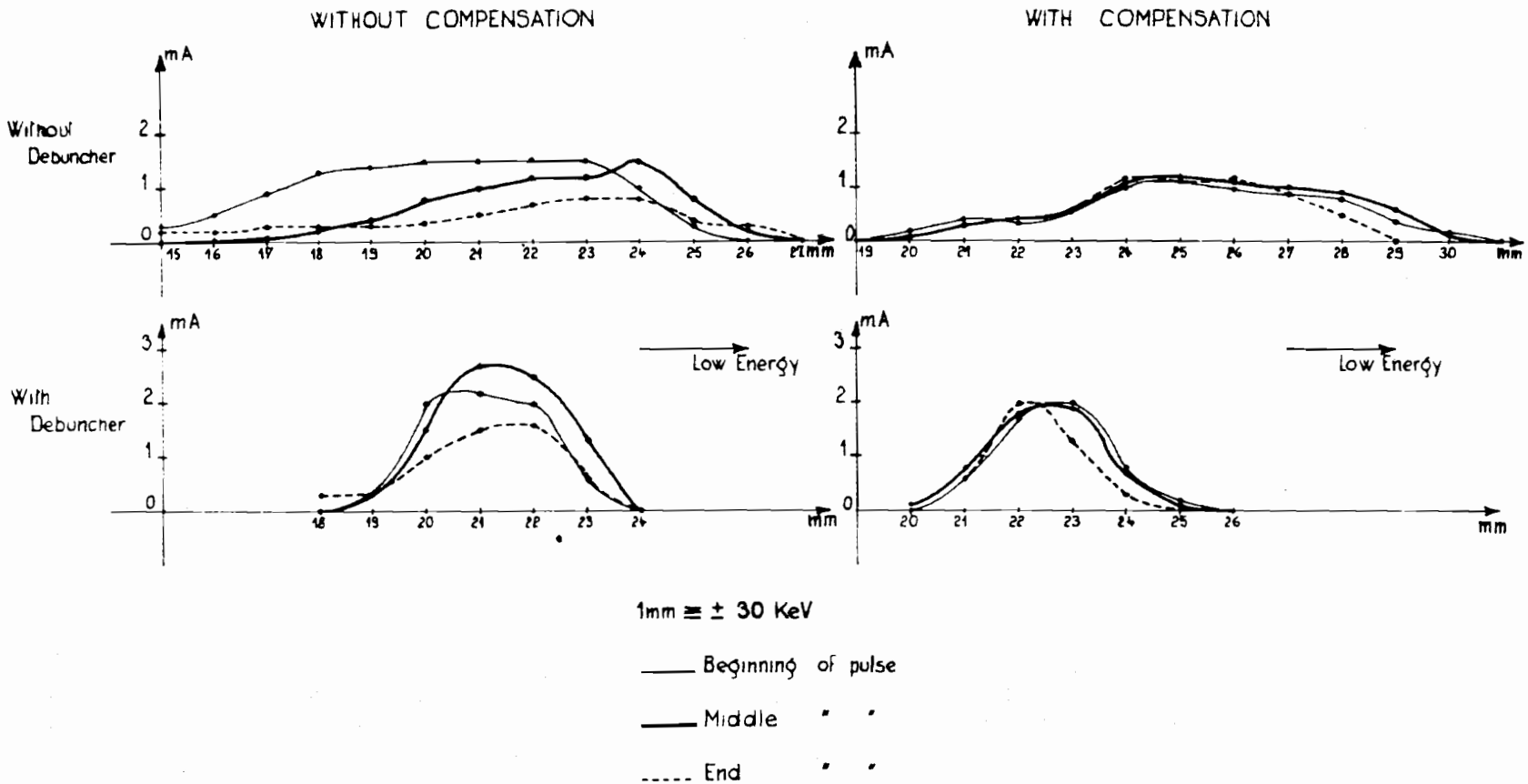

50 MeV ENERGY SPECTRA

Fig. 4A

duration of the beam pulse. We propose a hard-tube modulator for the beam power pulse, with the possibility of servo control from the beam current. One advantage of this system is that the phase of the beam power source can be varied with respect to that of the main source, i.e., power can be fed to the beam with the accelerating voltage in phase with the beam current Fourier fundamental φ_s from the crest.

The proposed scheme is shown in Fig. 5.

Preliminary tests of such a system have been made on the 30-50 MeV tank. The beam power amplifier was excited by rf power taken capacitively from the main loop feeder, and a modulator was modified to provide a short anode pulse (Fig. 6). Using the normal 200 μs pulse transformer, we could not obtain a very satisfactory rise time. Nevertheless full compensation of a 60 mA beam was obtained (Fig. 7). Unfortunately beam quality checks could not be made in the time available, apart from a quick measurement of energy spread which appeared to be normal.

V. PHASING BETWEEN TANKS

The three accelerating cavities are each held at a fixed phase by means of a phase servo loop. Line lengtheners in the final amplifier grid circuits are coupled mechanically to line lengtheners in the phase reference lines and this arrangement permits relative movement of the tank phases (see Fig. 8: Schematic of complete rf system).

A good beam can be obtained by a purely empirical adjustment of relative phases. Alternatively, one can employ a criterion based on the 3 φ_s trapping width. In the early experiments it was accepted a priori that the correct adjustment was the "in-phase" condition although some attempts to measure relative phases with hybrid ring bridges gave conflicting results. With, however, the installation of accurately adjusted cables and a lissajous figure type of phase comparison (Fig. 9), it has become fairly certain that the beam likes best to find the 10 and 50 MeV tanks in phase but the 30 MeV tank advanced by some 25°, that is, this dephasing produces the best energy spread.

There is as yet no satisfactory explanation of this effect. One possible contribution comes from the two-cell drift distance between the first and second tanks, combined with the fact that we normally inject our bunched beam into the first tank well above the center of the rf bucket in order to profit from the higher trapping. However, our step-by-step computations using the program developed at Harwell by Taylor and Carne show that the energy error resulting at 10 MeV is only about

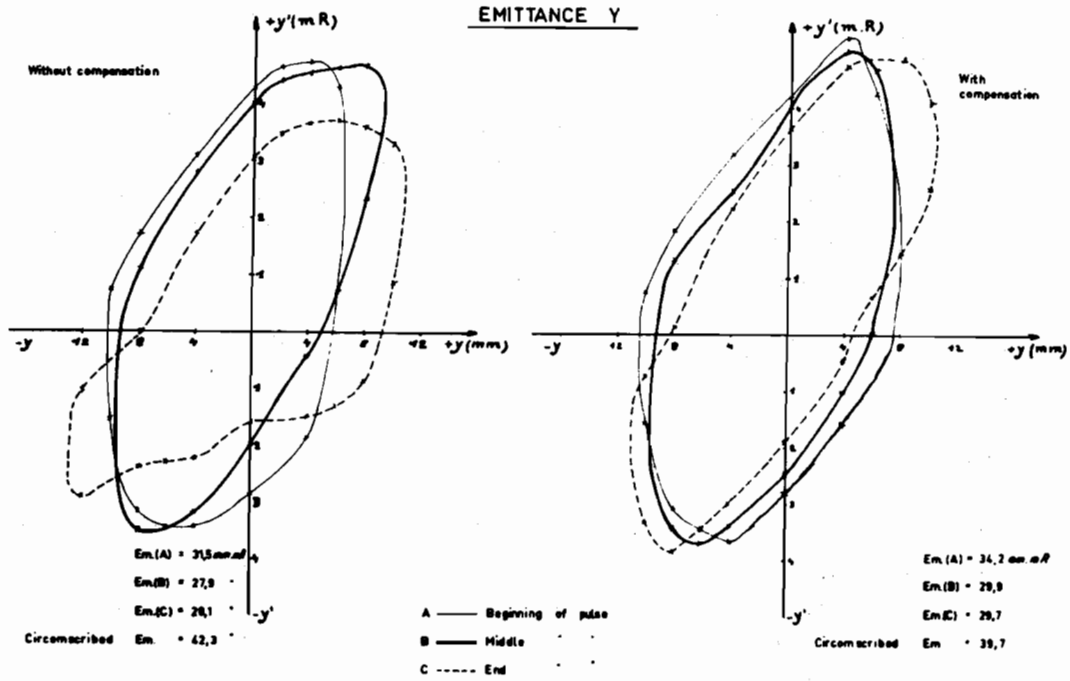
EMITTANCE Y
Without compensation
With compensation
+y'(m.R)
-y'
+y (mm)
-y
Em.(A) = 31,5 mm.mR
Em.(B) = 27,9
Em.(C) = 28,1
Circomscribed Em. = 42,3
Em.(A) = 34,2 mm.mR
Em.(B) = 29,9
Em.(C) = 29,7
Circomscribed Em = 39,7
A —— Beginning of pulse
B —— Middle
C ----- End

Fig. 4b

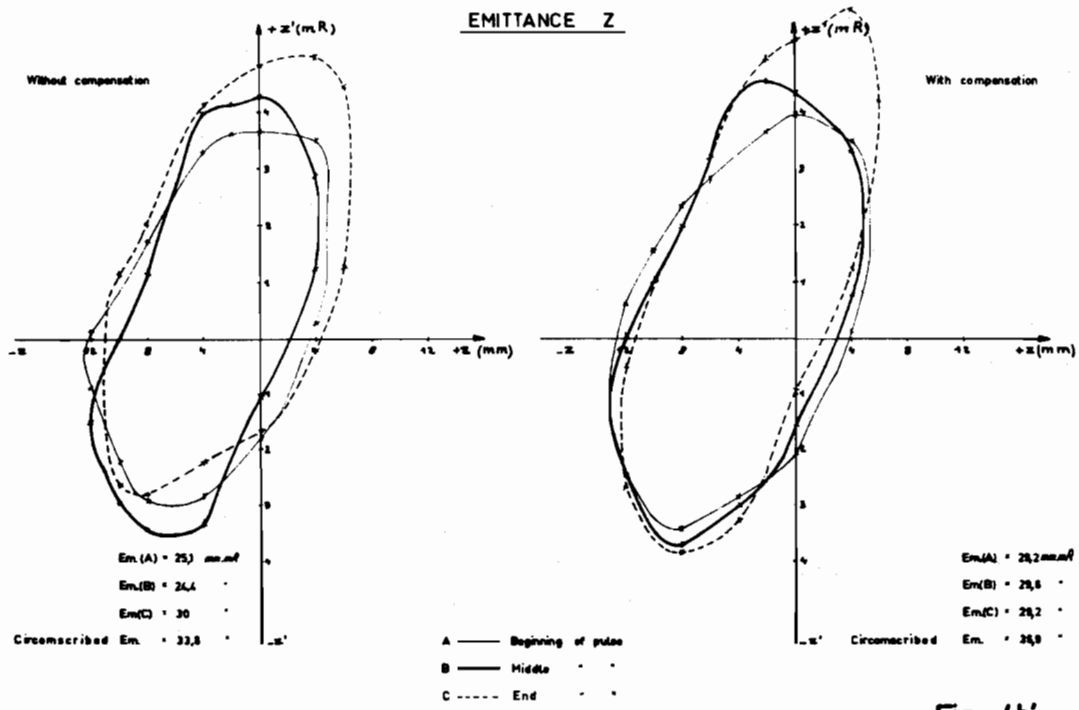
EMITTANCE Z
Without compensation
With compensation
+z'(m.R)
-z'
+z (mm)
-z
Em.(A) = 25,1 mm.mR
Em.(B) = 24,4
Em(C) = 30
Circomscribed Em. = 33,8
Em.(A) = 28,2 mm.mR
Em(B) = 29,6
Em.(C) = 29,2
Circomscribed Em. = 36,9
A —— Beginning of pulse
B —— Middle
C ----- End

Fig. 4b'

100 kV, and produces a phase error due to the drift distance of only 3 or 4 degrees.

Another possibility, which came out of a discussion with Teng and Lapostolle, is that we are exploiting the nonlinear region of the Tank II bucket to spread the bunch out, and then rotating this elongated bunch around to the position of minimum 50 MeV energy spread by adjustment at Tank II and III levels, thereby varying the number of phase oscillations in these tanks. This mechanism would require an integral number of wavelengths in Tank II and an odd number of quarter wavelengths in Tank III.

VI. PROPAGATION

Recent discussions of group velocities[2] have led us to compare the build-up of tank fields at the extremities of the 30-50 MeV tank (with power fed in at one end). Using the phase measurement loops and cables we have employed the chopped beam facility of an oscilloscope to superimpose the detected signals from both loops. In Fig. 10, we see the field signals and the initial build-up on a shorter time base. From these oscillograms one can put an upper limit of a microsecond on the delay and a lower limit of 10^7 m/sec on the corresponding velocity for field propagation along the cavity walls.

ACKNOWLEDGEMENTS

It is a pleasure to acknowledge the excellent contributions of Messrs. Block, Marti, Têtu and Weiss to the experimental work and computations.

TURNER: Could you repeat the specifications for the new FTH 515 tube you mentioned?

TAYLOR: 4 MW peak power; heater, 12 kW; anode dissipation, 11 kW. I think the drive power is 700 kW.

VAN STEENBERGEN: Do you have to make a modification to the tube cavity?

TAYLOR: No, the specification calls for a tube which is a mechanical plug-in replacement for the FTH-470. It will have the same anode volts but double the current. We will probably have to modify the loop and the coupling.

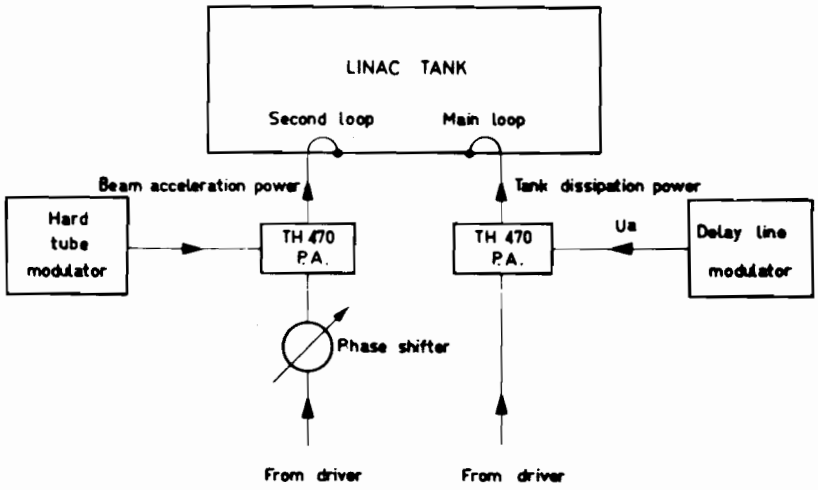

Fig. 5

Proposed scheme

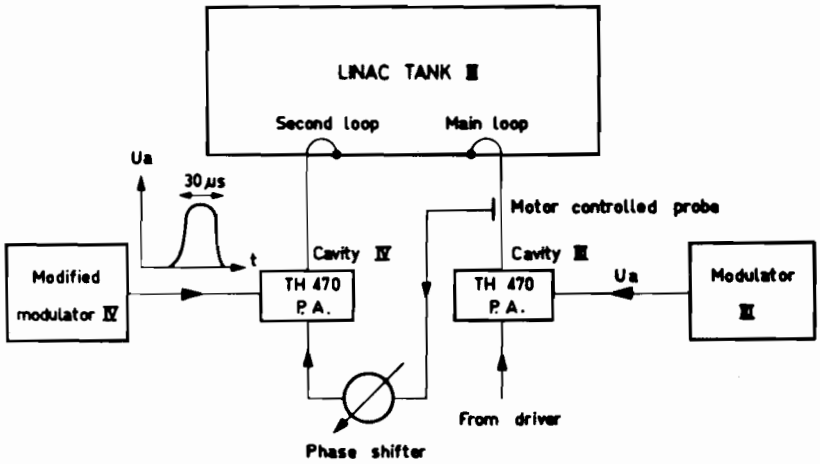

Fig. 6

Tested scheme

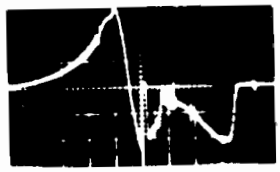

$\frac{dV}{dt}$ for a 50mA beam

Fig. 7

VAN STEENBERGEN: What is the promised delivery date on this tube?

TAYLOR: I think we should get a tube within about six months.

QUESTION: Have you watched some of the modeling on this tube?

TAYLOR: It is only just started. I might mention that the cost is something like $6, 500 per tube.

PERRY: I didn't understand the phase shift from 30° to 21°.

TAYLOR: This is simply the field going up and then dropping due to the presence of beam. This is equivalent to a change in the synchronous phase from 30° to 21°.

PERRY: When you have 50 mA beam loading and 8% droop, was the 30° to 21° the phase shift due to beam loading?

TAYLOR: The difference in cos φ_s was 8%.

KEANE: You mentioned that you had no phase or time delay in the field propagation along the tank. I have noted on Brookhaven's linac that we have at least 1-1/2 microsecond delay from the center drive point to both ends of the tank.

TAYLOR: In our measurement, the difference in path length is about 10 m. In your case it is 15 - 16 m.

MARTIN, J. H.: You used the term "compensated" and "uncompensated." Did that consist of anything besides just an additional bump at the end?

TAYLOR: No, that was simply a bump.

MARTIN: It had influence on the energy distribution and phase-space accommodation and so forth; did it have anything to do with the phase relations between the tanks?

TAYLOR: That occurs with a small beam. If we stop the beam down, we still have this effect.

MARTIN: So this effect is independent of beam loading?

TAYLOR: Yes.

KEANE: You mentioned that you used a separate amplifier for beam compensation. Did you have any trouble with power coupling between the loops of the two driving sources?

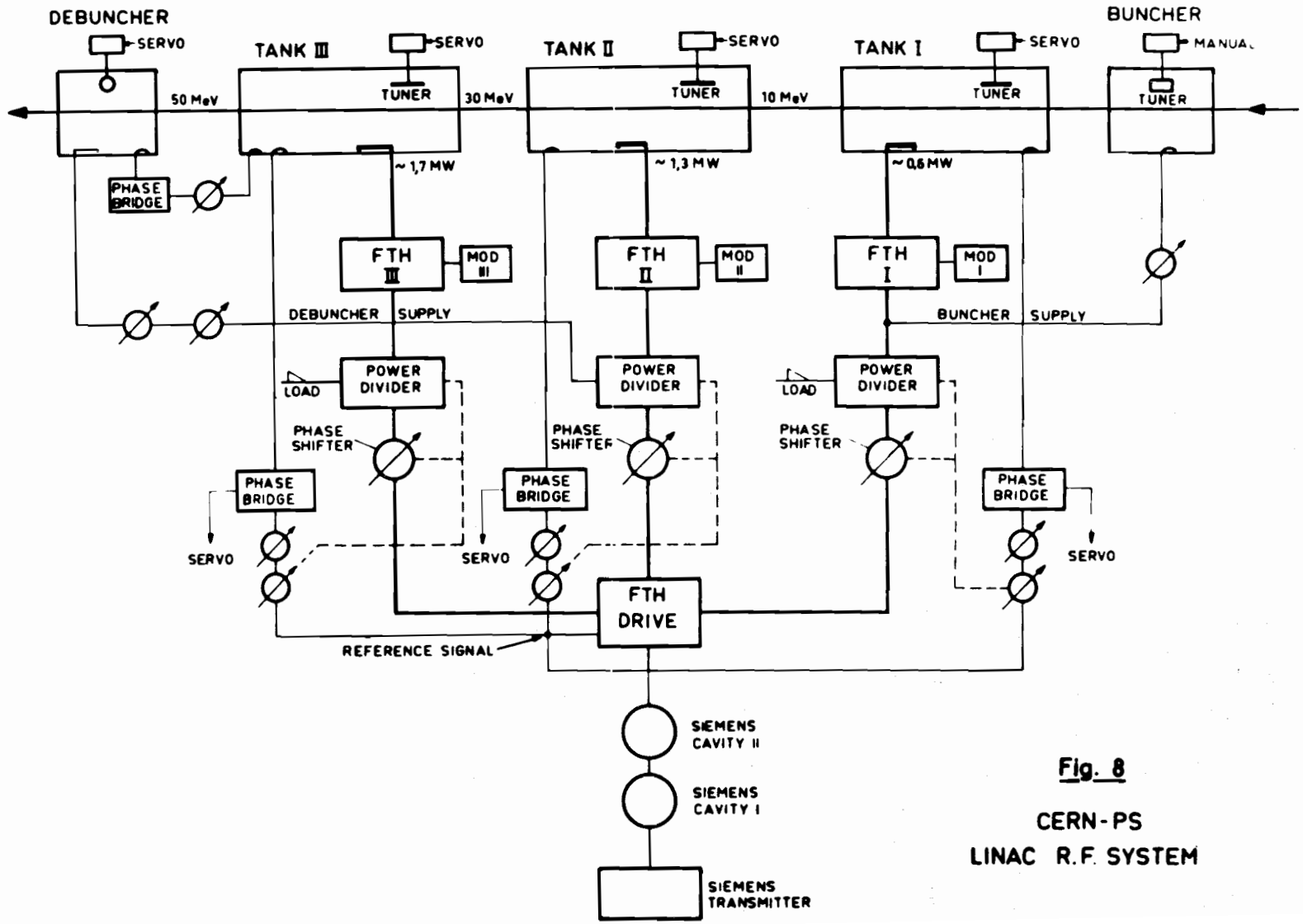

Fig. 8

CERN-PS
LINAC R.F. SYSTEM

TAYLOR: We were a little worried about this and our first move was to put a short circuit piston on the auxiliary loop. We made it as close to a short circuit in a tank as we could. Then we found that by moving this up and down, it made no difference. It is surprising. Then when we connected a FTH amplifier cavity in place of the short circuit, there was a tendency for it to "diode", and we found ourselves in a little bit of trouble getting enough power from the main amplifier.

KEANE: Were the loops the same?

TAYLOR: Exactly the same loop. It probably makes a terrible bump on the flattening, but so far we have not noticed it.

DICKSON: Going back to the phase changing in Tank 2, how do you find running all tanks in phase and adjusting the wave lengths of Tanks 2 and 3 together to get an integral half-wave length?

TAYLOR: We have tried to run them in phase and adjust the levels of all tanks together, but we went through a fair range and we could not find an energy spread as good as the energy spread which we get with the normal adjustment of the phasing.

REFERENCES

1. Y. Dupuis, Etude de la charge introduite par le faisceau dans les cavités H. F. du Linac du CPS. Internal report MPS/Int. LIN 36-8.

2. J. M. Dickson, Private communication.

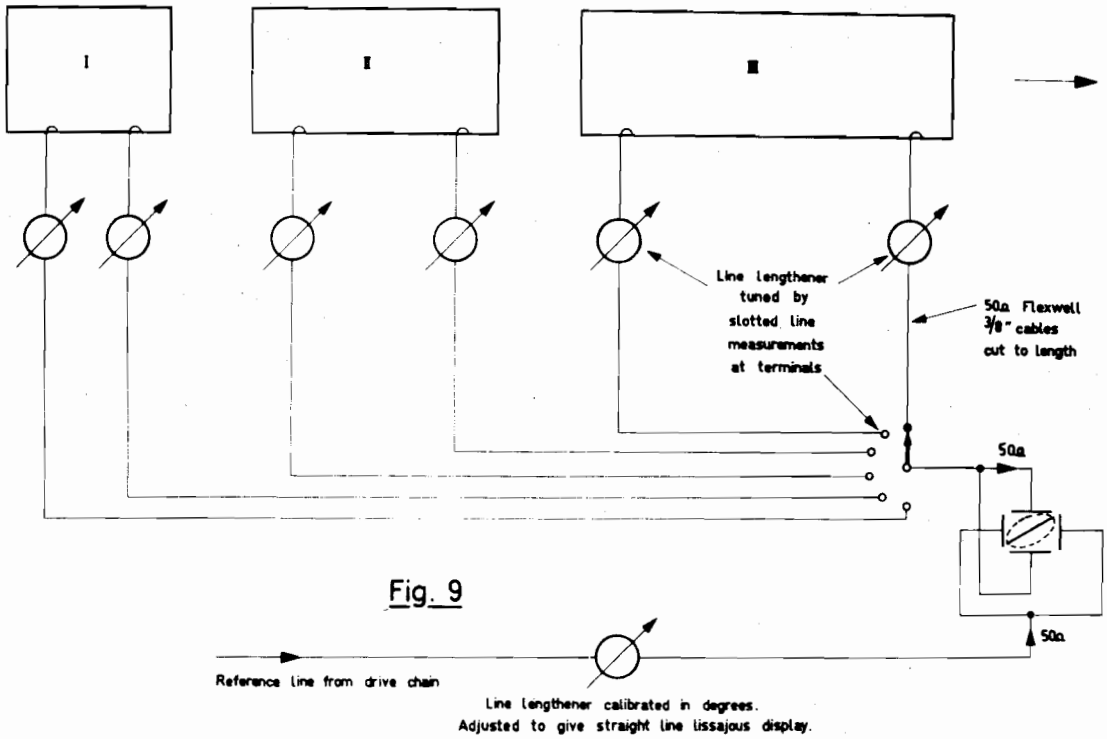

Fig. 9

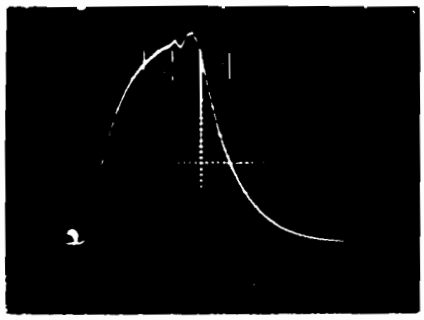

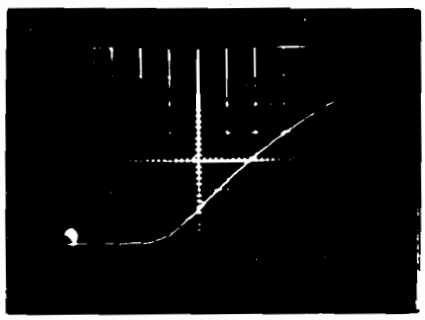

0.5 V/cm 50 μs/cm

Chopped beam.

Equalisation of detector outputs.

A

As Fig 10 A but 10μs/cm.

B

Fig. 10

MODEL MEASUREMENTS AND CORRECTION OF BEAM LOADING EFFECTS IN PROTON LINACS

S. Giordano
Brookhaven National Laboratory

When a proton beam is being accelerated in a linac, there is an interaction with the fields in the accelerator cavity. The effect of the beam on the cavity is referred to as beam loading. Beam loading affects the cavity in two ways: there is a real part which absorbs energy from the cavity, and a reactive part that detunes the cavity. Some estimates of the relative magnitude of these effects have been considered by a number of people, using an equivalent R, L, C circuit. It is the purpose of this paper to measure the effects of beam loading in a multiple-cell linac structure, and to determine the relative magnitude of these effects for two structures of different bandwidths.

It was first necessary to devise some method which would duplicate beam loading in a model cavity. It should be pointed out that the method to be described considers only the steady-state beam-loading effects, and is based on the premise that the beam-loading effects are uniformly distributed along the length of a cavity.

If all the cells of a cavity were detuned by a fixed amount, and the drive was kept at the original resonant frequency, then the effect upon the cavity would be the same as a uniformly distributed reactive component of beam loading. The same results can be obtained by detuning the frequency of the rf drive by a fixed amount. It should be emphasized that the above method results in simulating only the reactive component of beam loading.

The real component of beam loading can be duplicated in a cavity by increasing the losses (decreasing the Q) of all the cells uniformly. The Q is decreased by placing a strand of cotton thread that has been loaded with graphite,* down the axis of a cavity. The cotton thread has a very small reactive effect, which only slightly detunes the cavity. Since the reactive detuning of the loaded cotton thread is uniformly distributed along the cavity, its effects can be eliminated by adjusting the

---

*A piece of cotton thread is soaked in a graphite alcohol suspension. The thread is then squeezed to eliminate excess liquid and hung to dry. By varying the concentration of graphite and alcohol, the losses introduced by the thread can be varied.

perturbation tunes in each cell. Rather than adjusting the tuners, the same results are achieved by changing the frequency of the rf drive to the new resonant frequency of the loaded cavity. It should be pointed out that this simulates only the real component of beam loading.

We now see that it is possible to separate the effects of both the reactive part and the real part of beam loading. It is also possible to combine both of these effects, by simultaneously introducing the loaded string and detuning the drive frequency.

Measurements were made on two different cavities shown in Figs. 1 and 2. Figure 1 shows a shaped iris cavity having a center frequency ($\pi/2$ mode) of 880 Mc and a bandwidth of 2.7 Mc (bandwidth is defined as the difference in frequency between the "0" mode and the π mode). Figure 2 shows a slotted iris cavity (reported by this author in these minutes) having a center frequency of 824 Mc and a bandwidth of 72 Mc. Both the above cavities had pickup loops and perturbation tuners in each cell.

All measurements reported in this paper were made in the "π" mode at $\beta \approx 0.5$. Of interest is the phase and amplitude variations of the electric and magnetic fields along the cavity, as a function of beam loading. In all the measurements to be discussed, the cavity was first tuned to have a flat field (no amplitude variation). The Q and frequency of the drive were then varied in steps, representing different magnitudes of beam loading. Measurements were also made with two different drive conditions:

(1) A single drive at one end of the cavity.
(2) Two separate drives, both in phase, one at each end of the cavity.

Figures 4, 5, 6 and 7 show the results of the measurements made on the shaped iris cavity. These measurements were made for the unloaded Q. Because of the very narrow bandwidth of the shaped iris structure, any attempts to reduce the Q resulted in the overlapping of adjacent modes. Figures 4 and 6 show the amplitude variations along the cavity at three different frequencies for the one-drive and two-drive case. Figures 5 and 7 show the phase variations along the cavity at three different frequencies for both the one-drive and two-drive case. (All phase measurements were made by measuring the phase of each cell relative to one of the end cells.) For the two-drive case we see a considerable reduction of the relative phase change along the cavity, as compared to the single-drive case.

Figures 8 through 21 are the results of the measurement of phase and amplitude variations for the slotted iris structure. Figures 8, 10 and 12, are for Q values of 12,000, 5,000 and 3,000, with a single drive,

and show the variations of the field amplitude for different frequencies. In the above-mentioned figures, it is interesting to note that changes in the amplitude of the field are very sensitive to changes in frequency. It should be pointed out that changing the Q from 12,000 to 5,000 and to 3,000, had only a small effect on the variations of the amplitude.

Figures 9, 11 and 13 are for Q values of 12,000, 5,000 and 3,000, with a single drive, and show the relative phase variations along the cavity. It is interesting to note the relative insensitivity of the phase to changes in frequency, as compared to the large changes in phase due to the changes in Q. In Figs. 9, 11 and 13, when the Q is varied from 12,000 to 5,000 and to 3,000, the relative phase difference between the ends of the cavity varies from 3°, 10° and 14° respectively.

Figures 14, 16 and 18 are for Q values of 12,000, 5,000 and 3,000, with two drives, and show variations of field amplitude for different frequencies. Figures 15, 17 and 19 show the relative phase variations along the cavity, for the same conditions mentioned above.

It is interesting to compare the relative phase and amplitude variations for both the single and double-drive cases. Figure 20 is a plot of the over-all phase difference between the ends of the cavity vs Q, at f_o, $f_o + 150$ kc, and $f_o - 150$ kc, for both the single and double drive cases. For the same above-mentioned conditions, Fig. 21 is a plot of $\frac{\Delta E}{E_{av}}$ vs Q. ($\frac{\Delta E}{E_{av}} = \frac{E_{max} - E_{min}}{2\,E_{av}}$, where E_{max} is the maximum field in the cavity, E_{min} is the minimum field, and E_{av} is the average field.) Figures 20 and 21 closely show that there is a considerable reduction in both the amplitude and the relative phase changes with respect to beam loading changes.

In comparing the narrow band-shaped iris cavity to the wider band-slotted iris cavity, we see that the narrow band structure is considerably more sensitive to beam-loading effects.

Figure 3 shows a hollow cylinder which is to be operated in the TM_{010} mode. Work was recently started on this structure, and measurements are to be made in the near future.

VAN STEENBERGEN: In that diagram you showed a tilt in the tank amplitude. Could you not correct this tilt in the amplitude by changing the frequency?

GIORDANO: There are two reasons that could cause a tilt: (1) a change in the drive frequency as you have indicated, (2) a local detuning of the cavity which can be caused by a change in the thermal gradient along the cavity.

VAN STEENBERGEN: Don't these two effects amount to the same thing?

GIORDANO: No.

LEISS: Your resistive string represents only the beam loading which is 180° out of phase with the field in the tank. A beam of particles is at the equilibrium phase and not at the peak of the radio-frequency voltage, and so there is an additional phase shift due to this.

GIORDANO: We are only considering the steady-state condition and assuming that the beam-loading effects are uniformly distributed along the cavity. The resistive string represents the real component of beam loading, and the reactive component is obtained by changing the frequency of the drive.

LEISS: When you speak of reactive part, what you really mean is that the beam is not running at the peak of the wave, and as such we have an in-phase component and out-of-phase component, so that it is not really right to represent this by a frequency shift.

GIORDANO: What you call an out-of-phase component, I call the reactive part. This reactive component actually causes a detuning of the cavity, which I have duplicated by shifting the frequency of the drive. In Fig. 20, I have shown the effect by varying the frequency from f_o + 150 kc to f_o - 150 kc, and we see that the effect is small. It should be pointed out that this frequency variation is considerably greater than one would expect from a beam of 50 mA.

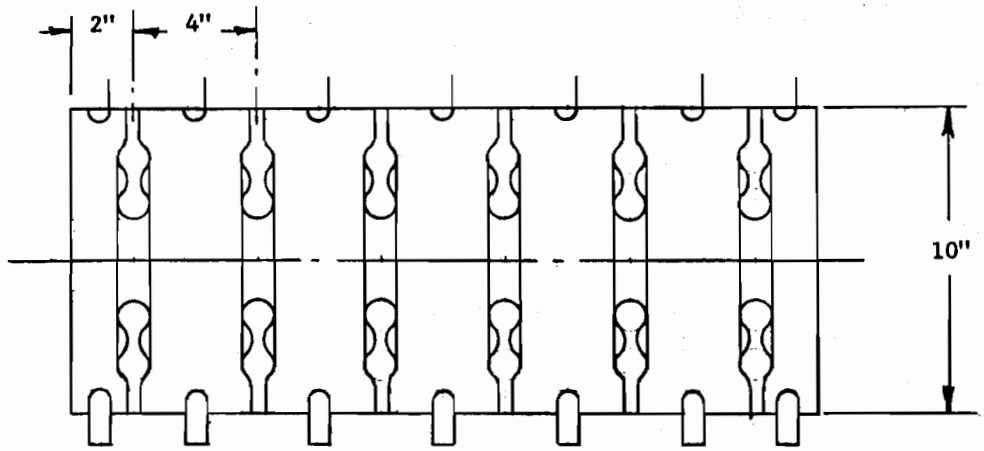

Fig. 1 Shaped Iris

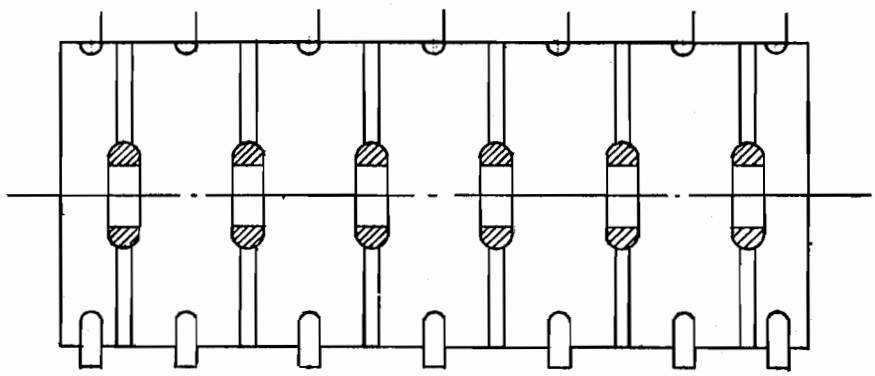

Fig. 2 Slotted Iris

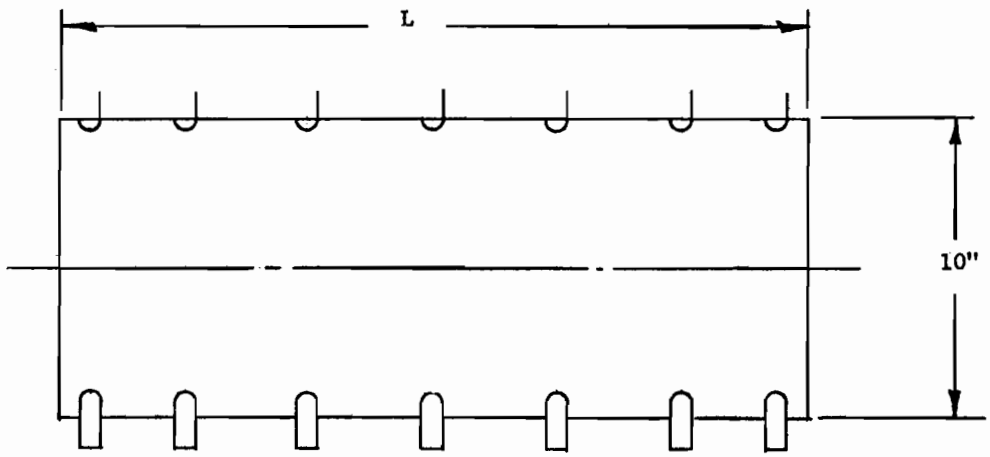

Fig. 3 Hollow Structure

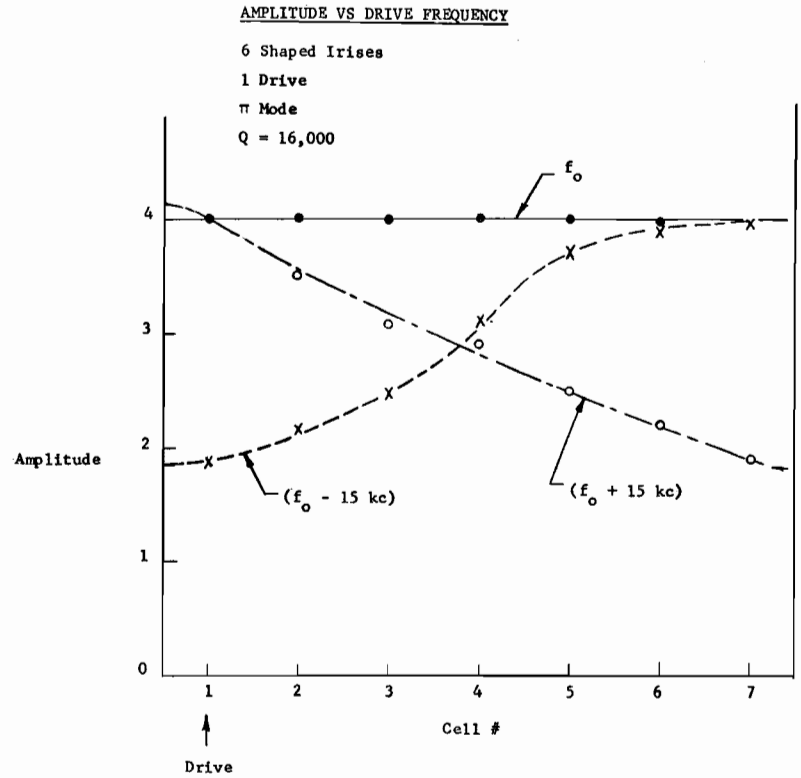
AMPLITUDE VS DRIVE FREQUENCY
6 Shaped Irises
1 Drive
π Mode
Q = 16,000
f_o
$(f_o - 15\ kc)$
$(f_o + 15\ kc)$
Amplitude
0
1
2
3
4
1
2
3
4
5
6
7
Cell #
Drive

Fig. 4

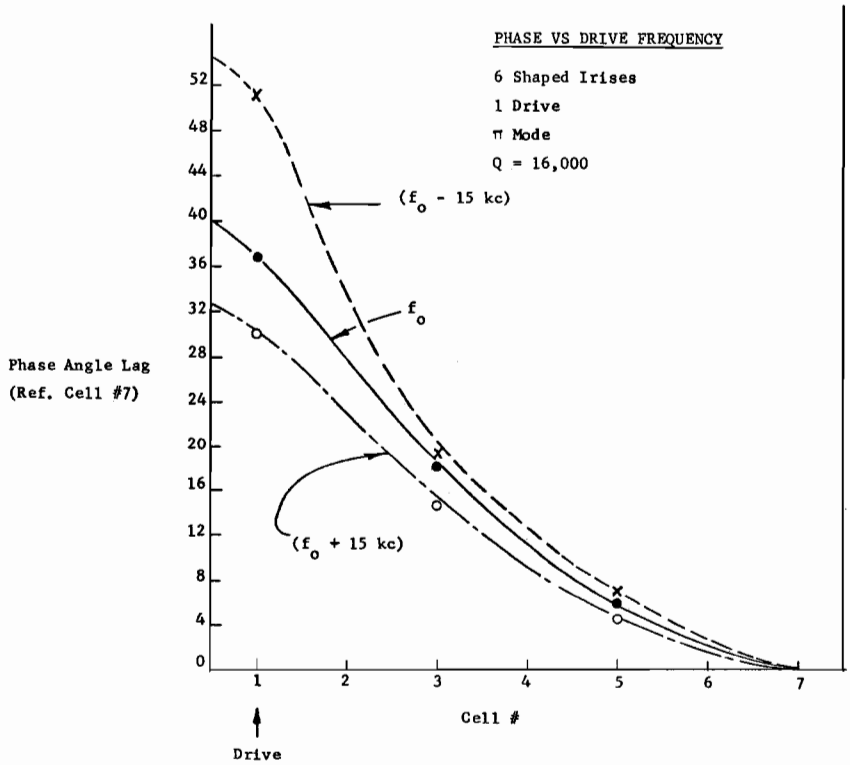
PHASE VS DRIVE FREQUENCY
6 Shaped Irises
1 Drive
π Mode
Q = 16,000
$(f_o - 15\ kc)$
f_o
$(f_o + 15\ kc)$
Phase Angle Lag
(Ref. Cell #7)
0
4
8
12
16
20
24
28
32
36
40
44
48
52
1
2
3
4
5
6
7
Cell #
Drive

Fig. 5

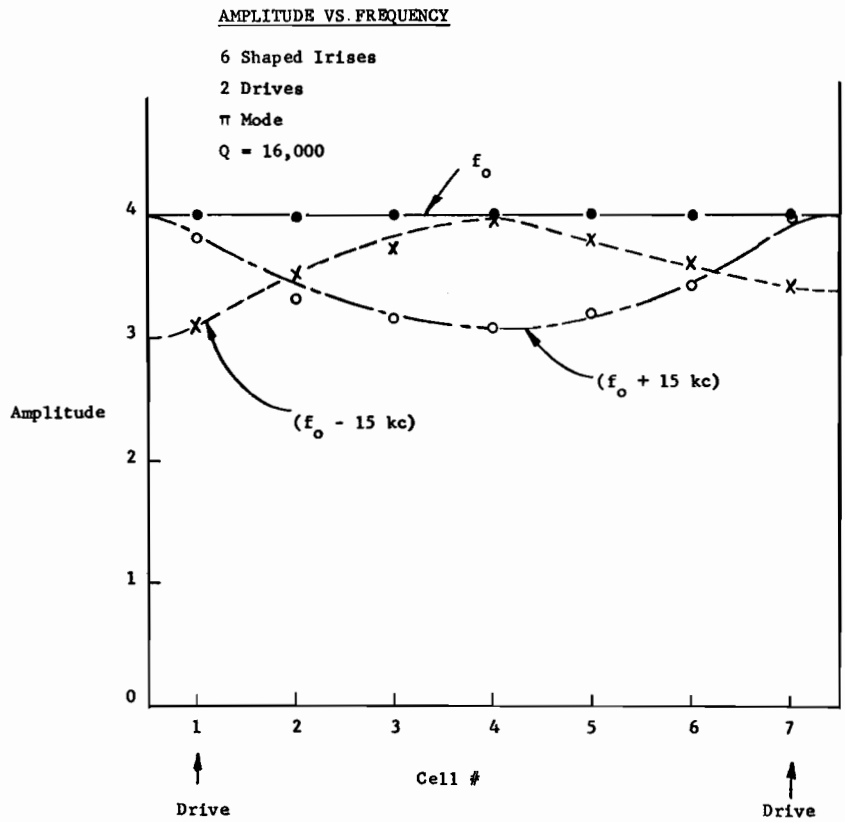
AMPLITUDE VS. FREQUENCY
6 Shaped Irises
2 Drives
π Mode
Q = 16,000
f_o
$(f_o + 15$ kc)
$(f_o - 15$ kc)
Amplitude
0
1
2
3
4
1
2
3
4
5
6
7
Cell #
Drive
Drive

Fig. 6

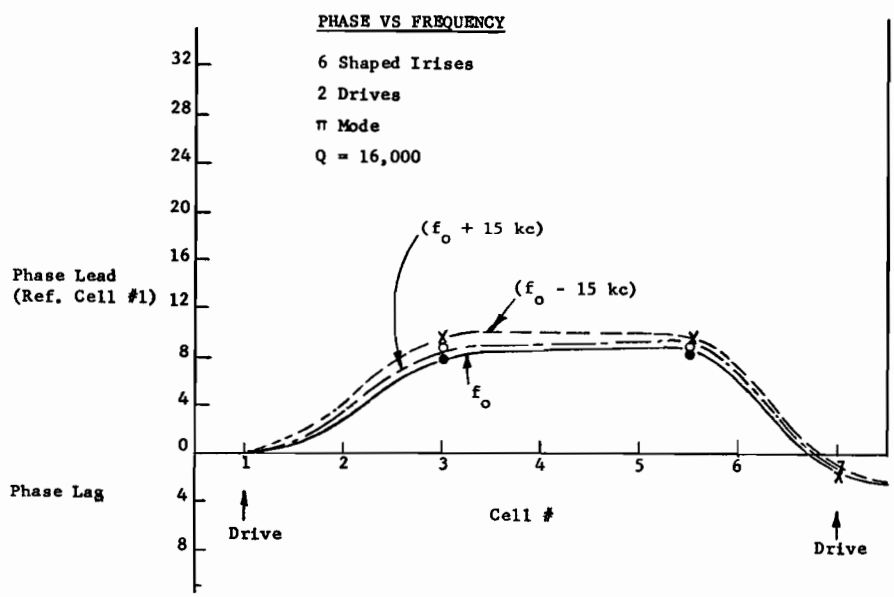
PHASE VS FREQUENCY
6 Shaped Irises
2 Drives
π Mode
Q = 16,000
$(f_o + 15$ kc)
$(f_o - 15$ kc)
f_o
Phase Lead
(Ref. Cell #1)
Phase Lag
32
28
24
20
16
12
8
4
0
4
8
1
2
3
4
5
6
Cell #
Drive
Drive

Fig. 7

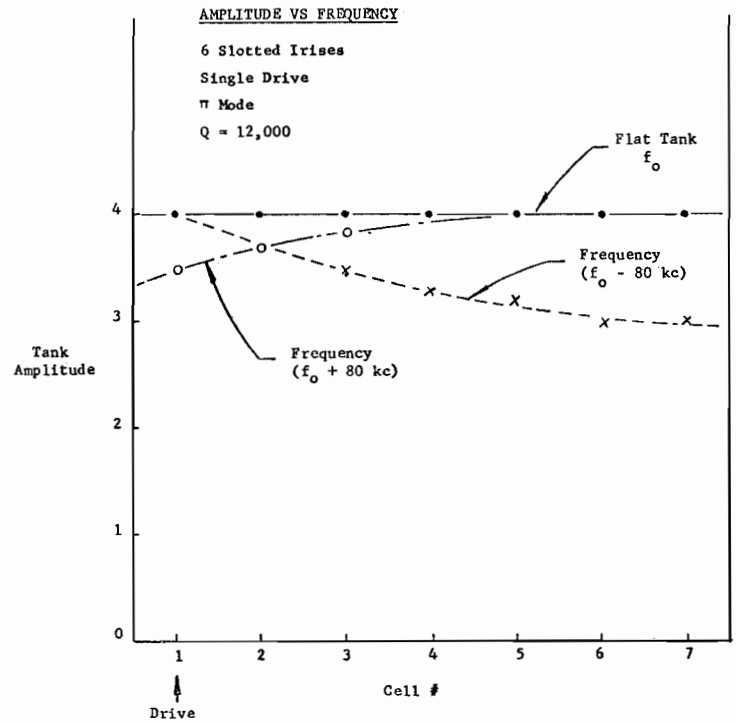
AMPLITUDE VS FREQUENCY
6 Slotted Irises
Single Drive
π Mode
Q = 12,000
Flat Tank
f_o
Frequency
(f_o - 80 kc)
Frequency
(f_o + 80 kc)
Tank
Amplitude
0
1
2
3
4
1
2
3
4
5
6
7
Cell #
Drive

Fig. 8

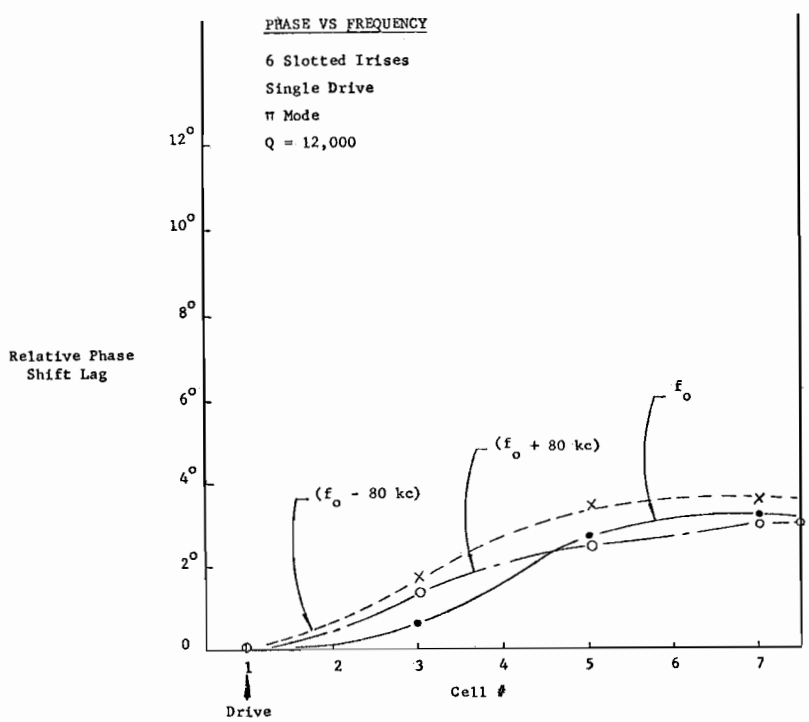
PHASE VS FREQUENCY
6 Slotted Irises
Single Drive
π Mode
Q = 12,000
Relative Phase
Shift Lag
0
2°
4°
6°
8°
10°
12°
f_o
(f_o + 80 kc)
(f_o - 80 kc)
1
2
3
4
5
6
7
Cell #
Drive

Fig. 9

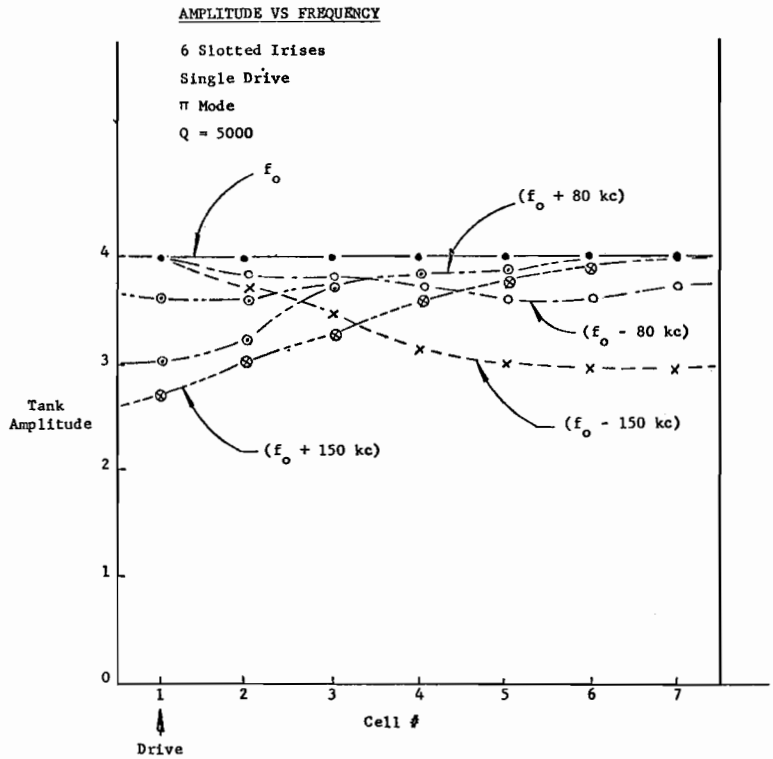
AMPLITUDE VS FREQUENCY
6 Slotted Irises
Single Drive
π Mode
Q = 5000
f_o
$(f_o + 80$ kc)
$(f_o - 80$ kc)
$(f_o - 150$ kc)
$(f_o + 150$ kc)
Tank Amplitude
0
1
2
3
4
1
2
3
4
5
6
7
Cell #
Drive

Fig. 10

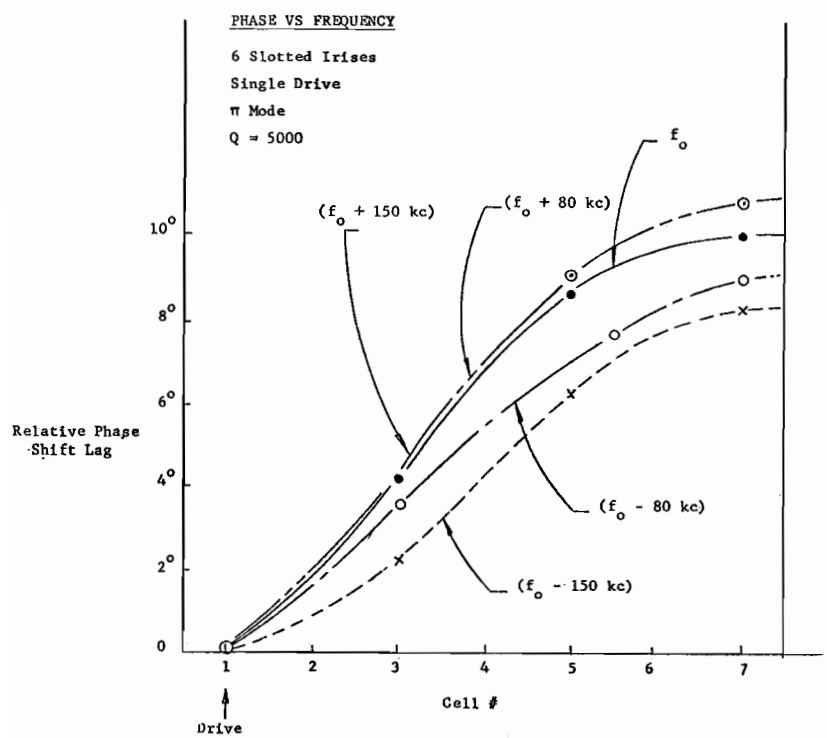
PHASE VS FREQUENCY
6 Slotted Irises
Single Drive
π Mode
Q = 5000
f_o
$(f_o + 150$ kc)
$(f_o + 80$ kc)
$(f_o - 80$ kc)
$(f_o - 150$ kc)
Relative Phase Shift Lag
0
2°
4°
6°
8°
10°
1
2
3
4
5
6
7
Cell #
Drive

Fig. 11

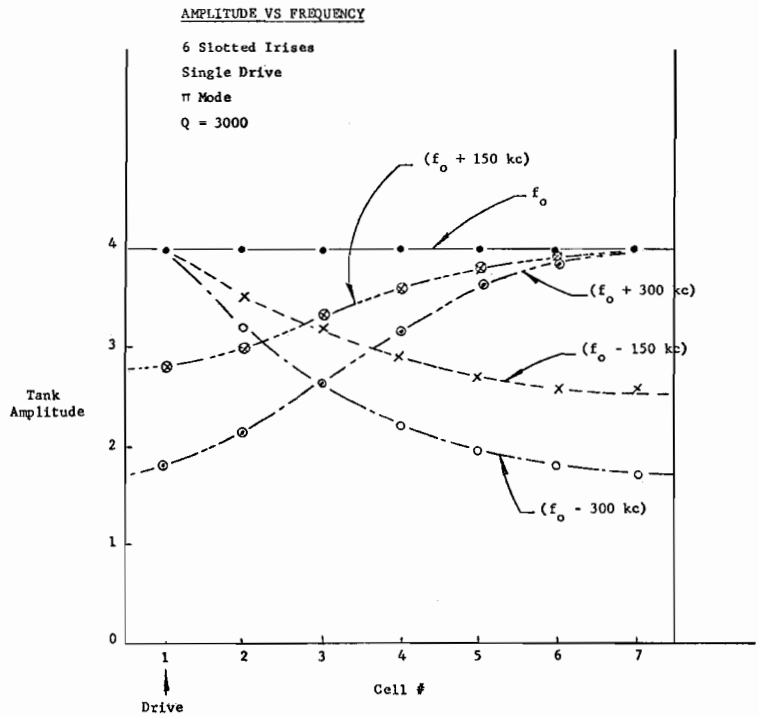
AMPLITUDE VS FREQUENCY
6 Slotted Irises
Single Drive
π Mode
Q = 3000
(f_o + 150 kc)
f_o
(f_o + 300 kc)
(f_o - 150 kc)
(f_o - 300 kc)
Tank Amplitude
0
1
2
3
4
1
2
3
4
5
6
7
Drive
Cell #

Fig. 12

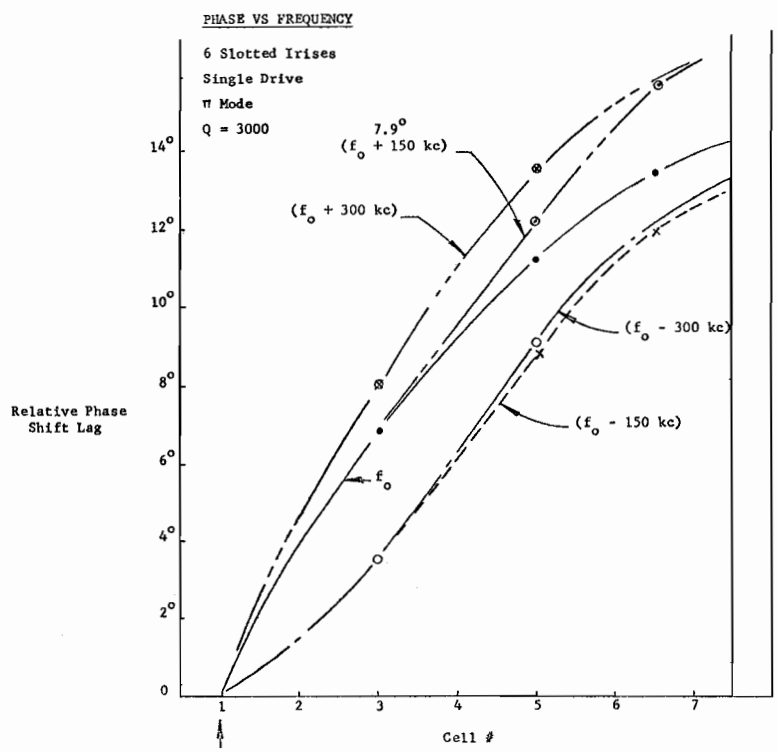
PHASE VS FREQUENCY
6 Slotted Irises
Single Drive
π Mode
Q = 3000
7.9°
(f_o + 150 kc)
(f_o + 300 kc)
(f_o - 300 kc)
(f_o - 150 kc)
f_o
Relative Phase Shift Lag
0
2°
4°
6°
8°
10°
12°
14°
1
2
3
4
5
6
7
Drive
Cell #

Fig. 13

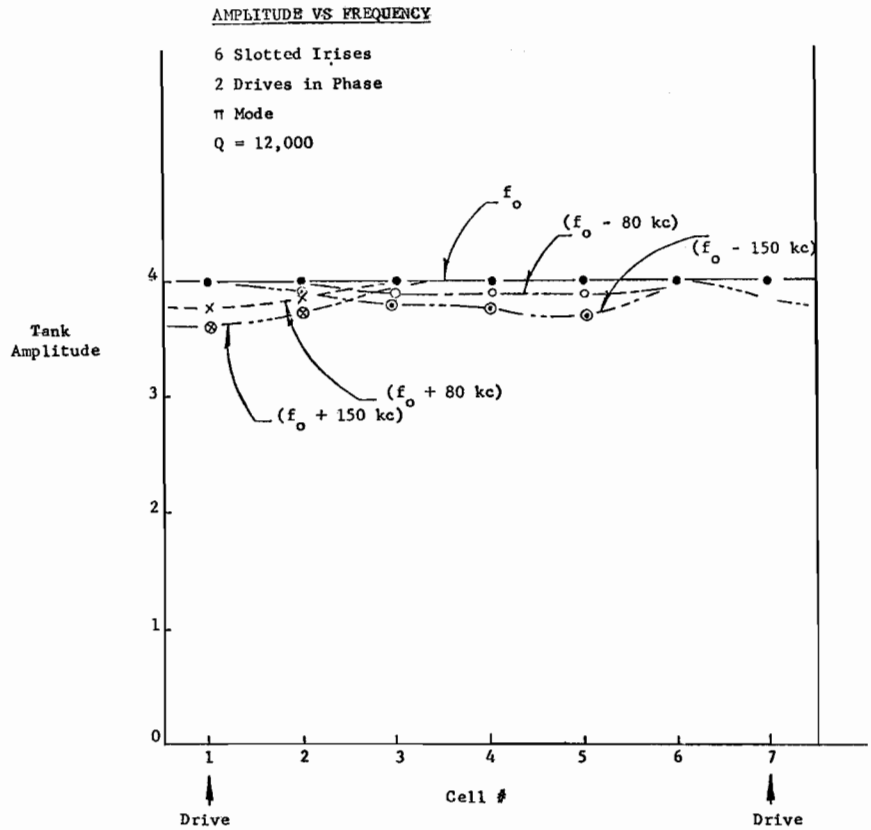
AMPLITUDE VS FREQUENCY
6 Slotted Irises
2 Drives in Phase
π Mode
Q = 12,000
f_o
$(f_o$ - 80 kc)
$(f_o$ - 150 kc)
$(f_o$ + 80 kc)
$(f_o$ + 150 kc)
Tank Amplitude
0
1
2
3
4
1
2
3
4
5
6
7
Cell #
Drive
Drive

Fig. 14

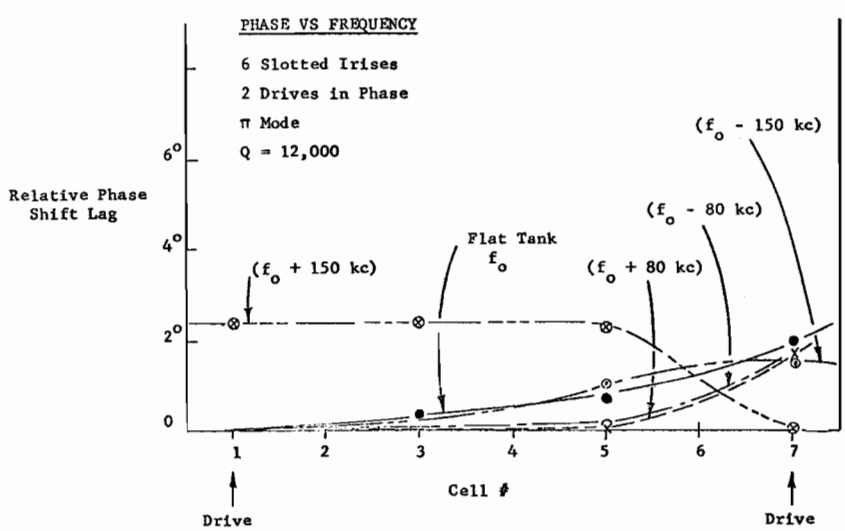
PHASE VS FREQUENCY
6 Slotted Irises
2 Drives in Phase
π Mode
Q = 12,000
$(f_o$ - 150 kc)
$(f_o$ - 80 kc)
Flat Tank f_o
$(f_o$ + 150 kc)
$(f_o$ + 80 kc)
Relative Phase Shift Lag
0
2°
4°
6°
1
2
3
4
5
6
7
Cell #
Drive
Drive

Fig. 15

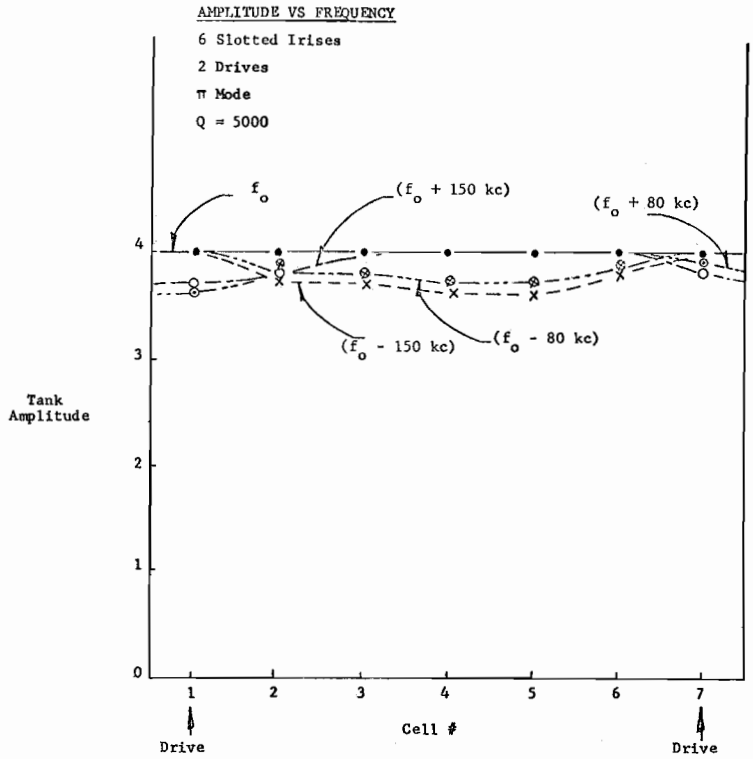
AMPLITUDE VS FREQUENCY
6 Slotted Irises
2 Drives
π Mode
Q = 5000
f_o
$(f_o + 150$ kc)
$(f_o + 80$ kc)
$(f_o - 150$ kc)
$(f_o - 80$ kc)
Tank Amplitude
0
1
2
3
4
1
2
3
4
5
6
7
Cell #
Drive
Drive

Fig. 16

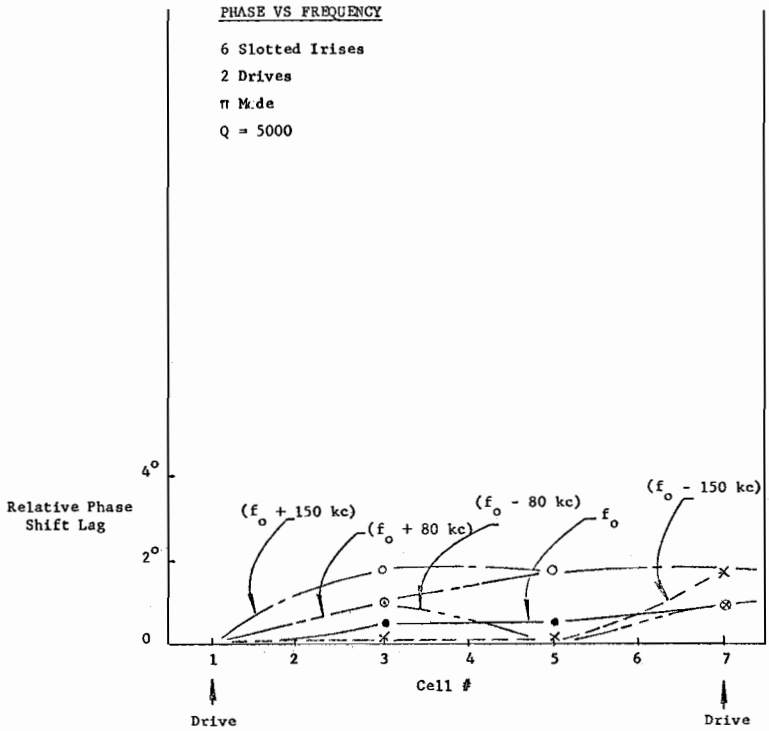
PHASE VS FREQUENCY
6 Slotted Irises
2 Drives
π Mode
Q = 5000
$(f_o + 150$ kc)
$(f_o + 80$ kc)
$(f_o - 80$ kc)
f_o
$(f_o - 150$ kc)
Relative Phase Shift Lag
0
2°
4°
1
2
3
4
5
6
7
Cell #
Drive
Drive

Fig. 17

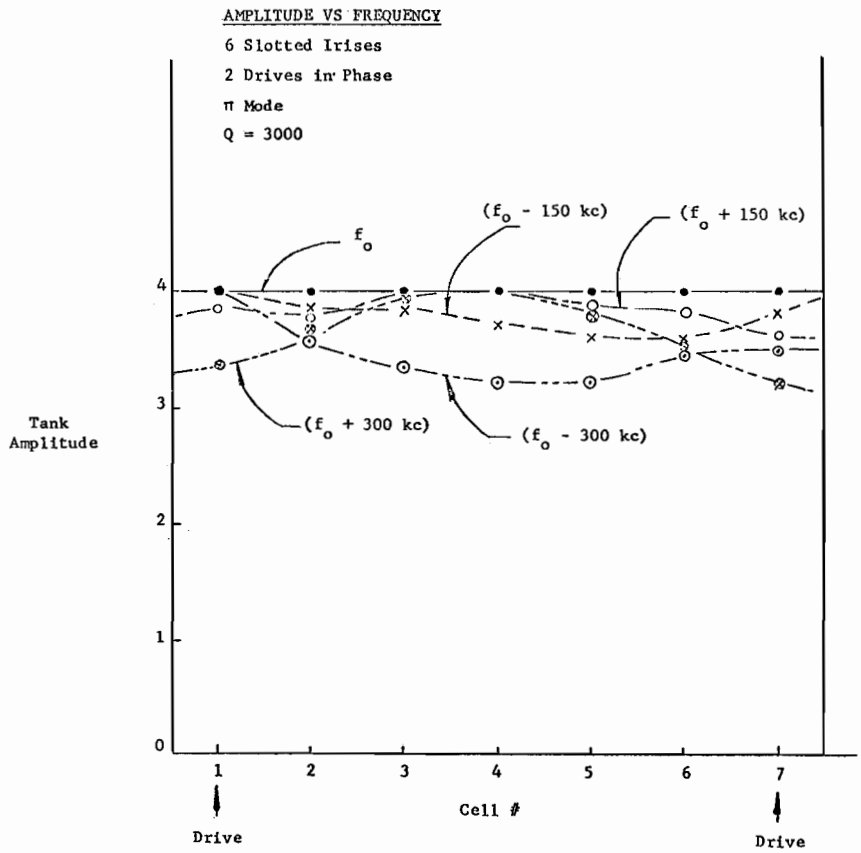
AMPLITUDE VS FREQUENCY
6 Slotted Irises
2 Drives in Phase
π Mode
Q = 3000
f_o
$(f_o - 150\ kc)$
$(f_o + 150\ kc)$
$(f_o + 300\ kc)$
$(f_o - 300\ kc)$
Tank Amplitude
0
1
2
3
4
1
2
3
4
5
6
7
Cell #
Drive
Drive

Fig. 18

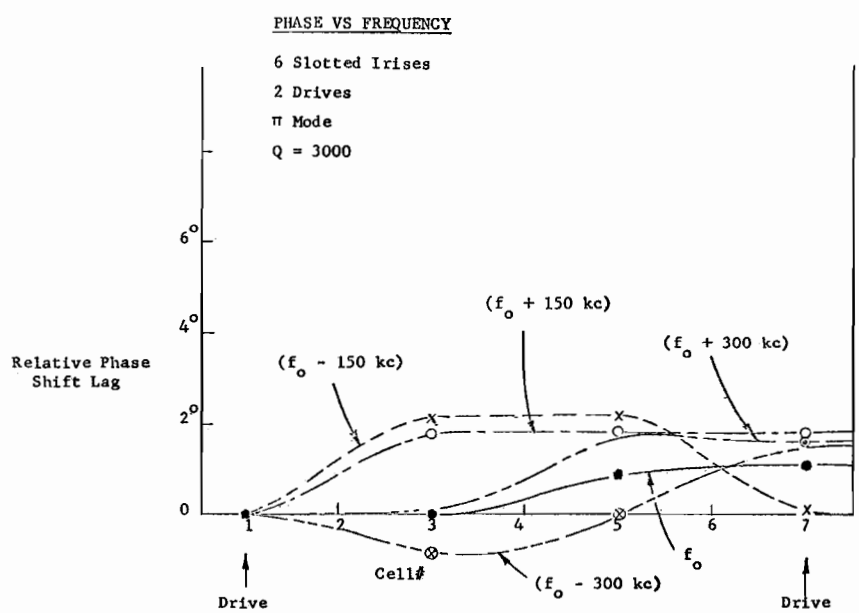
PHASE VS FREQUENCY
6 Slotted Irises
2 Drives
π Mode
Q = 3000
6°
4°
2°
0
Relative Phase Shift Lag
$(f_o + 150\ kc)$
$(f_o + 300\ kc)$
$(f_o - 150\ kc)$
f_o
$(f_o - 300\ kc)$
1
2
3
4
5
6
7
Cell#
Drive
Drive

Fig. 19

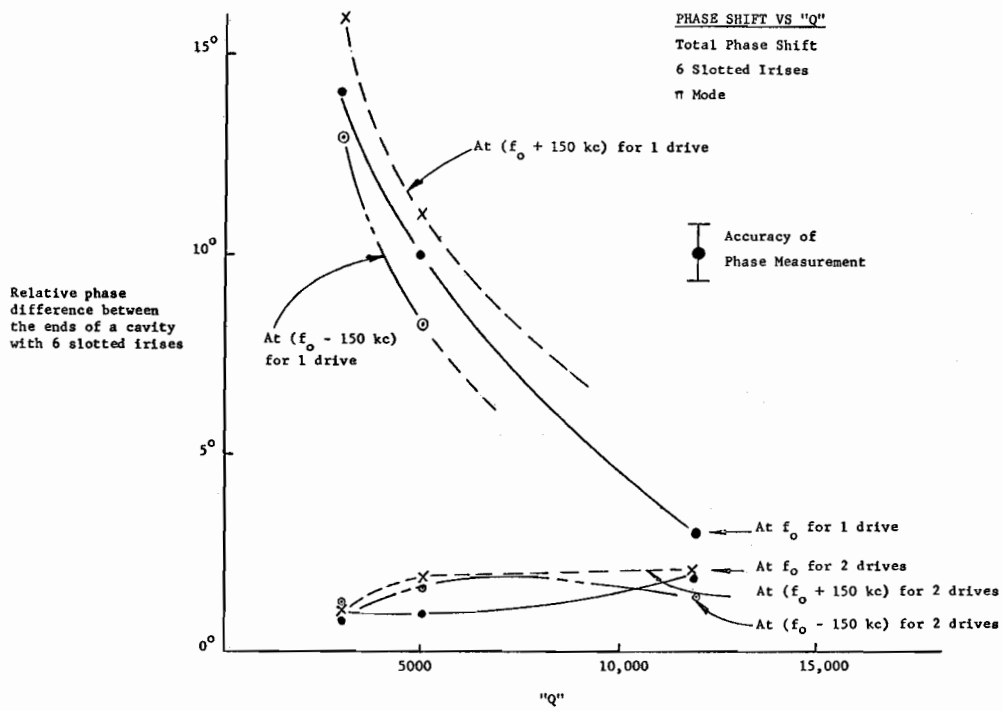
PHASE SHIFT VS "Q"
Total Phase Shift
6 Slotted Irises
π Mode
At (f_o + 150 kc) for 1 drive
Accuracy of
Phase Measurement
Relative phase
difference between
the ends of a cavity
with 6 slotted irises
At (f_o - 150 kc)
for 1 drive
At f_o for 1 drive
At f_o for 2 drives
At (f_o + 150 kc) for 2 drives
At (f_o - 150 kc) for 2 drives
15°
10°
5°
0°
5000
10,000
15,000
"Q"

Fig. 20

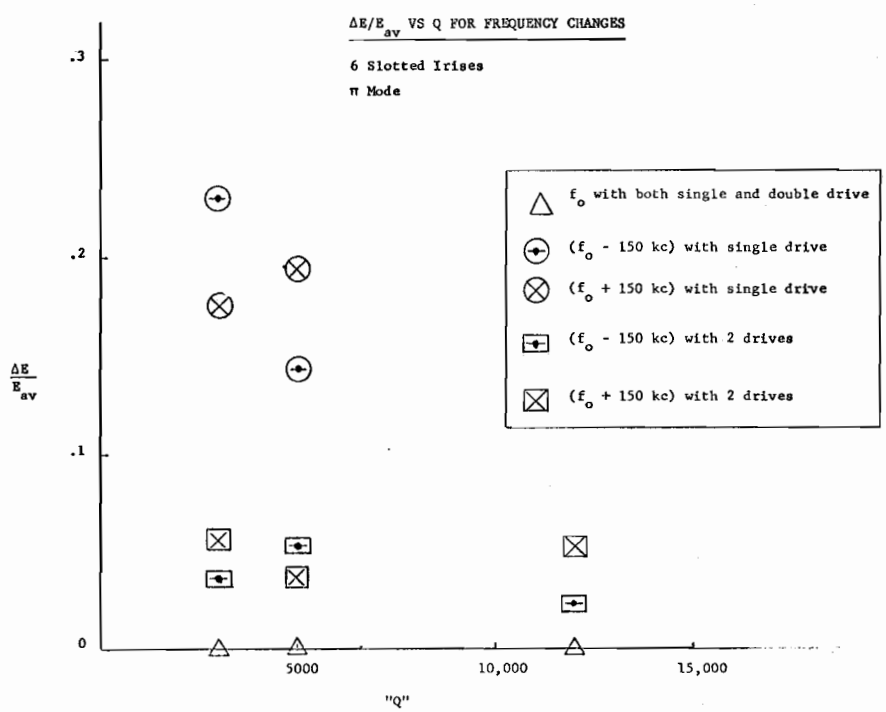
$\Delta E/E_{av}$ VS Q FOR FREQUENCY CHANGES
6 Slotted Irises
π Mode
f_o with both single and double drive
(f_o - 150 kc) with single drive
(f_o + 150 kc) with single drive
(f_o - 150 kc) with 2 drives
(f_o + 150 kc) with 2 drives
$\frac{\Delta E}{E_{av}}$
.3
.2
.1
0
5000
10,000
15,000
"Q"

Fig. 21

PARTICLE MOTIONS AND THE FOCUSING SYSTEM IN PROTON LINACS*

S. Ohnuma
Yale University

Introduction

Last year, at the conference on proton linacs, computer programs developed at Yale for particle motions and some of their preliminary results were presented.[1] Since then, there have been a number of modifications in our design parameters, particularly in the iris-loaded section. The results here are mostly based on the design parameters of the proposed 500 MeV injector for the AGS in Brookhaven which was presented by G. W. Wheeler. The computer programs are essentially the same as the one discussed in Ref. (1).

Buncher

No change has been made to the buncher which was presented last year .[2] The essential requirement here is that the beam must be tightly bunched near the synchronous point ($\Delta\varphi = \Delta\gamma = 0$). The distribution of particles from a double buncher is shown in Fig. 1. If the ion source can produce 100 mA, about 79 mA will be confined to within $\Delta\varphi = \pm 14^{\circ}$ and $\Delta W = \pm 20$ keV. On the other hand, there are still particles near the boundary ($\sim$ .5 mA) which come out of the drift tube section with relatively large values of ($\Delta\varphi$, $\Delta\gamma$). For a linac of higher intensity, a bunching scheme that gives very small fraction of beams near the boundary would become important.

Drift Tube Section

Phase and transverse oscillations of particles 1 and 2 in Fig. 1 are given in Figs. 2-3 together with those of the synchronous particle. The focusing system used here is shown in Fig. 4. Two different doublet arrangements, (A) and (B), have been tried in the last two tanks to see the change in the emittance shape. In Tanks No. 1 and No. 2, the strengths of quadrupole magnets are chosen such that they correspond to optimum values for the synchronous particle. For non-synchronous particles, the optimum condition is different and the amplitude of the transverse oscillation may increase instead of damping down. (see Fig. 3.) Since the

---

* The work reported here has been done by R. Bakeman, T. W. Ludlam, J. N. Vitale and S. Ohnuma.

Particle Distribution from
Double buncher

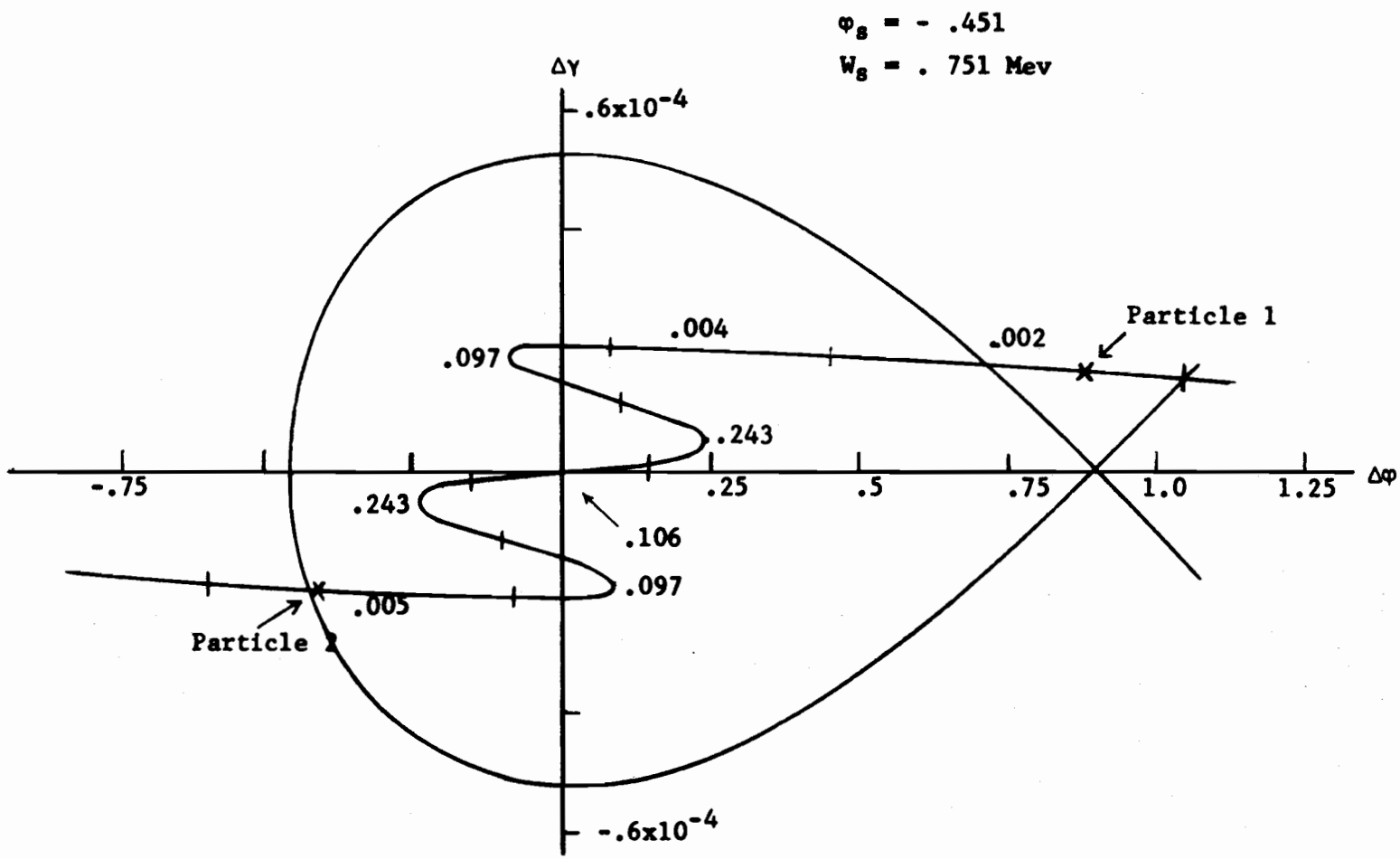

FIG. 1

focusing system is continuous from Tank No. 1 to Tank No. 2 with a very short drift space, no matching magnet is required. This, however, is not true between Tank No. 3 and No. 4 where the system suddenly changes. At least one set of triplet is necessary in order to achieve a near perfect matching in x- as well as y-direction. After that, the system is continuous (i.e., the change is "adiabatic") and the matching system can be eliminated entirely.

The acceptance in x - x' space of the drift tube section for the synchronous particle is shown in Fig. 5. When the smallest bore radius is .75 cm, the area is 17π cm-mrad. For most of the non-synchronous particles, the acceptance area remains fairly close to the 17π cm-mrad but the shapes are quite different. Thus, if the input beam is matched to the shape given in Fig. 5, the effective acceptance value for particles in ($\Delta\varphi = \pm 14^{\circ}$, $\Delta\gamma = \pm 20$ keV) region is reduced to $\sim 16\pi$ cm-mrad. For particles 1 and 2, the shaded area in Fig. 5 is not acceptable and the area is less than 15π cm-mrad. It is, of course, possible to get a larger acceptance by simply taking a larger bore radius. This, however, will give a larger output bunch in ($\Delta\varphi$) - ($\Delta\gamma$) space and may cause particle loss when the frequency is increased in the high energy section. If (NNSS) configuration is used instead of (NSNS) type, the acceptance for the synchronous particle is 14π cm-mrad. The change of the acceptance shape for non-synchronous particle from that of the synchronous particle is more serious than (NSNS) configuration.

The maximum radial excursion of the beam in Tanks No. 3 - No. 7 will be substantially smaller than shown in Fig. 3 if the focusing system is (NSNS) throughout instead of doublets with gradually increasing repeat lengths taken here. The particular advantage of the doublet system will be discussed later.

It would be useful for the purpose of shielding designs to see where particles are lost radially. The location depends on the initial position of particles in x - x', y - y' and ($\Delta\varphi$) - ($\Delta\gamma$) spaces. For example, most of the particle 1 in the shaded area in Fig. 5 are lost at drift tubes No. 7, No. 9, and No. 13 of the first tank and at drift tubes No. 2 and No. 6 of the second tank, whereas the particle 2 are lost at drift tubes No. 5 and No. 7 of the first tank and No. 2 of the second tank. By assuming a particle distribution, one can calculate the distribution of lost particles along the drift tube section. However, extensive study of this problem has not been made so far. The results we have accumulated clearly indicate that the loss will be entirely in the first two tanks and most likely below $\sim$ 20 MeV.

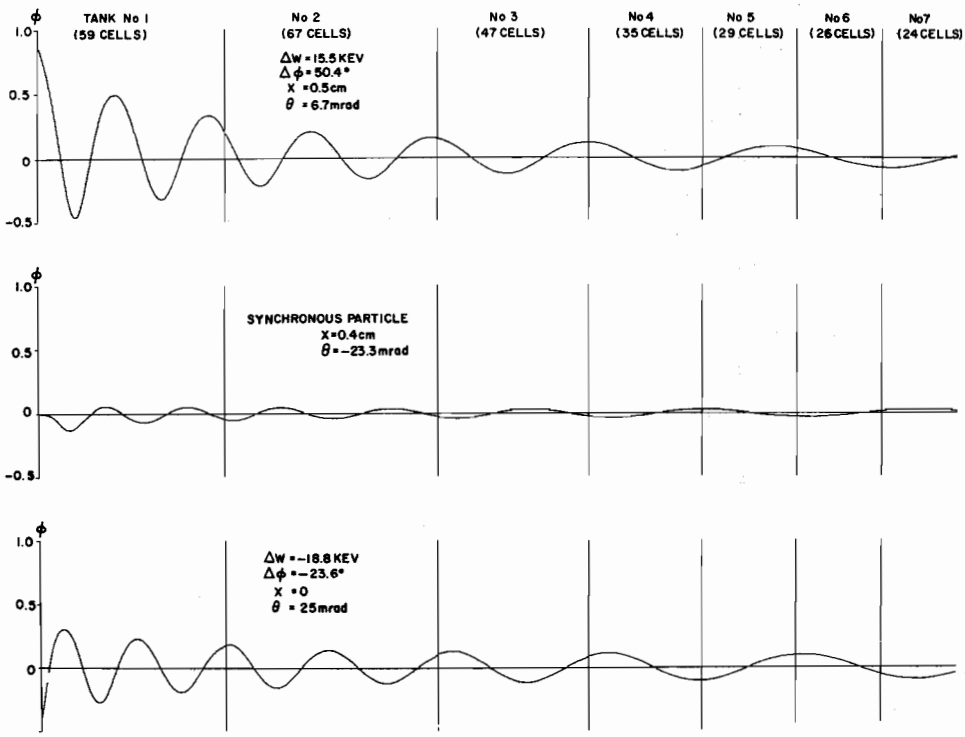
φ
TANK No I
(59 CELLS)
No 2
(67 CELLS)
No 3
(47 CELLS)
No 4
(35 CELLS)
No 5
(29 CELLS)
No 6
(26 CELLS)
No 7
(24 CELLS)
ΔW = 15.5 KEV
Δφ = 50.4°
X = 0.5 cm
θ = 6.7 mrad
SYNCHRONOUS PARTICLE
X = 0.4 cm
θ = −23.3 mrad
ΔW = −18.8 KEV
Δφ = −23.6°
X = 0
θ = 25 mrad
1.0
0.5
0
−0.5

FIG. 2

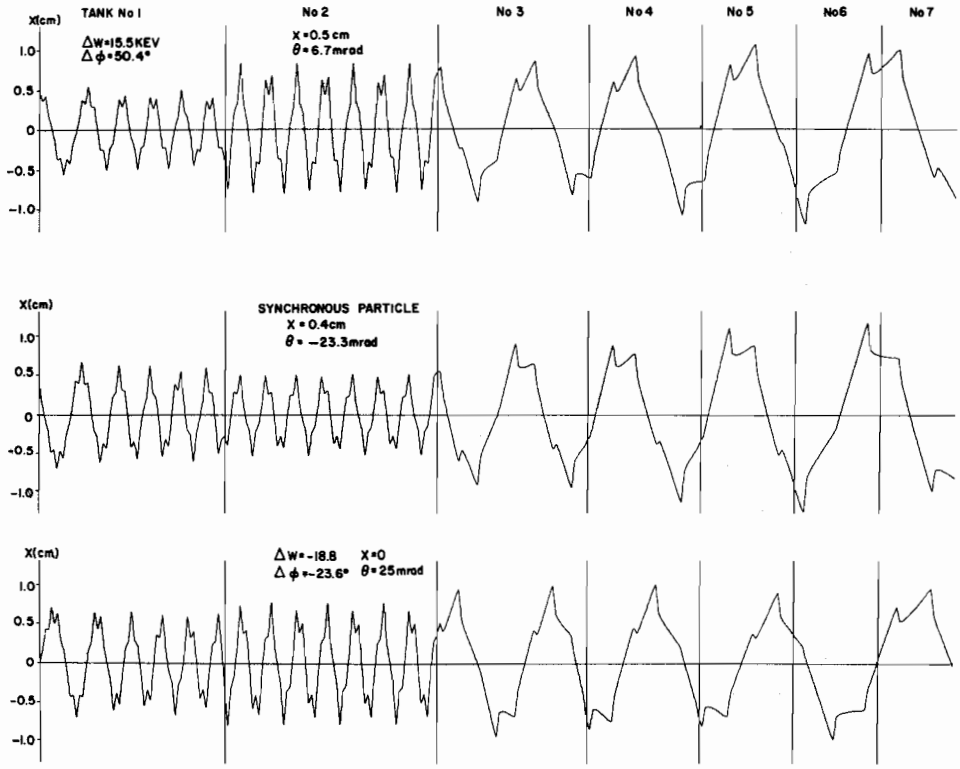
X(cm)
TANK No I
ΔW = 15.5 KEV
Δφ = 50.4°
No 2
X = 0.5 cm
θ = 6.7 mrad
No 3
No 4
No 5
No 6
No 7
SYNCHRONOUS PARTICLE
X = 0.4 cm
θ = −23.3 mrad
ΔW = −18.8
Δφ = −23.6°
X = 0
θ = 25 mrad
1.0
0.5
0
−0.5
−1.0

FIG. 3

In the $(\Delta\varphi)$ - $(\Delta\gamma)$ space, particles coming out of the drift tube section with the final energy of 187 MeV are all contained in the tilted ellipse shown in Fig. 6. Several dots are those particles with $(\Delta\varphi) \gtrsim 1.0$ or $(\Delta\varphi) \lesssim -.6$ at the injection. Since their "effective" transverse acceptance is very small ($0 - 3\pi$ cm-mrad), the total intensity of these stray particles is less than 5×10^{-5} of the main output current (i.e., the ellipse in Fig. 6). The other ellipse in Fig. 6 is the particle bunch assumed in calculating particle motions in the iris section.

Fig. 7 shows the emittance from the drift tube section in x - x' space. The area is very close to π cm-mrad. (A) and (B) correspond, respectively, to the doublet configuration (A) and (B) shown in Fig. 4.

In the low energy region ($\beta \lesssim .2$) where the rate of the change of β is large, the accuracy of the calculation is not too good. As has been already suggested previously[3], it may be necessary to integrate the equations of motion point by point. This, however, requires a detailed information on electric and magnetic fields at every point. When there is no bore hole, the fields of the shaped drift tube[4] are accurately known but the effect of the bore is difficult to evaluate. It is hoped that the calculation at MURA and at Los Alamos ("MESSY MESH")[5] will eventually give the fields with the desired accuracy.

Matching between Drift Tube and Iris Sections

It is clear from Fig. 6 that a long drift space between the two sections must be avoided in order to keep the resulting phase spread as small as possible. Although β here is large (.55), the spread could be as large as $\pm 2.6^{\circ}/m$ (for $\Delta\gamma = \pm .8 \times 10^{-3}$) so that a drift space longer than $\sim$ 4m will definitely cause trouble. This is particularly serious for a linac injector of a large synchrotron where a small momentum spread ($\Delta p/p$) is essential in getting a high capture efficiency. On the other hand, it is highly desirable to have a bending magnet (to guide the beam for the energy measurement), one or two slit boxes (for measuring the beam shape in x and y-space), and one or two current transformers. If, in addition to these, two or three sets of quadrupole triplet are required to match the beam shape in both x and y-direction simultaneously, a 4m long space does not seem to be sufficient. Two schemes have been tried to solve this problem.

The first is to employ a matching scheme in the longitudinal phase space that is based on the principle of the strong focusing[6]. A tank operated at the stable synchronous phase $\varphi = \varphi_s$ acts as a "focusing lens" and a tank operated at $\varphi = -\varphi_s$ as a "defocusing lens". The drift space

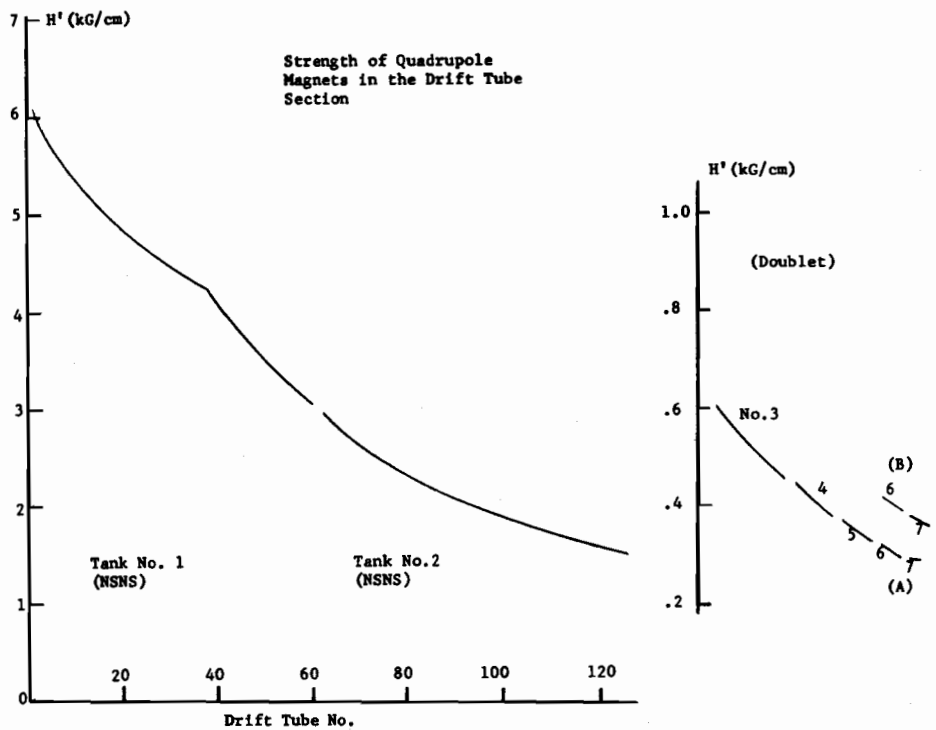
H' (kG/cm)
Strength of Quadrupole Magnets in the Drift Tube Section
Tank No. 1 (NSNS)
Tank No.2 (NSNS)
Drift Tube No.
H' (kG/cm)
(Doublet)
No.3
(B)
(A)

FIG. 4

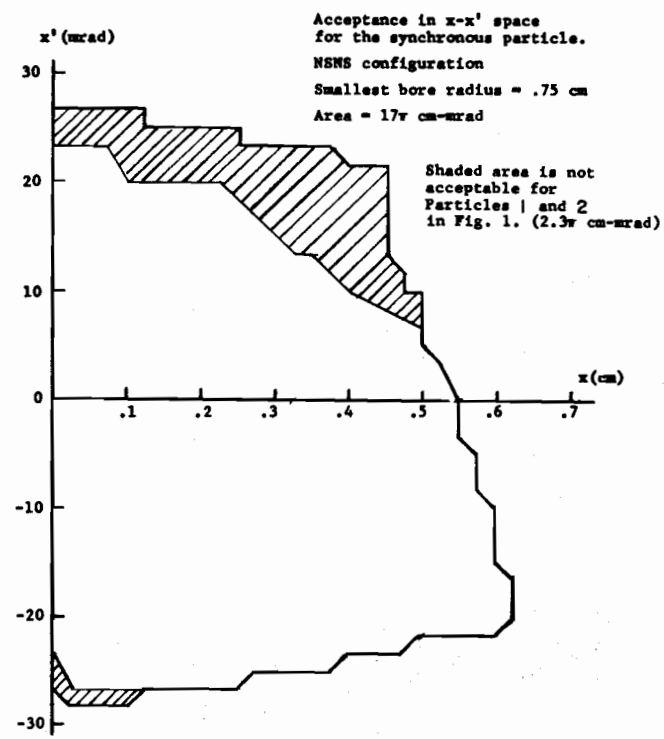
x' (mrad)
Acceptance in x-x' space for the synchronous particle.
NSNS configuration
Smallest bore radius = .75 cm
Area = 17π cm-mrad
Shaded area is not acceptable for Particles 1 and 2 in Fig. 1. (2.3π cm-mrad)
x(cm)

FIG. 5

then will be an element of the matching optical system and does not necessarily have to be short. The system will be composed of 10 – 15 regular tanks with reasonable values of rf level. Based on the linear theory, we found that we can achieve an almost 100% matching even with a 10 m drift space. However, numerical calculation has shown that the non-linear effects are so serious as to make the scheme rather impractical. It may be possible to design an elaborate system composed of very special tanks just for the matching purpose but this does not seem too easy.

The second choice is to eliminate the matching magnets for two transverse directions entirely, or use only one doublet. This means that the focusing system in the drift tube section (at least in the last two tanks or so) must be joined continuously to that in the iris section. Otherwise, one doublet or triplet cannot give a perfect matching in the both directions simultaneously. Since a doublet is used after each even-numbered tank in the iris section, one doublet just before the first tank together with a properly spaced doublet system in Tanks No. 6 and No. 7 will achieve the desirable matching. With 3.5 m space between two sections, we have found that the matching efficiency could be as large as 95% in both directions. It will be even better if two or three auxiliary magnets are placed in the last few drift tubes to make adjustments.

Iris Section

Various systems of quadrupole doublets and triplets to be used for the focusing in the high-energy section have been investigated in order to get the necessary information for the choice of multiplet type[7]. The doublet system used in the calculation and its acceptance shape are shown in Fig. 8 while the strength of magnets and the maximum (theoretical) excursions are given in Fig. 9. If the transverse phase space area is 10π cm-mrad at the injection (.75 MeV), the area at 187 MeV is $.6\pi$ cm-mrad. One advantage of doublet system is the relatively large space available between two magnets for a given drift space (1 m in this design). The maximum x or y excursion at 500 MeV is 68% of the excursion at 187 MeV. This is due to the increase of the momentum and the decrease of (Courant-Snyder) β_{max}[8]. It is, of course, possible to take longer magnet repeat lengths gradually as the energy increases. This, however, will increase the value of β_{max} and, for β_{max} (500 MeV)/ β_{max} (187 MeV) = 1.75, the maximum excursion stays constant. If, on the other hand, the focusing system is changed at some points, some kind of matching device will be required.

A good matching at the entrance is essential in achieving the smallest possible x_{max} or y_{max}. Different systems require different acceptance shapes so that a particular point in x-x' space leads to an entirely different maximum excursion. In connection with the matching, a device that can

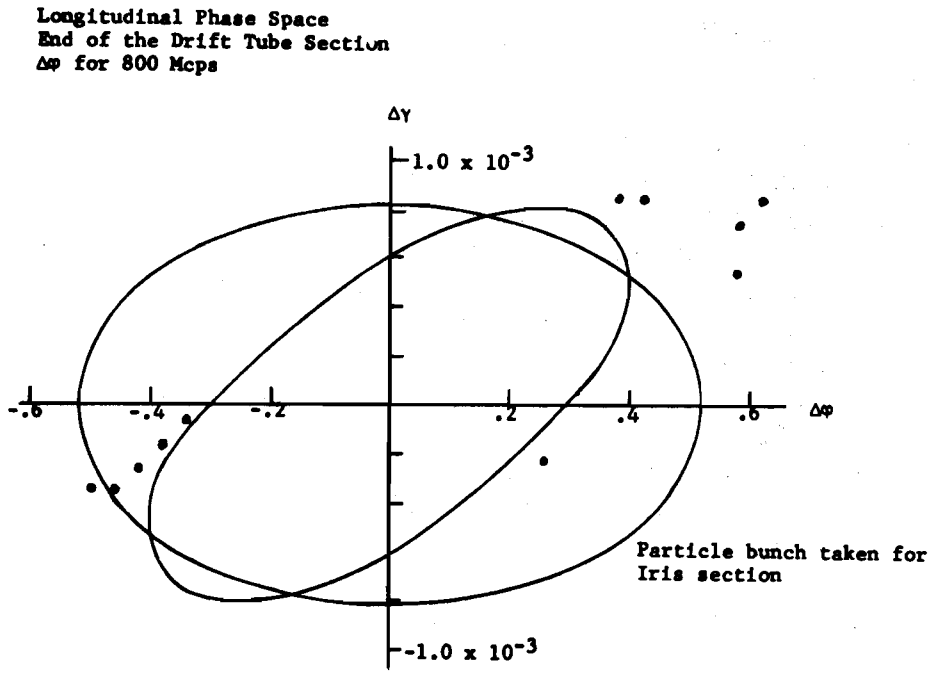
Longitudinal Phase Space
End of the Drift Tube Section
Δφ for 800 Mcps
Δγ
1.0 x 10^-3
-1.0 x 10^-3
-.6
-.4
-.2
.2
.4
.6
Δφ
Particle bunch taken for
Iris section

FIG. 6

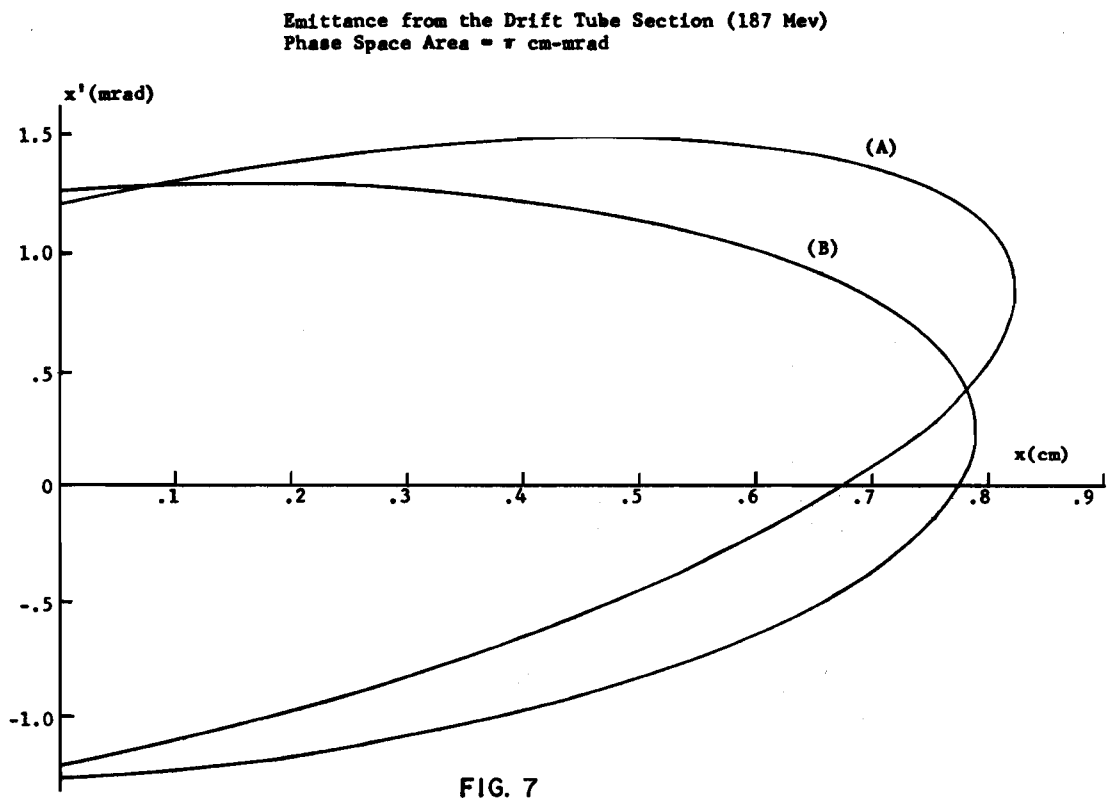
Emittance from the Drift Tube Section (187 Mev)
Phase Space Area = π cm-mrad
x'(mrad)
1.5
1.0
.5
0
-.5
-1.0
(A)
(B)
x(cm)
.1
.2
.3
.4
.5
.6
.7
.8
.9

FIG. 7

accurately measure the beam shape in x-x' and y-y' space will be extremely useful.

The theoretical maximum excursions in Fig. 9 are computed for synchronous particles. For non-synchronous particles, the acceptance shape is slightly different from those given in Fig. 8. This slight mismatching would, in general, give larger excursions for non-synchronous particles. The largest deviation recorded from the theoretical value is .25 cm. Of course, only those particles which are near the boundary of the acceptance ellipse in Fig. 8 deviate from the theoretical maximum excursion. For example, particles within an ellipse of size $.63\pi$ cm-mrad in x-x' space are not lost if, in $(\Delta\varphi) - (\Delta\gamma)$ space, they are inside of the (larger) ellipse in Fig. 6. On the other hand, it seems very difficult to keep the iris aperture smaller than 1 cm (radius) and still not lose particles. One obvious solution would be shorter tanks at the beginning to reduce the magnet repeat length. Since a smaller iris aperture gives a smaller power loss for the same structure, further studies of this point may be called for in the future.

The choice of the doublet arrangement instead of a triplet was made because of the better over-all quality in focusing the high energy beam.[7] Triplet arrangements (+) (-) (+) (rf tanks) (+) (-) (+) are not symmetric in x and y directions so that the best operating point in one direction is very close to the stability boundary in another direction. This situation is shown in Fig. 10(*) where g_s is related to H' by

$$H' \text{ (kG/cm)} = .313\,(\gamma\beta)\, g_s^{\,2}$$

and the parameter Ω for each curve is

$$\Omega = \left[\frac{\pi\, eE_o \sin|\varphi|}{m_p c^2 \lambda\, (\gamma\beta)^3}\right]^{1/2} \quad ; \quad \frac{d\gamma}{dz} = \frac{eE_o}{m_p c^2} \cos\varphi$$

Symmetric arrangements (+) (-) (+) (rf tanks) (-) (+) (-) give a very narrow stability range with large values of β_{max} as can be seen from Fig. 11(*). There is a possibility of using an upper stability region

---

(*) Figs. 10 and 11 are taken from Ref. (7). Tank length is 2.5 m instead of 3 m here and β_{max} is slightly smaller than for 3 m tanks.

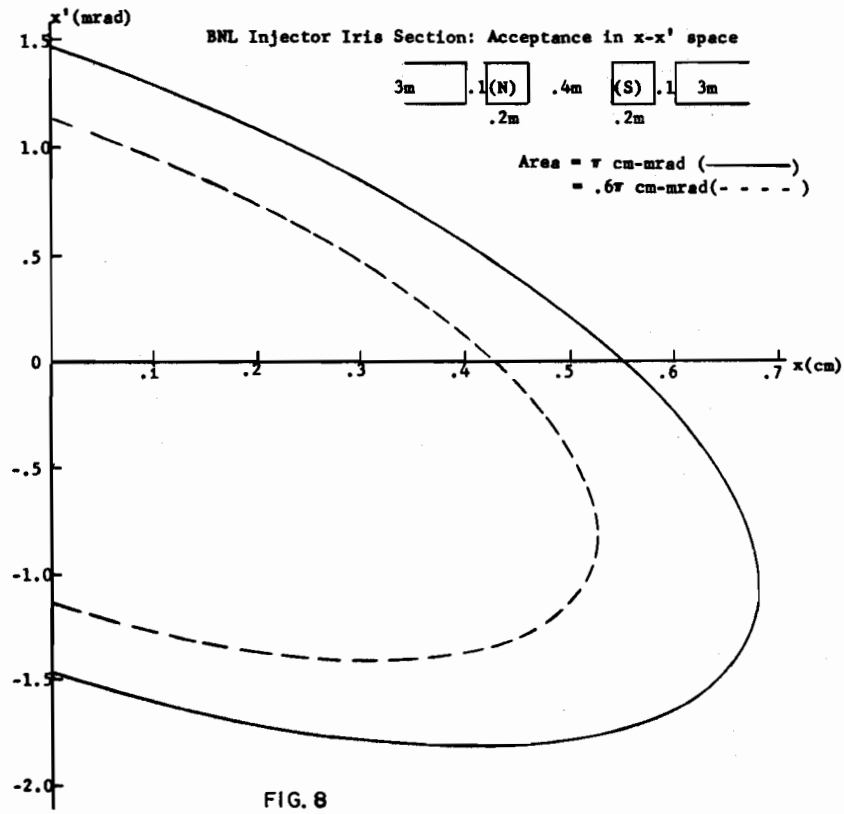
x'(mrad)
BNL Injector Iris Section: Acceptance in x-x' space
3m
.1
(N)
.2m
.4m
(S)
.2m
.1
3m
Area = π cm-mrad (———)
= .6π cm-mrad(- - - -)
1.5
1.0
.5
0
-.5
-1.0
-1.5
-2.0
.1
.2
.3
.4
.5
.6
.7
x(cm)

FIG. 8

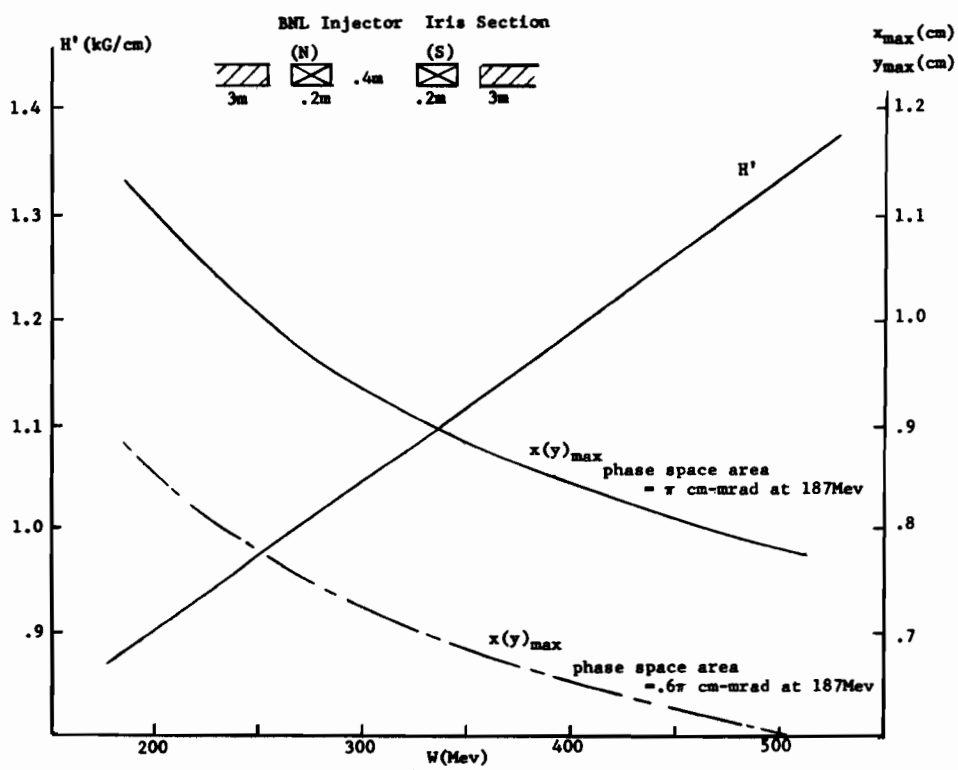
H'(kG/cm)
BNL Injector Iris Section
(N)
(S)
3m
.2m
.4m
.2m
3m
x_{max}(cm)
y_{max}(cm)
1.4
1.3
1.2
1.1
1.0
.9
1.2
1.1
1.0
.9
.8
.7
H'
x(y)max
phase space area
= π cm-mrad at 187Mev
x(y)max
phase space area
=.6π cm-mrad at 187Mev
200
300
400
500
W(Mev)

FIG. 9

where β_{max} are much smaller. However, aside from large magnetic fields required in the high energy region, non-synchronous particles may spend some time near the stability boundary or even cross the boundary into the stopband and get a large radial excursion. Unless an extensive numerical calculation is done, it does not seem safe to design the focusing system operating in upper stability regions.

The only remaining question is whether tolerance requirements for doublets are too difficult to achieve in the proton linac, as they appear to be in the Stanford two-mile electron linac[9], so that one is forced to take triplets. This has also been investigated in a semi-analytic fashion in Ref. (7). The method used there is outlined by R. L. Gluckstern.[10] As has been discussed in Ref. (9) and Ref. (10), the advantage of triplets is the possibility of "bench alignment" which makes the effect of magnet displacements entirely negligible (maximum tolerances are order of 100 mils). For doublets, bench alignment offers no improvement as far as the tolerance of "skew" (rotation about transverse axes) is concerned. On the other hand, it does not seem at all difficult to achieve the required tolerances for doublets (as well as for triplets) with the help of aligning monuments.[10] [11] A computer program has also been used to check the validity of the semi-analytic results. All together 50 random sets of misaligned doublets have been investigated at 400 MeV, 580 MeV, and 750 MeV. The displacements in x and y direction (individually) are larger than the analytic results in 5 cases at 400 MeV, 7 cases at 580 MeV, and 2 cases at 750 MeV. However, the radial displacements

$$(\sqrt{x^2 + y^2})$$

are always smaller than the expected values. Since these 50 runs are performed for a particular particle, we will have to repeat the similar calculation for many different particles. Nevertheless, we feel that the tolerance requirements for doublets are not too stringent to achieve.

Loss of Particles due to Failures of rf Tanks and Focusing Magnets[12]

The computer program for particle motions in the iris section can be used to find out whether the loss of particles is, in general, localized or extended over a long distance when certain tanks or a pair of focusing magnets fail.

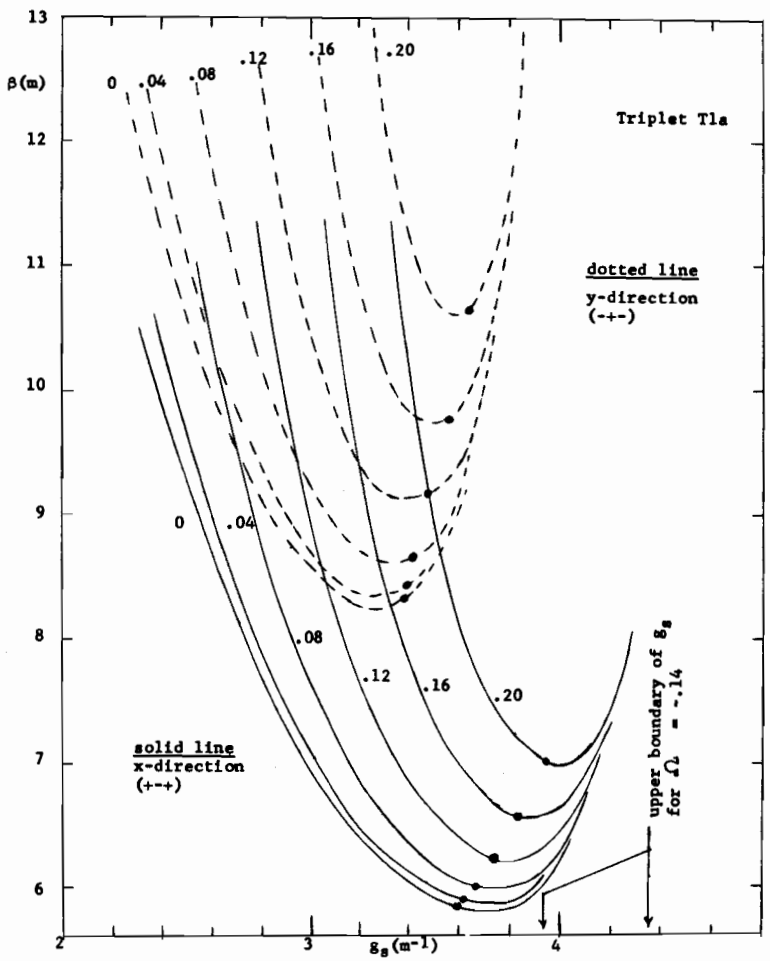
β(m)
13
12
11
10
9
8
7
6
2
3
4
g_s (m⁻¹)
0
.04
.08
.12
.16
.20
Triplet T1a
dotted line
y-direction
(-+-)
solid line
x-direction
(+-+)
upper boundary of g_s
for $\Delta\Omega$ = -.14

FIG. 10

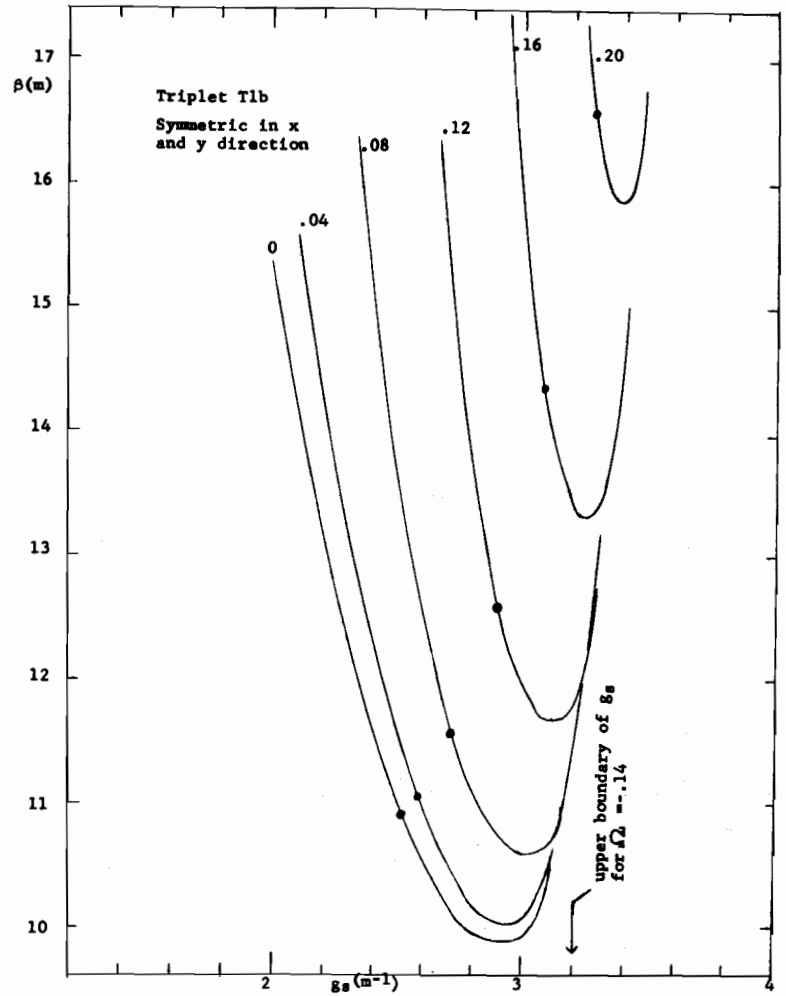
β(m)
17
16
15
14
13
12
11
10
2
3
4
g_s (m⁻¹)
0
.04
.08
.12
.16
.20
Triplet T1b
Symmetric in x
and y direction
upper boundary of g_s
for $\Delta\Omega$ = -.14

FIG. 11

If an amplifier tube fails, two consecutive tanks will be de-excited and there will be no increase in particle energy. The energy gain through two tanks are, in general, greater than the size of the "fish" (in $\Delta\gamma$ direction) so that all particles will become longitudinally unstable after passing de-excited tanks. The energy of such particles fluctuates around a certain value that is very close to what they had just before becoming unstable. For all practical purposes, the problem is then reduced to the transportation of particles with a constant momentum (in z direction) through a focusing system that is optimized for particles with increasing momenta. This means that we can predict where particles will be lost from the stability diagram of the focusing system. A detailed numerical calculation has confirmed this but it has also shown that particles are lost in a relatively long area ($\sim$ 100 m). Particles with 400 MeV or more energy are not expected to be lost at all. It is not possible to retain the bunch inside the longitudinal stability region by simply increasing the rf level in nearby tanks[13].

Since two quadrupole magnets will be getting power from the same source, the problem in case of magnet failures is to find the increase of the transverse amplitudes (A_x, A_y) when one pair of doublet is missing. At the "optical" centers, (x, x') and (y, y') will satisfy

$$x^2 + \beta_{max} x'^2 = A_x^2 \; ; \; y^2 + \beta_{max}^2 y'^2 = A_y^2$$

with $$A_x \leq \sqrt{\beta_{max} W_x} \quad , \quad A_y \leq \sqrt{\beta_{max} W_y} \; .$$

W_x and W_y are the phase space area divided by π in x and y direction, respectively. Because of the missing pair, these ellipses will be distorted to other forms (without changing the size):

$$ax^2 + bx'^2 + 2hxx' = 1 \quad , \quad a'y^2 + b'y'^2 + 2h'yy' = 1$$

where $1/\sqrt{ab-h^2} = A_x^2/\beta_{max}$ and $1/\sqrt{a'b' - h'^2} = A_y^2/\beta_{max}$.

If these distorted ellipses are entirely inside the ellipse

$$x^2 + \beta_{max} x'^2 = R^2 \text{ or } y^2 + \beta_{max}^2 y'^2 = R^2$$

with R = quadrupole aperture, there will be no loss of particles. For R = 2 cm and $A_x = A_y = 1.5$ cm, the fractional loss in both x and y directions changes from 30% at 200 MeV to 20% at 500 – 700 MeV. For R = 1.5 cm and $A_x = A_y = 1.0$ cm, corresponding figures are 40% and 30%, respectively. The important feature here is that most of these particles are lost in a relatively localized region ($\sim$ 15 m) because they can travel the distance which is at most one-half of the transverse wave length (29m) before getting the maximum excursions. Again it is not possible to adjust the strength of adjacent doublets (*) such that the loss would be decreased substantially. Preliminary results of numerical calculations show the recovery of only 5% or less at all energies.

VISSCHER: What is the radius of the aperture in your iris section calculations?

OHNUMA: The aperture radius really does not affect the calculation. It simply gives a criterion when you are concerned about the beam loss. Theoretically, the size of the beam would be about 1.5 cm or less. In calculating the misalignment effects, we used 2 cm radius.

VISSCHER: The value π cm-mrad of the transverse phase-space area you are using must have been based on some aperture radius.

OHNUMA: No. That is what we get out of the drift tube section independent of the iris section. The acceptance of the iris section is of course much larger. The calculation is a continuous one for both sections.

LAPOSTOLLE: About the possibility of a correction of the missing gap and drift spaces between tanks, especially in the Alvarez section, I think that, for transverse motions, it is possible to compensate with a slight correction of the quadrupole magnets. I wonder whether, for the longitudinal motion, it would not be possible also to compensate by a slight displacement of the accelerating gaps in order to change the phase when the bunch crosses the gap and modify the phase-focusing condition. Did you think about the idea of trying to compensate for any disturbance due to spaces between tanks, possibly by some modification at the end of the tank?

(*) Here it is assumed that the strength of two magnets of a doublet can be changed only simultaneously.

OHNUMA: We have not studied this problem in any detail in the Alvarez section. I believe that in the actual operation one must always make fine adjustments of the focusing magnets. As to the compensation for the longitudinal motion, it seems very difficult to adjust unless we can accurately measure the position of the bunch relative to the rf field in tanks. In the iris section, unless you change the strength of each magnet independently, even the transverse adjustment is not easy. You must remember that each doublet is 7 m apart. If one tank is out of operation, the bunch is completely out of the longitudinal stability region and there is no way of recovering it into the bucket. Of course, the focusing system still could transport this low energy beam down to the end without any beam loss. It depends on the energy acceptance of your focusing system.

KNAPP: You have two drift tubes close to one another that have magnets in them and then you have a large series of drift tubes with no magnet in them. Could you describe the distribution of magnets in the last four tanks of the Alvarez section?

OHNUMA: In Tank No. 3, there are 14 pairs for 46 full drift tubes; in No. 4, 6 pairs for 34; in No. 5, 4 pairs for 28; in No. 6, 3 pairs for 25; in No. 7, 3 pairs for 23 full drift tubes. The distance between the center of a focusing magnet to the next one, the magnet repeat length, ranges from 0.89 m to 7.3 m. The value of β_{max} changes gradually from 1.45 m to 12.5 m.

TENG: About the longitudinal phase space matching between the drift tube section and the iris section, have you considered the use of dispersive magnets? The distortion of the bunch in the longitudinal phase space due to the drift space can be compensated by such magnets.

OHNUMA: No, we have not thought about it. I don't know how wise it is to construct a special section or system just for this particular purpose. If we can use some regular sections as an option, it will be all right. Besides, such a system would require additional transverse matching systems and might not be desirable to have for the overall matching purpose.

TENG: You might have to bend the beam so that the drift tube section and the iris section are at an angle to one another. As far as the transverse phase space matching is concerned, you can always do that by a number of quadrupole magnets.

WHEELER: The figure of 10 m, which we have been using, was a somewhat arbitrary number which would allow us to have ample space between the sections. We have not looked carefully at how far down we can bring

this distance. I expect that it can be brought down quite a lot further, far enough so that it will satisfy beam dynamics requirements.

LEISS: Isn't it true of course that the reason for a short distance is removed if you do put a phase compression system such as Teng was talking about?

WHEELER: Yes, but I would rather try for a shorter distance than to try to put in a major magnet system which would be expensive, because of a longer tunnel length and require additional complex equipment and be consuming in manpower.

WALKINSHAW: Have you looked at the possible advantages of coming down in frequency to 600 Mc or even to 400 Mc where, I think, this problem would be less serious?

WHEELER: It would be nice to come down to 600 or 400 Mc for the purpose of solving this problem but the cost is going up proportionately. I think we are caught here in an attempt to keep the cost down but still meet the dynamics requirements. Based on our numerical calculations, we feel that we can operate at 800 Mc.

REFERENCES

1. Ohnuma, S., Minutes of the Conference on Proton Linear Accelerators at Yale University, October 1963, p. 14.

2. Ohnuma, S., ibid., p. 273.

3. Comment by R. Beringer in Ref. 1 above.

4. Gluckstern, R. L., Internal Reports Y-1 and Y-4, April and September, 1961, Yale University.

5. For example, see Edwards, T. W., MURA Report No. 622, June 15, 1961.

6. Teng, L. C., 1961 International Conference on High Energy Accelerators, Brookhaven National Laboratory, September 6-12, 1961, p. 212.

7. Ohnuma, S., Internal Report Y-10, March 1964, Yale University.

8. Courant, E. D., and Snyder, H. S., Annals of Physics, 3, 1 (1958).

9. Helm, R. H., Technical Report SLAC-15, March 1963, Stanford Linear Accelerator Center.

10. Gluckstern, R. L., Internal Report Y-7, January 24, 1964, Yale University.

11. Courant, E. D., Internal Report IA-3, EDC-43 (1961), Brookhaven National Laboratory.

12. Ohnuma, S., Technical Note S0-5, April 14, 1964, Accelerator Design Study, Yale University.

13. Wheeler, G. W., and Ludlam, T. W., Minutes of the Conference on Proton Linear Accelerators at Yale University, October 1963, p. 29.

NUMERICAL STUDY OF PARTICLE DYNAMICS IN A HIGH-ENERGY PROTON LINEAR ACCELERATOR*

M. Jakobson** and W. M. Visscher
Los Alamos Scientific Laboratory, University of California
Los Alamos, New Mexico

I. Introduction

We report here on the current status of a beam-dynamical calculation which has been evolving at Los Alamos for nearly a year. This paper should be considered as an addendum to and partial summary of a Los Alamos internal memo[1] which was written at the end of April. That report is considerably more complete and detailed than this one; we shall emphasize here the improvements and extensions which have been made since then.

At that time, most of our calculations had been made for a fictitious accelerator with plane symmetry, although some had utilized cylindrical symmetry in the accelerator sections with the beam constrained to move in only one of the transverse planes. Plane symmetry exaggerates the transverse defocusing and radial-phase coupling by a factor of two over the cylindrical case; it was therefore thought that conclusions valid for the plane problem would be pessimistic ones to apply to the cylindrical case. Our subsequent experience with the latter has borne this out.

The principal advance which has been made since our earlier report is the incorporation into the computer code of the other transverse dimension enabling us to calculate the real three-dimensional orbits of the protons as contrasted to 2 or 2-1/2 dimensions before. By 2-1/2 dimensions we mean three-dimensional fields with orbits constrained to two dimensions. We now take proper account of such things as x-y interaction and the effects of random rotations of the quads about the longitudinal axis. The addition of the third dimension has, unfortunately, nearly doubled the running time on the computer, but machine time has not been a serious problem as yet.

Another change which has been made is in the part of the code which designs the accelerator sections. Instead of designing them with a constant rf gradient, as before, we now design them with a constant power

*Work performed under the auspices of the U. S. Atomic Energy Commission.

**Permanent address: Department of Physics, Montana State University, Missoula, Montana.

consumption, for an obvious practical reason. The number of cells per section is, as before, a constant.

II. Method

We give here only a very sketchy description of the method used in the calculation; the interested reader can find much more detail in reference 1.

The π-mode rf field effective in accelerating the beam is assumed to be only that standing wave made up of components which have phase velocities equal to $\pm$ the synchronous particle velocity, and the impulse received by each particle in crossing a cell is approximated by that received by a particle moving across the cell in a straight line parallel the axis at constant speed. We call this the impulse approximation. The justification for these procedures is discussed in reference 1, and seems to be quite solid for the proton energies with which we are concerned.

The longitudinal and radial impulses calculated in this way are

$$I_z = \frac{\pi E_0}{2\omega} I_0(\kappa r) \cos\varphi \tag{1}$$

$$I_r = -\frac{\pi E_0}{2\omega} I_1(\kappa r) \sin\varphi ,$$

where I_0 and I_1 are Bessel functions of imaginary argument, E_0 is the maximum amplitude of the synchronous component of the rf field, $\kappa = \pi / L\gamma$, and φ is the phase of the proton entering the gap relative to the time at which the E field is a maximum. Our convention is to take the synchronous phase <u>negative</u>; thus Eqs. (1) predict a radial defocusing of the synchronous particle as is required by Earnshaw's theorem.

The acceleration received by each particle in each cell is computed by Eqs. (1), and the bunch is thus transported to the end of the section. At this point it enters a magnetic quadrupole lens system, which can be a singlet, doublet, or triplet. On the assumption that the transverse velocity is small compared to the longitudinal velocity, the x and v_x coordinates of a particle, on passing through a quad, are changed to

$$x' = \frac{v_x}{\Omega} \begin{matrix}\sin\\ \sinh\end{matrix} (\Omega t) + x \begin{matrix}\cos\\ \cosh\end{matrix} (\Omega t) \tag{2}$$

$$v_x' = v_x \begin{matrix}\cos\\ \cosh\end{matrix} (\Omega t) \mp \Omega x \begin{matrix}\sin\\ \sinh\end{matrix} (\Omega t) ,$$

where t is the time spent in the quad, and the upper (lower) signs and symbols refer to a focusing (defocusing) magnet. Similar equations are obtained for y' and v_y', with the upper and lower signs and symbols interchanged. Ω is the natural transverse oscillation frequency of a particle passing through the magnet, and is given by

$$(\Omega / \omega)^2 = 3.22 \left(\frac{\lambda}{2\pi}\right)^2 \frac{v_z}{\gamma c} H' \text{ (kilogauss/cm)} \tag{3}$$

for protons.

The bunch is transported through the quadrupoles by Eqs. (2), and allowed to drift through any drift spaces which may be present. Then the computer designs the next section and the process is repeated.

III. Calculations

Perhaps the most efficient way to explain the features of the code is to display the input parameters and the form of the output graphs. Figure 2 shows the input parameters for the current version of our 7094 Fortran code. This problem simulates an accelerator of 50 sections, each 40 cells long, separated by magnet systems of length equal to 4 cell lengths. The magnet systems can be singlet, doublet, or triplet; the 4 cell lengths include the internal drift spaces for the doublet and the triplet. As is illustrated in Fig. 1, this setup allows no space between the sections and the lens system for installation of plumbing or probes; we therefore have made provision for some extra drift space before the beginning of the magnet system. This extra drift space input also allows study of the effect of the necessary gap in the accelerator at the frequency transition point, and of a gap for a possible intermediate energy station.

The magnet systems have length proportional to β (line 1); but the quads themselves are, say 10 cm (line 5) long for the whole length of the machine. It takes two quads to make a doublet; four (10-20-10 cm) to make a triplet. This means that the effective strength of the lens increases with the energy if the quad strength stays constant. Line 5 and line 6 of Fig. 2 contain the rest of the focusing system parameters, contained in

$$H' = H_0' \; (1 + c\,E^n)/(1 + c\,E_0^n) \; . \tag{4}$$

c in Eq. (4) is the "quad coefficient", the synchronous energy E is raised to the "quad exponent" n, and H_0' is the field gradient (in kG/cm) of the quads at the beginning of the machine. We have not made an exhaustive study of variations in c and n; what we have done, however, indicates that the optimum is near c = n = 0.

In the 7th line are two remaining parameters which complete the description of the focusing system. The orientation of the first quad encountered by the beam is specified by saying whether it is converging or diverging in x. The repeat length is the periodicity of the lens system. For example, a doublet system with 4 section repeat length would be, schematically,

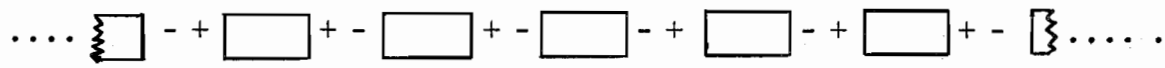

A repeat length between 6 and 12 sections seems best for triplets, and an infinite repeat length does well for doublets. Short repeat lengths give rise to unstable intervals in the stable range of quad strength.

More parameters to determine the geometry are in line 3 of Fig. 2. Synchronous input energy and design phase are self-explanatory. Phase shift and design beam load are numbers which describe the energy flow along the section, from cell to cell. We refer to reference 1 for discussion of them; here we only say that these and other effects which cause variation in phase velocity of the rf in time and position seem to cause no serious trouble. We have studied machines with constant cell length within a section, rather than phase velocity = "synchronous" particle velocity everywhere, which is what the code usually requires. Constant cell length has no noticeable deleterious effect for 40 cells per section; for much longer sections, however, it reduces the phase acceptance.

The hole radius has no effect on the fields, since we use only the lowest Fourier component; its only function is to provide criterion for deciding whether a given proton is still in the machine. We throw out particles when their radii exceed R_o, and only then. Particles often spill out of the phase-energy bucket and stay in the machine to the end due to the action of the quads. Our results indicate, in fact, that the rf can be turned off in a couple of sections near the start, resulting in the loss of the entire beam from the bucket, but the entire beam will be transported to the target. Also, the rf can be turned off entirely beginning at any point and the beam will coast out, or a few sections can be run with reversed rf and all subsequent ones with rf off. In this latter case a 600 MeV beam, say, can be made to come out at the 800 MeV end of the machine with the microstructure wholly debunched and a spread of 20 MeV. The drift length is shorter if a higher energy spread is allowable, and vice versa. Thus a variable energy machine could be designed with a maximum energy of 800 MeV (no debunching) and a completely debunched beam available from 700 MeV on down. Reference 1 contains a more quantitative discussion of this point.

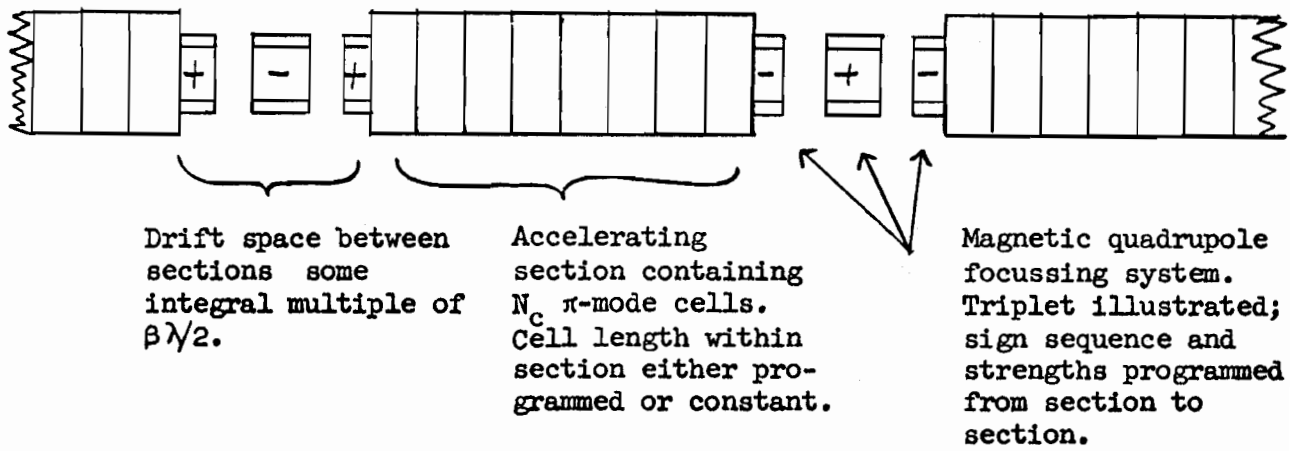

Figure 1. Schematic diagram of accelerator structure.

50 SECTIONS 40 CELLS PER SECTION 200 PROTONS IN BUNCH MAGNET SYSTEMS 4 CELLS LONG

DRIFT SPACE OF LENGTH 2 CELL LENGTHS AFTER THE 100TH SECTION REPEATED EVERY 1TH SECTION

INPUT ENERGY= 1.765E 02 DESIGN PHASE= -3.000E 01 PHASE SHIFT= 0. DESIGN BEAM LOAD= -0.

HOLE RADIUS= 2.000E-02 SECTION POWER= 5.000E-01 RANDOM START AT 1.900E 01

INITIAL QUAD GRADIENT= 3.000E 00 QUAD LENGTH= 1.000E-01 FREE SPACE WAVELENGTH= 3.750E-01

QUAD COEFFICIENT= -0. QUAD EXPONENT= -0

TRIPLET LENS SYSTEMS FIRST QUAD DIVERGING IN X 12 SECTION REPEAT LENGTH

SECTIONWISE AMPLITUDE ERROR= -0. CELLWISE AMPLITUDE ERROR= -0. SECTIONWISE PHASE ERROR= -0.

QUAD FIELD ERROR= -0. QUAD DISPLACEMENT= 10.000E-04 SECTION TWIST= -0. QUAD ROTATION= -0.

RF AMPLITUDE MULTIPLIED BY 0. FOR 0 SECTIONS STARTING WITH NUMBER 100

ENERGY LIMITS 1.765E 02, 1.765E 02 PHASE LIMITS -6.000E 01, 3.000E 01

X LIMITS -2.000E-02, 2.000E-02 Y LIMITS -2.000E-02, 2.000E-02

VR LIMITS -4.000E-03, 2.000E-03 VTH LIMITS -0, , -0.

Figure 2. Input Parameters for Computer Code.

Section power (megawatts) is in the input because rf gradient isn't. The sections are designed to consume a given amount of power with a 20 mA proton current and a ZT^2 given by an empirical formula for the cloverleaf structure (Knapp, LASL)

$$ZT^2 = 65\,\beta/(\beta + 0.76)\ \mathrm{M}\Omega/\mathrm{m}\,. \tag{5}$$

We chose 1/2 Megawatt as the section power because the power supplies envisioned at LASL will deliver ~ 1 Megawatt and splitting between two sections is feasible and will give sections of reasonable lengths and rf gradient; namely, 40 cells (4 meters up to 6 meters at 800 MeV) and 1.35 at 175 down to 1.20 MV/m synchronous particle energy gain at 800 MeV. The code designs each section with a synchronous phase velocity and converges on a given section power iteratively.

Random start has nothing to do with the machine or beam dynamics; it merely tells where to start reading the random number table. Random numbers are used for generating the seven "standard" kinds of random errors (uniformly distributed) listed in lines 8 and 9 (we have studied the effects of a number of other errors, besides those listed here), and also for generating the proton bunch. The bunch parameters are those in the last 3 lines of Fig. 2. It is characterized by upper and lower energy limits, phase limits, x and y, v_r and v_θ limits. All the particle coordinates but phase are chosen by the random number generator.

IV. Results

Our code should be able to given an answer to the question, "Are doublets or triplets better at focusing the beam in the high-energy linac?" The answer, we think, is that triplets are. Triplets give an acceptance zone in transverse phase space about 50% bigger than doublets in the example shown on Fig. 3. π milliradian-cm corresponds to the area of the small rectangle; we see therefore that either doublets or triplets are easily capable of accepting the transverse output thought to emanate from the drift tube section. Random errors of 1 mm in displacement of the lens system parallel to the axis cut the acceptance area by about 30% for each case. Radial beam confinement as reflected by the rms radii for the bunch seems about the same for triplets as for doublets; this is shown for triplets on the bottom curve on Fig. 4. Our tentative conclusion is that on the basis of simplicity and lower cost, doublets are preferable, unless doublet tilt or independent quad alignment tolerances prove to be excessively stringent, or very large transverse acceptance turns out to be necessary.

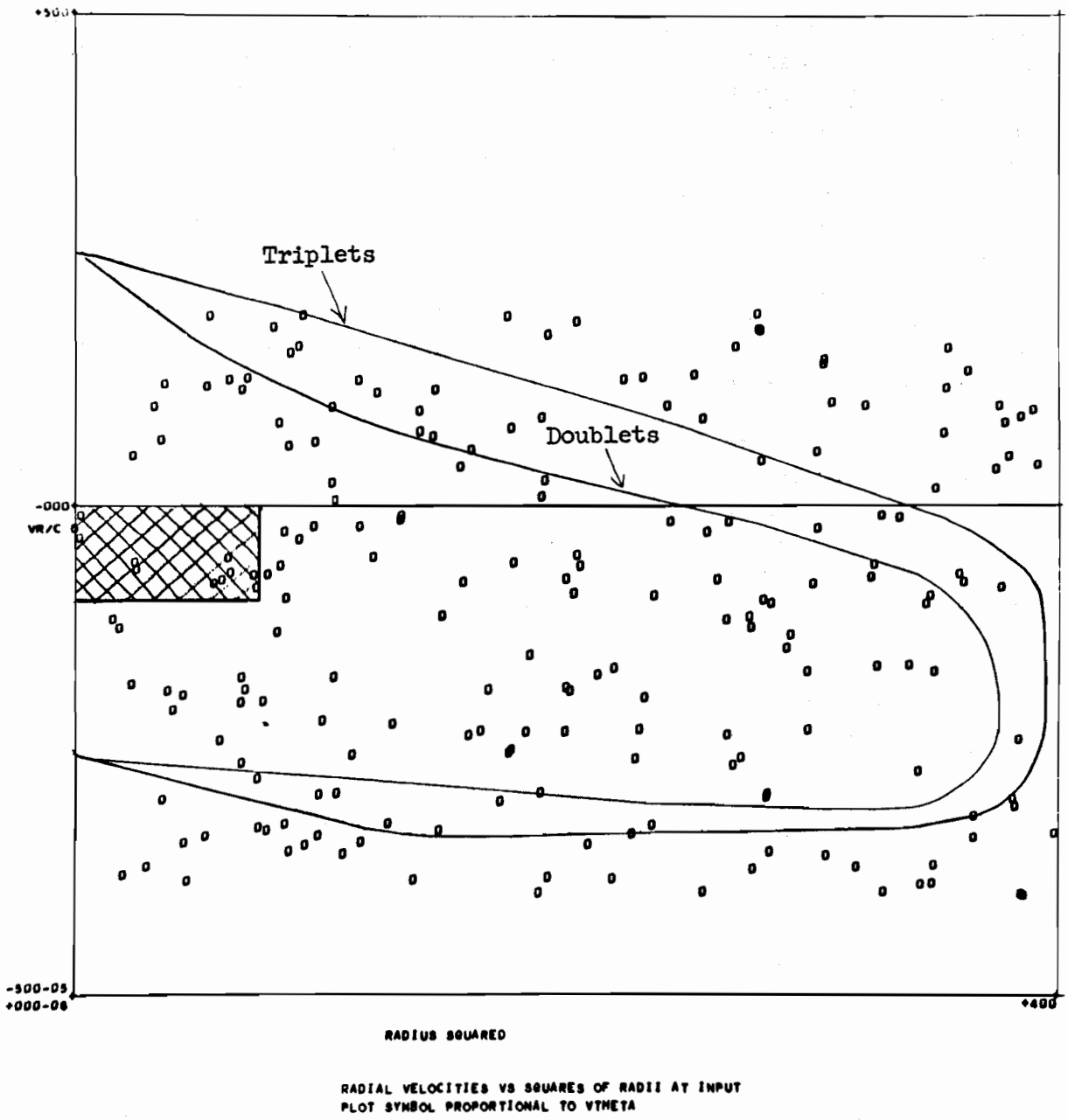

Fig. 3: Approximate acceptance envelopes in transverse sphase space for doublet and triplet focussing systems, both without errors. Crosshatched rectangle encloses π milliradian-centimeter beam area.

As an example of how the effect of a particular kind of error may be evaluated, we take a run for which the elements of the triplets are independently and randomly rotated about the longitudinal axis, up to a maximum angle of $\pm 0.5^{\circ}$. Figure 5 shows the transverse input, a rectangle in x, y space translated to r^2, v_r. Figures 6a, 6b, 6c are a series of phase-energy plots of the bunch as it progresses down the machine. Figure 7a, finally, is the summary plot, showing the rms radius and phase deviation from synchronous of the bunch, radius and phase of a particular particle, and the total number of surviving protons, all as a function of section number. Especially interesting here is the rms radius, which should be compared with Figs. 7b, 7c, which show the same for 0 and 1° quad rotation, respectively. See also Fig. 8, which is the summary graph for doublets with 1° quad rotations.

The effects of the other kinds of errors which we have studied (and are enumerated and discussed in reference 1) can be summarized by saying that no obviously impossible tolerances are imposed by beam dynamical requirements on the geometrical and electromagnetic parameters which we have varied. For example, sectionwise rf amplitude and phase tolerances are of the order of 2% and 2°. Tank axes can be a millimeter out of alignment (for 2 cm radius aperture), while the allowable spread in individual quadrupole field gradients is about 1%. Bench alignment tolerances for the triplet lens systems are a few mils; we have not yet determined them for doublets.

LAPOSTOLLE: You mentioned the possibility of debunching the beam in the last sections, especially when you use your machine for a slightly lower energy. I think that for some experiments it might be interesting not to debunch but to use an rf structure, very short bunches. Would it be possible to keep the rf structure even at a lower energy.

VISSCHER: Yes, well it depends on what energy you want. It is not possible to get the rf structure out if we let it drift all the way from, let's say, 300 MeV, because then the energy spread in the bunch will itself be sufficient to debunch, I think.

WALKINSHAW: You could keep your rf on and change the respective phasing along the tanks if you recalibrate your phasing.

LAPOSTOLLE: That was my original question.

VISSCHER: Yes, but it wouldn't be something simple like just turning off the rf.

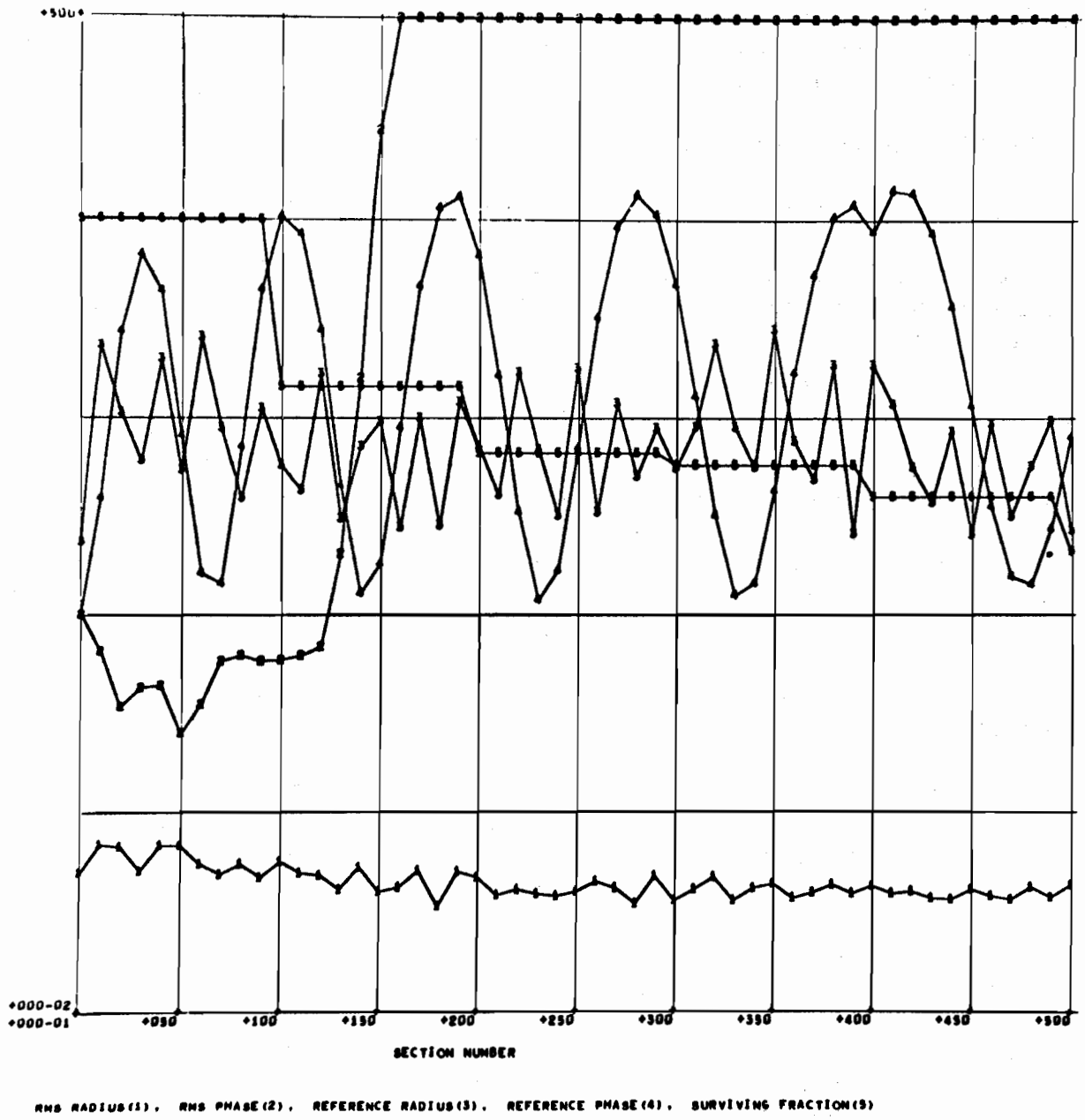

Fig. 4: Summary graph for triplet system. Particles are rejected for excessively large radius every 10 sections; the r.m.s. phase goes off scale because protons are lost from the phase bucket without blowing up radially. The "reference particle" is always that proton whose initial phase is smallest among the surviving particles. Quad displacement error for this run was 1 mm.

TENG: It would be possible only if the sections were short enough.

VISSCHER: Maybe it wouldn't be possible because the section length and the cell length wouldn't at all correspond with the beta of the particle that is drifting through.

WALKINSHAW: I don't think that matters.

TENG: Well it doesn't matter if it is short enough, but are they?

VISSCHER: In order for an accelerator section to be of any use in retaining the bunch structure, the number of cells in the section has to be less than about

$$N < \frac{\gamma(\gamma - 1)(\gamma + 1)}{4\,\Delta\gamma},$$

where $\Delta\gamma$ is the difference (mass units) between the synchronous energy and the beam energy. Thus, for example, in order to use a 700 MeV section to retain rf structure in a 600 MeV beam, the section length would be limited to 27 cells. (Otherwise the phase change of the beam within the section will exceed 180°.) For an energy difference of 300 MeV, say, this restriction becomes impossibly stringent. The beam could be coasted out with a bunched structure by inserting special rf bunchers between sections, but I don't think the accelerating sections themselves could be used for this prupose.

WALKINSHAW: Could you give a figure for the growth in transverse phase space area (with misalignment errors) relative to the phase space area of the synchronous particle? That is the increase in the transverse phase space area when errors are introduced.

VISSCHER: We have not yet made extensive studies of the transverse motions in three dimensions, but from those we have done combined with some extrapolations from the two-dimensional runs, I would expect the transverse phase space area of the beam to increase by less than a factor of two from 200 to 800 MeV with reasonable errors in quad alignment and rotation and section tilt.

REFERENCES

1. Informal report, "A Numerical Study of Radial and Phase Stability in a High-Energy Proton Linear Accelerator," Los Alamos, 30 April 1964.

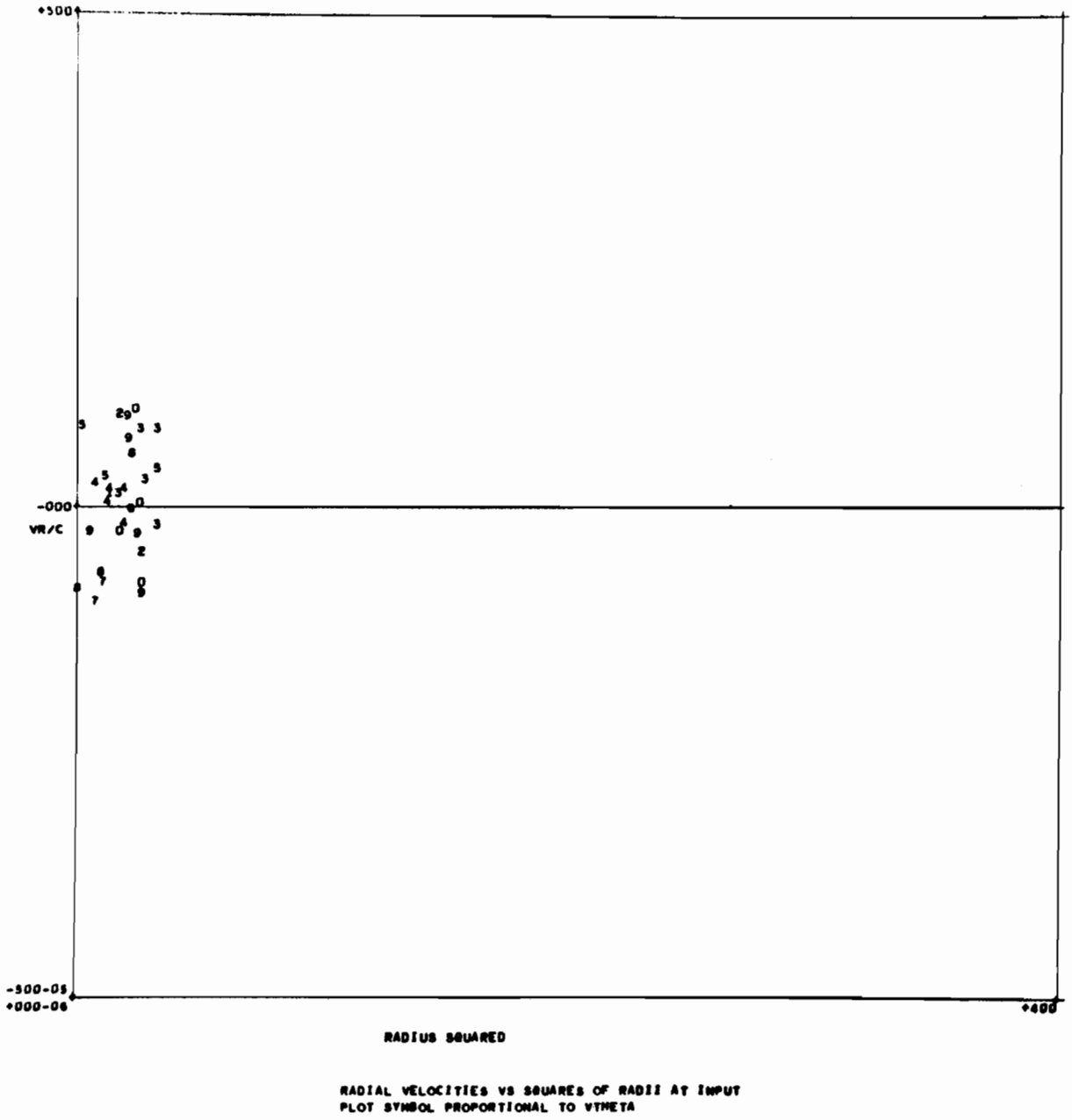

Fig. 5: Transverse input for quad rotation run. Area corresponds to 4 milliradian-cm. A plot symbol n means that $n/10 \leq v_\theta/v_{\theta\ max} < (n + 1)/10$.

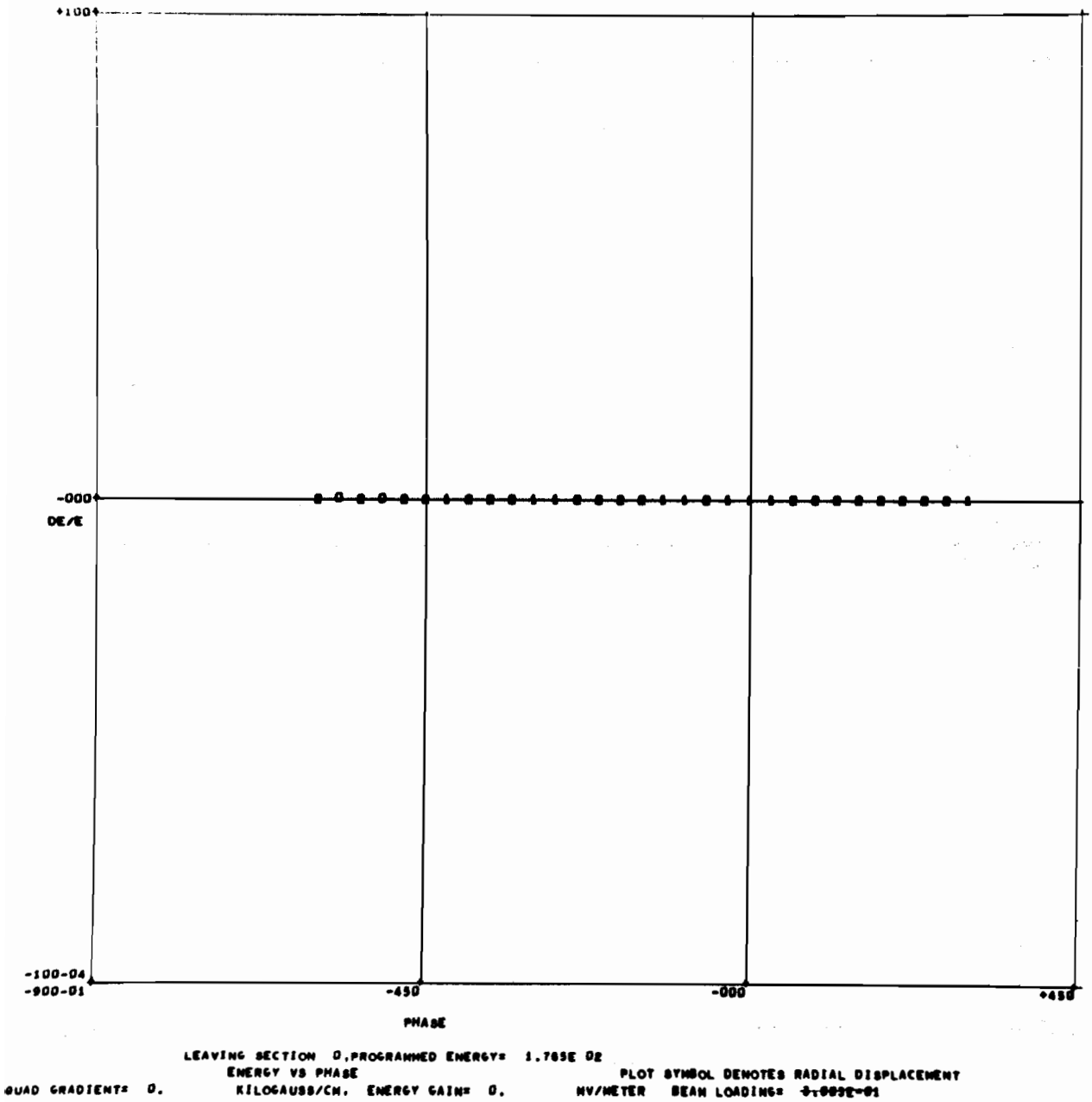

Fig. 6a: Phase-energy input for quad rotation run. Phase interval is 3 times synchronous phase; energy interval is zero, but the points will fill most of the range of the ordinate after the first section, since the phase oscillation wavelength is less than 3 sections for near-synchronous particles. A plot symbol n means the proton has $n/10 \leq r/R_0 < (n + 1)/10$.

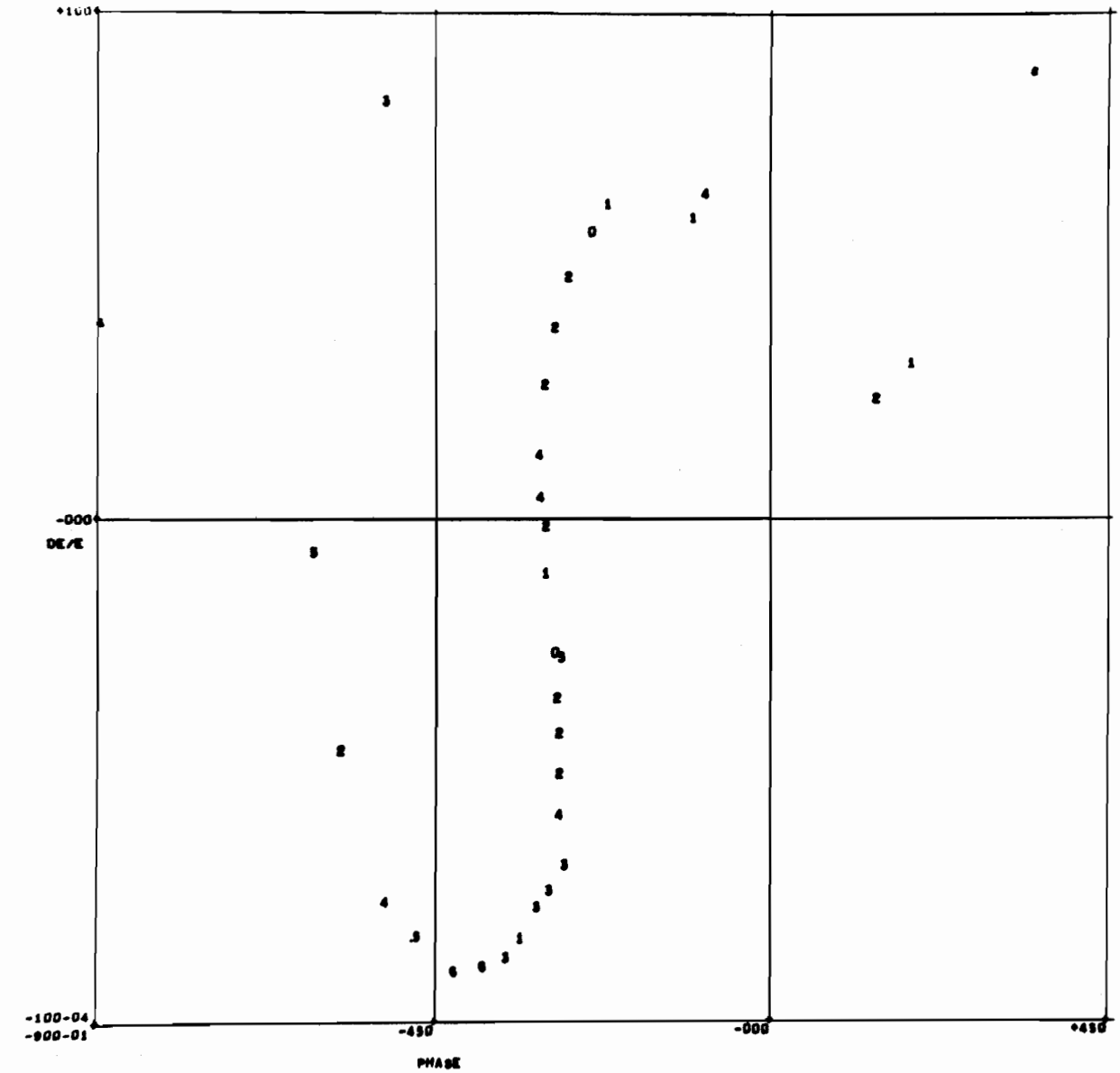

Fig. 6b: The same as Fig. 6a, but after 5 sections. The points would lie on a smooth curve were it not for the radial-phase interaction which causes the phase development to depend on the (initially random) transverse position. At this point the pattern has already rotated more than $1\frac{3}{4}$ times.

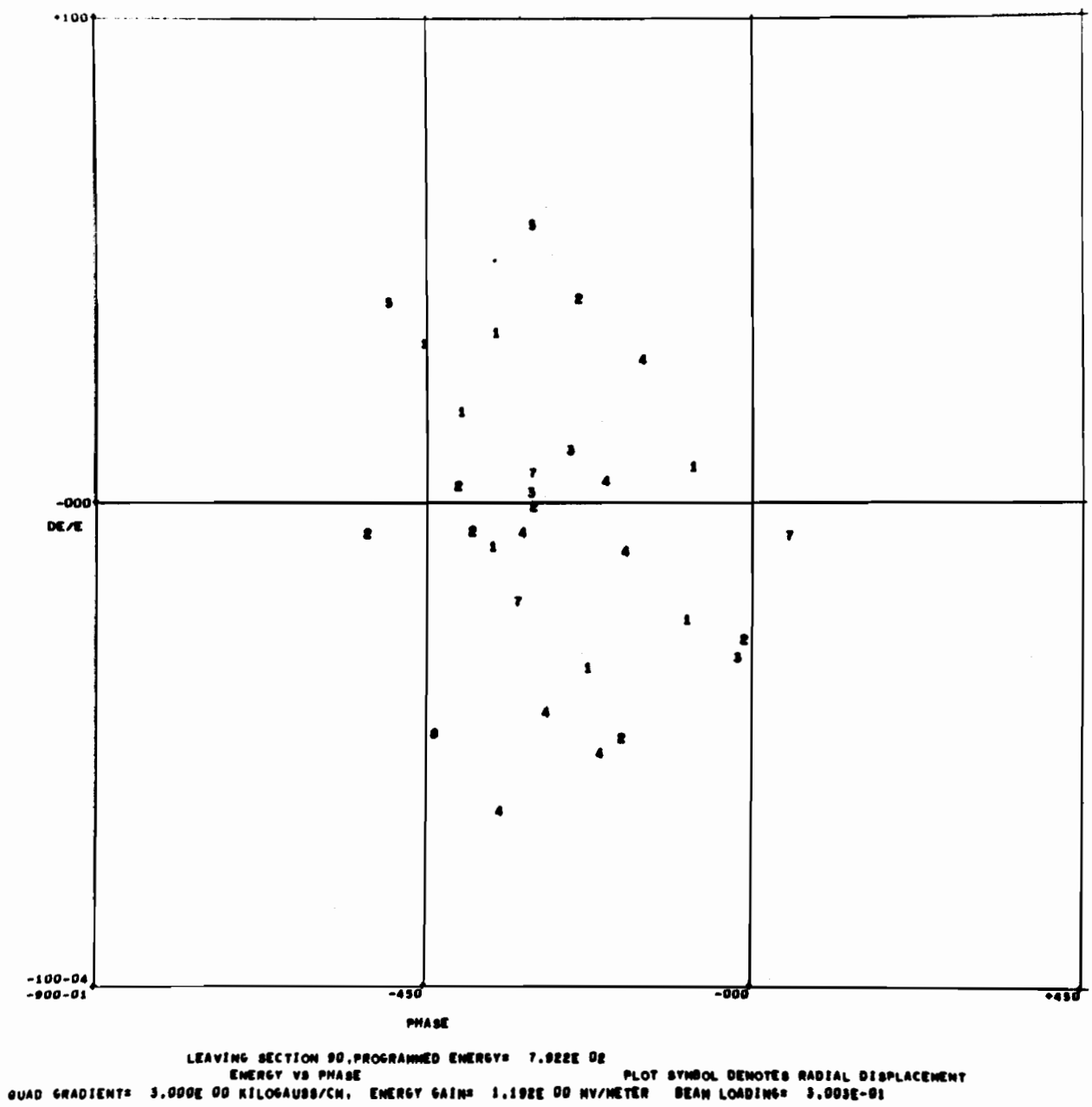

Fig. 6c: Same as Fig. 6b, but after 90 sections. Phase compression is noticeable; the wrapped-up line of the input is still recognizable.

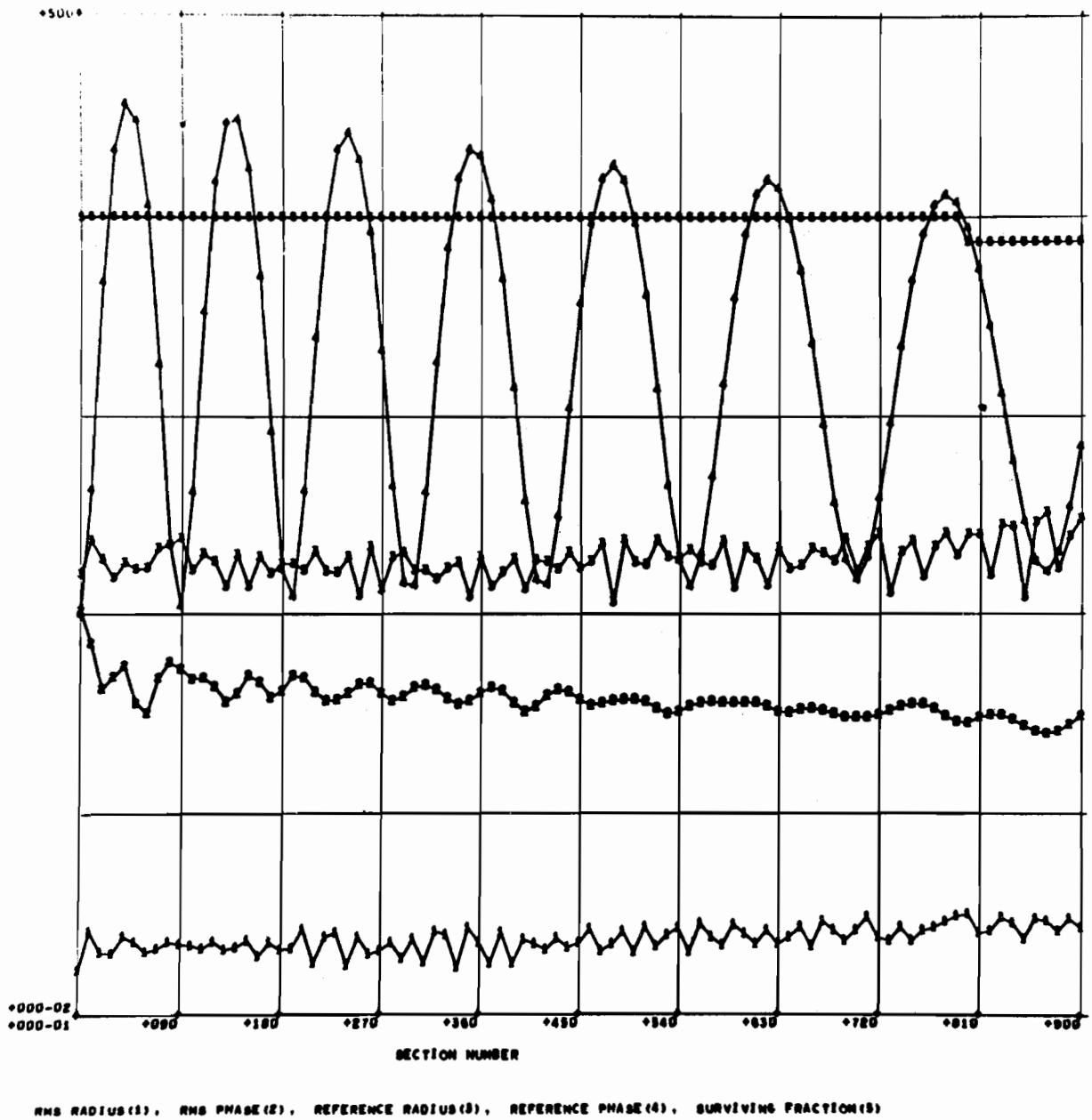

Fig. 7a: Summary plot for run with quad rotation errors of 0.5°. The r.m.s. radius shows a slight buildup, and a particle is lost radially at section 80.

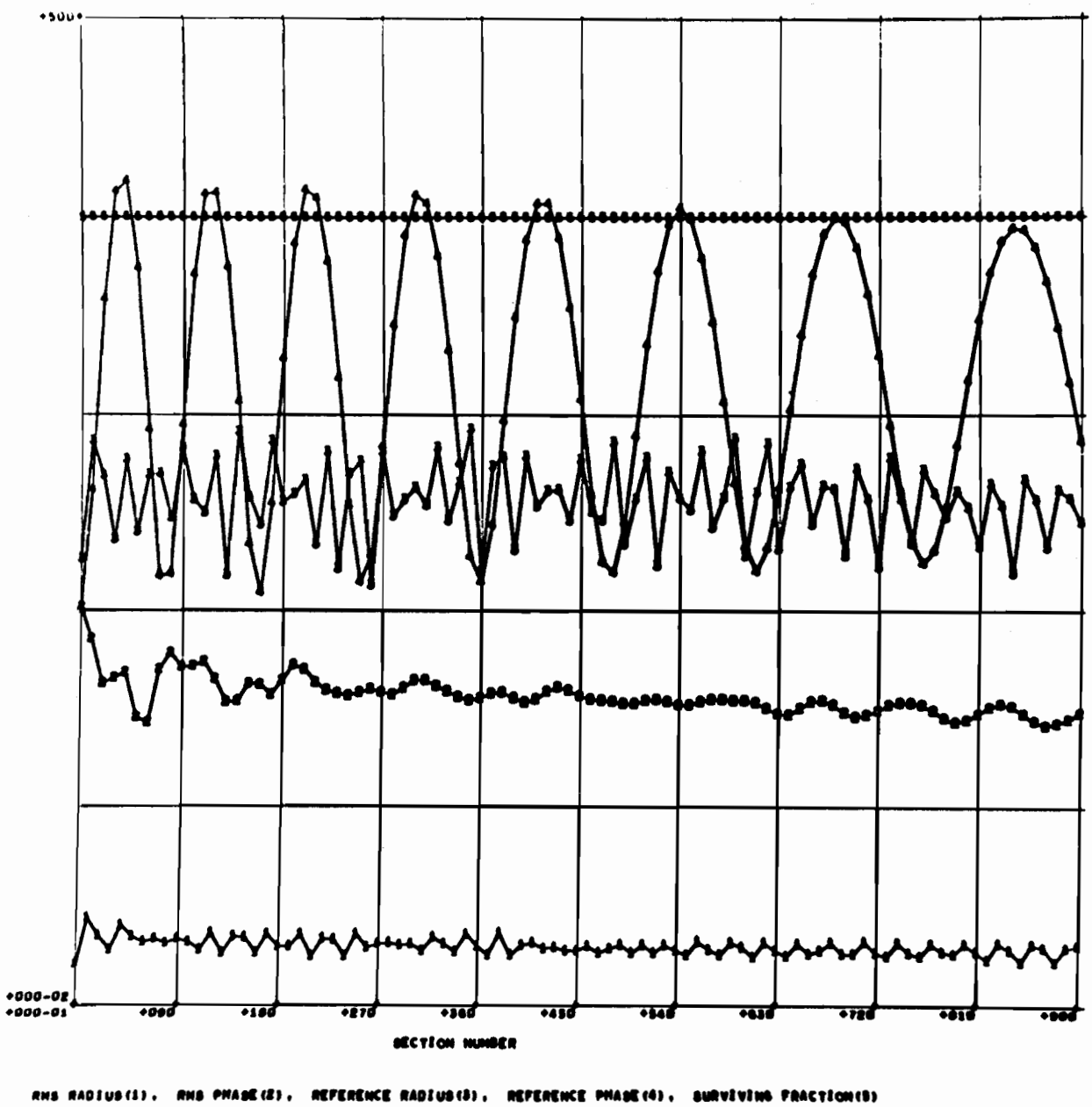

Fig. 7b: Same as Fig. 7a, but with no errors. R.M.S. radius is quite flat.

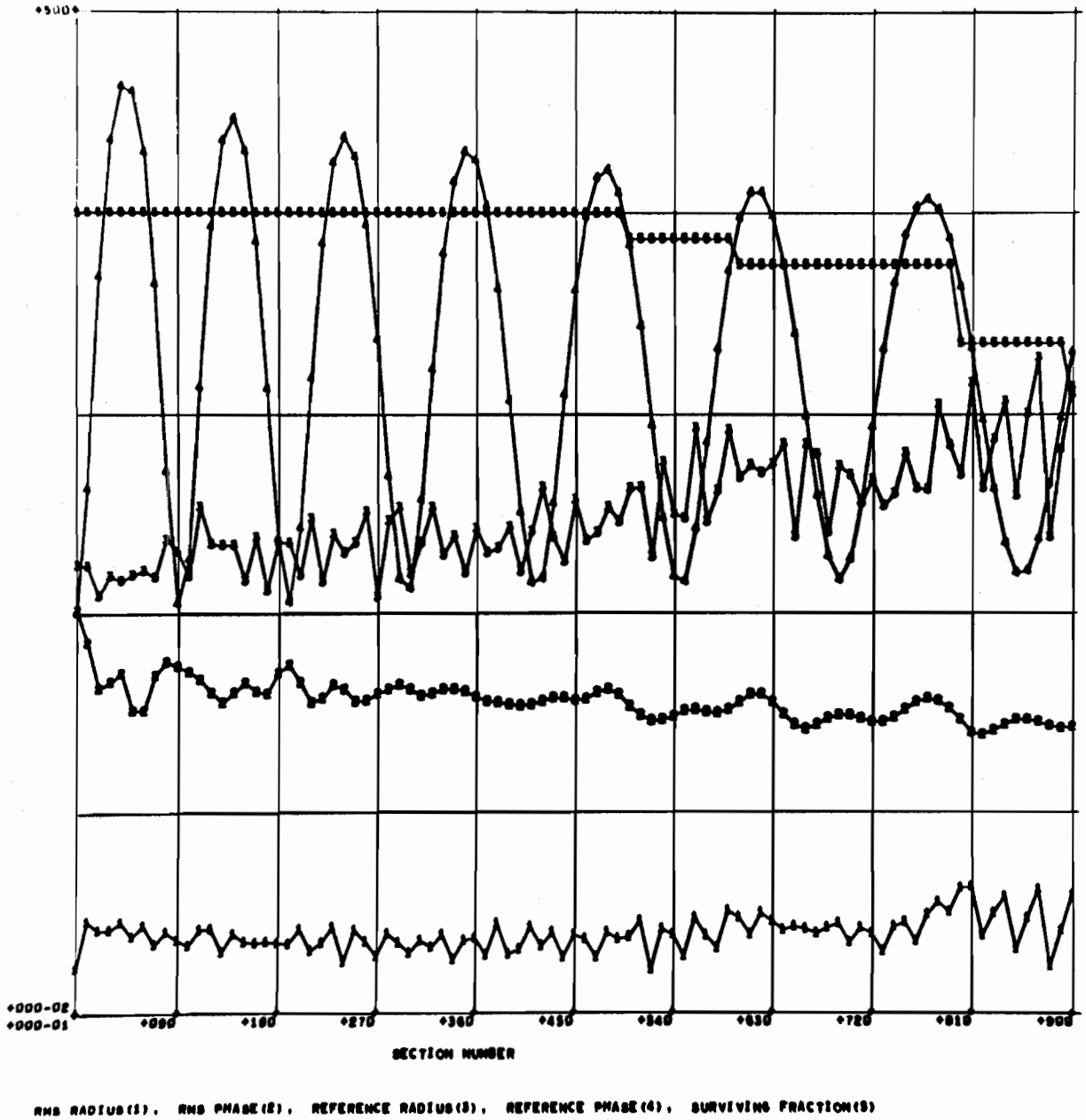

Fig. 7c: Same as Fig. 7a, but with 1° rather than 0.5° quad rotation errors.

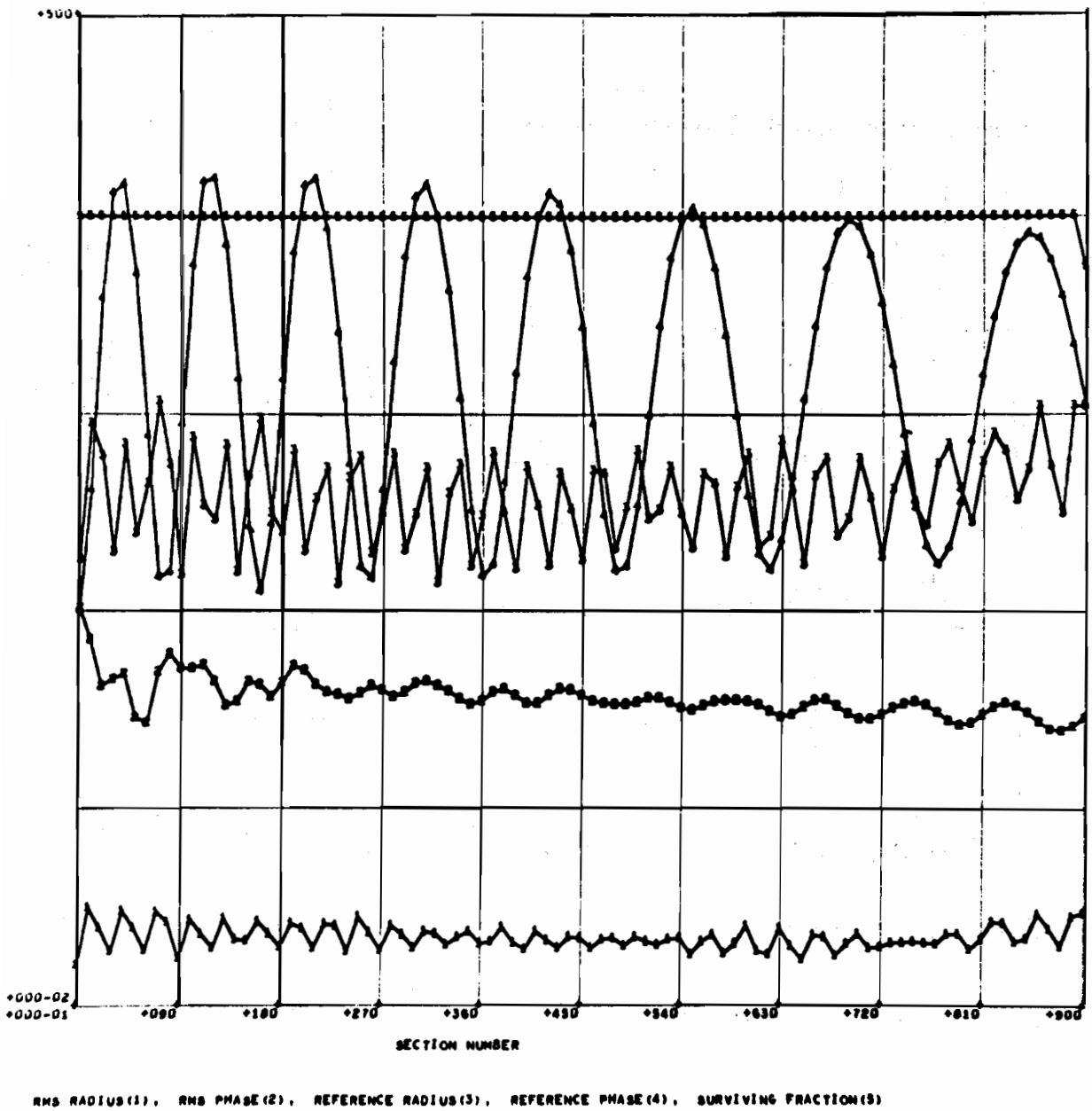

Fig. 8: Summary plot for doublets with quad rotation errors of 1°,

CONSTANT PHASE VELOCITY ACCELERATION SECTIONS IN A PROTON LINAC*

J. Parain
Centre D'Etudes Nucleaires De Saclay

For an accelerator with constant phase velocity acceleration sections, it is not possible to define a synchronous particle. One can however define a reference particle such that the motion of all particles might be related to this reference particle (1).

1 - Motion in one acceleration section

The equations of the motion in one acceleration section are:

$$\frac{dE}{ds} = e\,\xi\,\sin\varphi$$

$$\frac{d\varphi}{ds} = \frac{2\pi}{\lambda}\left(\frac{1}{\beta} - \frac{1}{\beta_r}\right)$$

where s is the direction of the motion, E the energy, ξ the electric field, φ the phase with respect to the accelerating field, λ the wavelength, β the relative velocity and β_r the phase velocity of the accelerating field in the section.

By writing $E - E_r = \Delta E$, the hamiltonian of the motion may be written

$$H = -\frac{\pi}{\lambda}\,\frac{E_o^2}{\left[E_r^2 - E_o^2\right]^{3/2}}\,\Delta E^2 + e\,\xi\,\cos\varphi$$

E_o is the rest energy of the particle.

---

* This work was started at the CERN.

A new variable energy may be defined by:

$$W = \frac{\Delta E}{e} A_o \quad \text{with } A_o = \left[\frac{2\pi}{\xi \lambda \frac{Eo}{e} \beta_r^3 \gamma_r^3} \right]^{1/2}$$

The trajectories in the (W, φ) space will be the curves having for equation

$$\left(\frac{W}{2}\right)^2 + \sin^2 \frac{\varphi}{2} = ct$$

The length of an acceleration section is

$$L = \pm \frac{1}{\Omega_o} \int_{\alpha_o}^{\alpha_e} \frac{d\theta}{(1 - k^2 \sin^2 \theta)^{1/2}}$$

with $\Omega_o = \left[\frac{2\pi\xi}{\lambda \frac{Eo}{e} \beta_r^3 \gamma_r^3} \right]^{1/2}$ $\quad k^2 = \left(\frac{W}{2}\right)^2 + \sin^2 \frac{\varphi}{2}, \sin\alpha = \frac{\sin \frac{\varphi}{2}}{k}$

This equation may be solved by introducing the $F(\alpha, k)$ elliptic integral of first kind. If $\phi = \Omega_o L$, one gets

$$\phi = \pm \left[F(\alpha_e, k) - F(\alpha_o, k) \right]$$

2 - The reference particle

The reference particle has for velocity the phase velocity in the middle of the section. At the beginning of the section, the initial conditions for this reference particle are $(\varphi_r, -W_r)$, the final conditions will be $(\varphi_r, +W_r)$. W will then increase by $2 W_r$. . From W, φ diagram, two points may have this property, one of them will be stable, the other one unstable.

The phase of the reference particle is variable all the way through the section; in the middle of the section, the phase will have its maximum value φ_m,

$$\text{with} \quad \sin \frac{\varphi_m}{2} = \left[\sin^2 \frac{\varphi_r}{2} + \left(\frac{W_r}{2} \right)^2 \right]^{1/2} .$$

One can compute the length of the acceleration section corresponding to the motion of the reference particle.

$$\phi = 2 \left[F \left(\frac{\pi}{2}, k_r \right) - F \left(\alpha_r, k_r \right) \right]$$

Figure No. 1 gives the curve ϕ = ct in the (W, φ) space. If the length of the section is small, the phase does not vary much, and the motion will be the same as in an accelerator with a synchronous particle, $\varphi_r \simeq \varphi_s$.

3 - Efficiency

For the reference particle, the energy increased in a section will be

$$2 \frac{\Delta E}{e} = \frac{2 W_r}{A_o}$$

If L is the length of the section, and ξ the electric field, the efficiency of the section may be written as

$$\eta = \frac{2 \frac{\Delta E}{e}}{\xi L}$$

Using reduced variables $\eta = \dfrac{2 W_r}{\phi}$

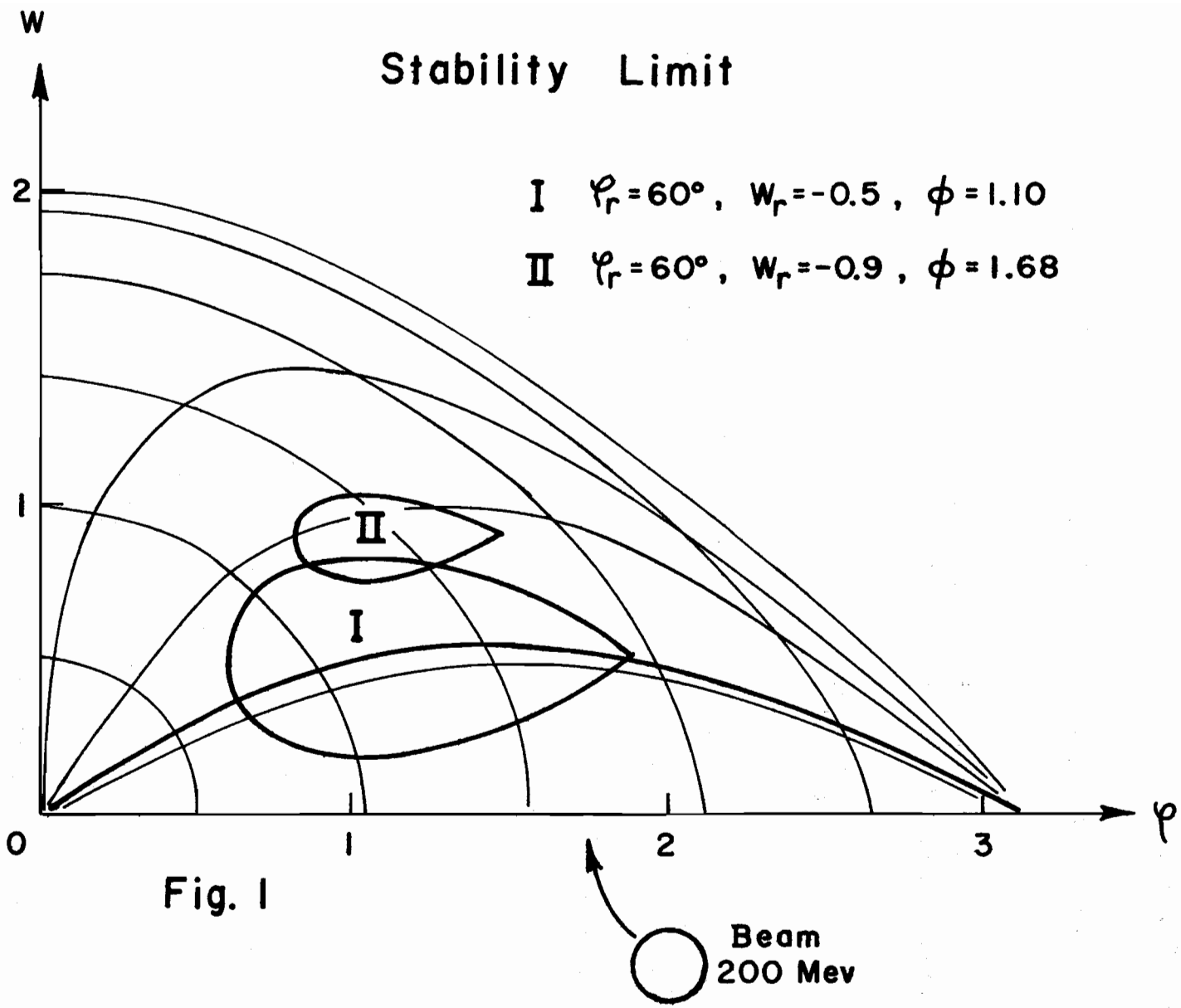
W
Stability Limit
I $\varphi_r = 60°$, $W_r = -0.5$, $\phi = 1.10$
II $\varphi_r = 60°$, $W_r = -0.9$, $\phi = 1.68$
2
1
0
1
2
3
φ
II
I
Beam
200 Mev

Fig. I

Figure No. 2 gives the curves η = ct in the (W, φ) space. For each value of ϕ , a maximum value of efficiency may be found such that

$$\eta_{max} = \frac{2\ (W_r)max}{\phi}$$

for smaller values of ϕ , η max = 1, for ϕ = 2, η max = 0.99 but η_{max} decreases rapidly for $\phi > 2$.

4 - Motion of a particle around the reference particle

Let us now consider a particle with initial conditions (φ_1, W_1). Since this particle will travel the same length in the linac, one may compute the conditions at the end of the section.

$$F\ (\alpha_2, k) = 2\ F\ (\frac{\pi}{2}, k) - F\ (\alpha_1, k) - \phi$$

with $\sin \alpha_i = \dfrac{\sin \frac{\varphi_i}{2}}{k}$ and $k^2 = \sin^2 \dfrac{\varphi_i}{2} + \left(\dfrac{W_i}{2}\right)^2$

This expression gives φ_2 and W_2 , that is the position of the particle at the end of the section. When entering the next acceleration section, the particle has the same phase, but the phase velocity of the new section is different, so that

$$(\varphi_1)_{j+1} = (\varphi_2)_j \text{ and } (W_1)_{j+1} = (W_2)_j - 2W_r .$$

The j indices are for the conditions in the jth section. In all of this, no consideration has been given to the adiabatic evolution.

5 - Stability Area

If one computes the position of one particle at the end of each section by using the relation in Section 4, one can find that the consecutive positions of the particle are plotted on a curve in the (W, φ) space.

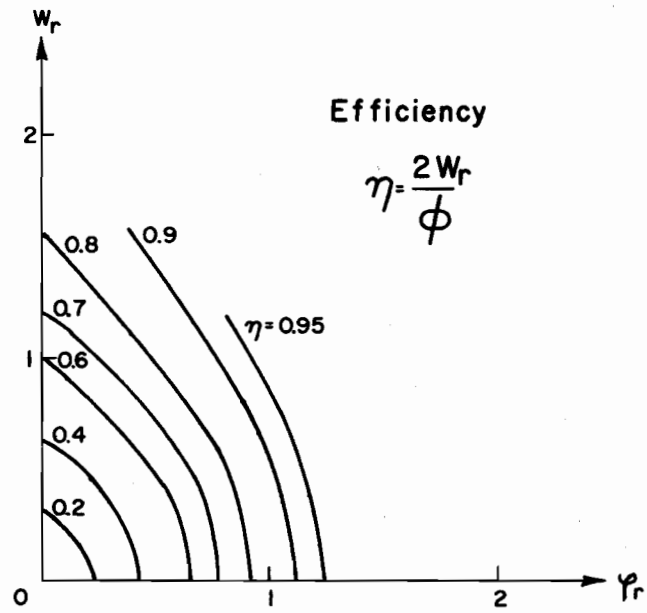
W_r
Efficiency
$\eta = \frac{2W_r}{\phi}$
0.8
0.9
0.7
$\eta = 0.95$
0.6
0.4
0.2
2
1
0
1
2
φ_r

Fig. 2

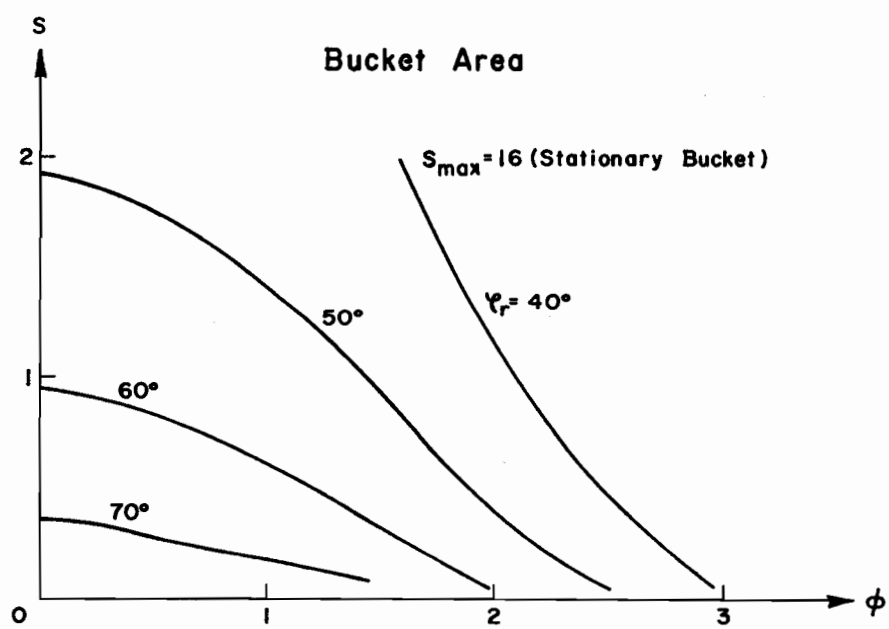
S
Bucket Area
$S_{max} = 16$ (Stationary Bucket)
$\varphi_r = 40°$
50°
60°
70°
2
1
0
1
2
3
ϕ

Fig. 3

For a small ϕ, one finds the curve of limit stability that is well known for an accelerator with synchronous particle. For greater ϕ, but ϕ still smaller than two, the curves have the same shape, the limit stability curves still go through the unstable point. Figure No. 1 shows the stability area for two values of ϕ.

For ϕ greater than two, that is for a number of synchrotron oscillations per section $\nu = \phi/2\pi$ of the order of 0.3 the motion is more complicated. For small amplitudes, the consecutive positions of the particle do not shape an ellipse centered on the stable point anymore. For larger amplitudes, the particle may become unstable after a few runs around the stable point. This case has not been thoroughly studied, since it is out of the limits of application.

The curves in Figure No. 3 give the surface of the limit stability curves versus ϕ for different values of φ_r. For ϕ smaller than two, it can be seen that the surface is the same as in accelerator with a synchronous particle the phase of which being such that $\eta = \sin\varphi_s$. For ϕ greater than two, the surfaces are smaller than it could be found from this approximation.

6 - Application

We shall now study a 200 MeV beam in a proton linac. For parameters defined in reference (2) that is $\xi = 2\times10^6$ V/m, $\lambda = 0.75$ m and an acceleration section length of 6 m, one finds $\phi = 1.4$. One still has to make choice of a reference phase such that all the particles might be contained inside the stability area. The 200 MeV beam has, in the (ΔE, φ) phase space, an area of 75.6×10^3 V.rd. In order to get a simpler image, one might admit that the adapted beam is a circle in the (W, φ) space, in that case

$$\Delta\varphi = \frac{A_0 S(\Delta E, \Delta\varphi)}{\Delta W}. \quad \text{Hence} \quad \Delta\varphi \simeq 0.1 \text{ rd.}$$

The Figure No. 1 gives the cross section of the beam. For $\varphi_r = 60^\circ$, the stability limit area is still 10 times greater than the beam area. This might be necessary to take care of phase and amplitude errors of electric field. The value of ϕ decreases for increasing energies, it is then possible either to keep constant the length of the section and to increase the efficiency or to increase the section length by increasing the number of identical sections, for example. The following table gives the length L and its corresponding value of ϕ, as a function of energy.

Energy BeV	L m	ϕ
0.2	6	1.42
0.4	6	0.80
0.4	12	1.60
1.0	12	0.66
1.0	24	1.32
2.0	24	0.63
2.0	48	1.25
3.0	48	0.78

These lengths still fit the quadrupole doublet radial focusing requirements. One might think of starting with a 50 MeV beam and 3 m long sections, ξ being 2 10^6 V/m and ξ = 1.5 m, ϕ would then still be = 1.5.

7 - Conclusion

It is possible to use constant phase velocity acceleration sections in a linac if the number of synchrotron oscillations per section is smaller than 0.3. With this condition, it is possible to obtain a large enough area of stability and an efficiency of about 0.9 for a proton linac of energy between 200 MeV and 3 BeV.

References

(1) SMITH, L. - Stepped phase velocity linacs
Conference on linear accelerators for high energies.
Brookhaven August 1962

(2) SHERSBY-HARVIE, R. B. R. - Tentative proposal for a 3 Gev Linac injector - CERN AR/Int. SG/63-18 - 24th October 1963

FOCUSING OF AN ALVAREZ LINAC BY USE OF MAGNETIC QUADRUPOLES ORIENTED AT 45°

D. T. Tran
CSF - Compagnie générale de télégraphie Sans Fil
Centre De Physique Electronique Et Corpusculaire
Domaine de Corbeville ORSAY (S. &. O.)

(Presented by M. G. Guilbaud)

Introduction

Strong focusing as used currently in Proton Linacs is made by quadrupoles in the N. S. N. S. or N. N. S. S. arrangement.

According to some authors (1), (2), (3), the acceptance of the system can be increased if the axis of the successive quadrupoles are oriented some angle, different from 90°. We have tried to analyze the situation when successive quadrupoles are at a 45° angle one from next.

We have taken the quadrupoles to be thin lenses, and assumed that the rf. defocusing is also that of a cylindrical thin lens, located at the middle of the gap.

Stability

Fig. 1 shows the equivalent mesh, starting at the middle of an R. F. gap. d and 2g are the respective convergence and divergence of the quadrupoles and rf. gap. R represents the rotation of the lens.

---

(1) Krienen, F. CERN - SC. 57-28 (1957).

(2) Morpurgo, M. CERN - SC. 141 Bis (1957).

(3) Septier, A. Advances in Electronics and Electron Physics. Academic Press - Vol. XIV - 1961.

The transfer matrix of vector

$$(1) \qquad \vec{V} = \begin{pmatrix} x \\ y \\ x' \\ y' \end{pmatrix}$$

is, for a diverging lens,

$$(2) \quad \left[d\right] = \begin{pmatrix} 1 & 0 & 0 & 0 \\ 0 & 1 & 0 & 0 \\ d & 0 & 1 & 0 \\ 0 & -d & 0 & 1 \end{pmatrix} = \begin{pmatrix} \left[1\right] & \left[0\right] \\ D & \left[1\right] \end{pmatrix}$$

where

$$(3) \quad D = d \begin{bmatrix} 1 & 0 \\ 0 & -1 \end{bmatrix} = d\,\pi \quad , \text{ where } \quad \pi^2 = \left[1\right] \quad .$$

For an accelerating gap:

$$(4) \quad \left[g\right] = \begin{bmatrix} 1 & 0 & 0 & 0 \\ 0 & 1 & 0 & 0 \\ 2g & 0 & 1 & 0 \\ 0 & +2g & 0 & 1 \end{bmatrix} = \begin{bmatrix} \left[1\right] & \left[0\right] \\ 2G & \left[1\right] \end{bmatrix}$$

where

$$G = g \left[1\right]$$

since the rf . is defocusing both in the x and y directions.

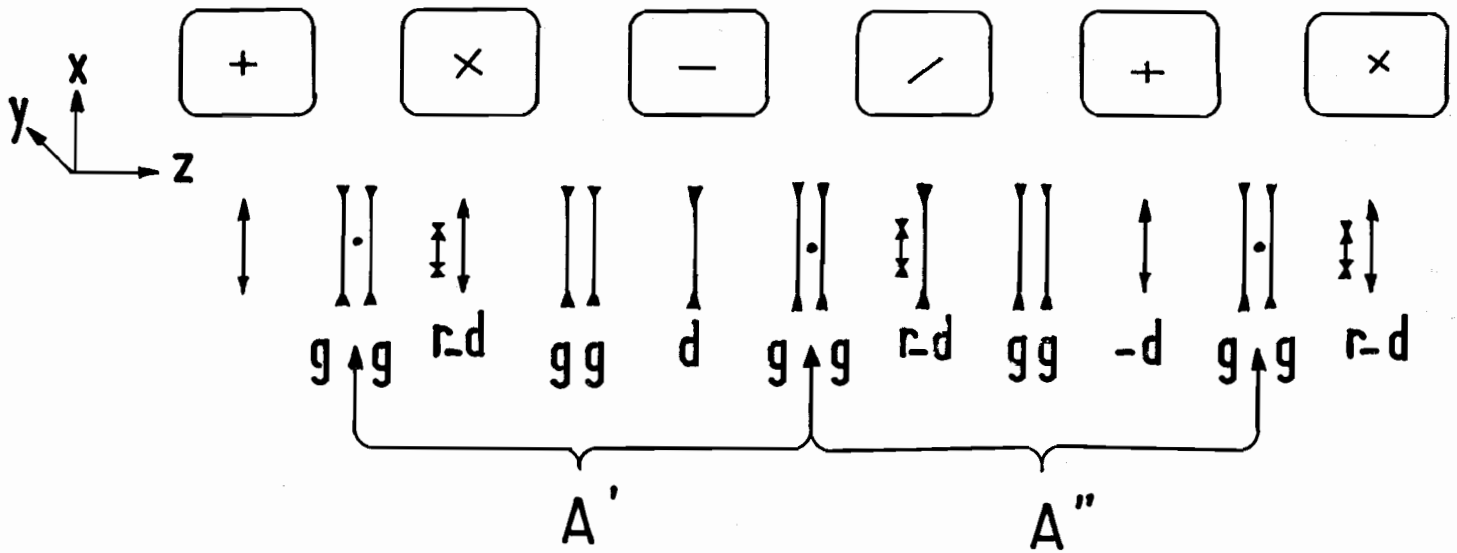

Fig 1 DISPOSITION SCHEMATIQUE

The zero field gap is represented by

$$(5)\quad [\ell] = \begin{pmatrix} 1 & 0 & \ell & 0 \\ 0 & 1 & 0 & \ell \\ 0 & 0 & 1 & 0 \\ 0 & 0 & 0 & 1 \end{pmatrix} = \begin{pmatrix} [1] & L \\ [0] & [1] \end{pmatrix}$$

where

$$(6)\quad L = \begin{pmatrix} \ell & 0 \\ 0 & \ell \end{pmatrix} = \begin{pmatrix} 1 & 0 \\ 0 & 1 \end{pmatrix}$$

if half a cell length is taken as the unit length.

The rotation comes to:

$$(7)\quad R = \begin{pmatrix} \cos\alpha & \sin\alpha & 0 & 0 \\ -\sin\alpha & \cos\alpha & 0 & 0 \\ 0 & 0 & \cos\alpha & \sin\alpha \\ 0 & 0 & -\sin\alpha & \cos\alpha \end{pmatrix}$$

In our case

$$(8)\quad R = \frac{1}{\sqrt{2}} \begin{pmatrix} 1 & 1 & 0 & 0 \\ -1 & 1 & 0 & 0 \\ 0 & 0 & 1 & 1 \\ 0 & 0 & -1 & 1 \end{pmatrix}$$

we write this

$$(9) \qquad R = \begin{pmatrix} \sqrt{J} & [0] \\ [0] & \sqrt{J} \end{pmatrix}$$

where

$$(10) \qquad \sqrt{J} = \frac{1}{\sqrt{2}} \begin{pmatrix} 1 & 1 \\ -1 & 1 \end{pmatrix}$$

Let us note that

$$(11) \qquad J = \left(\sqrt{J}\right)^2 = \begin{pmatrix} 0 & 1 \\ -1 & 0 \end{pmatrix} \quad \text{and } J^2 = -\begin{pmatrix} 1 & 0 \\ 0 & 1 \end{pmatrix} = -[1]$$

If A' and A'' are the transfer matrices of the mesh halves, the matrix is

$$A = A'' \circ A'.$$

where

$$A' = \begin{pmatrix} [1] & [0] \\ G & [1] \end{pmatrix}\begin{pmatrix} [1] & [1] \\ [0] & [1] \end{pmatrix}\begin{pmatrix} [1] & [0] \\ D & [1] \end{pmatrix}\begin{pmatrix} [1] & [1] \\ [0] & [1] \end{pmatrix}\begin{pmatrix} [1] & [0] \\ 2G & [1] \end{pmatrix}\begin{pmatrix} [1] & [1] \\ [0] & [1] \end{pmatrix}\begin{pmatrix} [1] & [0] \\ -D & [1] \end{pmatrix}$$

(12)

$$\begin{pmatrix} \sqrt{J} & [0] \\ [0] & \sqrt{J} \end{pmatrix}\begin{pmatrix} [1] & [1] \\ [0] & [1] \end{pmatrix}\begin{pmatrix} [1] & [0] \\ G & [1] \end{pmatrix}$$

A'' is obtained from A' by changing the sign of d.

This notation allows us to multiply 4 x 4 matrices as if they were 2 x 2.

Let us note also that since matrices $\sqrt{J}$, $\left[1\right]$ and G are commutative, we can write,

(13) $$A'(90^{o}) = A'(0^{o}) \cdot \sqrt{J}$$

(14) $$A(90^{o}) = A''(0^{o}) \cdot \sqrt{J} \cdot A'(0^{o}) \cdot \sqrt{J}.$$

So,

(15) $$A(0^{o}) = \begin{pmatrix} (a^2 - b^2 + c\,\delta)\left[1\right] & 2c(a\left[1\right] + b\,\pi) \\ 2\,\delta\,(a\left[1\right] - b\,\pi) & (a^2 - b^2 + c\,\delta)\left[1\right] \end{pmatrix}$$

(16) $$A\left(\frac{\pi}{4}\right) = \left(\begin{array}{c|c} (a^2 + c\,\delta)\,J - b^2\left[1\right] - ab\,\pi + ab\,\pi J & c(2a\,J + b(\pi + \pi J)) \\ \hline \delta(2a\,J - b\,(\pi + \pi J) & (a^2 + c\,\delta)\,J - b^2\left[1\right] - ab\,\pi + ab\,\pi\,J \end{array}\right)$$

If

(17) $$\vec{V} = \begin{pmatrix} x \\ x' \\ y \\ y' \end{pmatrix}$$

we can write matrices:

(18)

$a^2 - b^2 + c\delta$	$2c(a+b)$	0	0
$2\delta(a-b)$	$a^2 - b^2 + c\delta$	0	0
0	0	$a^2 - b^2 + c\delta$	$2c(a-b)$
0	0	$2\delta(a+b)$	$a^2 - b^2 + c\delta$

$\mathcal{A}(90^\circ) =$

(19)

$-b(a+b)$	bc	$a(a+b) + c\delta$	$c(2a+b)$
$-\delta b$	$+b(a-b)$	$\delta(2a-b)$	$a(a-b) + c\delta$
$-(a(a-b) + c\delta)$	$-c(2a-b)$	$b(a-b)$	$-bc$
$-\delta(2a+b)$	$-\left[a(a+b) + c\delta\right]$	δb	$-b(a+b)$

where

$$
(20)\quad \begin{cases}
a = 1 + 8g - 2d^2 + 8g^2 - 4d^2 g - 2g^2 d^2 \\
b = 2d(g+1) \\
c = 4 + 8g - 2d^2 - 2g d^2 \\
\delta = 4g + 12g^2 - 2d^2 - 6g d^2 + 8g^3 - 3g^2 d^2 - 2g^3 d^2.
\end{cases}
$$

In the classical focusing arrangement, x and y motions are uncoupled, and have the same trace:

(20 bis) $$Tx = Ty = 2\,(a^2 - b^2 + c\,\delta)$$

And the stability condition is:

(21) $$\left| 2\,(a^2 - b^2) - 1 \right| < 1$$

In our case, the characteristic equation is:

(22) $$\Delta(\lambda I - \mathcal{A}(90^\circ)) = 0$$

And this gives

(23) $$\lambda^4 + 4\,b^2\,(\lambda^3 + \lambda) + \left[4\,(2\,a^2 - b^2)^2 - 16a^2 + 2\right]\lambda^2 + 1 = 0.$$

It is a 4th degree reciprocal equation, the roots of which are two inverse groups:

(24) $$\lambda_1\,,\quad \lambda_1^{-1}\quad ;\quad \lambda_2\,,\quad \lambda_2^{-1}$$

If we write:

(25) $$\lambda_1 = e^{i\mu_1}$$

$$\lambda_2 = e^{i\mu_2}$$

we get

(26) $$\cos\mu_1 = -b^2 + 2\sqrt{a^2\,(1 + b^2 - a^2)}$$

$$\cos\mu_2 = -b^2 - 2\sqrt{a^2\,(1 + b^2 - a^2)}$$

The stability conditions write then:

$$
(27) \qquad \boxed{\begin{array}{lcl} 1 - b^2 & > & 0 \\ 1 + b^2 - a^2 & \geq & 0 \\ 4\,a^2\,(1 + b^2 - a^2) & < & (1 - b^2)^2 \end{array}}
$$

Relations (21) and (27) allow to draw the curves of fig. 2. The stability region of classical case is between curves 1 and 2, whereas for our case, it is between 1 and 4. It is much narrower.

From the point of view of stability, our arrangement is disadvantageous.

Acceptance

Let us consider the case when the four eigen-values λ_k are different (in the classical case, they make two identical couples).

Let

$$
(28) \qquad \vec{V_i} = \begin{pmatrix} X_i \\ X'_i \\ Y_i \\ Y'_i \end{pmatrix}
$$

be the ith eigen-vector.

A trajectory can be expressed as

$$
(29) \qquad \vec{v} = \begin{pmatrix} x \\ x' \\ y \\ y' \end{pmatrix} = \sum_i A_i \, \vec{V_i} \qquad i = 1, 2, 3, 4
$$

when A_i depend only on the initial conditions:

$$(30)\quad \begin{cases} A_1 = \dfrac{W(xy;2)}{W(1;2)} & A_2 = A_1^* = \dfrac{W(xy;1)}{W(1;2)} \\[2ex] A_3 = \dfrac{W(xy;4)}{W(3;4)} & A_4 = A_3^* = \dfrac{W(xy;3)}{W(3;4)} \end{cases}$$

where

$$(31)\quad \begin{cases} W(xy;i) = \begin{vmatrix} x & X \\ x' & X'_i \end{vmatrix} + \begin{vmatrix} y & Y_i \\ y' & Y'_i \end{vmatrix} = \vec{v}\ S\ \vec{V}_i \\[2ex] W(i;j) = \begin{vmatrix} X_i & X_j \\ X'_i & X'_j \end{vmatrix} + \begin{vmatrix} Y_i & Y_j \\ Y'_i & Y'_j \end{vmatrix} = \vec{V}_i\ S\ \vec{V}_j \end{cases}$$

are the classical Wronskians, and

$$(32)\quad S = \begin{pmatrix} 0 & -1 & 0 & 0 \\ 1 & 0 & 0 & 0 \\ 0 & 0 & 0 & -1 \\ 0 & 0 & 1 & 0 \end{pmatrix}$$

this yields

$$(33)\quad \begin{cases} x = A_1 X_1 + A_1^* X_1^* + A_3 X_3 + A_3^* X_3^* \\[2ex] y = A_1 Y_1 + A_1^* Y_1^* + A_3 Y_3 + A_3^* Y_3^* \end{cases}$$

or

$$(34)\quad \begin{cases} |x|_{max} = 2\ \mathrm{Max}\ \left(|A_1|\ |X_1| + |A_3|\,|X_3| \right) \\ |y|_{max} = 2\ \mathrm{Max}\ \left(|A_1|\ |Y_1| + |A_3|\,|Y_3| \right) \end{cases}$$

The eigen-values X_i and Y_i are determined as follows: let x_1, x_2, x_3, x_4, and y_1, y_2, y_3, y_4 be four different particular solutions, which can be determined from adequate initial conditions and by using the matrix of mesh $\mathcal{Q}(a_{ij})$.

We can write:

$$(35)\quad \begin{cases} X_i = \sum_j \sigma_{ij}\, x_j \\ X'_i = \sum_j \sigma_{ij}\, x'_j \\ Y_i = \sum_j \sigma_{ij}\, y_j \\ Y'_i = \sum_j \sigma_{ij}\, y'_j \end{cases}$$

Which yields, if

$x_{10} = 1$	$x_{20} = 0$	$x_{30} = 0$	$x_{40} = 0$
$x'_{10} = 0$	$x'_{20} = 1$	$x'_{30} = 0$	$x'_{40} = 0$
$y_{10} = 0$	$y_{20} = 0$	$y_{30} = 1$	$y_{40} = 0$
$y'_{10} = 0$	$y'_{20} = 0$	$y'_{30} = 0$	$y'_{40} = 1$

and since

$$\begin{bmatrix} X_i \\ Y_i \end{bmatrix}_{out} = \lambda_i \begin{bmatrix} X_i \\ Y_i \end{bmatrix}_{in}$$

four homogeneous equations:

$$(36) \qquad \left(\mathcal{A}(a_{ij}) - \lambda_i \, I \right) \begin{pmatrix} \sigma_{i1} \\ \sigma_{i2} \\ \sigma_{i3} \\ \sigma_{i4} \end{pmatrix} = 0 \qquad i = 1, 2, 3, 4.$$

This gives the characteristic equation (23) and coefficients σ_{ij}. So, from (34), we can determine the maximum amplitude of a trajectory corresponding to given initial conditions. Inversely, since the problem is linear, one can determine, at each point of the mesh, the bounding surface of initial conditions which yields trajectories which do not deviate from the axis by more than the hole radius. The volume bounded by this hypersurface is the system acceptance. According to Liouville's theorem, this volume deforms but is of a constant value. As the motion is Hamiltonian, and, due to the symmetry of the system, this volume is an hyperellipsoid.

Results

We shall consider points A, B, C, and D on fig. 2. A, B, C are stable both in the classical arrangement and in our arrangement. D is stable only in the classical one. D is close to the line of maximum acceptance of the classical system, A is close to the line of maximum acceptance of ours.

To make the comparison, we have drawn the intersection of the hypervolume with the phase planes (x , x') and (y , y'). These are ellipses (fig. 3, 4, 5, 6, 7, 8), the area of which is the acceptance of the system in said phase plane. We have chosen that the particles do not deviate from the axis by more than 10 mm.

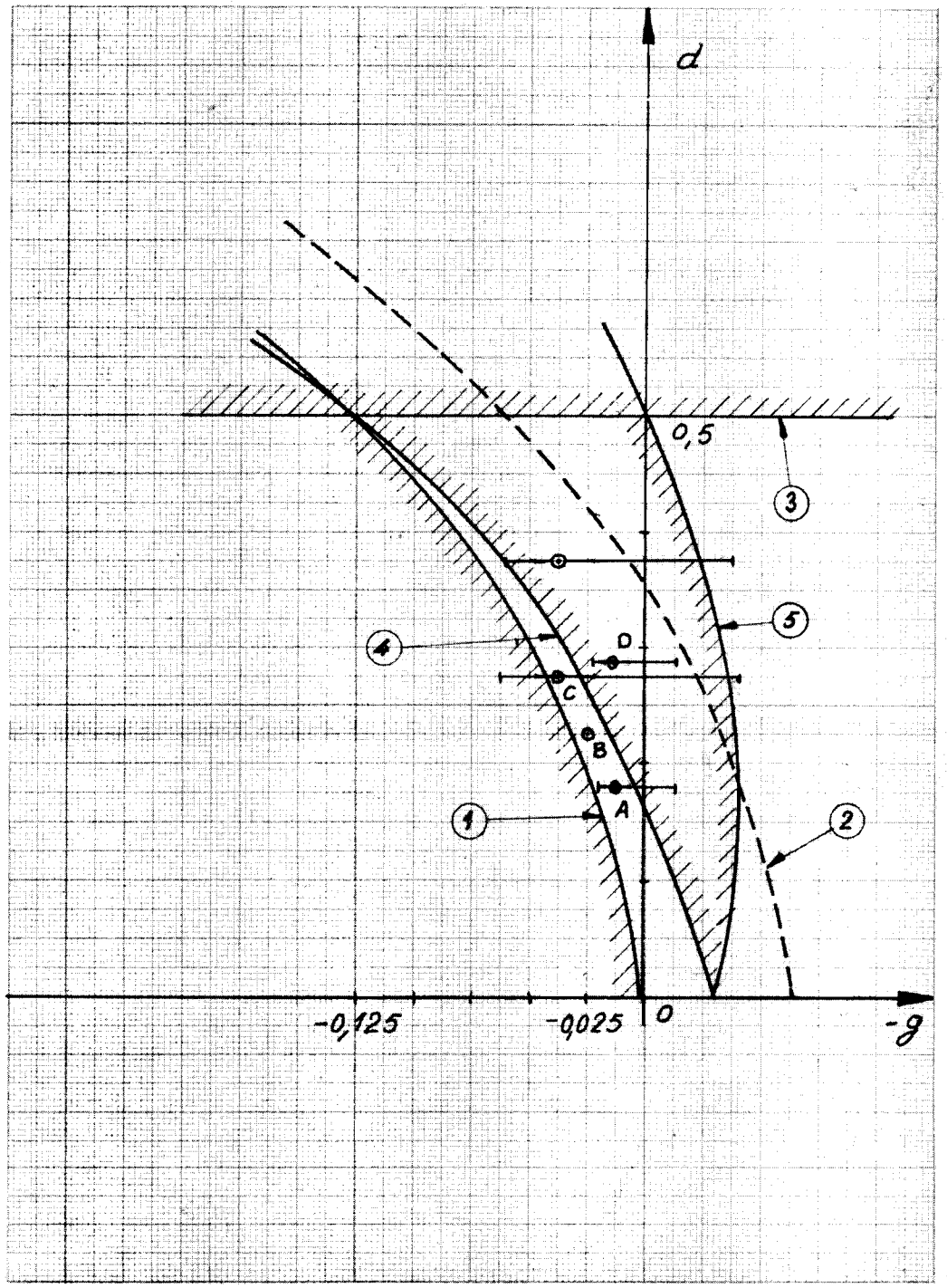

411 404-64

csf

STABILITY DIAGRAMM

Fig. 2

INT 2011

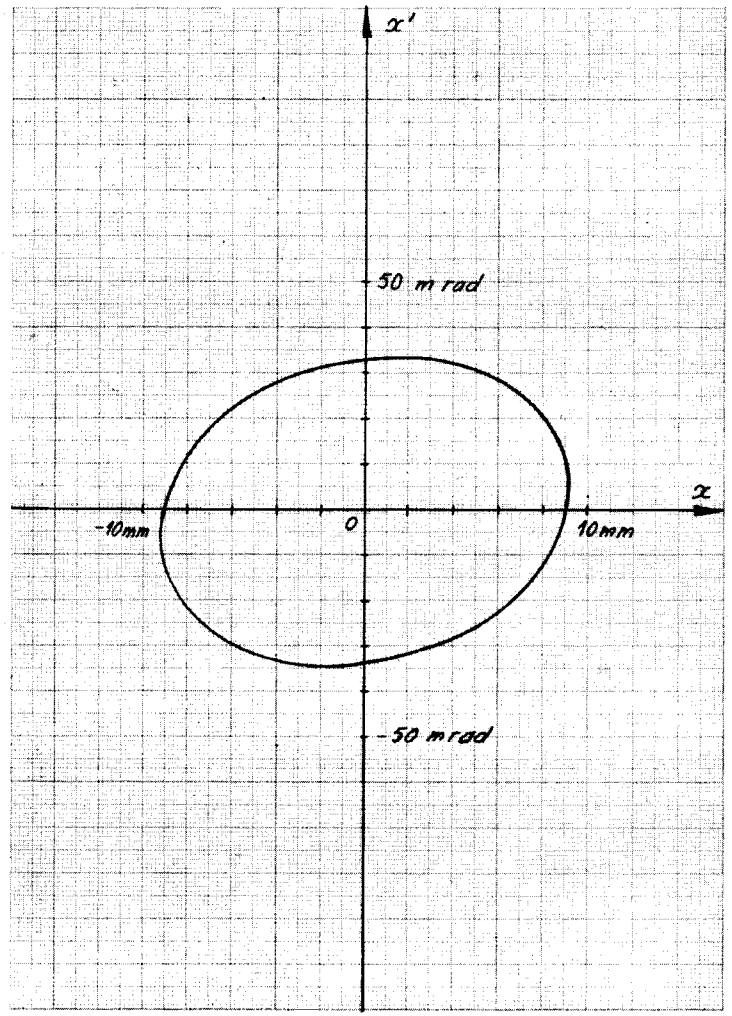

411 403-64

csf Point A
d = 0,1750 $\cos\mu_1$ = 0,32557 $a = \pi\, 350\, 10^{-6}$ rad m
g = 0,0125 $\cos\mu_2$ = −0,5767

Fig: 3

INT 2011

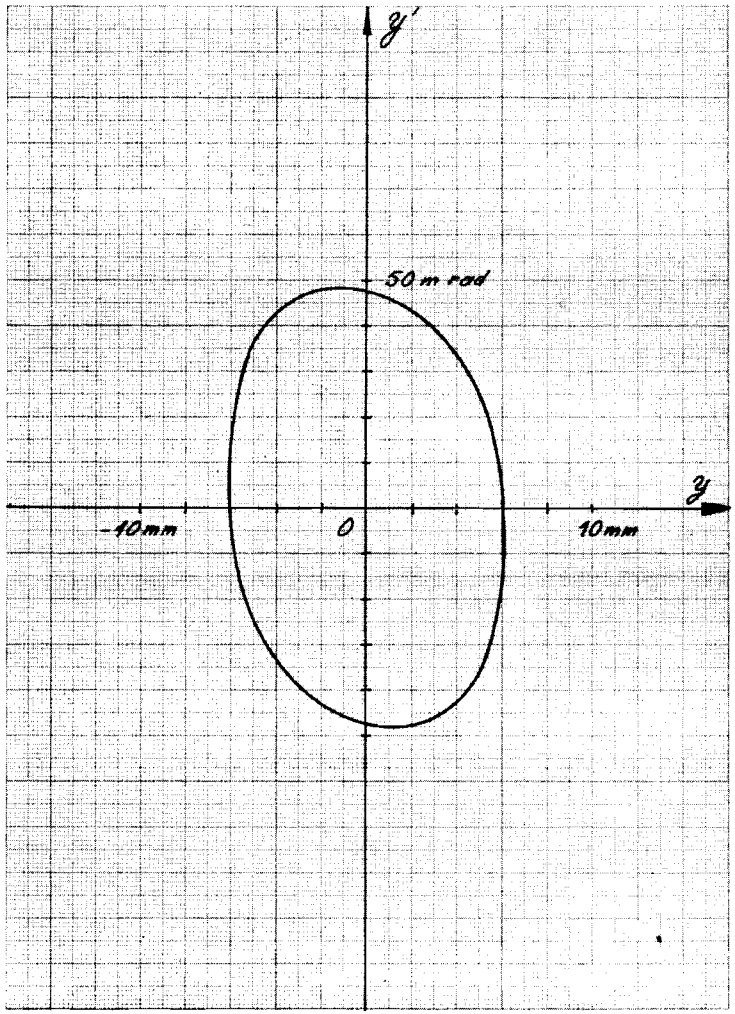

411 402-64

csf Point A d = 0,1750
g = 0,0125

Fig: 4

INT 2011

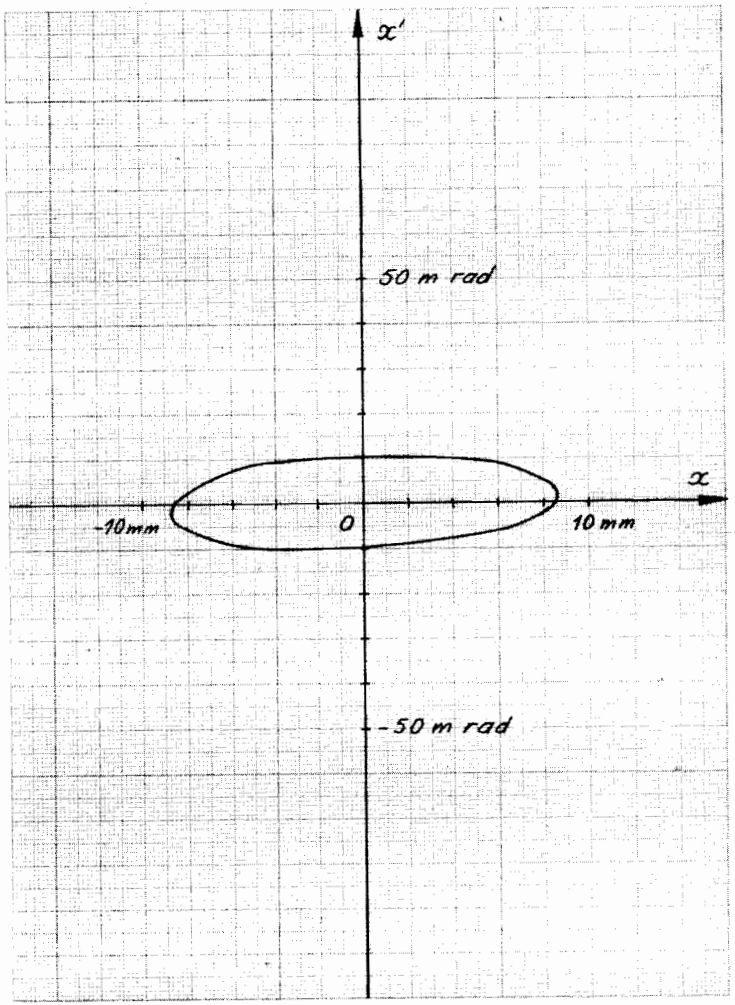

411 406-64

Point B
d=0,2250
g=0,0250

Demi trace
cos μ1 = -0,045754
cos μ2 = -0,37975
a=87π 10⁻⁶ rad m

Fig: 5

INT 2011

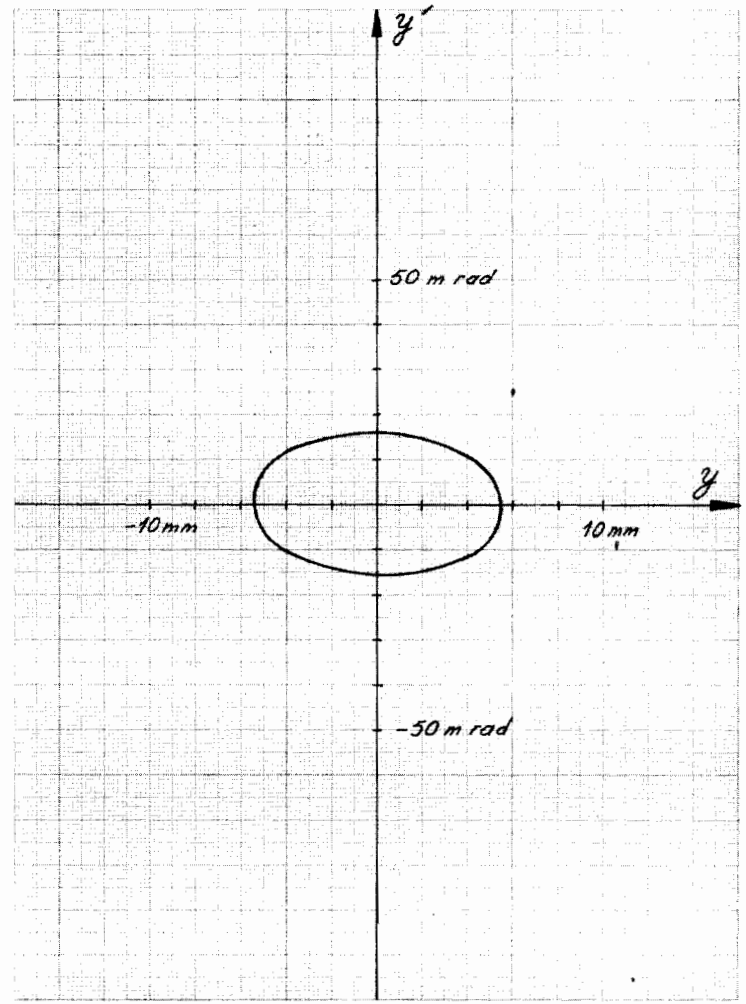

411 407-64

Point B

Fig: 6

INT 2011

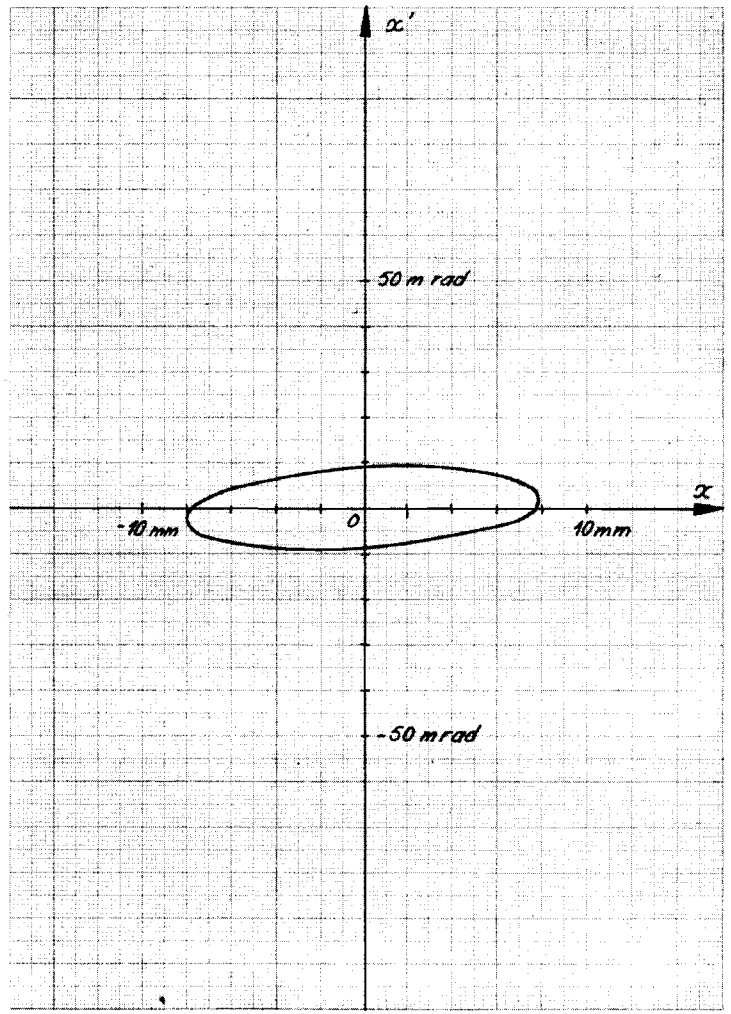

411 408-64

csf | Point C | Demi trace | Fig: 7
d = 0,2750 | cos μ1 = -0,13774 | a = 7,27 · 10⁻⁶ rad m
g = 0,0375 | cos μ2 = -0,51349

INT 2011

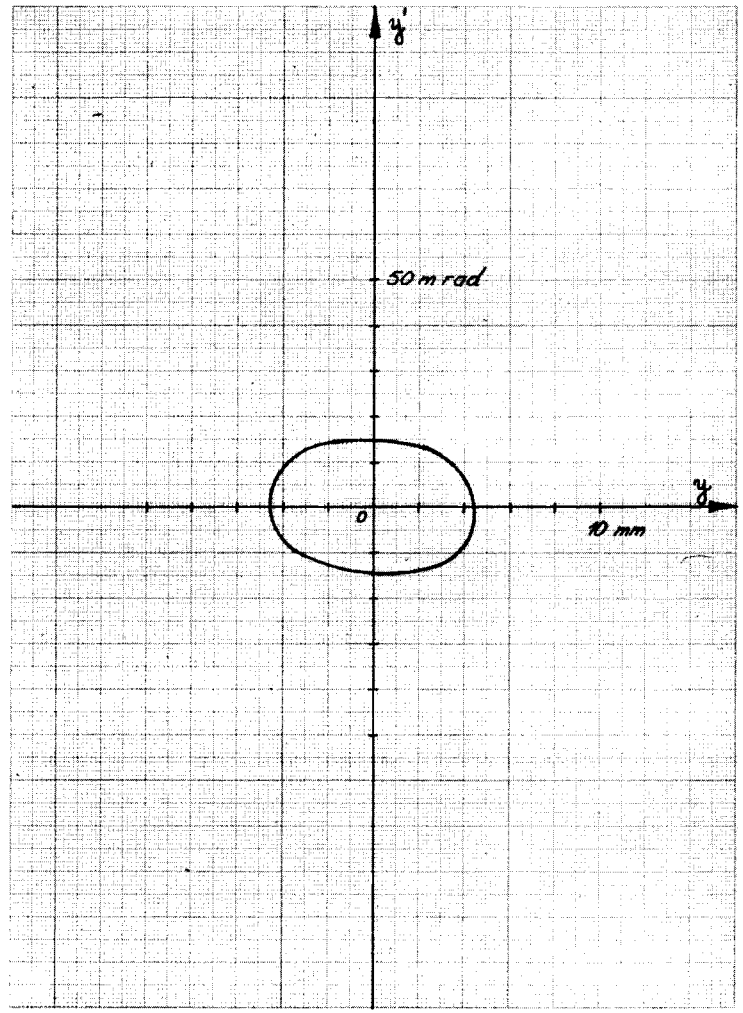

411 409-64

csf | Point C | Fig. 8

INT 2011

From (19), one obtains, for the classical case:

$$\cos \mu = 2\,(a^2 - b^2) - 1$$

$$\beta = \frac{2c\,(a+b)}{\sin \mu} = \frac{c\,(a+b)}{\sqrt{(a^2 - b^2)\left[1 - (a^2 - b^2)\right]}}$$

Since we have chosen that the mesh starts where β is maximum,

$$A_c = \frac{\pi a_o^2}{\beta \frac{L}{2}} = \frac{2\,\pi a_o^2 \sqrt{(a^2 - b^2)\left[1 - (a^2 - b^2)\right]}}{L\,c\,(a+b)}$$

In the table, we compare results obtained, by use of an IBM 7090 computer of Saclay, for a classical arrangement Ac, and the helicoidal arrangement A_H.

Table I(*)

Point A	Point B	Point C	Point D
Energie: 3, 5 MeV	Energie: 0, 9 MeV	Energie: 0, 750 MeV	Energie: 2 MeV
d = 0, 1750	d = 0, 2250	d = 0, 2750	d = 0, 2880
g = 0, 0125	g = 0, 0250	g = 0, 0375	g = 0, 0175
$A_c = 59\,\pi\,10^{-6}$ rad m	$A_c = 39,4\pi\,10^{-6}$ rad m	$A_c = 46,5\,\pi\,10^{-6}$ rad m	$A_c = 140\,\pi\,10^{-6}$ rad m
$A_H = 350\,\pi\,10^{-6}$ rad m	$A_H = 87\,\pi\,10^{-6}$ rad m	$A_H = 72\,\pi\,10^{-6}$ rad m	

(*). These results correspond to an electric field of 1, 75 MV/m, and a synchronous phase of - 30°.

To make a better comparison, we should evaluate, in both cases, the volume of the hyperellipsoid. In the classical case, where the x and y motions are uncoupled, it is equal to the product of the acceptances in the two principal planes (x , x') and (y, y'), whereas in the case of any orthogonal sections, this volume is the upper limit of the products of the acceptances for any two planes. This means that the acceptances listed in Table I are lower than the acceptance of the system.

Conclusion

It can be seen that the proposed system leads to an acceptance gain of 2, 4 for a quadrupole strength reduced by 1, 6. fig. 2.

If one were to operate at the same points of the diagram in the two cases, the acceptance gain would be 6 at point A, 2, 2 at point B and 1, 55 at point C. This could be expected since A, B and C are relatively closer to the stability limit in the classifical arrangement than in the helicoidal one.

The disadvantage of the proposed helicoidal system is the reduced stability region. To make a thorough evaluation, account should be taken of the phase oscillations. Fig. 2 shows a rough evaluation of the effect of these phase oscillations. It is smaller for higher energies.

BLEWETT: It seemed to me that this 45° rotation is just a step in the direction of a continuous rotation which could be solvable analytically. Have you looked at that?

GUILBAUD: We have looked; we have wondered about taking other angles and we were afraid of the complication of it, but there might be a continuous analytical formulation of the problem.

SYMON: Kerst has looked at something like this where you have a continuous twist in connection with the design of a probe for plasmas. One interesting thing, if you have continuous twist, is that you no longer have alternating gradient equations but you can transform to a twisting coordinate system and reduce the equations to equations with constant coefficients.

GUILBAUD: That's interesting; has that work been published?

SYMON: I don't think so as yet, but it probably will be.

WALKINSHAW: John Bell did a similar transformation many years ago. That was published. It had exactly the same equations.

TENG: When you compare the acceptances, are you comparing the acceptances for the classical case and this case at the same point?

GUILBAUD: Yes, at the entrance.

TENG: The point A, for instance, is rather close to the edge of the stability band for the classical case. I am wondering if you move the point A to the middle of the classical stability band, how will they compare?

LAPOSTOLLE: You cannot go into the middle of the classical band because here it is unstable.

TENG: It's unstable for this case but not for the classical case.

GUILBAUD: No, the acceptance was computed in both cases for the same point. But on Fig. 7 we can compare points A and D. D is in the middle of the classical case, and then for 2 MeV the acceptance was $140\ \pi\ 10^{-6}$ radian meters, and A for 3.5 MeV was 59 in the classical case. Now in our case, it was 350, so you see it is still better than D, but only by a factor of 2.2 but for weaker quadrupole strengths.

LAPOSTOLLE: Well, I might add something. I think that all these figures of acceptance are lower values in fact, since the product of any two normal cross sections is always lower than the hypervolume.

GLUCKSTERN: Is the classical case to which you compared a north-south north-south or a north-north south-south?

GUILBAUD: North-north south-south.

LAPOSTOLLE: Let me say that in principle, what you gain in acceptance, you may have to pay for by tighter tolerances.

APPLICATION OF CALCULATED FIELDS TO THE STUDY OF PARTICLE DYNAMICS

D. A. Swenson
Midwestern Universities Research Association

We have used a computer program by the name of PARMILA to study certain aspects of the phase and radial motion of particles in linear accelerators. Until recently, we have used expressions for the transit time factor and the radial impulse at the gap, which were derived from the simplest approximation of the field in the gap, that is, a field which is uniform across the geometrical length of the gap, and zero in the drift tube bore.

We have a great deal of information available to us on the actual distribution of fields in the entire linac cell in the form of output from our MESSYMESH program. It is possible to reduce these calculated field distributions to a few coefficients which reflect more precisely the effect of these fields on the particle motion.

I should say that this work was done primarily by Fred Mills and Don Young at a time when I was absent from the laboratory. More recently, I have gone over this work, and I have incorporated it into the PARMILA program.

Let $\vec{\mathcal{E}}(r, z, t)$ be the electric field vector at radius r, longitudinal position z, and time t. The fields through which the particles travel, that is the fields near the axis of the linac, can be expressed in terms of the axial component of the electric field on the axis, $\mathcal{E}_z(0, z, t)$. At this point we take the time dependence to be sinusoidal and we define $E_z(z)$ so that

$$\mathcal{E}_z(0, z, t) = E_z(z) \cos(\omega t + \phi) .$$

It is instructive to compare the actual field distribution $E_z(z)$ with the simple uniform distributions of field. Figures 1, 2, 3, and 4 facilitate this comparison for typical linac geometries at 50, 100, 150, and 200 MeV. Both curves in each figure are scaled so that

$$\frac{1}{L}\int_0^L E_z(z)\, dz \text{ is unity.}$$

Maxwell's equation, in gaussian units, for cylindrical coordinates in a charge-free space, with the further restriction that $B_r = B_z = E_\theta = 0$, yield the following set of nontrivial equations.

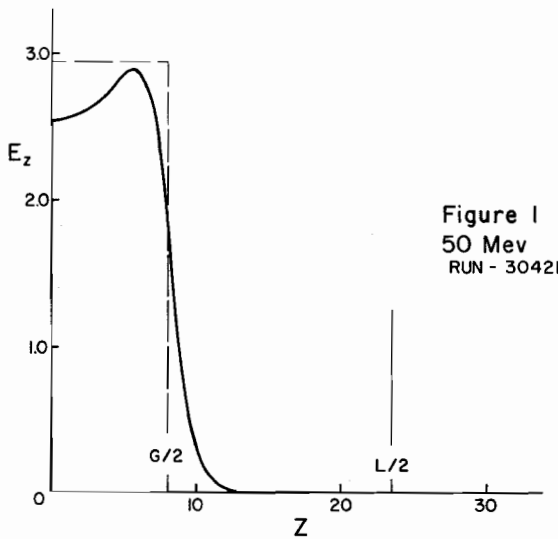

Figure 1
50 Mev
RUN - 30421

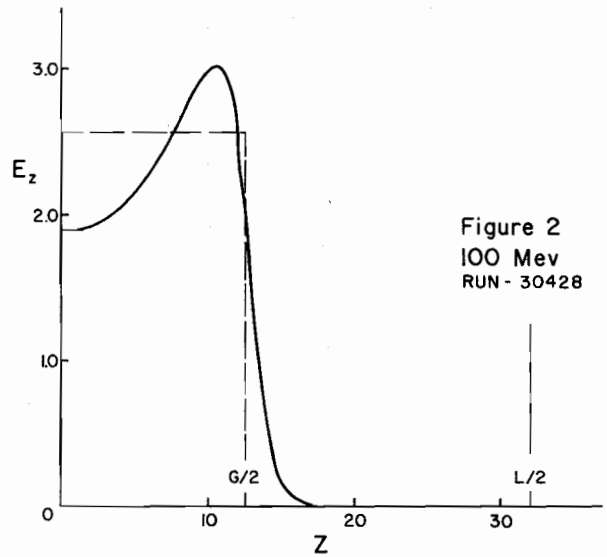

Figure 2
100 Mev
RUN - 30428

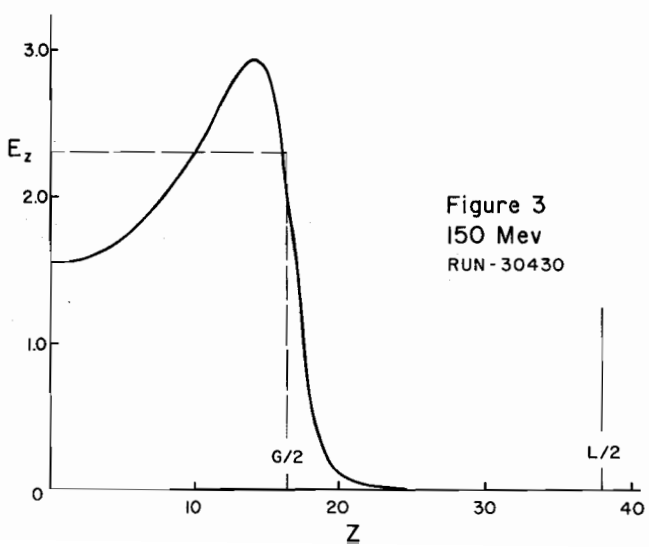

Figure 3
150 Mev
RUN - 30430

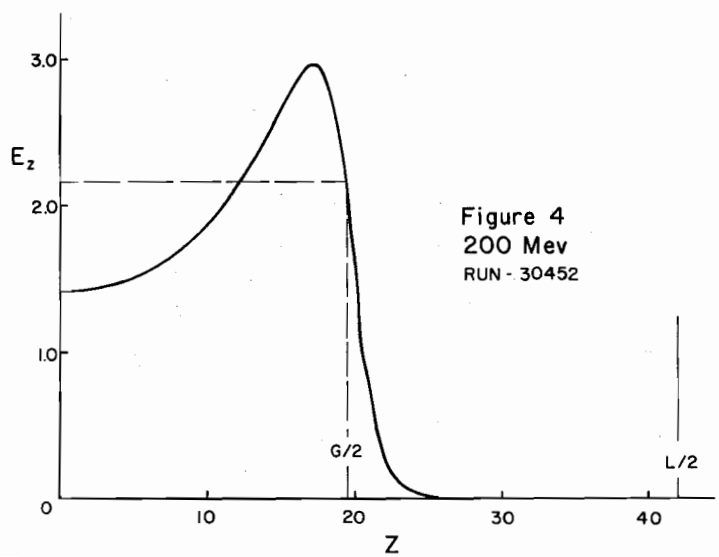

Figure 4
200 Mev
RUN - 30452

$$\frac{\partial E_r}{\partial z} - \frac{\partial E_z}{\partial r} = -\frac{1}{c}\frac{\partial B_\theta}{\partial t} \tag{1}$$

$$\frac{1}{r}\frac{\partial}{\partial r}(r\,E_r) + \frac{\partial E_z}{\partial z} = 0 \tag{2}$$

$$-\frac{\partial B_\theta}{\partial z} = \frac{1}{c}\frac{\partial E_r}{\partial t} \tag{3}$$

$$\frac{1}{r}\frac{\partial (r\,B_\theta)}{\partial r} = \frac{1}{c}\frac{\partial E_z}{\partial t} \quad . \tag{4}$$

We now assume that we know the fields on the axis of the linac [i.e., $\mathcal{E}_z\,(0, z, t)$] , and we attempt to get a satisfactory expression for the fields off the axis in terms of $\mathcal{E}_z\,(0, z, t)$. We employ an iterative procedure to get the nth order field in terms of the $n - 1^{st}$ order solution. This procedure yields the following expressions for $\mathcal{E}_z\,(r, z, t)$, $\mathcal{E}_r\,(r, z, t)$ and $B_\theta\,(r, z, t)$.

$$\mathcal{E}_z\,(r, z, t) = \mathcal{E}_z\,(0, z, t) - \frac{r^2}{4}\left(\frac{\partial^2\,\mathcal{E}_z\,(0, z, t)}{\partial z^2} - \frac{1}{c^2}\frac{\partial^2\,\mathcal{E}_z\,(0, z, t)}{\partial t^2}\right) \tag{5}$$

$$+ \text{ terms in } r^4 \text{ and higher}$$

$$\mathcal{E}_r\,(r, z, t) = -\frac{r}{2}\frac{\partial \mathcal{E}_z\,(0, z, t)}{\partial z} + \frac{r^3}{16}\frac{\partial}{\partial z}\left(\frac{\partial^2\,\mathcal{E}_z\,(0, z, t)}{\partial z^2} - \frac{1}{c^2}\frac{\partial^2\,\mathcal{E}_z\,(0, z, t)}{\partial t^2}\right) \tag{6}$$

$$+ \text{ terms in } r^5 \text{ and higher}$$

$$B_\theta\,(r, z, t) = \frac{r}{2\,c}\frac{\partial\,\mathcal{E}_z\,(0, z, t)}{\partial t} - \frac{r^3}{16\,c}\frac{\partial}{\partial t}\left(\frac{\partial^2\,\mathcal{E}_z\,(0, z, t)}{\partial z^2} - \frac{1}{c^2}\frac{\partial^2\,\mathcal{E}_z\,(0, z, t)}{\partial t^2}\right) \tag{7}$$

$$+ \text{ terms in } r^5 \text{ and higher .}$$

We now proceed to use these fields to evaluate the energy gain and the radial impulse imparted to a particle on traversing a particular linac cell.

The energy gain ΔE is

$$\Delta E = \int_{path} \vec{\mathcal{E}} \cdot \vec{ds} = \int_{path} (\mathcal{E}_z \, dz + \mathcal{E}_r \, dr)$$

which can be written, with the fields above, as

$$\Delta E = \mathcal{E}_z (0, z, t) \, dz - \frac{r^2}{4} \int \left(\frac{\partial^2 \mathcal{E}_z (0, z, t)}{\partial z^2} - \frac{1}{c^2} \frac{\partial^2 \mathcal{E}_z (0, z, t)}{\partial t^2} \right) dz - \int \frac{r}{2} \frac{\partial \mathcal{E}_z (0, z, t)}{\partial z} \, dr \, . \tag{8}$$

Before evaluating these integrals, we make a few definitions. We define the cavity length L and the average axial electric field E_o by

$$\int_{cell} dz = L$$

and

$$\int E_z (z) \, dz = E_o L \, .$$

We define the origin of z by requiring

$$\int E_z (z) \sin \frac{2 \pi z}{L} \, dz = 0 \, .$$

We define the transit time T by the relation

$$\int E_z (z) \cos \frac{2 \pi z}{L} \, dz = E_o L T$$

and we define an S factor by

$$\int z\, E_z\,(z) \sin \frac{2\,\pi\, z}{L}\, dz \;=\; E_o\, L^2\, S\,.$$

I will outline the evaluation of the first integral on the right-hand side of Eq. (8) to illuminate the meaning of the terms α and S.

$$\int \mathcal{E}_z\,(0, z, t)\, dz \;=\; \int E_z\,(z) \cos\,(\omega t + \phi)\, dz$$

where $t = \frac{z}{V}$. Let $\frac{1}{V} = \frac{1}{V_s}\,(1 + \alpha)$, where V_s is the velocity of the synchronous particle. Noting that $\omega t = \frac{2\,\pi\, z}{L}(1 + \alpha)$, we write

$$\int \mathcal{E}_z\,(0, z, t)\, dz \;=\; \int E_z\,(z) \cos\,(\frac{2\,\pi\, z}{L} + \phi + \frac{2\,\pi\, z\alpha}{L})\, dz$$

$$= \int E_z\,(z) \left[\cos\,(\frac{2\,\pi\, z}{L} + \phi) \cos \frac{2\,\pi\, z\alpha}{L} - \sin\,(\frac{2\,\pi\, z}{L} + \phi) \sin \frac{2\,\pi\, z\alpha}{L}\right] dz$$

$$= \int E_z\,(z) \Big[(\cos \frac{2\,\pi\, z}{L} \cos \phi - \sin \frac{2\,\pi\, z}{L} \sin \phi) -$$

$$- \frac{2\,\pi\, z\alpha}{L}\,(\sin \frac{2\,\pi\, z}{L} \cos \phi + \cos \frac{2\,\pi\, z}{L} \sin \phi)\Big]\, dz$$

where we have let $\cos \frac{2\,\pi\, z\alpha}{L} = 1$ and $\sin \frac{2\,\pi\, z\alpha}{L} = \frac{2\,\pi\, z\alpha}{L}$.

For a symmetric gap where $E_z\,(z)$ is an even function of z, two of the four terms in the latter expression integrate to zero, and we are left with

$$\int \mathcal{E}_z\,(0, z, t)\, dz \;=\; E_o\, L\,(T - 2\,\pi\,\alpha\, S) \cos \phi\,.$$

The factor $(T - 2\,\pi\,\alpha\, S)$ can be interpreted as a transit time factor for particles whose velocity is different from the synchronous velocity (i.e., for $\alpha \neq 0$).

When we evaluate the other two integrals on the right-hand side of Eq. (8), the expression for the energy gain for one linac cell is

$$\Delta E = E_o L \left\{ \left(1 + \frac{\pi^2 r^2}{\lambda^2 \beta^2 \gamma^2}\right) (T - 2\pi\alpha S) \cos\phi - \frac{r r' \pi}{\beta\lambda} T \sin\phi \right\}. \tag{9}$$

To evaluate the radial impulse imparted to the particle on crossing a gap, we write

$$\Delta p_r = \int_{path} |\vec{F}_r| \, dt = \int_{path} e \left(\mathcal{E}_r - \frac{V B_\theta}{c} \right) dt . \tag{10}$$

Using the expression for the fields given in Eqs. (6) and (7), and eliminating third and higher orders in the variable r, we find the expression for $\Delta r'$ to be

$$\Delta r' = - \frac{e\pi}{m_o c^2 \lambda} \frac{E_o L}{\beta^3 \gamma^3} r \sin\phi \, (T - 2\pi\alpha S) \tag{11}$$

where $\Delta r' = \dfrac{\Delta p_r}{m_o c \beta\gamma}$.

It is of interest now to compared the factor $T_a - 2\pi\alpha S_a$ with the transit time function for a uniform field distribution. The analytic expression for the transit time factor for uniform field distribution perturbed by a bore hole of radius "a",

$$T_u = \frac{\sin \frac{\pi G}{\beta\lambda}}{\frac{\pi G}{\beta\lambda}} \frac{I_o \left(\frac{2\pi r}{\gamma_s L} \right)}{I_o \left(\frac{2\pi a}{\gamma_s L} \right)} ,$$

can be expressed as

$$(T_u - 2\pi\alpha S_u) \, I_o \left(\frac{2\pi r}{\gamma_s L} \right) \tag{12}$$

where

$$T_u = \frac{\sin \frac{\pi G}{L}}{\frac{\pi G}{L}} \quad \frac{1}{I_o\left(\frac{2\pi a}{\gamma_s L}\right)}$$

and

$$S_u = \frac{1}{2\pi I_o\left(\frac{2\pi a}{\gamma_s L}\right)} \left(\frac{\sin \frac{\pi G}{L}}{\frac{\pi G}{L}} - \cos \frac{\pi G}{L} \right)$$

and α has the same meaning as above.

First of all, we note that the radial dependence of Eq. (12) is the same as that of the first term in Eq. (9). Secondly, it is of interest to compare the T_a and S_a obtained from the actual field distribution with the T_u and S_u derived from the uniform field distribution. A comparison is given in the Table I for some typical linac geometries ranging in energy from 2 to 200 MeV.

TABLE I

MESSYMESH Run Number	Energy (MeV)	L cm	G cm	A cm	T_a	S_a	T_u	S_u
25003	2.16	10	2.5	1	0.7354	0.0727	0.8198	0.0280
30243	18.21	29	10	1	0.7726	0.0663	0.8066	0.0546
30421	49.80	47	16	1.5	0.7775	0.0655	0.8126	0.0535
30428	97.73	64	25	1.5	0.7101	0.0839	0.7641	0.0682
30430	148.05	76	33	2	0.6262	0.1055	0.7139	0.0811
30452	195.41	84	39	2	0.5636	0.1183	0.6786	0.0902

From the Table I, one can see that the T_a is from 5 to 16% lower than T_u, and that S_a is 20 to 30% higher than S_u with exception of the 2 MeV results in which S_a is 150% higher than S_u. The actual field distributions, shown in Figs. 1 through 4, were obtained from the last four MESSYMESH runs presented in Table I.

I have made some exploratory runs to determine the transverse acceptance and the phase acceptance for an eight-tank 200 MeV linac. A brief description of the linac is given in Table II. It is described in more detail in MURA Technical Note 472 by Young and Austin. The results of

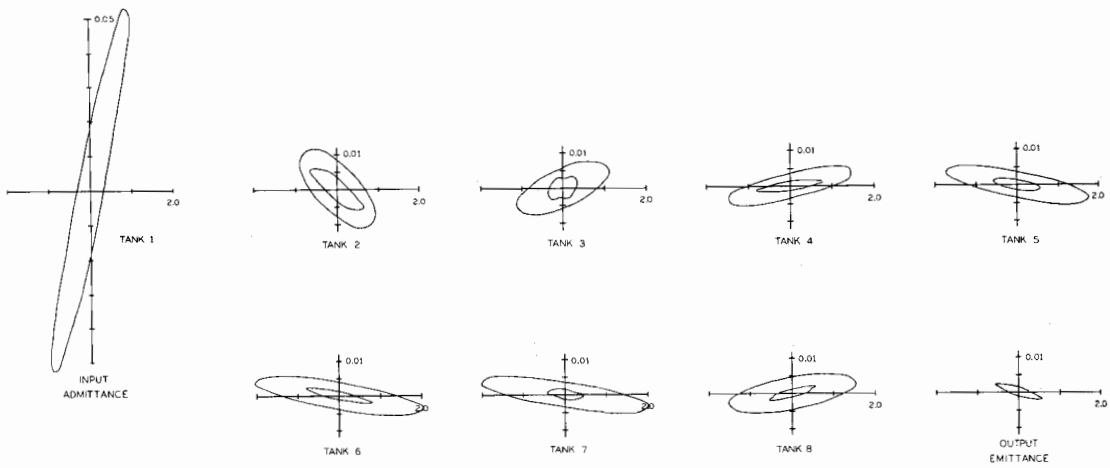

Figure 5 TRANSVERSE PHASE SPACE PLOTS

OUTER CURVE ADMITTANCE OF TANK N

INNER CURVE EMITTANCE OF LINAC THROUGH TANK N-1

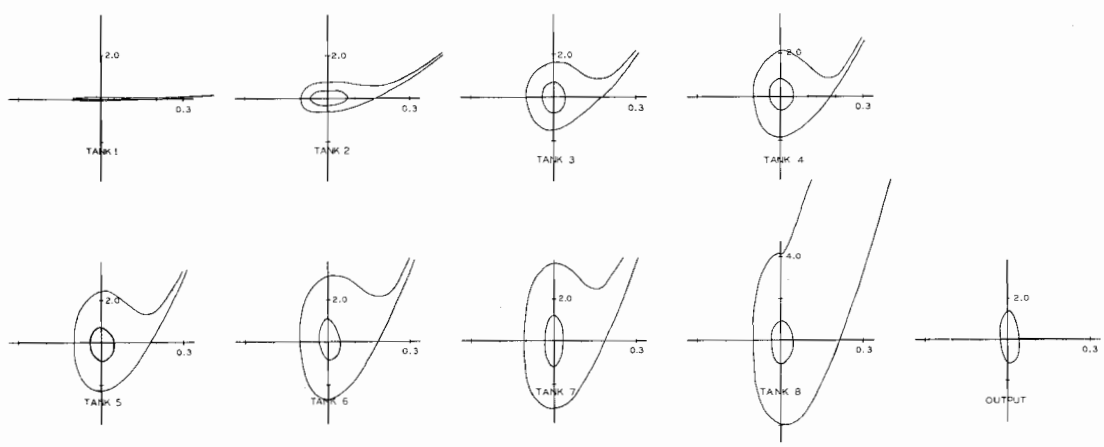

Figure 6 PHASE ACCEPTANCE PLOTS

OUTER CURVE ACCEPTANCE OF TANK N

INNER CURVE PHASE PLOT OF LINAC ACCEPTANCE TRANSFORMED THROUGH TANK N-1

these investigations, which I think are self-explanatory, are shown in Figs. 5, 6, 7, and 8.

TABLE II

Tank No.	1	2	3	4	5	6	7	8
Energy (MeV)	15	46	75	102	128	153	177	200
E_0 (MeV/m)	2.0	2.8	2.8	2.7	2.6	2.5	2.4	2.3
Length (m)	9.4	14.8	14.4	15.4	16.3	17.1	17.6	18.5
Power Actual (MW)	2.25	4.95	4.92	4.82	4.96	4.96	4.95	4.79
	Total Length			123.5 m				
	Total Power			36.6 MW				

WALKINSHAW: If you ignore the change in velocity of the particle across a gap and do the analysis as you have done, then you can show that the correct formula is E_0 L times that next term in the brackets I_0 of some factor of r, then the transit time factor and then cos ϕ . I don't understand where the term in α S comes in unless you are assuming that the particle velocity was changing as it crossed the gap.

SWENSON: The factor $(T - 2\pi\alpha S)$ is effectively a transit time factor for particles of energy E near the synchronous energy E_s. T is the transit time factor for the synchronous particle. The parameter α is defined in the text, but is a function of $(E - E_s)$. α is zero for $E = E_s$.

MILLS: Let me make some comments about this work. About four years ago when we became interested in linacs we began looking mostly for means for computational studies. Our starting point was the report by Panofsky published in 1953. You can see that these formulae are extensions of those in his report.

WALKINSHAW: There is in fact a paradox in some of his formulas.

MILLS: Your specific question about the second term can be answered the following way: In Panofsky's work, only the part of the fields that are traveling with the particle are included. This work includes all the other harmonics in the gap also. About two years ago, Phil Morton began his more complete treatment of the problem which many of you have seen.

WALKINSHAW: I think you will find that Panofsky now would accept that this formula is wrong.

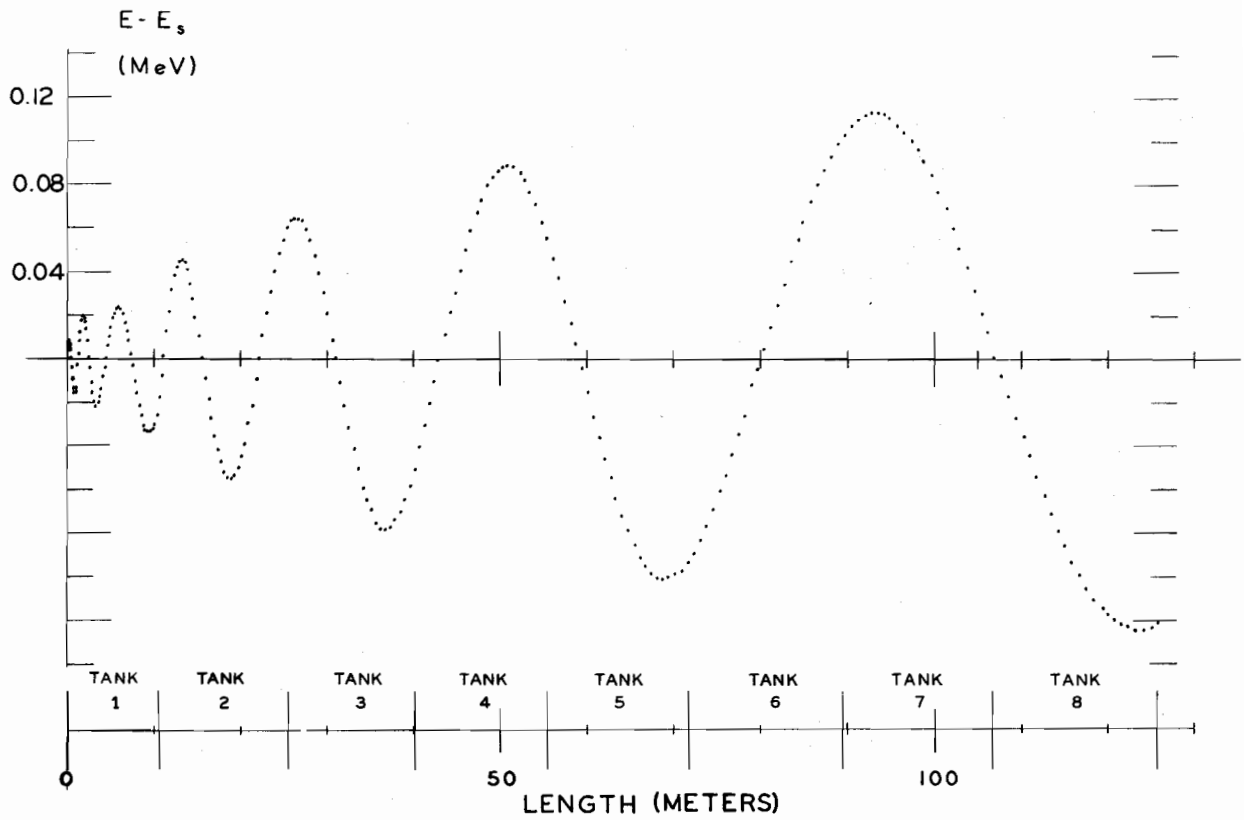

Figure 7 ENERGY OSCILLATION

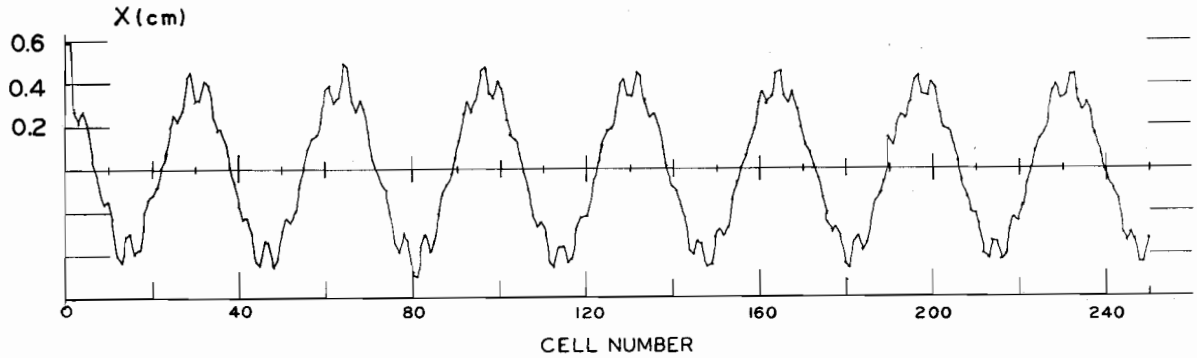

Figure 8 TRANSVERSE OSCILLATION

MILLS: I am not sure which one you mean.

WALKINSHAW: Well, I think that in calculating his transit time factor he put in a term which was dependent on the velocity. This is probably all right when you consider one gap, but when you change this into a differential equation, and consider the phase oscillations of the particle, you find that the phase damping is different from that in a harmonic traveling wave case. This is very curious because you are saying that the harmonic terms are causing some kind of extra phase damping. We wondered once if this was caused by some curious alternating gradient. Then we carried out the gap approximations, and discovered that there are indeed other second-order terms which cancel out the first one, and you come back to the simple approximation.

MILLS: The primary motivation here is the investigation of coupling between the axial and transverse motions. This is only intended to be an expansion in the next leading terms. There is another separate question which I think is related to what you said and that was the following: How adiabatic is the motion? This is a question which was investigated separately by Young and reported in 1961. Indeed the phase motion is not adiabatic in the low energy part of the linac.

WALKINSHAW: I think that the correct answer is the one that you get when you take the harmonic component only. We are quite sure of this. We spent a long time on this and corresponded with Panofsky. He agreed that there was this curious effect. It is quite complicated. What Panofsky was doing here was to integrate across one gap. You have to change this into the differential equation. If you do this by matrix techniques keeping in all higher order terms, including velocity variation, you find the modification to all the terms will cancel exactly the term you have on the board. The explanation that you are tempted to look for is that the higher harmonics, in some curious way, are causing some coherent effect on the linac. This is what started us off; we couldn't really see why this should be so. I think you will find that if you do this properly the harmonic term will in fact give you as accurate an answer as you want.

MILLS: I believe this is done properly in Morton's thesis. I did check to see the nature of the next order term and in fact when one totals up all the harmonics, just those present in this term are there.

OHNUMA: What kind of γ and β do you use? The γ and β are changing continuously across the gap.

SWENSON: We neglect the change of velocity across the gap and use for γ and β some sort of mean value.

OHNUMA: Another question. As I mentioned when I talked, this kind of effect or this kind of calculation might be important when energy is, say, below 50 MeV. But then I seriously doubt, aside from the academic question, in a practical design what the real importance of this kind of calculation would be. This is a point which is not completely clear, because there are all kinds of factors coming into the beam dynamics. Unless the effect is very serious, I do not see the particular importance in an exact point-by-point integration.

GLUCKSTERN: With regard to the point that Bill Walkinshaw made, I think there is another motivation for trying to include some velocity dependence in the formula. I agree with you in what you say in that, if the particle is trapped, then the only thing that can matter is the wave component which is traveling with the velocity of the particle. But an additional quantity of interest, if particles escape longitudinally, is the place where they strike the bore or the irises and cause radioactivity. To answer this question, I think one has to worry about the other wave components. If a particle escapes from a fish, if it is near the border, it will act as if it is stable for quite a way. And not until it gets far enough away so that all the waves average to zero can you take it as not having a change in energy.

WALKINSHAW: Well, I think if you truly analyze your performance, the higher order harmonics are traveling at such a vastly different phase velocity from the particle itself that the effect averages very quickly.

GLUCKSTERN: That is as long as the particle is traveling with the bunch.

WALKINSHAW: Oh, I see. You are saying you may trap them in some of the others.

GLUCKSTERN: No, I was referring to the fundamental wave component only, but for a particle traveling with almost the right velocity. When a particle escapes from a bucket, until it gets to a position where it does not oscillate very much, I think that the effects of the other waves will have to be taken into account.

WALKINSHAW: (Continuation of earlier discussion.) This paradox is a very interesting and amusing one really, because when we saw that the phase damping is different from the harmonic traveling wave case, we started to look for a physical explanation, and you can find one. The reason is this: if you look at the energy gained going across the gap, it will depend on the time it takes across the gap. Now if the particle is making phase oscillations, this means that it is taking different times during its phase oscillation. Part of the time it is going faster across

the gap, in which case it gains more energy, and then when it spins through half its oscillation, it gains less and you feel that you have some kind of integrated effect that could cause an increase in the rate of damping. Now that appears to be an explanation, but is the wrong explanation.

SYMON: I do not understand how two different approximations can give two different rates of damping because you can calculate the damping independently of any approximation just from the fact that the area on an energy time plot is rigorously constant independent of any approximations. That means that if the formula gives you a value which disagrees with that, it must be incorrect.

WALKINSHAW: I agree. That is where we started. We got two different rates of damping according to two approximations and then we tried to find out which one is correct and we decided it was the harmonic traveling wave approximation.

SYMON: But you can decide which one is correct by which one gives you the correct area in the end?

WALKINSHAW: Yes, quite so.

FEATHERSTONE: Regarding Dr. Ohnuma's question as to the value of this sort of calculation, I am sort of on the outside here, but looking at the figures over there, for ΔE, the difference between the flat and actual case amounts to more than 10%, which for the person who has to run these things means more than 20% in rf power. I think this is quite significant.

SWENSON: I believe Dr. Ohnuma questioned the significance of the velocity dependent term rather than the term which gives 10% effect which you mentioned. That really results from a better calculation of the transit time factor based on the actual fields in the gap.

BEAM DYNAMICS CALCULATIONS FOR ALVAREZ-TYPE LINEAR ACCELERATORS*

Marvin Rich
Los Alamos Scientific Laboratory, University of California
Los Alamos, New Mexico

I. Introduction

Detailed beam dynamics studies for Alvarez-type linear accelerators have generally been done on high speed computers using impulse-type approximations to simulate the particle acceleration within a gap or direct numerical integrations of the equations of motion. In this summary we would like to describe a procedure for studying such beam dynamics which retains most of the accuracy of the numerical integration without an excessive loss of computational speed as compared to the impulse approximation method. In addition, the results of some calculations for the proposed LASL meson factory will be presented.

Briefly, the procedure which has been used consists of assuming that the axial electric field within a gap between drift tubes is spatially constant and zero within the drift tubes. (A more general axial field could be used but with added complications.) This is as opposed to the more usual procedure of using the principal harmonic of the axial field within the gap. Using Maxwell's equations and the axial field form, the off-axis electric and magnetic fields can be obtained as a power series in the radial coordinate, r. This has been done through terms in r^3. In addition, one obtains radial and longitudinal impulsive terms which a particle will experience on entering or leaving a gap. Using the electromagnetic fields obtained in this way, an approximate solution to the relativistic equations of motion for a particle within a gap has been constructed. The impulses at the extremities of the gap are, of course, easily treated.

Comparisons of accelerator calculations using the approximate solutions mentioned above and an accurate numerical integration of the particle equations of motion have been made. Agreement to about four significant figures in energy and phase (absolute phase, not phase relative to the accelerator design particle) was found after passage of particles through 250 gaps. Similar comparisons using an impulse approximation treatment with the same accelerator design were noticeably poorer, particularly with respect to the final phase.

---

*Work performed under the auspices of the U. S. Atomic Energy Commission.

II. Method of Calculation

Only an outline of the computational procedure will be given. This may be divided into three parts:

(a) the form for the electromagnetic fields within a gap;
(b) the approximate solution of the particle equations of motion;
(c) the beam dynamics code.

A. The Gap Fields

For the purpose of the calculation it is assumed that the z-component of the electric field has the following spatial form on the axis, $r = 0$:

$$\begin{aligned} E_z(0,z) &= 0 && -L/2 \le z < -g/2 \\ &= E_0\, f(z) && -g/2 \le z \le g/2 \\ &= 0 && g/2 < z \le L/2 \end{aligned} \tag{1}$$

where L is the distance between drift tube centers as illustrated in Fig. 1 and g is the gap length. The field may be thought of as periodic with period L and its time dependence is taken as $\cos \omega t$.

Using the knowledge of the E_z field at $r = 0$ and Maxwell's equations, the off-axis fields in the gap may be obtained as a power series in r, the first few terms of which give

$$\left.\begin{aligned} E_z(r,z,t) &= E_0\, F(r,z) \cos \omega t \\ E_r(r,z,t) &= -E_0\, G(r,z) \cos \omega t \\ B_\theta(r,z,t) &= -E_0\, Q(r,z) \sin \omega t \end{aligned}\right\} \quad -g/2 \le z \le g/2 \tag{2}$$

where

$$\begin{aligned} F(r,z) &= f(z) + \frac{1}{4} r^2 S(z) \\ G(r,z) &= \frac{1}{2} r \left[\delta(z+g/2)\, f(z) - \delta(z-g/2)\, f(z) + \frac{df}{dz}\right] \\ &\quad + \frac{1}{16} r^3 \frac{dS(z)}{dz} \\ Q(r,z) &= \frac{1}{2} r \frac{\omega}{c^2} f(z) + \frac{1}{16} r^3 \frac{\omega}{c^2} S(z) \end{aligned} \tag{3}$$

and

$$S(z) = -\frac{\omega^2}{c^2} f(z) - \frac{d}{dz}\left[\delta(z + g/2)\, f(z) - \delta(z - g/2)\, f(z)\right] .$$

If the δ-functions are treated as slightly smeared δ-functions, representing the fall off of the fields within the drift tube hole, and it is assumed that a particle does not change its position or velocity appreciably over the fall-off region, then these terms merely contribute an impulse to a particle on entering and leaving a gap. The approximate effect of this impulse is given below in Eq. (7). Neglecting the impulse producing terms, the fields within a gap are

$$\left.\begin{aligned} E_z &= E_0\, f(z) \left[1 - \frac{1}{4}\frac{\omega^2}{c^2} r^2\right] \cos \omega t \\ E_r &= -E_0 \frac{df(z)}{dz}\left[\frac{1}{2} r - \frac{1}{16}\frac{\omega^2}{c^2} r^3\right] \cos \omega t \\ B_\theta &= -E_0 \frac{\omega}{c^2} f(z) \left[\frac{1}{2} r - \frac{1}{16}\frac{\omega^2}{c^2} r^3\right] \sin \omega t \end{aligned}\right\} \quad -g/2 < z < g/2 . \quad (4)$$

In the following, $f(z)$ has been taken equal to unity, giving $E_r = 0$ within the gap.

B. Approximate Solution of the Equations of Motion

In Cartesian coordinates, the relativistic equations of motion for a particle moving in an electromagnetic field of the sort given in Eq. (3) are

$$\left.\begin{aligned} \frac{du_1}{dt} &= \frac{e}{m}\left[E_r - v_3 B_\theta\right] \frac{x_1}{r} \\ \frac{du_2}{dr} &= \frac{e}{m}\left[E_r - v_3 B_\theta\right] \frac{x_2}{r} \\ \frac{du_3}{dt} &= \frac{e}{m}\left[E_z + (v_1 x_1 + v_2 x_2) B_\theta / r\right] \end{aligned}\right\} \quad (5)$$

$$\frac{dx_i}{dt} = u_i/\gamma = v_i \qquad i = 1, 2, 3 \quad (6)$$

where indices 1, 2, and 3 correspond to the x, y, and z directions, respectively, $r = \sqrt{x_1^2 + x_2^2}$, and $\gamma = \sqrt{1 + \vec{u}^2/c^2}$. From Eqs. (2), (3), and (5) it can be shown that the change in u_i due to the impulse occurring on entering a gap is approximately

$$\Delta u_1 = -\frac{e}{m} E_0 f(-g/2)\, x_1 \left(\frac{1}{2} - \frac{1}{16}\frac{\omega^2}{u_3^2} r^2\right)\frac{\gamma}{u_3} \cos \omega t$$

$$\Delta u_2 = -\frac{e}{m} E_0 f(-g/2)\, x_2 \left(\frac{1}{2} - \frac{1}{16}\frac{\omega^2}{u_3^2} r^2\right)\frac{\gamma}{u_3} \cos \omega t \qquad (7)$$

$$\Delta u_3 = -\frac{e}{m} E_0 f(-g/2)\frac{\gamma}{u_3}\left(\frac{1}{4} r^2 \omega \gamma / u_3 \sin \omega t + \frac{1}{16}\frac{\omega^2}{c^2} r^2 \frac{u_1 x_1 + u_2 x_2}{u_3} \cos \omega t\right)$$

where the coordinates, u components, and time are those corresponding to the arrival at the gap. Similar equations with opposite signs apply on leaving the gap.

A relatively accurate approximate solution of the equations of motion across the gap can be obtained by assuming that the components of velocity may be written in the form

$$v_i(t) = v_0^{(i)} + v_1^{(i)} t + f^{(i)}\left[\cos(\omega t + \psi_0) - \cos \psi_0\right] + g^{(i)}\left[\sin(\omega t + \psi_0) - \sin \psi_0\right] \qquad (8)$$

where ψ_0 is the phase of the cavity field when the particle enters the gap and the z-coordinate and time at the beginning of the gap are taken as $z = 0$ and $t = 0$. Equation (8) is actually part of a more general ansatz that can be made for the velocity. The coordinates are then approximately

$$x_i(t) = x_0^{(i)} + \left[v_0^{(i)} - f^{(i)} \cos \psi_0 - g^{(i)} \sin \psi_0\right] t + \frac{1}{\omega} f^{(i)}\left[\sin(\omega t + \psi_0) - \sin \psi_0\right] - \frac{1}{\omega} g^{(i)}\left[\cos(\omega t + \psi_0) - \cos \psi_0\right]. \qquad (9)$$

If the coordinates and velocities given in Eqs. (8) and (9) are inserted into Eq. (5) for the u_i, using the previously described fields with $f(z) = 1$, the u_i can be obtained upon integration. These values of u_i and the relation $v_i = u_i/\sqrt{1 + \vec{u}^2/c^2}$ may then be used to identify the coefficients $v_1^{(i)}$, $f^{(i)}$, and $g^{(i)}$. When small terms are neglected, one obtains

$$
\begin{aligned}
v_1^{(i)} &= \left[u_1^{(i)} - v_0^{(i)}\, \vec{v}_0 \cdot \vec{u}_1/c^2\right]/\gamma_0 \qquad i = 1, 2, 3 \\
f^{(1,2)} &= a^{(1,2)}/\gamma_0 \\
f^{(3)} &= -v_0^{(3)}\, \vec{v}_0 \cdot \vec{a}/(\gamma_0\, c^2) \\
g^{(1,2)} &= -v_0^{(1,2)}\, \vec{v}_0 \cdot \vec{b}/(\gamma_0\, c^2) \\
g^{(3)} &= b^{(3)}/\gamma_0 - v_0^{(3)}\, \vec{v}_0 \cdot \vec{b}/(\gamma_0\, c^2)
\end{aligned}
\tag{10}
$$

where

$$\gamma_0 = 1/\sqrt{1 - \vec{v}_0^{\,2}/c^2} \quad , \quad \text{and}$$

$$
\begin{aligned}
u_1^{(i)} &= -\frac{e}{m} E_0 \frac{\cos \omega_0}{c^2} \left\{\left(\frac{1}{2} - \frac{1}{16}\frac{\omega^2}{c^2} r^2\right) v_0^{(i)} - \frac{1}{8} v_0^{(3)} x_0^{(i)} \frac{\omega^2}{c^2} \sum_{k=1}^{2} x_0^{(k)} v_0^{(k)}\right\} \\
a^{(i)} &= -\frac{e}{m} E_0 \frac{v_0^{(2)}}{c^2} x_0^{(i)} \left(\frac{1}{2} - \frac{1}{16}\frac{\omega^2}{c^2} r_0^2\right) \qquad i = 1, 2 \\
b^{(i)} &= \frac{e}{m} E_0 \frac{v_0^{(3)}}{\omega c^2} v_0^{(i)} \left(\frac{1}{2} - \frac{1}{16}\frac{\omega^2}{c^2} r_0^2\right) \\
u_1^{(3)} &= -\frac{e}{m} E_0 \frac{\sin \psi_0}{c^2} \left\{\frac{\omega}{2} \sum_{k=1}^{2} x_0^{(k)} v_0^{(k)} - \left(\frac{1}{2} - \frac{1}{16}\frac{\omega^2}{c^2} r_0^2\right) \sum_{k=1}^{2} v_0^{(k)2}\right\} \\
a^{(3)} &= 0 \\
b^{(3)} &= \frac{e}{m} E_0 \frac{1}{\omega} \left(1 - \frac{1}{4}\frac{\omega^2}{c^2} r_0^2\right) .
\end{aligned}
\tag{11}
$$

In the limit of pure phase motion one has

$$
\begin{aligned}
u_3 &= u_0^{(3)} + \frac{e}{m} E_0 \frac{1}{\omega}\left[\sin(\omega t + \psi_0) - \sin \psi_0\right] \\
v_3 &= v_0^{(3)} + \frac{e}{m} E_0 \frac{1}{\omega \gamma_0^3}\left[\sin(\omega t + \psi_0) - \sin \psi_0\right] \\
x_3 &= x_0^{(3)} + \left[v_0^{(3)} - \frac{e}{m} E_0 \frac{1}{\omega \gamma_0^3} \sin \psi_0\right] t - \frac{e}{m} E_0 \frac{1}{\omega^2 \gamma_0^3}\left[\cos(\omega t + \psi_0) - \cos \psi_0\right] .
\end{aligned}
\tag{12}
$$

C. The Beam Dynamics Code

The beam dynamics code which has been written using the above results is essentially the same as most such codes. However, the method for specification of the accelerator geometry is perhaps somewhat different from what is usual and should be described. Here, input values of stable phases and the g/L sequences for each tank are used to define an entering and an exiting phase of the "stable particle" in any gap, say gap n, by

$$\psi_{in}(n) = \psi_{stable} - \pi(g/L)_n$$

$$\psi_{out}(n) = \psi_{stable} + \pi(g/L)_n \ .$$

Starting at the end of the $(n-1)^{th}$ gap with longitudinal velocity v_{n-1}, the length of the $(n-1)^{th}$ drift tube is taken as

$$d_{n-1} = (\psi_{in}(n) - \psi_{out}(n-1) + 2\pi) \cdot v_{n-1}/\omega \ .$$

The length of the nth gap and the velocity v_n at the end of this gap are obtained from Eq. (12), where the time to be used is $t = (\psi_{in}(n) - \psi_{out}(n))/\omega$ since the field was assumed to have phase $\psi_{in}(n)$ when the particle entered the gap and phase $\psi_{out}(n)$ when it left. If ϵ_0 is the energy gain per meter in the tank containing gap n, the constant E_0 appearing in Eq. (12) is

$$E_0(n) = 2\pi\epsilon_0 / \left[\sin\psi_{out}(n) - \sin\psi_{in}(n)\right] .$$

When the geometry of the accelerator has been determined, particles with varying initial energy, phase, and off-axis position and velocity can be carried through the structure using Eqs. (8) through (11). The time required to cross a gap is first obtained by iterating the $z \equiv x_3$-coordinate equation in the form

$$t_{k+1} = \left\{ g + \frac{f^{(3)}}{\omega}\left[\sin(\omega t_k + \psi_0) - \sin\psi_0\right] - \frac{g^{(3)}}{\omega}\left[\cos(\omega t_k + \psi_0) - \cos\psi_0\right]\right\} \times \left[v_0^{(3)} - f^{(3)}\cos\psi_0 - g^{(3)}\sin\psi_0\right]^{-1}$$

using an initial guess of $t_0 = (\psi_{in} - \psi_{out})/\omega$. It has been found that two to three iterations are required for four-digit convergence. With this time interval, the remaining particle parameters are found by substitution into the remaining equations. Transit through quadrupole

magnets in drift tube sections is accomplished by the standard linear approximation.

The code also contains provisions for studying random errors in tank phase, tank or gap field amplitudes, drift tube and quadrupole misalignment, and quadrupole field magnitude.

III. Some Preliminary Results

Very little has been done as yet with regard to radial motion studies using the code described above. However, fairly extensive phase motion calculations have been made on a number of accelerator designs. In these, phase-energy acceptance "fishes" have been obtained with and without various types and combinations of random alignment and field errors, and output phase and energy spreads have been examined. A few examples of these results are given below for a geometry corresponding to the present design of the LASL meson factory. A definite statement about the effect of random errors will not be made since error studies for this geometry with many different sets of random inputs have not been completed.

Figure 2 shows a comparison of the phase and energy oscillations for a sample particle, using a numerical integration of the equations of motion (upper graph) and using Eqs. (12) (lower graph). The oscillatory solid lines give the phase motion and the dotted lines the energy deviations with respect to the stable particle. In Fig. 3 the acceptance fish for the design in Table I is shown (solid line) along with that when a particular set of random errors, specified in Table II, are introduced (dashed line). The effects of certain type errors, as tank-to-tank phase or field amplitude errors, have been found to have a more drastic effect on the acceptance region than when they are present as gap-to-gap errors. The remaining figures show the maximum phase and energy oscillation amplitudes of particles leaving the machine as a function of input phase and energy with and without the errors of Table II.

TABLE I

Specifications of the Drift Tube Portion of the LASL Linear Accelerator

Tank Number	1	2	3	4	5
Initial Energy	0.75	10.75	60.35	102.0	141.5
Final Energy	10.75	60.35	102.0	141.5	176.5
Stable Phase	-26°	-26°	-26°	-26°	-26°
Energy gain/meter (MeV/m)	1.11	1.65	1.42	1.28	1.16
g/L Range	.2-.3	.19-.33	.35-.42	.40-.44	.43-.46
Drift Space (meters)	0.305	0.610	0.610	0.610	

TABLE II

Maximum Field and Alignment Errors for the Sample Problem	
Axial Drift Tube Displacement Error	$\pm$ 0.001 m
Field Error for Drift Tube Gaps	$\pm$ 2%
Tank Field Error	$\pm$ 2%
Tank Phase Error	$\pm 1^{\circ}$

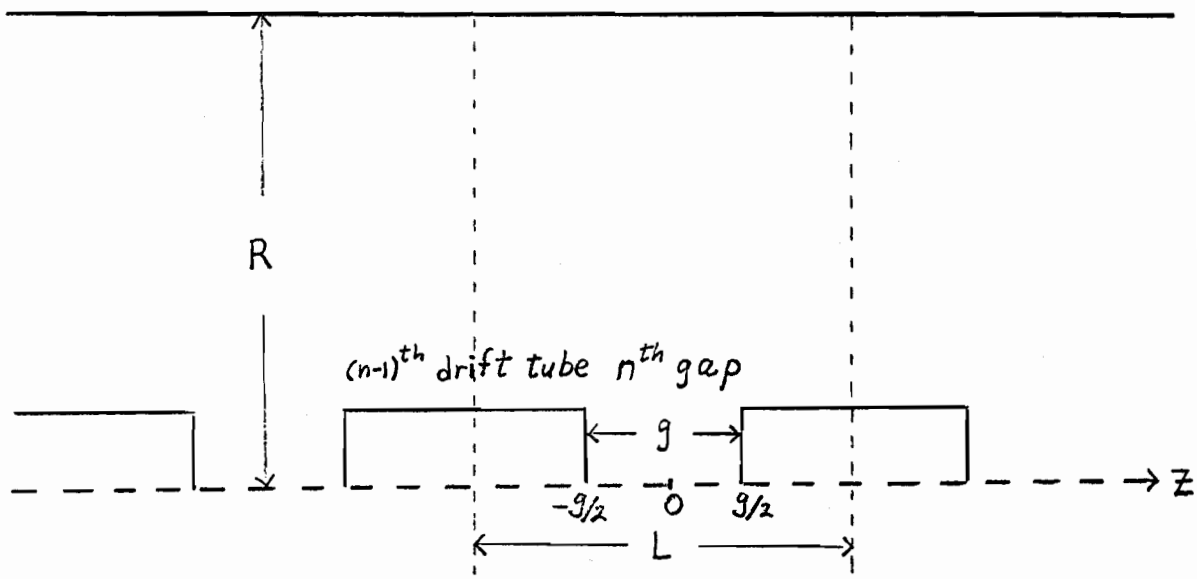

Figure 1: Schematic diagram of a drift tube section

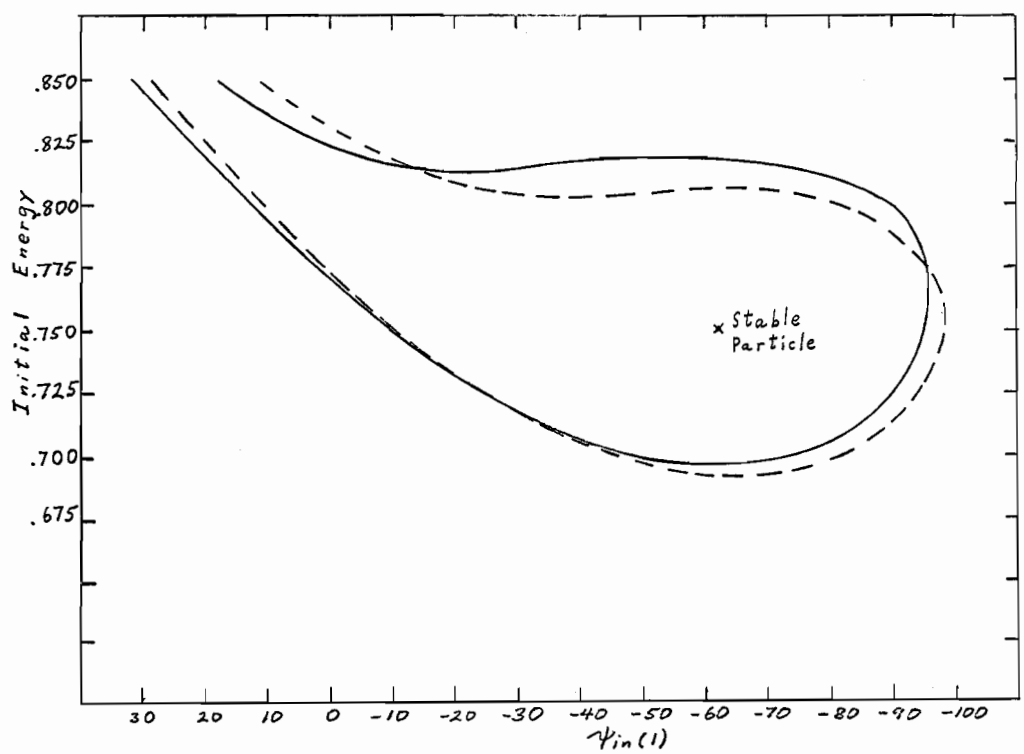

Figure 3: Phase-energy acceptance region for the accelerator geometry specified by Table I. The solid curve shows the acceptance when no errors are present and the dashed curve gives the acceptance for the errors of Table II.

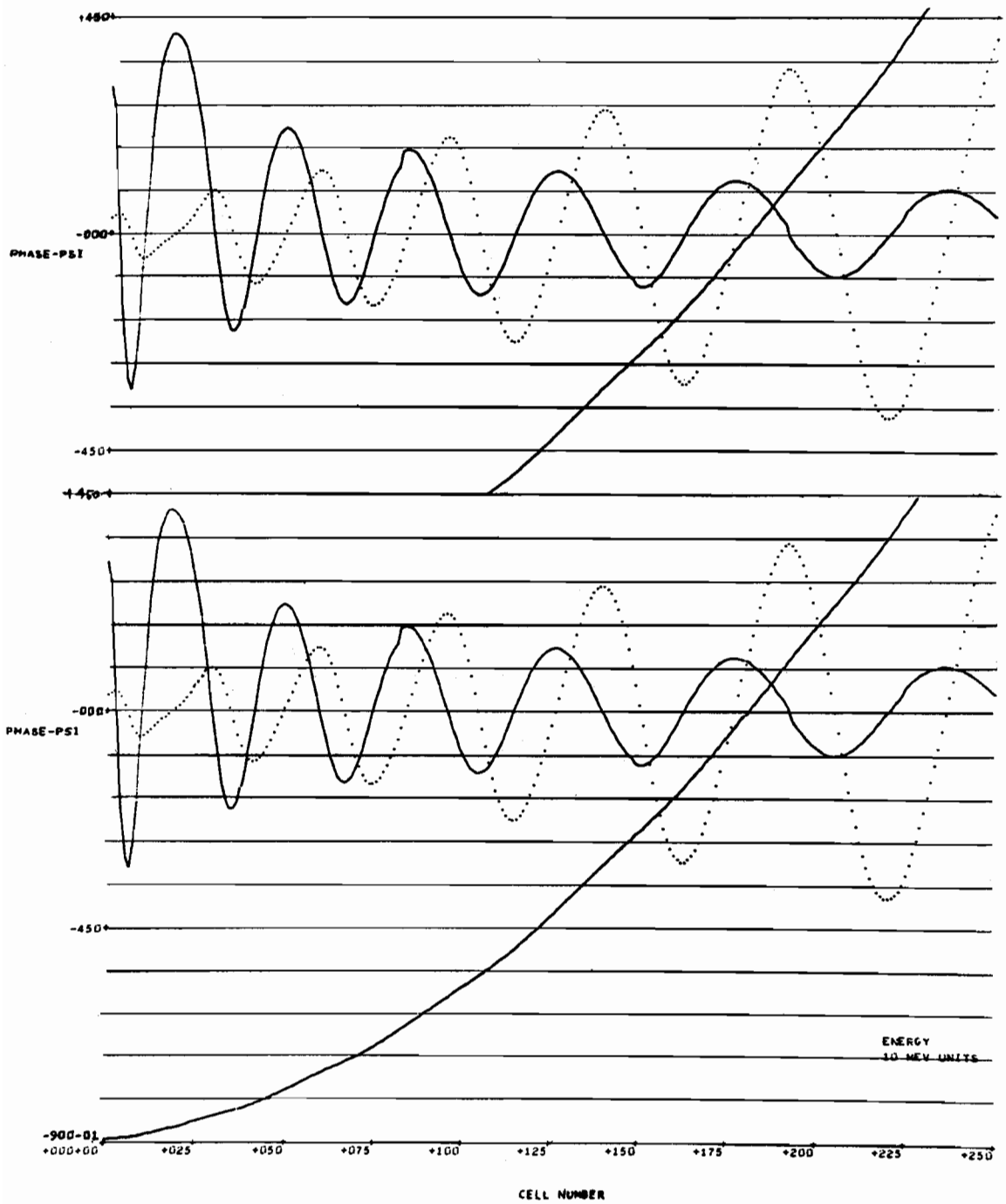

Figure 2: Comparison of phase and energy oscillations for a sample particle using a numerical integration of the particle equation of motion and using Equations (12).

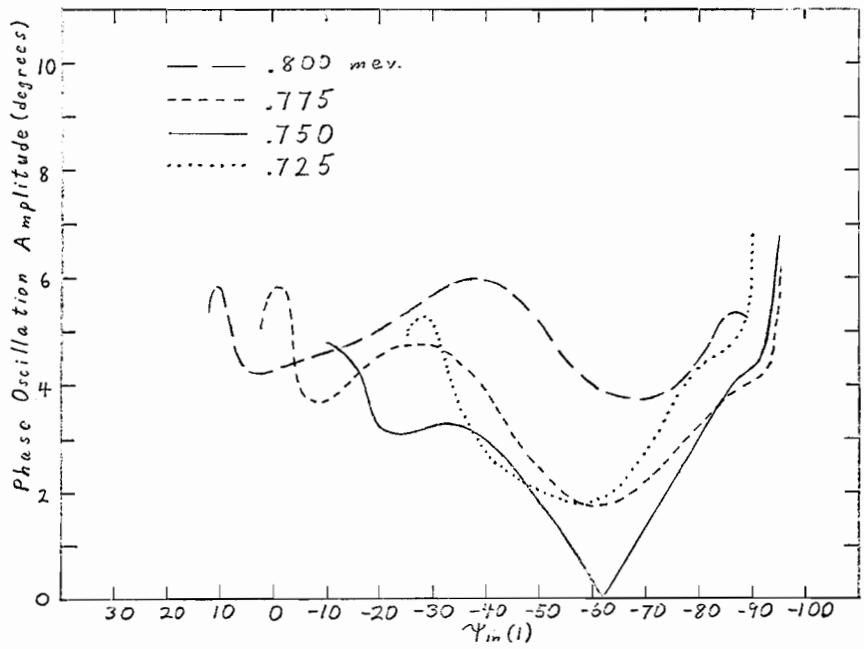

Figure 4: Final phase oscillation amplitude as a function of initial phase, $\psi_{in}(1)$, for various initial energies no errors are present.

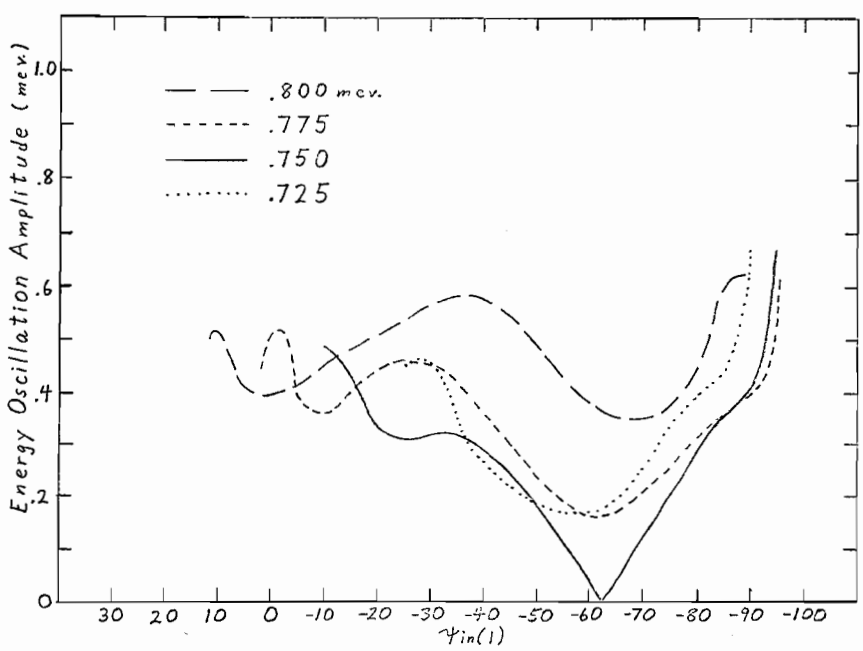

Figure 5: Final energy oscillation amplitude as a function of initial phase, $\psi_{in}(1)$, for various initial energies when no errors are present.

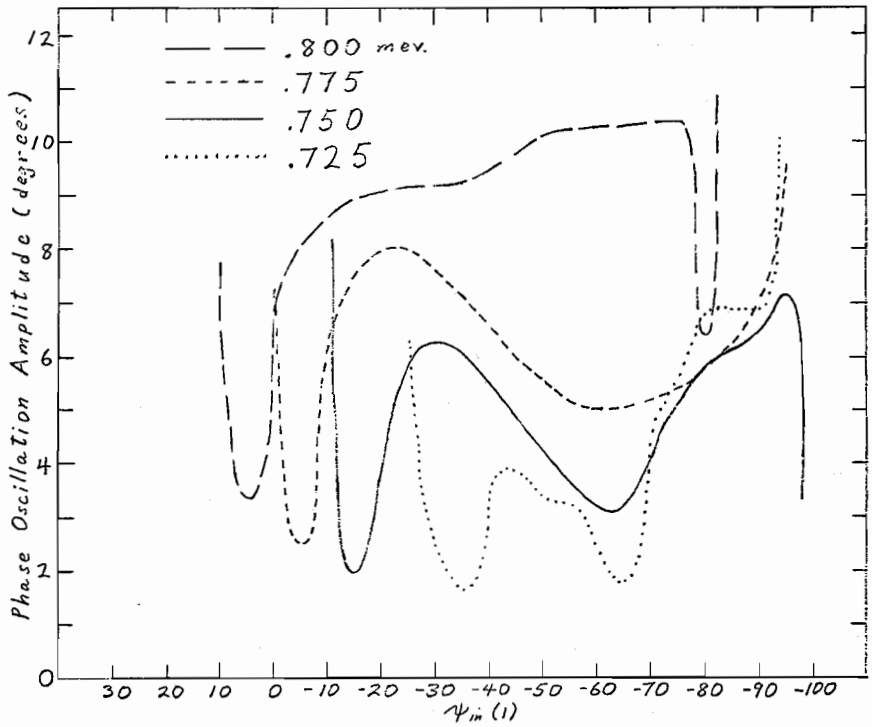

Figure 6: Final phase oscillation amplitude as a function of initial phase, $\psi_{in}(1)$, for various initial energies when the errors of Table II are present.

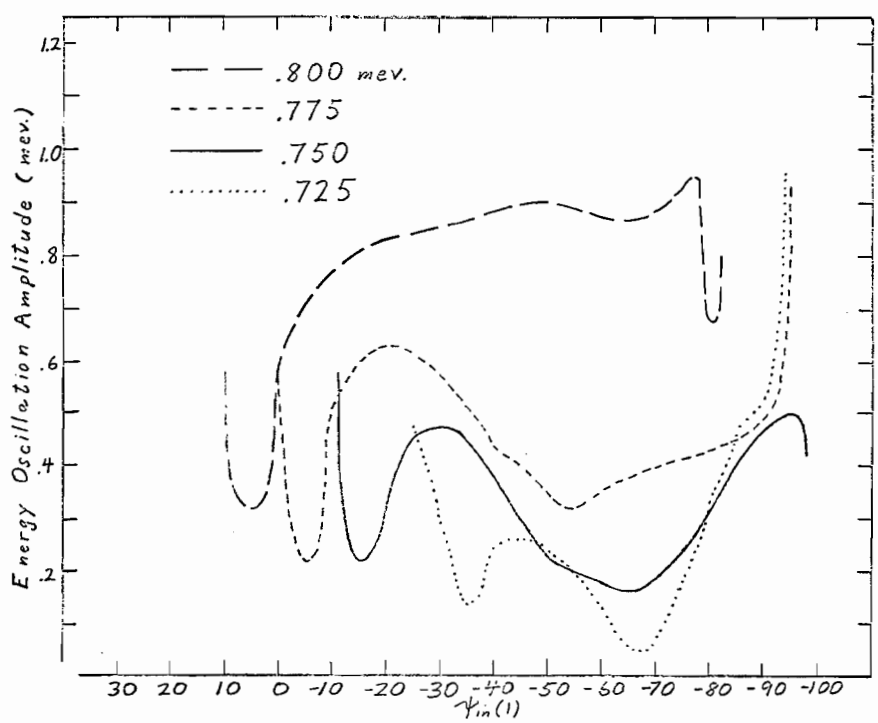

Figure 7: Final energy oscillation amplitude as a function of initial phase, $\psi_{in}(1)$, for various initial energies when the errors of Table II are present.

PERFORMANCE OF THE PS LINAC

C. S. Taylor
CERN

I. INTRODUCTION

With the exception of a recent increase of peak current to 75 mA the machine's characteristics remain much as reported at Dubna.[1] It has, however, revealed an appetite for deuterons.[2]

In these notes we shall mention briefly the minor changes which have taken place, describe some of the developments in the duoplasmatron and short column studies and in instrumentation, and conclude with some of the practical aspects of operation.

II. PREINJECTOR

1. RF Ion Source

Reductions in the height of the cathode protection brought increases in the source output current, with more than 300 mA observed in the laboratory. Further reductions however produced instability. A normal working current is 220 mA.

A miniature Faraday cup was used to scan the beam 30 mm from the source outlet and indicated a roughly triangular current density distribution.

2. Focusing and Beam Transport

The maximum current observed till now at the earth end of the column was 220 mA, but only 140 mA reached the input of the first tank.

The emittance "blow-up" factor of 2 to 3 in the lens and column is largely responsible for this loss, and is believed to be due in part to a time dependence. Recently we rearranged the column electrodes for greater acceleration at the source end with the object of reducing the lens strength required and hence of increasing the minimum particle velocity in the lens. This only reduced the 500 keV emittance by 10% for the same current.

It is believed that aperture limitation in the first triplet also contributes to the beam loss, and so the triplet diameter will shortly be in-

creased from 40 to 50 mm. The increase in peak current to 75 mA followed the widening of the second triplet aperture from 40 to 50 mm and the buncher aperture from 30 to 40 mm.

3. High Tension

New control circuits were installed towards the end of last year to permit:

(i) Automatic formation of the column, 0-500 kV in 3 hours, advisable after extended work on the column at atmospheric pressure.

(ii) Manual formation to 250 kV and automatic to 500 kV in 2 hours.

(iii) Fast automatic voltage rise 0-500 kV in 3 minutes.

Other items of interest are:

(a) An automatic restart circuit, which tries twice to reapply full H. T. after breakdowns and then shuts down the H. T. set. The breakdown rate averaged over 2-week runs varies between 1 and 3 per day.

(b) A multi-channel pen recorder for the continuous monitoring of voltage, column current and vacuum pressure simultaneously. A fourth channel is available for other parameters as required.

As a routine check on the state of the H. T. set, power factor is measured twice a month, and a precision measurement at the column divider resistor chain is made monthly in order to detect any incipient fault in this component. The present chain has been in operation for 2 years without trouble.

III. ADDITIONAL 500 KEV ELEMENTS

1. Harmonic Buncher

A second harmonic cavity has been added to the 200 Mc/s buncher cavity but awaits completion of the 400 Mc/s generator.

2. Chopper

An electrostatic deflector and power supply has been built to permit chopping of the 500 keV beam at the P.S. injection frequency (3 Mc/s) with variable mark to space ratio. This should relieve the linac rf system of charge which would lie between the synchrotron rf buckets and would be lost anyway. This will be installed and tested shortly.

IV. DUOPLASMATRON AND SHORT COLUMN DEVELOPMENTS

Following the plasma expansion cup developments in Leningrad, we have made some tests on different cup and extraction geometries. These were encouraging and the best beam for which we have complete figures was 450 mA at 100 kV in a phase volume of 0.59 cm mrad, giving a brightness of 130 mA cm^{-2} $sterad^{-1}$.

Assuming that high gradients are useful in controlling beam blow-up along the accelerating column, we have also been exploring the behaviour of different electrode materials in a re-entrant column arrangement. Use of a conventional column for these tests (13 - 40 kV sections)) enables us to put aside the air breakdown aspect of a short column for the time being while profiting from the range of potentials available for supplying intermediate electrodes.

The test setup consisted of the column within which two electrodes of the new material, carefully cleaned and polished, could be separated by a known gap. Cathode current, anode current, anode temperature, radiation level and voltage were monitored. The best materials were found to be low carbon stainless steel and titanium alloy as used for supersonic aircraft. At a pressure of 2×10^{-6} mm Hg provided by a mercury pump and liquid nitrogen baffle, we could hold 500 kV over a 10 cm gap.

Preparations are being made for testing the combination of duoplasmatron and high gradient gap in the laboratory. If successful, we plan to install it on the linac early in 1965.

V. INSTRUMENTATION

For emittance measurements the aperture-lens-aperture method is used where quick checks are required or where time dependence is suspected. Formerly it held another advantage in that it also yielded density distribution across the phase space, but the photographic emulsion method has now been developed to the point where the emulsion can be calibrated and made to supply contours as well as envelopes. These developments are described in references 3, 4.

The method was recently adopted for measurements of the first turn in the P.S., one wavelength downstream from the point of injection. A series of 24 exposures was made for different injection conditions, permitting estimates to be made of aberrations in the first P.S. wavelength, the acceptance of this section, and the matching achieved.

VI. OPERATION

1. Machine Reliability

The scheduled P.S. time which is lost due to linac faults remains at around 2% in spite of a fairly serious breakdown in May when 48 hours were lost in stripping down on FTH cavity and replacing the input loop which had flashed across at a metal-epoxy joint.

The FTH 470 tubes themselves have averaged 7000 hours, with one lasting for 11,000 hours.

2. Machine Stability

The pulse-to-pulse stability remains good but the P.S. is rather sensitive to mains voltage variations. The linac contribution to this seems to come from the modulators which are at present not regulating very efficiently.

There are certain major items of equipment which one expects to run without much attention, for example, the mercury vacuum pumps, the FTH cavities, the high-power phase shifters and power dividers, and the refrigerator compressors. After five years' running, however, we are finding that the pumps take longer to pull a tank down, and that breakdown occurs occasionally in the phase shifters and power dividers, provoking flash-over elsewhere in the rf system and reducing the range of adjustment, making the whole chain more critical of adjustment. We have also had the complete failure of an FTH cavity already mentioned, and recently the failure of a compressor.

We are therefore turning our attention to the overhaul of these items, one by one; this has involved for the mercury pumps the construction of a separate ventilated lab for cleaning and speed measurements on a dummy tank.

3. Setting-Up

The present rhythm of P.S. operation allows us from Sunday through Tuesday twice a month for maintenance and repairs, source

changes and measurements, with machine start-up on Wednesday. In the absence of faults it is sufficient to take standard values for source, rf and focusing, and trim around these values by successive approximation, progressing along the machine. The final criteria are intensity and pulse shape at the point of injection into the synchrotron, and 50 MeV emittance and energy spread. The emittance at 500 keV is also measured as a routine procedure.

4. Running

When the beam is handed over to the P.S. Main Control Room for injection, certain controls are also transferred and the linac control position is abandoned. A linac operator remains "on call" for fault repairs and readjustment, but otherwise works normally within reach of a telephone in his laboratory or office during the day, or sleeps in the operators' dormitory at night.

The controls transferred include the bending magnets, triplets and the vertical steering coils in the inflector region, variable apertures and the tank levels. The transfer of tank level controls and indications is questionable in principle, but the retouching of tank levels by the M.C.R. operators seems justified with the present stability of the modulators.

VAN STEENBERGEN: When you saw an increase of current, did you see increase in emittance?

TAYLOR: It didn't make a great deal of difference; the 50 MeV emittance is always around about 3 cm milliradians and it did not change very much.

HUBBARD: These standard operating values that you use to start up after shutdown, are they a set of values that do not change over a long period of time or are they just the ones you used when you turned it off before?

TAYLOR: Actually, by the control position we have a little piece of paper with them all marked down; this has been around for a year or so, and it is still the one we use.

WROE: You mentioned right at the beginning that you had reduced the height of the cathode shield. Could you say how much you reduced it by and what difference it made?

TAYLOR: I can't give you the exact figures, but it was the order of 1 or 2 mm. This pushed us up to the 300 mA from the source. We had been previously in the 200's.

WROE: We tried it at one time and it did not make any difference.

BLEWETT: Do you have any evidence of x-ray emission?

TAYLOR: No.

NORDBY: I was wondering about the 3 Mc chopper. Do you have any information on its operation?

TAYLOR: It is a couple of parallel plates with about 10 kV across them. We haven't used it yet. We had some trouble getting sufficient power in the driver stage.

NORDBY: Also on that photograph method, do you have any trouble with the surface building up potential and giving you erroneous readings?

TAYLOR: No.

OHNUMA: You mentioned about the routine measurement of the beam shape in the transverse direction. To what extent can you use the results of those measurements for adjusting the focusing system between the preinjector and the linac?

TAYLOR: It is almost entirely an empirical type adjustment. We do it rather as a check on the performance of the preinjector.

OHNUMA: Is it something you could probably control by, say, on-line computers or anything like that?

TAYLOR: We have got for the normal method at 50 MeV this arrangement of the slit, lens and a slit. This defines in the phase plane of the first slit a strip like this, which is swung around through 90° by the lens and drift system to the second slit where we further limit to a small rectangle in the phase plane. Now what we have done recently is to make up a new set of slits from which we can take digital information, with the object of feeding this to a computer eventually.

VAN STEENBERGEN: Have you noticed at those high currents any beam intensity modulations? Have you noticed with the duoplasmatron source, any plasma boundary instabilities?

TAYLOR: No, not yet.

VAN STEENBERGEN: At the high currents, with the duoplasmatron source, one finds that the beam extracted from the ion source shows hash or intensity variations. Does this exist with the rf source?

TAYLOR: Apparently not. The pulse shapes are always very clean. In the early days we found in the synchrotron a 60 Mc component and it looked as though it was beating between the rf frequency of the source, which is 140 Mc, and the tank which is 200 Mc. But as far as hash is concerned, we have not observed any problem.

NORDBY: We found some hash in the Argonne duoplasmatron source and we got rid of it by putting a small capacitor on the extractor supply.

FEATHERSTONE: I wonder if you know approximately what proportion of the beam current you quoted from the source is protons?

TAYLOR: Yes, it is between 90 and 95%.

FEATHERSTONE: Excellent. Also, have you a feeling as to the kind of electron current that flows up the column to produce unwanted x rays at the top? In other words, if this is the actual proton or positive current going down the column, the person who designs the bouncer to maintain stability on your Cockroft-Walton system has to contend with the electron loading as well. And I haven't seen figures quoted on what this amount is on typical installations.

TAYLOR: We said a little in the Dubna report. We've got a fairly big capacitor across the generator. And I gave some results, I believe typically 4 kV drop during the pulse. Measurements over a long period show that normally we have about equal electron and proton currents, occasionally rising to electron currents twice the proton current.

VAN STEENBERGEN: I would like to add to this question of Featherstone's. At High Voltage Engineering they mentioned that they normally take a factor of 2 into account. If you take 100 mA proton beam down one way, you count on a 100 mA of electrons the other way. May I ask at the same time, with the duoplasmatron source and the expanded plasma, are there any figures existent yet on proton percentages?

ANSWER: No.

VAN STEENBERGEN: One might worry here that the proton percentage might be drastically down from the conventional duoplasmatron source.

GUILBAUD: Could I offer a comment that we made such a duoplasmatron in our laboratory with expanded cup and at 40 kV we measured about 300 mA but these were protons. We had a magnetic focusing which took only protons on the target. I think I remember the proton percentage was estimated to be somewhere around 75%, but I am not sure.

WADDELL: The other day when you were talking about the machine, you described there that the phase between the first and the third cavities was zero and that the second cavity turned out to have a phase difference. You indicated at that time that you got a sharper beam, less spread at the end, and I was wondering if you were tuned for maximum current, whether you arrived at a similar condition without looking for the sharper energy spread.

ANSWER: The current in fact is determined by the level of Tank one and the focusing and matching, and thereafter it stays pretty well constant through the machine. You have to move the tank level a long way to drop the current and by then you would have a completely unacceptable beam.

QUESTION: The other day you indicated that the second tank had a different phase than the others and that at that time you got better energy spread operating in that mode. Is this reflected in the overall current acceptance?

TAYLOR: If you put the tanks in phase, you get about the same sort of current, but worse energy spread.

FEATHERSTONE: I am also interested in your high voltage experiment at 500 kV. When you say you were holding this across 10 cm, would it represent a voltage reached after a succession of conditioning sparks had been permitted to occur, or would this system be something that just never sparked at all?

TAYLOR: This is something which you form watching the sparking. You bring the voltage up gently, and reach a level where you get a low frequency of sparking.

FEATHERSTONE: So the sparking rate essentially drops off exponentially and after a time it becomes a negligible matter.

TAYLOR: Yes.

MORGAN: I believe you mentioned that you had about 220 mA of current out of the source and about 200 mA at the 500 kV level. Do you have any idea what happens to this 20 mA difference?

TAYLOR: We've got 300 mA maximum coming from the source and 220 mA maximum at the bottom of the column, and we think that the difference is scraped off by the aperture limitation at the end of the column. We have our first focusing triplet actually integral with the first accelerating electrode of the column.

MORGAN: I believe you extracted the high current at 28 kV; have you tried extracting it at higher gradients or higher potential levels?

TAYLOR: Yes, but that is about the limit of stable operation.

HUBBARD: I would like to ask Van Steenbergen about the electron drain number he quoted from High Voltage Engineering. Is that with one of their new inclined gradient columns or is that with the old-fashioned kind?

VAN STEENBERGEN: I couldn't tell.

REFERENCES

1. C. S. Taylor. "High Current Performance of the CERN PS Linac" (Presented at the 1963 Dubna Conference). Available as CERN internal report MPS/Int. LIN 63-9.

2. Th. Sluyters. "A Theoretical and Experimental Comparison of Proton and Deuteron Acceleration in the CERN Linear Accelerator (C. L. A.)," CERN 64-22.

3. Th. Sluyters. "Radial Beam Studies Using an Emulsion Technique Applied to the CERN Linear Accelerator." Nuc. Instr. & Meth. 26, 999 (1964).

4. C. Bovet and M. Regler. "Etalonnage d'emulsions pour les mesures d'emittance." MPS/Int. LIN 64-2.

PERFORMANCE OF THE PLA

J. M. Dickson
Rutherford High Energy Laboratory

Availability

The PLA has been operating 24 hours per day since January, 1962 on a schedule of 10 days for operation and 4 days for maintenance and for the setting up of experiments. In late summer of each year there has been a shutdown of one to two months for major modifications, repairs and installations. The percentage of this scheduled operating time which has been lost by machine faults has decreased from 30% in 1962 to 12.5% in 1964 (January to June). During the 12 months, July, 1963 to June, 1964, the total number of hours available to the experimenters was 4638 hours and the total number of hours scheduled for operation was 5424; an availability of 85.5%. Figure 1 shows the monthly availability figures since the start of regular operation in April, 1960.

Faults

Analysis of the fault log of the machine shows that the lost time was due to rf amplifiers (grounded grid triodes) (15%), modulators (20%), accelerating structure (15%), polarized source (10%), coaxial lines (7%) and miscellaneous small items.

The grounded grid triodes, which are continuously pumped valves manufactured by AERE Harwell and tested and serviced by the PLA group, operate for a total of about 30,000 valve-hours per year.

The faults which cause loss of time are water leaks (in the grid), damage to some silvered mica condensers in the cathode assembly, broken rf windows, anode-to-grid sparking, and broken cathodes. Grid water leaks are normally caused by the accumulation of deposits in the fine bore stainless steel tubes of the grid. Control of the water conductivity to less than 10 μmho and filtering by scintered stainless steel filters has not eliminated the trouble. The mica condenser forms part of the cathode/grid resonant circuit, and carries about 90 amp rf. Spark erosion of the silver reduces the capacity, puts the cavity off tune and reduces the gain of the valve. Mica life is about 6000 hours. Six to ten valve changes per year are due to the above faults.

Modulator faults are often minor faults now and have become less frequent since the main switch valves were changed from ignitrons to deuterium thyratrons (CV 3336). The basic circuit of the modulators is

P.L A AVAILABILITY 1960 – 1964

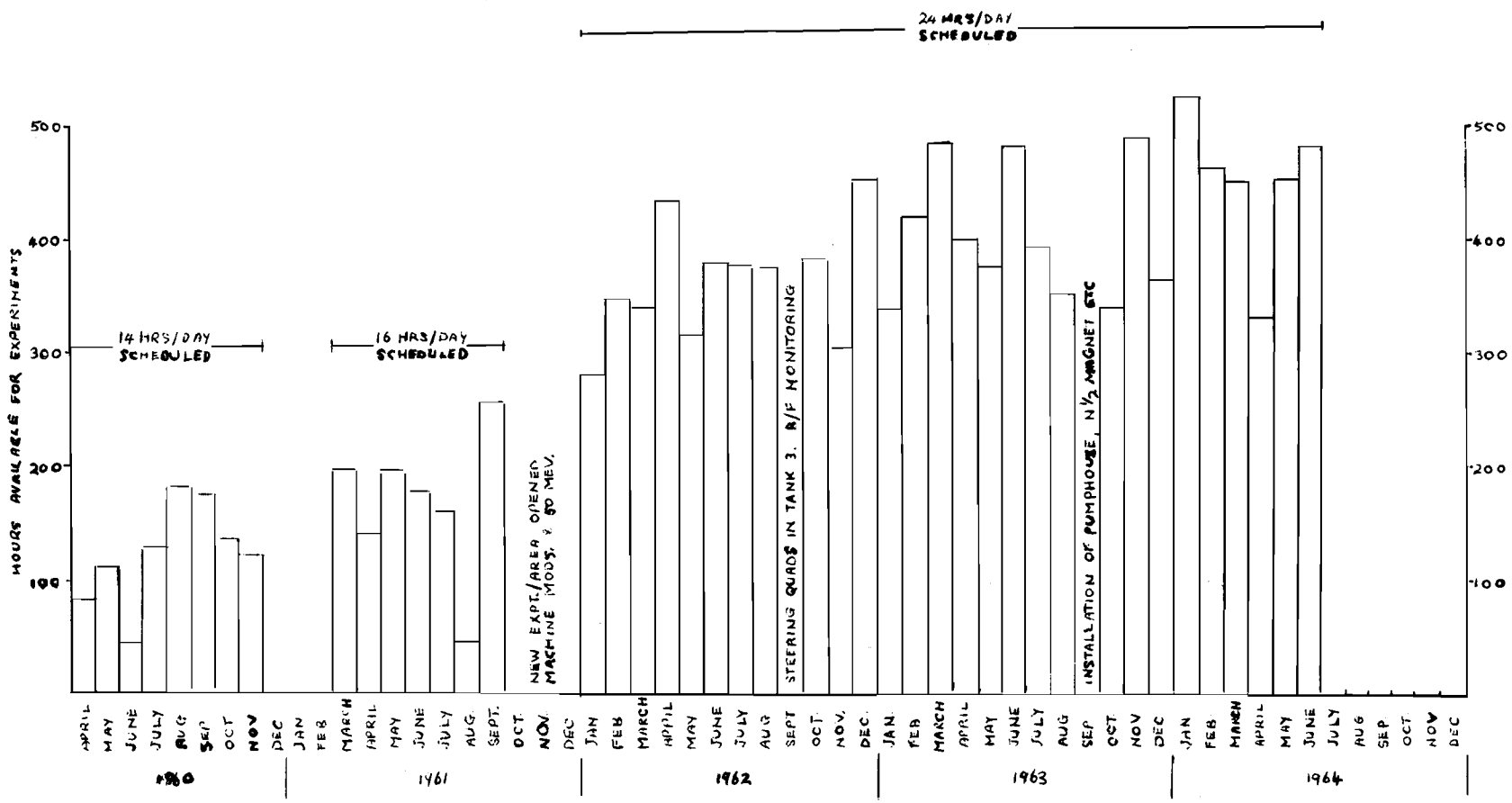

FIG. 1

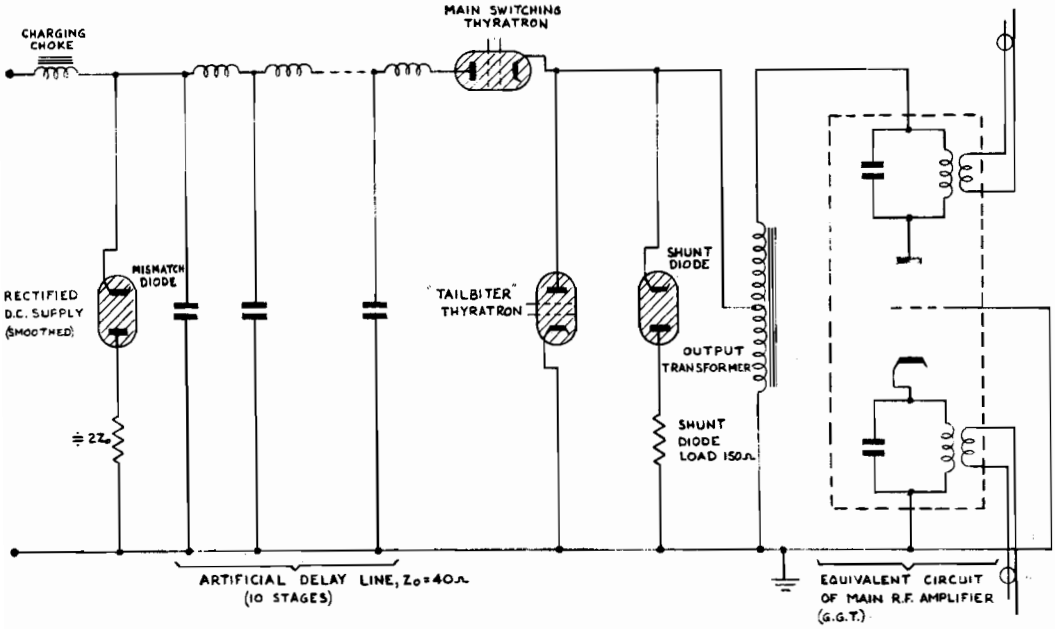

BASIC CIRCUIT OF PLA MODULATOR
FIG. 2

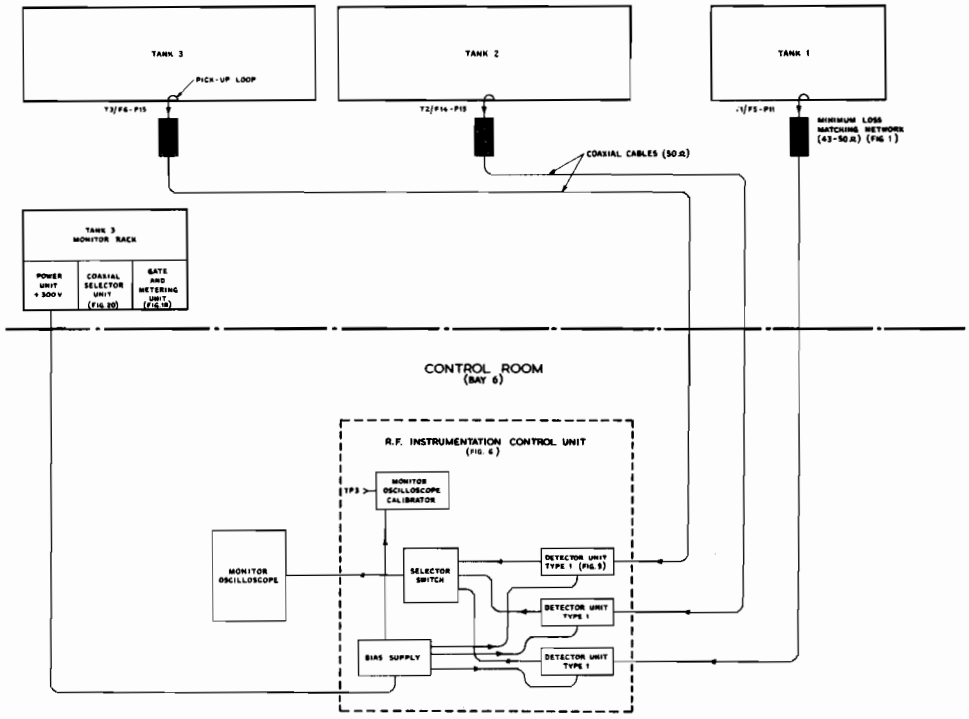

FIG. 3 BLOCK SCHEMATIC DIAGRAM OF ACCURATE R.F. LEVEL MONITOR

shown in Fig. 2. Protection against high impedance mismatch conditions of the modulator load is provided by the "tail-biter" thyratron which is triggered near the end of each modulator pulse. A negative voltage swing on the delay line results and the mismatch diode (a deuterium triggered diode) fires. Subsequently the main switch tube and tail biter are extinquished by the reflected wave. Low impedance mismatches are absorbed by the mismatch diode. The CV 3336 thyratrons have run well, one for over 10,000 hours without a fault. Some have had partial heater failures and some have had gas pressure trouble. These faults have caused very little lost time and are mostly due to preproduction difficulties with the valve and are being cured.

Lost time on the accelerating structure has been due to some water leaks in the drift tube and liner cooling circuits. These have all been "repaired" by pumping a weak solution of resin varnish through the faulty circuit.

Coaxial line faults are nearly always due to fractures in soft soldered joints or to accidental damage to joints during assembly. Peak powers of over 1 Mw (2% duty cycle) cannot be reliably carried by 50 ohm coaxial lines of 3" OD. The use of 4-1/2" and 6" lines and copper plating of all surfaces has improved the reliability very significantly. For further descriptions of the faults, see NIRL R/55 and R/60.

RF Monitoring

The basic requirement here is to obtain for each tank a measure of the rf accelerating field, the phase and the "tilt." Rf amplitudes are measured by loops in the cavity walls which transmit an rf signal to the control room to a matched and biased diode detector (Fig. 3). The bias voltage ($\sim$ 7 V) to give a 0.2 V residual pulse is read off the dial of a helipot. The accuracy of the measurement is $\pm$ 0.1% and the long term stability is about 0.2%. A measurement of the tilt of a cavity is obtained from several loops along the cavity; the calibration of each loop must be obtained by comparison with a perturbation measurement of the tilt. This comparison has only been completed for tank 1, where a perturbation measurement was performed recently. This showed that, for the same position of the tilt tuners, the tilt had changed greatly over the past four years. The tilt can now be checked from time to time to look for long term changes in the cavity. The tanks are individually servo tuned to maintain the cavity phase in a constant relation to the phase of the input power. The intertank phase is controlled manually and is monitored by a phase bridge with thermocouple detectors and a meter indication (Fig. 4). This system can detect small phase changes ($\sim 0.1^{\circ}$), but it is sensitive to changes in the shape of the rf pulses in the tanks,

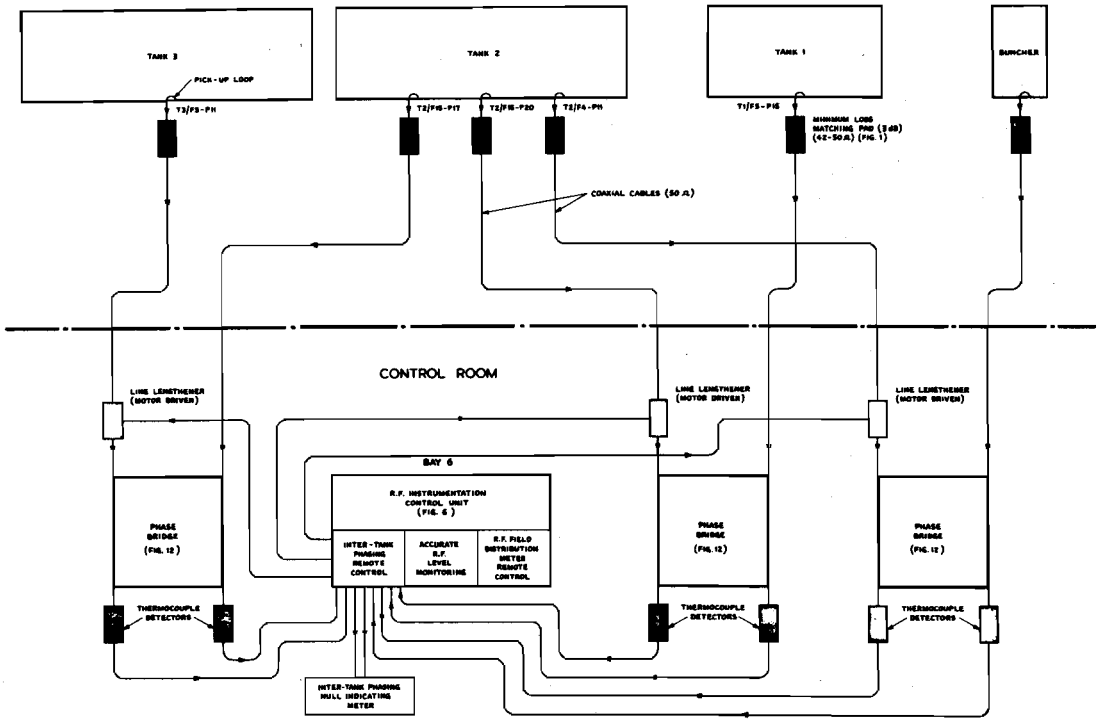

FIG. 4 BLOCK SCHEMATIC DIAGRAM OF INTER-TANK PHASE MONITORING SYSTEM

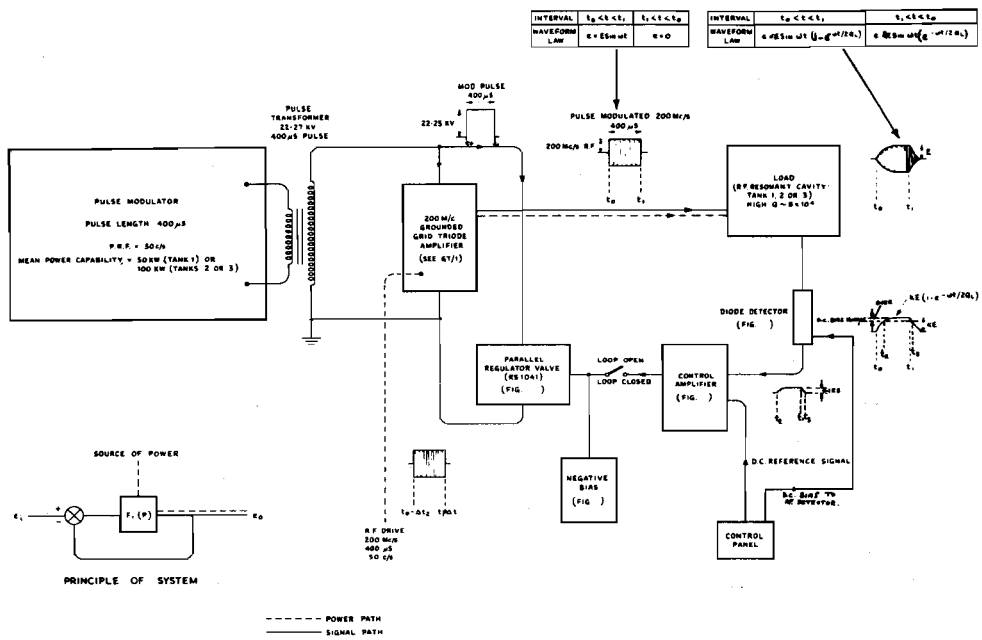

SIMPLIFIED BLOCK SCHEMATIC DIAGRAM OF CAVITY R.F. FIELD STABILISER

FIG. 5

in particular to the build-up rate, which can be affected by changes of amplifier valves or their associated coaxial line components. It is hoped that by using diode detectors that better long term stability can be achieved.

RF Stabilization

It is important for many experimenters on the PLA that the output beam energy of the machine should remain constant over long periods and that it should be constant throughout each beam pulse. Slow acting stabilization of the rf could satisfy the first requirement, but the second is more demanding. The rf field stabilizer shown in the block diagram, Fig. 5, produces a nearly flat-topped rf pulse; variation along the pulse is about 0.1% and $\pm$ 5% changes in field can be corrected by a factor of 50. Variation of the modulator mains or H. T. voltages produces a variation in the length of the flat top of the stabilized pulse. This is particularly noticeable, when the Nimrod magnet is being pulsed at full power, but it is not embarrassing operationally.

Beam Energy Monitor

Beam energy measurements by the time of flight method, by momentum and by range measurement have all been used to observe the dependence of beam energy on machine parameters. The range measurement method has the advantage of requiring relatively simple appartus and in the arrangement used it imposes only one restriction on the beam, that it should have a peak current of 10^{-6} to 10^{-9} A. The beam energy monitor is located about 6 feet from the end of tank 3 and can be moved in an out of the beam by remote control.

Figure 6 shows the principal parts of the device. Ion chambers A and B form a differential ion chamber with a common collector which is connected to a vibrating reed electrometer. The thin degrader is equivalent in thickness to two standard deviations of the nearly Gaussian range distribution. The relative thicknesses of A and B is such that the larger number of protons passing through A is compensated by the greater ionization loss per proton in B, to produce equal currents in A and B when the mean range of the protons is coincident with the center of the thin degrader. The thick degrader is removed for measurements at 30 MeV. The variable wedge degrader is motor driven and arranged to give a digital read-out of its position. The ion current as a function of the wedge position (results for a prototype with a dial reading only) is shown in Fig. 7. The zero cross-over point can be repeatedly found to be better than the equivalent of $\pm$ 10 keV for 30 and 50 MeV beams; its position is insensitive to changes in the ion chamber voltages under the recommended operating conditions.

This energy monitor needs to be calibrated at one energy near 50 MeV and one near 30 MeV. The incremental energy calibration can be obtained from range energy tables and the mechanical movement of the wedge degrader; it has also been checked against time of flight energy measurements. The monitor measures the mean energy of the beam and it is insensitive to the energy spectrum provided it is not too wide (less than 1 MeV). The most important advantages of this instrument is that it is always available for measuring the beam energy, whatever experiment is scheduled and its calibration remains unchanged since it depends only on one measurement of degrader thickness.

Beam Loss in Tanks 2 and 3

When the PLA was first operated, there was practically 100% transmission of beam current from the end of tank 1 (10 MeV) to the output of tank 3 (50 MeV). Recent measurements showed that the transmission had deteriorated to about 60%. Part of this loss was found to be due to a fault in the quadrupole current wiring in tank 2 which had increased the current in one of the quadrupoles by 40%. When this fault was cleared, the transmission increased to about 75%. Further measurements of quadrupole currents showed that there was a rms deviation from a $1/\beta$ quadrupole gradient law of 7%, which would produce an rms increase in beam spot size of 3 mm radius. This fault alone would not account for the beam loss, but it is also known that the mechanical alignment of the quadrupoles is not perfect and this will cause a radial oscillation of the beam, which now appears to be sufficient to cause the beam to be intercepted by the drift tubes. After a run at $1\,\mu$A mean beam current for a few hours, radioactivity of the drift tubes can be detected by a γ-ray monitor outside the vacuum envelope. Two peaks, at approximately a half-wave radial oscillation interval, are found, one of 2 mr/hr near the output end of tank 2 and one of 10 mr/hr in tank 3.

The majority of the neutron radiation, measured outside the shielding walls of the machine, is due to this beam loss, since the irradiated material here is copper, while all beam degraders, collimators and beam stoppers in the experimental areas are carbon. Experiments on the relative neutron yields from various materials are planned, which will give useful data for the control of radiation from machines of around 50 MeV.

SHAYLOR: I was interested to see that you are using a simple shunt type modulator to regulate rf amplitudes. Are you happy that just regulating the drive in the way you are doing keeps the whole of one tank flat to 0.1%? Don't you think that you may be regulating the rf level at the point where the detector is, but not elsewhere in the tank?

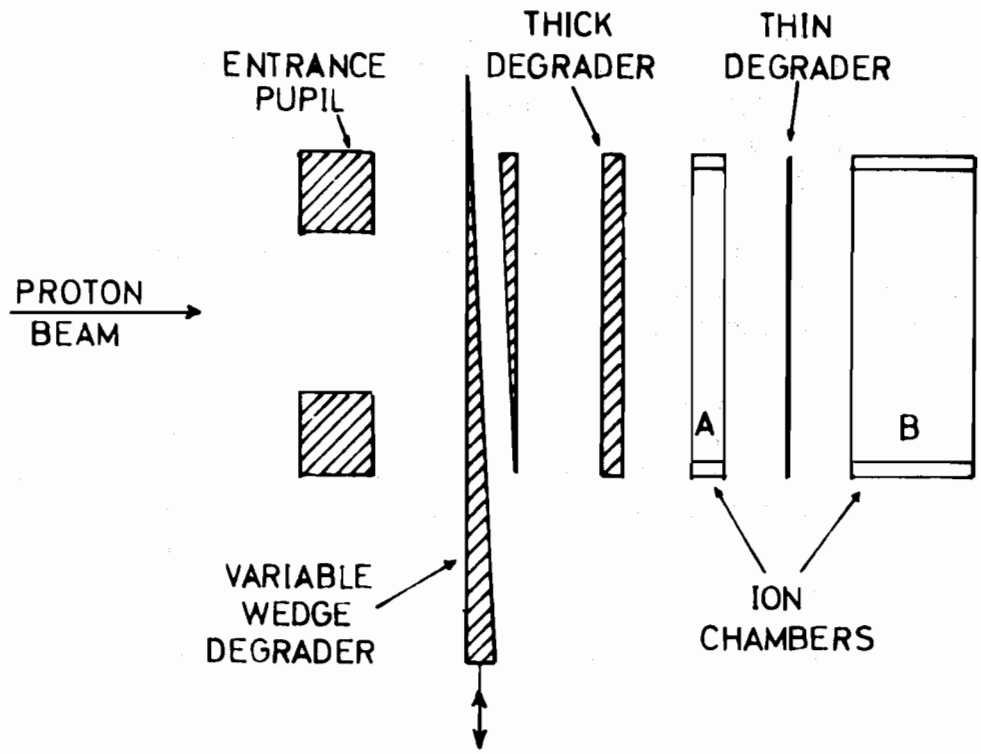

Fig. 6 Layout of Beam Energy Monitor.

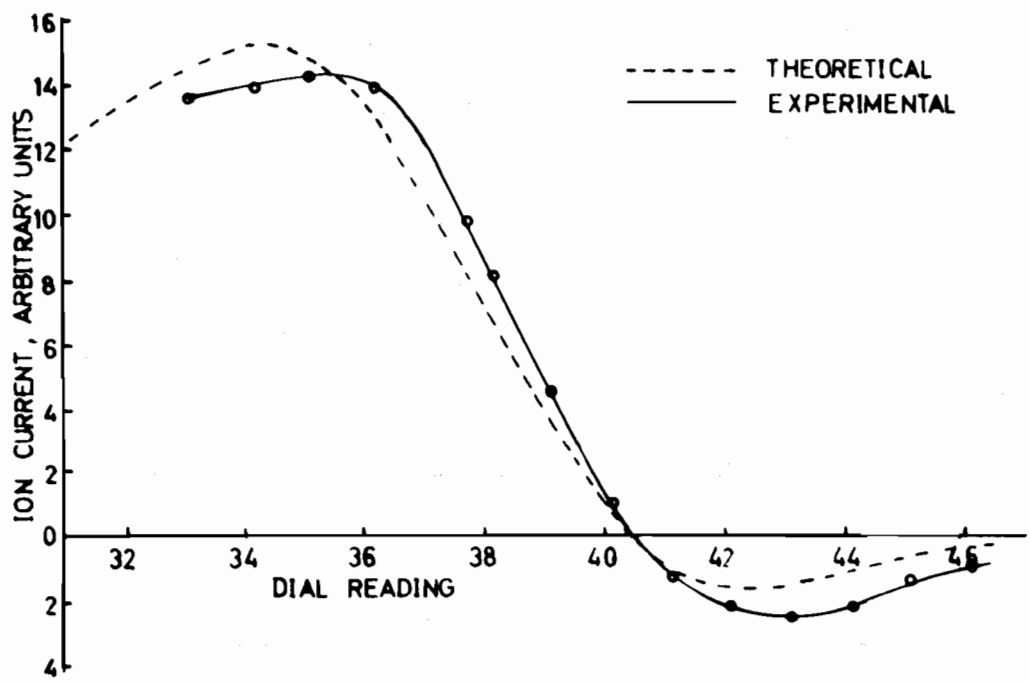

Fig. 7. Response Curve of Beam Energy Monitor.

DICKSON: I haven't seen any trouble like this, no. I have not looked at this very carefully, but we have got some evidence on this because the pickup for the stabilizer is at one part of the tank (I think in the middle), and the pickup for some other monitoring is in another part of the tank. They both flatten together.

SLUYTERS: We have done also at CERN these radiation measurements along the tank, but we have not found these bumps. Everything was very equal all along the tanks.

PRIEST: You have a nice servo mechanism there which keeps the pulse flat. I would like to know more about what it tells you. I think you are talking about the last part of the pulse after the beam is injected into the machine. And this corresponds with what Taylor was talking about. Have you got a measure of the extra amount of power that you have to put in when the beam is turned on?

DICKSON: Very little in our case. We are only running with at the most a peak current of around 200 μA. Beam loading doesn't worry us.

TENG: Do you have any experience similar to CERN that you can reduce the energy spread by detuning the phase of the second tank.

DICKSON: Can we leave that till Carne gives his paper? We have not measured the absolute phase between tanks.

HUBBARD: Can you not affect beam loss as you have indicated by adjusting the quadrupole magnet strengths?

DICKSON: I hope we can. We have not tried this yet. The adjustment is not so easy since the adjusting resistors are in boxes right underneath the tanks and there are a whole lot of things built in front of them all the way along. It is a slow and tedious business, but it probably has been done by now, since there was a shutdown last week. I hope that it has been fixed.

PERRY: Do you contribute any significance to the second peak?

DICKSON: No.

FEATHERSTONE: I was interested in your experience on blocking the water passageway within one of your vacuum tubes. This is an experience we share in our resnatrons. In our case, it turned out to be largely copper compounds which apparently had been removed from other parts of the system, and we are now undertaking a program of deoxygenating

and filtering and hope to prevent recurrences of this sort. We have also been trying to go to a higher purity of water. Are these the measures that seem appropriate in view of your experience? First of all, was it copper that plugged up the passages in your case?

DICKSON: There is some copper in the water circuits. We used not to have very much but in the last three months it has been building up. We don't know why but we had this blockage of the grid tubes before that. One of the main components is silica in this blockage. I think there are all sorts of other components.

QUESTION: What was the conductivity of the water.

DICKSON: 10 micromhos.

BEAM ENERGY MEASUREMENTS ON THE RUTHERFORD LABORATORY P. L. A.

K. Batchelor, A. Carne, J. M. Dickson, D. J. Warner
Rutherford High Energy Laboratory

I. Introduction

The results to be described are from measurements made using the time-of-flight method described previously,[1] and are a continuation of the work reported at other accelerator conferences.[2,3] As a result of recent observations some of the work reported previously needs some qualification. In particular, the 10 MeV and 30 MeV spectra have previously been affected by the residual power in Tanks 2 and 3 which results from the drive power feeding through the grounded grid triode amplifiers into these cavities even though the E. H. T. is removed from the amplifiers. Also early comparison between theory and practice from the 10 MeV beam has been invalidated by the fact that the field law in Tank 1 was distorted from its original value, which was used in the computer program. These effects are discussed below.

II. Effect of Residual Power on the Beam

Figure 1 shows the layout of the rf system of the P. L. A., for reference. The effect on the 10 MeV beam of varying the amplitude of residual power in Tanks 2 and 3 respectively, with these tanks maintained at the correct resonant frequency, is shown in Figs. 2a and 2b. The level of residual power was varied by means of the variable attenuators Att 2, Att 3 in the power dividing network. The effect of varying phase was found by setting the attenuators at their normal operating values, and detuning each tank in turn. The resulting spectra are shown in Figs. 2c and 2d for detuning of Tank 2 and Tank 3 respectively. It can be seen that the residual power affects the spectrum shape and position quite considerably. For normal settings of attenuators and frequency tuners the residual voltages were 6.4% of operating value in Tank 2, and 8.8% in Tank 3 (see Fig. 2). An amplitude reduction by a factor 0.7 (to give 'half power point' amplitude) produced a doubling of the beam energy spread at FWHH, and a small shift of mean energy $\sim$50 keV by each tank. A detuning of $\pm$ (f/2 Q) $\equiv \pm 45^{\circ}$ (to give the same reduction in amplitude, but now plus a phase shift) produced a change in beam energy spread at FWHH by a factor 3 (+ 45°), 0.6 (- 45°) by Tank 2, and 3 (+ 45°), 0.5 (- 45°) by Tank 3, and a shift of mean energy of + 20 keV (+ 45°) by Tank 2, and - 40 keV (+45°), - 120 keV (- 45°) by Tank 3.

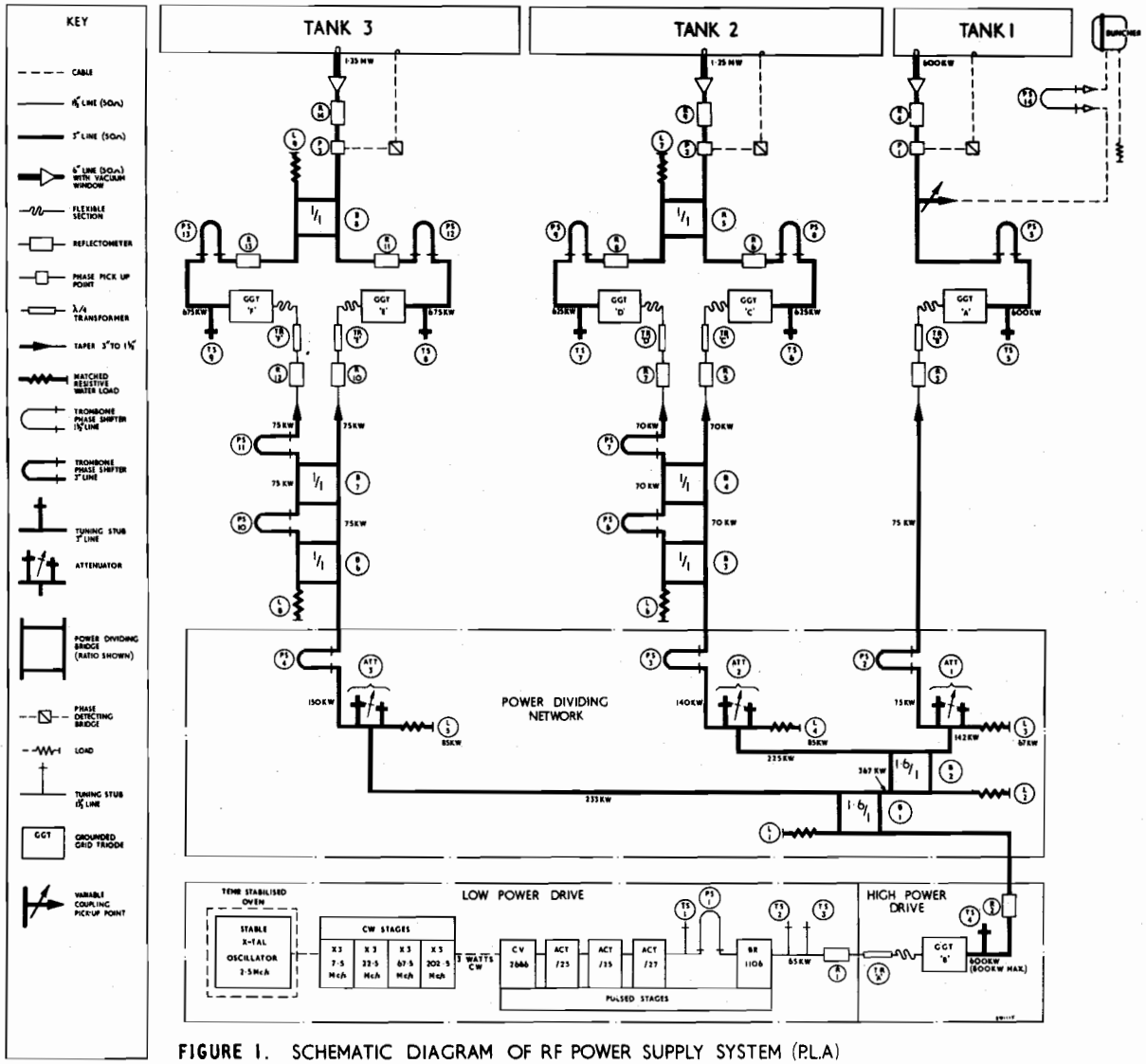

FIGURE 1. SCHEMATIC DIAGRAM OF RF POWER SUPPLY SYSTEM (P.L.A)

Figures 3a and 3b show the effect of residual power in Tank 3 on the the 30 MeV beam. For normal settings of the attenuator and frequency tuner of Tank 3, the residual voltage was 10% of operating value. An amplitude reduction by 0.7 produced little or no effect on the 30 MeV beam energy spread, but a shift of 120 keV. Detuning by $\pm 45^{o}$ produced marginal changes in energy spread, and a shift of mean energy - 350 keV ($+ 45^{o}$) and + 50 keV ($- 45^{o}$).

It is now normal operating procedure to reduce the residual power to a minimum in nonoperating cavities, this being achieved by detuning the tanks and insertion of maximum attenuation in the drive lines to the grounded grid triodes.

III. Measurements on Tank 1

Due to the discovery of the effect of residual power on the spectra it was decided that some of the early work on the 10 MeV beam should be repeated to try to improve the agreement between theory and practice which, at this energy, had not been good. Figure 4 shows some typical spectra for different injection energies and rf field levels, the tilt tuners being set at their assumed "flat field" setting (tilt 50-50). Computed spectra and phase acceptance did not agree well with measured values. Also the transparency of the tank was down by a factor 5 on its original value. It was therefore decided to remeasure the axial field in Tank 1 to see if this could be the cause of the disagreement. The field law measured for "tilt 50-50" is plotted in Fig. 5 and is compared with the field law measured when the cavity field was set up seven years ago (i.e., the field law used for computer calculations). It can be seen that gross distortion of the field has occurred, probably due to a change of dimensions caused by temperature cycling and periodic dismantling over the past seven years.

The actual measured field law has been used in the computer program to give comparison with some of the measured data of Fig. 4, and the computed spectra are given in Fig. 6. The experimental spectra of Fig. 4 do not show the same fine structure as the computed spectra, due to "smoothing out" by jitter in rf level and phase, and injection energy. But, with this proviso, comparison of corresponding spectra (A, B, C, etc.) now shows quite good agreement.

The field law has been restored to the proper value shown in Fig. 5. The transparency of Tank 1 has returned to its original value (i.e. 1/50). Results for the new field setting are not yet available.

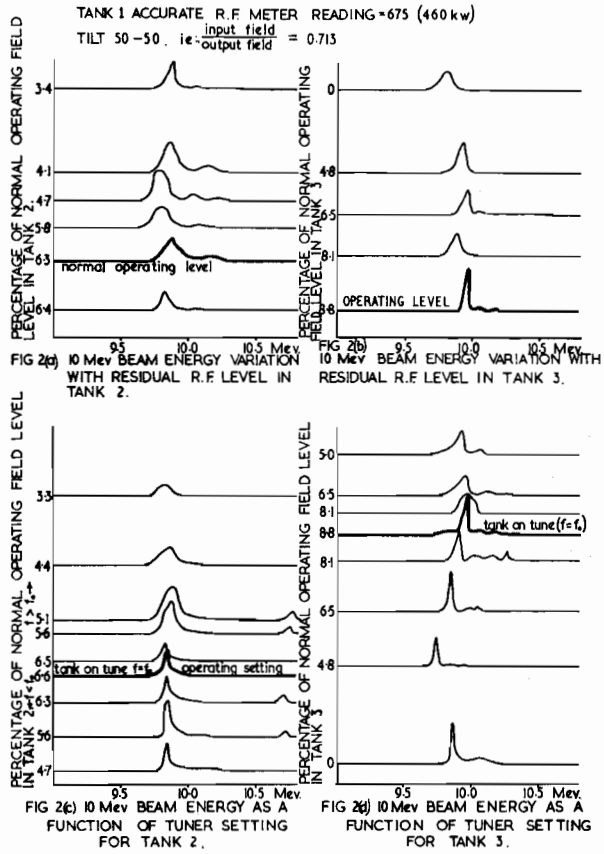
TANK 1 ACCURATE R.F. METER READING = 675 (460 kw)
TILT 50 – 50. ie. input field / output field = 0.713
PERCENTAGE OF NORMAL OPERATING FIELD LEVEL IN TANK 2
3·4
4·1
4·7
5·8
6·3
normal operating level
6·4
9·5
10·0
10·5 Mev.
FIG 2(a) 10 Mev BEAM ENERGY VARIATION WITH RESIDUAL R.F. LEVEL IN TANK 2.
PERCENTAGE OF NORMAL OPERATING FIELD LEVEL IN TANK 3
0
4·8
6·5
8·1
OPERATING LEVEL
8·8
9·5
10·0
10·5 Mev.
FIG 2(b) 10 Mev BEAM ENERGY VARIATION WITH RESIDUAL R.F. LEVEL IN TANK 3.
PERCENTAGE OF NORMAL OPERATING FIELD LEVEL IN TANK 2
f > f₀
3·3
4·4
5·1
5·6
6·5
tank on tune f = f₀
operating setting
6·6
f < f₀
6·3
5·6
4·7
9·5
10·0
10·5 Mev.
FIG 2(c) 10 Mev BEAM ENERGY AS A FUNCTION OF TUNER SETTING FOR TANK 2.
PERCENTAGE OF NORMAL OPERATING FIELD LEVEL IN TANK 3
5·0
6·5
8·1
8·8
tank on tune (f = f₀)
8·1
6·5
4·8
0
9·5
10·0
10·5 Mev.
FIG 2(d) 10 Mev BEAM ENERGY AS A FUNCTION OF TUNER SETTING FOR TANK 3.

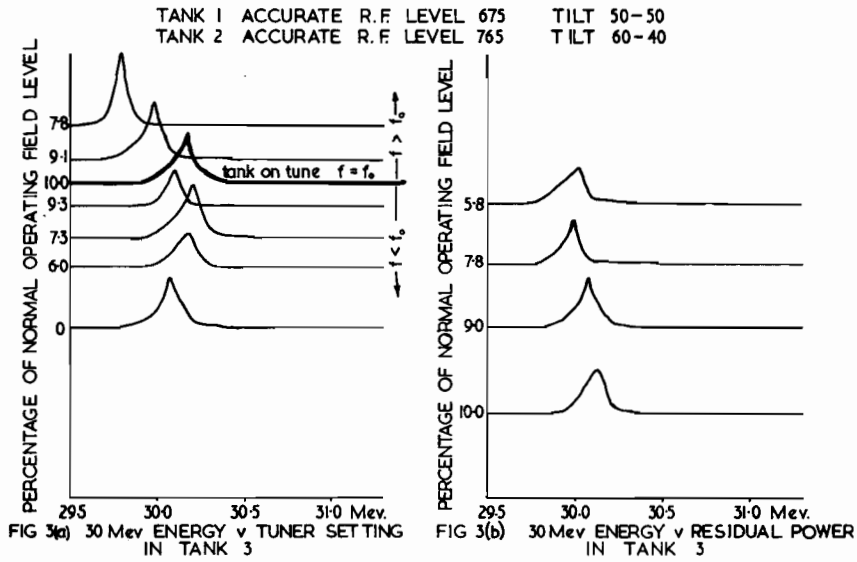
TANK 1 ACCURATE R.F. LEVEL 675 TILT 50 – 50
TANK 2 ACCURATE R.F. LEVEL 765 TILT 60 – 40
PERCENTAGE OF NORMAL OPERATING FIELD LEVEL
7·8
9·1
10·0
9·3
7·3
6·0
0
tank on tune f = f₀
f > f₀
f < f₀
29·5
30·0
30·5
31·0 Mev.
FIG 3(a) 30 Mev ENERGY v TUNER SETTING IN TANK 3
PERCENTAGE OF NORMAL OPERATING FIELD LEVEL
5·8
7·8
9·0
10·0
29·5
30·0
30·5
31·0 Mev.
FIG 3(b) 30 Mev ENERGY v RESIDUAL POWER IN TANK 3

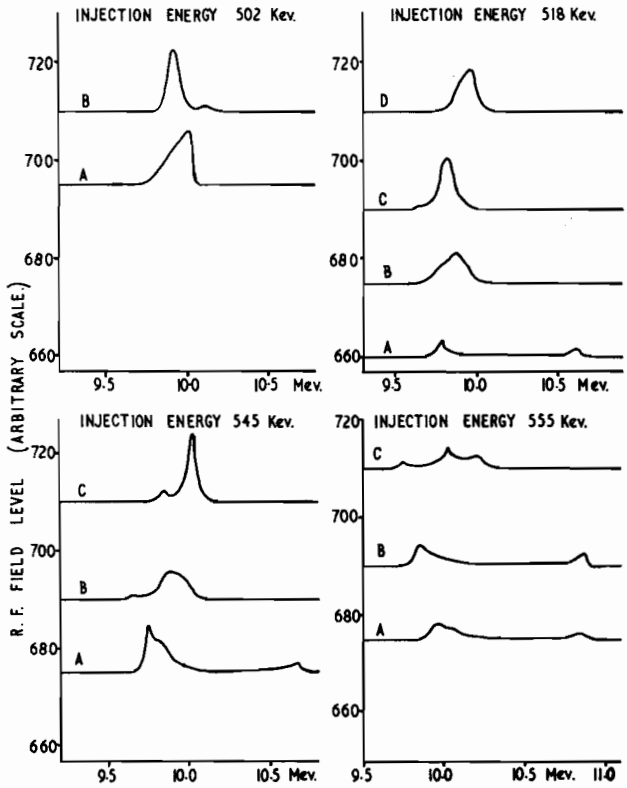

FIG 4. 10 Mev. ENERGY AS A FUNCTION OF R.F. LEVEL IN TANK 1 AND VARIOUS INJECTION ENERGIES.

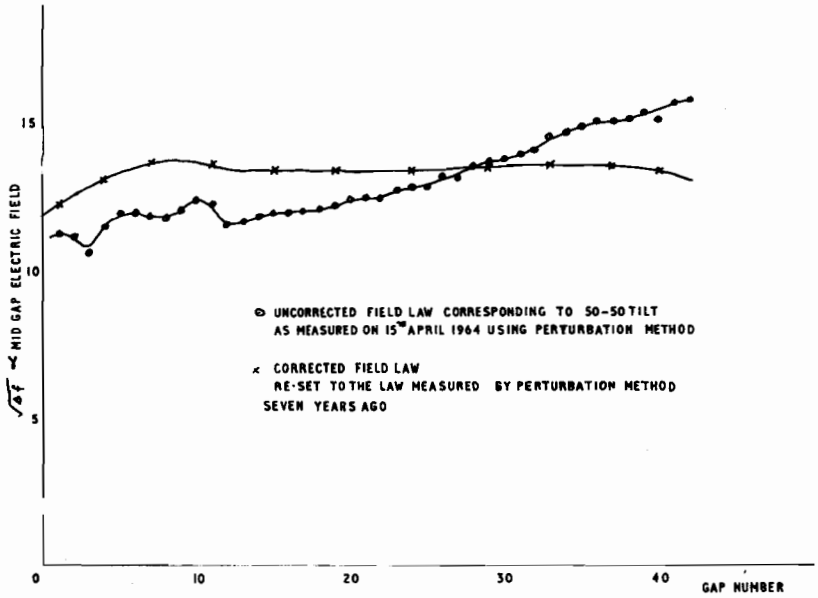

FIG 5. AXIAL FIELD LAWS FOR TANK I (BEFORE AND AFTER CORRECTION)

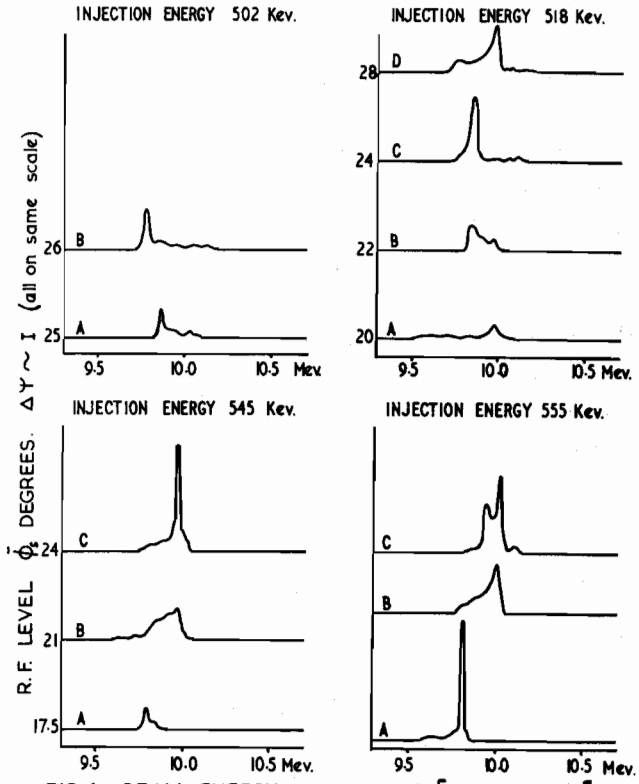

FIG 6. BEAM ENERGY IN TANK 1 [THEORETICAL]

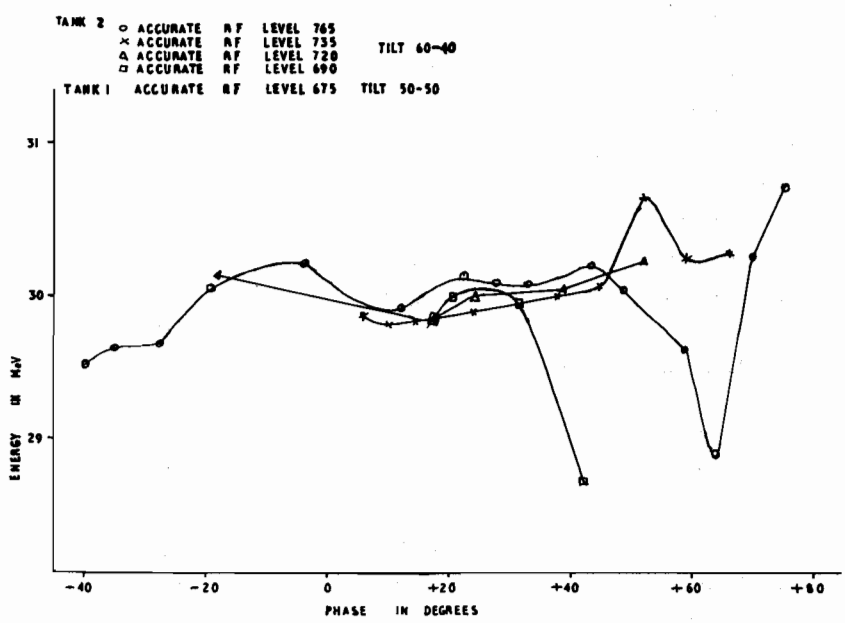

FIG 7 30 MeV ENERGY V INPUT PHASE

IV. Setting of Tanks 2 and 3

Before correcting the field law for Tank 1 measurements on the 30 MeV and 50 MeV beams were made to determine good operating levels of Tanks 2 and 3 for minimum energy spread in the beam. For the 30 MeV beam it is possible to run Tank 2 at an rf field level which gives an integral number of phase oscillation half wavelengths along the tank, and hence a flat energy vs. input phase region for the linear phase oscillation range of $\phi_s \pm 15^o$. Additionally it is required that the beam energy spectrum should be narrow. Figure 7 shows the variation of output energy with input phase: in particular, the rf level 735 is nearest to the required condition. The effect of input phase on output energy for the chosen rf level in Tank 2 (735) is plotted in Fig. 8, showing a roughly constant energy over the phase range, with little change in energy spread.

In Tank 3 it is not desirable to operate at a level corresponding to an integral number of phase oscillation half wavelengths, since the $\lambda_\phi/2$ level is too near threshold for acceleration, and the 2 $\lambda_\phi/2$ level is such that sparking would occur in the tank. Thus Tank 2 is operated at a different level (765) to give nearly integral number of phase oscillation half wavelengths between the input of Tank 2 and the output of Tank 3. The resulting 30 MeV spectra as a function of input phase to Tank 2 are shown in Fig. 9; the 50 MeV spectra versus input phase to Tank 3 is shown in Fig. 10. Finally Fig. 11 shows the energy spectra as a function of rf level in Tank 3.

V. Tank Tolerances

From the above results it is possible to make estimates of the stability of the output beam in terms of mean energy and energy spread as functions of machine parameters. Also use has been made of the Beam Energy Monitor described by Hanna and Hodges[4] to complete some of the results not determined by time-of-flight methods. This monitor, which utilizes a combination of degrading wedges for range determination, and a split ion chamber as a detector system, is very useful for determining mean energy, and can measure shifts of the order of 5 keV. A set of measurements with this monitor takes only a few minutes compared with several hours by time-of-flight methods. In the future the energy monitor will be used as a survey instrument to determine machine conditions worthy of further investigation by the longer method.

The following tables summarize the effect of injection energies, rf field levels and intertank phases on the output energies of the P. L. A., for the settings specified in Section IV.

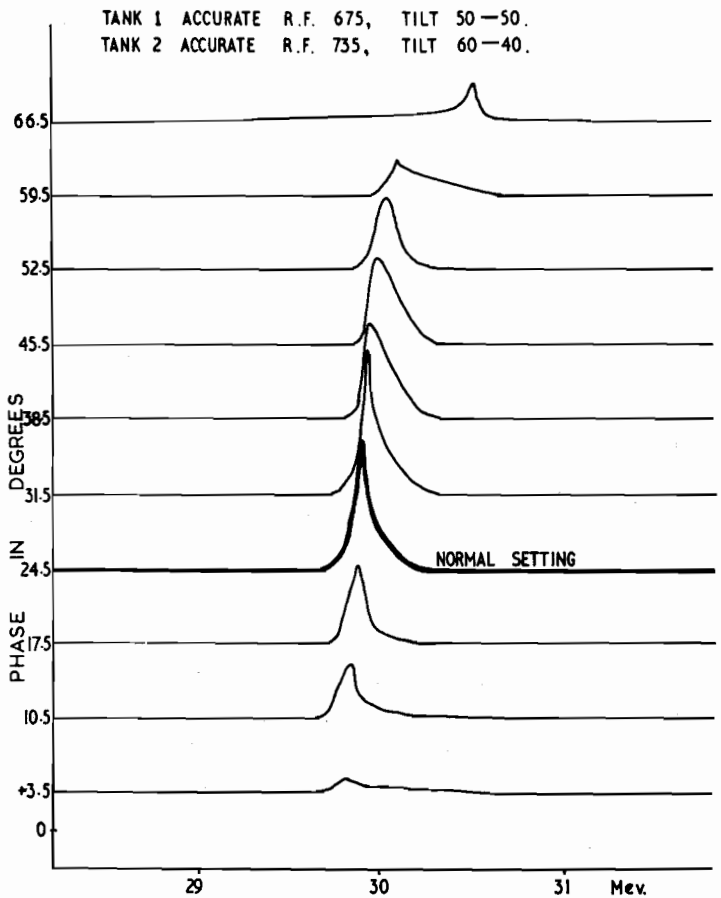

FIG 8 30 Mev. ENERGY v INPUT PHASE

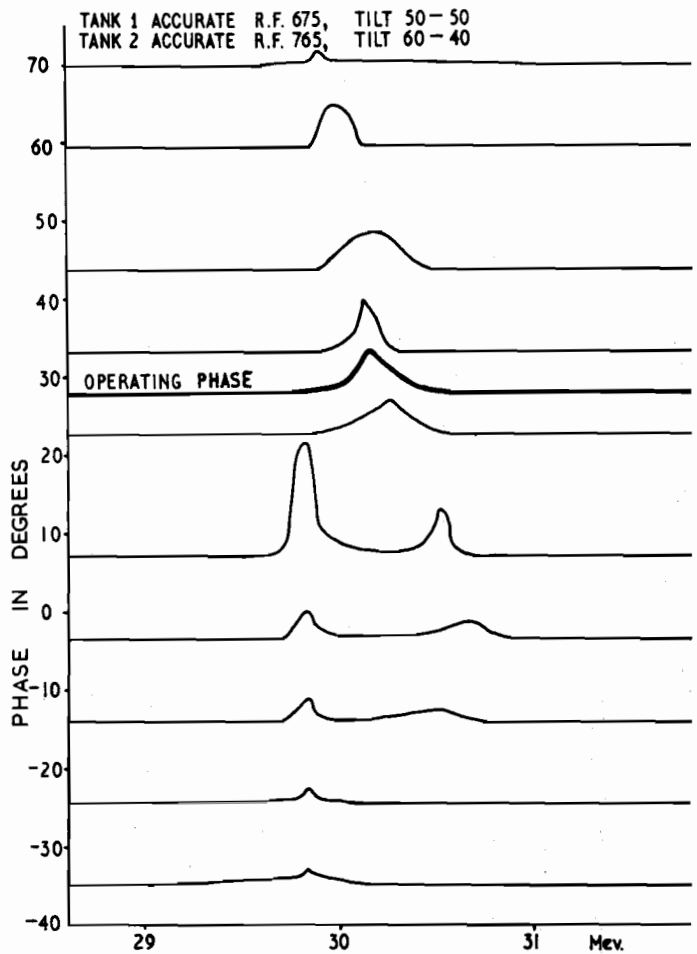

FIG 9. 30 Mev. ENERGY v INPUT PHASE

Tolerances on Various Machine Parameters Affecting the Output Energies of the P. L. A.

(a) Injection Energy

Change of Injection Energy %	Change of Injection Energy kV	Output Energy MeV	Change in Mean Energy keV	Measured by
		10 30	Not measured yet Not measured yet	
+1 -1	+5 -5	50 50	-12 (-0.024%) +12 (+0.024)	B. E. M.

(b) RF Levels

Change in RF %		Acc. RF	Output Energy MeV	Change in Mean Energy keV	Measured by
Tank 1	+1 -1	+5.5 -5.5	10 10	-30 (-0.3%) +30 (+0.3%)	T. o. F.
	+1 -1	+5.5 -5.5	30 30	-25 (-0.08%) +25 (+0.08%)	T. o. F.
			50 50	Not yet measured	
Tank 2	+1 -1	+8 -8	30 30	+80 (+0.27%) -80 (-0.27%)	B. E. M.
			50	Not yet measured	
Tank 3	+1 -1	+9 -9	50 50	0 -50 (-0.1%)	B. E. M.

(c) Intertank Phases

	Change in Intertank Phase. Degrees	Output Energy MeV	Change in Mean Energy keV	Measured by
Tanks 1/2	1° 1°	30 50	24 (0.08%) 18 (0.036%)	B. E. M. T. o. F.
Tanks 2/3	1°	50	45 (0.09%)	

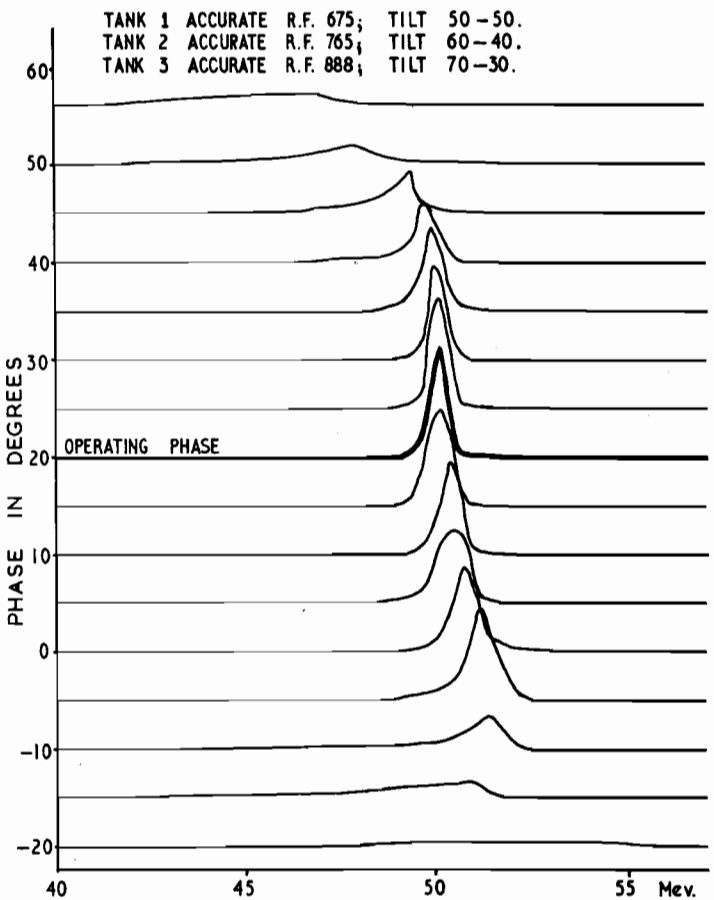

FIG 10. 50 Mev. ENERGY v INPUT PHASE

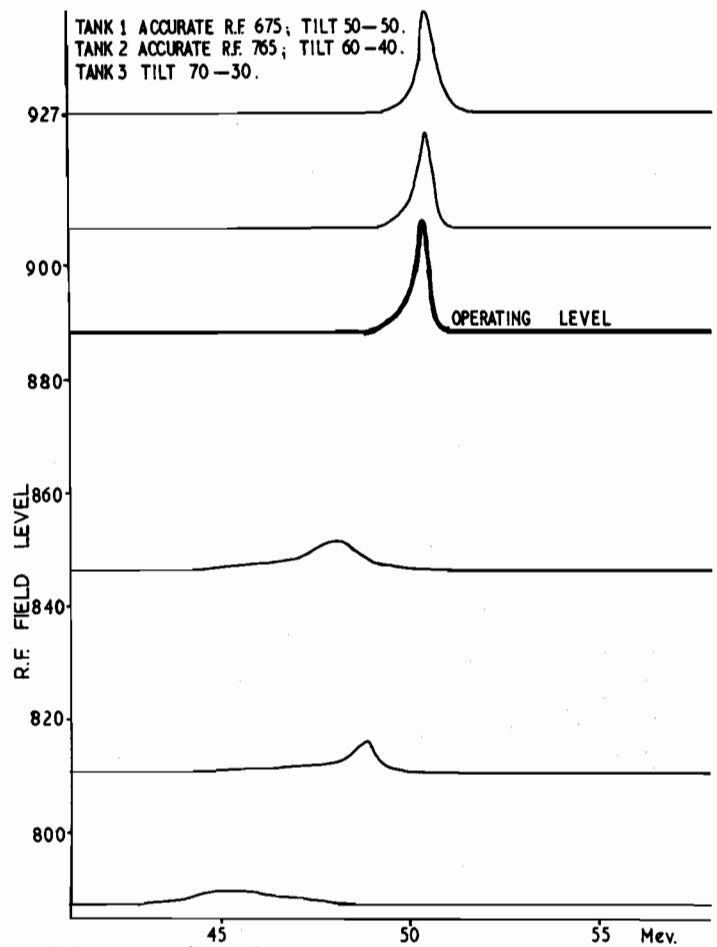

FIG 11. 50 Mev ENERGY AS A FUNCTION OF R.F. LEVEL IN TANK 3

Conclusions

The change of energy and energy spread in a beam drifted through a cavity containing some residual rf power has been shown to be such as to cause concern if a precise output spectrum is required.

Agreement between computation and experiment at 10 MeV has been improved, after finding the actual field law in Tank 1. This field law has now been set to its correct value, and it is intended to check the field laws in Tanks 2 and 3 in the near future.

The settings and tolerances given for the P. L. A. represent the state of the art at the present time. Detailed work is continuing, by the use of the Beam Energy Monitor and time-of-flight apparatus, to determine more closely the optimum operating conditions.

Acknowledgements

The authors wish to acknowledge the help of Messrs. A. P. Banford, D. H. Carpenter, E. M. Mott, and S. Webb during these measurements, and members of the P. L. A. Operating Staff.

TENG: Do you understand all these?

CARNE: Well, certainly the agreement between axial motion computations and the experiment is quite good. This is particularly true in the case of tanks two and three, where we have used a large signal calculation, that is, a 32 step-by-step integration per cell. The agreement in tank one is now quite good and we think we can improve the situation. We think in terms of phase oscillation wavelengths, and the picture ties up fairly well.

TENG: The shifts you are talking about are very large, 50 kV in 50 MeV.

CARNE: Sure that's alarming, but these figures in fact agree with equations given by Lloyd Smith some time ago in LS-3. These give quite tight tolerances.

WHEELER: When you change the level in a cavity by say 1%, did you change the phase between the cavities to compensate for the change in the position of the bucket?

CARNE: No.

LAPOSTOLLE: When you spoke about the inference of residual field in tanks two and three on measurements done at 10 MeV, do you think that even the field induced by the beam could affect such measurements?

CARNE: There could be some effect, but as John Dickson said earlier, we have a peak current of the order of 200 μA, so that fields induced by the beam are of the order of a factor 1000 down on the residual fields in the cavities, where there are still a few kilowatts of rf power.

TAYLOR: I will just mention that we have had exactly the same effect. Unless we drop the field to zero, we find that the measurements are turned about all over the place and we have a high current too.

REFERENCES

1. An Accurate Determination of the P. L. A. Beam Energy by a Time of Flight by C. J. Batty and D. J. Warner. NIRL/R/9.

2. Accurate Energy Measurements on a 50 MeV P. L. A. report submitted to 1963 Accelerator Conference in Dubna U. S. S. R. (Also P. L. A. Acc/Phys. 18).

3. Beam Observations in the P. L. A. by K. Batchelor, A. Carne, J. Dickson and D. J. Warner. Report on 1962 Conference on Linear Accelerators for High Energies at Brookhaven National Laboratory. BNL 6511.

4. A Beam Energy Monitor by R. C. Hanna and T. A. Hodges. P. L. A. Progress Report 1963 NIRL/R/50.

ZGS INJECTOR OBSERVATIONS

Philip V. Livdahl
Argonne National Laboratory

In considering the design of multicavity, high current linacs, the effects of beam loading on the cavity gradient are matters of greater concern as the beam currents become increasingly large. Presented in this discussion will be observations of these effects made on the ZGS, 50 MeV injector. Also some comments will be made on observations of group velocity and cavity phase acceptance.

Beam Loading

The 50 MeV beam from the ZGS injector is bent into the synchrotron through a 107° achromatic magnet system. At the center of the second bending magnet of the system there is a focus at the same point where the energy dispersion is greatest.[1] Therefore, by arranging to have a narrow (0.010") vertical slit (i.e., a slit which confines the beam to a vertical line) which can be positioned at any point in the transverse plane across the center of this magnet, it is possible to make analysis of the distribution of energies in the beam. The dispersion at this position is $\frac{\Delta E}{E} = 4.6\%$ per inch. Since the absolute value of the fields in the magnets have not been precisely determined, only relative observations can be made.

In using this slit for orbit measurements in the synchrotron under conditions of limited energy spread in the injected beam, it had been noted that there was a distinct variation of energy with time during the pulse under conditions of large beam loading as shown in Fig. 1.

This observation led to investigation of the variation of the mean energy and energy spread with rf gradient in the cavity. Figure 2 is a typical energy distribution as determined by sweeping the slit under a given set of conditions. The results of these measurements of the energy distributions at various rf levels are shown in Fig. 3.

By observation of the high energy and low energy extremes of the distriubtions (see Fig. 1) measured at each rf level, one can observe the variation of total energy spread with cavity gradient. This variation is shown in Fig. 4.

The operating conditions of the entire linac system were maintained constant while taking the data represented in Figs. 3 and 4; that is, there were no changes of preaccelerator conditions or focusing magnets made to

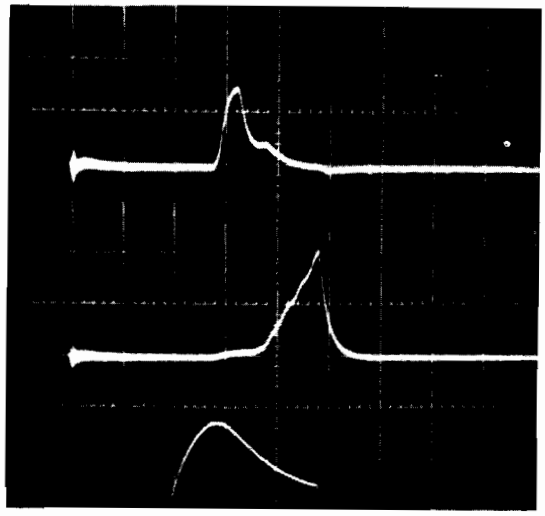

Beam pulse through slit on High Energy side of energy distribution.

Beam pulse through slit on Low Energy side of energy distribution.

Expanded rf pulse under heavy beam loading condition. 2% of rf gradient/cm, 100 μ sec/cm.

Fig. 1 Time Variation of Beam Energy Under Condition of Large Beam Loading

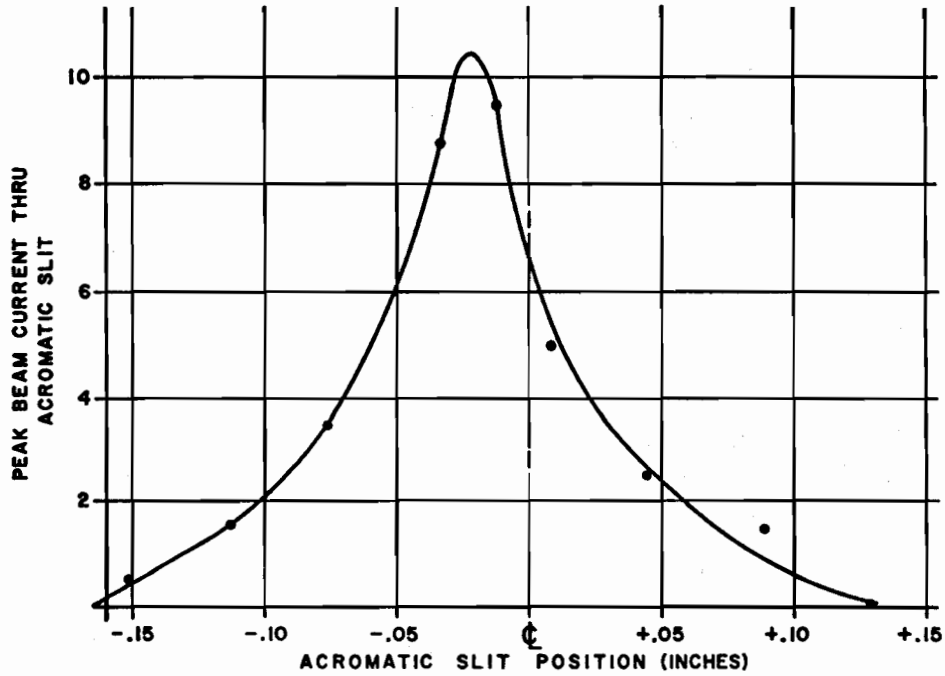

FIGURE 2 – ENERGY DISTRIBUTION AS OBSERVED BY SWEEPING ACROMATIC SLIT

adjust the injection matching conditions at the various rf levels. However, the cavity rf level was adjusted for each measurement so that there was no beam loading present.

We do not as yet understand the reasons that the mean energy and energy spread vary as observed, but will continue experiments to determine the reasons for this behavior.

Beam Loading Compensation

The ZGS injector rf system[2, 3] was designed with a series, hard tube modulator for regulation of the plate voltage to the output stage of the driven amplifier. This provides a means for delivering a variable amount of power to the linac cavity during the rf pulse for cavity voltage stabilization and beam loading compensation.

Ideally, the compensation is provided by a feedback system which regulates the power amplifier output for a constant rf cavity voltage through a closed loop servo system. Unfortunately, the servo loop of this system must include the final amplifier stage of the rf system and the characteristics of this stage are variable depending on tuning of the rf circuits. For this reason, the servo loop on the ZGS injector, as of this time, has been closed only under test conditions and not under operating conditions where its effects could be evaluated. This is not to imply that there is anything impossible about the task of establishing closed loop operation but rather that the tuning conditions of the power amplifier and the matching power amplifier to the cavity must be established as fixed conditions for the closed loop system to be satisfactory. This condition is being approached but has not yet been reached on the ZGS injector.

Beam loading is now compensated by an open loop system shown in the block diagram of Fig. 5. The operation of this open loop system is shown in the scope pictures of Figs. 6.1 through 6.8.

Measurements of pulse compensation voltages required for a cavity envelope which is flat during the time of the beam pulse with 50 mA of 50 MeV beam indicate that this should be within the capability of the system when such beam currents become available from the ZGS preinjector.

Questions had been raised from time to time of the ability of the beam loading compensation system to correct all parts of the cavity properly for beam loading. Figure 7.1 shows the cavity envelope near the low energy end, center and high energy end of the cavity under condition of heavy beam loading and Fig. 7.2 shows the same output loops under operation with the open loop correction of Fig. 5. These scope pictures

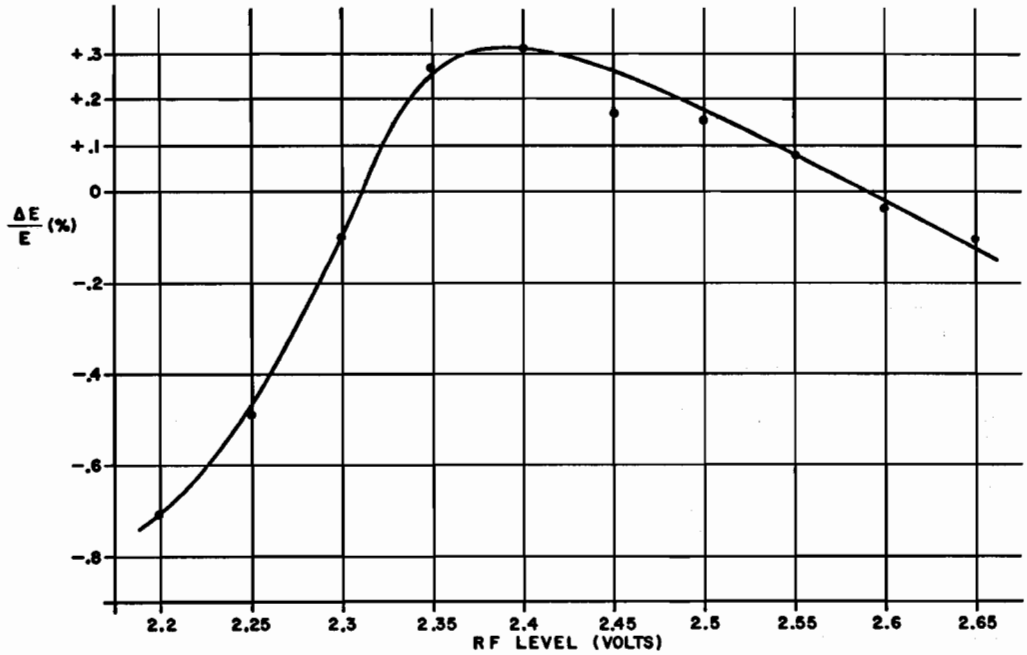

FIGURE 3 – VARIATION OF MEAN ENERGY WITH RF GRADIENT

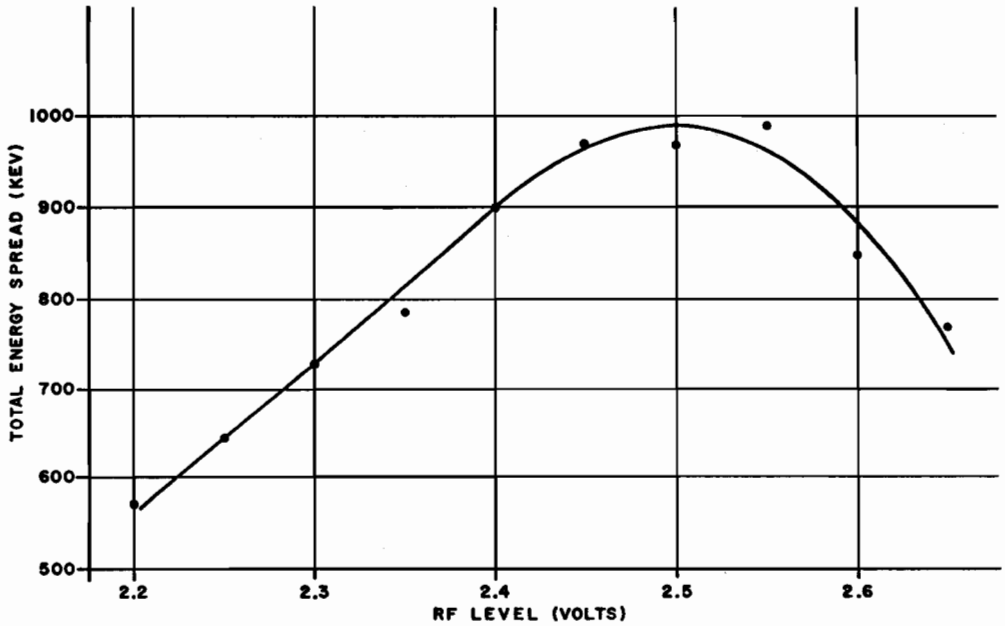

FIGURE 4 – VARIATION OF TOTAL ENERGY SPREAD WITH RF LEVEL

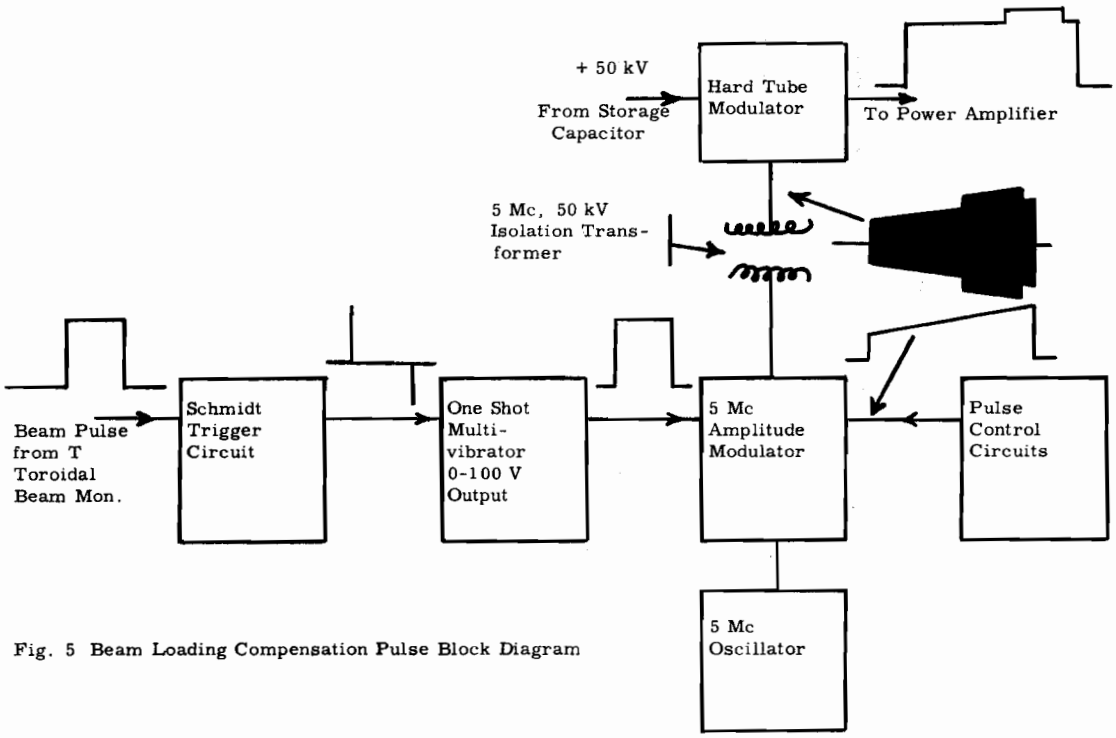

Fig. 5 Beam Loading Compensation Pulse Block Diagram

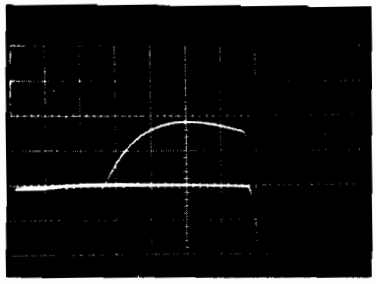

Fig. 6.1 No Beam through Cavity
No Compensation Pulse

Top Trace

Rectified cavity rf voltage.
.05 v/cm - zero suppressed.
(2.4 v is accel. gradient.)

Bottom Trace

Power amp. plate voltage.
10 kv/cm.
Sweep - 50 μ sec/cm.

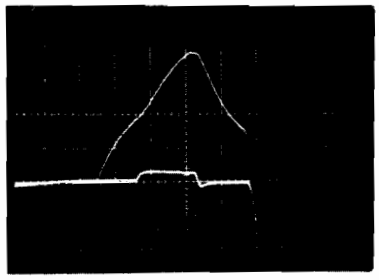

Fig. 6.2 No Beam through Cavity with
Compensation Pulse 3 kv

Top Trace

Rectified cavity rf voltage.
.05 v/cm - zero suppressed.
(2.4 v is accel. gradient.)

Bottom Trace

Power amp. plate voltage.
10 kv/cm.
Sweep - 50 μ sec/cm.

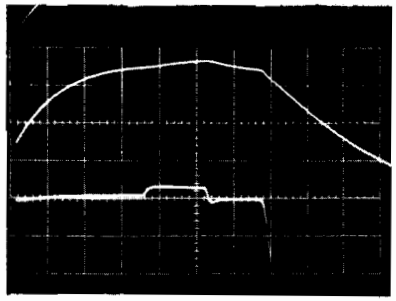

Top Trace

Rectified cavity rf without zero suppression.
1 v/cm.

Bottom Trace

Power amplifier plate voltage with 3 kv compensation.
10 kv/cm.
Sweep - 50 μ sec/cm.

Fig. 6.3 Same as 6.2, but without Expanded RF Scale

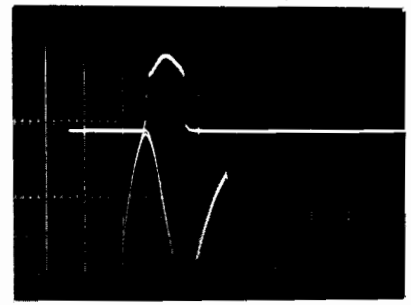

Top Trace

Beam pulse - 10 mA/cm.

Bottom Trace

Expanded rf voltage.
.05 v/cm.
Sweep - 100 μ sec/cm.

Fig. 6.5 Same as 6.4 with Expanded RF Voltage

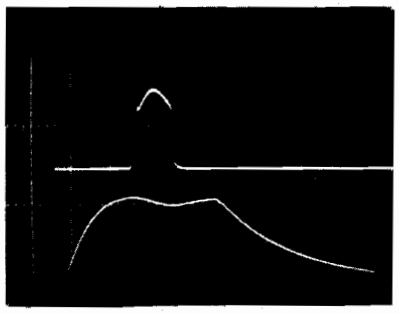

Top Trace

Beam pulse - 10 mA/cm.

Bottom Trace

Rectified cavity rf voltage.
1 v/cm.
Sweep - 100 μ sec/cm.

Fig. 6.4 20 mA Peak Beam Pulse RF Loading without Compensation

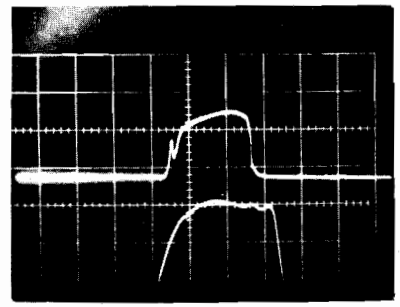

Top Trace

Beam pulse - 10 mA/cm.

Bottom Trace

Expanded rf voltage.
.05 v/cm.
Sweep - 50 μ sec/cm.

Fig. 6.6 Beam Pulse and Expanded RF Voltage with Compensation

(NOTE: Beam pulse shape changes from pictures 6.1 through 6.5, is not due to rf compensation but rather different injection conditions. 6.6 and subsequent pictures were taken on a different day.)

indicate that the cavity envelope is compensated everywhere, minor differences in the corrected waveform are due to the fact that they are not taken on the same pulse and there is some pulse-to-pulse variation when operating with the open loop system.

Group Velocity in the Linac Cavity

The group velocity, or rate of transfer of rf energy from the coupling loop to the extreme ends of the cavity, was observed in the following way. Using a dual beam scope, the output of the monitoring loops at the high and low energy ends of the cavity were compared at the time of initial cavity build-up with the rectified rf signal from an identical loop at the center of the cavity. (In this linac the rf feed loop is located at the center of the cavity.)

Figures 8.1 and 8.2 show the build-up of rf at the initial rise of the pulse. Figure 8.1 compares the center of the cavity (upper trace) with the low energy end. It is noted that the build-up of the field in the center of the cavity is very small until the rf energy has been propagated to the ends of the cavity where the initial build-up is much more rapid. The length of cavity between the two loops is 17.3 meters and the delay to start of build-up at the low energy loop is 9 μ seconds, giving a group velocity of 1.9 meters/μ second.

No explanation for the apparent initial negative slope of the center loop has been found; changing detectors, cables, etc., has not shown the reason to lie in the detection equipment.

Figure 8.2 compares similar waveforms at the high energy end. The length of cavity between loops is 15.7 meters and the delay of build-up to the high energy loop is 3 μ seconds. This results in a group velocity in this end of the cavity of 5.2 meters/μ second.

These observations raise the question of whether or not these numbers are characteristic of an unfilled cavity or if they do indeed remain the same in a cavity which is already excited. To observe this, the compensating pulse was applied to the power amplifier plate voltage after accelerating gradient in the cavity has been achieved and similar observations are then made of the changing rf level in the cavity due to the increased drive power. Figures 9.1 and 9.2 show the same loops as in Figs. 8.1 and 8.2 under excited cavity conditions using high gain, zero suppression plug-in units with delayed sweep.

These pictures indicate a delay of at most 2 μ seconds at the low energy end and about 1 μ second at the high energy end which would

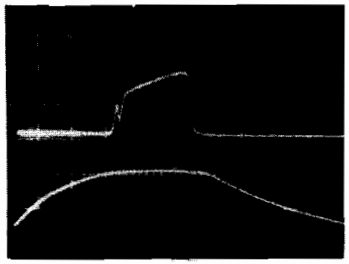

Top Trace

Beam pulse - 10 mA/cm.

Bottom Trace

Sweep - 50 μ sec/cm

Fig. 6.7. Same as 6.6, but without Expanded RF Waveform

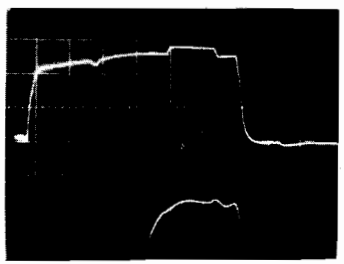

Top Trace

Power amplifier plate voltage with compensation pulse.
10 kv/cm.
Sweep - 50 μ sec/cm.

Bottom Trace

Rectified cavity rf voltage
.05 v/cm.

Fig. 6.8. RF Voltage Pulse and Plate Voltage Waveform with Compensation for Beam Loading

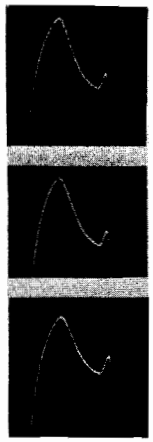

Low Energy End of cavity. Loop 9. 2%/cm, 50 μ sec/cm.

Center of cavity. Loop 42, 2%/cm. 50 μ sec/cm.

High Energy End of cavity. Loop 58, 2%/cm, 50 μ sec/cm.

Fig. 7.1. RF Envelope at 3 Cavity Positions Under Heavy Beam Loading Conditions

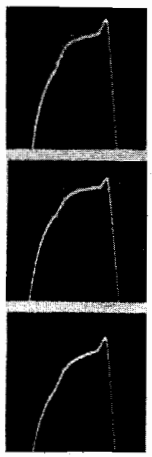

Low Energy End of cavity. Loop 9, 2%/cm, 50 μ sec/cm.

Center of cavity. Loop 42, 2%/cm, 50 μ sec/cm.

High Energy End of cavity. Loop 58, 2%/cm, 50 μ sec/cm.

Fig. 7.2. RF Envelope at 3 Cavity Positions With Open Loop Beam Loading Compensation

indicate group velocities which are greater by about a factor of 5 (8.6 meters/ μsecond) at the low energy end and 3 (15.7 meters/μ second) at the high energy end under the condition where the cavity is excited.

Linac Phase Acceptance

Phase acceptance measurements are made as the ratio of the peak beam current entering the bore of the first drift tube, as measured by a shielded toroid which measures only those particles which enter the bore of the first drift tube, to the peak beam current accelerated through the linac (as measured by either stopping the beam or by a toroid). The expected phased acceptance without buncher at the design synchronous phase angle and accelerating gradient is $\frac{3 \times 26^{o}}{360^{o}}$ or 22.6%. This phase acceptance, or transmission efficiency, is observed at an rf level of 2.35 volts (see Fig. 1) and the threshold for acceleration is 2.15 volts. Raising the rf level beyond 2.45 volts has not ever been observed to raise the transmission efficiency without buncher beyond 25%. One would expect it to continue to rise as the gradient is increased, provided appropriate compensation of quadrupole focusing fields were made. Efforts to achieve this have not been successful.

Measurements of phase acceptance as a function of preaccelerator injection energy have confirmed those measurements made at BNL.[4] Use of the first harmonic buncher has yielded transmission efficiencies as high at 65% (68% is the design expectation) but 55% to 60% is the usual day-to-day operating condition.

These phase acceptance measurements make no correction for proton percentage. In the ZGS system the two sets of triplet quadrupole matching lenses serve to separate such a large percentage of the molecular hydrogen and other heavy ions which are produced in the ion source that only a negligible amount of these ions are injected into the linac.

Conclusions

These observations show that very precise rf level control is necessary to meet the design requirements of a multicavity system to maintain the required injection energy as the beam progresses from section to section. In connection with the use of this particular linac as the injector for the ZGS, the data shows that by an appropriate programming of the rf level, it may be possible to use the changing energy characteristic to an advantage by providing an increasing injection energy with pulse length.

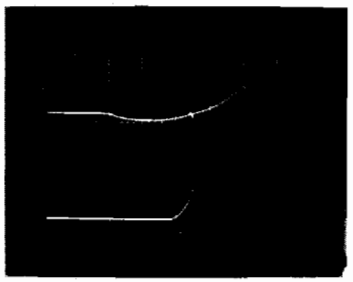

Top Trace

Loop 34 (center of cavity) time base 5 μ sec/cm.

Bottom Trace

Loop 1 (low energy end of cavity) time base 5 μ sec/cm.

Fig. 8.1 Initial Cavity Build Up at Center and Low Energy End of Cavity

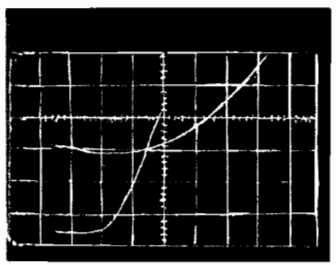

Top Trace

Loop 34 (center of cavity) time base 5 μ sec/cm.

Bottom Trace

Loop 64 (high energy end of cavity) time base 5 μ sec/cm.

Fig. 8.2 Initial Cavity Build Up at Center and High Energy End of Cavity

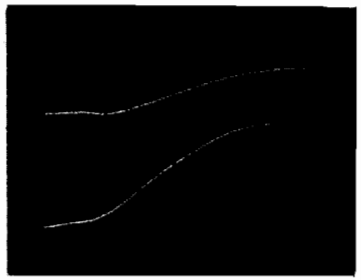

Top Trace

Loop 34 (center of cavity), 10 μ sec/cm.

Bottom Trace

Loop 1 (low energy end), 10 μ sec/cm.

Fig. 9.1 Change of Cavity RF Envelope Due to Spike on Power Amplifier Plate Voltage at Center and Low Energy End of Cavity

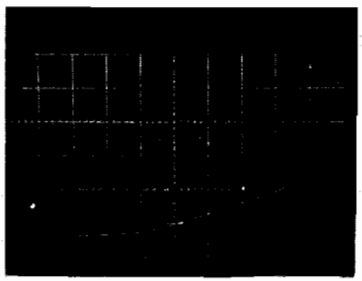

Top Trace

Loop 34 (center of cavity), 5 μ sec/cm.

Bottom Trace

Loop 64 (high energy), 5 μ sec/cm.

Fig. 9.2 As in Fig. 9.1 except comparing center and high energy end of the cavity.

Beam loading control with long pulse length at high beam current is certainly feasible but all of the engineering problems on our particular machine are not as yet solved.

SHAYLOR: I presume you are using a Tektronics 555 Scope for the double display work.

LIVDAHL: That is correct.

SHAYLOR: Until recently I was at Birmingham (England) and there we have very great difficulties with earth loops, due to certain peculiarities of our synchrotron. The 555 is particularly difficult to use in this respect since you can't selectively earth both signal inputs simultaneously unless you are using differential input amplifiers. So now one question is: Are you using differential input plug-ins? If not, what is the voltage you have at your probes so as to give us a feel for your pickup problems. Another question is, have you tried testing with the offending loop that goes negative short circuited, but still earthed in the normal way? I am looking for cross talk or trouble between the amplifiers. I am deeply suspicious of the negative-going curve, and if in fact the kick-off point is not where it starts to go negative but where it starts to go positive, then the time schedules of all these things are going to be significantly different.

LIVDAHL: In answer to your first question, differential plug-in units were not used. As a matter of fact, type Z, zero suppression plug-in units were used. I am not sure what type of units were used for the initial build-up.

CASTOR: They were the type Z used without the slide back.

LIVDAHL: In connection with the cabling to the loops, neither loop is grounded anywhere in the system. There is a teflon shield around the loop where it penetrates into the cavity so that there are no ac or grounding problems. It is a floating system all the way to the scope.

SHAYLOR: The type Z unit, the slide-back unit, has in fact a lot of hook diodes on its input, and I think that feeding a bit of the 200 Mc rf into it may produce some interesting effects.

ROWE: I would like to make a couple of remarks on this--an old user of Tektronics Scopes--I never noticed this particular difficulty with the type Z plug-in, but the CA plug-in has an obnoxious habit of ringing at very high frequency, far beyond the response of the scope proper. This seems

to be associated with the input attenuator and the first stage of the amplifier. And you can get some truly magnificent results under some condition; I was thinking along the same lines this gentleman was and I was wondering if maybe that might be the trouble. We got around some of these problems once by buying intentionally a poor scope.

LIVDAHL: Nevertheless, I believe that where you saw this negative-going trace was the point at which the pedestal was placed on the plate voltage waveform. For this reason I didn't worry about this because that was not what I was attempting to look at. The fact that the top trace came up at a delayed time relative to the lower trace and that we knew that this was synchronized within less than a microsecond with the pedestal on the waveform just did not seem like there was any reason to worry too much about the negative undershoot.

SHAYLOR: You were not trying to interpret anything from the point where the top trace rose above the base line?

LIVDAHL: That is correct. All of the numbers that I gave you were from this point to this point.

KEANE: I might have a different explanation on this same topic. I think I have seen the same thing and I think it is moding. We have scalloping on our waveform. I am going to talk about this next, but essentially because you have a variance from probe to probe, I feel it is not the scope itself but rather the existing modes in the tank.

PRIEST: If that is the case, what Shaylor suggested would prove it, would it not; if you short circuit the loop or rotate it so that it doesn't couple, this negative thing will disappear whether it is a mode or not, if it is an rf effect, it will disappear, but if it is some kind of an extraneous spurious effect, it won't disappear. At least it would be a check.

LEISS: We are probably pushing this a little bit too much. However, it is quite possible that it actually represents one of the things which we have calculated in the extreme transit behavior of the machine. This is the following. You probably have before your main pulse, for example through the grid drive, a small amount of rf in the cavity. Now when you turn the pulse on, you get some very interesting transients and phase oscillations. What you detect in your diode is the total field vector, which can have oscillations on it and these oscillations have actually been observed. I would suspect that this is actually a real phenomena that one can predict in the extreme transient behavior on this machine as you start filling it.

LIVDAHL: I just cannot believe this, Jim, because this is nothing but the rectified output of an rf envelope and this says that this loop has got to be taking power out of the cavity.

LEISS: Well, the point is that if you have a small amount of rf in there, which I suspect you do, because your grid drive is probably on before the plate voltage, then you have an offset zero and it really has not gone negative; it has just gone down closer to true zero.

LIVDAHL: Yes, the drive does come on about 10 microseconds before the plate pulse and I do not know that we have looked for this.

LEISS: There is another interesting example you can predict and which has been observed on a lot of machines. When you turn the rf off, instead of the detected rf signal going down it initially has a rise. This is again precisely the same thing. This is the phase oscillation that is induced when you make a sudden change in the rf level of the cavity.

JAMESON: I might comment on this last statement. We did some measurements on a cell iris-loaded structure in which we put in a square wave input and looked at the build-up with a sampling scope. We took the pictures and measured the 63% rise time, and these indicated that the structure filled from the back end first. We also saw the transient that you spoke of at pulse turn-off. This effect was greater the further away you got from the drive. Now, these measurements that we did were done at signal generator power levels and I have some reservations about the techniques as far as quantitative results are concerned. One thing was that we were coupling out more than we should have been with the measurement loops. However, the observed results were qualitatively exactly as predicted by the equivalent circuit theorem.

VAN STEENBERGEN: May I make one comment on the closing of the loop? Mr. Otis, together with John Keane, has worked on the rf stabilization loop at Brookhaven. So far he has succeeded in closing the loop and keeping a stable system for the cut-off frequencies up to 20 kc and loop gains up to 5. When he exceeded these limits of cut-off frequency and loop gain, he saw strong excitation of extramoding of the tank. We just could not work with a loop stabilization system which had a wider frequency band which means that if there were to be any corrections, they had to be of a very slow variety in our particularly long tank.

FEATHERSTONE: I think everybody here who is interested in rf systems would like a status report on life and performance of 7835's.

LIVDAHL: I knew that question would be asked, so I looked at the clock last week. At the present time our mode of operation is to start up at midnight on Wednesday night and run through the following Friday morning, a period of 25 shifts, with operation on the succeeding days as we need for maintenance, observation, development, etc. At this rate we build up a maximum of 500 hours per month, so we really do not have an awful lot of data on it yet. However, last November 21, we put a 7835 in the power amplifier; it has been in there since. The power amplifier has not been apart in that time and we have operated for 4,400 hours in that time and the tube had a little over a 100 hours on it before that. The other two tubes that we own have 2,000 and 2,200 hours on them. There is no reason to believe that any of the three tubes have changed characteristics in that time.

REFERENCES

1. Teng, L. C., "Achromatic Bending Magnet Systems", ANLAD 48, Argonne National Laboratory, April 8, 1958.

2. Abraham, J., et al., Operational Experience with the ZGS Injector, Argonne National Laboratory, July 9, 1963.

3. Livdahl, P. V., ZGS Injector Linac, Minutes of the Conference on Proton Linear Accelerators, Yale University, October 23, 1963, pp. 231-239.

4. Blewett, J. P., Phase Acceptance and Bunching in the AGS Linac, JPB-18, Brookhaven National Laboratory, March 27, 1963.

EXPERIMENTS ON RF FIELD PATTERNS IN THE BNL LINAC

J. T. Keane
Brookhaven National Laboratory

The major portion of this presentation will be concerned with the scallops observed on the rf probe patterns of the linac tank. Questions concerning this phenomena were brought up last year at Yale during Phil Livdahl's talk on the ZGS injector linac. It is contended that the cause of these scallops is due to excitation of higher order modal resonances. Figure 1 shows the scallops observed on the rf tank pattern. Note that this disturbance dies out as steady-state conditions are reached.

TANK VOLTAGE PATTERN WITH DISTORTION

TANK VOLTAGE PATTERN UN-DISTORTED

Figure 1

Before giving experimental proof of the cause of these scallops it seems appropriate to review the modes that can exist in a linac tank.

The wave types for a circular guide and their cutoff wavelengths are shown in Table I. It is seen that if as in a linac tank the diameter of the guide is adjusted for a cutoff frequency of 200 Mc in the TM_{01} mode (d = 1.15 meters), the TE_{11} mode is the only remaining mode above cutoff. As will be shown the frequency of resonance of the linac tank operating in the TE_{11} mode is 153 Mc. Since this is much lower than the excitation frequency of 200 Mc, this mode will provide little trouble.

Wave Type	Cutoff Wavelength	Cutoff Frequency if d = 1.15 m
TE_{11}	1.71 diameter (d)	153 Megacycles (Mc)
TM_{01}	1.31 d	200 Mc
TE_{01}	0.82 d	320 Mc
TE_{21}	1.03 d	255 Mc
TM_{11}	0.82 d	320 Mc

TABLE I. Modes in Circular Waveguides

NOTE: TM_{10} and TE_{10} modes impossible since zero tangential electric field at conducting walls requires 1 0.

For the TE_{11p} mode where p is the number of variations in the longitudinal direction the resonant wavelength is as shown below

$$\lambda = \frac{2}{\left[\left(\frac{p}{\ell}\right)^2 + \left(\frac{1}{1.706a}\right)^2\right]^{1/2}} \cong 2\,a\,(1.706) \text{ since } \ell \gg p$$

$$\therefore \lambda \cong 1.706\ d = 1.706\ (1.15) = 1.96 \text{ meters}$$

$\therefore$ all resonances = f $\cong$ 153 megacycles where ℓ = 33.5 meters, the length of present linac tank

a = radius of tank
d = diameter of tank .

Thus the majority of the TE_{11p} mode resonances for a long tank will be near 153 Mc.

The only remaining resonant modes needing consideration are the higher order TM_{01p} modes. Their resonant frequencies are given as follows.

$$\text{For } TM_{01p} = \frac{2}{\left[\left(\frac{p}{\ell}\right)^2 + \left(\frac{1}{1.306\ a}\right)^2\right]^{1/2}} \frac{1.5}{\left[1 + \left(\frac{0.75\ p}{33.5}\right)^2\right]^{1/2}}$$

where a = 0.575 meters
ℓ = 33.5 meters

$$\lambda \cong 1.5\left[1 - \left(\frac{0.75\,p}{\ell}\right)^2\right] = 1.5\left[1 - \left(\frac{0.75\ p}{33.5}\right)^2\right]$$

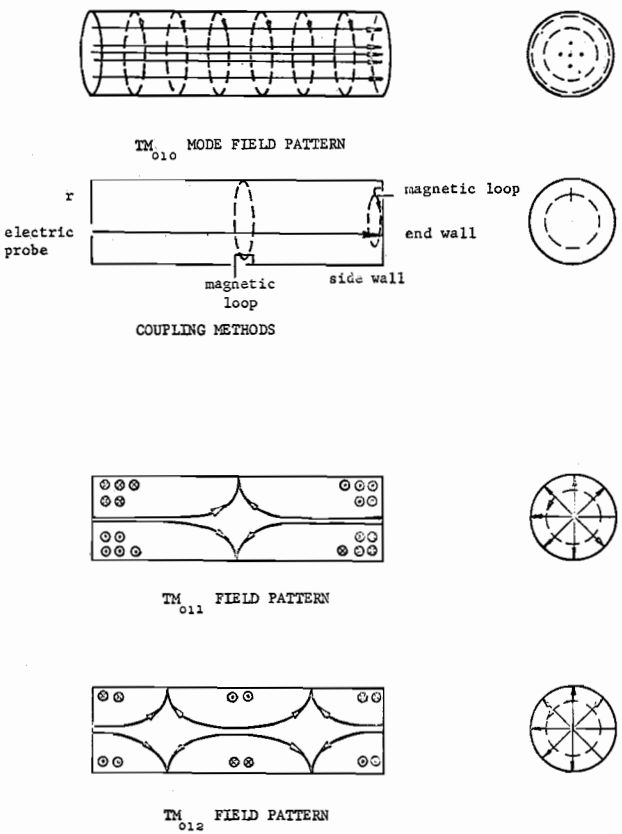
TM010 MODE FIELD PATTERN
r
electric probe
magnetic loop
end wall
side wall
magnetic loop
COUPLING METHODS
TM011 FIELD PATTERN
TM012 FIELD PATTERN

FIG. 2

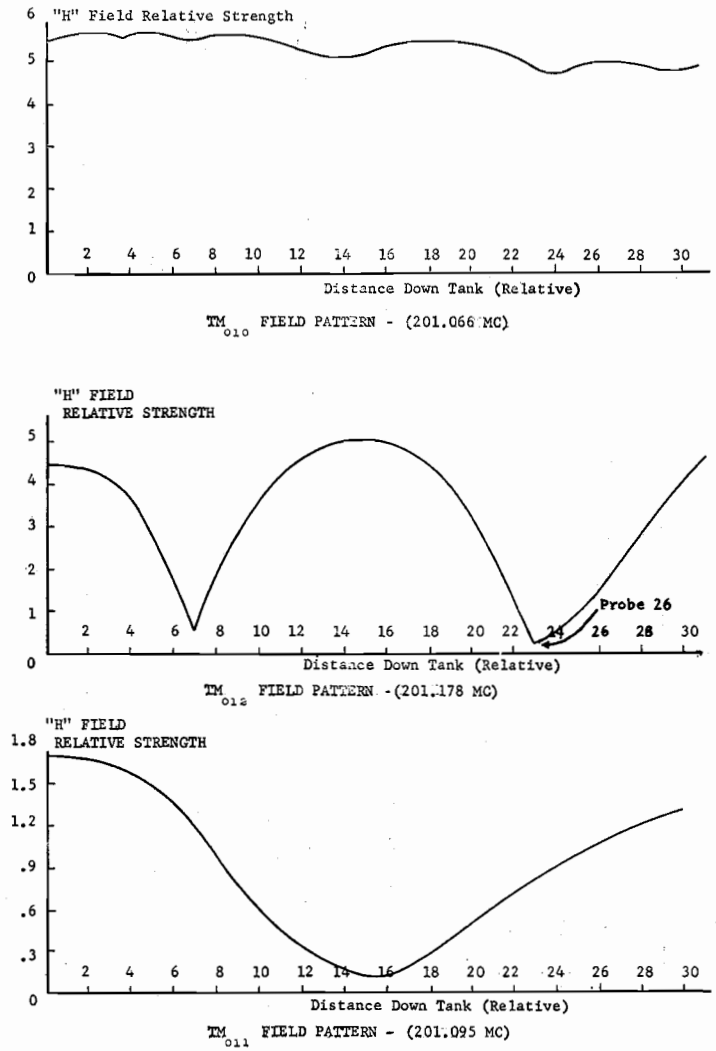
"H" Field Relative Strength
Distance Down Tank (Relative)
TM010 FIELD PATTERN - (201.066 MC)
"H" FIELD RELATIVE STRENGTH
Probe 26
Distance Down Tank (Relative)
TM012 FIELD PATTERN - (201.178 MC)
"H" FIELD RELATIVE STRENGTH
Distance Down Tank (Relative)
TM011 FIELD PATTERN - (201.095 MC)

FIG. 3

Note: Resonant wavelength for higher order modes approach that of TM_{010} as ℓ increases.

$$\Delta f = f \frac{\Delta\lambda}{\lambda} = 200 \times 10^6 \left(\frac{0.75\,p}{33.5}\right)^2 \left(\frac{1}{1.5}\right)$$ where Δf is cycles above the resonant frequency of TM_{010} mode.

$$\underline{\Delta f = p^2 \ (66.2 \times 10^3) \text{ cycles}}$$

TM_{011}: $p = 1 \therefore \Delta f = 66$ kilocycles (kc)
TM_{012}: $p = 2 \therefore \Delta f = 264$ kc
TM_{013}: $p = 3 \therefore \Delta f = 6$ megacycles (Mc)

It is thus seen that the TM_{011} and TM_{012} modes can be excited very readily in a linac structure. Of course, their strength will be highly dependent on the location of the coupling loop into the tank. If a single magnetic loop is used, its location can be unfavorable to either the TM_{012} mode or the TM_{011} mode but not both (see Fig. 2). Since BNL's loop provides magnetic coupling at a point centrally located along the tank length,

(a) weak coupling to the TM_{011} mode will result since this is a point of minimum "H" field for this mode;

(b) strong coupling to the TM_{012} mode will result since this is a point of maximum "H" field for this mode.

Having reviewed the possible modes that can exist in a linac tank we can get on with the results of modal studies on BNL's tank. The capability of a linac structure to support a TM_{011} and TM_{012} mode was vertified by changing the excitation frequency and looking for the characteristic modal configurations of the TM_{011} and TM_{012} waves along the length of the tank. These patterns were ascertained by use of 34 calibration loops located along the tank length. Essentially they measure the magnetic field strengths at the tank walls.

The results of the test are given in Table II below.

Mode	Frequency	Maximum Observed Field Strength Relative Reading	f	Calc. f
TM_{010}	201.066 Mc	5.7	0	0
TM_{011}	201.095 Mc	5	29 kc	66 kc
TM_{012}	201.178 Mc	1.65	112 kc	264 kc

TABLE II. Observed Modes in BNL Linac (see Fig. 2)

Since this linac is excited by a single magnetic loop centrally located, the results agree with theory. As was expected the field strength was strong for the TM_{012} mode but weak for the TM_{011} mode. It is noted, however, that the resonant frequencies of the TM_{011} and TM_{012} modes were closer to that of the TM_{010} mode than expected. This apparent deviation from theoretical findings is easily explained. The existence of varying length drift tubes and ball tuners should alter results expected from an unperturbed cylindrical guide analysis.

Figure 3 shows plots of the relative "H" field steady-state strength along the length of the tank for the normal TM_{010}, the TM_{012} and TM_{011} modes. Note that as expected the "H" field for the TM_{012} mode has a minimum at Probe 10 and Probe 26, also that the field strength of the TM_{011} mode is smaller than that of the other two.

Essentially the initial statement that the scallops on the rf patterns were due to moding is proved by the data just presented.

With the tank excited at its normal frequency the following observations were made.

1. At Probes 10 and 26 where the tangential magnetic field of the TM_{012} field pattern was minimum, the scalloping on the TM_{010} excited rf pattern was not present.

2. The relative magnitude of the scalloping on the TM_{010} rf pattern increased along the tank length in the same manner as the magnetic field intensity of the TM_{012} pattern.

3. The frequency of the scallops agreed closely to the difference frequency between the TM_{010} and TM_{012} resonances.

4. As the steady-state tank response to TM_{010} mode excitation is reached, the scalloping dies out.

From the above statements it is concluded that during the build-up time of the tank the TM_{012} resonant mode is excited. Due to two different frequency sources present the measuring loops detect a modulating signal whose frequency is equal to the difference frequency of the two sources ($TM_{010} + TM_{012}$).

It is well known that the Fourier power spectrum of an rf pulsed signal has frequency components around the center frequency. These frequency components serve as the source of the TM_{012} excitation during the build-up period and tend to die out once steady-state conditions are reached. Since BNL's method of coupling is favorable to the TM_{012} mode, the scallops are observed.

At this point we took a closer look at the probe patterns that did not have the noticeable scallops, namely Probes 10 and 26. It was noted that there was a slight modulation at 30 kc which indicated that the TM_{011} mode was also excited but to a much lesser extent than the TM_{012}.

Since this time, A. Otis of BNL has done work on an rf level stabilization loop. In his first attempts at closing a loop he had oscillations. Again the frequency of oscillation was the difference frequency of the (TM_{011} and TM_{012}) modes away from the TM_{010} mode.

Now that the existence of these modes has been verified, what does it mean? Certainly it will prove cumbersome to a closed loop system being controlled by a linac tank signal. Again since the tank is more susceptible to these undesired oscillations during transient periods, what effect will it have on beam compensation schemes? Both these modes have radial "E" field components that would prove detrimental to the beam. The big question which unfortunately I cannot answer is how strong can these defocusing fields be when 50 or 100 ma beams are passing through linac tanks? Hopefully they are weak enough to neglect. One way to lessen the effects of these resonances would be to keep the tank length down. Previously I showed a resonance equation that indicated that the frequency of these undesired oscillations moved further away from the TM_{010} mode resonance as tank length decreased. This would tend to decrease the power present in the side bands.

The scalloping just described is always present on BNL linac probes. We are blessed with another type of scalloping, however, that acts something like a phantom. It crops up suddenly and leaves just as suddenly. Fortunately it only stays for very short periods. The magnitude of these scallops are much larger than the ones just described. The scalloping frequency and distribution along the tank length indicates it is a TM_{011} modal excitation. Apparently it is caused by particles coming from the

Cockcroft-Walton generator. This is concluded by the fact that it can normally be eliminated by

1. Turning on beam chopper, or
2. Closing the valve at the linac tank entrance, or
3. Putting in a flag between the Cockcroft-Walton and linac tank.

We have done studies during one of its short stays recently and found that

1. It is independent of the buncher--the rf feedback loop from the tank was taken off and it still existed.

2. It is very sensitive to the Cockcroft-Walton voltage. It disappeared when the voltage is below 737 kV.

3. It is relatively insensitive to the linac tank rf power level. When the power is brought well below accelerating levels, it is unaffected--but if the level is brought above tank level, its magnitude starts to decline.

4. It is very sensitive to gas pressure. The tank is more prone to these scallops when the gas pressure is decreased.

Unfortunately this is as much as we know about these scallops and we will have to wait for its further reappearance before more data is accumulated.

DICKSON: On our closed loop stabilizer, I did not say that we had never seen scallops. We do see scallops at times but we can get rid of them and there seem to be two things that affect them. One is that if one tunes the tank so that it appears to be exactly on tune, I think this gives scalloping. If one tunes slightly off maximum, then the scalloping can be reduced to practically zero. The other thing that affects the scalloping is the length of coaxial line between the final amplifier and the tank. If one changes this line length, then the impedance presented to the tank by the amplifier changes and this has some effect on the scalloping as well. So we play with these two things and can get rid of the scalloping. We had not related the scalloping to the modes of the cavity in the way you have.

KEANE: We tried to move the resonant frequency of the higher modes. They are quite sensitive to ball tuners, etc. Anything in the line will tend to change the frequency to a greater extent than it changes the normal frequency.

TAYLOR: Can I just confuse the issue? When they are on tune, we see no scalloping and when we move off, we see a beating which corresponds to the beating between the drive frequency and the tank resonant frequency.

WADDELL: I would like to merely comment that this modal business, of course, was something that is seen in the original machine. That is, we have the original Alvarez accelerator and it differs from all the others that you are talking about in that it is a self-excited oscillator, and so during the tune-up procedure the operator has to essentially adjust the pre-exciters so that one is on the proper mode. It is possible to tune up the machine on the wrong mode and probably Earl White could speak on this, but what we do is instead of presenting a rectified waveform in the control room, we actually present the rf and then it is quite simple for the operator to look at this pattern and to simply tell what modes are being generated as the pre-exciter is being tuned.

KEANE: I would like to make one comment on this--these scallopings are very slight, small in amplitude; indeed if you detune, I can take my whole pattern and I have gigantic scallopings, but these scallopings do not attenuate. Essentially what I am saying is that these scallopings are more pronounced during the transient time and they die out once steady-state conditions are reached. Definitely if you detune, you get off frequency and you will get more violent scallopings.

JAMESON: Nagle and Knapp have pointed out the equivalent circuit theory that we are fond of at Los Alamos. I have extended this theory to a transient analysis, and I am going to talk about it tomorrow. It points out in a rigorous fashion how these scallops occur. It is the beating between the drive and the modes in the pass band, all of which are excited during transients. This beating dies out in the steady state. I have some runs also that show the behavior that you get when you drive off frequency where you get large transient bumps and then a settling back down to a steady state on which there are regular "scallops" produced by beating between the drive and the nearest mode frequency. It all comes out quite nicely in terms of the equivalent circuit theory.

BLEWETT: Something that bothers me about these higher order modes is the fact that,as John showed in his pictures, they all have radial components. Why aren't these shorted out by the drift tube stem? Our drift tube has got two stems at right angles to each other. I was wondering what sort of mode pattern you get if you had say four drift tube stems going out in all directions, or what these actual mode patterns look like in the present case.

KEANE: I will note one thing. The Q of the TM_{012} seemed to be much lower than that of the normal tank. The rise time looked to be in the order of 120 microseconds in the pattern.

LAMB: We did an experiment some years ago which is relevant to this problem. It was cleaner because there weren't any drift tubes--it was a cylindrical tank--it was resonant at around 200 Mc and into this tank we introduced the burst of electrons. The tank was surrounded by a solenoid and these electrons were just shot into the tank, and they had many Fourier components in their front. We did not detect any frequencies lower than the fundamental frequency, but we detected essentially every frequency from there on up and of course it varied where the probe was located as he pointed out. There were different ones in different places--TE's, TM's, and very high order modes. In order to suppress these modes so we could carry on with our experiments and see some electrical signal in this tank, we did the things that John just suggested. We tried to short certain modes out by putting conductors across the tank, and this would deQ this particular one, but the conductors would then look like an end wall to some other mode.

PERRY: I think there is no question that these modes do exist. In the tune-up stage of our machine we excited quite a number of these with a lock-on oscillator.

AUTOMATIC CONTROL AND STABILIZATION OF THE ORSAY LINAC

P. Brunet, L. Burnod and L. Lheritier
Ecole Normale Superieure - Orsay, France

Before speaking about automatic control, I would like to show briefly the present status of the Orsay linac. In this initial design the electron linac itself was built by the CSF Company. Since the end of 1961, the laboratory of the Orsay linac has the machine in charge for operating and improvements.

There are now four experimental areas (Fig. 1) available for physics experiments: one at 250 MeV in use since 1960, one at 500 MeV and one at 1 GeV in use since January, 1962, and the last one at 1.3 GeV is just finished now, including the deflecting system. Another experimental area is ready to receive the 500 MeV electron-positron storage ring, but the storage ring itself will be ready in 1965. The positrons will be extracted from a radiator located at the 700 MeV electron energy level and then accelerated from a few MeV to 250 MeV before injection. The electrons will be accelerated from another gun by the last part of the linac and injected in the ring at the same point as the positrons are.

We already accelerated a positron beam extracted at 200 MeV electron energy level. For a 700 MeV positron beam, the ratio of the positron intensity in 3% energy spread to the electron intensity on the target is 10^{-4}.

Now there is another proposal to extend the electron energy from 1.3 to 2.8 GeV by doubling the length of the machine, and to increase the duty factor by a factor of 3, from 50 pps to 150 pps. In this case, the new part of the machine will be built at the front of the present linac, the shielding of the 1.3 GeV experimental area being sufficient for a 3 GeV beam.

Operating a multisection electron linac for physics experiments requires a high stability for both beam current and energy.

It is quite easy to obtain 50% of the beam current in a 1% energy spread, if the transient beam loading is compensated for by early injection or changing the modulator timing.

However, it is difficult to maintain these adjustments over a long period of time, and in addition, the setup time is long unless automatic controls are incorporated.

The influence of variations in the main machine parameters such as High Voltage, Frequency, Temperature, etc., are well known.

It is my intention here to speak only about some of the systems which have improved the Orsay accelerator and some systems which will be incorporated in the machine extension from 1.3 to 2.8 GeV.

I. Klystrons High Voltage

In the initial design, the klystrons and modulators were supplied from a single ac power supply controlled by an induction regulator with a stability of $\pm$ 1%. Such a long term stability may be sufficient if the operator can control the long term energy fluctuation. However, with a short term stability of the same magnitude, every fluctuation in the power lines is transmitted to the klystron high voltage resulting in beam energy variations of the same order. With a narrow energy spectrum and energy defining slits, excessive variations in the analyzed beam current result. Furthermore, for the induction regulator which was used, the response to the power lines transients is very slow, of the order of one second, which means that the short term stability was much worse than 1%.

In order to overcome this short term instability, we are now using a motor generator set with an ac voltage regulator of $\pm$ 1%. We now get a short term stability better than 0.1% due to the large inertia of the set. Such a system can keep approximately 2×10^{11} electrons/pulse within a 2% energy spread for several hours with current variations less than $\pm$ 5%. The long term stability can be further improved by controlling the alternator output not from the ac output voltage but rather from the charging voltage of the pulse-forming network. This means we can also adjust the klystrons high voltage by the inductor of the alternator.

II. Phasing

An automatic phasing system is already installed on five sections, or 300 MeV, of the present accelerator and it is yet working but it is under test too.

The rf phase of the section input signal is compared to the beam phase obtained from a low Q cavity excited by the beam (Fig. 2). The electronic length of the rf comparison circuit is set up so that a null on the phase detector is obtained for the optimum rf phase (Fig. 3). This optimum rf phase is determined by means of a beam energy measurement and fixed by a phase shifter. The phase detector is a magic T with two linear rf diodes (or one diode and a phase wobbling system). The two diode voltages are stretched to a dc voltage and compared in a

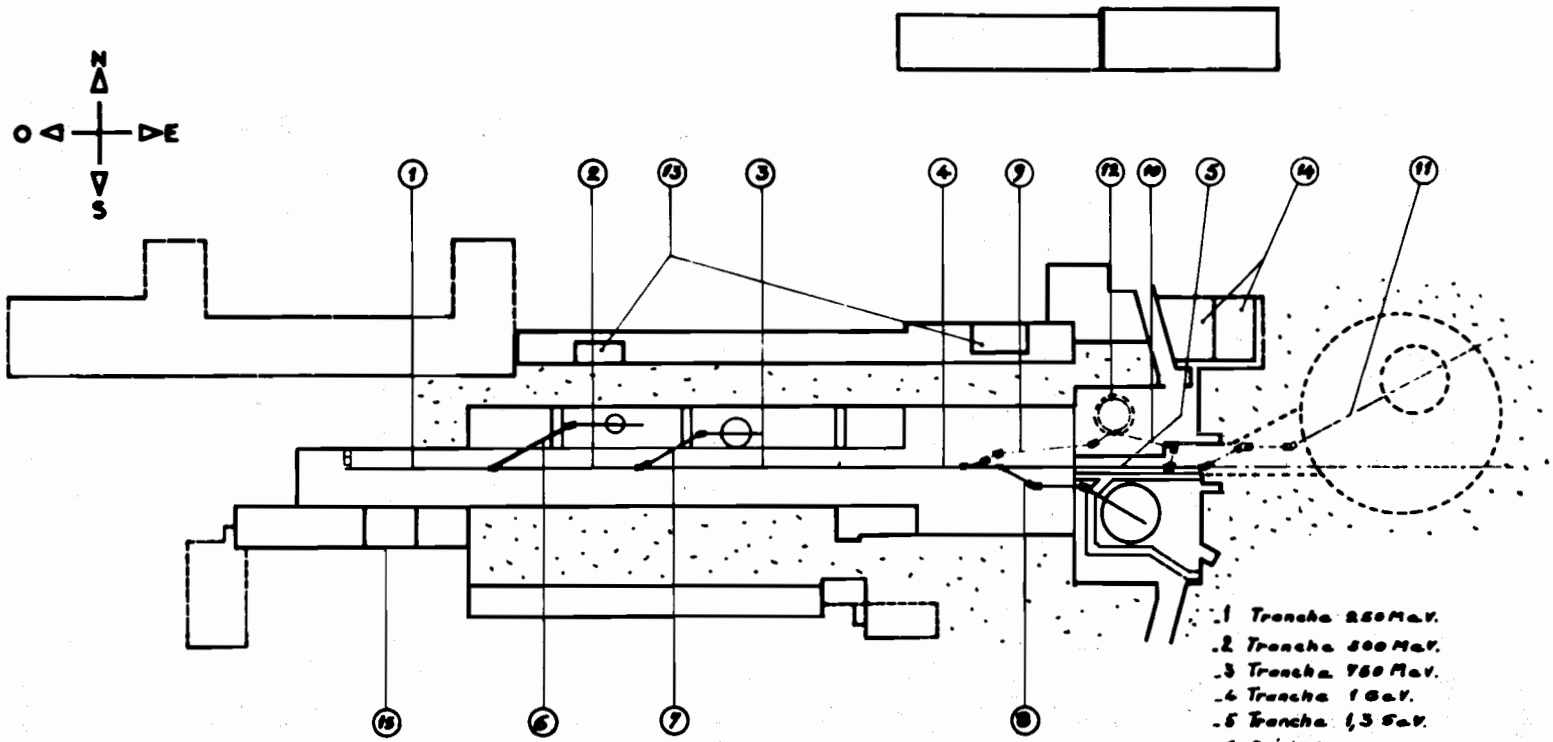

.1 Tranche 250 MeV.
.2 Tranche 500 MeV.
.3 Tranche 750 MeV.
.4 Tranche 1 GeV.
.5 Tranche 1,3 GeV.
.6 Déviation et salle 250 MeV.
.7 Déviation et salle 500 MeV.
.8 Déviation et salle 1 GeV Sud.
.9 Déviation Positrons. Anneau.
.10 Déviation électrons anneau.
.11 Déviation et salle de cible 1,3 GeV.
.12 Anneau.
.13 Salles de contrôles Physiciens.
14 Salles de contrôles Anneau et 1,3 GeV.
15 Salle de contrôle accélérateur.

Note

Les parties dessinées en pointillés ne sont pas encore construites

terre de protection

Fig: 1

differential dc amplifier which controls the phase of the rf klystron input. A transmission cavity in one arm of the rf comparison circuit, temperature locked to the section, compensates for small frequency and temperature variations.

With such a system we can control the phase within $\pm 3^{o}$ with a range of beam intensity from 20 to 80 mA and a 3 db klystron power range (10 to 20 MW). However, we do not know yet the behavior of the system over a long period of time, let us say for more than one month, without a new energy calibration.

It seems feasible that such a long term stability can be obtained with the following improvements.

(a) Increasing the phase stability of the rf comparison system by choosing rigid and short transmission lines.
(b) Broadening the range of operation to a 10 to 1 variation in the beam current and 6 db for the klystron power.
(c) Achieving a more simple and accurate phase calibration for example, by adjusting the set: Section + Cavity + Rf Comparison Circuit in a separate room set up for this purpose.

The disadvantages of the system are:

(a) A complete system is required yet for each section (cavities, rf comparison circuit, electronic).
(b) We must trust the phase stability of the rf phase comparison system.

The advantages are:

(a) It does not require a special accelerator triggering system nor sections with output couplers, i.e., it can be adapted on the present machine.
(b) It is a continuously operating system.

Assuming the rf driver frequency is stable, there are still two other control systems which must be incorporated if stable and reliable operation of the linac is to be obtained. These are temperature and beam position controls.

III. Temperature

The rf power level in each section is controlled by means of the klystron high voltage and is set to give the optimum performance of

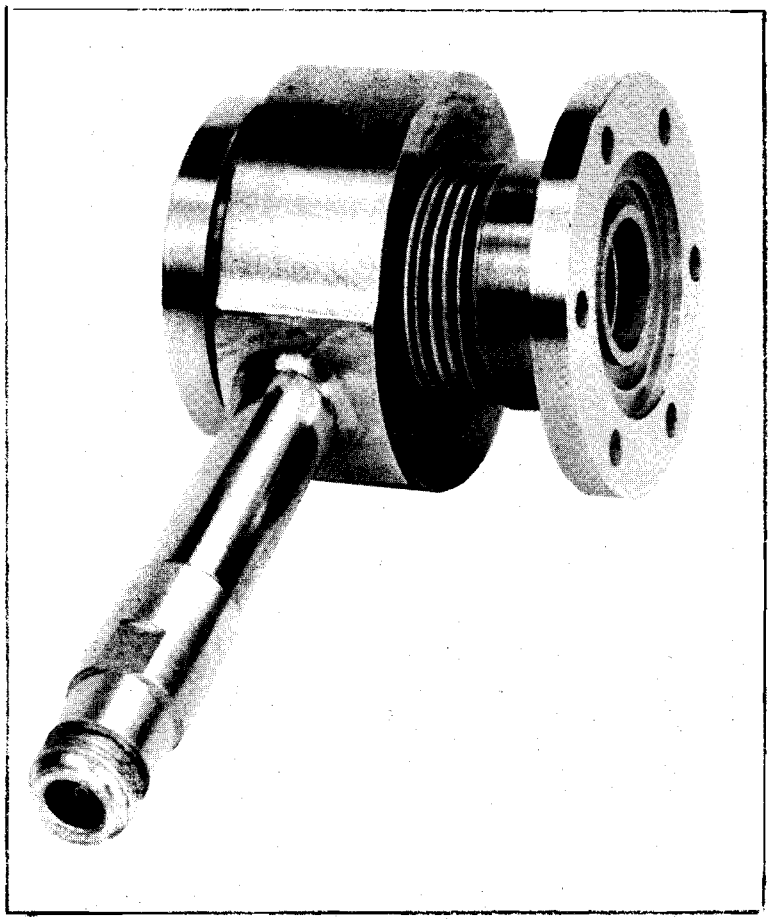

Fig. 2

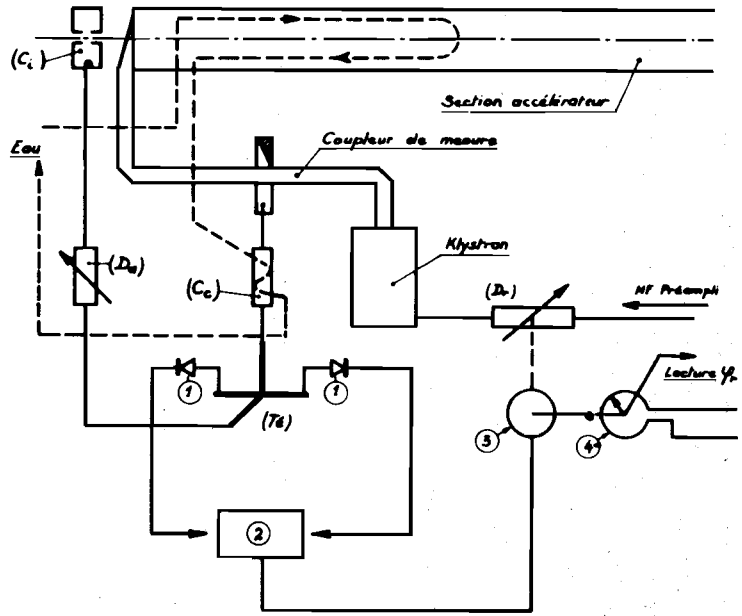

① Détecteur HF
② Circuit d'asservissement
③ Moteur de commande de (D_r)
④ Potentiomètre de lecture

Réglage automatique des phases hyperfréquence
Schéma synoptique

Fig. 3

section and klystron. Preliminary measurements on the heat transfer between the sections and the water indicated that the temperature gradient between the copper and water is not independent of the power. This means that the cooling of each section has to be independently adjusted. This can be achieved by controlling the rf phase between the input and output of the section.

This comparison can be seen to be extremely sensitive, since

$$\Delta\phi = \alpha\omega\tau \cdot \Delta\theta$$

where

α is the coefficient of linear expansion of copper
ω is 2π x frequency
τ is the filling time of the section
$\Delta\theta$ is the temperature change

For example, with

$\omega = 2\pi \times 3 \times 10^9$
$\tau = 10^{-6}$ seconds
$\alpha = 1.6 \times 10^{-5}$

$$\underline{\Delta\phi = 17 \text{ degrees/degree C.}}$$

IV. Beam Position Control

For a high power beam, it is very important to keep the beam on the axis. A steering system which is really independent of energy and stray magnetic fields appears difficult to build. However, for a single beam operation it should be possible to use an error signal derived from a beam position monitor to control steering dipoles and keep the beam on axis; after phasing a given sector, the beam can be steered and the position monitored. This sequence of events is then carried out on each successive sector.

Despite the multiplicity of parameters affecting the beam dynamics, it should be possible to design in such a way an automatic beam steering system.

In this stage we still prefer to put local control loops, better than a central computer, and to increase the stability of the components.

In conclusion, at Orsay the present philosophy is always to manually control the accelerator with the exception of the automatic systems which I have described.

BLEWETT: Could you give an estimate of the ultimate that you could achieve in the control of phase?

BURNOD: With the electronics which we have now, because we use a mechanical phase shifter, we think that $\pm 3^{\circ}$ is a limit we cannot improve. If we use a ferrite phase shifter instead of a mechanical one, we can have a continuous variation of the phase and a better short-term stability, but of course using such a ferrite device we will lose in long-term stability due to the ferrite and its power supply.

JAMESON: What kind of short-term phase stability are you talking about?

BURNOD: Oh, the phase stability is now $\pm 3^{\circ}$ over several hours. There is no problem for the short-term stability using a mechanical phase shifter.

FEATHERSTONE: Must you control the temperature of the transmission lines which bring the phase information to your control devices?

BURNOD: It is not done yet, but we must do it.

PROGRESS IN HIGH INTENSITY ION SOURCE AND ACCELERATOR COLUMN DEVELOPMENT

A. van Steenbergen
Brookhaven National Laboratory

Recent work on ion sources has shown a gradual increase of proton beam intensities obtainable from preinjector systems. In general, together with an increase in beam intensity an increase of the beam emittance was observed. Up to the space-charge limit in the BNL AGS, this will become most likely the determining factor in AGS beam intensity. This will be especially so when multiple turn injection will be used at the AGS, which is scheduled to be completed during the next month.

Further, preinjector intensities for the proposed BNL 500 MeV linac injector will be of the order of 500 mA in order to obtain linac beam intensities of at least 100 mA.

Only recently have ion sources been developed capable of total beam outputs of this order of magnitude and being suitable at the same time for use in conjunction with particle accelerators because of emittance characteristics. For completeness sake a short enumeration of these sources follows:

1) PIG Ion Source. Here a plasma is obtained by means of a gas discharge in a simple two electrode structure. Secondary electron emission to sustain the discharge is obtained by means of ion impact on the cold cathodes. Electron oscillation between the two cathodes is maintained for high ionization efficiency by means of the anode-cathode electrical field and an axial magnetic field.

2) Rf Ion Source. An electrodeless ("magnetically" excited) discharge, by means of a radio-frequency field is obtained in a ceramic or pyrex source "pot." An extra electrode in the plasma chamber is used to establish a field in a ceramic channel for ion extraction from the plasma boundary located within the source pot.

3) Duoplasmatron Source. A hot cathode (emission layer coated cathode or a tungsten cathode) is used for the production of electrons for gas ionization in a three-electrode structure. With a conical geometry of the extra electrode between cathode and anode some plasma compression is obtained. Further compaction, between the extra electrode and the anode is accomplished by means of magnetic mirror fields around the

interspace of these electrodes. For higher output currents, a specially shaped aperture button makes it possible to obtain ion emission from a larger area than the source aperture opening (small plasma cup).

4) Lamb-Lofgren Source.* This source is a version of the "magnetic" ion source, i.e., a hot cathode discharge type source with plasma concentration by means of an axial magnetic field. Here, instead of a single aperture hole, a multiple of apertures is used to let the plasma expand in a large cylindrical plasma expansion cup. With the extraction field a concave plasma sheath is formed within the relatively large plasma expansion cup.

5) "Modified" Duoplasmatron Ion Source (Solnyshkov, et al). A large plasma expansion cup is attached to the basic duoplasmatron source and ion extraction takes place from a shaped plasma boundary sheath.

6) "Modified" PIG Source (Gabovich, et al). This is the basic PIG source with hot cathode and large plasma expansion cup.

In order to establish some criteria by which to compare these various ion sources, it is useful to define source brightness and related beam emittance again. The momentum normalized beam emittance, as related to the two-dimensional phase space projection is given by,

$$v = \beta\gamma \frac{\iint F(x, \alpha_x)\, dx\, d\alpha_x}{\pi} = \beta\gamma E$$

where v is the emittance invariant and $F(x, \alpha_x)$ represents the two-dimensional transverse phase space boundary for a proton beam, determined at a particular energy.

The source "brightness" may now be defined as:

$$B = \frac{I}{\pi^2 v^2},$$

---

*Ion extraction from a large plasma boundary and plasma boundary shaping ("plasma boundary focusing") by means of grids or extraction fields, as applied in the "modified" duoplasmatron source and "modified" PIG source were first incorporated in this particular ion source design.

which specifies the particles per unit time density in four-dimensional phase space, assuming a simplified E, t distribution.[1,2] This definition is identical to the statement that the source brightness is the particle flux (current density) per unit solid angle.

Referring now to the conventional duoplasmatron source, the rf source and the PIG source, these sources showed generally the behavior that the emittance increased linearly with the output beam current. This was observed at BNL for the PIG source and conventional duoplasmatron source and similarly at CERN for the rf source. This behavior is expressed as:

$$v = \frac{I}{\pi \delta}$$

and consequently,

$$B = \frac{\delta^2}{I} ,$$

with δ a constant.*

It was rather disturbing to observe that the four-dimensional phase space density decreased with extraction of higher beam intensities from the ion source. Regarding this, it is useful to consider the optimum expected ion source emittance versus output beam intensity.

The minimum emittance is determined by the transverse velocity components existing at the plasma boundary from which beam extraction takes place. The magnitude of the transverse components is determined by the plasma temperature.

Taking the simplest case of a plane plasma boundary and homogeneous particle density filling of the plasma of N ions per unit volume, then for ion extraction from an area a^2 one finds for the emittance

$$v = \frac{2}{\pi} \beta \gamma \, a \, p_x/p_z = \frac{2 \beta \gamma \, a \, m_o \bar{v}_x}{\pi \beta \gamma \, m_o c} = \frac{2 \, a \, \bar{v}_x}{\pi c} .$$

Using a simple cut-off of the Maxwell-Boltzmann momentum distribution and assuming plasma equilibrium, i.e., $T_i \cong T_e$, one finds[3]

---

*The brightness as defined here refers to four-dimensional phase space only, the time structure of the beam may change the δ and B values.

$$\bar{\nu}_x \leq \left(\frac{k\,T_i}{m_o}\right)^{1/2} .$$

Here $\bar{\nu}_x$ is the x component of the mean velocity of the ions near the plasma boundary.

Further, the total beam extracted from the plasma boundary for a space-charge limited beam may be obtained from the diffusion equation:

$$I = a^2\,Ne\,\bar{\nu}_z$$

or similarly

$$a = I^{1/2}\left[N^{1/2}\,e^{1/2}\left(\frac{k\,T_i}{m_o}\right)^{1/4}\right]^{-1} .$$

Actually, because of limitations in beam extraction due to space-charge effects, a more practical expression for a would be given by Langmuir's equation:

$$a = I^{1/2}\left[\frac{4\,\epsilon_o}{9}\;\frac{2\,e}{m_o}\;\frac{V_{extr.}{}^{3/2}}{g^2}\right]^{-1/2} .$$

Comparison of the two expressions indicates that a practical upper limit exists for N. For higher values of N and a given extraction field and geometry the plasma boundary takes on such a shape that unacceptable optical conditions result. Therefore, for any practical system, the maximum value of N may not be determined by the ion source capabilities only, but, especially with recent ion source developments, by limitations in $(V_{extr.}{}^{3/2}/g^2)$.

For the present argument the first expression for a will be used. Substitution of a and $\bar{\nu}_x$ yields:

$$v = \left(\frac{1}{\pi\,B_o{}^{1/2}}\right)\,I^{1/2}$$

with B_o a constant,

$$\left[\text{or } v = \frac{2\,a}{\pi}\left(\frac{k\,T_i}{m_o c^2}\right)^{1/2}\right]$$

and by definition $B = \frac{I}{\pi^2 v^2}$, therefore

$$B = B_o = \frac{N e c}{4 \left(\frac{k T_i}{m_o c^2} \right)^{1/2}} .$$

Contrary to experimentally observed behavior, theoretically the source brightness would be independent of output current, as it should be.

The foregoing approach may be enforced by substituting some practical values for T and N in the expression for B_o. An expanded plasma from a pulsed high-intensity PIG source with hot cathode was studied by Gabovich et al.[4] Here, a plasma expansion system, similar to that used by A. I. Solnyshkov[5] for the duoplasmatron ion source, was used. Typical values for N and T in the expanded plasma are $10^{12}/cm^3$ and 10^5 °K, respectively. This substituted yiel ds for B_o:

$$B_o = 1.2 \times 10^{10} \frac{ma}{cm^2\text{-}rad^2} .$$

This value is indicat ed in Fig. 1. Also given here are values for B and v derived from Solnyshkov's results obtained with a modified duoplasmatron source. Through these points lines have been drawn in the log-log emittance current plot of "suggested" output current dependence of the modified duoplasmatron source. At the present time this is only supported by the assumption that with extraction from a relatively large plasma boundary area the theoretical expected current dependence of v and B may be approached.

The B_o value as calculated is of the same order of magnitude as the approximate B value obtained from Solnyshkov's experimental results.

The experimental observed behavior of v and B as a function of I for the conventional duoplasmatron source, rf source and PIG source is also given in this figure. Further the range of some recent results for v and B with the modified duoplasmatron source as obtained by B. Vosicki at CERN and L. Oleksiuk at BNL are also indicated. These results will be discussed in detail by L. Oleksiuk.

The foregoing approach suggests immediately that it is desirable to keep the plasma temperature low in order to obtain high B_o values and low v values. It also explains the reason for the encouraging results obtained with the sources with large plasma expansion.

419

$$V = \beta\gamma \frac{\text{Area } F(x, \alpha_x)}{\pi} = \beta\gamma E \; ; \; B = \frac{B(p_z^2)}{\beta^2 \gamma^2} \; ; \text{ for } \delta \text{ definition, see text.}$$

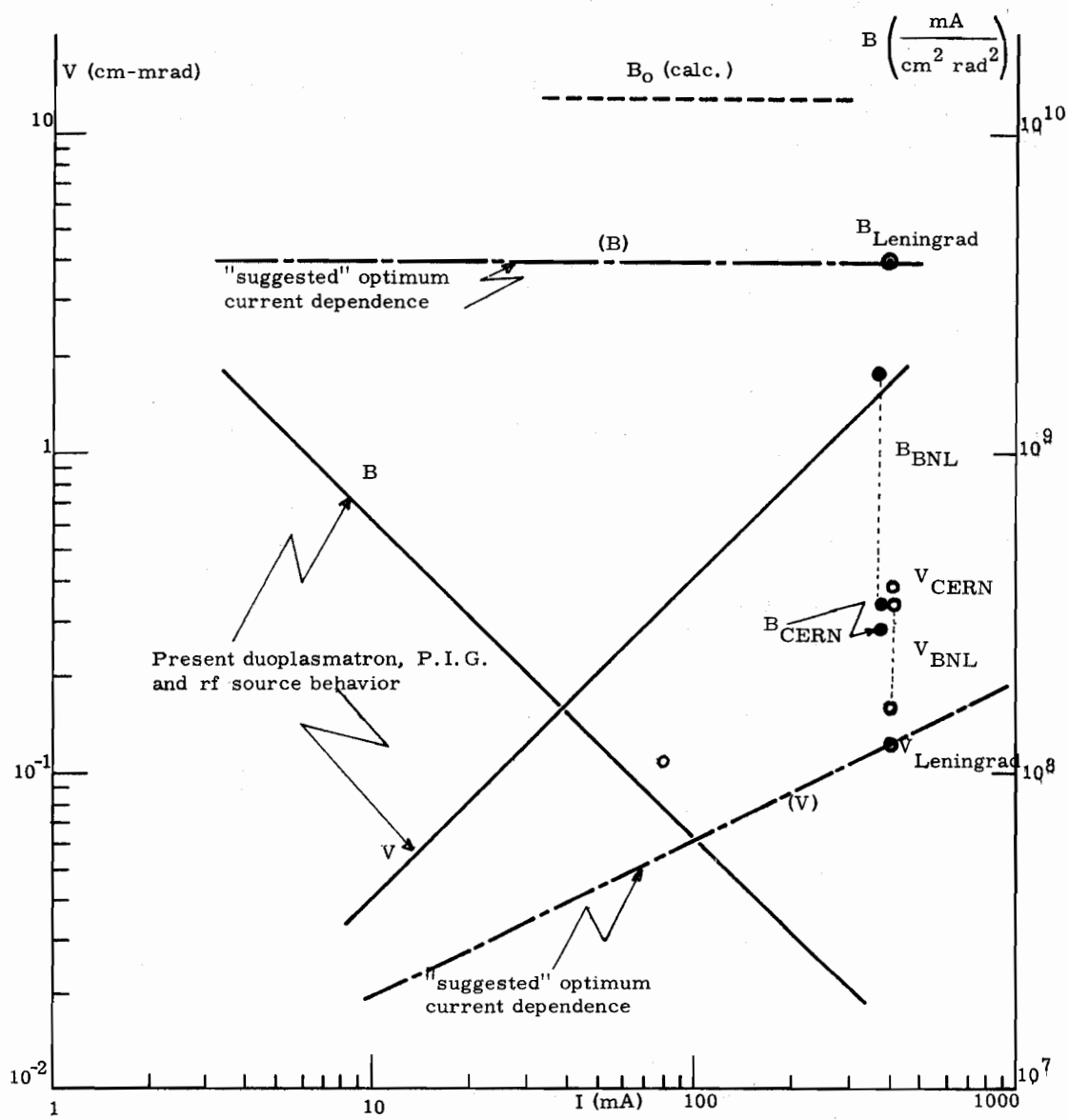

Fig. 1. **ION SOURCE CHARACTERISTICS**

It is evident that the ion sources using plasma expansion and plasma boundary focusing may substantially improve present ion source (PIG, rf and duoplasmatron) brightness figures. With these sources, beam intensities of the order of 500 mA are readily obtained. It is in a sense secondary how the expanded plasma is established, as long as the appropriate plasma temperature and density may be obtained. Therefore, in a first approach several of the above mentioned ion sources will be suitable. Some pertinent parameters of these sources have been collected from the literature and from BNL experience. These are given in Table I. The figures given are meant for comparison only and all values given should be considered to be approximate only. There should be no clear cut choice between the modified PIG souce, the Lamb-Lofgren "magnetic" source and the modified duoplasmatron source. However, with the duoplasmatron a high density primary plasma is obtained in a rather efficient way. This source is therefore more suitable to produce an expanded plasma without actually enlarging the ion source aperture to any appreciable extent, which should be avoided to the extent possible because of neutral gas flow into the acceleration column.

Some thought has been given to the most desirable shape of the plasma boundary in the modified duoplasmatron source. This is illustrated in an oversimplified way in Fig. 2. The possibility of positive aberration and also space-charge blow-up with a consequent equivalent negative aberration in the proton beam should be avoided to reduce effective phase space dilution. Presently, the first case illustrated, i.e., that of an essentially flat boundary is being considered as a desirable configuration together with a high gradient column approach as will be further detailed below.

In Fig. 2 is also indicated the possible reason for the experimentally observed emittance-current behavior in the conventional duoplasmatron source ($v = C_1 I$ instead of $v = C_2 I^{1/2}$ as expected). As illustrated the measured emittance would be

$$v \cong \beta\gamma a \alpha .$$

From elementary electron optics $\alpha = C_3 I^{1/2}$, further, Langmuir's equation gives $a = C_4 I^{1/2}$, consequently $v = I/\pi\delta$.

Even though the source brightness values obtained with the Solnyshkov source are promising one might say that developments are not so far advanced yet that one could speak of an operational source at present. Some problems are mentioned:

TABLE I

Evaluation of High Intensity Ion Sources		P.I.G. Source	RF Source	Duo-plasma-tron Source	With large plasma expansion and plasma boundary focusing: Lamb-Lofgren "Magnetic" Source	P.I.G Source With Hot Cathode	Modified Duoplasmatron Source
Reported maximum	units						
Ion currents: after single electrode acceleration	mA	150	350	1000	1000	1000	800
after C-W acceleration	mA	90	250	150	-	-	400
Ion source brightness: B^* (for definition see text)	$\frac{A}{(m.\ rad)^2}$	5.10^8	5.10^8	5.10^8	$\geq 5.10^7$	-	5.10^{10}
Expectation of approaching $B = B_o$ instead of $B = \delta^2/I$		neg.	neg.	neg.	pos.	pos.	pos.
Physical characteristics:							
beam energy spread	eV	< 10	10	< 1	-	-	-
typical maximum proton percent	%	50-80	60-90	60-90	95	-	-
Characteristics related to complexity of auxiliary equipment: gas consumption	Ncm^3/h	10-100	10-100	50	2000	1000	100-200
power input** / duty factor	kW	0.5-5	1-10	0.5-2	5-10	5	1-5
power for solenoids etc.	kW	1	0.5	0.5	10	1	0.5
cathode heating	kW	-	-	0.1-0.5	1	0.1-0.5	0.1-0.5
discharge current	A	1-5	-	10-40	100	40	20-100

*Because of the measured current dependence (or possible current dependence), the value given refers to the cited current after C-W acceleration.

**Related to source discharge current only.

a. With the large plasma boundary extraction use is made of plasma boundary focusing, i.e., the beam optics will depend on the boundary shape. This in turn depends sensitively on extraction field, its distribution and plasma density. Slight variations in source parameters are expected to affect beam optics substantially. In this connection also the nonuniform plasma density is a problem resulting in complex emittance patterns. For plasma boundary shaping a shaped grid might be used. This is shown in Fig. 3 together with a version of the modified duoplasmatron source. If a grid is used on the extraction electrode scattering of protons due to the fine structure of the local fields might prove to be causing effective dilution of phase space. This is presently being studied at BNL.

b. Plasma oscillations and boundary instabilities. With the conventional duoplasmatron source, beam intensity modulations with frequencies up to 30 Mc/s and even higher have been observed with the wide band frequency system of the AGS. At times, beam intensity modulations of nearly 75% have been observed, while under optimum conditions this was still of the order of 5% to 10%.

c. Further measurements are needed on proton percentage from an expanded, lower temperature, plasma with the Solnyshkov source.

With conventional Cockcroft-Walton acceleration columns the voltage gradients are such that a relatively large diameter column aperture is needed in order to be able to transfer of the order of 400 mA total beam. Also, with a larger diameter beam, problems connected with aberrations would be more serious.

An alternative is to try to improve the accelerator column gradient. Further, with the possibility of extracting beams from large plasma boundary diameters and actually also the desirability of doing so in connection with beam emittance and source brightness, it becomes attractive to consider again the "Pierce" approach of beam formation. In the small beam diameter case, an unpractical high voltage gradient is required to support the "rectilinear: beams; this because of the higher current densities involved, i.e., $\cong$ 1 A/cm^2. With current densities of the order of 0.1 A/cm^2 the required fields approach practical values again. Various text books on electron optics detail the "Pierce" approach. Here only the resulting formulas will be given:

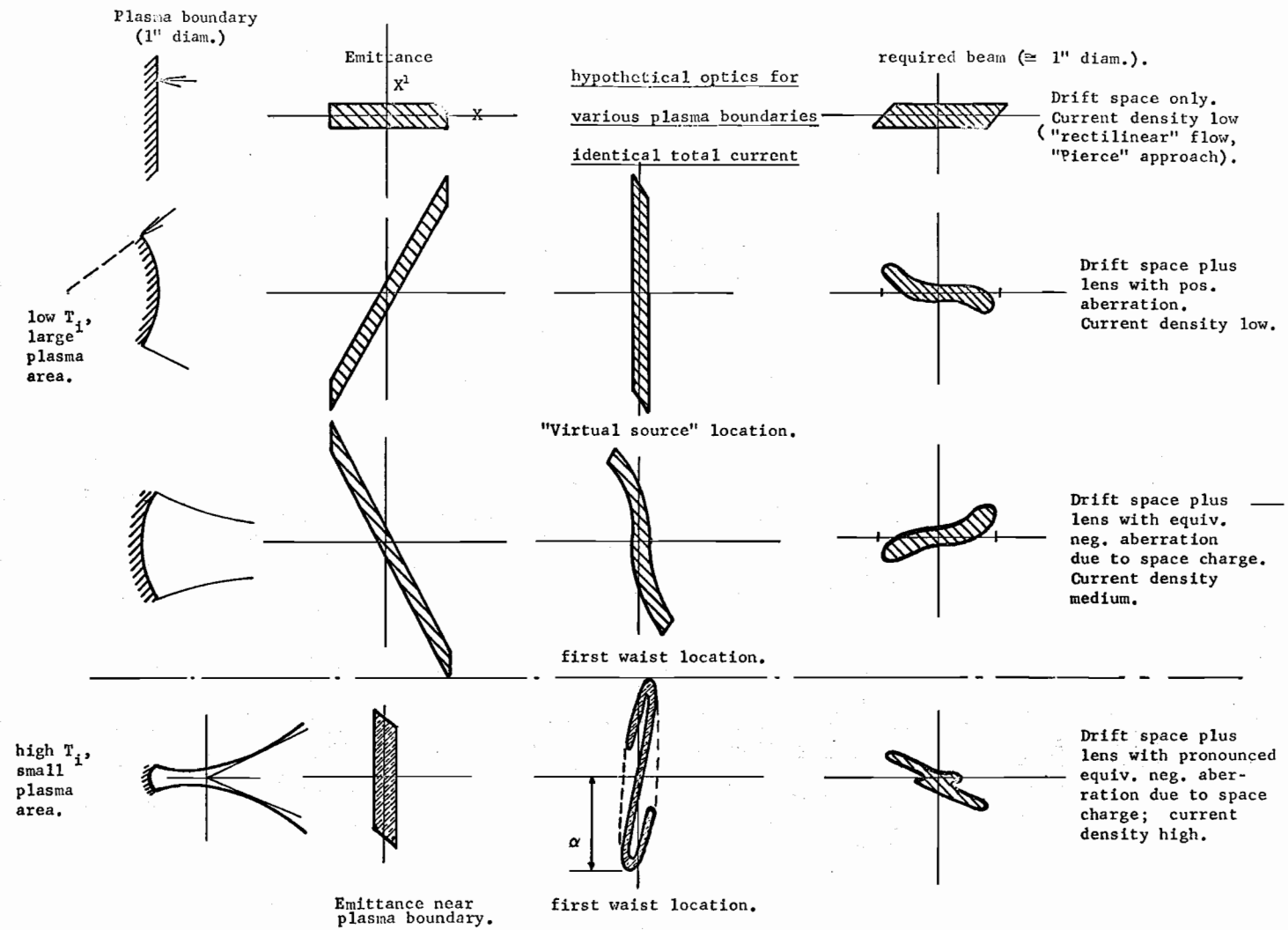
Plasma boundary
(1" diam.)
Emittance
X^1
X
hypothetical optics for
various plasma boundaries
identical total current
required beam (≅ 1" diam.).
Drift space only.
Current density low
("rectilinear" flow,
"Pierce" approach).
low T_i,
large
plasma
area.
Drift space plus
lens with pos.
aberration.
Current density low.
"Virtual source" location.
Drift space plus
lens with equiv.
neg. aberration
due to space charge.
Current density
medium.
first waist location.
high T_i,
small
plasma
area.
Drift space plus
lens with pronounced
equiv. neg. aber-
ration due to space
charge; current
density high.
α
Emittance near
plasma boundary.
first waist location.

Fig. 2

For a "rectilinear"* flow with cylindrical boundaries the axial potential distribution is given by

$$U_{z,o} = A_i Z^{4/3}$$

with

$$A_i = \left(\frac{m_p}{m_e}\right)^{1/3} A_e \qquad \text{and} \qquad A_e = 5.7 \quad 10^3 \; j^{2/3} .$$

For a plasma boundary of 1 inch diameter and 500 mA total current one obtains $j_o = 0.1 \text{ A/cm}^2$ and

$$U_{z,o} = 1.5 \quad 10^4 \; Z^{4/3} .$$

The potential distribution outside the beam boundary has to match this distribution at the beam boundary. This has been obtained analytically and can be approached for practical electrode shapes with an electrolytic tank. The axial distribution together with the required fields as a function of axial location are given in Fig. 4. In this case the extraction electrode held at 50 kV is matched at the proper location and given the proper shape. Consequently 700 kV will be held across a gap of approximately 16.5 cm. The maximum axial field indicated is $\cong$ 50 kV/cm. Similarly some parameters for the spherical case, i.e., a beam cone cut out of the inner space between two spheres has been explored. Again a plasma boundary diameter of 1 inch and total beam of 500 mA have been assumed. The axial potential distribution is given by

$$I_{op} = 2.4 \quad 10^{-6} \; \frac{\sin^2 \frac{\theta}{2}}{\alpha^2} \; U_{z,o}^{\;3/2}$$

with $\alpha^2 = f\,(R/R_{\text{plasma boundary}})$, a known function. The results, matched again to the extraction electrode, are also shown in Fig. 4. The field has been limited to 10 MV/m, resulting in a slight deviation from the required potential distribution above 650 kV. This is not thought to be serious.

As a first approach the "rectilinear" beam with cylindrical beam boundaries have been considered. An electrode system enforcing the required potential distribution has been designed and at present, first

---

*This would constitute a beam emittance of zero value, which does not occur in practice. Nevertheless the approach is useful.

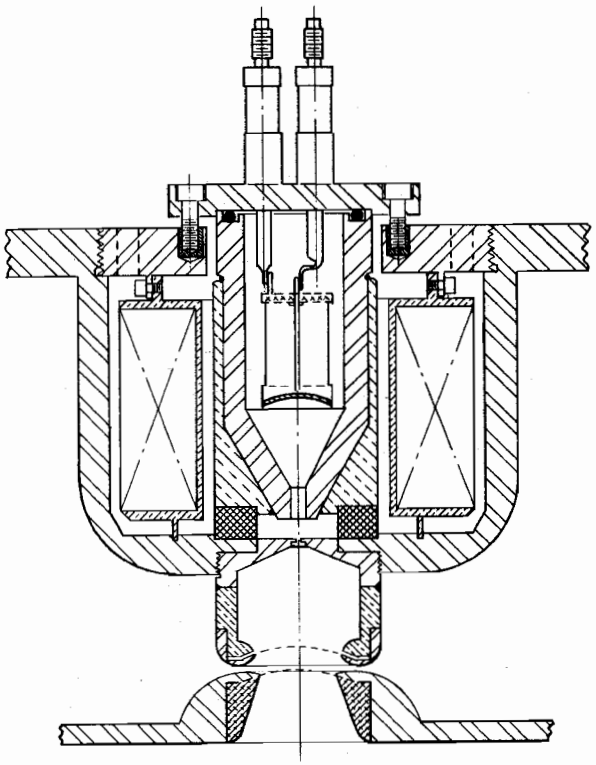

Fig. 3 Modified Duoplasmatron

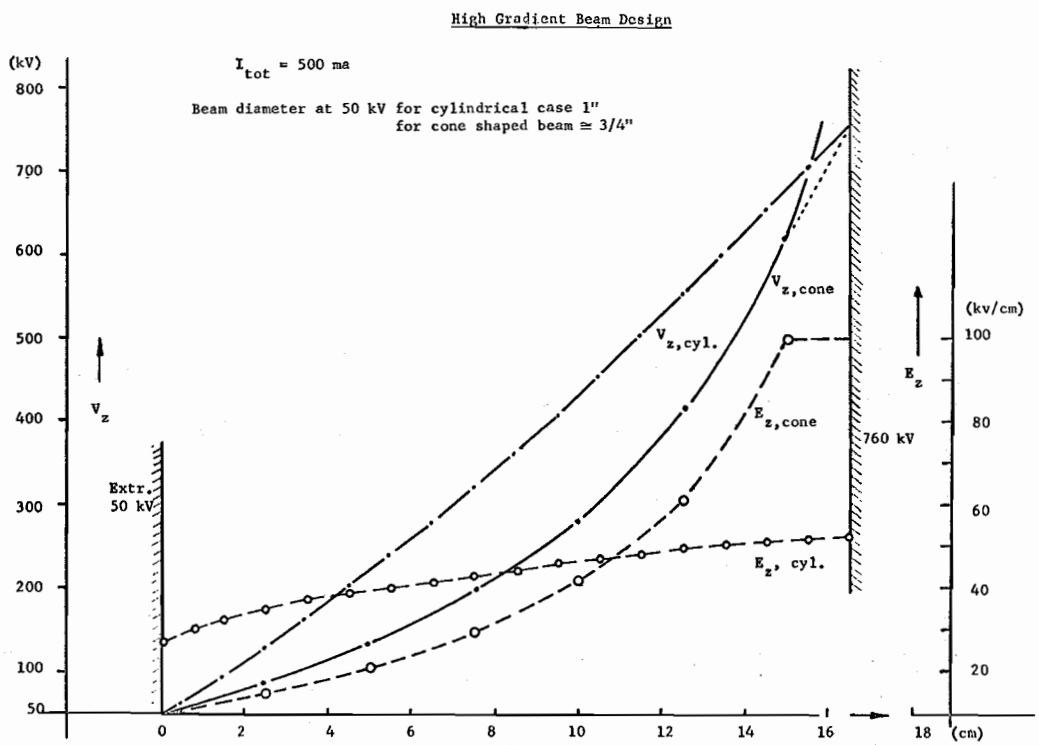

Fig. 4

approach equipotential measurements have been done with a semi-automatic equipotential plotter. An electrolytic tank of 30" x 24" and the plotter have been built by Mr. A. Soukas, who also did some of the measurements, an example of which is given in Fig. 5.

The finally synthesized electrode structure will be mounted in a high gradient large diameter column structure, as shown in Fig. 6. This is a double walled structure with the possibility of conditioned and cooled gas mixture flow in the interspace for cooling of the voltage dividing resistors and improved voltage rating. The total length of the column is about 40 inches for 750 kV. A test section is presently being built up to evaluate some of the design approaches in more detail. The over-all preinjector arrangement as envisaged at present is shown in Fig. 7.

LAPOSTOLLE: I would like to ask you two questions. First, what type of aberration do you consider due to space charge? Is that due to non-uniform density or to the potential drop inside the beam?

VAN STEENBERGEN: I have talked in terms of equivalent negative aberration, because the space-charge effects, even in a homogeneous beam with potential drop inside the beam, tend to distort the two-dimensional phase-space boundary in a sense opposite to that due to spherical aberration. I assume that boundary distortion due to space-charge in a nonhomogeneous beam would tend to be more serious and lead to more equivalent negative aberration.

LAPOSTOLLE: Now, I have the second question, which was about your high gradient column design where you try to have a field distribution which fits the space-charge law in some way. That of course only applies for a given current density.

VAN STEENBERGEN: The equipotential distribution at the boundary is correct for one value of current density only. Therefore, at present the preliminary design is for a particular total current, i.e., 500 mA only; it is not expected to suit typically a 50 mA total beam.

MORGAN: In your high gradient column design, did you worry about regions of electron oscillation in the stray field of the solenoid lens which is right beneath the column? We found this to be real critical in the design of our column.

VAN STEENBERGEN: We did not consider this yet.

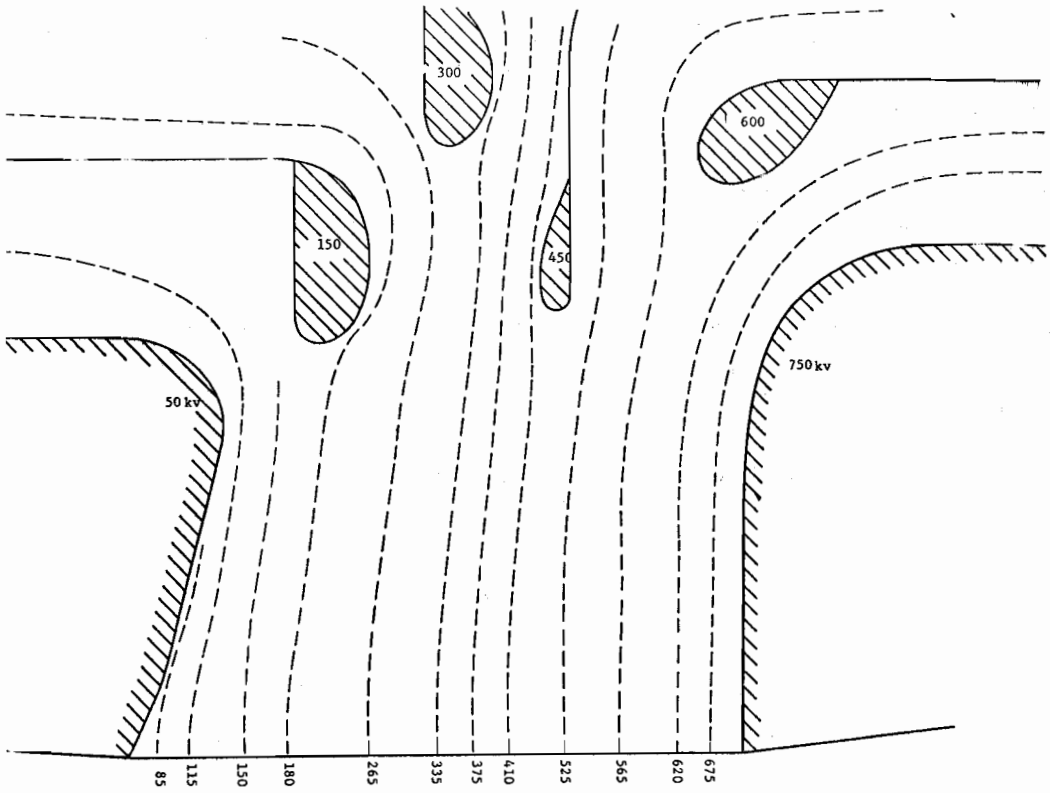

Fig. 5

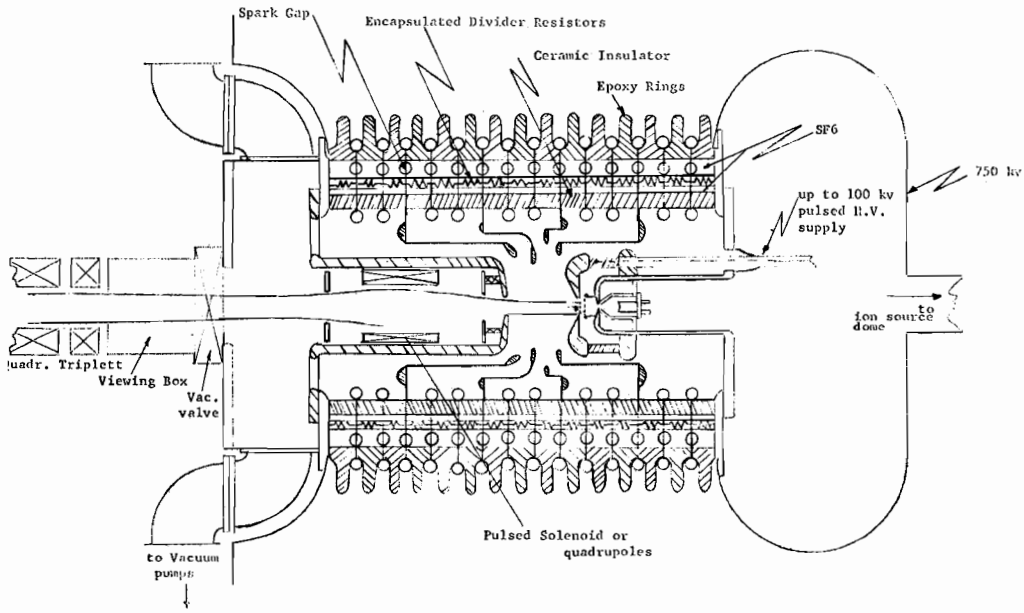

Fig. 7 High Gradient Accelerator Column Arrangement

TAYLOR: Have you plotted trajectories through on a computer? And if so, I want to ask you what sort of program you use and how you included the space charge?

VAN STEENBERGEN: We hope to start using the Kirstein program but have not done so yet. I recognize completely that the equipotential tank leads to a first approximation only.

WROE: Would you say a bit more about those ion temperatures you quoted? I notice you wrote down 10^5 °K and 10^{12} ions per cm^3. Is this a measured value?

VAN STEENBERGEN: This was a measured value by Gabovich with an expansion cup attached to a hot cathode P.I.G. source.

REFERENCES

1. A. van Steenbergen et al. Proceedings of the International Conference on High Energy Accelerators, Dubna, August 1963.

2. A. van Steenbergen, BNL Internal Report, AADD-29, March 1964.

3. A. Guthrie and R. W. Wakerling, "The Characteristics of Electrical Discharges in Magnetic Fields", McGraw-Hill, May 1949.

4. M. D. Gabovich et al. Soviet Physics-Technical Physics, Vol. 6, March 1, 1961, p. 766.

5. A. I. Solnyshkov et al., Proceedings of the Conference on High Energy Accelerators, Dubna, August 1963.

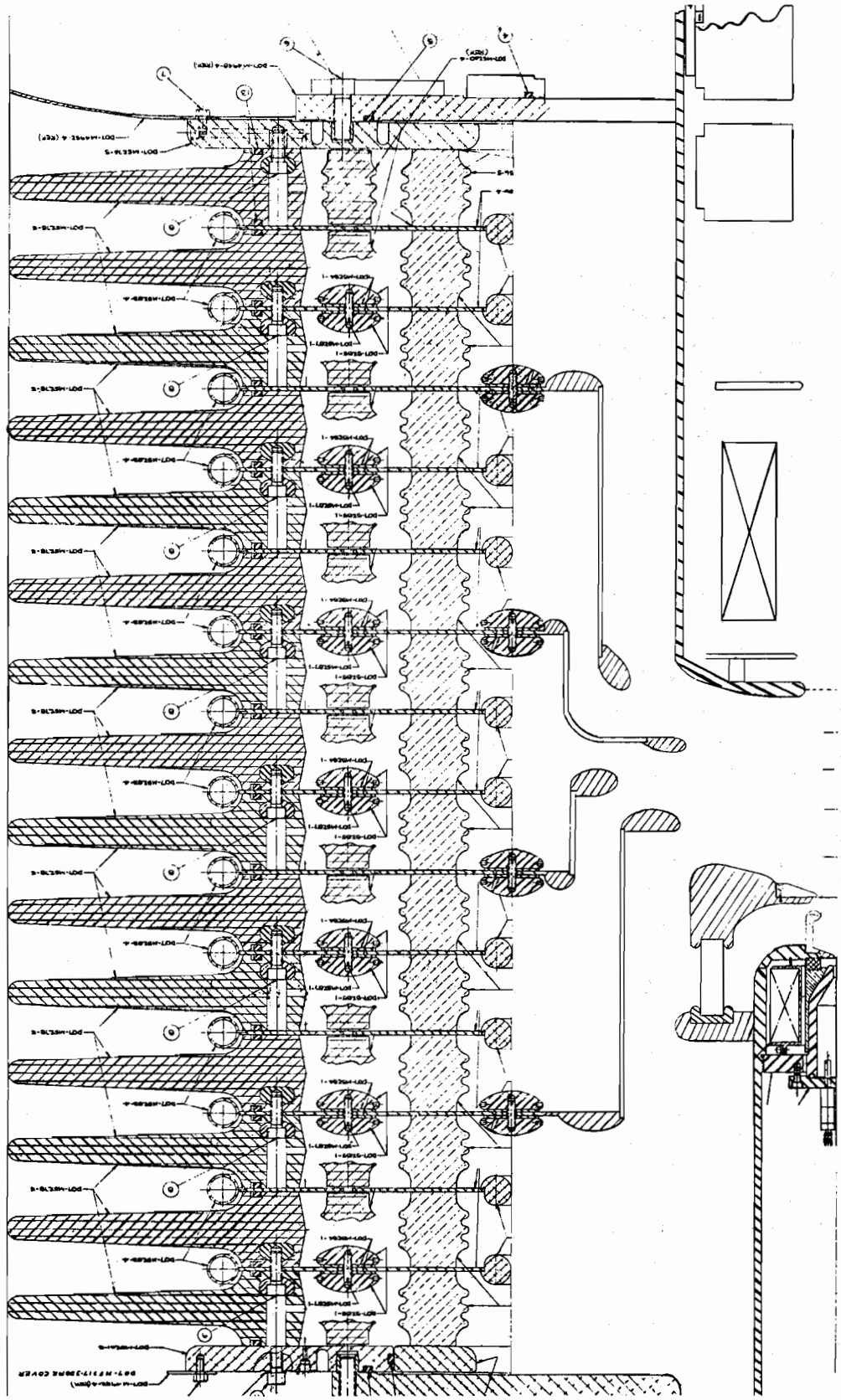

Fig. 6

RECENT DEVELOPMENTS IN RF PROTON SOURCES

H. Wroe
Rutherford High Energy Laboratory

1. Introduction

An rf ion source of the Schneider type[1] was originally developed for Nimrod, but it suffered severely from internal breakdown when delivering intense beams with a pulse length of 1 millisecond. The onset of breakdown marked the end of the useful life of the source which was often short and unpredictable. The breakdown problem was never solved in spite of intense effort and eventually the Schneider source was abandoned in favor of an arrangement similar to that described by Thonemann and Harrison.[2] This source has been reliable in operation on Nimrod and some of its characteristics are given below.

2. Description of Nimrod RF Source

The source is shown in Fig. 1. It is mounted on a mild steel base plate, 1, which carries the invar cathode, 2, on an accurate register. The source pot 7 is made from a piece of standard 1" bore QVF pyrex pipe line with one end sealed, and ground parallel to the lower end. The pot is mounted on the dural extraction plate, 4, which is insulated from the cathode by the pyrex ring, 6. A pyrex disc, 5, almost completely covers the top surface of the extraction plate so as to reduce the area of metal exposed to the plasma to a minimum. Extraction of ions is achieved by pulsing the extraction plate (and therefore the plasma also) to a positive potential. To prevent discharges between the source pot and rf coil, which is "earthy", the insulating envelope, 10, is pumped up with compressed air to about 30 lbs/in^2. This also prevents breakdown from the extraction plate to the base plate over the outside of the ring, 6, at high extraction voltage.

The rf circuit consists simply of a 50 Ω coaxial line stretcher and stub connected directly to the coil, as shown in Fig. 2. The lengths of the line stretcher and the short circuited stub shown in Fig. 2 are typical values. When a 50 Ω power meter is connected in place of the tuner and source, a maximum pulse power of 20 kW can be obtained. The frequency is 125 Mc/s.

Hydrogen is fed into the source through a hole in the base plate via a nickel leak.[3]

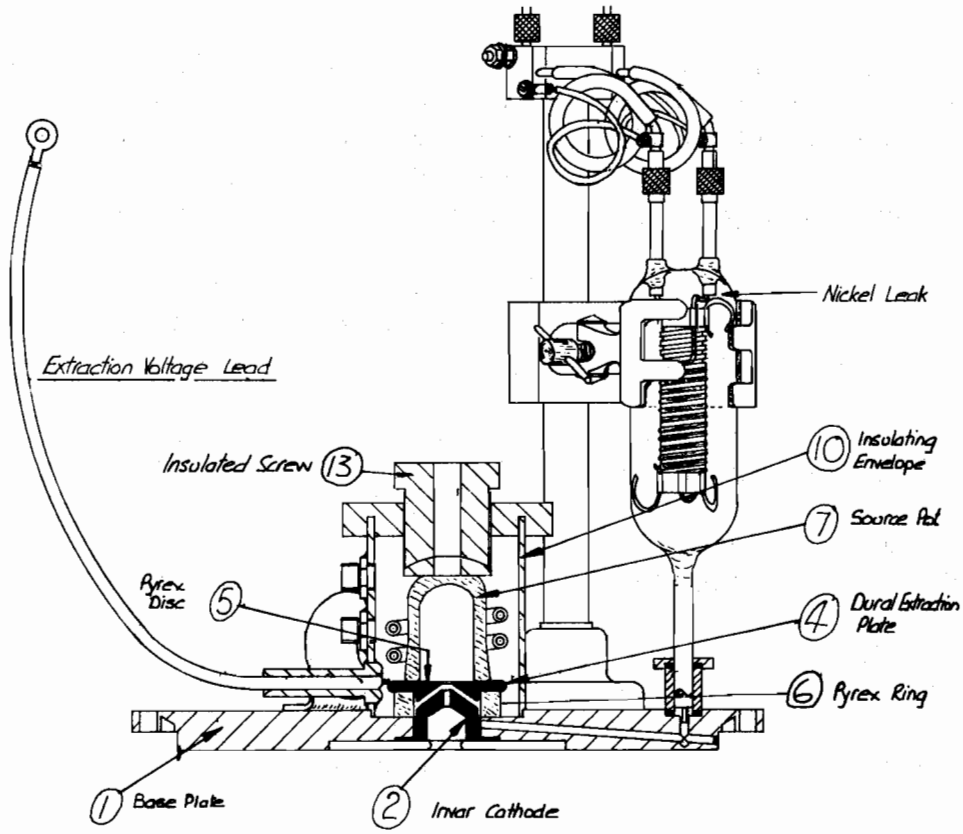

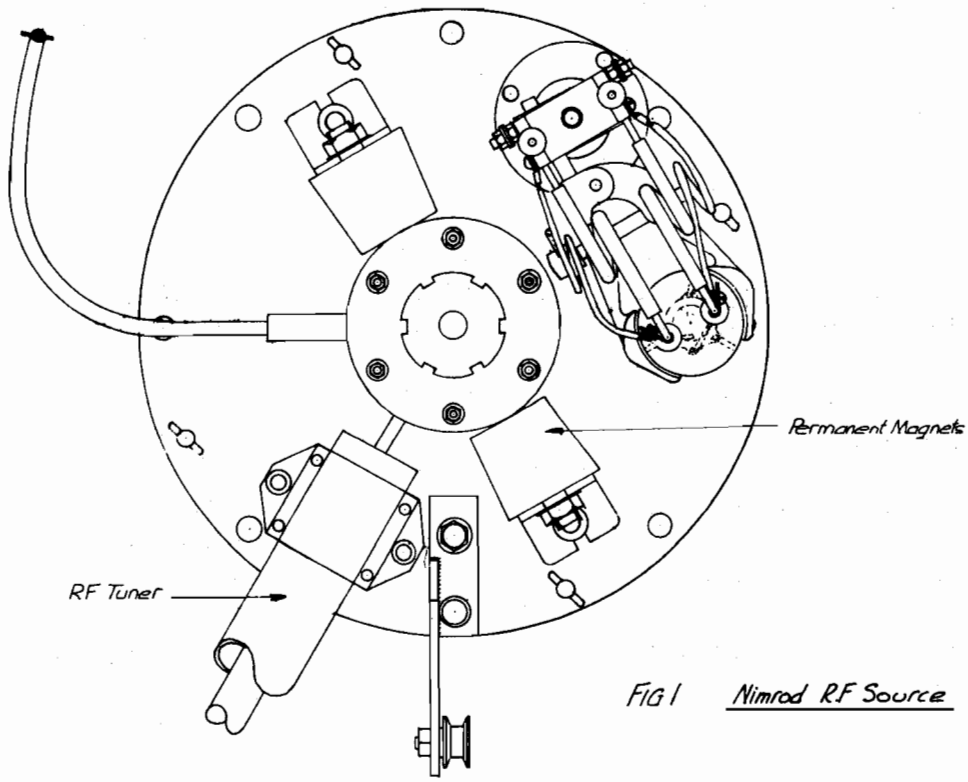

FIG 1 Nimrod R.F Source

The vacuum seals on the source itself are 1/32" diameter indium wire compressed to a thickness of 0.004". Considerable pressure is required and this is achieved by a strong insulated screw, 13, on top of the outer envelope. A pressure pad with a spherical upper surface takes up slight misalignment between the screw and source pot.

Two permanent magnets provide a roughly transverse magnetic field of about 50 gauss which greatly increases the ion density in the plasma, for a given rf power input.

The dimensions of the extraction gap used at present on Nimrod are shown in Fig. 3. Alignment of the extraction plate and cathode is critical. It will be seen that the insulating pyrex ring is well shielded from the beam and plasma and this is considered to be an important contribution to the high breakdown voltages achieved in operation.

Figure 4 is a photograph of a source assembly and Fig. 5 is a view of the source in position on the Nimrod preinjector.

3. Performance of the Source on a Laboratory Rig

3.1 Source Pressure

A special source pot was made up with a Pirani gauge head mounted on top. The variation of source pressure with the nickel leak current is shown in Fig. 6. The pressure readings are corrected for hydrogen. Normal operating pressure is about 10^{-2} Torr and the power consumption of the nickel leak at this level is 36 watts.

3.2 Output Current

A reliable current measuring device has been developed, which combines electrical and calorimetric methods, as shown in Fig. 7. The principle of the calorimeter is the same as that of Harrison.[4]

A collector cup, made in 2 mil copper foil to reduce its thermal capacity, is mounted on a double "stem" of copper strip 3/8" wide and 0.020 thick. A transverse magnetic field of about 200 gauss is applied to the cup, by permanent magnets, to suppress secondary electrons and a michrome wire heating coil is wound on it for calibration purposes. Thermistors are used for temperature measurement. Figure 8 shows a general view of the device. Both the calorimeter and the bridge circuit used to measure the resistance of the thermistors are well screened as shown in Fig. 10.

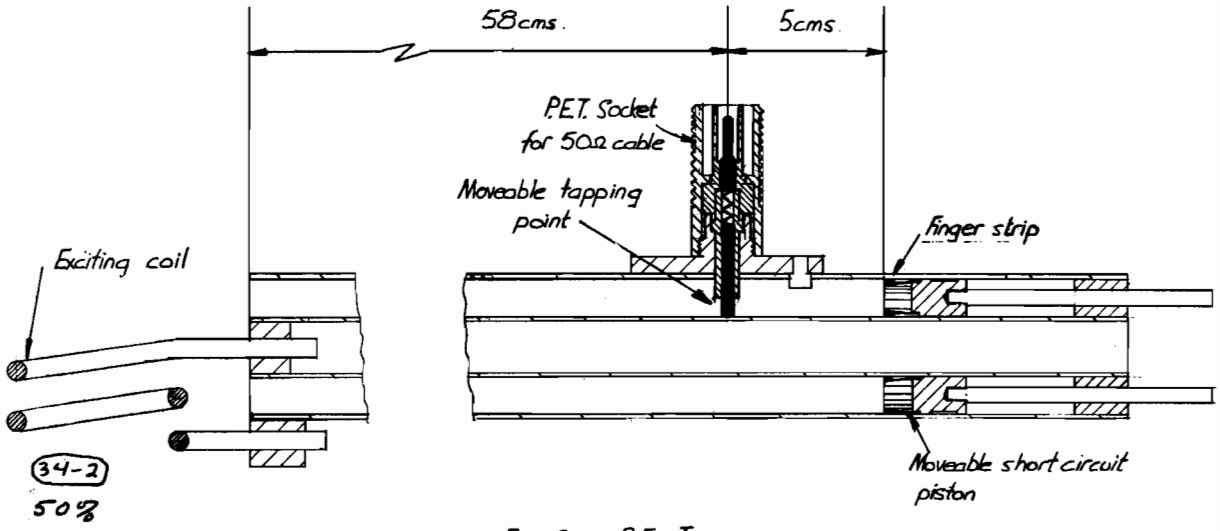

FIG. 2 R.F. Tuner

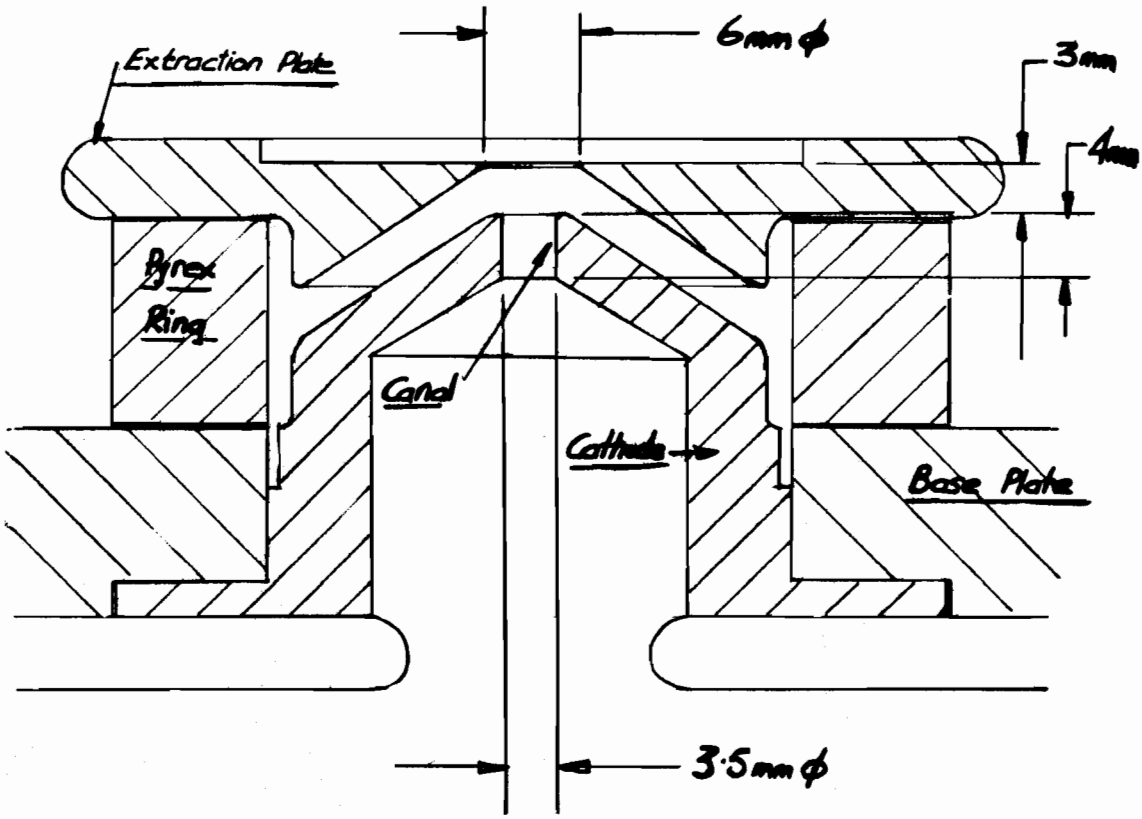

FIG. 3 Extraction Gap Dimensions

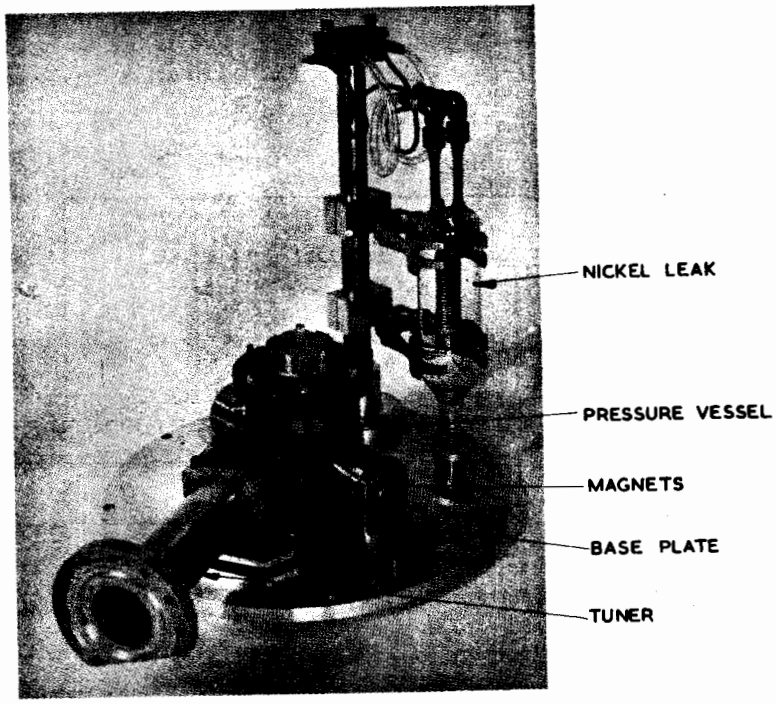

FIGURE 4 GENERAL VIEW OF SOURCE ASSEMBLY

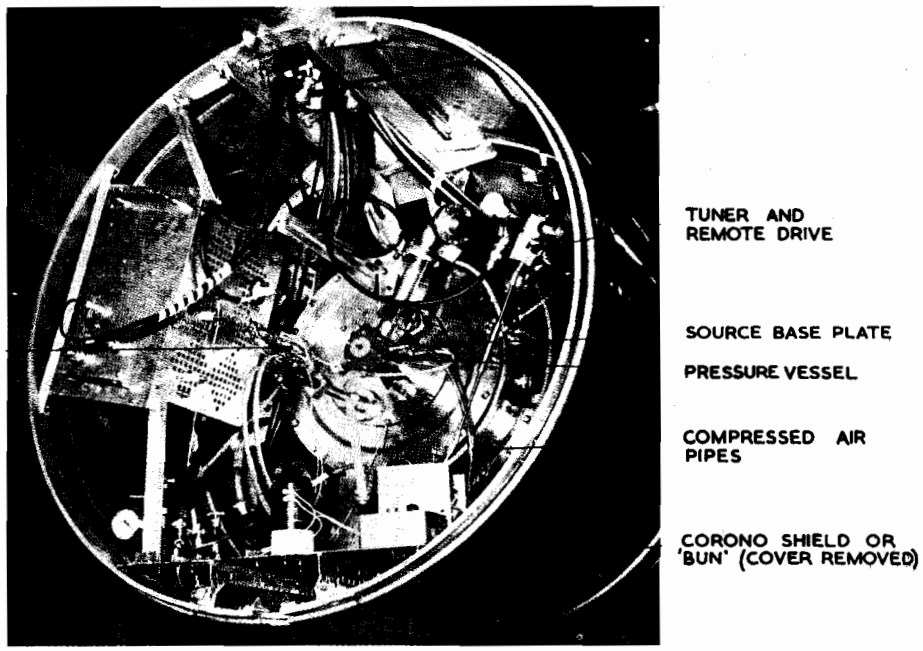

FIGURE 5 GENERAL VIEW OF SOURCE FITTED TO THE NIMROD PREINJECTOR

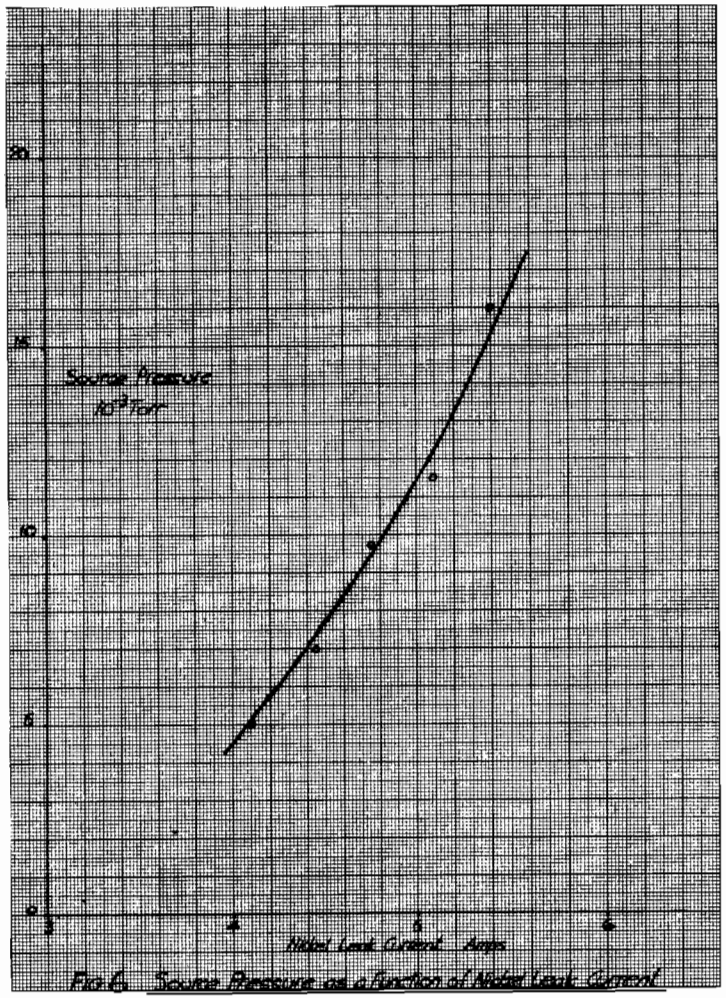

FIG. 6 Source Pressure as a function of Nickel leak Current

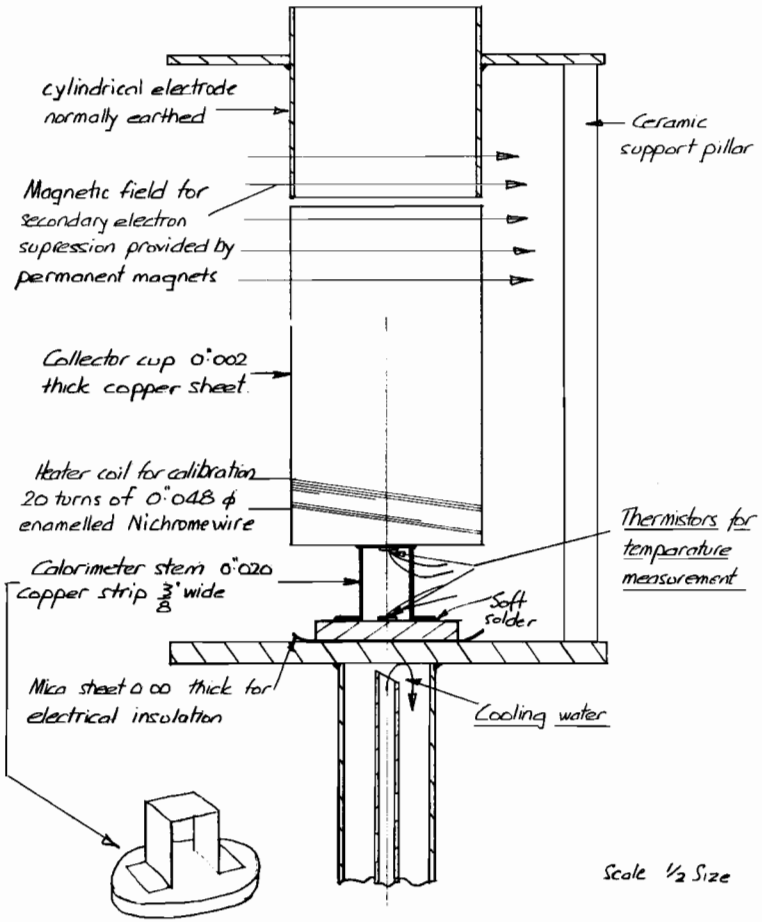

FIG. 7 Combined calorimeter & collector cup for beam current measurements.

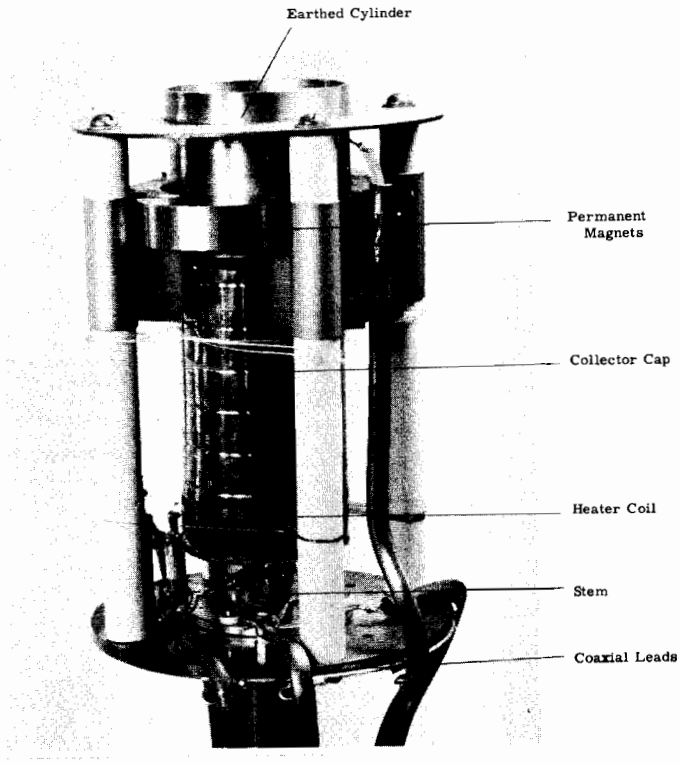

FIG 8 Current Measuring Device

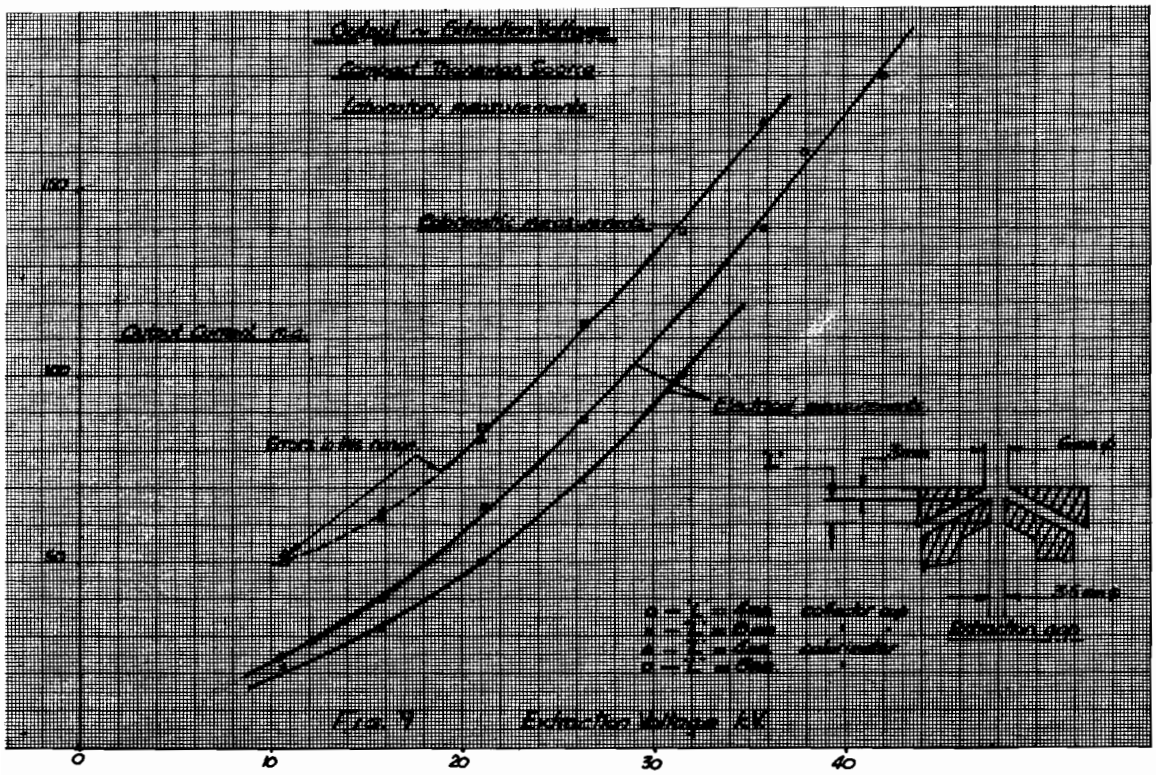

FIG. 9 Extraction Voltage E.V.

Curves of output current against extraction voltage for two different canal lengths are shown in Fig. 9. The rf power level was adjusted to give a maximum output current at each value of extraction voltage. The difference between the calorimetric and electrical measurements is probably due to the neutral content of the beam, i.e. the total ion current crossing the plasma boundary under given conditions is the same for each canal length but the number of charge exchange events occurring in the beam is greater for the longer canal. Thus the charged component of the beam is smaller for the longer canal. The dotted part of the calorimetric curve in Fig. 9 is in error due to direct pickup of rf power by the thermistors--this result was obtained before the screening arrangements were fitted.

3.3 Multiwire Target

Preliminary experiments have been carried out using a technique for rapid measurement of beam properties such as diameter, current density distribution or emittance. The device is a target consisting of 25 tungsten wires, 0.2 mm diameter, spaced 2 mm apart and insulated from each other, each wire being connected to a condenser. When exposed to a beam, the charge collected by each wire produces a proportional voltage on its condenser. The latter are then "scanned" by a mechanical commutator which discharges each in turn through a resistor. Thus, a series of spikes is produced, the height of each one proportional to the charge collected by the wire in the first place.

This is illustrated in Fig. 11 where the target was used to measure the diameter of the beam at various axial distances from the source. The target itself is shown in Fig. 12.

Permanent magnets are built into the target to provide a magnetic field for suppression of secondary electrons, but they are not very effective and there is evidence that the space charge in the beam is at least partially neutralized by secondary electrons. Thus the dotted curve in Fig. 11 is not a real beam profile. The four positions of the target probably gave rise to four different beams, though the source conditions were the same.

It is hoped to extend this technique to the measurement of emittance.

3.4 Source Emittance Measurements

Some measurements of emittance of the beam immediately below the source have been made using the slotted plate and copy paper method.[5]

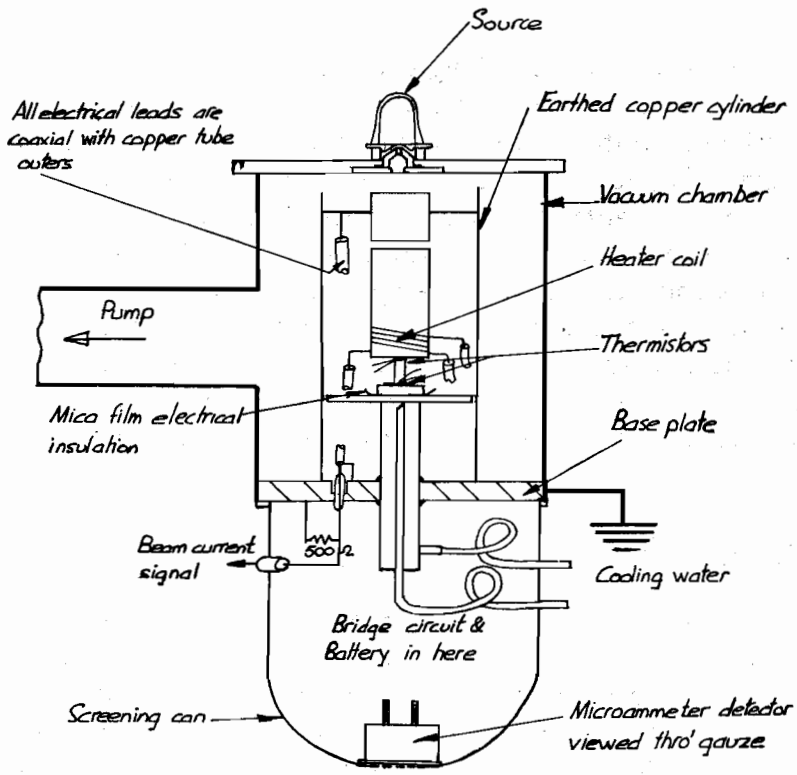

FIG 10 Screening arrangements for calorimeter

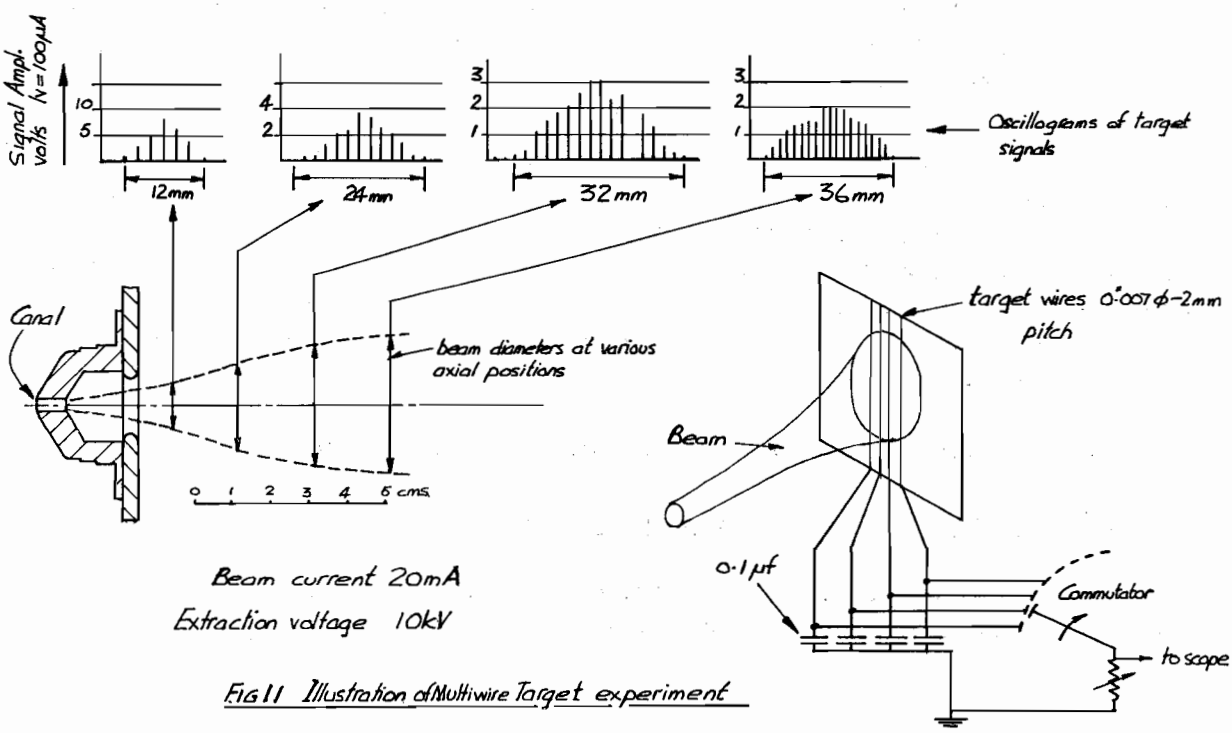

FIG 11 Illustration of Multiwire Target experiment

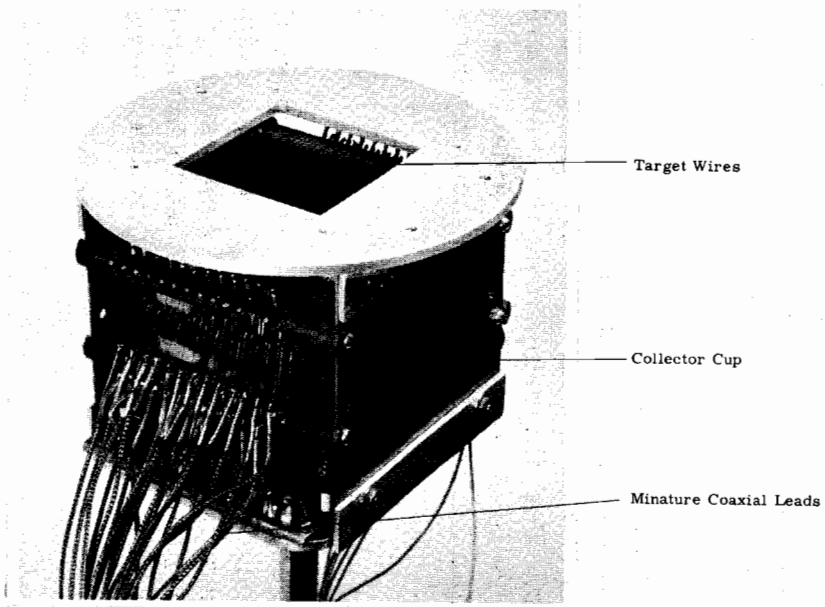

FIG 12 Multiwire Target

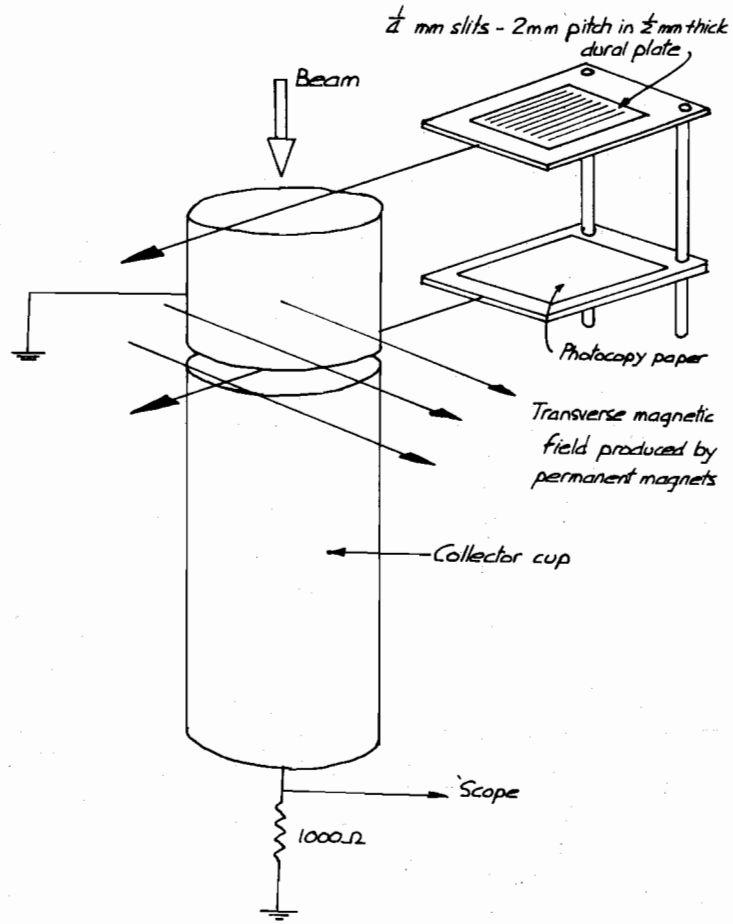

FIG 13 Emittance Measuring Device

The slits used were 1/4 mm wide, spaced 2 mm apart, in a 1/2 mm thick dural plate and they were built into a standard collector cup as shown in Fig. 13. The beam current was first measured with the plate and copy paper withdrawn, then they were pushed into the beam and the exposure made. A typical image is shown in Fig. 14 and preliminary plots of emittance are shown in Figs. 15 and 16. Both the area of the diagrams and the details of the images are closely similar to those obtained by Tallgren[5] with a Schneider type source. There seems to be a dense central region to each image which may well correspond to a large fraction of the beam.

Less dense markings, at larger values of divergence are often completely separated from the main "spectrum." The explanation of these effects is not yet clear, but they are not peculiar to the Schneider type source. They may well be common to all high intensity rf sources.

4. Source Performance on Nimrod

The source has proved reliable and consistent on Nimrod during a period of over a year. The present normal beam current is about 38 mA. At this level the useful life of the source is not yet known but a unit has been in service on Nimrod for four months of routine operation without detectable deterioration. The period of operation, to the time of writing, is about 1000 hours "beam-on" time.

The curve of output current against extraction voltage is shown in Fig. 17. The beam current was measured at 600 kV using the beam monitor system and the values shown were optimized at each value of extraction voltage.

Figure 18 shows an emittance diagram of a 40 mA beam which was obtained by using two 4-jaw apertures in the low energy drift space of the Nimrod injector as shown in Fig. 19. The apertures were set to 1 mm wide vertical slits. The diagram shows the distribution of current in phase space. There is evidence that the "side arms" on the diagram are due to the molecular ion component of the beam which was separated out by the quadrupole.

5. Future Developments

The present objective is to discover the upper limit of the performance of the source. Improved rf screening (with higher rf power inputs) is being incorporated and compressed sulphur hexafluoride is being substituted for compressed air so as to improve the external insulation. It is hoped to increase the extraction voltage to 50 kV.

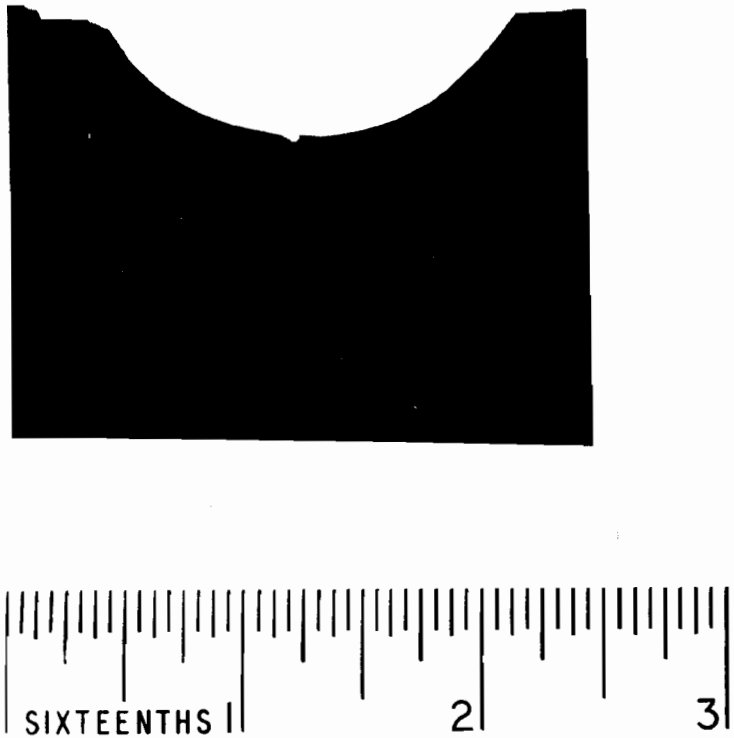

BEAM CURRENT 100 ma. EXTRACTION VOLTAGE 20 KV.
0·5ms PULSE LENGTH. EXPOSURE 120 PULSES.

FIGURE 14 IMAGE PRODUCED ON PHOTO COPY PAPER DURING EMITTANCE MEASUREMENT

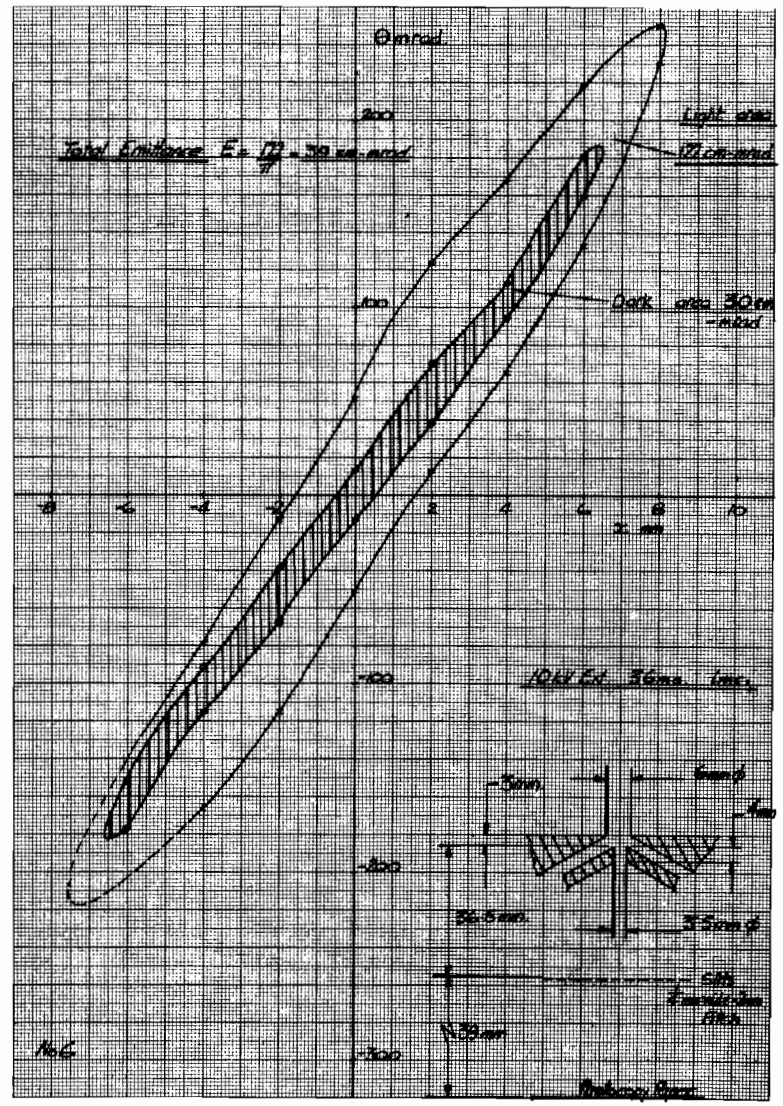

FIG 15 Emittance of 36 ma Beam at the Ion Source

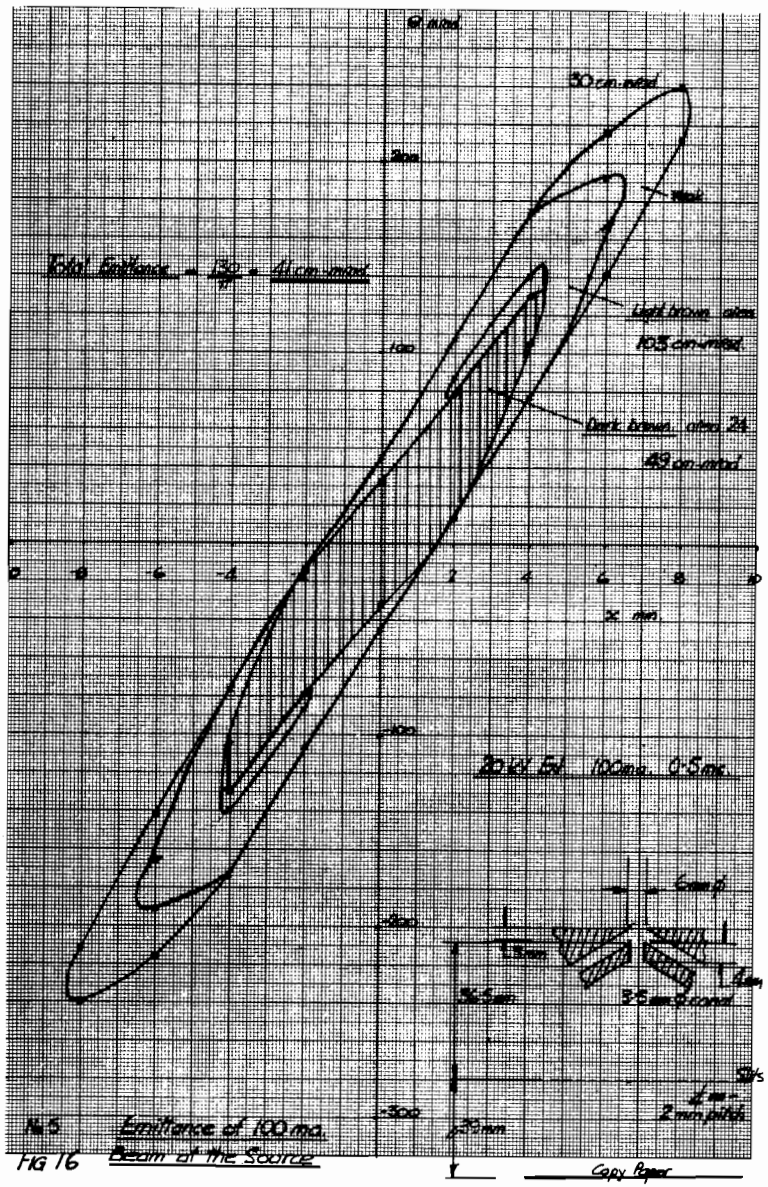

No 5 Emittance of 100 ma. Beam of the Source
FIG 16

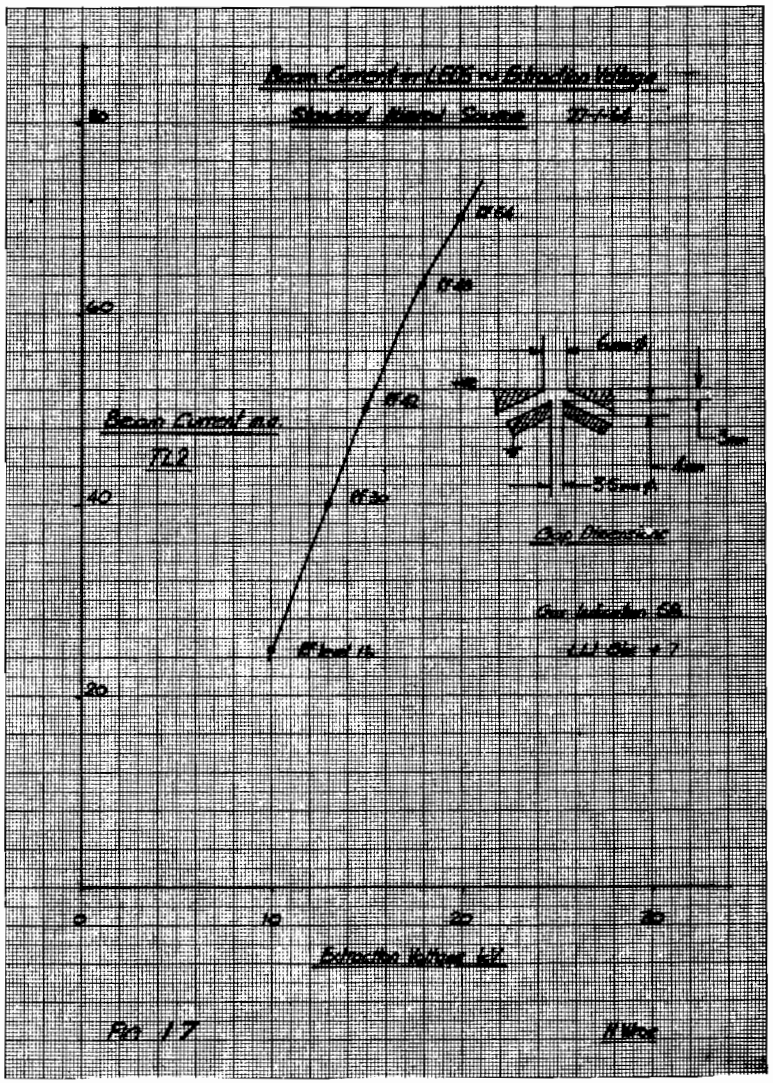

FIG 17

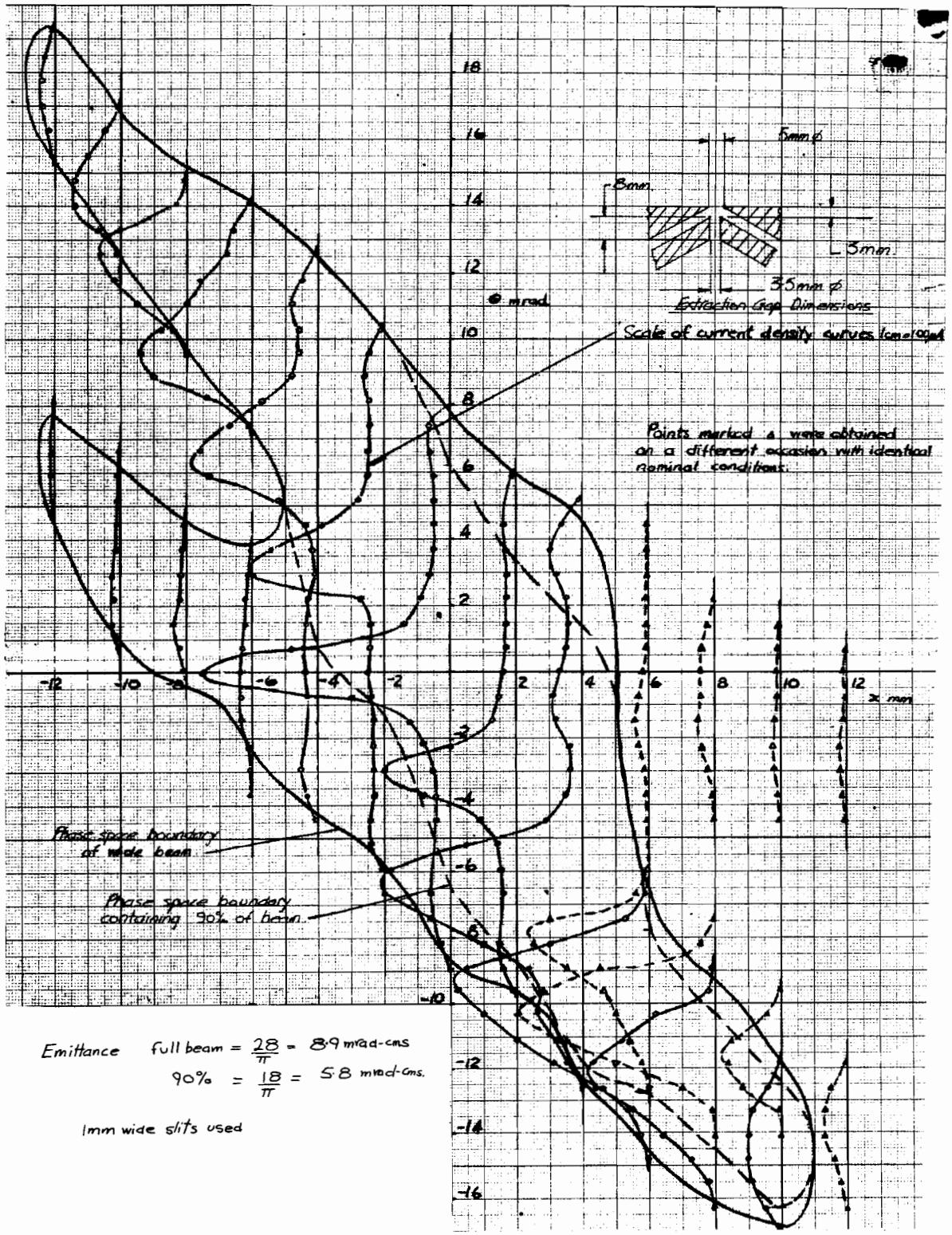

FIG 18 Emittance Diagram 40 mA Beam at 600 kV [Horiz Plane]

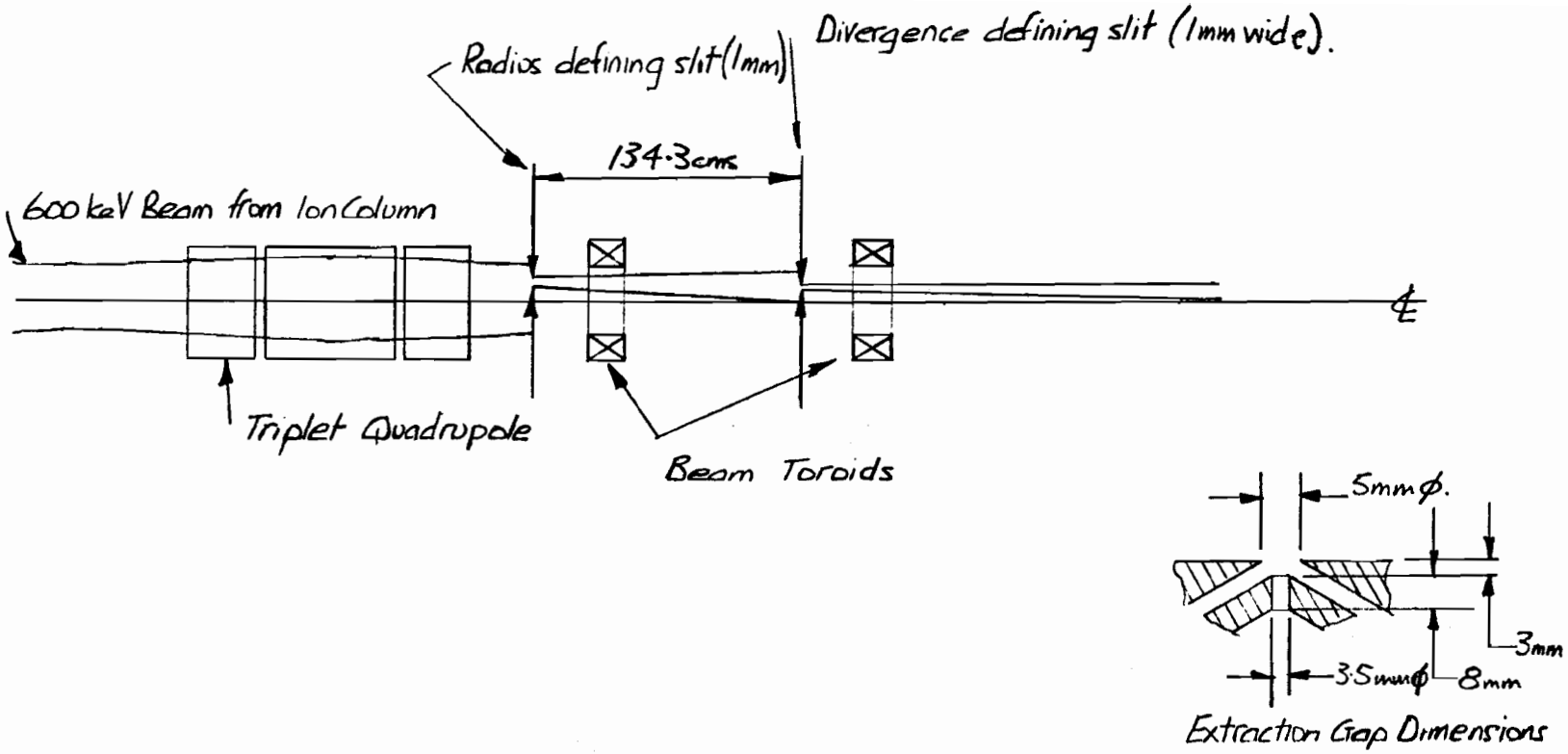

FIG. 19 Arrangement for Emittance Measurements at 600 kV

LAPOSTOLLE: I would like to make a comment and ask you a question about the various parts in the emittance diagrams you have shown or, in other terms, the existence of several beams. First, I would like to say that what you observed in the rf source exists in many sources; it is for instance the same in the PIG source. Now I would like to ask, what is your explanation?

WROE: Well, I haven't got one of course. There are so many things it could be. For instance, this technique gives you the integrated beam which strikes the film. You cannot distinguish any changes with time. Now we have evidence that changes of emittance occur during a pulse. If you examine waveforms of beam pulses through a set of emittance measuring slits, they are hardly ever square and flat topped, though the waveform of the whole beam is. It looks as if beam is shifting about in phase space.

LAPOSTOLLE: You then think that it might come from different parts of the pulse?

WROE: Yes. We are going to look at this sort of thing in more detail on the source itself. This measurement I have just told you about was done at 600 kV. I really cannot offer any serious explanation yet.

HUBBARD: With respect to this wire target you use for measuring emittance, how do you handle the secondary electrons from the wires?

WROE: What we intended to do is just put the magnetic field along the wires. There is a field on this present target, a weak magnetic field. It doesn't seem to do very much good. What we are thinking of now is to make a target in the form of a stack of thin plates with insulation between and a fairly strong magnetic field along the plates. If the field falls off rapidly enough as you move away from the target, then it will not affect the trajectories of the ions. The idea is to cause an electron liberated from a plate to be returned to that plate and not a nearby plate.

SHAYLOR: I wondered if you could do anything successful in that line by putting a potential on the wires you are not using adjacent to the wires you are using?

WROE: I do not like electrostatic means of suppression you see, and we have got experience of incredible things that secondary electrons seem able to do in a field of this sort. I don't like it at all.

SHAYLOR: But you are quite happy with magnetic techniques?

WROE: Yes.

VAN STEENBERGEN: You have measured only current distribution, not emittance?

WROE: That is right.

HUBBARD: You measured the current distribution after a slit?

WROE: The idea of the wire target was simply to substitute it for the photocopy paper, so that you have a series of slits and you get out of the wire target a series of profiles in a single pulse, which you can interpret in terms of divergence angle. That is the idea.

REFERENCES

1. The CERN Proton Synchrotron (2nd Part) Chapter V, Injection, CERN 60-26 (1960), p. 22.

2. P. C. Thonemann and E. R. Harrison. AERE Report No. GP/R 1190.

3. L. C. W. Hobbis and E. R. Harrison. Rev. Sci. Instr. 26, 303 (1955).

4. E. R. Harrison. Jour. Sci. Instr. 30, 242-244 (1957).

5. U. Tallgren. MPS/Int. LIN. 62-3, 1962.

RECENT MEASUREMENTS ON THE DUOPLASMATRON SOURCE

L. W. Oleksiuk*
Brookhaven National Laboratory

At Brookhaven interest has been expressed in determining the phase space densities for the conventional duoplasmatron ion source beam as well as studying the effects of extracting the duoplasmatron ion beam from an expanded plasma.

It was hoped that measurements of the beam brightness in the ion source extraction region would indicate the maximum attainable beam that could be injected into the linac and that by varying the plasma surface from which the beam is extracted some insight could be gained into the factors controlling ion source brightness.

Figure 1 shows a typical brightness profile for the BNL conventional (Mark I) duoplasmatron beam after acceleration to 750 kV. The measurements were performed by A. Van Steenbergen using a 4-slit method. It can be seen that the filling of four-dimensional transverse phase space is poor, and much of the linac acceptance is populated only by the tail of the brightness profile. The brightness "B_{MI}" could theoretically put in about 1000 mA in the present linac acceptance if all the transverse phase space were filled at this brightness.

Emittance measurements were performed on the conventional (Mark I) duoplasmatron as shown schematically in Fig. 2. Measurements were also performed using photocopying paper. The slit width of 0.010 inches produced beam images on the fluorescent screen, and these were photographed and measured to yield emittance values for the beam. Current measurements were performed by collecting current from the slit plate and from the current transformer. Corrections were made for secondary electron emission, these corrections yielding an uncertainty of $\pm$ 20% in the current measurements. Slit images for a 25 kV 200 mA (40 microsecond pulse width) beam are shown in Fig. 3, and the resulting phase space plot is shown in Fig. 4.

Preliminary measurements (see Fig. 5) for a range of extracted currents from the Mark I duoplasmatron from 30 mA to 400 mA indicate that the brightness of the Mark I, as measured by our techniques is

---

*Now at the University of Toronto, Toronto, Ontario, Canada.

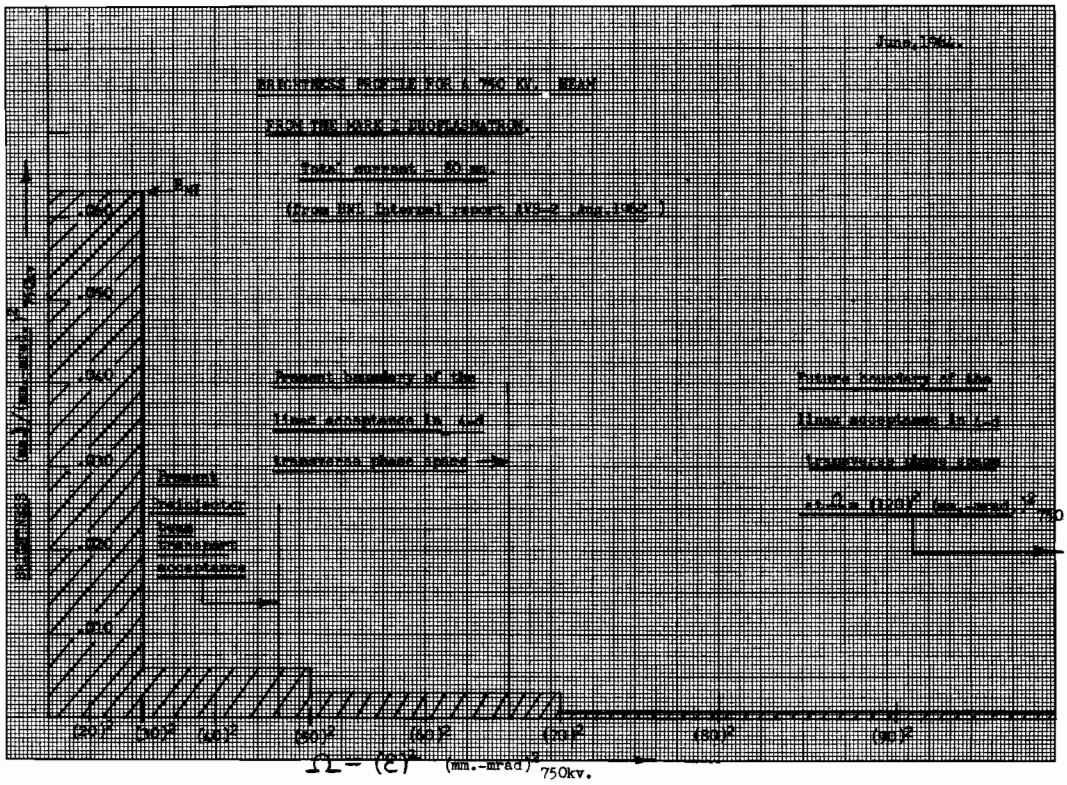

Fig. 1

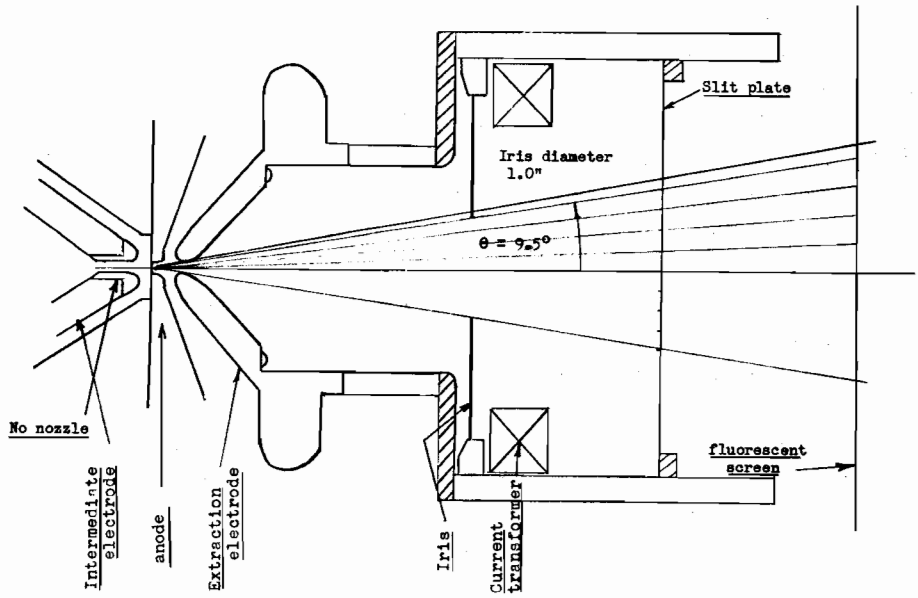

Fig. 2 Mark I duoplasmatron beam study geometry.

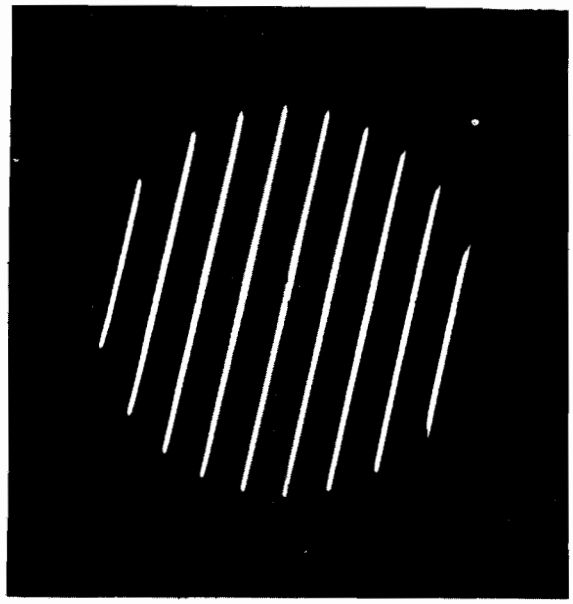

Fig. 3 Mark I duoplasmatrom beam: slit images for a 200 mA. beam.

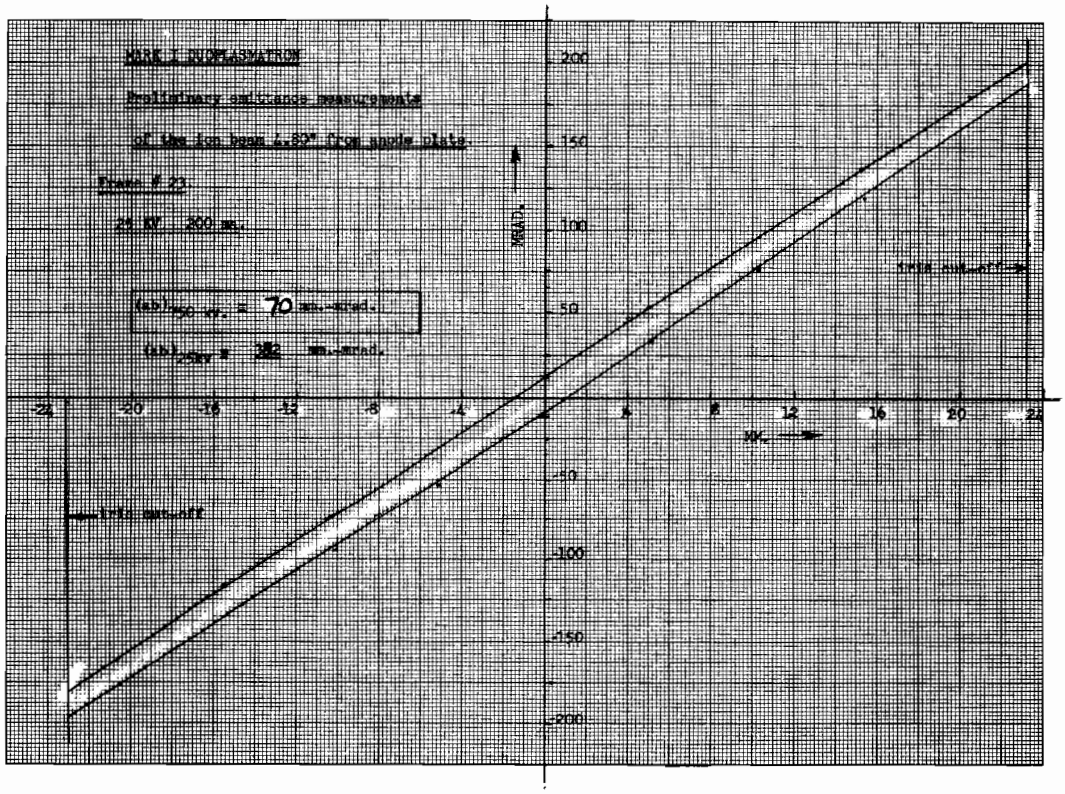

Fig. 4

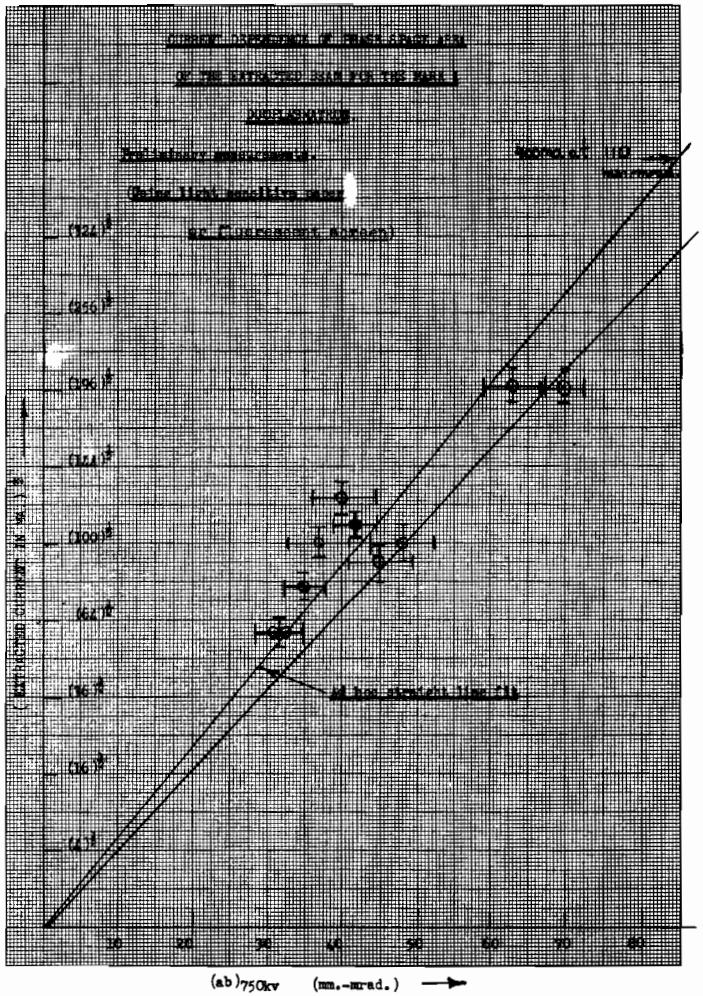

Fig. 5

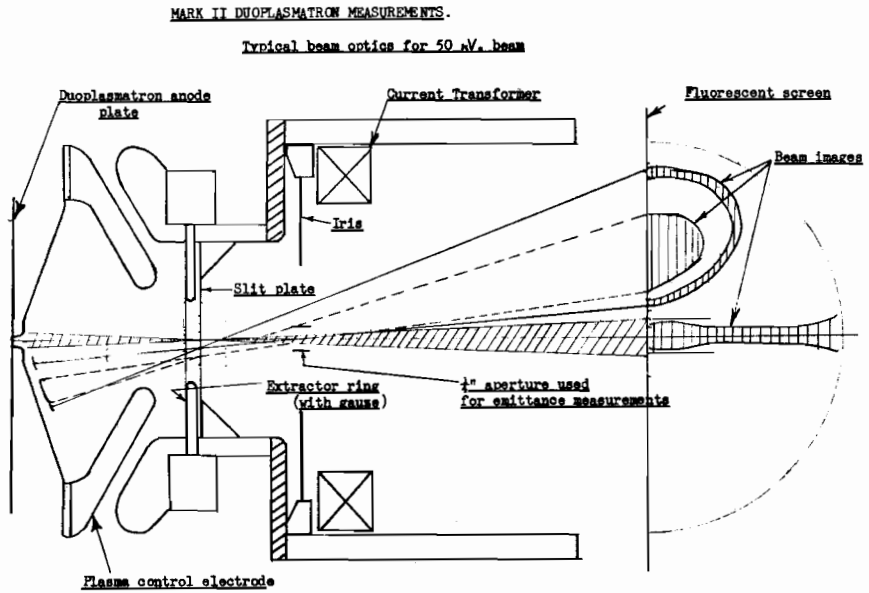

Fig. 6 Mark II duoplasmatron beam extraction geometry using the plasma expansion cup.

between 0.04 and 0.06 mA/(mm-mrad)^2 750 kV which corresponds approximately to the region B_{MI} in Fig. 1. Since the uncertainties in defining the cut-off point on the brightness profile are large for this kind of measurement, it can be assumed that the measurements described here represent only the highly dense portion of the brightness profile.

The duoplasmatron extraction region was modified to incorporate an area for the expansion of the arc plasma through the anode aperture. This modification has been shown to be potentially capable of giving larger extracted beams of high brightness from a hot cathode arc discharge. The first model of this method of beam extraction at Brookhaven was the Mark II duoplasmatron, consisting of a Mark I ion source with a modified extraction geometry shown in Fig. 6. The beam optics for a 50 kV beam are also shown, indicating the existence of a beam crossover just upstream from the iris position. The plasma control electrode was biased approximately 20 - 30 volts positive from the anode plate to prevent the plasma from expanding too close to this electrode. This bias had a significant effect on the intensity of extracted beam and in some modes of operation it could increase the extracted beam intensity by a factor of 3 over the beam intensity without bias. The extraction electrode had a fine tungsten wire gauze across its aperture to increase the focusing at the extractor electrode.

A set of emittance measurements were performed for the Mark II extractor geometry using slits placed near the extractor ring and 1.25 inches from the end of the Faraday cup. By narrowing the intermediate electrode channel to 0.10 inches diameter it was found possible to expand the anode aperture to 0.060 inches and get large extracted beams of the order 600-700 mA.

A typical emittance measurement is shown in Fig. 7 for a 60 kV - 710 mA beam extracted from the Mark II setup. Evidence for the existence of two phase space areas is shown in which the smaller area has probably the higher current density. The ion source was pulsing for a 40 microsecond pulse width and a 55 A discharge current for this measurement.

A summary of recent emittance measurements for the duoplasmatron type of ion source is given in Fig. 8. It can be seen that in general higher extracted currents with better brightness qualities can be obtained with the plasma expansion mode of extraction. It is expected that future trends for high accelerator beam intensities will be satisfied by means of careful attention to the ion extraction mechanism in ion source plasmas.

VAN STEENBERGEN: More in terms of a remark, it seems possible to change the magnitude of the plasma cup and get the same plasma density for a lower discharge current.

OLEKSIUK: That is right. I think the density is really dependent on discharge current. I believe that discharge current tells you how many neutrals you have relative to ionized particles in the plasma and this is perhaps where the strong dependence arises. If you are trying to control an ion density, I believe that this is the place to do it. The control of the plasma area I think will be perhaps a control on the aperture of the anode. We did get larger extracted currents, of course, using larger apertures, but the increase in brightness appears to come from the discharge current.

VAN STEENBERGEN: I remember Solnyshkov's results whereby he used 150 A discharge current for typically a 10-cm diameter plasma cup. He got equivalent results at least in emittance when he used, say 50 A with a 3-cm cup. It was as though the plasma density in both those cases was similar but he did not expand the plasma as far in the latter case.

OLEKSIUK: Yes, that sounds reasonable. In fact this may be the other way of doing it, that is, keeping the plasma expansion down to a certain finite degree.

VAN STEENBERGEN: Yes. This, of course, might limit the total current. You might not get 700 mA then.

OLEKSIUK: This would be for the same brightness figures. The brightness figures would not change radically--that is a possibility. We used only the one extraction geometry at this stage and, of course, there is a lot more work to be done that way.

MORGAN: On the 700 mA emittance work at 50 kV, I believe you say you used only 600 to 900 V bias on the target. Did you actually check this current calorimetrically. With a beam like this, this field would probably be insufficient for containing the electrons.

OLEKSIUK: The two readings we had were the current transformer and the Faraday cup. No calorimetric readings were obtained. We see what is hitting the iris and what is being collected in the cup and what the current transformer reads. We are biased for secondaries and we have a small area that the back-streaming electrons see anyway to get out. So it seemed that we were fairly safe in the current measurements.

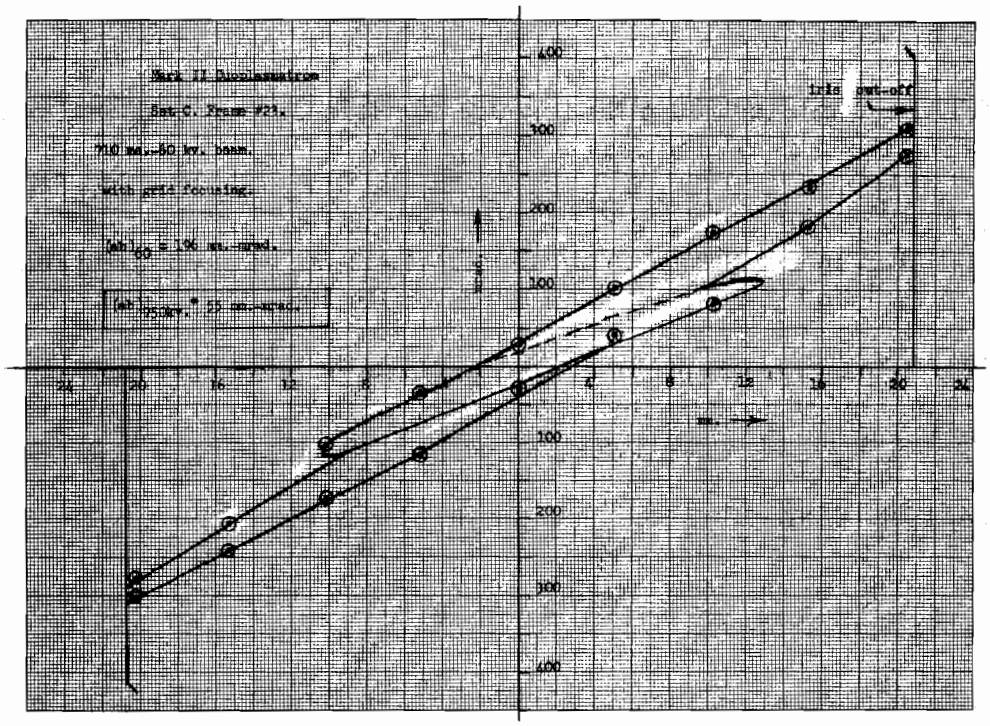

Fig. 7 Emittance of a 710 mA beam extracted from the Mark II configuration.

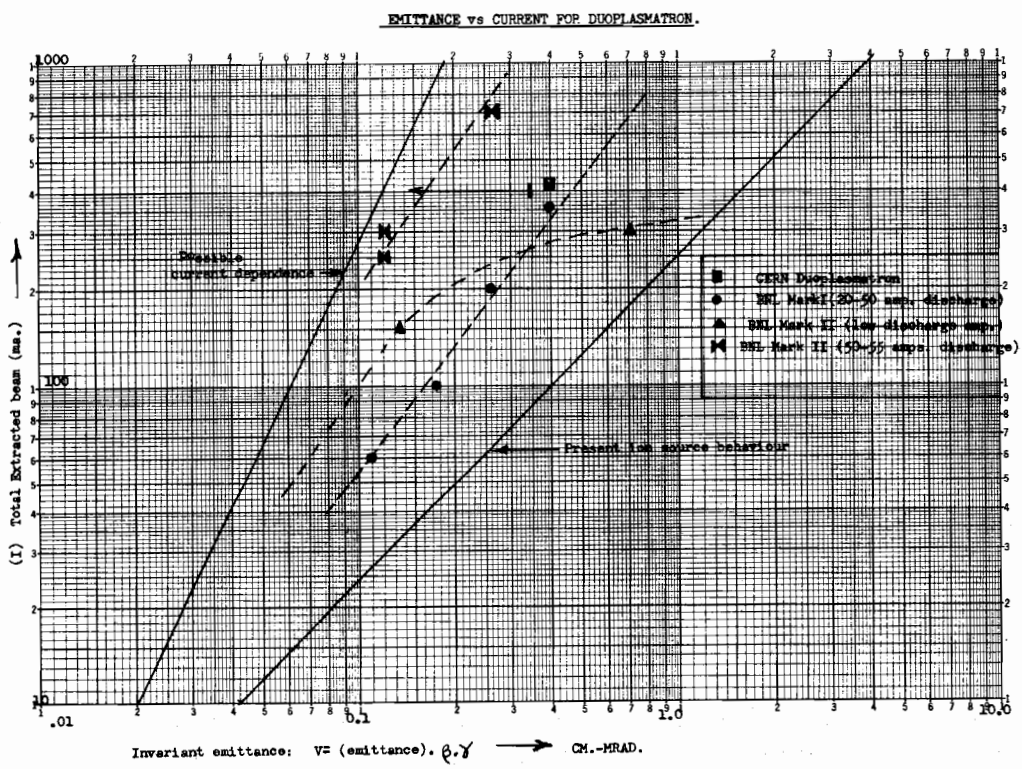

Fig. 8 Recent beam emittance values for the duoplasmatron type ion source.

MORGAN: Were the 700 mils through the iris or was that the total current, including the loss on the iris?

OLEKSIUK: The 700 mils were through the iris. There were possibly about 100 mils cutting in on the iris itself. So we measured the collected slit current and checked it with the transformer.

WROE: I just wanted to check on variation of emittance with arc current. Were you saying toward the end that the emittance you measure went down as the arc current went up?

OLEKSIUK: Yes.

WROE: This seems the wrong way around if you attribute the emittance to an ion temperature.

OLEKSIUK: Well, in fact, we do not know what the temperature does. One may be just changing ion density. Of course, I don't know how the plasma would see this. But, in fact, just looking qualitatively at the way this bright spot appears, I think we are introducing some sort of a new area in the plasma from the high discharge and this dense area is perhaps contributing to the large effects we are seeing in the brightness. Extraction from this new bright area may be giving us the high brightness numbers.

LAPOSTOLLE: You tested your source with and without grids. Could you say what you think is best?

OLEKSIUK: The grids tended to dilute the beam emittance a little bit. The emittance numbers were perhaps 20% higher for the same current extracted using the grids.

LAPOSTOLLE: Is it one or two grids?

OLEKSIUK: It is one grid. The grid changed the optics a bit as was expected. The other effect was that with the grid I could extract higher currents. That is, without grid I would be limited to perhaps 350 to 400 mA. Then by putting in the grid I could go up to 700 or 710 mA of beam under the same ion source conditions. So I think the grid is contributing secondaries which are neutralizing space charge, or something to this effect. It does have a good effect on the extraction.

VAN STEENBERGEN: It is interesting to note that at HVEC indications have been obtained that the various shapes in the emittance diagram

would be related to two kinds of beam shapes or beam profiles. The high intensity central core would come from a lower density plasma at the periphery of the plasma boundary and the rather wider beam of lower intensity, which constitutes the lower density filled distorted shape in the emittance diagram , would come from the central part. Thus there seem to be indications of an inhomogeneous density distribution at the plasma boundary. I don't know how this would tie in with the observation of a preponderance of heavy ions in the distorted shapes. Possibly beams from a lower density region with a lower plasma temperature might show a different proton percentage.

OLEKSIUK: I should really mention ion source oscillations; we get evidence of about a 10-12 Mc oscillation in the extracted beam and I believe this is due to ion sound-wave oscillations; one can estimate the frequency using the parameters in the discharge and get reasonable agreement with this range. I found it possible for the oscillation to disappear, due mainly to change in the aperture of the anode plate, that is, for large anode plate apertures the oscillation completely disappeared.

ION SOURCE AND COLUMN PERFORMANCE AT ORNL*

G. G. Kelley and O. B. Morgan
Oak Ridge National Laboratory

Most of the experimental work in controlled fusion in Oak Ridge is based on the trapping of high energy molecular ions in a magnetic "bottle" by dissociation of the ions in the bottle. For the past six years our group has been concerned with the development of injectors for these experiments. Large dc currents are needed and large current densities are desirable. Since we are not interested in short pulse performance and do not have to match emittance shape to an accelerator, our approach has been different from that of the people making preinjectors. We have not been measuring emittance but have concerned ourselves with passing a beam through the smallest possible channel in specific geometries. Our beams are pulsed on and off, but generally we are not concerned with the first 100 μsec after turn-on or turn-off. On the other hand, we have the problem of dissipation of very large amounts of power at high power densities.

Two power supplies and two test stands have been used for our studies. One test location is in a small laboratory. It has available up to 100 kV at 3 amp. Here we have made source studies and have done magnetic deflection beam analysis. The other test facility is in a large open area and is coupled to a 600 kV, 1 amp supply. At this site we have tested accelerator tubes and made studies of beam profile and of targets.

We have been using the duoplasmatron of von Ardenne. We started with what was practically a Chinese copy of a source described in his books, but we could not get sufficient heat transfer from the tungsten anode insert to the anode to permit operation at high dc arc currents. A current of about 5 amp was the most that could be maintained reliably for long periods. After we found that we could get good performance with nonmagnetic anodes, we changed to solid copper. A solid molybdenum should work somewhat better, but it is less convenient to use. One other change had to be made to permit operation at steady arc currents greater than 10 amp. The tip of the intermediate electrode needs to be cooled very well to prevent heating beyond the curie temperature. A water-cooled copper block is brazed to this electrode just beyond the tip. Figure 1 is

*Research sponsored by the U. S. Atomic Energy Commission under contract with the Union Carbide Corporation.

a cross-sectional view of one of our present sources. We are using filaments of a type designed by C. D. Moak of the Physics Division of ORNL. They are made from 40 mil tantalum wire covered with a platinum gauze and wrapped in a bi-filar spiral. Care is taken to see that no part of the finished filament is directly on the axis of the assembly. The filaments are then dipped in a barium strontium carbonate solution, the standard cathode dip used in tube manufacture. They require no activation procedure but should be outgassed in a separate system to prevent dirtying the source. Operating current is about 20 amp. These filaments have a life in the hundreds of hours when they are kept away from the high energy electrons which stream back through the anode aperture from the accelerating gap.

The methods we have used for determining the mass ratios in the plasma from the source will be described later. Our main interest has been in the production of molecular ions. When a source is run with a small spacing between intermediate electrode and anode--about 1/16 of an inch--and if the source is run gas starved, i.e., at sufficient arc voltage and at low enough source pressure that the desired output current is insensitive to variations in arc voltage, then the H_2^+ ion component is at least 60% up to 100 mA and at least 95 mA of H_2^+ has been obtained at correspondingly higher total currents. The proton yield can be increased by increasing the intermediate electrode to anode spacing to at least 1/4 inch, and by the use of high electron densities--by reduced anode aperture size and increased arc current for a given output. A relative proton yield of 90% has been obtained at moderate current, and proton yield seems to be even more favored at higher currents. Triatomic ions are produced by operating at high gas pressures and low arc voltage. A maximum of 37 mA of H_3^+ has been produced.

The plasma streaming through the anode aperture in the source consists of rather energetic electrons--up to 100 eV--and considerably lower energy ions. The ions have a directed energy of the order of about typically 8 V. When a strong electric field is created in the region beyond the aperture, the electrons are repelled and the ions accelerated. There results a plasma-beam boundary which forms at such a place that the space charge of the ion beam shields the plasma surface from the extracting field. Since the current density of ions in the anode aperture may be as high as 100 amp/sq cm (it is kept high to make the gas efficiency of the source high--typically greater than 90%) and since the maximum current density that can be supported with physically realizable extracting fields is under about 2 amp/sq cm, the plasma will expand into the region below the aperture. For a long time we thought that the arrangement using the highest possible field and correspondingly the smallest amount of expansion was most desirable. Recently we have

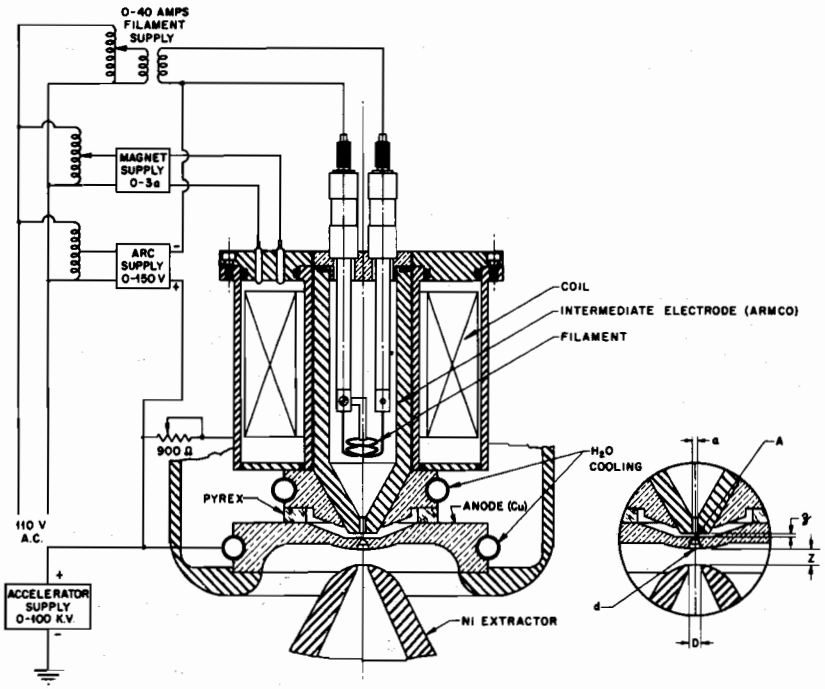

FIG. 1 MODIFIED DUOPLASMATRON ION SOURCE

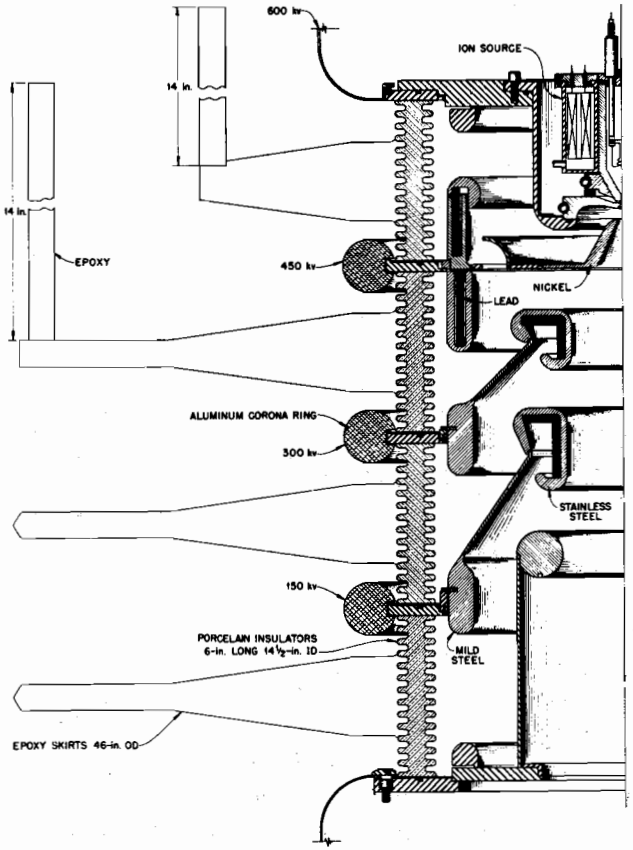

FIG. 2 600 KV ACCELERATOR TUBE

been experimenting with large cup arrangements found to give better beam quality by the Leningrad group and others.* This arrangement has the further advantage of more reliable voltage breakdown characteristics.

The maximum current that can be obtained with a given maximum allowable divergence of the beam after extracting depends only on the extraction voltage. Since the current density for space-charge limited current is given, for an infinite plane beam, and for a parallel cylindrical beam using Pierce geometry, by the expression

$$j = \frac{5.44 \times 10^{-8}\, \phi^{3/2}}{M^{1/2}\, Z^2}$$

where M is the mass number, j is in amp/sq cm, ϕ is in volts, and z is the electrode spacing in centimeters, the total current depends only on ϕ for a given ratio of spacing to beam diameter. We have found that this expression predicts the maximum current density even when the electrode shape is far from that which would be expected to produce a parallel beam according to the derivation of Pierce. (To get good agreement, however, it is necessary to make an empirical correction which consists of increasing the value of z by the radius of the aperture in the accelerating electrode.) For a spacing of twice the radius of the beam which seems to be a reasonable choice, the maximum current is given by $I = 19\, V^{3/2}$ where I is in mA and V is tens of kV for protons. The maximum current then which can be obtained in a beam of moderate divergence at 150 kV is slightly over 1 amp.

A current of 500 mA has been extracted from a source on the small test stand at 100 kV. A current of 400 mA was extracted from this source continuously for a period of four hours.

Our 600 kV supply has a 170 mA bleeder with taps at 150 kV, 300 kV, and 450 kV. We extract from the source plasma at 150 kV and accelerate the beam in three more 150 kV high-gradient, close-spaced steps. An ion from the source is accelerated to the full voltage in approximately 12 inches. Figure 2 is a cross-sectional view of the accelerator tube. There

---

*A. I. Solnyshkov et al., "Current Injector for a Strong Focused Linac," Proceedings of the Dubna Conference (1963). See M. D. Gabovich, Review Article, "Extraction of Ions from Plasma Ion Sources and Primary Formation of Ion Beams," Instruments and Experimental Techniques, No. 2, pp. 195-206 (March-April, 1963). See also N. B. Brooks et al., "Production of Low Divergence Positive Ion Beams of High Intensity," Rev. Sci. Instr. 35, 894 (July 1964).

are four alumina insulators six inches high by fourteen inches ID. These are fastened to stainless steel rings by the vinyl seal technique. The rings provide electrical connection and alignment. Viton O-rings are used between the metal pieces. Skirts of unfilled epoxy molded to the insulator sections provide a large external breakdown path. Some of these skirts have been in use for over two years with no trouble due to breakdown through the interface between epoxy and ceramic. The electrodes are designed to keep the metal surface area having a strong field at a minimum. We made tests which showed that voltage cleanup problems become much greater when the linear dimension of the surface at high field is large compared to the electrode spacing. A solenoid focusing magnet is provided just below the accelerator tube to converge the beam. It is capable of operation at 2.4×10^5 amp turns and has six-inch diameter throat.

The site of the development of this tube is shown in Fig. 3 and Fig. 4. The beam is passed into a long cylindrical tank where probe studies and visual observation can be made. By means of an extension on the bottom of this tank the beam can be allowed to travel about 17 feet before striking a target. A profile measurement at a number of points along the beam gave an extrapolated value of 2.9 inches for the diameter of the beam in the lens at a total beam current of 180 mA. This measurement was made quite some time ago. We believe now that with large source cups we can make the beam considerably smaller. Large beam currents can be mass analyzed by this test facility by making use of the different focal lengths of the magnetic lens for the different mass components. These can be focused successively through a small aperture and the power on a target beyond measured calorimetrically. There is an essentially complete self-neutralization of the space charge of the beam by electron trapping. The beam profile shows no space charge spreading down to the lowest operating pressure which can be obtained in the system--2×10^{-6} mm Hg. We found, however, that the beam cannot be passed through a crossover in the region below the lens without being seriously disrupted. When a beam component is focused in the observation tank, it appears to get brighter as it gets smaller down to a diameter of about 1 cm and then becomes less bright but continues to converge to a sharp point. Nothing is seen of the beam below this point. When the beam is allowed to fall on a target and the lens strength is increased, the spot size becomes smaller and smaller and more and more intense down to no more than a pin point. With a further increase in lens strength, the spot disappears. We intend to study this phenomenon in greater detail.

We have operated this accelerator at a total power supply drain of 330 mA. At the same time we were able to account calorimetrically for about 300 mA. We do not know what became of the other 30 mA. It did not flow to any of the electrodes in the tube. These currents were

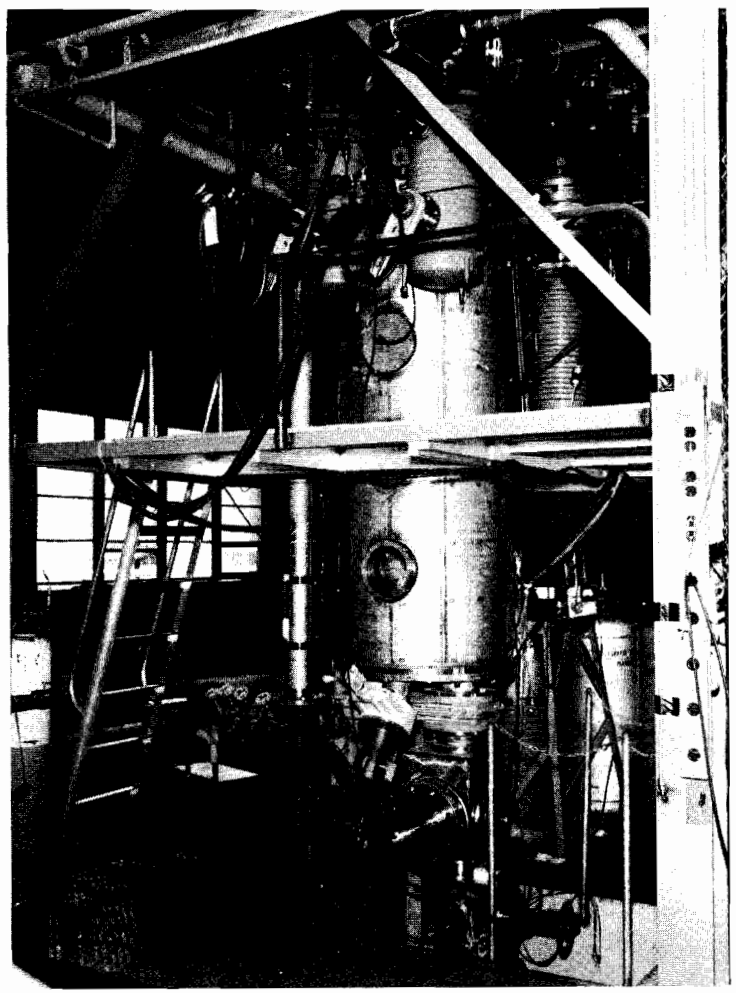

FIG. 3 VACUUM CHAMBER FOR ACCELERATOR TEST STAND

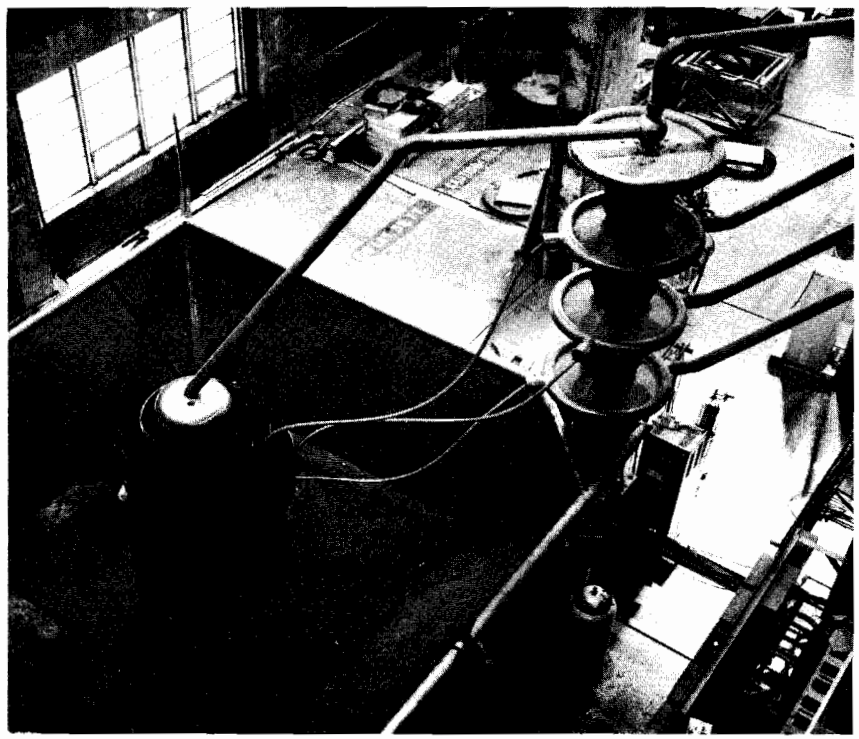

FIG. 4 TOP VIEW OF ACCELERATOR TEST STAND

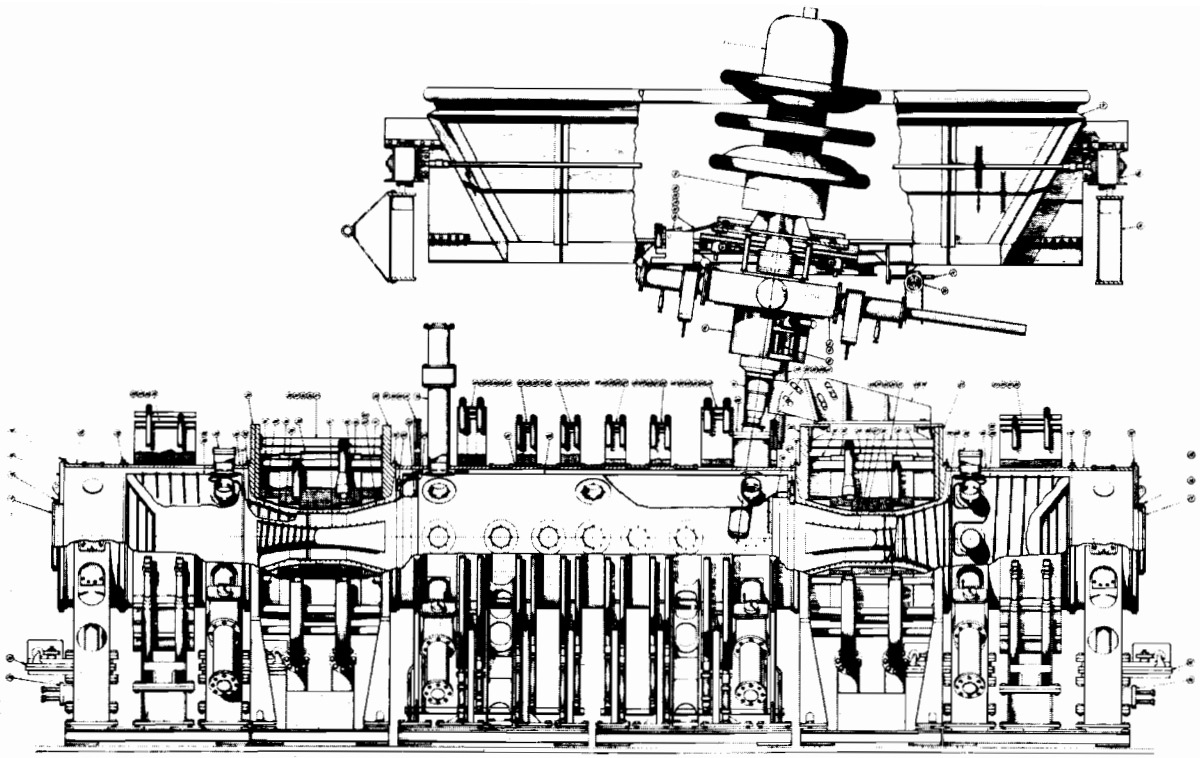

FIG. 5 CUTAWAY VIEW OF DCX-2

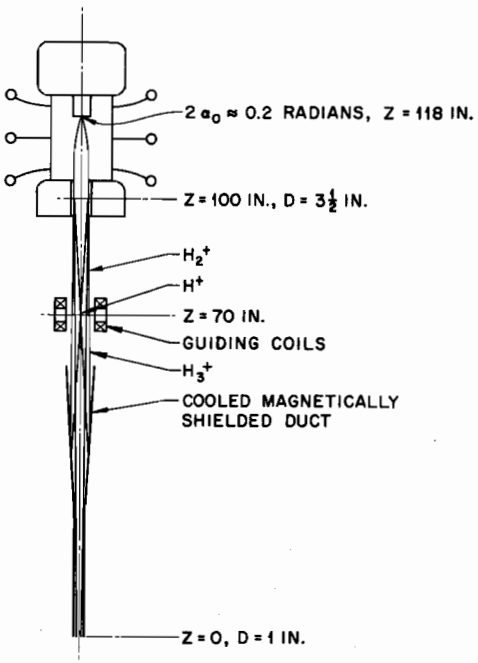

FIG. 6 DCX-2 INJECTION SYSTEM

measured to be no larger than 1 mA. At the same time the power dissipated by the source anode was being monitored. An electron current of 0.5 mA at the full energy should have been detectable. No power difference was measured when the accelerating voltage was turned on or off.

The beam can be switched on and off by an electronic switching device in the source-arc supply. This switch is operated through a crater lamp-photomultiplier light beam link between ground and the 600 kV level. The beam can be turned on and off in less than 2 μsec.

The instantaneous beam current is transmitted from the 600 kV level to ground through a FM radio link. The system uses two commercial FM receivers having AFC, with slight modification. The arrangement has excellent linearity and low drift and has a time resolution of about 13 msec.

We have found, as have others, that an accel-decel arrangement can be used to permit neutralization of an ion beam. To be successful the arrangement must provide an electron-repelling field only in a small region around the beam. The exit electrode should be at ground potential and the beam beyond should not be able to "see" other potentials. We have neutralized a 50 mA, 70 kV beam after the beam had passed through an Einzel lens. A potential of - 3 kV, with aperture sizes of 1 to 1.5 inches, was enough to prevent electron loss from the beam.

Figure 5 shows a cutaway view of DCX-2, the largest of the experimental devices at Oak Ridge. In this device 600 keV H_2^+ ions are injected through a magnetically shielded channel into a uniform 12 kilogauss field. This field increases to 39 kilogauss at points 81 inches either side of the midplane. Ions enter the field 9 inches from the longitudinal axis at such an angle that they have a helical trajectory passing from a point near one magnetic mirror to slightly beyond a corresponding point near the other mirror. The orbit diameter is 10.3 inches. These ions reflect and return to the injector after having traveled a distance of the order of 100 meters. During their flight some of them are dissociated either by background gas and plasma or by a vacuum arc run between electrodes at opposite ends of the machine. The protons resulting circulate between reflection points and precess at each reflection, but some of them are deposited in the field in such a way that they do not return to the injector in spite of this precession. The mechanical and magnetic design of the injection channel is quite difficult. It consists of a hyperco cylinder with overlaid windings which compensate externally for the effect of the cylinder and also cancel the longitudinal component of magnetic field along the cylinder. The problems of design of the in-

jection duct make a small channel very desirable. The value chosen was 1-5/8 inches. Figure 6 is a schematic view of the beam path. Steering magnetic fields are provided in the pumping chamber just below the lens to compensate for small misalignments and for the effect of the stray magnetic field. This field is reduced along the beam path by the use of ferromagnetic materials in the electrodes and in other hardware wherever possible. It probably is the effect of the small residual field which has prevented injection of more than 50 mA of H_2^+ into DCX-2 in spite of the fact that, as has been said above, 95 mA have been passed through an identical structure in the test stand. The losses probably will be reduced by repair of the 600 kV supply which has been producing an abnormally large voltage ripple.

WROE: Could you just say quickly what type of resistors you used for grading the column?

KELLEY: I don't know the brand. They are just very many wire-wound resistors in an oil-filled column.

FEATHERSTONE: I was interested in your 1 A continuous 600 kV supply. Is it possible to keep the stored energy in the capacities fairly low, or do you worry about damage to electrodes in the column when a spark occurs?

KELLEY: Well, we worried about it until we found in practice that it did not cause us trouble. We have a 0.0125 μf condenser and then a 14,000 Ω series resistor between the condenser and the output, which consists of the isolation transformer capacity which I think mounts up to about 700 $\mu\mu$f .

THE PLA POLARIZED PROTON SOURCE

J. M. Dickson
Rutherford High Energy Laboratory

History

The design work on the polarized source was started in 1957. It was developed into a functioning source by 1959 and was first operated on the PLA in February 1961. The time during which a polarized beam has been available for nuclear physics experiments now totals 4670 hours, comprising 500 hours in 1961, 1500 in 1962, 1725 in 1963 and 945 in the first six months of 1964. The operational reliability of the source has been such that the percentage fault time of the P. L. A. has been only marginally lower with a polarized beam compared with thatof the normal unpolarized beam.

Development

Engineering development of the source has been a continuing process during its life and has been aimed at eliminating weaknesses in the original design, notably, lack of sufficient cooling, unreliability of control mechanisms between ground and the 500 kV platform, and alignment difficulties. The original ionizer was inefficient, gave an annoying inequality of "spin-up" and "spin-down" polarizations and intensities, and produced a beam which was not parallel to the axis of the injector. Two successive redesigns of the ionizer eliminated the polarization inequality and provided electrical steering of the beam. The ionizer now used is shown in Fig. 1. It has an ionization efficiency of about 10^{-3}, as used, but by modifying the extraction electrode and the ion mirror a factor 5 improvement might be achieved. The ionizer is followed by two pairs of deflector electrodes similar to the X, Y plates of an oscilloscope.

Surrounding the ionizer there are three pairs of coils arranged in the general form of Helmholtz coils. These are used to produce a low field (3 to 10 Oe) in the ionization region to orient the polarized atomic beam in the desired direction. This system is very convenient to use and very flexible, in that any desired direction of proton polarization can be produced and the direction can be precisely reversed by reversing the current in one or two of these pairs of coils. For horizontal transverse polarization the Helmholtz coils need not be used since the sextupole magnet of the atomic beam system was designed to give a stray dipole field at the ionizer and the sextupole polarity can be reversed.

The atomic beam intensity has been increased by a factor of 1.5 by a new collimator in the dissociator. This collimator consists of a large number (~1000) fine bore pyrex tubes of uniform cross section (length ~1 mm, bore ~0.1 mm). It is similar in concept to the original collimator but the individual tubes are more uniform in size and the assembly technique produced much better alignment of the tubes.

Polarization and Intensity

The accelerated beam of protons, measured at the output end of tank 3, has normally a polarization of 0.40 and a mean intensity of 2×10^8 protons/sec (at 1% duty cycle). The polarization and intensity cannot be measured at any other point along the accelerator. This leads to some slight difficulty during operation of the accelerator and in locating some faults. The total beam current from the injector is about 20 times the proton current and the polarization cannot be measured at low energy. However, the rf and other parameters of the PLA are now well enough monitored to overcome nearly all these difficulties.

There is now rather good instrumentation for measuring the polarization and intensity of the output beam (the mean energy can also be measured to good accuracy). The polarization is measured by degrading the beam energy to 15 MeV (mean) and scattering the protons at 45° by a 2 MeV thick carbon target into four scintillation counters placed up, down, left and right of the proton beam. The degrader and target are mounted on a wheel rotating at 2.5 revs./sec. Variation of the number of degrader-target pairs from 2 up to 10 allows sampling of from one proton pulse in ten up to alternate pulses. In general two 50 MeV and two 30 MeV degrader-target pairs have been mounted, so that on changing machine energy from 50 MeV to 30 MeV the only change required is an adjustment to the gating circuits to ensure that counts from the appropriate target are registered. A signal from the rotating wheel is used to trigger the accelerator timing system and ensures synchronization of the target wheel and the proton pulses. Elastically scattered protons from the carbon target are selected by discriminators in the counting system. More details of this apparatus are given in the 1962 and 1963 PLA Progress Reports.

This system enables one to measure the transverse (vertical and horizontal) components of the beam polarization continuously. During a typical experiment, running for several hundred hours, the measured beam polarization varied by only $\pm$ 0.01 (standard deviation) per counting cycle, each of which had a statistical counting error of $\pm$ 0.002. At the same time the horizontal component of the polarization varied between - 0.008 and + 0.003 $\pm$ 0.002 and averaged - 0.002.

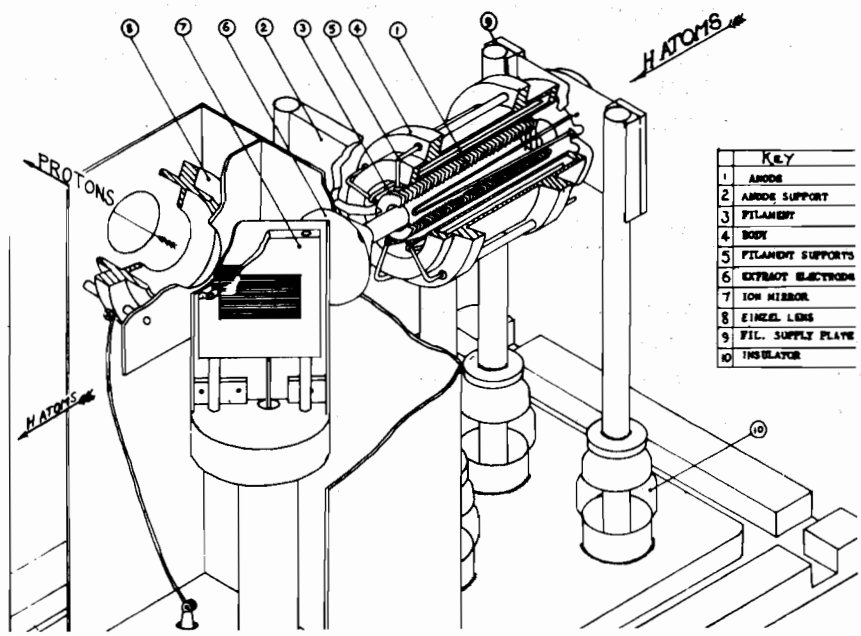

Fig. 1. Ionizer

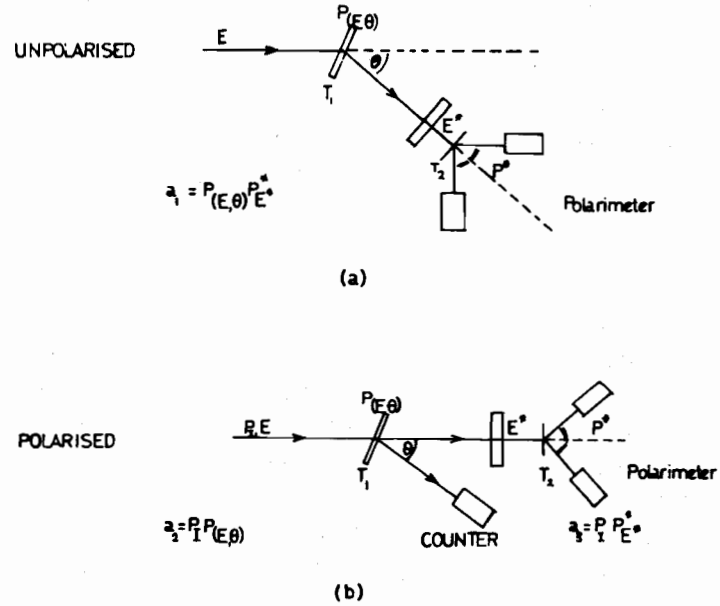

Fig. 2. Scattering Geometry for the Measurement of the Carbon Polarimeter Analysing Power.

The beam intensity is measured in an ion chamber filled with 1 atmosphere argon + 10% methane mixture. Mean proton currents down to 10^4 protons/sec can be measured using a dc amplifier and peak pulse currents of 10^7 protons/sec can be detected in a pulse amplifier.

Absolute Calibration of Polarization

The polarimeter described above could be calibrated from data available in the literature for (p-C) polarization at about 15 MeV but it was thought desirable that an absolute calibration measurement should be performed. The apparatus for this calibration is shown schematically in Fig. 2. From the three asymmetries measured with a polarized and an unpolarized beam the polarization of the beam is found from the relation

$$P^2 = a_2 a_3 / a_1 .$$

From the asymmetry a' measured by the continuous polarimeter its analyzing power $P' = a'/P$ can be found, $P' = 0.562 \pm 0.006$ at 50 MeV. The analyzing power, however, is a function of the mean proton energy incident on the polarimeter target so a correction factor had to be calculated from the results of a subsidiary experiment to enable one to measure the beam polarization for energies other than that used during the calibration. The absolute value of the beam polarization can be measured to an accuracy of $\pm$ 0.005 (standard deviation).

To obtain a beam with zero polarization it has been found necessary not just to switch off the sextupole magnet of the PPS, but to degauss the magnet by reversing the current several times while decreasing it. Otherwise residual polarizations of 0.01 may be observed.

Future Modifications

Since the statistical accuracy of polarization measurements depends on P^2, it is always desirable to increase the beam polarization. The present source has a theoretical maximum polarization of 0.50 so not much improvement can be expected. However, by using the adiabatic passage "spin-flip" technique first described by Abragam and Winter and so successfully exploited by the Saclay cyclotron group a factor of two improvement can be achieved. The necessary modifications to the source are now being proposed for installation later this year.

If the atomic beam, after selection of the $J = +\frac{1}{2}$ states in the sextupole magnet, is passed through an rf field in a low magnetic field,

which varies slowly through resonance, the $I = +\frac{1}{2}$ state can be completely converted into a $I = -\frac{1}{2}$ state. If the beam is then ionized in a strong magnetic field (~1000 Oe), a theoretical proton polarization of 1.0 can be achieved. Since ionization in a strong field is more efficient, the proton current will also be increased. It is expected that a polarization of 0.80 at an intensity of about 10^9 protons/sec will be obtained.

One disadvantage of the modified source will be that the present Helmholtz coil system cannot be used. The polarization direction will be vertical initially, but it can be rotated in the transverse plane by a solenoid, located in the 500 kV terminal. To obtain longitudinal polarization a crossed electric and magnetic field spin rotator will have to be installed.

Scheduling of experimental time on the PLA is handicapped by the fact that the unpolarized beam intensity obtainable from the PPS is lower than most experimenters require, and changing over to the normal source requires at least a 24-hour shutdown. It is desirable, therefore, to combine in the same vacuum system the PPS and a proton source of a few mA peak current.

Acknowledgements

D. A. G. Broad has been responsible for the recent development work on the polarized source. He has been assisted by R. C. Carter and A. G. D. Payne in the laboratory and the engineering has been the responsibility of K. McAinsh and J. A. Taylor.

MARTIN, J. H.: What was the pulsing rate of the machine?

DICKSON: It is 50 pulses per second and the pulse length is 200 μs.

FEATHERSTONE: Are you using the high frequency rf transition at about 1400 Mc or are you using the low frequency?

DICKSON: We are using the low frequency transition at about 10 G and 8 Mc/s which gives a transition from state 1 to state 3 by the adiabatic passage method.

ION SOURCE WORK AT ANL

D. H. Nordby
Argonne National Laboratory

I. Column

In the pursuit of higher beam currents with lower emittance a 500 kV test facility has been constructed. It has been built in such a way that various columns and ion sources can be tried with ease. Figure 1 shows the layout of the development room. Figure 2 shows a column that is presently being tested. It is a 15-inch long constant acceleration type column which is planned for the first section of a future 750 kV column (see Fig. 3). The column section is designed to run at about 250 kV, but as yet has only reached 175 kV.

II. Ion Source

This source shown in Fig. 4 was designed to be small enough to fit in a re-entrant column with an inside diameter of 10 inches. This requirement was met by using formvar-coated copper tubing in the magnet and a small diameter insulator. We use an oxide-coated cathode as has been used in the ZGS preaccelerator for the past two years. The expansion cup has been wound with formvar-coated copper tubing to give us another tuning parameter. The arc modulator is made in two sections so that the filament and intermediate anode voltage can be varied with respect to the anode independently. The modulator is transistorized and has a current capability of 30 A from the intermediate anode to anode. Source parameters are shown in Table I.

We have gotten over 600 mA with this source on a test stand.

III. Results

The column and ion source combination has been run at 575 mA and 120 kV. Crude emittance measurements were made which seem to indicate a beam quality improvement of a factor of 8-10 with a beam intensity increase of a factor of four over our present 750 kV preaccelerator. We expect to make more accurate measurements at various beam conditions later this month.

TABLE I

SOURCE PARAMETERS

Filament Current	15.5 A
Filament Voltage	5.9 V
Magnet Current	130.0 A
Extraction Voltage	20.0 kV
Focus Voltage	40.0 kV
Filament - Anode Voltage	200.0 V
Intermediate Anode - Anode Voltage	70.0 V
Filament - Intermediate Anode Current	12.0 A
Intermediate Anode - Anode Current	24.0 A
Source Press	0.2 Torr
Beam Current	400.0 mA
Acceleration Voltage	130.0 kV
Aperture	Nickel with Copper Tungsten Insert

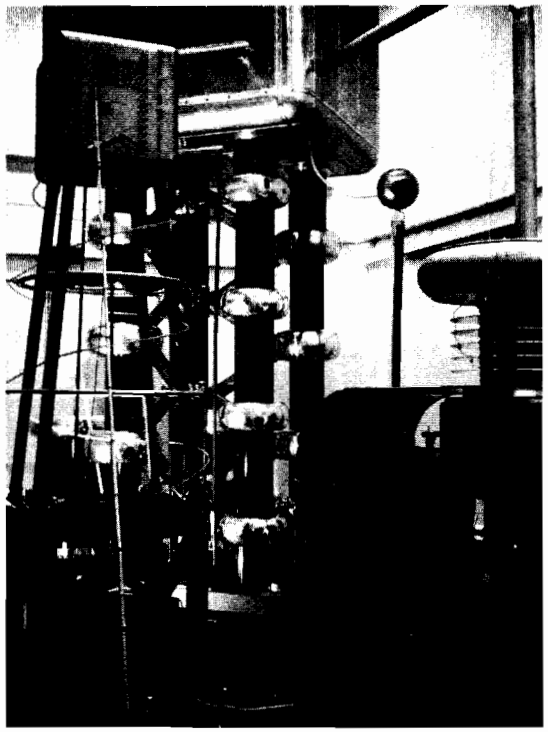

FIG. 1

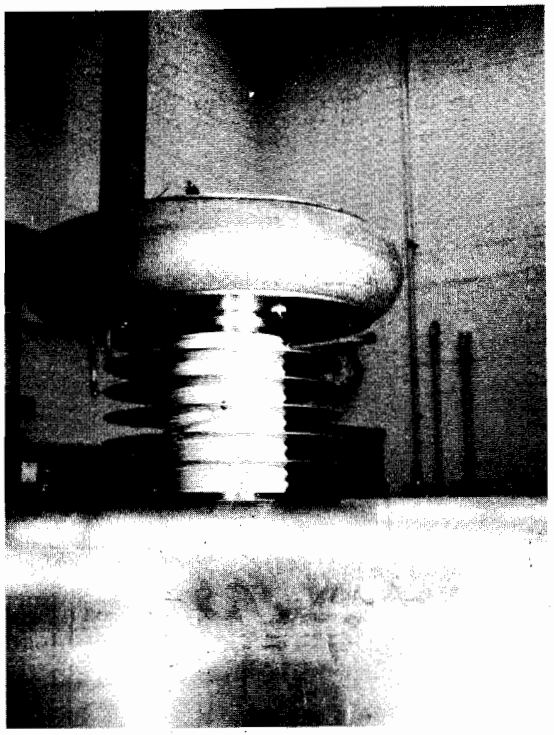

FIG. 2

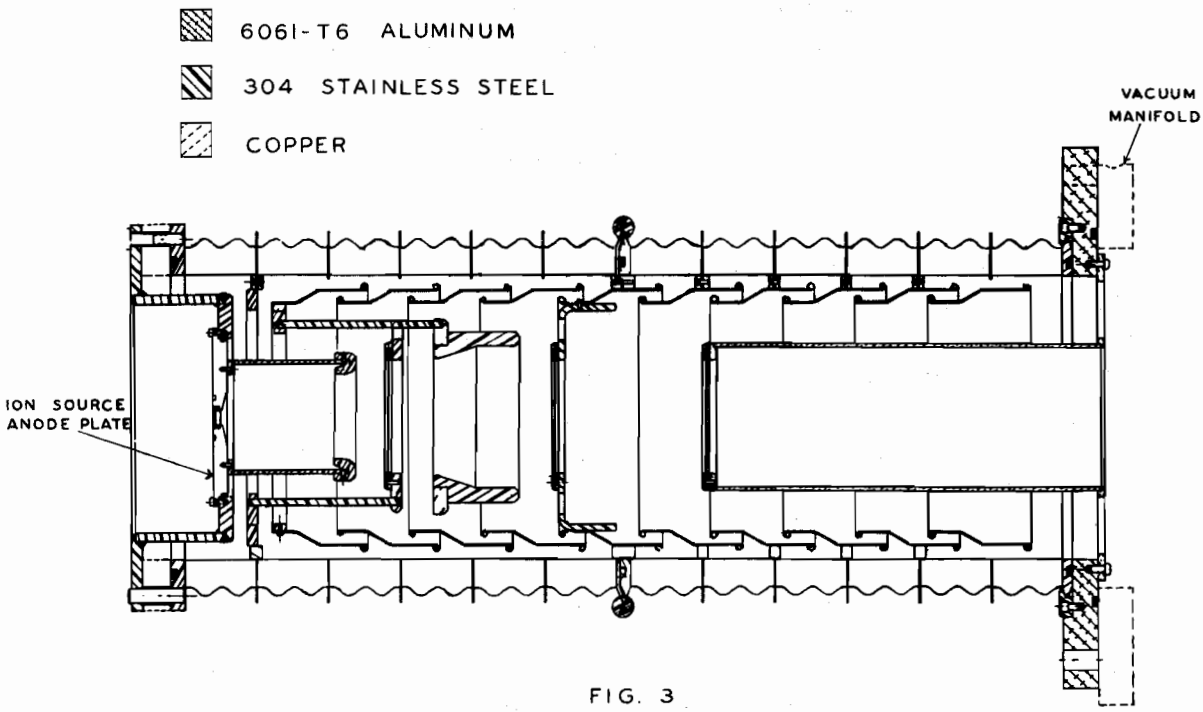
6061-T6 ALUMINUM
304 STAINLESS STEEL
COPPER
VACUUM MANIFOLD
ION SOURCE ANODE PLATE

FIG. 3

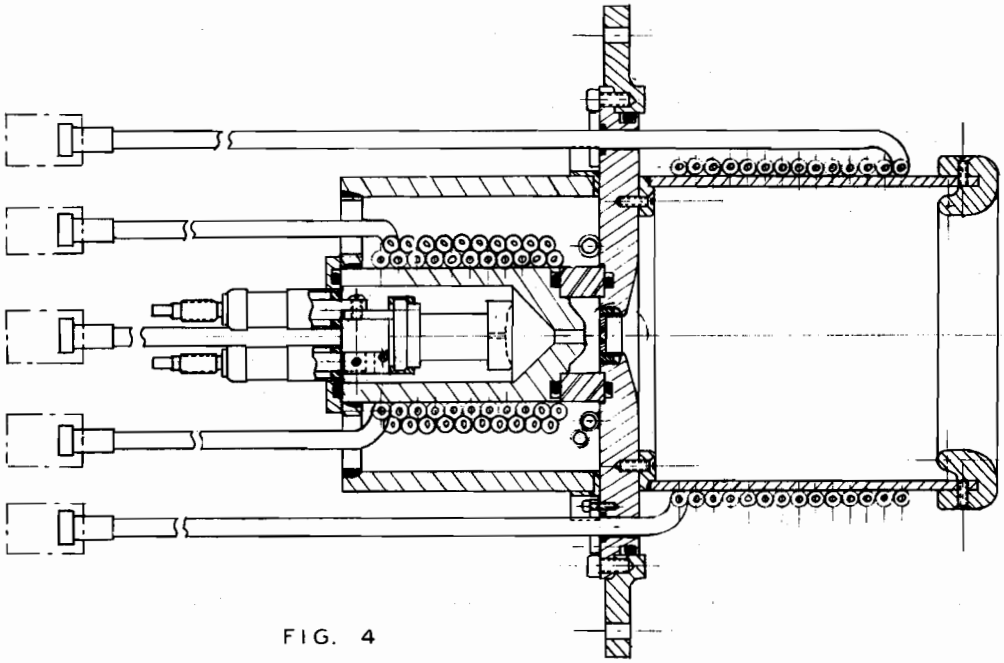

FIG. 4

AN EXTENDED RF ION SOURCE WITH SMALL PHASE SPACE EMITTANCE AREA

Rolland Perry
Argonne National Laboratory

Several types of ion sources have been designed for use on particle accelerators, and considerable effort has been devoted to attaining large beam currents. Somewhat less work has been done in the direction of reducing the beam divergence or of minimizing the effects of space charge. Since the latter effects are greatest in the region of low beam velocity, and since the emittance properties are established at the source, the present work is aimed at making some improvements in these two respects, without sacrificing intensity.

Historically, the first concepts were stimulated by a discussion of an electron gun for an electron microscope by A. V. Crewe, and the results are applicable to electrons as well as ions, except in different methods of production. Moreover, while the present design is based on the use of an rf excitation of a plasma, one might possibly adapt other methods of plasma production and extraction to achieve similar results.

The general arrangement of the source is simply that of a hollow donut-shaped cavity excited by an rf power source as shown in Fig. 1. Ions are extracted from the cavity by means of a dc field applied across a diameter between A and C, and the ions must traverse a narrow channel or slit arrangement which restricts their divergence angle. Since the slit extends all the way around the circular length of the donut, the area of extraction may be large even though the width w is made small, thus permitting almost arbitrarily large beam extraction.

The beam exit direction may be oriented at any arbitrary angle , which may be chosen to be compatible with some focusing and accelerating system.

First we look at the case of $\varphi = \pi/2$ in which case the central rays from all points around the circumference of the circular slit are emitted parallel to the axis of symmetry. The noncentral rays will have maximum divergence angle

$$\Delta\varphi = \frac{w}{\ell}$$

where ℓ is the length of the extraction channel. The area in phase space is

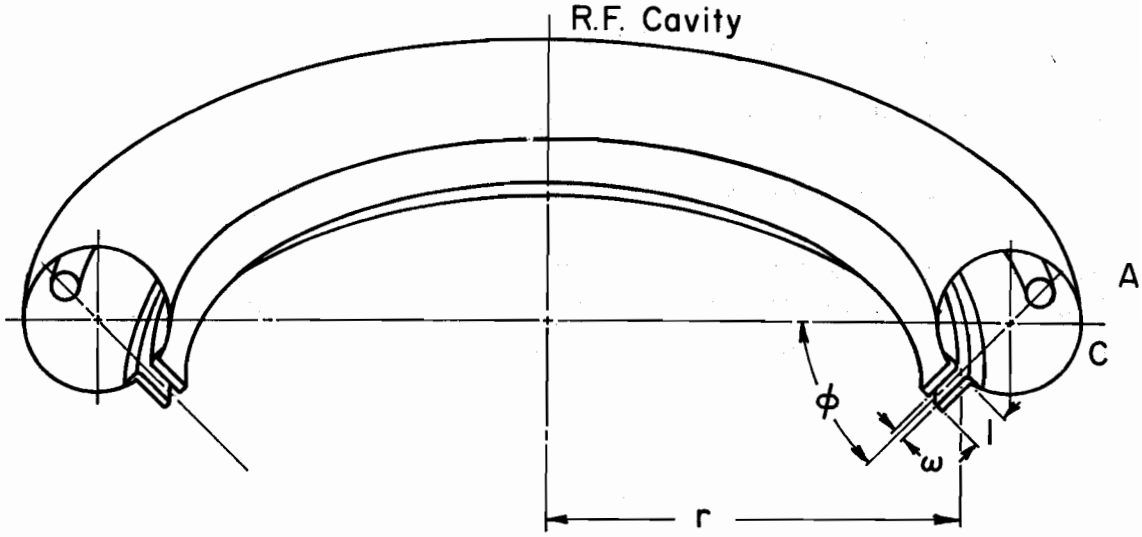

FIG. 1

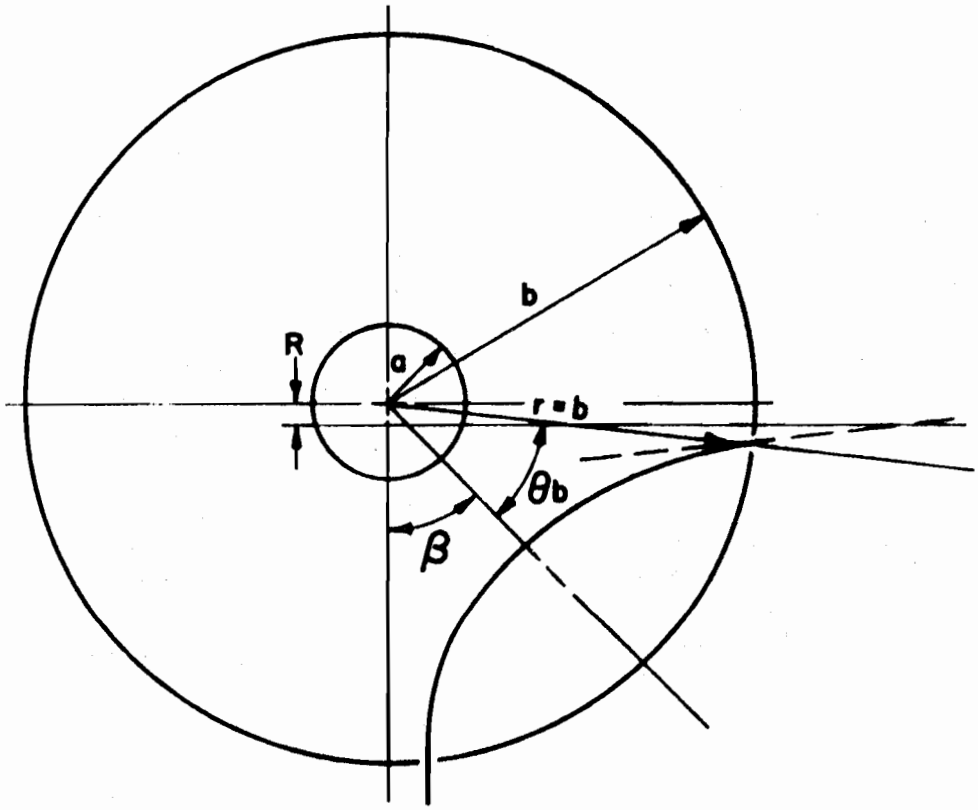

FIG. 2

$$A_x' \equiv r\alpha\pi = r\Delta\varphi\pi \quad .$$

Let w = 0.010", ℓ = 1", r = 7.5 cm. Then

$$A_x = r\,\Delta\varphi\,\pi = 7.5 \times 0.01\pi = 75\,\pi \text{ cm mrad}$$

at an extraction voltage of 20 or 30 kV which is typical for an rf source. This becomes about 12.5 π cm mrad at 750 keV or 15 π cm mrad at 500 keV. The extraction area for this condition is

$$S = 2\,\pi\,r\,w$$

$$= 2\,\pi \times 7.5 \times 0.025$$

$$= 1.18 \text{ cm}^2.$$

Compare these numbers with the corresponding values for rf sources of the CERN type, where

$$A_x \simeq 20\,\pi \text{ cm mrad at 500 keV}$$

$$S \simeq \pi\,(0.2)^2 = 0.125 \text{ cm}^2.$$

Now the geometry of accelerating tubes may not be compatible with a beam diameter as large as 15 cm, so the diameter may be chosen to satisfy this limitation. Likewise one may wish to inject into the accelerating tube at some arbitrary focusing angle. This may be done either by choosing the angle to meet the requirements, or, if this is not otherwise compatible, by injecting into a spherical condenser cavity and deflecting it by means of the electrostatic field in the cavity to form a hollow beam of arbitrary diameter and convergence angle.

The requirements for accomplishing this are as follows: The central ray from the slit must enter the spherical cavity at r = b tangent to a hyperbolic path shown in Fig. 2 and described by the relation

$$\frac{1}{r} = \frac{\sqrt{\left(V_a \frac{ab}{b-a}\right)^2 + 4\,R^2\,V_e + \left(V_a \frac{a}{b-a}\right)^2} \cos\theta - V_a \frac{ab}{b-a}}{2\,R^2\left[V_e + V_a \frac{a}{b-a}\right]}$$

This is a solution of the equations of motion for a particle of mass m and charge e moving in a central force field:

$$m\left[\ddot{r} - r\dot{\theta}^2\right] = \frac{Qe}{r^2}$$

$$m\left[2\dot{r}\dot{\theta} + r\ddot{\theta}\right] = 0 \quad .$$

The quantities in the trajectory equation are as follows:

a = radius of inner sphere

b = radius of condenser cavity

R = distance from center of sphere to asymptotic line toward which the hyperbola tends at infinity

V_a = potential on inner sphere

V_e = extraction voltage which corresponds to the kinetic energy the particle must have as it enters the chamber, i.e.,

$$e\,V_e = \frac{1}{2}\,m\,U_i^2 + \int_{\infty}^{b} \frac{Qe}{r^2}\,dr = e\,V_i - e\,V_b; \qquad V_b \equiv V_a\,\frac{a}{b-a} \quad .$$

The asymptotes are defined by

$$\tan\beta = \frac{2\,R\left[V_e + V_a\,\frac{a}{b-a}\right]}{V_a\,\frac{ab}{b-a}} \quad .$$

There are two benefits to be expected from using a hollow cylindrical or conical beam, viz

1. Since space-charge effects are more nearly the same for all particles due to the $\frac{1}{r}$ dependence, the distortion of the phase space figure due to space charge will be minimized, and

2. Since all particles traversing an axially symmetric lens will see essentially the same field configuration, lens aberrations should be minimized, thus reducing growth of phase space area from this cause.

A number of problems need to be examined in connection with the rf source as described. Figure 3 shows a conceptual design for such a source together with a spherical condenser lens system. The rf cavity would be driven in the TM_{010} mode from a wave guide coupling through

an iris into the cavity. For a cavity diameter of about 4 cm the frequency would be about 5000-6000 Mc/sec. Peak power requirements would be a few hundred watts.

CURTIS: With respect to your concern about violating Liouville's theorem, should I understand from your numbers that density in the region of phase space occupied by the particles has increased in the deflected beam over what it was in the converging ring of beam?

PERRY: One is concentrating the beam into a smaller diameter in the deflected beam. One might expect from Liouville's theorem that the divergence angle would actually go up in the process. The divergence angle does go up but it apparently does not increase in proportion to the reduction of beam radius according to my simple calculations which I am pretty sure are questionable.

LAPOSTOLLE: That worries me, and I also have some doubts about your estimated emittance. It is clear that, having a narrow slit, you can reduce very much the angle of divergence in the direction perpendicular to the slit. But in the direction parallel to the slit the emittance can be very large. The two directions cannot be considered independently in your bending system and I think that this could explain the apparent disagreement with Liouville's theorem.

PERRY: The extraction field has no component in the parallel direction, so the component of velocity in this direction is only the thermal component, which would be small in comparison.

LAPOSTOLLE: But there is no focusing in this direction from your deflecting system.

CURTIS: There would actually be divergence in this direction from the deflecting system.

PERRY: Yes, this is true. I cannot vouch for anything at present in terms of actual magnitude of emittance.

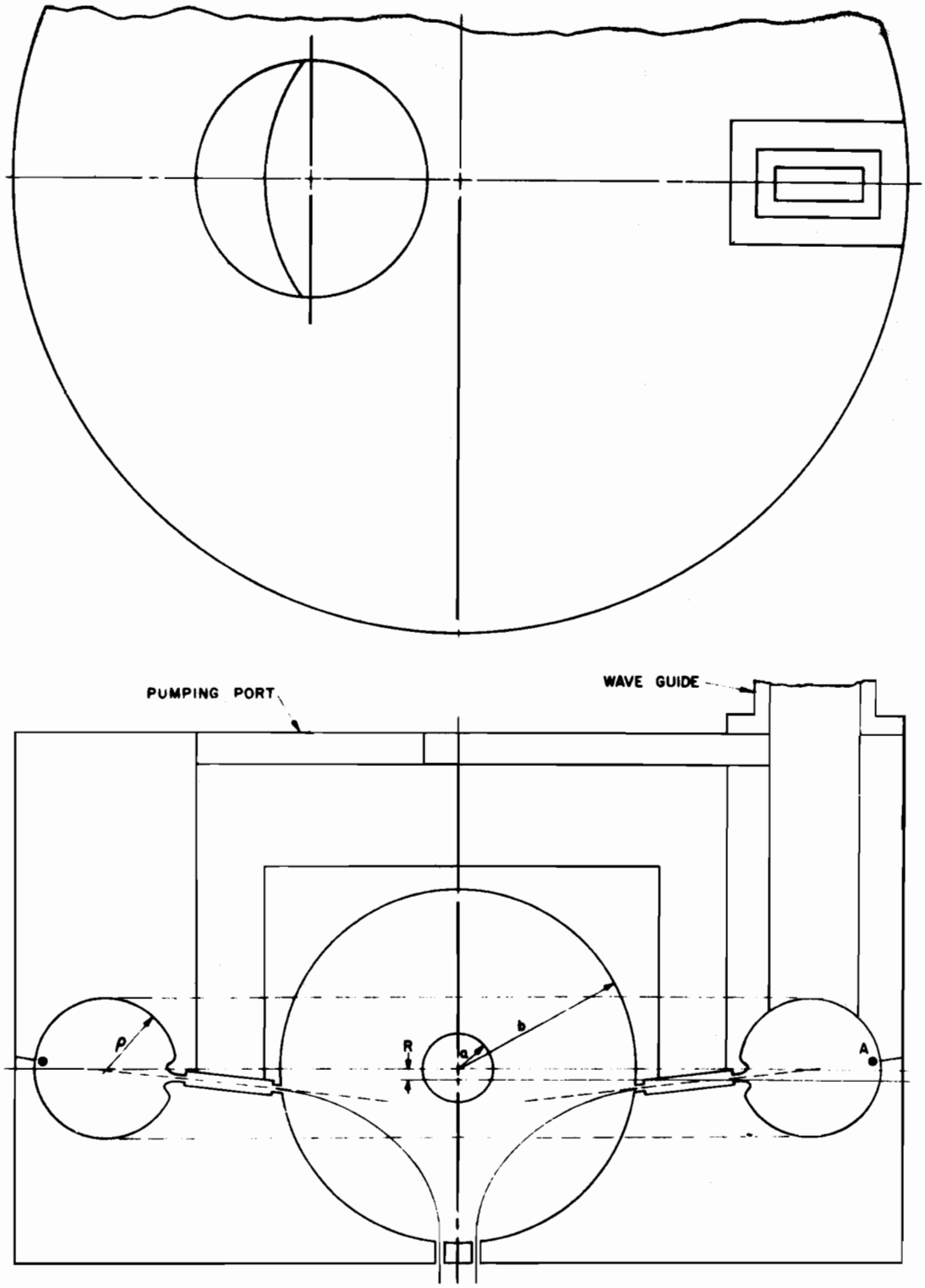

FIG. 3 EXTENDED RF ION SOURCE

A NEW APPROACH TO PREINJECTORS

H. Wroe
Rutherford High Energy Laboratory

1. Introduction

It has been realized for some time that the conventional preinjector, consisting of an ion source and focusing electrodes followed by a long accelerating column, could be simplified. If the vacuum breakdown problems could be overcome, then acceleration to the final energy in one step, across a single gap, has many advantages. Focusing could be done at earth potential thus reducing the quantity of equipment which has to be operated on the high voltage platform. The beam would be accelerated rapidly thus minimizing the effects of space charge.

Some work on the principle of single gap acceleration is described below.

2. A Single Gap Acceleration Experiment

An obvious first step is to arrange a pair of electrodes in a vacuum vessel and have a conventional ion source in the high voltage electrode. As a quick preliminary experiment, the apparatus illustrated in Fig. 1 was set up. In this case a standard rf source was operated at earth potential and the beam was accelerated to a negative potential across a single gap. This circumvented the need for the high voltage electrode. The latter contained a collector cup with a transverse magnetic field for secondary electron suppression, the only measure of beam current being a resistor on the low voltage side of the energy storage capacitor, as shown.

With no beam present the "pressure effect" was observed when a voltage was applied to the gap. The steady loading currents of several hundred μA which occurred at 3×10^{-5} Torr dropped to a negligible value at a pressure of about 5×10^{-4} Torr.

A beam current of about 40 mA (pulse length 1 ms) was accelerated to - 220 kV without breakdown of the gap at a pressure of 10^{-3} Torr in hydrogen. These values were the maximum available from the various power supplies at the time.

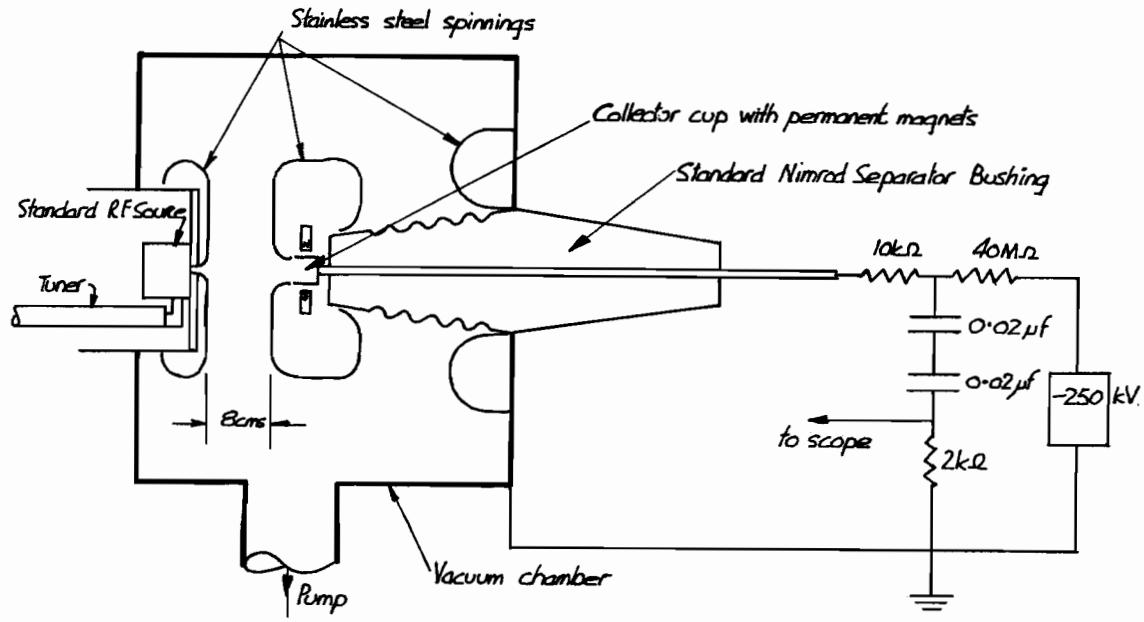

Not to scale

FIG. 1 Diagram of single gap experiment

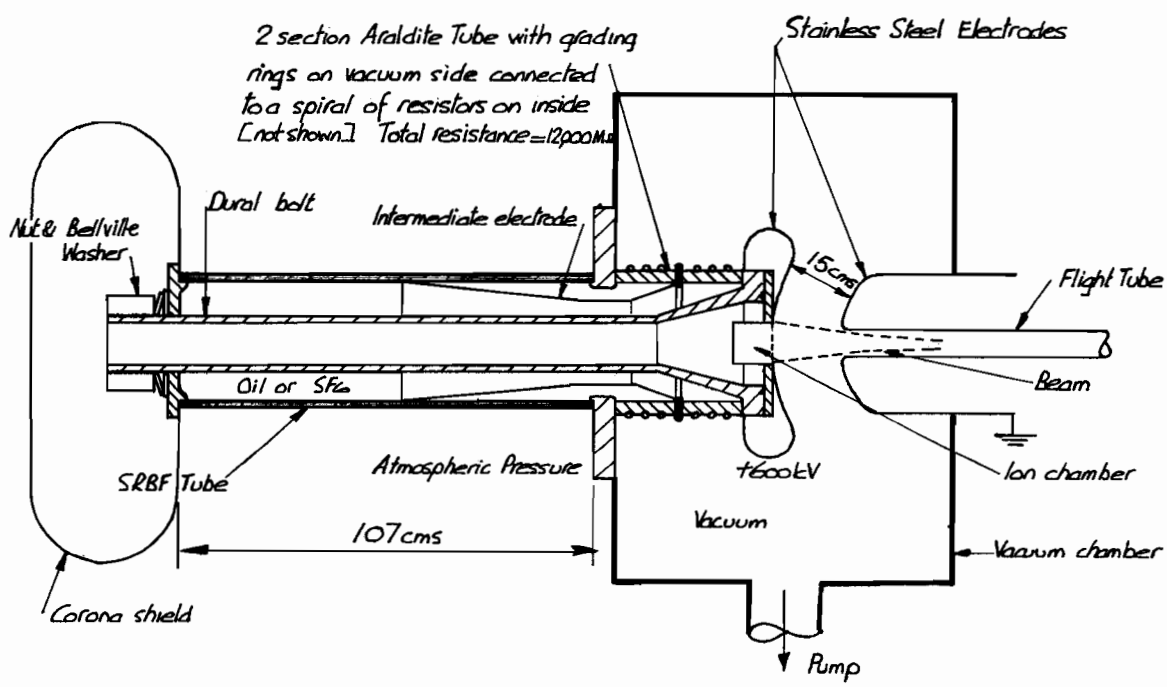

FIG. 2 Scaled-up Ion Source with 600 kV Lead-in Bushing

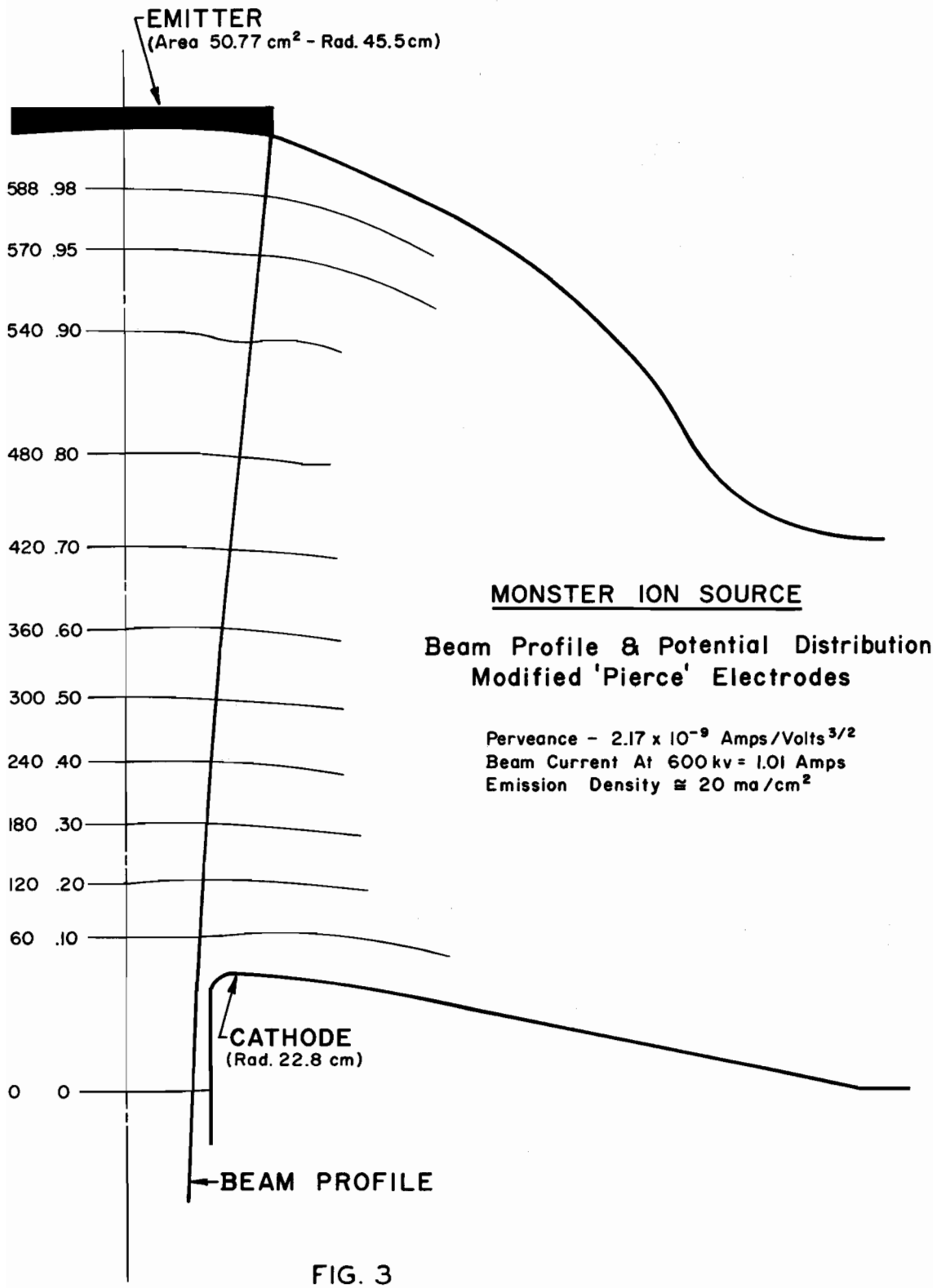
EMITTER
(Area 50.77 cm² - Rad. 45.5cm)
588 .98
570 .95
540 .90
480 .80
420 .70
360 .60
300 .50
240 .40
180 .30
120 .20
60 .10
0 0
CATHODE
(Rad. 22.8 cm)
BEAM PROFILE
MONSTER ION SOURCE
Beam Profile & Potential Distribution
Modified 'Pierce' Electrodes
Perveance - 2.17 x 10⁻⁹ Amps/Volts^3/2
Beam Current At 600 kv = 1.01 Amps
Emission Density ≅ 20 ma/cm²

FIG. 3

3. A Scaled Up Ion Source

The "pressure effect" makes it feasible to operate some sort of ion chamber and an accelerating gap at the same pressure, thus avoiding the canal or orifice needed in conventional sources to limit gas flow. The ions could be extracted over a large area at low current density from a discharge operating in the pressure range 10^{-3} - 10^{-4} Torr.

Work is proceeding on a device utilizing this principle as shown in Fig. 2.

A discharge chamber is housed in the end of a lead-in bushing. It has a gridded aperture 8 cm in diameter through which the ions are extracted. The extraction voltage corresponds to the accelerating voltage of a conventional preinjector, 600 kV in this case. The electrodes of the single gap have surfaces which are parts of concentric spheres. The radii of the anode and cathode are 30 cm and 15 cm respectively. With an ion emitting aperture of 8 cm diameter, assuming spherical space-charge flow and ignoring the hole in the cathode, the perveance is 3.6×10^{-9} $A/V^{3/2}$ for protons. Thus at 600 kV the space-charge limited proton current would be 1.7 A, requiring an emission current density at the plasma boundary of 30 mA/cm^2. The optics in the accelerating gap is illustrated in Fig. 3.

Two possible low pressure discharges are being examined as plasma sources--a Penning type and a discharge using an electrostatic electron trap.[1]

The design of the lead-in bushing is a major technological problem. The design shown in Fig. 2 consists of four parts, a mounting flange, an epoxy resin cylinder about 30 cm long and 34 cm diameter projecting into the vacuum chamber, a bakelite tube 107 cm long and the same diameter, and finally a strong tubular tie bolt down the center to hold the assembly together and give access for electrical leads to the ion chamber. The space between the bolt and the tubes is filled with transformer oil (and possibly compressed SF_6 at a later date). The surface of the epoxy resin tube is electrically graded by means of 8 metal rings on the outside (i.e. the vacuum side) connected through the epoxy resin to a spiral of resistors on the inside (i.e. immersed in oil). The total resistance is 12,000 M . The outside of the bakelite tube (i.e. in air at atmospheric pressure) may also be graded. An intermediate electrode is incorporated into the bushing as shown to make the radial potential distribution more uniform in the gap between the bolt and mounting flange.

Acknowledgements

The author wishes to acknowledge the valuable assistance of Mr. R. G. Fowler, Mr. D. G. Moneypenny and Mr. S. C. Sutherland and Mr. J. Ellis in the above work.

VAN STEENBERGEN: In your figure you show an H.V. electrode aperture about equal to the beam diameter at that location. The rectilinear beam is of course a zero emittance approximation, which is not true in practice. A certain fraction of the beam will end up outside the beam periphery determined with the "Pierce" approach. As a consequence, one would expect secondary electron production on the H.V. electrode when the aperture diameter is close to the theoretical beam diameter.

WROE: Yes.

CURTIS: What was the distance across the gap? If the gradient is high enough, that angular divergence due to thermal motion would not be very large, would it?

WROE: It shouldn't be. The gap is 23 cm and the beam radius 4 cm.

MORGAN: A comment. As you know we normally extracted at 150 kV from a duoplasmatron ion source. We have also extracted at 300 kV with a 1-cm gap. This is for either a 50% duty cycle or dc operation. There are other possible complications, but there is no indication of it being advantageous to operate in an increased pressure range. In fact a lower pressure range of $\sim 3 \times 10^{-6}$ torr is better for stability in our case.

WROE: Well there is a feeling these days in the vacuum breakdown field that you can divide the phenomena into two parts: short gaps where the fields are high and gaps several centimeters long where the mean fields are quite low. The pressure effect is observed in the long gap case.

HUBBARD: How do you supply the power to the ion source?

WROE: Down the tube--the bolt that holds the whole thing together is hollow. The idea is to use such a simple ion chamber that few supplies will be necessary. However, if you put a duoplasmatron in there with many supplies needed, there will be some difficulty. However, there is a 2-1/2-inch hole down the bolt which holds the assembly together.

HUBBARD: But then you have to have it up at high voltage in the back end? You need a platform just like a conventional machine?

WROE: Oh sure, you need a platform.

KELLEY: you say a PIG source, for example, looks like a good thing. I was wondering, in making your ions in the ion source, how are you sure that you have an essentially zero energy cathode. You said everything was calculated for zero initial velocities.

WROE: Yes it is. That is what the computer program assumes, though it won't be true in practice. The ions will have initial velocities. But the initial energy is quite small compared to the total potential of the gap.

VAN STEENBERGEN: I am interested in hearing the pressure effect mentioned here in connection with voltage breakdown. This came up some time ago when the pressure in the linac was being discussed. I wonder if it could be useful in a linac to improve the maximum attainable gradient, say by running the linac at a pressure of 10^{-4} mm Hg instead of 10^{-6} mm Hg.

WROE: Well, I won't be sure about that. This phenomenon seems to manifest itself in the case of long gaps at low pressure. I am not sure this has been observed in impulse or rf breakdown--just dc. The theory of this is nowhere near as advanced as the short gap case. There are some quite acceptable theories in the short gap case of breakdown where the mean fields are high and you can invoke some sort of field emission at the cathode to start the thing off. The mean fields here, across these gaps, are nowhere anywhere big enough for that. In the old days one of the earliest theories was that you have a particle interchange; an electron or negative ion is emitted here, crosses the gap, and liberates an ion which comes back and a chain reaction is set up. The effect of putting gas in as far as I understand it is just that you might get an occasional charge exchange event or scattering which interferes with this particle interchange. There are also micro discharges which you probably know about. If you observe the current through this gap, even though it is not breaking down, you see bursts of current. These micro discharges are also suppressed while working in this pressure range. I think there is no doubt that it occurs for the dc case.

NORDBY: I would be afraid in linacs at 10^{-4} mm Hg that your mean free path goes down pretty fast.

WROE: Well, it is true that it will be close to the gap dimensions. You are working in a rather critical position, if you put the pressure up too

high, you come onto the low pressure side of the Paschen curve. You have to try to ride this rather tricky edge between the two.

NORDBY: I think you are all right at 23 cm, but in a couple hundred-foot tank things might be bad.

WROE: Yes, that is true.

FEATHERSTONE: We do observe in the Minnesota tanks that sparking becomes a problem when we get much above 10^{-5} torr.

BLEWETT: I guess this suppression of breakdown by gas pressures is observed mostly in dc separators. I believe the gas that is conventionally used is nitrogen. Are you sure this is true of hydrogen?

WROE: I talked to the Bevatron people and they use argon and they do not think it would make much difference what gas was used. Fundamentally, if the idea of charge exchange is correct, I don't really see why it should make much difference.

CURTIS: I think there is some information on that from the people at Ion Physics Corporation, who have used various gasses in their dc gaps, and they observed the improvement with all of these. They do not really prefer one gas over another, particularly, I think.

OLEKSIUK: Did you mention what you expected the sheath thickness to be?

WROE: It is just given by this formula. This is a very simple calculation for the one-dimensional case.

OLEKSIUK: This is just the Debye length that people talk about?

WROE: No, it would depend on the voltage you apply between the plasma and the cathode, you see.

PREACCELERATOR COLUMN DESIGN

C. D. Curtis and G. M. Lee
Midwestern Universities Research Association

I. REQUIREMENTS

There are three principal requirements that we should like to meet in the design of a high current accelerating system. The first is that the undesirable effects of space-charge forces within the beam on beam emittance be removed or rendered insignificant. One practical approach to accomplish this is to use a beam from the source which is initially large in diameter to reduce the self-forces and which can be accelerated very quickly to reduce the time for the forces to act. Another approach is to use a Pierce-type field geometry to balance out the self-forces. Both approaches lead to a high field gradient in the accelerating gap or column. A second requirement is for reliability of operation against breakdown. Because of the premium placed on high field strength capability here, we wish, if possible, to design the overall system so that the chance of breakdown due to conditions external to the accelerating gap is small. Our principal concern then is the voltage-holding properties within the column. The third requirement is for ion source accessibility. Under the assumption that servicing of the ion source is a major cause of down time on a preaccelerator, it is important to provide for fast access and change capability. In particular, on an experimental facility where frequent changes may be needed, this is important. The use of two preinjectors with one on standby can be considered, of course, to give increased reliability in the case of accelerator operation.

II. ELECTRODE DESIGN

To provide for a large diameter beam we have chosen to use the scheme of a plasma expansion cup attached to a conventional duoplasmatron source, following the example of Solnyskov[1] and others. We propose that the extraction grid be the first electrode of the high gradient acceleration region. The beam will thus be accelerated quickly without the delay required in passing first through a focusing lens. The hope is that one can control the focal properties of the beam to some extent for any given current intensity by simultaneous adjustment of the plasma density and the extraction voltage. Use of a fine mesh grid to shape the boundary would be a welcome addition, if successful. A properly concave plasma surface will render the beam

initially converging. The source position is shown in Fig. 1. The exact configuration of the source cup and extraction grid are subject to experimental change.

Unless one uses an accelerating field of the appropriate shape to counteract the space-charge forces, there will be some divergence of the beam. We can obtain some idea of the dependence on beam size and field gradient by assuming a uniform accelerating field. If one further assumes a cylindrical beam of radius R and of uniform charge density, which remains uniform across the beam diameter, one can derive an expression for the divergence of the ion beam after acceleration through some potential drop. This is given approximately for a particle at the edge of the beam by

$$\theta = \frac{I}{ER} \sqrt{\frac{m}{-2\,eV}} \ln \frac{V}{V_o}$$

for a long beam with neglect of end effects. The beam here is assumed parallel as it crosses the surface of potential V_o relative to the source. For a given final potential V one notes the divergence angle to be proportional to beam current I and inversely proportional to beam radius and to field strength E. For constant gradient and variable V there is a maximum θ for $\ln V/V_o = 2$. As an example we may consider a beam of 4 cm radius accelerated through a column or gap of 30 cm length. If the initial potential of the parallel beam is $V_o = -50$ kV and the final potential V is -500 kV, the angle θ becomes 6×10^{-3} radians. If V is changed to - 1000 kV, θ becomes 2.6×10^{-3} radians. This divergence is comparable with the spreading which results from thermal motion of the ions at the source but does not play the same role in determining beam emittance.

When a short high gradient accelerating column is considered, one is led to wonder if a single-gap two-electrode accelerator is feasible. If the field in such a gap were converging, it would tend to offset the beam divergence due to space-charge forces, to the diverging aperture lens at the gap exit and to the absence of focusing electrodes between source and gap entrance. A simple converging field geometry, not of the Pierce type, is given by concentric spherical electrodes as shown in Fig. 2.

The optics of the system is given by the formulas in the figure where f is the focal length of the exit aperture lens and F is the distance of focus from this aperture for a beam, which, starting from rest, is accelerated radially between the spheres. The drawing is for the special

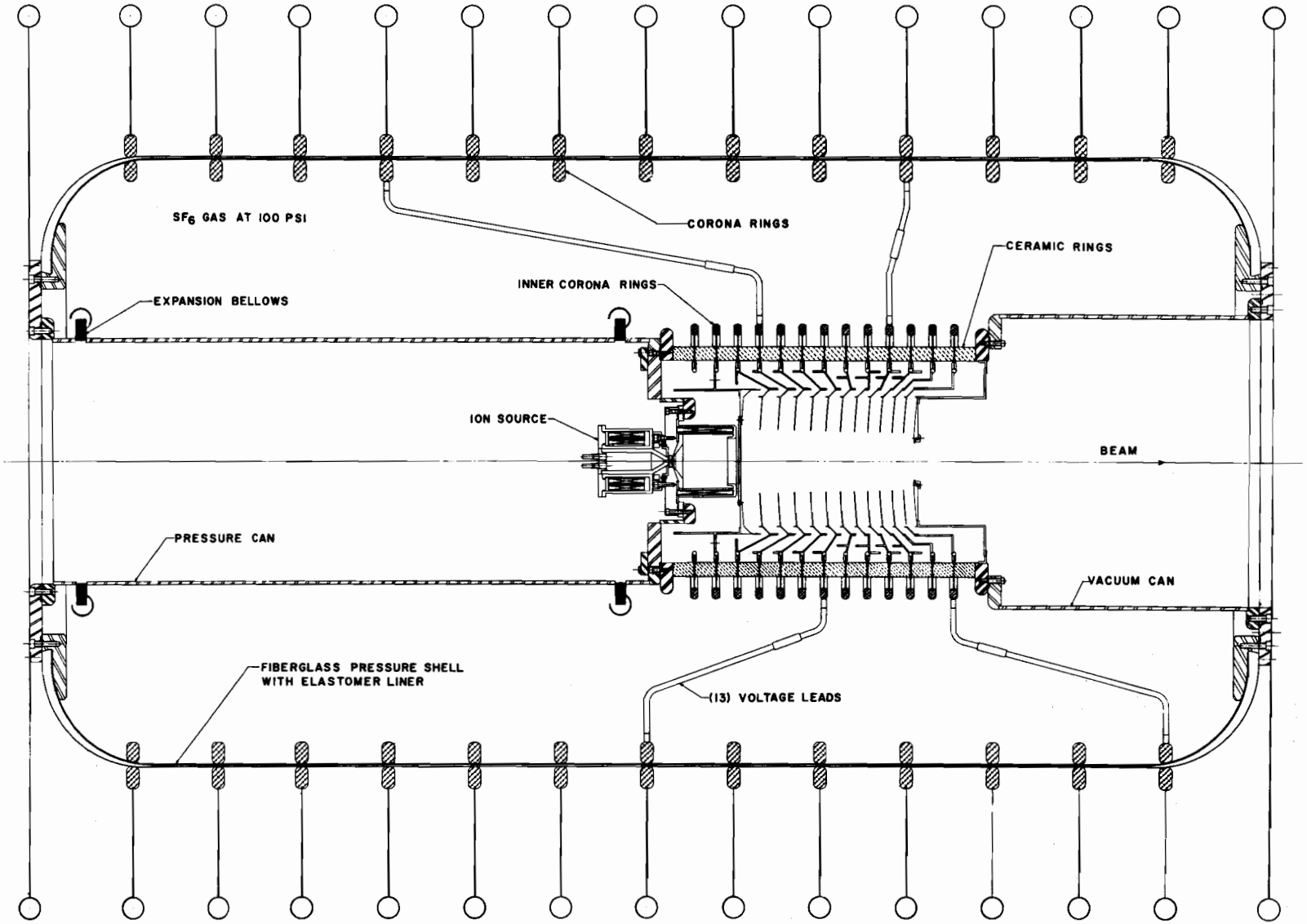
SF6 GAS AT 100 PSI
CORONA RINGS
CERAMIC RINGS
INNER CORONA RINGS
EXPANSION BELLOWS
ION SOURCE
BEAM
PRESSURE CAN
VACUUM CAN
FIBERGLASS PRESSURE SHELL
WITH ELASTOMER LINER
(13) VOLTAGE LEADS

FIG 1

case of the sphere radii having the ratio of 4/3, which renders the beam parallel beyond the exit.

Aside from the question of adequate voltage insulation between the electrodes in vacuum, there is the problem of insulation at the boundary between vacuum and external pressure. One approach is to take the beam out through a grounded tube which passes through a high voltage bushing support for the high potential sphere. Another approach is to distort the electrode shapes to give a spherical field in the beam region when the grounded electrode is bent back to surround the high voltage electrode as shown in Fig. 2. The shapes given there were determined in an electrolytic tank and give closely the required field shape. A similar geometry, except for cylindrical electrodes, is used successfully as an electron gun[2] on the MURA 50 MeV accelerator. In this arrangement, the source leads enter through a high voltage bushing which supports the high voltage electrode.

Of prime concern in such a two-electrode system for the 500 to 1000 kV range is the large area of the electrodes in vacuum. Through the "area effect", one can expect to hold less voltage for large than for small area. For small gaps between stainless steel electrodes withstanding of the order of 100 kV, the breakdown voltage varies with area[3] approximately as $\frac{V}{V'} = \left(\frac{A'}{A}\right)^{0.15}$.

A way to reduce the electrode area required is to use a multi-electrode design, the usual practice, to aid in distributions of the potential across the gap. If one does this but keeps the re-entrant electrode shape suggested by Fig. 2, one obtains a design shown, in principle, in Fig. 3. The electrode area exposed to the total voltage difference is now greatly reduced, although the area of each electrode is still quite large. The "total voltage effect", however, whereby the breakdown voltage above 100 kV is approximately proportional to square root of electrode separation, is not now so severe. The voltage is divided across the several gaps of Fig. 3 by an external voltage divider (not shown). A further benefit resulting from use of the intermediate electrodes should be a reduction in x-ray intensity. It is clear that there exists good shielding of the ceramic rings from the beam.

There are certain problems of mechanical design associated with the sketch of Fig. 3. In addition, access to the ion source is limited, allowing removal of no more than the filament holder through the high voltage bushing. A large diameter access channel would be possible by this route only by use of ceramic rings of quite large diameter.

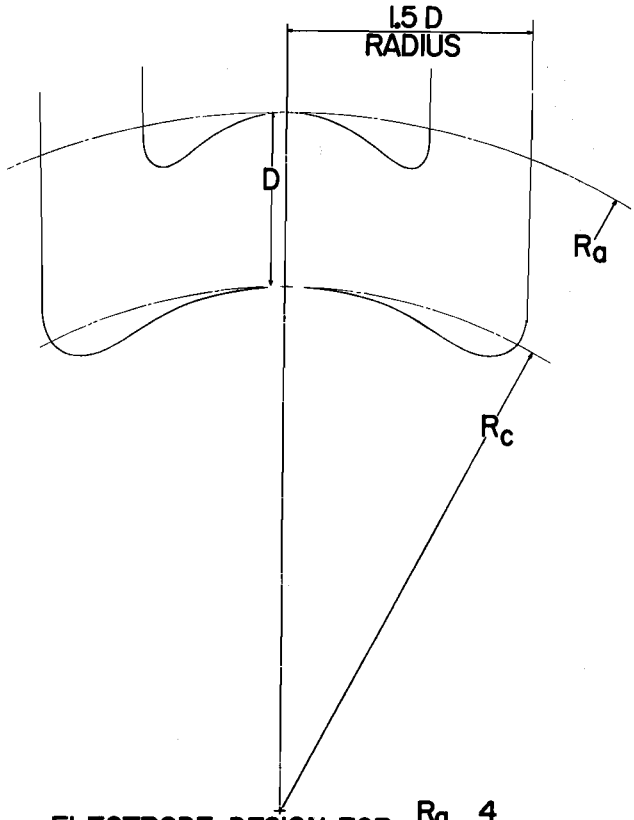

$$\frac{1}{F} = \frac{1}{R_c} + \frac{1}{f}$$

$$\frac{1}{f} = \frac{\Delta E}{4V} = -\frac{R_a/R_c}{4(R_a - R_c)}$$

$$\frac{1}{F} = \frac{3R_a/R_c - 4}{4(R_a - R_c)}$$

ELECTRODE DESIGN FOR $\frac{R_a}{R_c} = \frac{4}{3}$

FIG 2

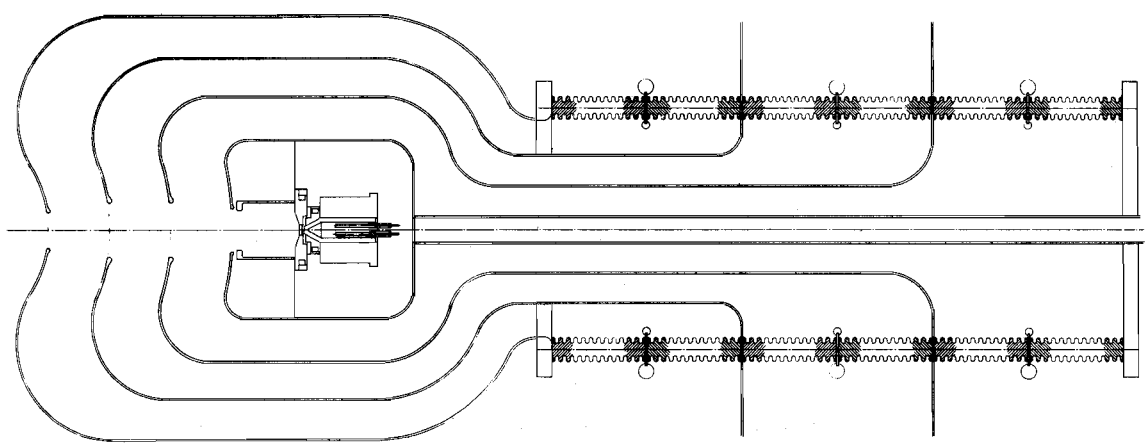

FIG 3

In the interest of achieving a high gradient column with good accessibility to the ion source as well as to the exit beam, we considered it prudent for the present to use a multi-electrode design with a more nearly conventional arrangement of the ceramic insulators. This is the design of Fig. 1, which still retains a converging field with the optics of Fig. 2. The accelerating gap is 30 cm long. The thin spherical electrodes have supports which flare out to a longer ceramic column of 21-inch length having 14 sections. A variable extraction voltage is applied across the first two sections while the other sections have an equal voltage difference across them.

The required field was achieved in an electrolytic tank by John Spooner with only the top and bottom spherical electrodes in place together with the z-shaped portions of the other eleven electrodes. This meant that the remaining electrodes of spherical shape could be placed along already existing equipotential surfaces. One can thereby hope that with accurate placement, the thin electrode edges will not be prone to voltage breakdown and will offer only a small perturbation in the field distribution due to finite electrode thickness. The thickness planned is 1/16 inch.

If the exit aperture in the last electrode is covered by a grid, the beam optics will, of course, be changed. The exit lens action is removed and an otherwise parallel beam will converge, except for space-charge effects, toward a minimum at the center of the spheres.

The electrode material having the best voltage holding properties in the 100 kV range that has come to our attention is a titanium alloy, Ti-7 Al-4 Mo. Furthermore, since it has a thermal coefficient of expansion which closely matches that of the ceramic rings, it becomes a good ring spacer material. Certain voltage tests which we have carried out on 304 stainless steel indicate that this also may be suitable. These included tests of a 0.9 cm gap between the end of a thin-walled right circular cylinder of 10-inch diameter and a plane. A cylinder of 1/16-inch wall held dc voltages well beyond 100 kV without breakdown when the gap was paralleled with a 0.02 μf capacitor. In the column a voltage gradient of 75 kV per gap, where the minimum spacing is 1 cm, would give over 900 kV for the total accelerating voltage.

The ceramic rings are 16 inches outer diameter. Each ring is 1-inch thick by 1-15/32 inches high and is recessed at the ends as may be seen in Fig. 1. This is to take advantage of any improvement in ability to hold voltage, as observed by others[4] when the cathode end is recessed. The rings will be vinyl sealed together.

In assembly the electrodes will be inserted into the column through the high voltage end. A jigging arrangement will permit accurate positioning of each spherical electrode with its attached z-shaped portion before it is connected to its conical support.

III. PRESSURIZED SHELL ASSEMBLY

In order to diminish the possibility of voltage breakdown outside the accelerator column, we decided to enclose the column in a pressurized atmosphere. A practical way to do this is to use a filament-wound fiberglass vessel as shown in Fig. 1. Such items are commercially made in a variety of sizes for rocket motor cases and chemical tanks. The vessel we plan to use is wound onto end flanges that were machined here at MURA. The wall thickness is 1/8 inch with an additional 1/16-inch butyl rubber liner to seal the fiberglass for SF_6 up to 100 lbs/in^2. The rubber can be made semiconductive to allow accumulated charge on the wall to drain off. The vessel is 42 inches inside diameter and 84 inches long.

There is a 17-inch diameter access channel to the source, which remains at atmospheric pressure. Bellows in this tube allow for some stretching of the pressurized tank. The column is under compression when evacuated and approximately neutral when up to air. Source changes are thus possible without the need to disturb tank pressure.

Each column electrode is connected to external corona rings on the fiberglass shell. A resistor string, not shown, divides the voltage here. The resistors can readily be changed if one should wish to alter the field distribution within the column. The position of the column within the tank can be changed, of course, from that shown by changing the electrode leads and the relative lengths of the source and beam exit channels.

Should one wish to test other electrode configurations, the tank should be capable of accommodating designs which vary greatly in electrode and insulator structure from that described here.

KELLEY: It looks as though there are several places in that design, first of all where electrons can be trapped from the magnetic field that you use for shaping the plasma surface. And I think you might get pigging trouble in those regions. Have you tested this?

CURTIS: No, this design has not been tested. The magnetic field indicated in the region of the cup may be undesirable and perhaps unnecessary.

KELLEY: We don't find it necessary to have a labyrinth sort of arrangement with a many bounce path between column and the beam. It seems that just barely shadowing is all that is necessary.

CURTIS: We wondered if this was really necessary and thought that the design might be a bit conservative in this respect.

KELLEY: Did I understand that your thin sheets now along equipotentials were there so that when you have the beam you will still force equipotentials at those places? Otherwise you don't need any electrode surface there.

CURTIS: One should not need any electrodes, except that they do reduce the area of the total gap and may therefore aid the voltage-holding ability. They also should reduce the x-ray level. We may actually remove them, depending on what experience tells us.

VAN STEENBERGEN: Does it make much difference in equipotential distribution outside, say, the beam region, if the high intensity beam is present or not? Are the electrodes at the correct place with beam?

CURTIS: They are in the correct place without beam as designed. It doesn't make a lot of difference whether the beam is present or not. This, of course, depends on the magnitude of beam current. For a 200 mA beam of 4 cm radius, the potential at the center of the beam increases by a few hundred volts. One can compare this with a voltage gradient of approximately 20 kV/cm for a total voltage of 600 kV to determine the displacement of the equipotential surfaces. Now it is possible, by varying the voltage on these electrodes to push the potential surfaces around quite freely. So I think it may be possible to adjust the voltage distribution externally and adequately correct any trouble resulting from displacement of the potential surfaces by the beam.

PRIEST: Lamb was saying that he had done exactly what you are saying and we have done it too. We vary the potential on these electrodes and get very good beam control and then having found out what the potential distribution is we then redesign the thing so that it doesn't need this variation. There is one comment I would like to make. It may be applicable in this case, I am not sure. In electron guns which are at all sophisticated where we really want to get a clean beam and the minimum amount of interception at the anode and so forth, we find we have to pay very special attention to the geometry at the edge of the cathode. And the thing we call the focus electrode, which is the element that does the field shaping, which surrounds the cathode and normally is at the same potential, has to be put in exactly the right place. I mean within a mil

or so or you get into trouble. We found that we have to pay very good attention to this, and a trick we found we can play to overcome the effect of poor tolerances or misalignment is to insulate this electrode so that in the case of electrons we can put a little negative voltage on it, maybe 20 or 30 V. This does wonders to clean up the beam and I suppose if you put a positive voltage on this in your case it might do the same.

CURTIS: Is this again with a Pierce-type geometry?

PRIEST: Yes, I have seen several of these drawn here in the course of the day.

CURTIS: We also found that similar electrode biasing in a Pierce electron gun we once built was quite effective.

MARTIN, J. H.: In regard to breakdown, how much better is this titanium alloy than some good stainless steels?

CURTIS: Of course, different people who make measurements on the same materials do not always obtain the same results. Comparison measurements were made by Ion Physics Corporation people. At the same time that they reached 80 kV across a 1 mm gap for buff-polished Ti alloy electrodes of 20 cm^2 area, they could hold only 60 kV for 304 stainless steel. They achieved, I believe, 110 kV for optically polished Ti alloy.

WROE: I am thoroughly convinced that there is this difference between long and short gaps and I wouldn't consider extrapolating that result into a long gap for instance. I mean that this difference in materials may not apply either.

CURTIS: Yes, I am quite aware of that. We may be just as well off with stainless as with titanium alloy for long gaps. These short gap figures are just the only comparative information I have. There are, of course, several relatively high field short interelectrode gaps in the column design which I have described.

REFERENCES

1. A. J. Solnyshkov et al., Proceedings of the International Conference on High Energy Accelerators, Dubna (Atomizdat, Moscow, 1964), p. 507.

2. C. D. Curtis et al., Rev. Sci. Instr. 35, 1447 (1964).

3. A. S. Denholm, F. J. McCoy, and C. N. Coenroods, Proceedings of the Symposium on Electrostatic Energy Conversion (Power Information Center, Philadelphia, April, 1963), p. 3-1.

4. Thomas J. Holce, 1962 Transactions of the Ninth National Vacuum Symposium of the American Vacuum Society (The Macmillan Co., New York, 1962), p. 376.

THOUGHTS ON MODE DISTRIBUTION IN RF MANIFOLDS

F. Voelker
Lawrence Radiation Laboratory

I first reported on this idea of an rf manifold at the Yale meeting. I want to add to these ideas some further work we have done regarding the mode structure of an rf manifold system. For the benefit of those who are not familiar with it, I will describe such a system. If we have a long linear accelerator cavity which we want to excite, we parallel it with a transmission line or wave guide. At the ends we short circuit the transmission line so that there are an integral number of half-wave lengths along its length at the operating frequency of the linac. This defines a number of E_{max} points along the length of the transmission line. It is permissible to connect to these E_{max} points, but all other points are forbidden.

Now the linac may be divided up into N parts, and let each section be connected to an adjacent E_{max} point on the transmission line so that there are n half-wave lengths between load points. Thus the whole system is $nN\ \lambda_g/2$ in length.

We have let the section of linac be a π-mode rf cavity. See Fig. 1. This figure shows the $\omega - \beta\ell$ diagram for such a cavity and the equivalent circuit for one of the resonances. L_m, C_m, G_m and M_m are the circuit parameters defined at the input loop to the cavity.

Since the cavity must be coupled to the transmission line (or rf manifold), we will arrange the length such that the value of M_m is tuned out and the parallel circuit appears at the E_{max} or load point. This is a very tight coupling to the manifold. The next several modes to the desired one are so close in frequency to ω_o that the value of M_m is effectively tuned out for these also.

We have let these values of

$$Y_{L,m} = G_m (1 + j\,2\,\delta_m Q_m) \quad \text{where} \quad \delta_m \equiv 1 - \frac{\omega^2}{\omega_m^2} .$$

Now we represent the rf manifold in this way.

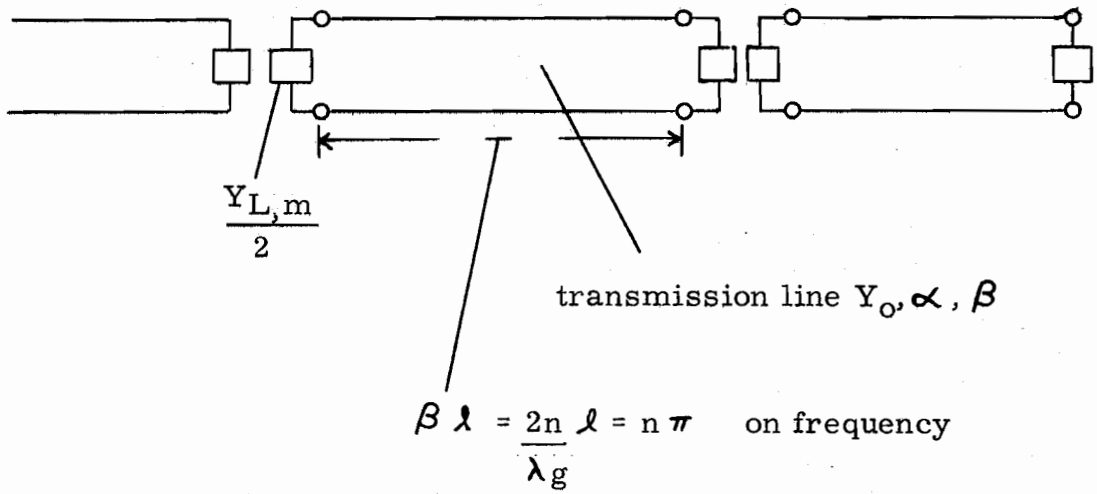

The loaded manifold is now a loaded transmission line, and we will let it have the parameters α_L, β_L, and it has a characteristic admittance Y_{o_L}. The equation governing the values of α_L, β_L as a function of α and β is the following.

$$\cosh \nu_L \ell \equiv \cosh \nu \ell + \frac{Y_L}{2\, Y_o} \sinh \nu \ell,$$

where $\nu_L = \alpha_L + j\,\beta_L$ and $\nu = \alpha + j\,\beta$. These lead to the equations

$$\cosh \alpha_L \ell \cdot \cos \beta_L \ell = \cosh \alpha \ell \cdot \cos \beta \ell + \frac{G_m}{2\, Y_o} \Big[\sinh \alpha \ell \cdot \cos \beta \ell - 2\, Q_m\, \delta_m \cosh \alpha \ell \cdot \sin \beta \ell \Big]$$

$$\sinh \alpha_L \ell \cdot \sin \beta_L \ell = \sinh \alpha \ell \cdot \sin \beta \ell + \frac{G_m}{2\, Y_o} \Big[\cosh \alpha \ell \cdot \sin \beta \ell + 2\, Q_m\, \delta_m \sinh \alpha \ell \cdot \cos \beta \ell \Big]$$

In order for the transmission line to have the properties we want for a manifold, we let the following be true.

$$\alpha \ell << 1 \text{ so that } \cosh \alpha \ell \cong 1 \text{ and } \sinh \alpha \ell \cong \alpha \ell .$$

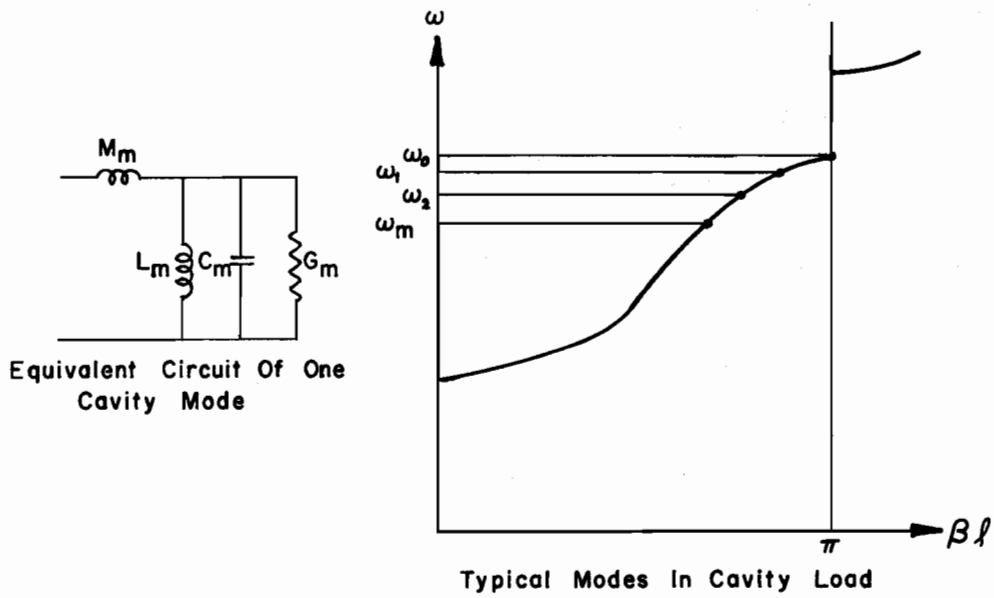
M_m
L_m
C_m
G_m
Equivalent Circuit Of One Cavity Mode
ω
ω_0
ω_1
ω_2
ω_m
π
$\beta\ell$
Typical Modes In Cavity Load

FIG. 1

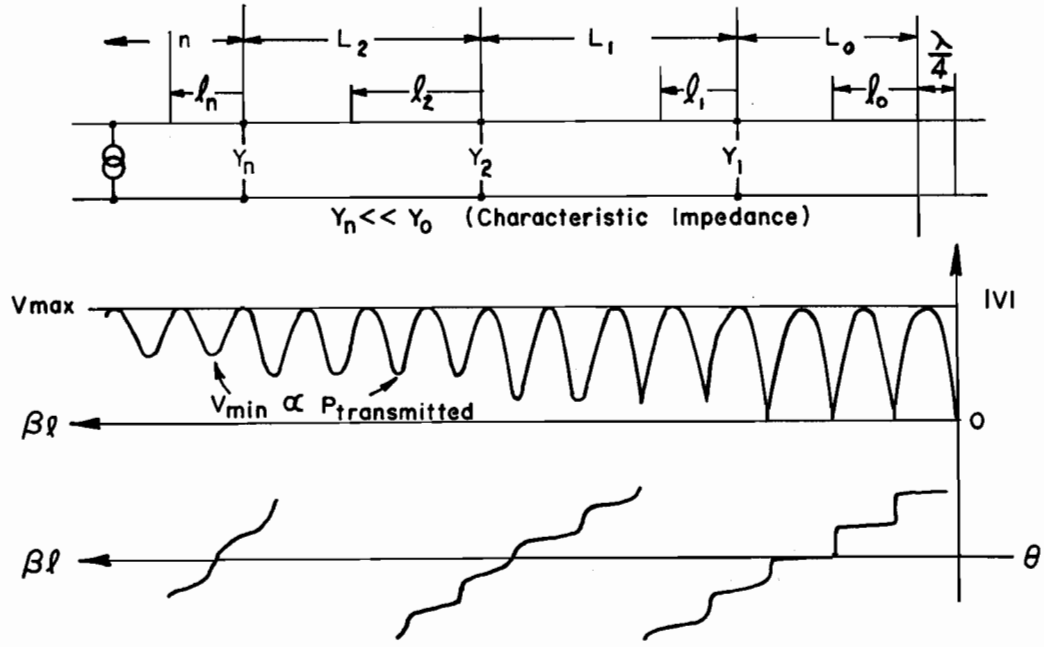
n
L_2
L_1
L_0
$\frac{\lambda}{4}$
ℓ_n
ℓ_2
ℓ_1
ℓ_0
Y_n
Y_2
Y_1
$Y_n << Y_0$ (Characteristic Impedance)
Vmax
|V|
$V_{min} \propto P_{transmitted}$
$\beta\ell$
0
$\beta\ell$
θ

FIG. 2

Also we require that $\beta = n\pi(1 + \delta_o)$ where δ_o is a small quantity. Then

$$\sin\beta \cong \pm \delta_o n\pi$$

$$\cos\beta \cong \pm \left[1 - \frac{1}{2}(\delta_o n\pi)^2\right] .$$

The above equations then reduce to

$$\cosh\alpha_L\ell \cdot \cos\beta_L\ell = \left[1 - \frac{(\delta_o n\pi)^2}{2}\right]\left\{1 + \frac{G_m}{2Y_o}\cdot\alpha\ell\right\}$$

$$- \delta_o n\pi\left\{\frac{G_m}{2Y_o}\ 2\ \delta_m Q_m\right\}$$

$$\sinh\alpha_L\ell \cdot \sin\beta_L\ell = \delta_o n\pi\left\{\alpha\ell + \frac{G_m}{2Y_o}\right\}$$

$$+ \left[1 - \frac{(\delta_o n\pi)^2}{2}\right]\ 2\ \delta_m Q_m \frac{G_m}{2Y_o} .$$

Solving these equations simultaneously will give values for α_L and β_L, the propagation coefficients for the loaded manifold.

I have not solved them. There are two cases of interest, that are easy to solve.

Let $\omega = \omega_o$ so that $\delta_o = 0$. Then the two equations become

$$\cosh\alpha_L\ell \cdot \cos\beta_L\ell \cong 1 + \frac{G_o}{2Y_o}\alpha\ell$$

$$\sinh\alpha_L\ell \cdot \sin\beta_L\ell \cong 0 .$$

The solutions are $\beta_L\ell = n\pi$ and $\alpha_L\ell \cong \sqrt{\frac{G_o}{Y_o}\alpha\ell}$.

Since $\beta_L\ell = n\pi$, the voltage at each E_{max} point differs from that at each other in phase by zero or π, and in amplitude by a factor

$$e^{\sqrt{\frac{G_o}{Y_o}\alpha l}\,M}$$

If $\frac{G_o}{Y_o}$ is a small number which we desire for other reasons and if the α of the transmission line is low which we naturally try to achieve, then the amplitudes are very nearly the same unless we allow the value of ℓ to be too large. Another way of putting this is that if we have a preconceived value that is acceptable,

$$e^{\sqrt{\frac{G_o}{Y_o}\alpha l}\,N}$$

will be limited to some value.

A generator can be introduced at any E_{max} point on the manifold, but the nearer the generator is to the loads the smaller the argument above will be, and the more tightly coupled the loads will be to the generator. If more than one generator is added, they are effectively in parallel (making sure that the sign of the phase is correct), and, if they act as current generators, will share the load depending on their drive. Figure 2 shows a section of a manifold with several loads and one generator.

I might explain that since the E_{max} are all locked together, and since $P_{transmitted} = \frac{V_{max}\,V_{min}}{2\,Z_o}$, then the value of V_{min} is proportional to the power transmitted at a given point on the manifold. If there is a plane of symmetry or end wall that no power flows past, $V_{min} = 0$, and V_{min} grows larger as one moves past each load point.

In practice each cavity will have its phase servoed to a reference line from the same master oscillator that drives the amplifiers. Then if the cavities do not wander <u>too</u> far from their correct resonant frequency, each cavity will have its fields locked in phase and in amplitude to each other cavity. If the cavities are not quite at resonance, the amplifiers must supply the reactive energy necessary to keep the cavities in phase. They will be able to do this because

1) the various load cavities should tend to average out the reactive energy required, and

2) in order to overdrive the linac in order to obtain fast rise time, the amplifiers must have considerable surplus of energy available, which can go to supply reactive energy.

An amplitude servo will be required to increase the drive so that beam loading can be supplied by the amplifier tubes. Probably it will be desirable to servo the phase of the drive line to the phase of the anode line, to minimize the losses in the amplifier tubes.

The immediate worry one has when one first sees this scheme is, "what about the other modes"? By going back to these original equations and looking at what happens near $\omega = \omega_o$ or $\delta_m = \delta_o$, the equations become

$$\cos \beta_L \ell \cong 1 - \frac{(\delta_o n \pi)^2}{2} \left[1 + \frac{2}{n\pi} \frac{G_o Q_o}{Y_o} \right]$$

$$\alpha_L \ell \cdot \sin \beta_L \ell \cong \delta_o n \pi \left[\alpha \ell + \frac{G_o}{Y_o} + \frac{2}{n\pi} \frac{G_o Q_o}{Y_o} \right] .$$

The solutions to these equations are

$$\beta_L \ell \cong \delta_o n \pi \left[1 + \frac{2}{n\pi} \frac{G_o Q_o}{Y_o} \right]^{1/2}$$

$$\alpha_L \ell \cong \alpha \ell + \frac{G_o}{Y_o} + \frac{2}{n\pi} \frac{G_o Q_o}{Y_o} .$$

See Fig. 3. Note the slope of the $\omega - \beta\ell$ curve and that there is a stop band adjacent to ω_1, the next cavity mode.

Analogous to the modes along the $\omega - \beta\ell$ curve for the π cavity (see Fig. 1), there will be modes along this $\omega - \beta\ell$ curve if the value Nn is too large. The limits of the frequency where this first permissible point can be found will vary between

$$\frac{1}{nN} < \delta_A < \frac{1}{nN \left[1 + \frac{2}{n\pi} \frac{Q_o G_o}{Y_o} \right]^{1/2}} \; ; \quad \delta_A = \frac{\omega_A - \omega_o}{\omega_A}$$

depending where it falls on the $\omega - \beta\ell$ curve.

Next consider a long cavity in the π mode. Panofsky's formula says that the mode next to the operating frequency is given by $\delta_I = \frac{\lambda^2}{8 M^2 \ell_o^2}$ where $\ell_o = \beta_{particle} \frac{\lambda}{2}$. The total length

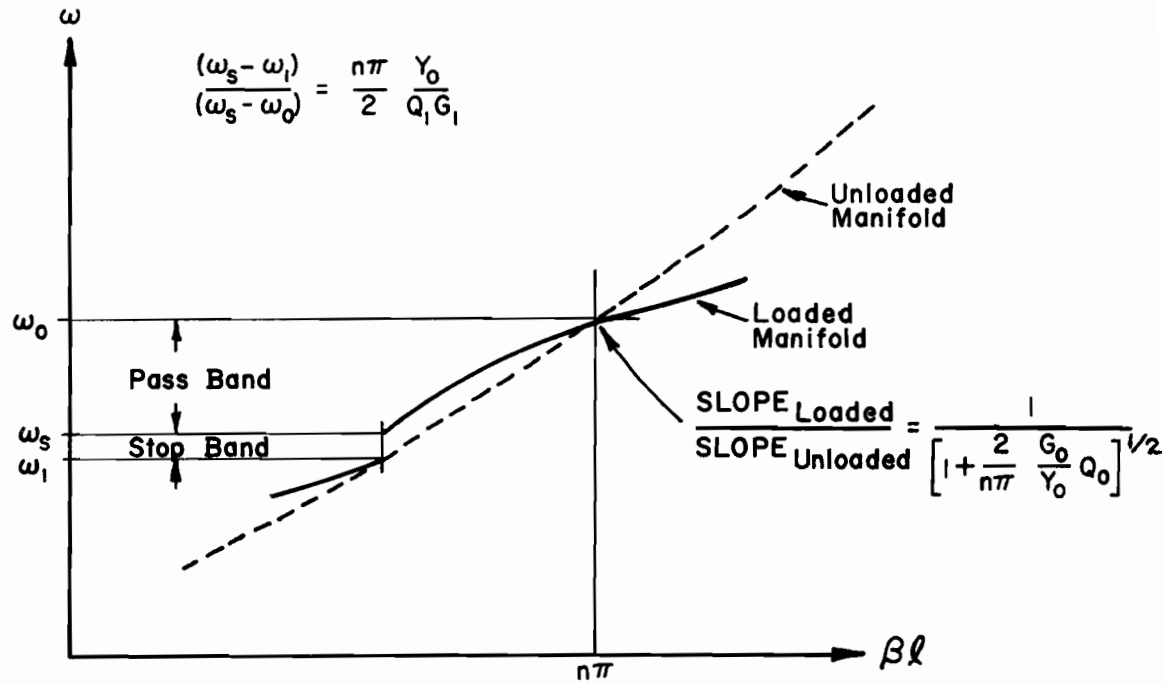
ω
$\frac{(\omega_s - \omega_1)}{(\omega_s - \omega_0)} = \frac{n\pi}{2} \frac{Y_0}{Q_1 G_1}$
Unloaded Manifold
Loaded Manifold
ω_0
Pass Band
ω_s
Stop Band
ω_1
$\frac{\text{SLOPE}_{\text{Loaded}}}{\text{SLOPE}_{\text{Unloaded}}} = \frac{1}{\left[1 + \frac{2}{n\pi} \frac{G_0}{Y_0} Q_0\right]^{1/2}}$
$n\pi$
$\beta\ell$

FIG. 3

$\ell_T = M\ell_c$ and also equals $nN \frac{\lambda g}{2}$, so that it can be written as $\delta_I = \frac{1}{2\, n^2 N^2} \frac{\lambda^2}{\lambda_g{}^2}$. If the manifold is a coaxial line as it might well be at 200 Mc, then $\frac{\lambda}{\lambda g} = 1$, and $\delta_I = \frac{1}{2\, n^2 N^2}$. This is to be compared with δ_A which varies as the first power of nN.

Also note that if N = 1, it gives the value of ω_1 in Fig. 3.

RF PHASE AND AMPLITUDE CONTROL*

Robert A. Jameson
Los Alamos Scientific Laboratory, University of California
Los Alamos, New Mexico

Basic Specifications

From beam dynamics

Phase - Average tank phase, measured over a period of ~10 μsec, to remain within a $\pm 2^{\circ}$ square well around the reference phase.

Since the short-term phase instabilities will include random effects, the above specification must be redefined as a mean deviation such that a random phase jitter of Gaussian distribution remains in the $\pm 2^{\circ}$ square well some percentage of the time:

Percent of Time Within Square Well	σ
99%	0.8°
95%	1.0°
90%	1.2°

Amplitude - $\pm$ 2%

From power amplifier

The HPA (Coaxitron) has transit time phase shifts of the order of $2.5^{\circ}/1\%$ change in plate voltage. This indicates the necessity for amplitude control to less than 0.5%, if operating open loop.

The transit time problem is further complicated by the necessity of increasing of power output to match increasing beam loading as the beam is turned on. The effects of various load configurations on the amplifier are being studied to determine how great this effect is.

General Layout -- Figure 1

Comments

1. After initial setup, tanks n and n' are ganged together with sensing from one tank.

*Work performed under the auspices of the U. S. Atomic Energy Commission.

2. Both fast and slow phase shifters may be required, depending on range available from fast shifter. Survey of existing mechanical, ferroelectric and varactor phase shifters indicate fast phase control must be done at power levels like 10 watts CW or less.

Quotations have been received for development work on ferroelectric shifters capable of handling 100 W CW (1700 W at 6% duty), shifting $\pm 10^{\circ}$ in 1-2 μsec. This is already a development task--shifters capable of handling higher power levels would require major development.

Basic Control Loops - Block Diagrams--Figure 2

1. Coupling Effects

a. Major coupling from IPA and HPA plate voltage changes to phase of Coaxitron output, as mentioned earlier. Effect is nonlinear, given approximately by:

Transit time, cathode to plate $\dfrac{3\ dcg + dgp}{5.93 \times 10^{7}\sqrt{\dfrac{V_{po}}{10}}}$ sec.

where dcg and dgp are cathode-to-grid and grid-plate distances in centimeters, and $\dfrac{V_{po}}{10} = V_p \min = V_g \max$.

b. Second-order couplings between amplitude and phase in tank. More on this later.

2. Other Nonlinearities

a. Phase comparator output proportional to the sine of the phase error.

b. Nonlinear phase shifter characteristics.

c. Tank behavior nonlinear for large signals.

3. The effect of beam loading on the loop must be included.

4. Basic Frequency Stability Requirements

It is interesting to note what frequency stability is required of a standard in order that the short-term stability of the standard itself does not introduce phase disturbances which exceed the specified tolerances. Assume that the characteristic time constant in the transfer function from the reference phase to the tank phase

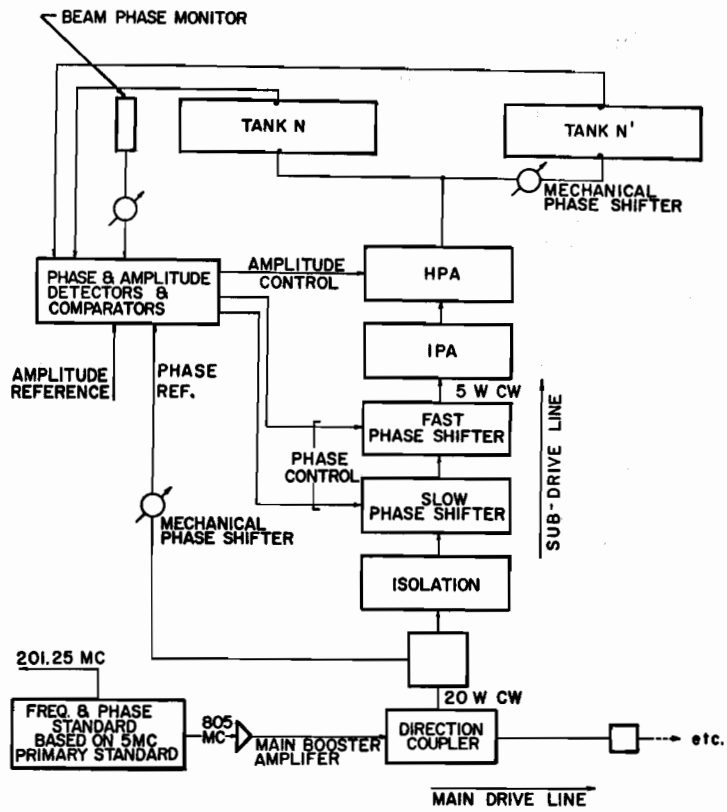

FIG. 1 **GENERAL LAYOUT**

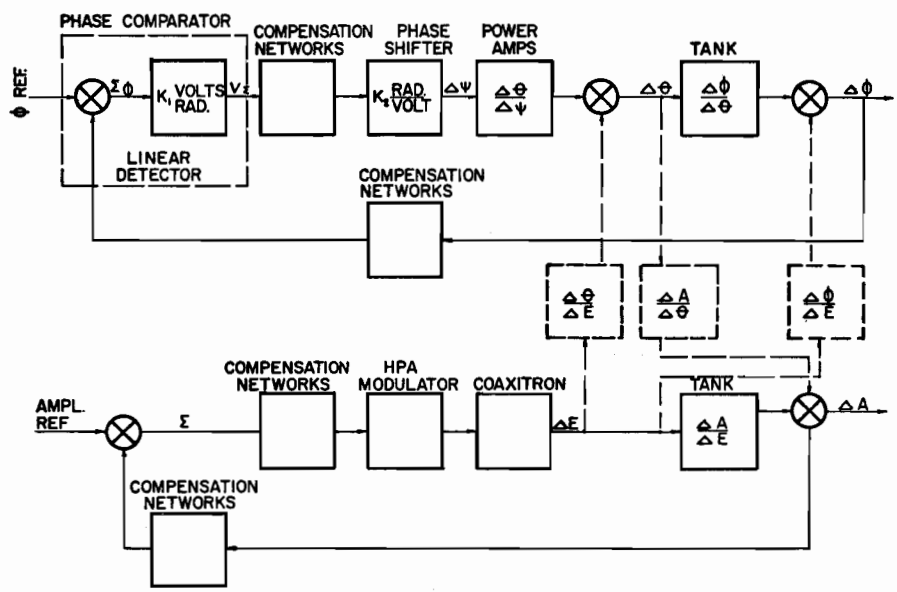

FIG. 2 **BASIC CONTROL LOOPS — BLOCK DIAGRAMS**

is that of the tank--in the order of 10 μsec. We are thus interested in phase perturbations that occur at rates of ~16 kc or less. The relation for frequency uncertainty due to a short-term phase instability is

$$\frac{\Delta f}{f} = \frac{\Delta\theta}{2\pi N}$$

where $\frac{\Delta\theta}{2\pi}$ = phase stability, proportional to noise-to-signal ratio

N = number of periods used for measurement

$$\frac{\Delta f}{f} = \frac{2^{\circ}}{360^{\circ} \times 800 \times 10^{6} \times 10^{-5}} = 7 \times 10^{-7} \text{ for 10 } \mu\text{sec measurement at 800 Mc.}$$

$$= \frac{7 \times 10^{-7}}{100} = 5 \times 10^{-9} \text{ for 10 } \mu\text{sec measurement at 5 Mc.}$$

Thus the primary frequency source which will provide the reference and drive signals must be very precise--in fact somewhat better than any source advertised at this date.

5. Measurement Techniques

The state-of-the-art nature of the stability requirements and some of the hardware promise difficulties in obtaining accurate and repeatable measurements.

Transfer Functions--Phase Loop

1. Phase Comparator

The simplest comparators use the rf signals directly, without converting to intermediate frequencies, etc. Because of their simplicity and reliability, this type is being considered in the early studies.

The comparator might thus be a quadrature mixer whose two outputs are linearly detected and differenced to form the error signal:

$$V_E = \pm k\sqrt{2}\ E_2 \sin \epsilon_\varphi$$

where k = detector efficiencies
E_1 = unknown signal
E_2 = reference signal
$E_1 \gg E_2$

$$\cong \pm k\sqrt{2}\ E_2\, \epsilon_\varphi \quad \text{for } \epsilon_\varphi \ll 1 .$$

2. Phase Shifter

At this time, it is proposed to use a varactor controlled phase shifter. Indications from industry are that these devices will soon be available at the desired power levels (~10 W CW), with phase shift ranges of greater than $\pm 90^{\circ}$. The phase shift vs. bias voltage characteristic is nonlinear, tending to saturate at the high end. A linear approximation may be used for small phase swings.

3. Power Amps

The chain is treated as a single resonant cavity, with the envelope responses characterized by an exponential rise to a step input; e.g.

$$\frac{\text{Output Amplitude}}{\text{Input Amplitude}} = \frac{\alpha}{s+\alpha}$$

$$\frac{\text{Output Phase}}{\text{Input Phase}} = \frac{\alpha}{s+\alpha} .$$

The phase transfer function is good for small signals only, becoming an inverse tangent function in the time domain for large signals, which introduces a nonlinearity.

4. Tank[1]

The tank transfer functions are derived from the transient analysis of a lumped parameter equivalent circuit for the accelerator cavity:

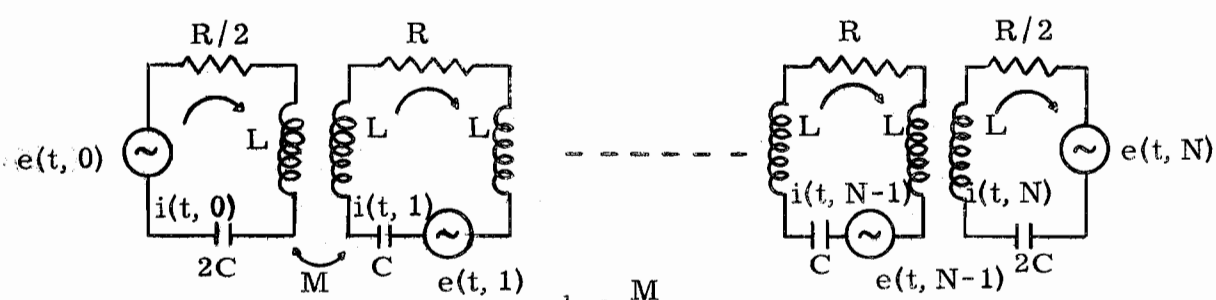

$$k = \frac{M}{L}$$

$$\omega_o = 1/\sqrt{2LC}$$

$$Q = 2\ \omega_o L/R$$

[1]These results are summarized from LASL Tech Memos P-11/RAJ-3 and P-11/RAJ-4.

The steady-state theory for this circuit has been developed by Nagle and Knapp--some results of this were given in Knapp's talk earlier.

The matrix equations for the circuit were written using Laplace transforms, transforming first with respect to time, and then, after using jump functions to express the repetitive nature of the cells, again with respect to the cell number. The solution of the homogeneous equation gives the characteristic equation and the n dependence. The inhomogeneous equation is then solved using an orthogonality relation based on the n dependence. The complete solution for the current in any cell is:

$$I(s,n) = \sum_{d=0}^{N} \sum_{q=0}^{N} \frac{2 \cos \frac{\pi n q}{N} \cos \frac{\pi d q}{N} W_1(q)\, s\, E(s,d)}{N\left(1 + k \cos \frac{\pi q}{N}\right)\left[s^2 + \frac{\omega_o}{Q(1 + k \cos \frac{\pi q}{N})} s + \frac{\omega_o^2}{(1 + k \cos \frac{\pi q}{N})}\right]}$$

where d = index on rf drive, e.g. $E(s,d)$ is a drive in the dth cell

q = mode number

n = cell number

$E(s,d)$ = drive term normalized by $1/2\,L$

$$W_1(q) = \frac{1}{\delta_{n,o} + \delta_{n,N} + 1} .$$

The transfer function with respect to a particular drive is

$$\frac{I(s,n)}{E(s,d)} = G(s,n,d) =$$

$$= \sum_{q=o}^{N} \frac{2 \cos \frac{\pi n q}{N} \cos \frac{\pi d q}{N} W_1(q)\, s}{N\left(1 + k \cos \frac{\pi q}{N}\right)\left[s^2 + \frac{\omega_o}{Q\left(1 + k \cos \frac{\pi q}{N}\right)} s + \frac{\omega_o^2}{1 + k \cos \frac{\pi q}{N}}\right]}$$

For example, the time response to a single sinusoidal drive in the dth cell started at $t = 0$:

$$e(t,d) = u(t) \sin \omega t)$$

$$i(t,n) \cong \sum_{q=0}^{N} K_q \left[\sin(\omega t + \Phi_\omega) + e^{-\alpha_q t} \sin(\omega_q t + \Phi_{\omega_q})\right]$$

where

$$K_q = \frac{2\,\omega\,(|\text{Magnitude of drive}|)\,W_1(q)\cos\frac{\pi d q}{N}\cos\frac{\pi n q}{N}}{N\left(\left[\omega^2\left(1 + k\cos\frac{\pi q}{N}\right) - \omega_o^2\right]^2 + \left[\frac{\omega_o \omega}{Q}\right]^2\right)^{1/2}}$$

$$\Phi_\omega = \tan^{-1}\frac{-Q\left[\omega^2\left(1 + k\cos\frac{\pi q}{N}\right) - \omega_o^2\right]}{\omega_o\,\omega}$$

$$\Phi_{\omega_q} = \tan^{-1}\frac{\sqrt{4Q^2\left(1 + k\cos\frac{\pi q}{N}\right) - 1}\left[\omega^2\left(1 + k\cos\frac{\pi q}{N}\right) - \omega_o^2\right]}{-\left[\omega^2\left(1 + k\cos\frac{\pi q}{N}\right) + \omega_o^2\right]}$$

$$\alpha_q = \frac{\omega_o}{2Q\left(1 + k\cos\frac{\pi q}{N}\right)}$$

$$\omega_q = \frac{\omega_o}{\left(1 + k\cos\frac{\pi q}{N}\right)}\sqrt{\left(1 + k\cos\frac{\pi q}{N}\right) - \frac{1}{4Q^2}}$$

and the approximation results from retaining only the first term of the expansion of the factor $\dfrac{1}{\sqrt{1 - \frac{1}{4Q^2}\left(1 + k\cos\frac{\pi q}{N}\right)}}$ which modified the transient part of the solution.

Discussion

1. The steady-state solution says that the steady-state current at any particular drive frequency is the sum of components from each mode. If the drive is at a mode resonant frequency, that component has its maximum amplitude and is in phase with the drive. The other components are present because of the losses in the system. They are driven far from resonance and thus have small amplitudes and are about 90° out of phase with the drive.

2. The natural frequencies and damping factors are apparent as the transient terms. The initial amplitudes are very nearly the same as for the corresponding steady-state term, and the initial angles are almost 180° out of phase with the steady-state angles. The amplitude and phase variations during the transient period both die out with the same time constants.

3. The cos (dq/N) and cos (nq/N) terms add 180° to the phase when they are negative. Note that a drive in an end cell excites all the modes, while a drive in the center (N even) cell excites only the even numbered modes. Placing drives at node points to suppress various modes can be used effectively to increase the apparent "mode separation."

Envelope Responses

The transfer functions of real interest are those of the amplitude and phase envelopes:

From Input Amplitude to Output Amplitude
From Input Amplitude to Output Phase
From Input Phase to Output Phase
From Input Phase to Output Amplitude .

We write the response to the desired drive (in this case amplitude or phase step changes in a sinusoidal drive) as follows:

$$i\,(t,n) = \sum_{q=0}^{N} \mathcal{I}m \left\{ \left[a_q\,(t)\, e^{i\,\phi_q(t)} \right] e^{i\omega t} \right\}$$

where $a_q(t)$ = amplitude envelope function
$\phi_q(t)$ = phase envelope function .

Examples, the time response to a sinusoidal drive started at t = 0, used before:

$$i\,(t,n) = \sum_{q=0}^{N} \mathcal{I}m \left\{ K_q\, e^{i\omega t} \left[e^{i\Phi_\omega} + e^{-\alpha_q t}\, e^{i\left[(\omega_q-\omega)t + \Phi_{\omega_q}\right]} \right] \right\} .$$

Two types of approximation to the response are considered:

a. The components of the response are taken as the driven mode component and an out-of-phase component. The latter is found by first assuming that each off-resonance component is exactly $\pm 90^{\circ}$ out of phase with the driven mode component at steady state. The amplitude is then taken to be the vector sum of these steady-state amplitudes, and called ΣK_q. The damping term is taken to be that of the driven mode α_N for π-mode drive. The beat frequency $\beta = \omega_q - \omega$ is taken to be that produced by the

nearest mode frequency to the drive frequency that is present in the tank.

b. Response of the driven mode component only. The steady-state amplitude of this component for π mode drive is K_N.

The results for the first approximation are listed below, for π - mode drive. Simplification to the second follows by letting $\Sigma K_q = 0$. The exact responses have been found using a computer program. The approximate responses have been superimposed on the exact in Figs. 3 - 10.

1. Response to pulse turn-on (Large amplitude step).

$$a(t) = \left\{\left[K_N (1 - e^{-\alpha_N t}) - \Sigma K_q \, e^{-\alpha_N t} \sin \beta t\right]^2 + \left[\Sigma K_q \, (1 - e^{-\alpha_N t} \cos \beta t)^2\right]\right\}^{1/2}$$

$$\phi(t) = \tan^{-1} \frac{-\Sigma K_q \, (1 - e^{-\alpha_N t} \cos \beta t)}{K_N (1 - e^{-\alpha_N t}) - \Sigma K_q \, e^{-\alpha_N t} \sin \beta t}$$

2. Response to small amplitude step = k from steady state; $k \ll 1$:

$$a(t) = \sqrt{K_N^2 + (\Sigma K_q)^2} \left[1 + k\left(\frac{K_N^2 (1 - e^{-\alpha_N t}) - K_N \Sigma K_q \, e^{-\alpha_N t} \sin \beta t + (\Sigma K_q)^2 (1 - e^{-\alpha_N t} \cos \beta t)}{K_N^2 + (\Sigma K_q)^2}\right)\right]$$

$$\phi(t) = -\frac{\Sigma K_q}{K_N}\left[1 + k\, e^{-\alpha_N t} (1 - \cos \beta t)\right] ; \quad \frac{\Sigma K_q}{K_N} \ll 1$$

Small signal transfer functions:

$$\frac{\Delta A(s)}{\Delta E(s)} = \frac{\alpha_N \sqrt{K_N^2 + (\Sigma K_q)^2}}{S + \alpha_N} - \frac{\Sigma K_q \, \beta S}{(S + \alpha_N)^2 + \beta^2}$$

$$\frac{\Delta \phi(s)}{\Delta E(s)} = -\frac{\Sigma K_q}{K_N}\left[\frac{\beta^2 S}{(S + \alpha_N)\left[(S + \alpha_N)^2 + \beta^2\right]}\right]$$

3. Response to step phase change of φ radius from steady state:

$$a(t) = \Big\{ K_N^2 \left[1 - 2\, e^{-\alpha_N t} (1 - \cos\varphi)(1 - e^{-\alpha_N t}) \right] + 2\, K_N \Sigma Kq \left[(1 - \cos\varphi)\, e^{-\alpha_N t} (2\, e^{-\alpha_N t} - 1) \sin\beta t + \sin e^{-\alpha_N t} (1 - \cos\beta t) \right] + (\Sigma Kq)^2 \left[1 + 2\, e^{-\alpha_N t} (\sin\varphi \sin\beta t - (1 - \cos\varphi) \cos\beta t) + 2\,(1 - \cos\varphi)\, e^{-2\alpha_N t} \right] \Big\}^{1/2}$$

$$\phi(t) = \tan^{-1} \frac{K_N \left[(1 - e^{-\alpha_N t}) \sin\varphi \right] - \Sigma Kq \left[\cos\varphi + e^{-\alpha_N t} ((1 - \cos\varphi)\cos\beta t + \sin\varphi \sin\beta t) \right]}{K_N \left[\cos\varphi + e^{-\alpha_N t} (1 - \cos\varphi) \right] + \Sigma Kq \left[\sin\varphi + e^{-\alpha_N t} ((1 - \cos\varphi)\sin\beta t - \sin\varphi \cos\beta t) \right]}$$

Small signal transfer functions:

$$\frac{\Delta A(S)}{\Delta\theta(S)} = \frac{K_N \Sigma Kq}{\sqrt{K_N^2 + (\Sigma Kq)^2}} \left[\frac{\beta^2 S}{(S + \alpha_N) \left[(S + \alpha_N)^2 + \beta^2 \right]} \right]$$

$$\frac{\Delta\phi(S)}{\Delta\theta(S)} = \frac{\alpha_N}{S + \alpha_N} - \frac{\Sigma Kq}{K_N} \frac{\beta S}{(S + \alpha_N)^2 + \beta^2}$$

KEANE: This is a very nice piece of work. One comment; you did not take into consideration the response for each particular mode. As a matter of fact for what I was talking about, the next mode would be the TM_{011}. Because of my weak coupling to that mode, I had very slight scalloping. To the mode where I had strong coupling, namely the TM_{012}, the scalloping was much more pronounced.

RESPONSE OF CELL 00 TO PULSE TURN-ON
ON-RESONANCE DRIVE AT CELL 00

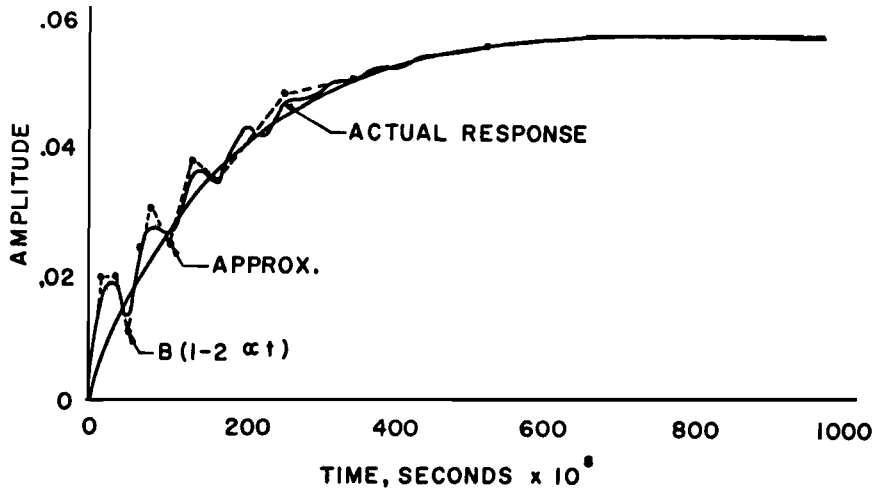

FIG. 3

RESPONSE OF CELL 00 TO PULSE TURN-ON
ON-RESONANCE DRIVE AT CELL 00

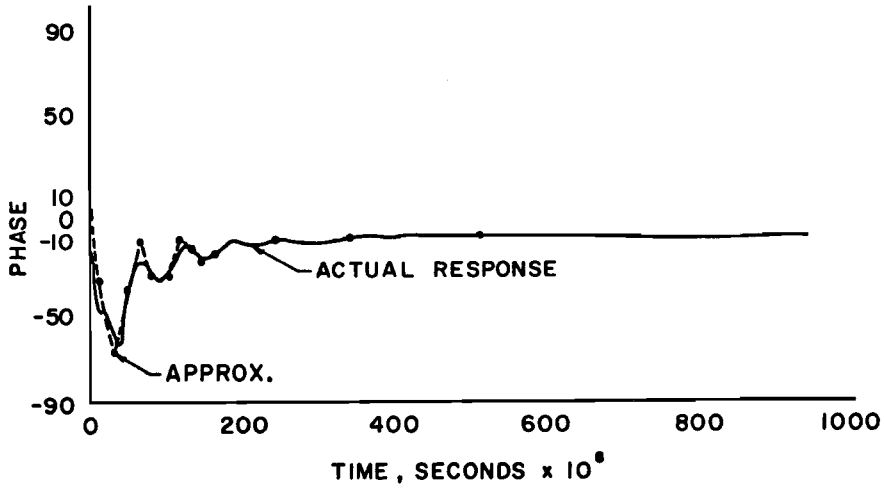

FIG. 4

RESPONSE OF CELL 00 TO +2 PERCENT AMPLITUDE STEP APPLIED TO STEADY-STATE ON-RESONANCE DRIVE AT CELL 00

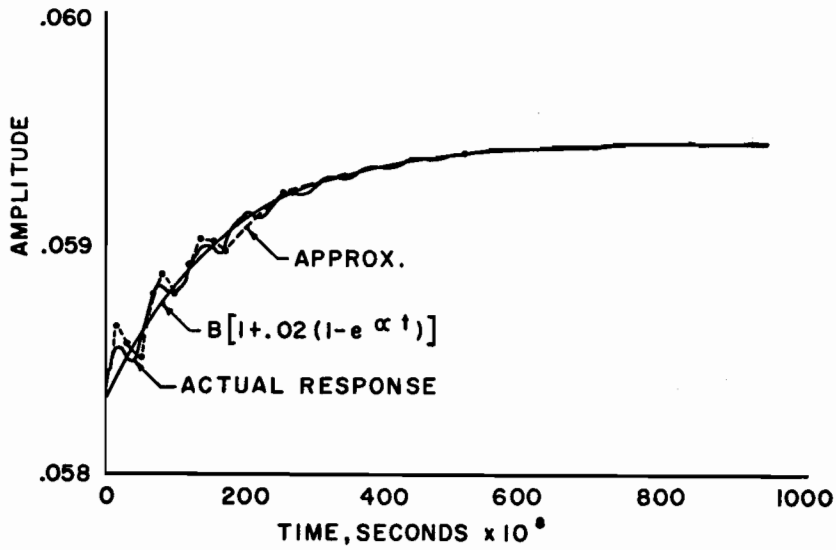

FIG. 5

RESPONSE OF CELL 00 TO +2 PERCENT AMPLITUDE STEP APPLIED TO STEADY-STATE ON-RESONANCE DRIVE AT CELL 00

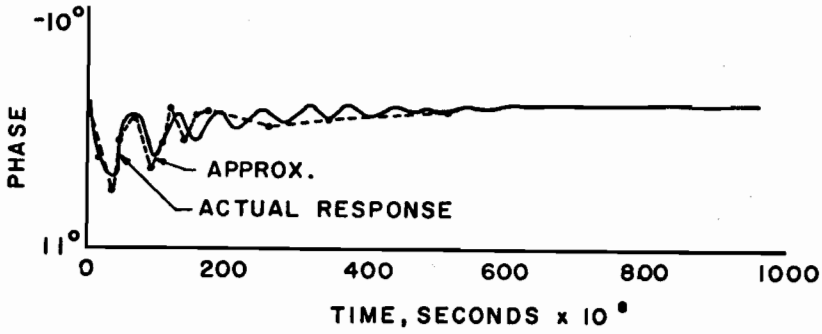

FIG. 6

RESPONSE OF CELL 00 TO 180° PHASE STEP APPLIED TO STEADY-STATE ON-RESONANCE DRIVE AT CELL 00

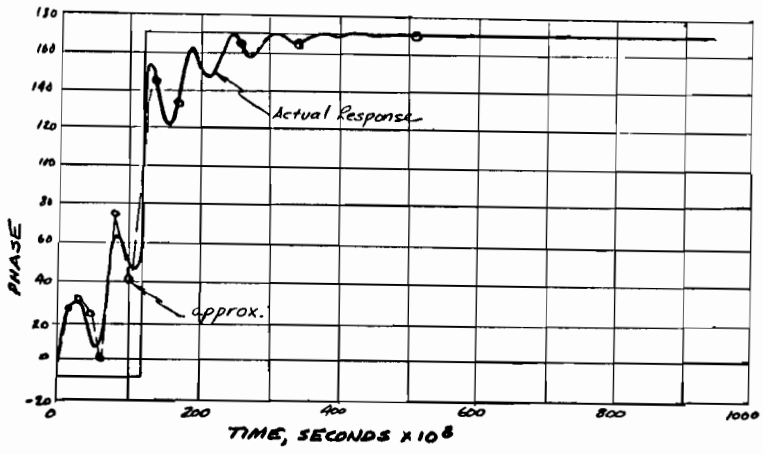

FIG. 7

RESPONSE OF CELL 00 TO 180° PHASE STEP APPLIED TO STEADY-STATE ON-RESONANCE DRIVE AT CELL 00

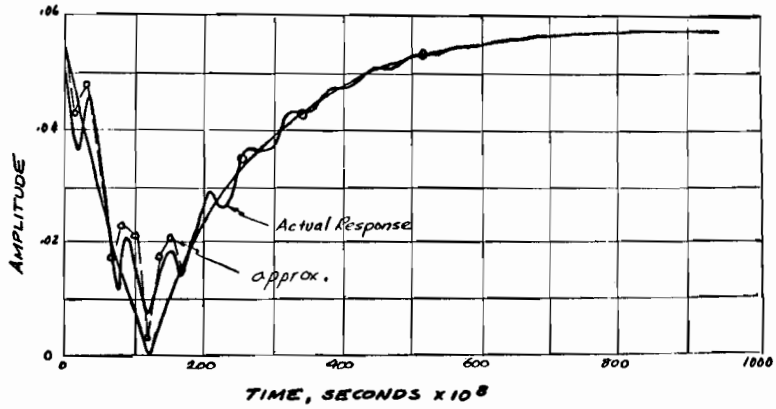

FIG. 8

RESPONSE OF CELL 00 TO +2 DEGREE
PHASE STEP APPLIED TO STEADY-STATE
ON-RESONANCE DRIVE AT CELL 00

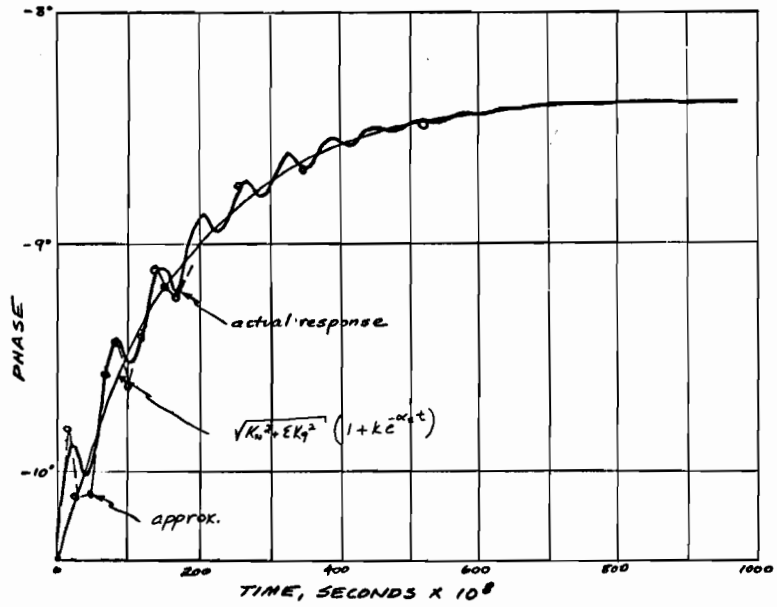

FIG. 9

RESPONSE OF CELL 00 TO +2 DEGREE
PHASE STEP APPLIED TO STEADY-STATE
ON-RESONANCE DRIVE AT CELL 00

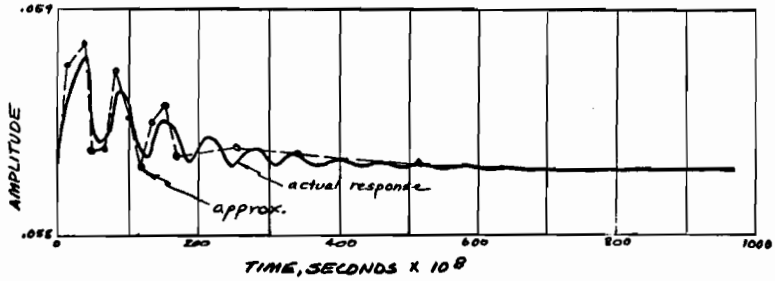

FIG. 10

JAMESON: That is not true. The answer for the current in any cell shows the dependence on the location of the drive, or drives, as well as the modal dependence. It shows that if you pick the right place to drive, the mode separation problem becomes easier. For instance, at the center you don't excite any of the odd number modes; you excite only the even number modes. So that helps you out by a factor two.

VOELKER: I want to mention our experience on the HILAC. We had two tanks coupled together with a coupling line and the scallop was directly related to the difference in frequency between the two cavities so that we used this as a rough tuning. When we took off the coupling line and began to drive from a separate amplifier, we found that we no longer had phase lock; we had as much as 10° between the two tanks during the pulse. On some experiments the beam would go away during the early part of the pulse. In the last few months we have put in a phase servo with a veractor in a low level stage and have reduced the phase shift from about 10° to 2° .

JAMESON: You do have to take into account the fact that these other modes are there even though the effect is very small. Below is a picture of output from an 11-cell iris-loaded tank, which we drove at signal level frequencies. That is the input pulse on the upper left-hand corner. Then I used the sampling scope to look at the output of the tank in the various cells of the tank. This allows us to look at the rf directly and you can see the scallops that arise. This tank has a Q of 8300, a coupling of 2%, N was equal to 10 in the theory, and it was driven at the center. It shows quite well what the effect is. We also drove at the end of the same tank, and in the cells furthest away from the drive we observed, at the turn-off of the pulse, the pip where the energy actually goes up for an instant before it comes back down. Jim Leiss mentioned this yesterday.

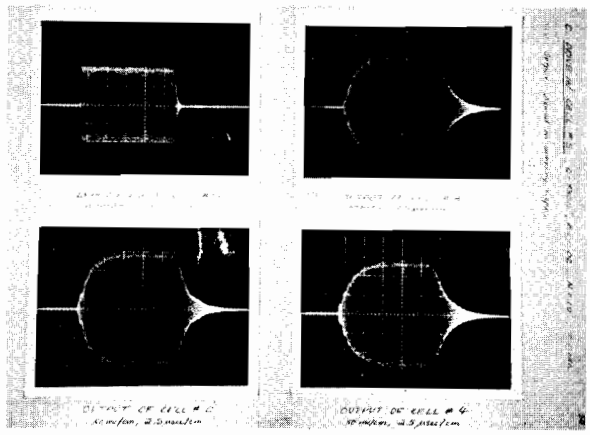

RECHARGING LARGE CAPACITOR BANKS

H. R. Shaylor
Brookhaven National Laboratory

The power bill for a large linac such as that proposed for the AGS conversion would be in the order of $100,000 per year. This is for an 0.6 msec pulse length and 30 pps, and an 8,000 hour year. It also assumes fairly high efficiency in the rf power stages. A typical "meson factory" would involve a power bill ten times as great.

A simple method of recharging a modulator condenser bank or storage line from zero volts to a given voltage would be to use a standard dc power supply and a series resistance to limit the current. Such a circuit would dissipate as much energy in the resistance as it supplied to the condenser bank, and the power bill would then be doubled.

Clearly then it is very worthwhile to design condenser recharging circuits with view to achieving a high recharge efficiency, any improvement of a few per cent or more will be significant.

The modulator energy storage system usually takes the form either of a delay line or a single capacitor bank. After considering the alternatives it was decided that the single capacitor bank is the most suitable alternative when (a) the pulse length was too long to permit the use of a pulse transformer, and (b) it was necessary to modulate the dc plate voltage on the rf amplifier in order to control the rf amplitude in the linac tank, (c) the rf power amplifier was some sort of triode with a dc plate voltage around 30 kV. The reasons for this choice will not be enumerated here. Further practical considerations show that the optimum choice of capacitor bank size is not one which stores twice the energy delivered to the load, although this is the smallest bank in terms of energy stored. A capacitor bank that droops about 10% during the discharge, and stores about five times the energy delivered to the load is a better choice.

Recharge Analysis

The basic circuit upon which the analysis has been made is shown in the circuit diagram:

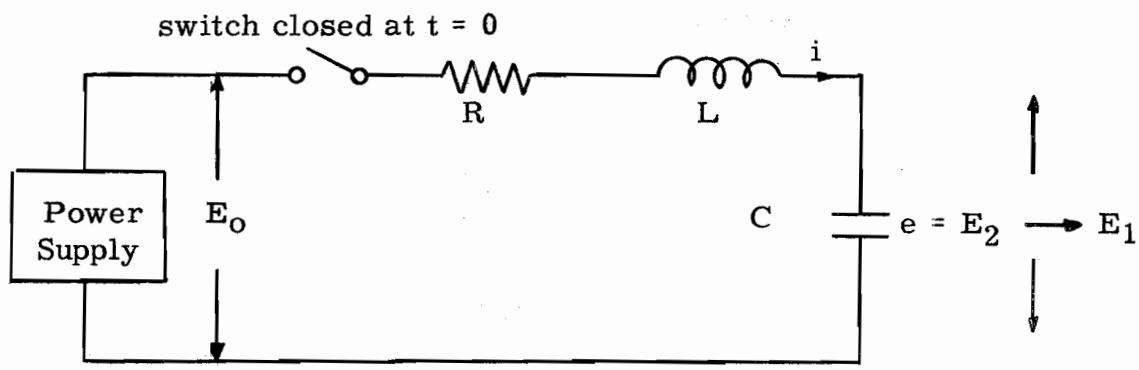

Circuit Diagram

The condenser is discharged by the load circuit (not shown) to voltage E_2. The recharge is effected by closing the switch at time t = 0. A variable current i flows and the condenser voltage e rises from E_2 at t = 0 to E_1 at t = T. At time T the current flow is interrupted either by opening the switch, or by some other means. The power supply voltage is E_o, and the energy dissipated in the circuit from time 0 to time T is U_R.

Arrangement of formula

In order to show that the analysis is dependent only upon the relative values of L, C and R, the results have been normalized. The capacitor current i becomes a dimensionless quantity

$$n_i = \frac{i}{(E_1 - E_2)} \frac{T}{C} ,$$

the capacitor voltage e becomes

$$n_e = \frac{e - E_2}{E_1 - E_2}$$

and the energy dissipated in the resistance U_R becomes

$$N_R = \frac{U_R}{(E_o - E_1)^2} \quad \frac{2}{C} \quad .$$

The efficiency of the recharging circuit can be obtaine directly from N_R since

$$\frac{\text{Energy dissipated}}{\text{Energy supplied to capacitor}} = N_R \frac{E_1 - E_2}{E_1 + E_2}$$

Thus for a capacitor with 10% voltage droop during discharge, an N_R value of 1 will give a 5% loss.

The circuit has been analyzed for the values of energy dissipated in R (N_R), the maximum capacitor voltage (N_C), the peak charging current (N_m), and the charging current at the end of the recharge period (N_T). The latter current is significant since it determines the rate of change of condenser voltage at switchoff, and hence the time tolerance requirements for a given voltage accuracy.

The analysis falls naturally into two cases, one when Q is greater than one-half, and the other when it is less. In the $Q > 1/2$ case, were it not for the power supply rectifiers, the capacitor voltage would be a damped periodic function of time; however, the decrease in capacitor voltage after the first peak is accompanied by a reversal of the charging current, and the rectifiers cut off at this point leaving the capacitor charged to the peak voltage. Thus, if the circuit is not interrupted by the switch, the recharge period will be one-half of the ringing period, the current at this time will be zero, and the capacitor voltage will be greater than (or in the limit equal to) the recharge voltage. The formula relating to the $Q > 1/2$ case assumes that the charge is terminated by current reversal at the end of the first half cycle, and shown in the first summary table.

SUMMARY

$$Q = \frac{1}{R}\sqrt{\frac{L}{C}} > \frac{1}{2}$$

$$\frac{\pi}{T} = \sqrt{\frac{1}{LC} - \frac{R^2}{4L^2}} \qquad P = \sqrt{\frac{4L}{R^2C} - 1} = \sqrt{4Q^2 - 1}$$

$$n_i = \frac{\pi}{N_c}\left(\frac{1}{P^2} + 1\right) e^{\frac{-\pi}{P}\frac{t}{T}} \sin\frac{\pi t}{T}$$

$$i = \frac{(E_1 - E_2)C}{T} n_i \qquad N_T \equiv 0$$

$$n_e = \frac{1}{N_c}\left(1 - e^{\frac{-\pi}{P}\frac{t}{T}}\left(\cos\frac{\pi t}{T} + \frac{1}{P}\sin\frac{\pi t}{T}\right)\right) = \frac{e - E_2}{E_1 - E_2}$$

$$N_c = \frac{E_1 - E_2}{E_o - E_2} = 1 + e^{\frac{-\pi}{P}}$$

$$N_R = \frac{1}{N_c^2}\left(1 - e^{\frac{-2\pi}{P}}\right)$$

$$U_R = \frac{(E_1 - E_2)^2 C}{2} N_R$$

Here P is a function of Q, and T is defined as half the natural periodicity of the circuit.

N_T, the value of n_i at time T is zero. N_c is the recharge voltage ratio. Both current and voltage are damped trigonometrical functions of time. N_R is a function of P (and hence Q) only.

In the $Q < 1/2$ case the capacitor voltage rises asymptotically towards the recharging voltage, so the recharge period is assumed to be terminated after time T by opening the switch. Thus there is a finite current flowing at time T and the final capacitor voltage is always less than the recharge voltage. The formula relating to the $Q < 1/2$ case is shown in the second summary table.

In this case the recharge period T is not uniquely determined by Q and C as in the $Q > 1/2$ case, so the period has to be specified. It has been normalized (somewhat arbitrarily) as the quantity $V = \frac{T}{RC}$. S is a function of Q, chosen so as to avoid the use of complex notation. The other symbols used are similar to the $Q > 1/2$ case. N_T may be found by putting $t = T$ in the n_i formula.

The current and voltage are exponential functions of time, and N_R is a function of Q and T.

Recharging Power Supply

A practical power supply would not deliver a smooth dc voltage as assumed in the analysis, but a rectified ac voltage. However, such a supply would be at least six phase and the ripple would be less than 15%, so results calculated for the dc case would be reasonably accurate.

The power supply would also have a finite internal impedance (generally inductive) and this impedance will, of course, add to any external resistance and inductance in the circuit.

The exact relationship of the power supply transformer leakage inductance and resistance to those values found as source impedance in a complete multiphase power supply is not clear, but it is probable that a resistance that would account for the supply dc regulation in series with the leakage inductance per rectifier phase would give the correct value of source impedance.

SUMMARY

$$Q = \frac{1}{R}\sqrt{\frac{L}{C}} < \frac{1}{2}$$

$$V = \frac{T}{RC} \qquad S = \sqrt{1 - \frac{4L}{R^2C}} = \sqrt{1 - 4Q^2}$$

$$n_i = \frac{V}{N_c S}\left(e^{\frac{-2V}{(1+S)T}t} - e^{\frac{-2V}{(1-S)T}t}\right)$$

$$i = \frac{(E_1 - E_2)C}{T} n_i$$

$$n_e = \frac{1}{N_c}\left[1 + \left(\frac{1}{S} - 1\right)\frac{e}{2}^{\frac{-2V}{(1-S)T}t} - \left(\frac{1}{S} + 1\right)\frac{e}{2}^{\frac{-2V}{(1+S)T}t}\right] = \frac{e - E_2}{E_1 - E_2}$$

$$N_c = \frac{E_1 - E_2}{E_o - E_2} = \left[1 + \left(\frac{1}{S} - 1\right)\frac{e}{2}^{\frac{-2V}{(1-S)}} - \left(\frac{1}{S} + 1\right)\frac{e}{2}^{\frac{-2V}{(1+S)}}\right]$$

$$N_R = \frac{1}{N_c^2 S^2}\left[(1 - S^2)\, e^{\frac{-4V}{(1-S^2)}} - (1 + S)\frac{e}{2}^{\frac{-4V}{(1+S)}} - (1 - S)\frac{e}{2}^{\frac{-4V}{(1-S)}} + S^2\right]$$

$$U_R = \frac{(E_1 - E_2)^2 C}{2} N_R$$

Evaluation of Results

Since the evaluation of formula by inspection is a difficult mental exercise, it was decided to program the Brookhaven computer to plot out the results. Copies of these results are shown in the next few diagrams.

Figure 1 shows the variation of current and voltage with time for Q values of 0.7 and 5. The Q = 5 case shows the current as a sine curve and the voltage as a cosine curve. The Q = 0.7 case shows heavily damped versions of the same curves. Figure 2 shows N_c, the recharge voltage ratio; N_m, the peak to average current ratio; and N_R, the loss factor; varying with Q for the Q > 1/2 case.

For the Q < 1/2 case, Figures 3, 4 and 5 show the variation of current with time. They show Q values of 0.5 and 0.12, and T/RC values of 0.5, 1 and 3. Note that the definition of T is quite different from that in the Q > 1/2 case, so the values of $\frac{t}{T}$ in the two cases have no correspondence. It will be seen that as the recharge period $\frac{T}{RC}$ is made shorter, the Q = 0.12 curve shapes approach the simple RC exponentials.

For the Q < 1/2 case the values of N_c, N_T, N_R and N_m are shown as functions of T/RC rather than Q, since the recharge period is the more significant parameter. Figure 6 shows N_c and N_T, and Figure 7 shows N_R and N_m.

It may be seen from the plots that the dissipation value N_R is always greater than one for Q < 1/2, and less than one for Q > 1/2. Two further points may be seen in the Q > 1/2 case; with increasing Q the dissipation decreases toward zero, and the maximum current during the recharge period I_m decreases toward $\pi/2$. This would seem to indicate that the highest attainable Q is the ideal situation. However, with high Q values the N_C ratio tends toward 2, and this leads to an unstable recharge voltage in that when the capacitor bank is discharged to an unusually low voltage (e.g. because of a partial breakdown) then the bank is recharged to a higher voltage than normal. In the extreme case consider a bank which normally has a 10% droop and would require a recharge voltage E_o of about 95% of the maximum capacitor voltage E_1. If such a circuit were discharged to zero voltage then the capacitor bank would theoretically recharge to 1.9 times the normal maximum voltage, which could be very dangerous.

A practical compromise would seem to be a circuit designed to give a Q a little above 0.5, say 0.75. This would give a dissipation value of 0.9, which means a power loss of 4.7% during the recharge of a 10% droop;

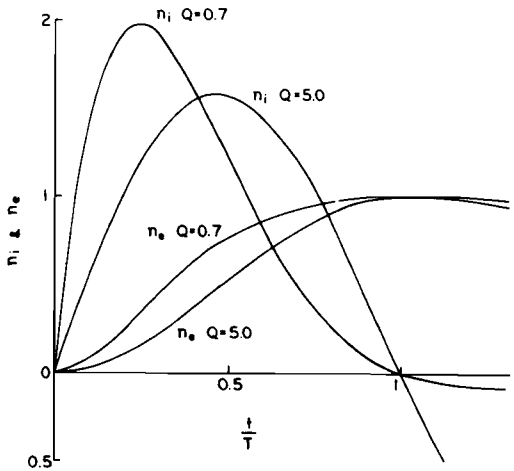

FIG. 1

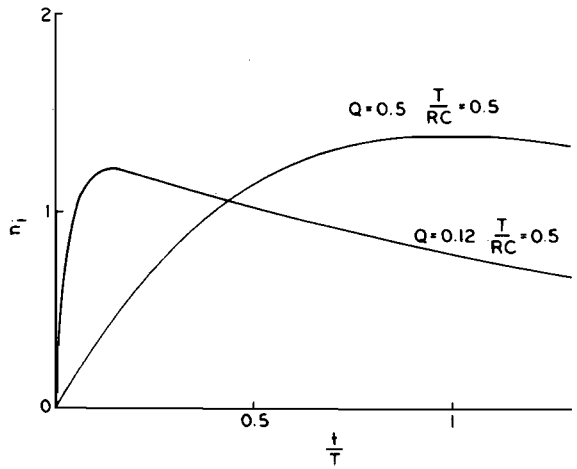

FIG. 3

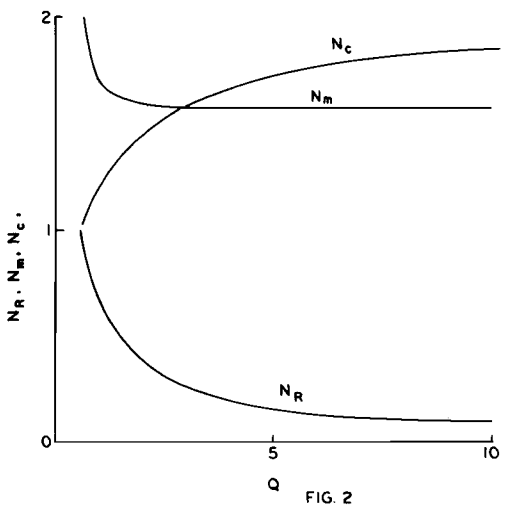

FIG. 2

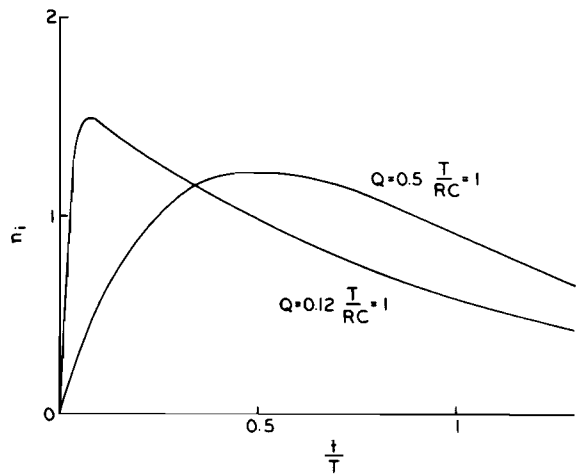

FIG. 4

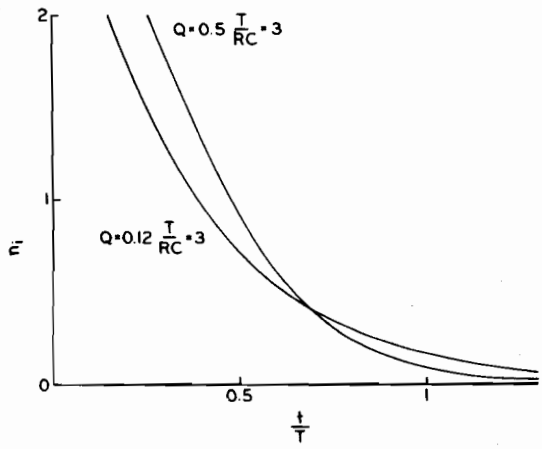

FIG. 5

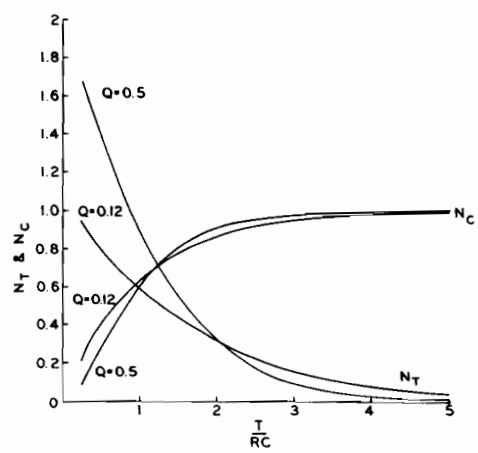

FIG. 6

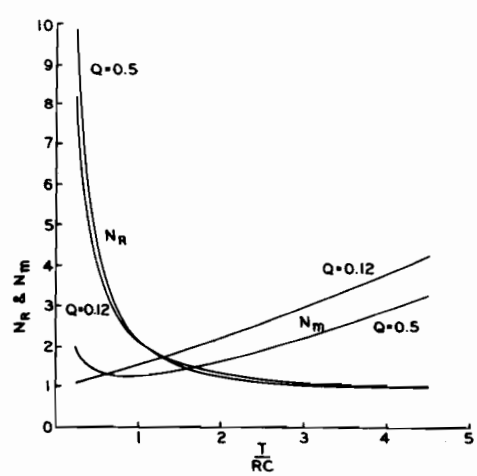

FIG. 7

and an N_C ratio of 1.06, so under conditions of complete discharge the condenser voltage would rise only 6% higher than normal. The maximum current for such a circuit would be 1.9 times the average current and the circuit would automatically cut off at zero current when the recharge is finished. Although the danger of over-volting the capacitors is now removed, there would still be the problem of high recharge current in the event of recharging from zero voltage, in which case the maximum current would tend to rise to 19 times the normal current. The recharge control equipment would have to have some provision for reducing such current in the event of a flashover or crowbar, and also at start-up times.

There seems to be no advantage in using the $Q < 1/2$ case, except on the grounds of simplicity, or perhaps to obtain a lower maximum recharge current at the expense of greater losses.

It is of interest to note that for the case of $Q < 1/2$ and $T/RC < 1$, N_R <u>increases</u> with increasing Q. This is because when the switch is opened with a finite current flowing, then the LI^2 energy in the inductance at that time is dissipated (presumably in the switching arc) and thus is lost to the circuit. When T/RC is less than one, the ratio of energy stored in the inductance to that dissipated in the resistance is such that increasing the Q also increases the total power loss.

Variable Resistance Recharging

Mr. J. F. Sheehan of Yale University has suggested a very interesting alternative to the LR current limiting network. This would replace the LR combination with a variable R, automatically controlled to keep the recharge current constant. The variable resistance would take the form of a hard tube.

The most useful case of this circuit would be when the recharge voltage E_o is equal to the maximum voltage E_1, and so the minimum variable resistance value is zero. This gives a dissipation value N_R of 1.0, so the power loss would be similar to the $Q = 0.75$ case outlined above. The maximum current ratio N_m is now the ideal value of 1.0, the N_C ratio is 1.0 and the current at the end of the charge is zero since there is no way for the capacitor voltage to rise above the recharge voltage.

Provided the current controlling action is automatic, the only effect of recharging a fully discharged bank would be to prolong the recharge period. The main disadvantage would be the complexity of such a circuit as compared with a passive LR combination.

Continuously Recharged Capacitor Systems

Some consideration has been given to the case which is often used; when recharge current is not zero at the start of the recharge period. This would occur if the switch was omitted in the $Q < 1/2$ case, or if the discharge repetition rate was greater than twice the ringing frequency in the $Q > 1/2$ case. An analysis of the recharge current in the latter case has been carried out.

The arrangement presents the difficulty that each recharge cycle depends upon the previous one, and there is no obvious indication as to how the current at the start of each recharge period will converge upon a steady value. Furthermore, this steady state will be upset by any irregularity in the pulsing rate. It is considered then that unless used with a $Q < 1/2$ and a large value of T/RC, in which case the initial recharge current will be very small, the continuous recharge system is likely to give less stable operation than one in which the recharge current is zero at the start of the recharge cycle. There would seem to be no real advantage of a continuous recharge circuit over one in which Q is a little greater than 1/2, and the recharge terminated by current reversal.

Conclusions

The optimum design of a circuit for recharging condenser banks of the type described above, would be one with a Q value about 0.75. If an active circuit is acceptable, then a constant current circuit would be preferable. It seems that a continuously recharged system would be less stable than one in which the recharge time is controlled.

WHEELER: If you look at the figure here, $I_m = 1.9$, and make a quick estimate of the peak power demand for a large installation, it turns out to be of the order of 60 MW for the instantaneous demand. This is reflected into the power line and the power companies will not be very happy about it. For this reason alone I think it may be necessary to go to a constant current-charging system.

STATUS REPORT ON THE COAXITRON DEVELOPMENT PROGRAM

G. W. Wheeler
Yale University

Several years ago, when the Yale Design Study Group proposed the use of 800 Mc/sec as the operating frequency for the waveguide section of the proton linac, it was recognized that suitable rf power sources were not available. Consideration was given immediately to this problem. It was generally agreed that negative grid triodes offer the best type of power source for proton linacs.

Work at RCA indicated that the "coaxitron" type of tube was promising. The coaxitron is a negative grid triode in which the resonant input and output circuits are contained within the vacuum envelope. The Yale and Los Alamos groups drew up and agreed on a set of performance specifications for an 800 Mc/sec coaxitron based on the estimated performance which RCA felt was reasonable. This has resulted in a fixed price contract between LASL and RCA for RCA to supply five prototype coaxitrons to meet certain performance specifications. The five tubes will be split between LASL and BNL for test and evaluation. The first tube is scheduled for delivery in November 1964 and then one tube per month.

The specifications for this tube are as follows. It is designated as the A15191.

Frequency (midband)	805 Mc/sec
Band width	15 Mc/sec
Gain	10 db (minimum)
Peak power output	1.25 MW
Pulse length	2.2 msec
Pulse rate	30 pps
Duty cycle	6.6%
Cathode	Thoriated tungsten filament
Output connector	Coax to waveguide transition
Input connector	1-5/8" Coax
Tuning adjustments	None
Operating mode	Zero bias, grounded grid
Plate output blocking capacitor	Internal
Plate voltage	~35 kV
Plate current	~100 A
Cathode area	~75 cm^2
Peak emission current	~300 A

The A15191 is scaled from the existing type A15038 which produces 5 MW peak power at 450 Mc/sec. At present, the A15191 design has progressed to the point where the cavity design has been verified by cold test measurements. The performance of the electronic circuitry has already been verified in other tubes. The grid-cathode structure is essentially identical with another coaxitron which exists. This is a 900 Mc/sec tube with the following demonstrated performance.

Frequency	~940 Mc/sec
Band width	~ 50 Mc/sec
Gain	11 db
Peak power output	1.4 MW
Pulse length	25 msec
Duty cycle	1%
Plate voltage	~35 kV
Plate current	~125 A
Cathode	Oxide Filament

MARTIN, J. H.: What is the average power output from the A15191?

WHEELER: Six per cent of 1-1/4 MW. This is hopefully conservative for the anode structure. The only experience we have is with the 400 Mc tube which does appear to be all right at that average power level.

VOELKER: You hope to get more gain than 10 db?

WHEELER: Yes. The more the better. They are already getting 11 db out of the 900 Mc/sec wide band tube and reducing the band width should improve the gain.

A POSSIBLE APPROACH TO THE INITIAL ADJUSTMENT OF A LONG LINAC

G. W. Wheeler and T. W. Ludlam
Yale University

In existing proton linacs, the maximum number of independent cavities is three. No serious problems have been encountered in adjusting the field level in each cavity and the relative phases of the cavities to the proper values. However, the initial adjustment of the multicavity linacs which are now being discussed[1] is a much more difficult problem. The reasons for this are clear. The effect of an improper adjustment at one point in the linac generally will not be observed until the beam has passed through several more cavities so that there is no direct way of determining the location of the improper adjustment. Furthermore, the adjustment of a particular cavity interacts with those for the following cavities. Initially, the setting of the quadrupole magnets is not very critical and it will be supposed that they can be set to the calculated values with sufficient accuracy to assure retention of the beam. Thus there are two major adjustments per cavity: the field level (E_o) in the cavity and its phase relative to the preceding cavity. Consequently, for the new linac injector proposed by the Brookhaven National Laboratory there are 122 adjustments.

There are two important stages in the adjustment. The first is an adjustment which is sufficiently good to assure the acceleration of the entire captured beam without the loss of particles at high energies. Numerical calculations indicate that if the field level is held to $\pm$ 1% and the intercavity phase to $\pm 2^o$, this situation will exist. The second stage of the adjustment involves reducing the beam energy spread and emittance to the smallest values which can be achieved. The success of these linacs particularly as injectors will be determined by the extent to which the adjustment errors can be reduced toward zero. It is generally agreed that the energy spread and emittance of a perfect linac would be entirely adequate for injection into a large synchrotron.

If all of the characteristics of the beam could be accurately measured at the end of each cavity, there would be no difficulty in adjustment. This unfortunately is impossible. The following quantities can be measured as indicated.

a) W and ΔW, the beam energy spread.

These quantities can be measured by magnetic analysis. Consequently the measurements can only be made at the injection point, at the

transition section and at the end of the accelerator. Beams of less than full energy may be drifted through the accelerator to the magnets without destroying the desired information. Accuracies of about 0.1% can be achieved. An alternative method involves time-of-flight techniques but requires considerable equipment and space.

b) I, the beam current.

Absolute measurement of the peak beam current is difficult but is not necessary for accelerator tune up. Relative measurements may be made with ease and considerable accuracy using beam current transformers. The transformer output is independent of energy and relative readings can be accurate to better than 1%. Thus if several transformers are calibrated relative to each other at one point, they may then be distributed along the accelerator and the differential outputs from them will be a sensitive measure of beam loss along the accelerator. However, the sensitivity of the transformers is only about 10 μA so that a peak beam current of at least 100 μA is needed for good measurements. Another sensitive method of detecting beam loss is to locate neutron or gamma detectors close to the structure to detect radiation due to lost beam. This system gives somewhat more detailed information as to the location of the beam loss.

c) The beam emittance.

The beam emittances can be fairly readily measured at low energies with considerable accuracy. At higher energies, the measurement can be done less readily. The measuring equipment is bulky and can be provided only at the injection point, at the transition and at the end of the accelerator. Some simpler systems which will give a rough measurement of x and y may be placed at more frequent intervals between cavities.

d) E_o, the average accelerating field in each cavity and φ_s, the synchronous phase.

An absolute measurement of E_o can be made to between 5 and 10% with carefully calibrated pickup loops in the cavities. A relative measurement of E_o between two cavities can probably be made to a few percent, and E_o may be held stable to 0.1%. There is no direct measurement of φ_s. If the energy gain in a cavity can be measured, then $E_o T \cos \varphi_s$ is known to the same accuracy. The transit time factor, T is fairly well known from cavity calculations. If E_o is decreased until $\varphi_s = 0$, it is possible in principle to measure the threshold value of E_o for which particles just gain the synchronous energy. This involves measuring a very small current and consequently has limited accuracy.

e) $\Delta\varphi$, the phase spread of the bunch.

The phase spread of the bunch can best be determined from a knowledge of ΔW. The center of the phase bunch may be measured with poor accuracy by observing the phase of a small resonant cavity between the accelerating cavities. This cavity will be excited by the beam at a phase corresponding to the "center of gravity" of the bunch.

f) $\Delta\varphi'$, the phase difference between adjacent cavities.

The phase difference between two cavities can be measured absolutely to a few degrees. The design value can be calculated accurately. The setting can be held to better than 1°.

The following general procedures will be followed in order to tune up the accelerator with a minimum of activation of the structure. Initially, short beam pulses and reduced repetition rate will be used. The peak beam current will be limited to about 100 μA to remove the beam loading problems from the first tune-up attempt. The drift tube section should be completely tuned up before a serious attempt is made to tune the waveguide section. All measurements of the output beam from the drift tube accelerator will be done in the transition region between the two sections.

In what follows, it will be assumed that the beam from the drift tube section of the linac has been adjusted for best quality and that the transverse focusing of the beam in the waveguide section is well enough adjusted so that all particles which are longitudinally stable will be radially stable. The following procedure is suggested as a possible method of adjusting the waveguide section of the linac. Very extensive numerical calculations are needed to demonstrate that the procedure will actually lead to the desired result. Some preliminary calculations have been made using a program[2] which treats only the longitudinal motion of the axial particle.

If the field level (E_o) in each cavity and the phase difference between cavities ($\Delta\varphi'$) are set by absolute measurements to the design values, it is to be expected that particles will be lost at various points along the accelerator because of the errors. However, if the size of the bucket in each cavity is substantially increased, the entire beam can be retained in spite of sizeable errors in $\Delta\varphi'$. Since the initial tune up will be carried out at low beam current, the amplifier output, which will ultimately be transferred to the beam, is available to increase E_o above the design value. Calculations have shown that if E_o is increased by 15%, the entire beam can be retained for errors in $\Delta\varphi'$ of $\pm 5^{o}$ or more.

Since the design value of E_o should be well below the sparking limit, a 15% increase in E_o is possible. This will increase the bucket width from about 77° to about 115°. Throughout this procedure, the beam current is carefully monitored at several points along the accelerator.

The next step is to gradually decrease E_o in the first cavity until a noticeable decrease in beam current occurs. It will be necessary at the same time to decrease E_o slightly in the next few cavities in order to prevent the recapture of the particles which have become unstable in the first cavity. When the bucket in the first cavity has been shrunk so that some particles are outside of the stable region in the first cavity, the setting of $\Delta\varphi'$ for the first cavity is varied to minimize the loss. Here, $\Delta\varphi'$ is the phase difference between the last 200 Mc/sec cavity and the first waveguide cavity. This centers the injected bunch optimally in the first cavity. Now, E_o in the first cavity can be increased by a calculated amount to the design value. This will only be approximate but the exact value is not important. It should be noted that changing E_o causes the bucket to expand or shrink around $\varphi = 0$ and not around φ_s. Consequently, the value of $\Delta\varphi'$ which was just determined is no longer correct. A reasonably good calculated correction can be set in $\Delta\varphi'$ because now we are making changes in the relative (rather than absolute) values of E_o and $\Delta\varphi'$ and this can be done with considerable accuracy for changes of this magnitude.

At this point, all but the first cavity are turned off and the energy gain of that cavity is measured. If the average energy gain does not correspond to the calculated value, the cavity field will have to be tipped to make it do so.

The whole procedure is then repeated for subsequent cavities in a sequential fashion. When measuring the beam current decrease due to shrinking the bucket in cavities near the high energy end, magnetic analysis of the output beam will be required to distinguish between particles which have become unstable and those which have not since all will emerge from the end of the accelerator.

Repeating this entire performance a second time should further improve the adjustment. Once values of E_o and $\Delta\varphi'$ have been established for each cavity, it is the job of the level and phase servos to hold them there.

Preliminary numerical calculations indicate that the phase errors can be reduced by this procedure on the first attempt. However, the measurement of beam loss is not extremely sensitive and it will be necessary to examine the beam quality in order to achieve better

adjustment. Nevertheless the procedure seems promising at first look and further computations will be carried out.

Once the whole accelerator has been tuned up in the unloaded condition, the beam current can be increased until the effects of beam loading are observed. The automatic level and phase control systems must be adjusted to maintain the correct settings. At each stage the necessary adjustments can be made until the full beam current is (hopefully) reached.

LEISS: In making this analysis, you have assumed that subsequent buckets are in the correct place. Now, if you have a systematic deviation of the location of the subsequent buckets, have you assured yourself that in fact you are not building in systematic errors which you are trying to satisfy rather than putting the beam where you would like it? It seems possible that there is a trap here. In other words, are you presupposing that the problem is already solved?

WHEELER: No, we have not presupposed a solution. It is true that we have used only random errors distributed about the correct value and have not looked at the effect of gross systematic errors. However, by increasing E_o by an amount which is greater than any reasonable systematic error we can assure ourselves that E_o is well above the design value. Our assumption of $\pm 5^o$ phase error would account for a systematic phase error up to that value. A systematic phase error larger than this could be troublesome but I think that the system is flexible enough to handle it. Let me emphasize that there is a lot more work to do before we fully understand how to apply this method of tune-up.

BLEWETT: I should think that if you have a gross systematic error, no beam will come out and you will say, "Ah ha, I have a systematic error", and will look for it.

WHEELER: Yes. I think that there are a number of ways that you can detect gross systematic errors before you turn on the beam which implies that such errors can be eliminated.

FEATHERSTONE: There are at least two possible methods of controlling the relative phase of the cavities in a long string of cavities. One is to refer all the cavities to a reference line and the other is to refer each cavity to the preceding one. Is there a preferred way of doing this when you consider the actual tune-up process?

WHEELER: Yes, I think there is although I am not sure which it is. My own opinion is that it is better to measure the phase directly between two adjacent cavities. In either case you can have a systematic error in the phase detector.

TAYLOR: For about 18 months, we have been trying to get a rather similar measurement to work but so far we have not gotten consistent results. We have tried the following measurements. You have the bunch coming from the first tank and then you collapse the bucket in the second tank until you trap only a small current. You define this as a threshold and then you raise the level a little and shift the phase of the second tank to get back to the threshold current. The lowest tank level achieved gives you approximately the $\varphi_S = 0$ level and then the other levels can be converted to the corresponding φ_S. Making certain assumptions, the result should be two straight lines ($\varphi_S = \varphi$ and $\varphi_S = \varphi/2$) and the intercepts give you the phase width of the bunch. We have tried this several times. The very first time, we got two straight lines which intercepted the axis and gave us a phase width which agreed quite well with simple theory. We repeated this later and got two more lines with different slopes which gave us different intercepts. We still think that there is some way to go before you can use this technique as a measurement for setting phases but I agree with you that it could be useful.

CARNE: I think that the success of this technique depends on the beam performing many phase oscillations in one tank.

WHEELER: This could be correct. We find from our numerical calculations that we must shrink the buckets in a group of about four tanks at a time in order to get a clear indication of particle loss. This corresponds to about one phase oscillation wavelength near 200 MeV.

DICKSON: One has to be careful about the detector used here. A current transformer will accept all energies. Some sort of threshold detector might be better.

WHEELER: When a particle becomes unstable in phase at an energy of about 300 MeV or more, it will emerge from the end of the accelerator, even though its energy is incorrect. Magnetic analysis can be used to determine when particles have not been fully accelerated, or one can use a threshold detector as you suggest.

TAYLOR: I want to point out that this setup problem may be with us in 5, 6 or 7 years but that in the meantime the methods of measuring beam properties may have advanced to the point where one can get all of the

information required for a rational setting up. It does make one wonder about the distance between the tanks and if there are some tricks that can be used such as changing the stability limit at the end of the previous tank, as Lapostolle has suggested, to allow a little more space between tanks. I think that this would pay off.

PERRY: It seems to me that one might start at the high energy end to measure the E field level and determine from the energy whether or not you are above the accelerating gradient and then go progressively up the line toward the front end to determine what accelerating gradient you must have.

WHEELER: I don't think you can learn much about the proper phase setting by this approach.

PERRY: This is true, but it seems to me that knowing this gradient to begin with before you start worrying about phase you have an easier job in the phasing problem. You know how high you have to go to get 15% above accelerating gradients, for example.

FEATHERSTONE: I wonder if Blewett's technique of using the upper tail of the fish as a rather precise probe could be adapted to this technique?

WHEELER: I think that it can be done and could be of additional help.

REFERENCES

1. See for example:
"Design of a High Current 200 MeV Proton Linear Accelerator," NIRL/R/55, RHEL, 3/64, p. 19.

"A Proposal for Increasing the Intensity of the Alternating Gradient Synchrotron at the Brookhaven National Laboratory", BNL 7956, 5/64, p. 153.

"A Final Report on the Design of a Very High Intensity Proton Linear Accelerator as a Meson Factory at an Energy of 750 MeV", Yale University Y-12, 9/64, p. 111-113.

2. G. W. Wheeler and T. W. Ludlam, Minutes of the Conference on Proton Linear Accelerators, Yale University, October 1963, p. 29.

RF SUPERCONDUCTIVITY MEASUREMENTS

J. M. Dickson
Rutherford High Energy Laboratory

The feasibility of designing a proton linear accelerator with superconducting cavities has been studied by A. P. Banford at the Rutherford Laboratory. The work has been mostly on the measurement of the surface resistivity of metals at 4.2°K, since it was realized that it was vital to this project that a workable means of producing large areas of superconducting surfaces had to be devised, and that nearly all the other problems were easy by comparison with this one with the notable exception of the problem of beam loading. The ideas formulated in the first papers on this subject were based on results obtained with small samples of pure metals. The rf measurement work has had two aims (1) to measure the surface resistivity of superconducting electroplated metals and of superconducting alloys and (2) to attempt to build a small superconducting resonant cavity with low surface resistance.

The rf measurements consisted of the measurement of the Q of resonant devices at 4.2°K and comparison of the results with Q of a dimensionally similar resonant device of copper measured at room temperature. The ratio of the two Q's gives the "improvement factor", which is the factor by which the rf power loss of a resonator would be reduced relative to a similar copper resonator. The approach has been to try to use plating or other techniques which would be applicable to large areas and not to try to relate the results to the physical state of the surface. Most of the work has been with simple $\lambda/4$ resonant lines in the form of a hairpin, weakly coupled to a pulsed rf source and a detector. The Q was estimated from the decay rate of the detected pulse. The result for several surfaces are as follows:

1. Lead, extrapolated onto copper with a standard commercial fluoborate solution, has given improvement factors up to 15,000 (the theoretical limit at 400 Mc/s is 40,000). Solid "Specpure" lead wire gave slightly worse results.

2. Solid niobium wire, after electropolishing, yielded improvement factors of up to 13,000.

3. Niobium deposited from $NbCl_5$ vapor, or electroplated from a molten salt gave results similar to (2) after electropolishing.

4. Inhomogeneous superconductors, such as Pb-Bi eutectic and Nb_3Sn gave very poor improvement factors (~ 50). This result can be explained by the filamentary nature of such materials, which is of course not a disadvantage when dc superconductivity is required.

5. Homogeneous alloys, such as Nb-Zr and Mo-Re gave improvement factors of about 2000. This can be explained simply by the fact that their resistivities fall rapidly below the critical temperature, but change very slowly above it, in contrast to the behavior of elementary metals.

Thus there seemed to be grounds for believing that large surfaces of lead or niobium could be prepared with suitably low surface resistivities. Some measurements on dielectrics at $4.2^{\circ}K$ showed that PTFE (teflon) was the least lossy material tested and that it had a tan δ of about 2.5×10^{-6}.

The type of resonant cavity chosen was a half-wave coaxial line, short circuited at each end and split perpendicular to the axis at the central current node. All the cavities were made by electroforming in copper and subsequent electroplating with lead. It was intended that these cavities should be used at high power and that current carrying joints would be tested, but all tests were in fact made at low power. Ten sets of tests were made but the best improvement factor measured was 2000, while all the others were less than 1000. Variations in plating techniques, ambient magnetic field, thermal contact and liquid helium level were all tried to attempt to eliminate the cause of the poor results. An improvement factor of 2000 would mean that a 50 MeV proton linac would have an rf dissipation of 1 kW. A $4.2^{\circ}K$ refrigerator for such a machine would cost about £ 400,000.

To account for the poor results one can postulate a residual resistivity to represent the unexpected extra losses, which can occur due to losses at joints, radiation through holes, etc. It can also include losses due to uncoated areas and parts of the surface held in the normal state magnetically or (unlikely) thermally. These areas would have an rf loss at 400 Mc/s about 4000 times larger than the ideal superconducting surface and if they totaled $1/200^{th}$ of the resonantor surface, the improvement factor would be reduced from the ideal 40,000 to the 2000 found experimentally. This degree of imperfection might also be expected to apply to the hairpin measurements, but it does not appear to do so. However, only the best results with hairpins have been quoted and some poor results (~ 4000) have been obtained with electroplated lead hairpins. Perhaps there is a statistical factor, which favors small surface areas.

These results can be compared with those obtained by other laboratories. At CERN Sussini using 260 Mc/s capacity loaded $\lambda/4$ coaxial resonators has never obtained improvement factors greater than 2000 to 3000 with lead and niobium. At Newcastle University Armitage using open ended 300 and 600 Mc/s $\lambda/2$ coaxial resonators has not exceeded an improvement factor of 40 yet with lead. At MIT Maxwell obtained an improvement factor of 50 with a 400 Mc/s coaxial resonator. At Stanford University Wilson obtained improvement factors of 2000 at 2856 Mc/s with a cavity which had a theoretical improvement factor of 3500. However, it must be noted that the normal (anomalous) surface resistivity scales as $f^{2/3}$ and the superconducting surface resistivity scales as f^2, so superconductivity of the whole surface is 14 times less important at this higher frequency. If $1/450^{th}$ of the surface was in the normal state, then the difference between 3500 and 2000 can be accounted for. Thus Wilson has been somewhat more successful in producing a homogeneous surface.

Other problems associated with a superconducting linear accelerator which have been studied include the effects of transient heat transfer and the relative merits of a conventional liquid nitrogen jacket and superinsulation. Thermal problems appear to be unimportant, even gross local overheating, whether steady or transient would not give trouble owing to the greatly enhanced diffusivity of metals at low temperatures. The extra cost of superinsulation would be offset by savings on liquid nitrogen after four years.

The rf tests have not been exhaustive and eventual success may yet be achieved by improved techniques and the expenditure of much time and effort. The results have, however, been sufficiently discouraging to inhibit further work on this problem at the Rutherford Laboratory, for the present.

SCHOPPER: I would like to comment on the beam loading problem. Gluckstern mentioned in the talk he gave here that according to his calculations, you get a limit of about 4 mA or several milliamperes, let us say.

DICKSON: Do you mean milliamperes or amperes?

SCHOPPER: Milliamperes instead of your 10 μA.

CARNE: Gluckstern gave 2 A as the limiting current for the new BNL injector for an estimated 1 M Ω/m for the deflecting mode, and, I think,

a frequency of 800 Mc/s. In view of the remarks of Walkinshaw, this current is probably of the order of 1 A. Now the limiting current varies inversely to shunt impedance of the deflecting mode, so that at a given frequency the limiting current will simply be reduced in ratio of the shunt impedances of the normal case and the superconducting case. Assuming that the deflecting mode exists at 400 Mc/s, where the improvement factor is 40,000, the limiting current will be down by the order of 40,000 from the limiting current of the normal situation, i.e. of the order of a few tens of microamps.

SCHOPPER: The main thing I want to point out is that you have an advantage in a superconducting linac in that you are working with CW which means that your peak current is equal to the average current. And so even 10 μA average current, I think, would not be too bad.

DICKSON: Well, one has the advantage as far as counting techniques are concerned. I think the advantage is probably a doubtful one in the case of CW beam loading. I don't think one is convinced that CW beam loading is any easier to cope with than pulse beam loading.

LEISS: I don't believe I can agree with this beam loading conclusion that you make. The beam loading is at a different frequency and it is not too hard to consider the possibility of a selective filter which keep the Q of that mode low and leaves the Q of the operating mode high. Admittedly with these leakage problems, it is nontrivial, but in principle it is probably no more difficult than many of the other problems involved. And so I just cannot see this limit.

CARNE: This selective loading may remove the deflecting mode, but in, for example, the disc-loaded guide, there are plenty of higher order modes which may cause deflection, and in CW operation there is time for them to build up. I doubt if one can load down all of them.

LEISS: I am sure that is true, but as you go higher and higher, you are almost guaranteed that the limiting currents go up. I agree there are many technical problems of a very formidable nature, but I don't believe that it is as discouraging as that.

DICKSON: Well, you see, the Rutherford Lab is in business for studying accelerators, not studying rf superconductivity as such. We feel that the present state of knowledge of the latter subject is sufficiently discouraging for us to abandon further work on a superconducting proton linac for the present. This is slightly changing the subject.

LEISS: But there are other people who are intensely interested in the ideas of superconducting machines.

DICKSON: Well, let them have a go.

ROWE: You were estimating what part of the surface area was a good surface in your cavities. Am I correct in thinking that what you did was make a copper cavity, say, and then cover it with lead, or were these cavities solid lead, for example?

DICKSON: The half-wave coaxial cavity we are talking about was one which was electroformed in copper over a plexiglass mold, in two halves, and then the mold was extracted and the inside of the copper cavity was electroplated. In all measurements a copper structure of the same physical dimensions was used for comparison and to find the improvement factor.

SCHOPPER: I want to mention another problem; that is the sparking. I think an advantage of a superconducting linac is that you can use high gradients. If you could go to higher gradients and somehow avoid sparking, then you could build a much shorter accelerator, which would be a saving.

DICKSON: O.K., but you put in two "ifs" which I do not think are really justified.

CARNE: You are suggesting that the sparking limit is a function of temperature. Now there may be something in this, but the sparking limit, we would like to say, is 17 MV per meter.

SCHOPPER: This was just my question. I was asking if anybody has any experience with sparking properties at low temperatures.

DICKSON: No, I haven't. There is one thing that can be said about sparking and it is just that you have still got the same stored energy in the cavity whether it is superconducting or not, because you have the same fields. So when you do get a spark, the same power will be dumped into the spark as in a normal machine, which is of the order of 50 Joules per 20 MeV cavity. 50 Joules might make a mark on the superconductor producing a normal area.

PERRY: The problem of sparking at low temperature, I think, is aggravated by the possibility of condensation of gasses on surfaces, which is an unknown quantity, I believe.

DICKSON: We have no data on this, but we recognize that is another problem.

DEUTERON ACCELERATION IN THE C. L. A. (CERN LINEAR ACCELERATOR)*

Th. Sluyters
Brookhaven National Laboratory

Acceleration of deuterons in the CLA using the 2π mode as employed for protons would require that the deuterons have the same velocity as the protons at every point along the linac structure. This would mean deuteron acceleration up to 100 MeV. This is far above any field level that is practically possible in the present machine. We can investigate the case where we use half the proton velocity in the 4π mode; so maintaining the same frequency of 202 Mc/s, the deuterons traverse one unit cell in two rf cycles. The alternating magnetic focusing properties are now identical for protons and deuterons, because the momenta of both particles are equal. Nonrelativistically speaking, this can be realized if the velocity of the deuteron is half the velocity of the proton; so the linac injection energy deuterons should be 270 keV instead of 540 keV for protons and linac final energy will be 25 MeV instead of 50 MeV for protons.

Approximately the energy gain for a synchronous particle per cell is:

$$W = e\bar{E}T\,L_n \cos \varphi_s$$

in which

e = electron charge

$\bar{E}$ = mean accelerating field

T = transit time factor

L_n = cell length

φ_s = synchronous phase angle.

Thus, for deuteron acceleration, the transit time factor T_D should be half the factor T_H for protons, if the other quantities are identical for both particles; if $T_D > 1/2\ T_H$, one has to diminish E and if $T_D < 1/2\ T_H$, one must look for means of increasing E.

---

*See: "A Theoretical and Experimental Comparison of Proton and Deuteron Acceleration in the CLA", CERN 64-22.

Courant (1962*) has calculated these ratios T_D/T_H for all gaps of the BLA, showing a reasonable drift tube geometry for deuteron acceleration.

Ratios of the energy gain per gap can be obtained by calculating the effective available voltage in the gaps for both particles, using theoretical values of the longitudinal electric field for the first cavity and experimental values for the second and third tanks:

$$R = \frac{\int_0^\infty E_x(x) \cos \frac{4\pi x}{\lambda} dx}{\int_0^\infty E_x(x) \cos \frac{2\pi x}{\lambda} dx} = \frac{\text{effective accelerating voltage for } D^+}{\text{effective accelerating voltage for } H^+} .$$

These ratios were evaluated for the first and last gap of each tank (see Table I). The results show a less optimistic situation compared with Courant's results for the BLA and they suggest, for deuteron acceleration, appreciable tilting of the electric field in each cavity.

TABLE I

Cavity I		Cavity II		Cavity III	
Gap 1	Gap 42	Gap 1	Gap 41	Gap 1	Gap 27
0.2625	0.5137	0.6345	0.3598	0.7613	0.4942

A more extended investigation of axial motion has been made by calculating linac phase acceptances for both particles as a function of mean accelerating field and tilt using a mercury autocode program for proton acceleration written by A. Carne of the Rutherford National Laboratory. The approximations in this program are: symmetric gap fields, constant drift tube radius in each cell and acceleration independent of radial excursions.

The phase acceptances have been calculated as follows: at first the ideal tilt factors of the first cavity have been determined so that phase oscillations around a given phase angle are as small as possible

---

*E. D. Courant, "A Study of Possible Deuteron Acceleration", Conference on Linear Accelerators for High Energies, BNL, August, 1962.

($< 1^{o}$); then one searches for stable phase oscillations in the phase space. The tilt factors for the first cavity for synchronous deuteron acceleration compared to the tilt factors used for synchronous proton acceleration are shown in Fig. 1. Using these tilt factors, the linac acceptance for deuterons has been calculated for a stable phase angle of - 25 degrees, (see Fig. 2). On the basis of phase acceptance alone (so without radial loss), and a buncher peak voltage of 10 keV, deuterons are trapped for 80% between the initial phases 30° and 314°.

In practice, the flatteners in our cavities are fixed for synchronous proton acceleration and one can only impose from the outside a "linear" tilt gradient with tilt tuners positioned at the input and output end of each cavity. So it is more realistic to investigate deuteron acceptances with a linear change of electric field along the cavity.

Let us define acceptances in the energy phase plane as a product of the height of a bucket (stable energy range ΔE) and width of the bucket at mean injection energy (stable phase range $\Delta\varphi$), (see Fig. 3).

Figure 4 represents now proton and deuteron acceptances as a function of mean accelerating field for a set of negative tilts in the first cavity.*

The curves show that an increase in field level is necessary for deuteron acceleration in this drift tube structure and radio frequency and that tilt increase is more effective for deuterons than for protons. In practice, the increase in field level (which affects the whole cavity) is limited by radial losses, whereas the optimum tilt has not been reached.

The relation between acceptances, level and tilt for the second and third cavities are of less interest, because one can expect that the bunches can be captured in the respective buckets at appropriate level and/or tilt. Figures 5a and 5b show two typical deuteron buckets of the second cavity inside which an ellipse around an ideal deuteron bunch is drawn. Deuteron acceptances are here much less dependent on tilt compared with the first cavity.

Experimental deuteron acceleration has been investigated with a standard rf ion source assembly, producing deuteron beam currents up to 100 mA (10 μs pulse and 90% D^{+}). The beam performance for optimum machine conditions is given in Table II.

---

*Tilt is defined as $\frac{\Delta E}{E}$ x 100% in which ΔE is the rf electric field at output end minus the electric field at the input end of the cavity.

TABLE II

Preinjector	Source current	100 mA
	Beam current after column	60 mA
	Total emittance ($\frac{\text{area}}{\pi}$)	20 cm-mrad
	Linac input current	40 mA
	Injection energy	268 keV
Linac	Output current after first cavity (4.9 MeV)	7 mA
	Output current after second cavity (14.6 MeV)	7 mA
	Output current after third cavity (22.9 MeV)	7 mA
Inflector	Total beam emittance (90%)	<3.0 cm-mrad
	Energy spread of 65% of the beam	<100 keV

In the first cavity, approximately 17% of the beam was trapped and no beam losses occurred in the second and third ones. The final deuteron energy was 23 MeV with an energy spread of around 60 keV for 65% of the beam. The remaining part had a wide energy spread concentrated around an energy of 7.2 MeV.

There are two reasons for low trapping in the first cavity:

a) Axial phase losses. The range of the tilt tuners is limited to - 14%. Increase of rf level (affecting the whole cavity) should also increase the axial phase acceptance, however an optimum was reached, which finds its origin in stronger radial defocusing forces across the accelerating gaps for higher electrical field; this could not be compensated with the quadrupole focusing.

NOTE: For deuterons, always stronger focusing than for protons is necessary; this can be explained by comparing the radial force constant across the accelerating gaps; this constant is - 1/2 the axial force constant ω_φ^2, which is the square of the frequency of phase oscillations per unit length (Smith and Gluckstern, 1955*). The first cavity yields $\omega_\varphi(D^+)/\omega_\varphi(H^+) \approx 1.5$, so the defocusing forces for deuterons across the gaps are somewhat more than twice as large as for protons under equal machine conditions.

b) Radial losses. An important part of the beam is lost by improper matching at injection due to a smaller instantaneous transverse

*L. Smith and R. L. Gluckstern, Rev. Sci. Instr. 26, 220 (1955).

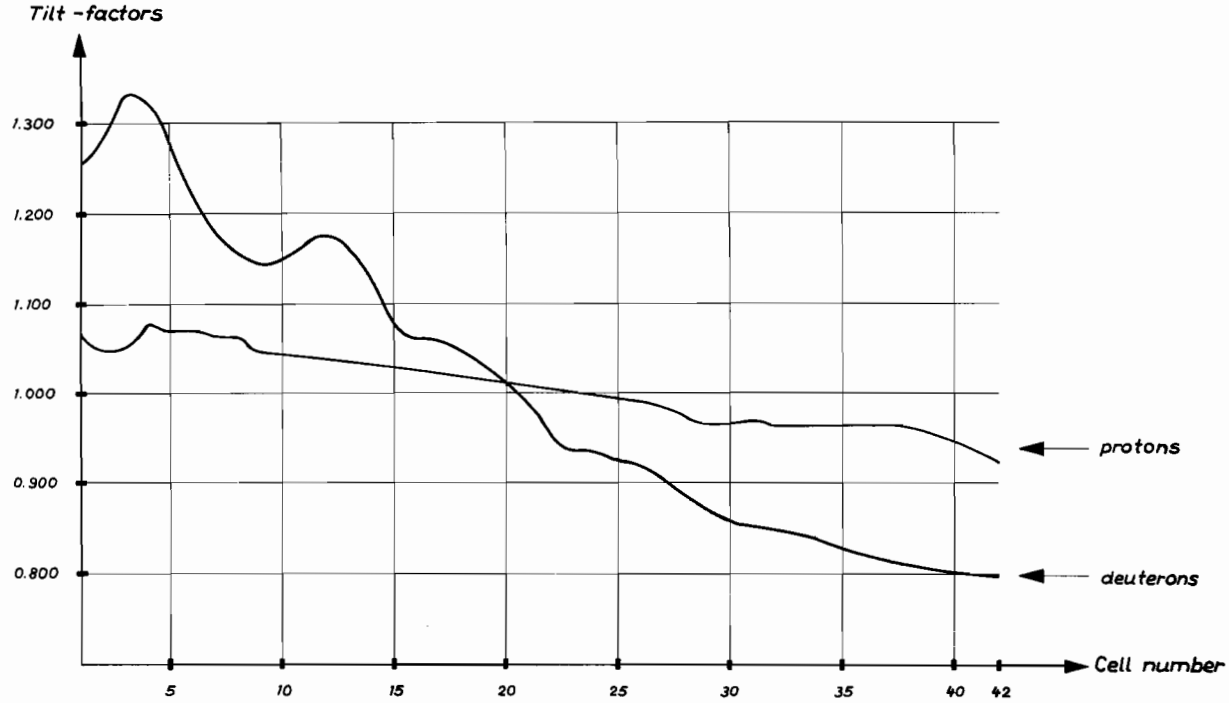

Fig. 1 Tilt factors for synchronous proton and deuteron acceleration in the first cavity.

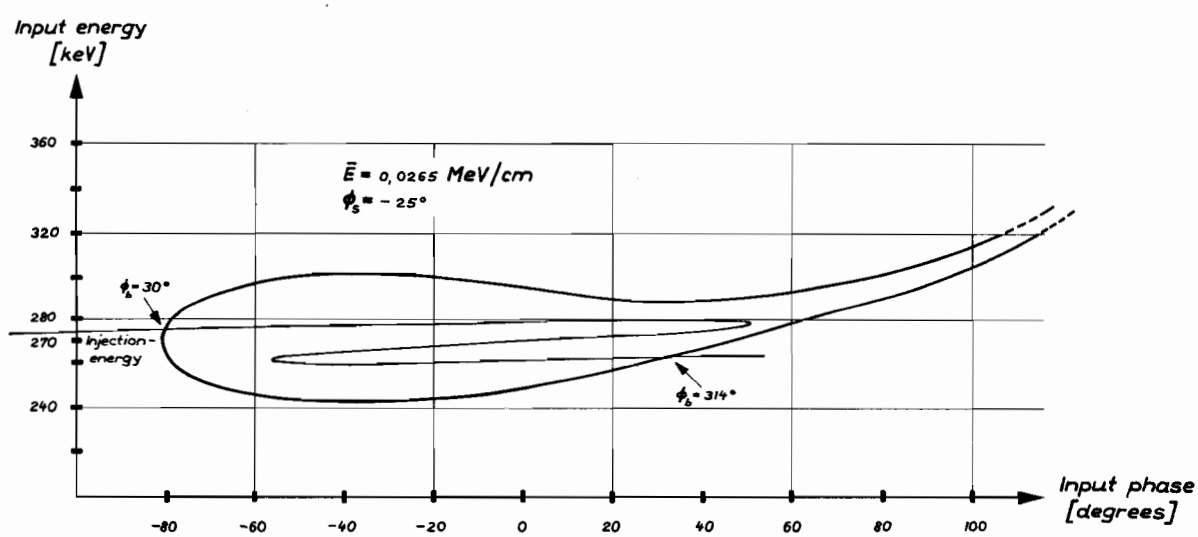

Fig. 2 Linac phase acceptance for deuterons with ideal tilt factors and a phase trapping curve for a buncher peak voltage of 10 keV. ϕ_b are particle phase angles at buncher position.

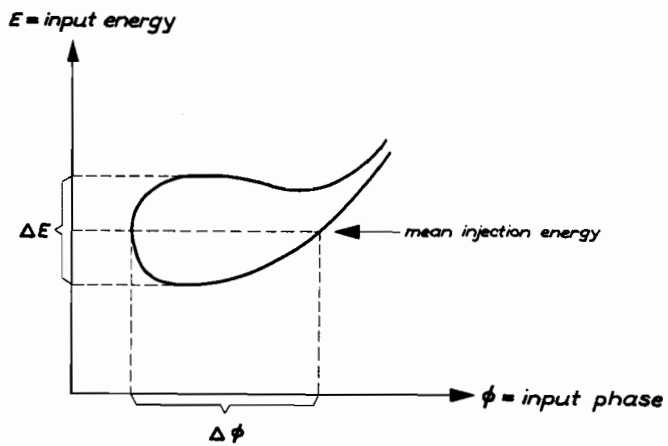

Fig. 3 Acceptance definition $\Delta E \cdot \Delta \phi$

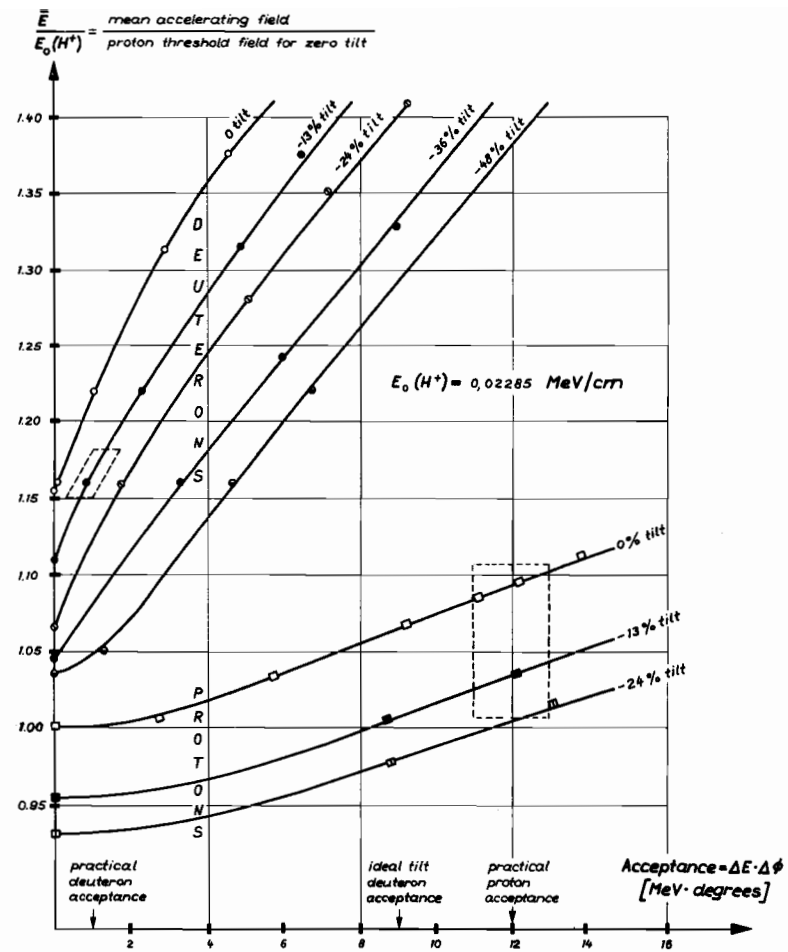

Fig. 4 Proton and deuteron acceptances as a function of accelerating field and linear negative tilt gradients in the first cavity. The parallelograms are actual working regions.

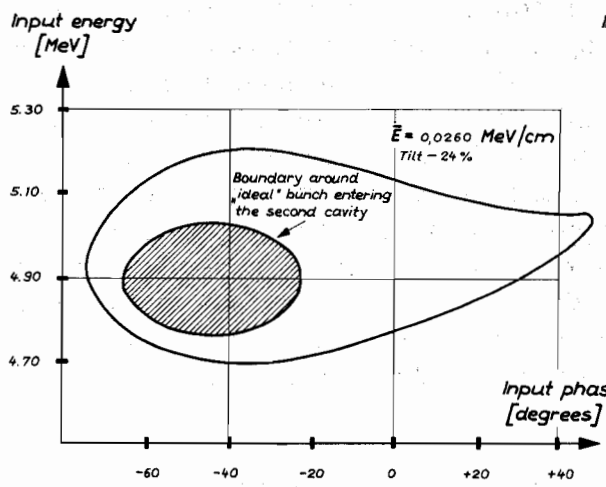

Fig. 5a Deuteron phase acceptance for the second cavity with positive tilt.

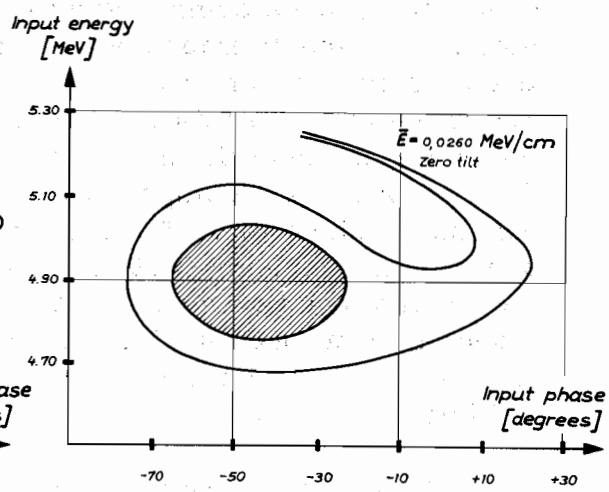

Fig. 5b Deuteron phase acceptance for the second cavity with flat field.

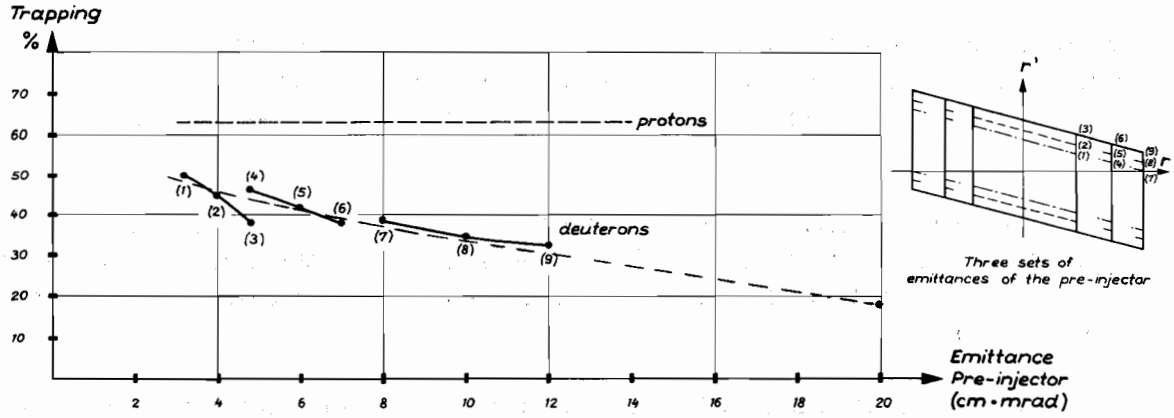

Fig. 6 Trapping for protons and deuterons as a function of injector emittances.

phase acceptance compared with protons. Therefore, smaller injector emittances should improve the trapping. Figure 6 shows an increase of trapping by a factor of three if the emittance diminishes to below 4.0 cm-mrad. At this injector emittance, the phase acceptance has been measured using optimum tilt and mean field conditions (see Fig. 7a). These results are compared with a theoretical phase acceptance. A buncher peak voltage of 7 keV suggests a theoretical trapping of 56%. In practice one measures 46%. The reasonable correspondence between theory and practice suggests that the present machine has an optimum trapping of around 50% for a preinjector emittance of around 4.0 cm-mrad; for this small emittance and low rf levels the radial focusing system is sufficient.

At the low energy side of the machine the radiation from deuteron interaction was 1 mrem/h or 7 n/cm^2/sec. This is a lower level than found from proton interaction with twice as much beam current. At the output end of the linac, a maximum dose rate of 20 mrem/h was measured.

SHAYLOR: I am very impressed with the fact that your ion source went well. We have a very elementary rf ion source in our Birmingham synchrotron and we started to accelerate deuterons about two years ago. Please don't ask me why. We had great trouble with the ion source; we had to get our witch doctor to say all sorts of interesting spells and to this day we don't really know why we cannot use commercial deuterium gas in it, but we have to use electrolyzed D_2O.

SLUYTERS: We have used commercial deuterium gas and normal operation of the source as if it were hydrogen gas except for the automatic flow control which was switched off.

SHAYLOR: I don't know why commercial gas would not work for us. Our injector is like your preinjector. We did not have trouble with the synchrotron, although it does not have beam control so we had to reprogram rf.

VAN STEENBERGEN: The emittance of the beam in the theoretical limit should be mass dependent. Was the emittance of the deuteron beam from the preinjector different from the corresponding emittance for an identical intensity of proton current?

SLUYTERS: Normalized to energy, the emittance was about twice as large as normal.

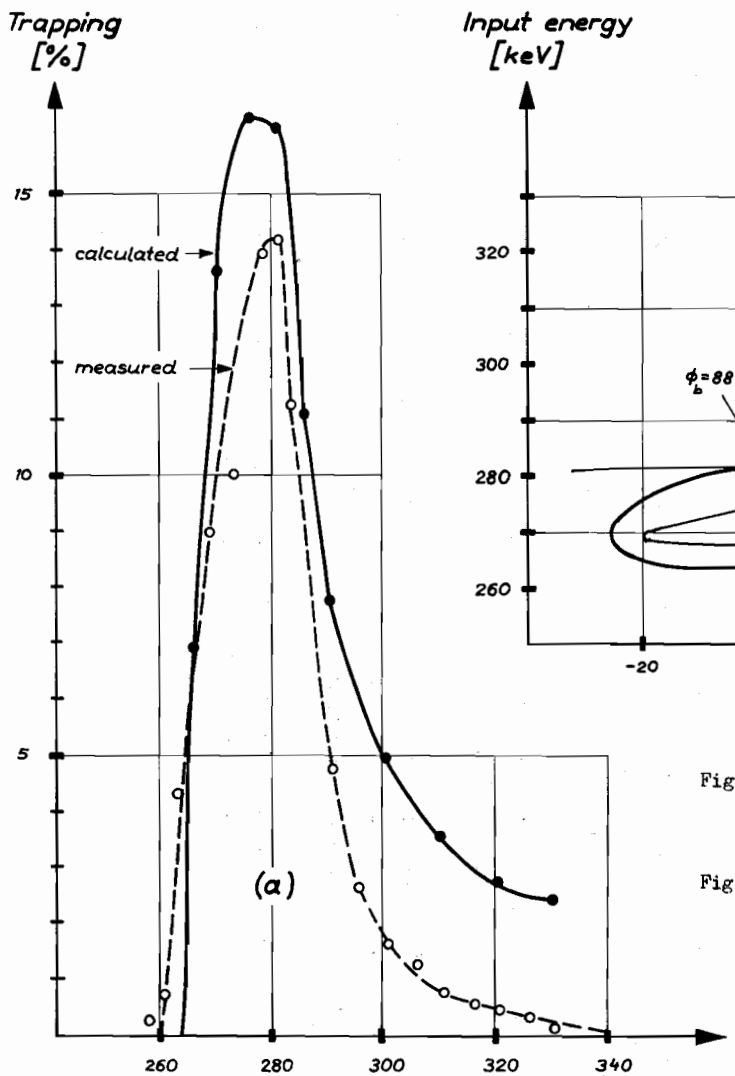

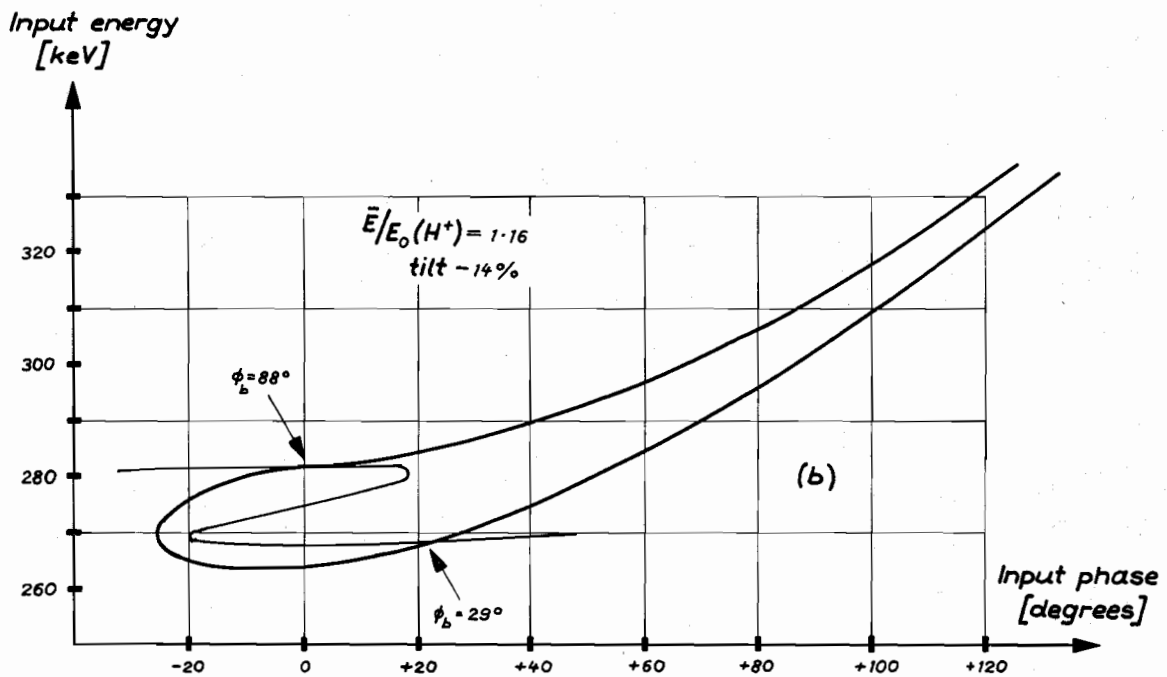

Fig. 7a Linac trapping for deuterons without buncher for an injector emittance of 4.0 cm mrad

Fig. 7b Linac phase acceptance for deuterons and a phase trapping curve for a buncher peak voltage of 7 keV.

VAN STEENBERGEN: The next question is regarding the longitudinal acceptance for deuterons. The calculated curve as shown here at a higher energy shows up the high energy acceptance tail in the fish diagram. The observed curve goes down to zero at the high energy end suggesting that you do not have a tail in the fish diagram.

SLUYTERS: There was a tail, but it was very low in intensity.

WADDELL: I was interested in your low background, when you were running the deuterons. I wonder, did you look for neutrons?

SLUYTER: Yes.

WADDELL: Then, does this not suggest that all of the loss was occurring essentially as one entered the machine, because certainly at energies of 4 or 5 MeV, the numbers of neutrons produced would have been very high.

BLEWETT: I think with protons the main capture loss is about 5 MeV, so with deuterons it should be about 1 MeV, should it not?

SLUYTERS: Yes. The main loss is during the first 10-15 drift tubes; this corresponds roughly with 1 MeV for deuteron acceleration. But, nevertheless, the background was much lower than we should expect.

FEATHERSTONE: I noticed in the first slide you showed us that the change of tilt required in going from accelerating protons to accelerating deuterons seemed to be in one sense in the first tank and in the opposite sense in the other two tanks. Do you use a constant g over ℓ ratio all the way through the machine as in the early Alvarez structures?

CARNE: In the first tank it is constant. Then the second two tanks have a varying g over ℓ .

FEATHERSTONE: So perhaps the fact that one had to change the tilt one way in the one tank and the other way in the other tanks is a reflection of the difference in design of the cavities.

SLUYTERS: In theory and in practice, the tilt has not an important influence on the capture as one can observe in Fig. 5.

THE ANL SECOND HARMONIC BUNCHER

W. Myers
Argonne National Laboratory

A multiple harmonic buncher system has been proposed for linacs by Dr. R. Perry[1] to improve the capture efficiency, or transmission, of the injected beam. With suitable choice of parameters, he has shown theoretically that it should be possible to secure an increase from 66% to 81% capture when using a second buncher operating at twice the linac frequency.

Such a buncher system has been designed and built, and this report will describe it briefly.

As is well known, a threefold improvement in capture over that provided normally by linac phase stability may be attained by bunching, i.e. applying a sinusoidal rf voltage across a gap where the rf phase is such that the synchronous particles undergo no energy change. Under these conditions, particles which differ in energy from the synchronous particles will be velocity modulated, and after traversal of a drift path, will arrive at the linac in a phase suitable for acceleration (see Fig. 1).

In order to increase the bunching efficiency still further one possibility is to replace the buncher sinusoid by a sawtooth wave of the form:

$$V = V_b \frac{\psi_b}{\pi} \qquad (-\pi \leq \psi_b \leq \pi) \qquad (1)$$

ψ_b = buncher phase

V_b = buncher gap voltage.

These two are plotted on the same scale in Fig. 2. It is seen that the sinusoid offers only a rough approximation to the optimum curve.

However, preliminary investigation of the nature of equipment required to generate a $\pm$ 20 kV sweep in 5 nsec, plus an ever faster retrace, indicated that an elaborate and expensive system would be needed if a sawtooth waveform were used.

Another possiblity would be to form a harmonic series approximation to the sawtooth, and this is the approach which we are developing. A total effective gap voltage V :

$$V = \sum_{1}^{K} \frac{(-1)^{n-1}}{n} \sin n\psi \qquad (2)$$

can be assembled across several individual buncher gaps, each one contributing a voltage term to the series. The net effect will be as if the total voltage were obtained in a single gap, since the individual gap separations will be small with respect to the drift distance. In Fig. 2b is shown the case where one buncher is running at the fundamental with another operating at the second harmonic. In Fig. 2d is the result when four gaps are driven at harmonically related frequencies. The gaps of such a system can be spaced closer together by locating the two higher frequency cavities inside the drift tubes of the others.

Theoretical phase space analyses to determine capture efficiencies have been made by plotting $\psi - \psi_s$ vs $W - W_s$ on an overlay of the ANL linac acceptance. The efficiency is found by dividing the absolute range of phase angle in radians enclosed in the linac acceptance by 2π (over total rf cycle). The equations relating the quantities plotted are for phase:

$$\psi - \psi_s = \psi_b - \frac{\psi_s T V_b}{2 V_o} \sum_{n=1}^{K} \frac{(-1)^{n-1}}{n} \sin n \psi_b \qquad (3)$$

and for energy:

$$W - W_s = e V_b T \sum_{n=1}^{K} \frac{(-1)^{n-1}}{n} \sin n \psi_b \qquad (4)$$

where

ψ =	particle phase	V_b =	buncher gap voltage
ψ_s =	linac synchronous phase	V_o =	potential of particle entering buncher
ψ_b =	particle phase at buncher	n =	order of harmonic
T =	buncher transit time factor		

Figure 3 shows the phase space diagram for a first plus second harmonic buncher system; the efficiency is about 81%. A similar plot for a four-harmonic buncher is shown in Fig. 4.

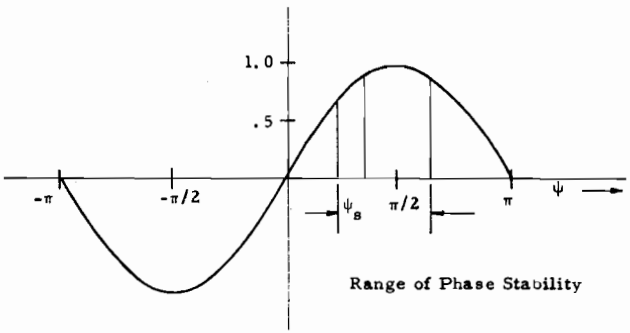

Linac RF Voltage Wave

Fig. 1

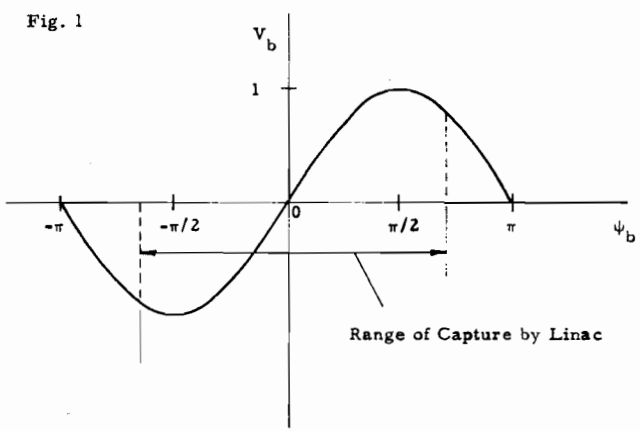

Sinusoidal Buncher Voltage

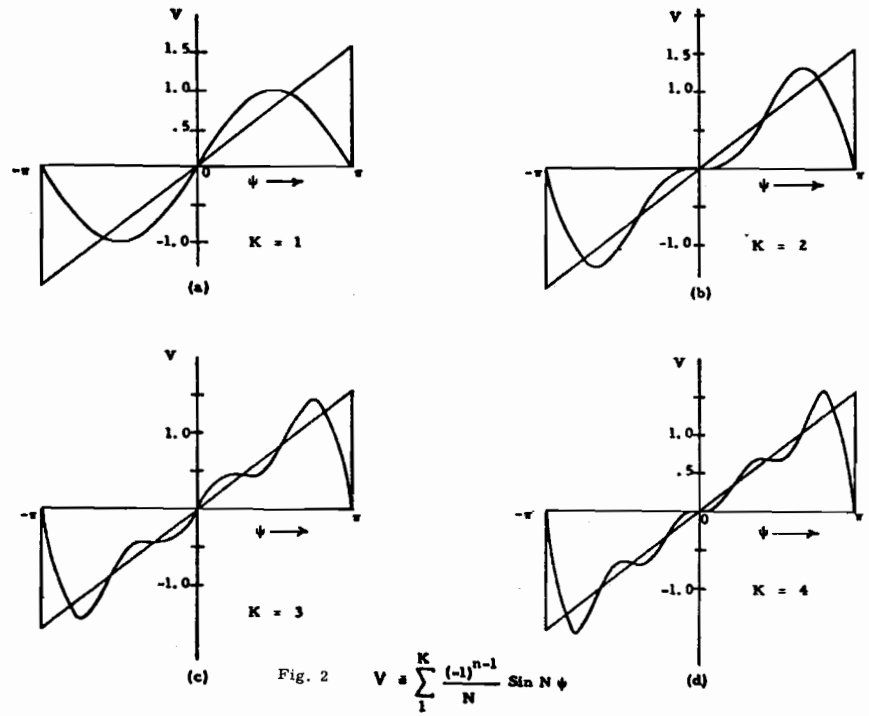

Fig. 2 $V = \sum_{1}^{K} \frac{(-1)^{n-1}}{N} \sin N\psi$

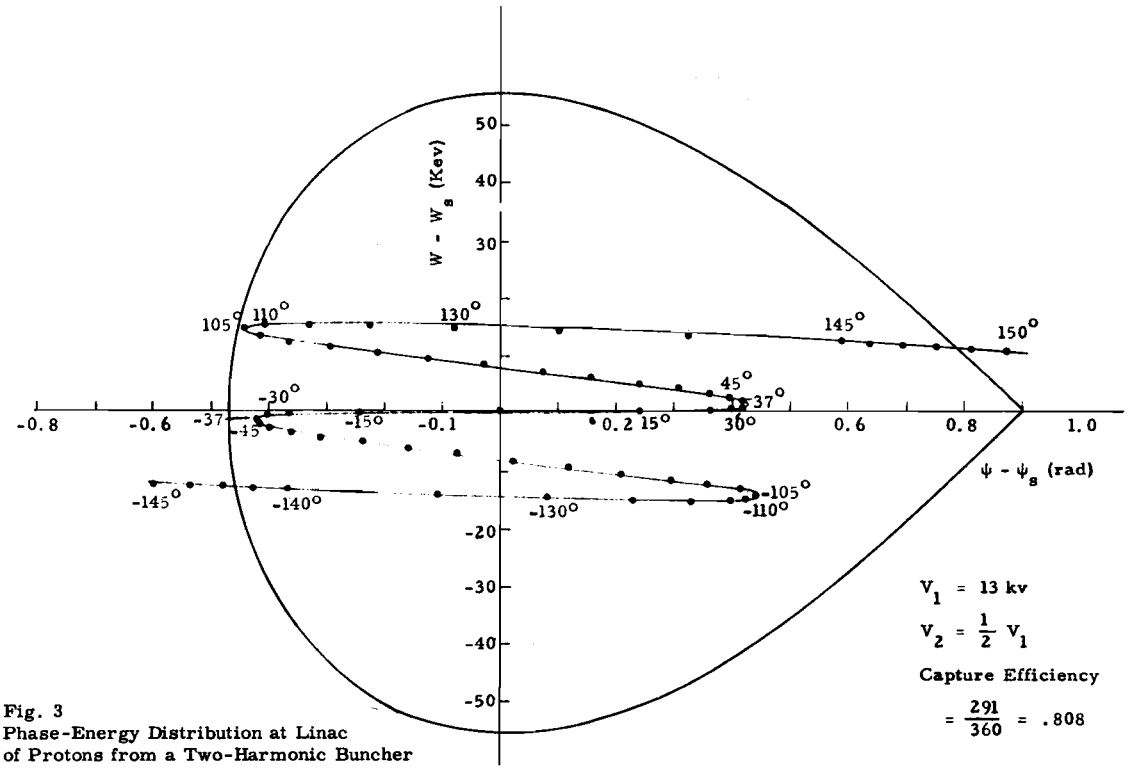

Fig. 3
Phase-Energy Distribution at Linac
of Protons from a Two-Harmonic Buncher

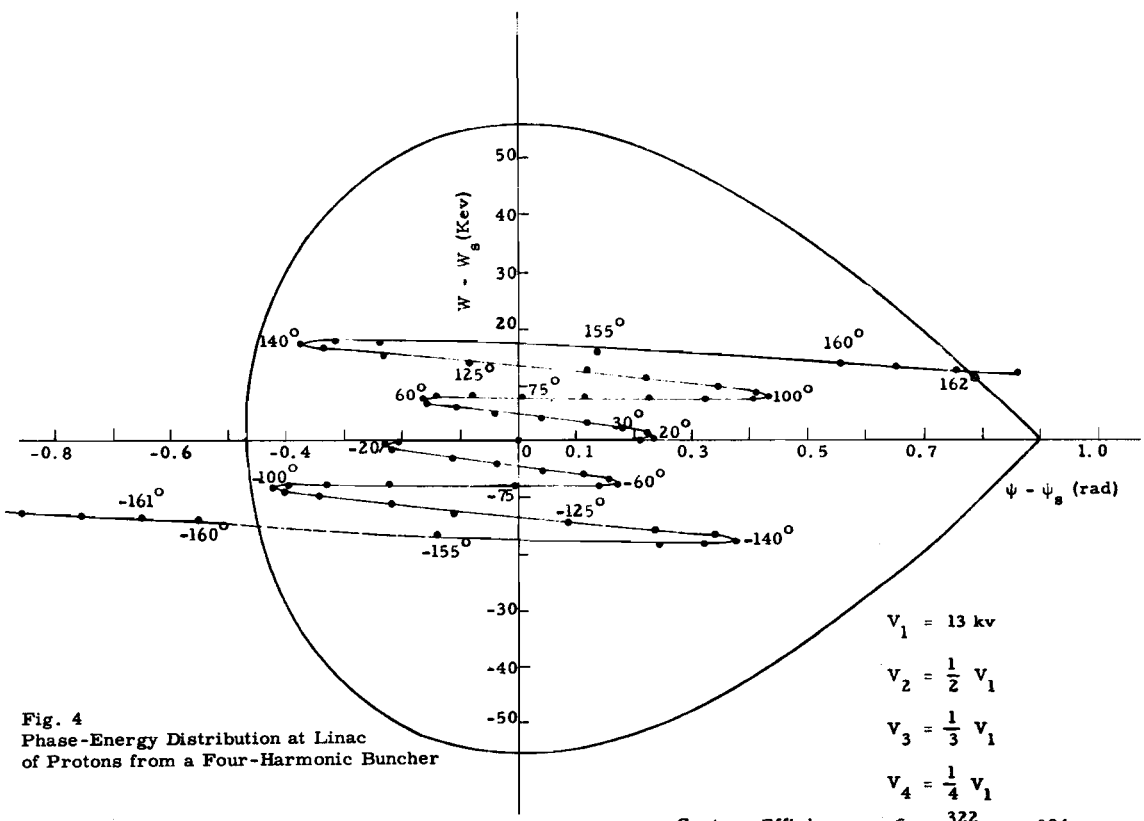

Fig. 4
Phase-Energy Distribution at Linac
of Protons from a Four-Harmonic Buncher

By noting that the first terms in Eq. (2) are the most important, it is not too surprising that a plot of capture versus number of bunchers (Fig. 5) taken from phase space data shows a pronounced roll-off after the second buncher is added. It was, therefore, decided to restrict the ANL system to the fundamental plus second harmonic. The complete second harmonic buncher system is shown in Fig. 6. The cavity was designed as a capacity-loaded radial line resonator; the dimensions and some details are shown in Fig. 7.

The cavity and the end plate were machined from OFHC copper. The end piece, which consists of a sandwich of two copper plates separated by a sheet of 1/16" teflon, provides for application of a 1 kV bias to prevent difficulties with multipactoring. Fine tuning of the cavity frequency is accomplished by rotating a 1" x 1/2" Cu "paddle." The level of rf excitation is observed by feeding a signal from the pickup loop to a diode detector and CRO. The gap is located approximately 2" from the first harmonic buncher gap.

The second harmonic buncher cavity is excited by a 400 Mc pulsed power doubler stage. The tube is an RCA type 7650 tetrode operated in the cathode drive configuration and delivers 500 watts output for 125 watts of drive. The input and output tank circuits are tuneable coaxial cavities. The plate power supply contains a large capacitor bank to obtain less than 0.5% droop during a 1 millisecond pulse, at a 10 pps repetition rate.

The source of 200 Mc drive power is a loop inserted near the low energy end of the linac. The phase shift control is placed in the drive line to avoid possible loading problems with the doubler, and to allow a slower tuning rate on the phase control.

In order to operate the doubler efficiently and obtain maximum power in the cavity, a double stub tuner is used to match the transmission line to the cavity. Transmission lines in most cases are RG8/U coaxial cable. The phase shifter is a standard General Radio unit, as are the stub tuner components.

Preliminary procedure for testing the SHB is to tune up the linac with the existing buncher for maximum transmission and observe the output current as the doubler is switched on and off.

It was anticipated that some preliminary results on the SHB would be available for presentation at this time. However, circumstances were such that no data was obtained in the limited time which was available for testing. Theoretically, 250 watts should suffice for cavity excitation;

however, no effect on the beam could be seen at levels of about 500 watts. The original estimate was based on the power taken by the first buncher, and may be low, since the Q of the present cavity is of the order of 1000. During the latest test, capture without the SHB was 55.5%.

No effect was observed on the beam as the doubler was switched on and off. The phase shift control has a range of $\sim 180^{\circ}$, so that the coupling loop may need to be rotated 180° to fall in the right phase range. Further trials will be made soon, and we expect to have it operational shortly.

OHNUMA: I don't know what kind of a beam your ZGS likes to receive from the linac, but unless you are very careful in designing this bunching system, the quality of the output beam could become lousy, because looking at the graph, the bunched beam is spread out very long, practically the entire area of the bucket. Since an increase in the phase spread automatically gives rise to an increase in the energy, unless you indeed require a very high intensity, sacrificing the beam quality, this may not be what you want. If you really want a very good quality of the beam, perhaps you should sacrifice the intensity a little bit, or capture efficiency of the buncher a little bit, and try to concentrate particles more around the center point.

MYERS: Yes, I can see what you mean. Our only thought here was just to try and see if it works basically as far as increasing the amount of beam that we can get. It may well be true that we experience an increase in phase space.

BLEWETT: Do you include grids in these buncher gaps?

MYERS: No, no grids.

BLEWETT: This is a question which we thought about a little at Brookhaven. We do have grids in the gaps of our first harmonic buncher for the reason that theoretically if you left the grids out you increased the emittance area by a factor of about two. Now I must admit that at one time the grids burned out, and the emittance area as far as we could see did not change.

HUBBARD: A comment on that too. We took the grids out of our buncher on the Highlac once also and the beam went down by quite a large factor, but I forget what it was.

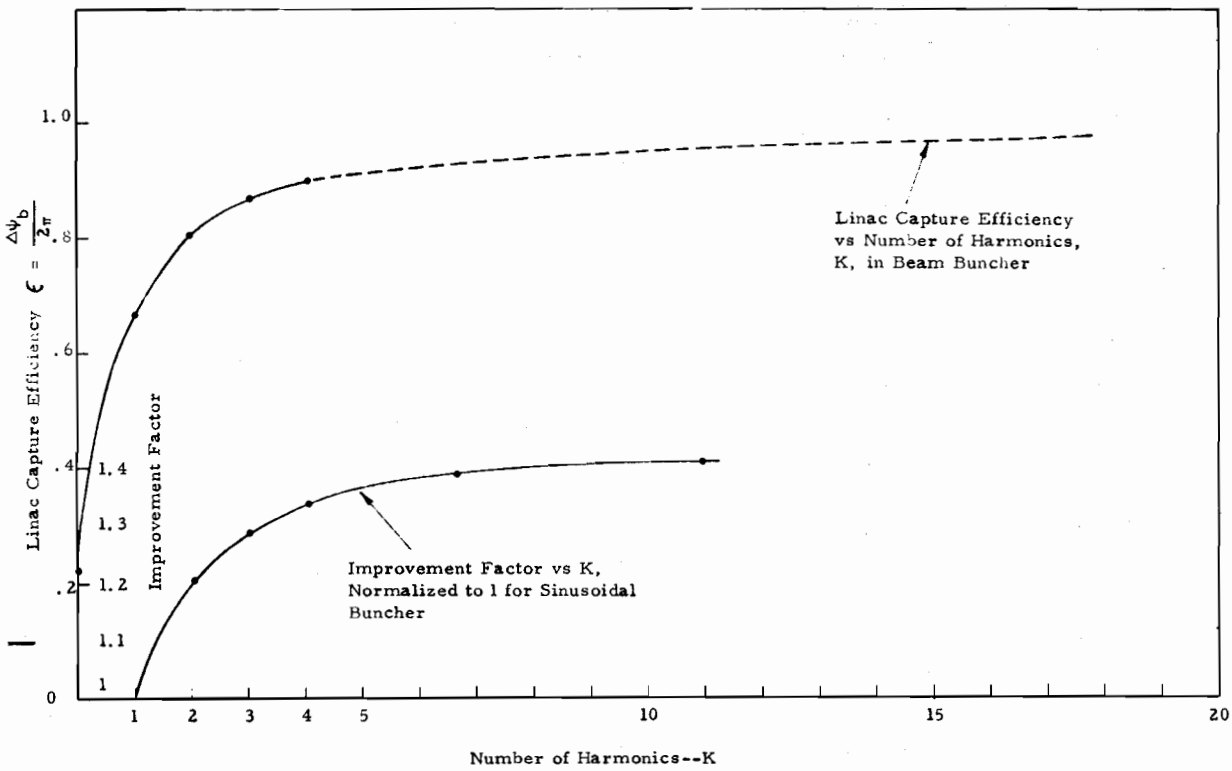
Linac Capture Efficiency $\epsilon = \frac{\Delta\psi_b}{2\pi}$
1.0
.8
.6
.4
.2
0
Improvement Factor
1.4
1.3
1.2
1.1
1
Linac Capture Efficiency vs Number of Harmonics, K, in Beam Buncher
Improvement Factor vs K, Normalized to 1 for Sinusoidal Buncher
1
2
3
4
5
10
15
20
Number of Harmonics--K

FIG. 5

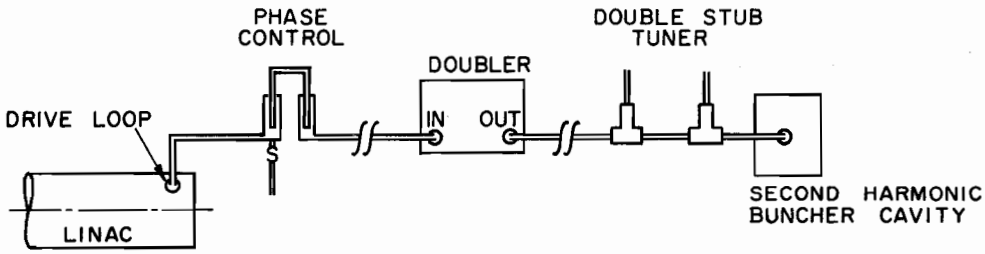
PHASE CONTROL
DOUBLE STUB TUNER
DOUBLER
DRIVE LOOP
IN
OUT
LINAC
SECOND HARMONIC BUNCHER CAVITY

FIG. 6

VAN STEENBERGEN: Do you have grids in the buncher of the 20 MeV linac injector for the Bevatron.

HUBBARD: Yes, there are grids.

PERRY: I would like to ask Ed, is it not possible to compensate for this divergence without grids by adjusting the matching quadrupoles?

HUBBARD: No, because it puts in a radial dependence of the change in energy of the beam you are putting in with the buncher.

BLEWETT: There is a Brookhaven internal report on this which should be in your files.

HUBBARD: Our buncher incidentally has a fairly large aperture, so we do not have to align it carefully in the transverse direction. This means that without grids we have a large radial dependence of the transit-time factor across it and this is why we think the grids are necessary.

VAN STEENBERGEN: I would like to make just one short comment to Rolland Perry with respect to the theoretical paper John mentioned. The focal length of the buncher gap lens, although modulated with the buncher frequency, is typically relatively long. If one has adjacent to the buncher a beam transport system with rather short focal lengths, then the buncher gap lens influence might be rather small. Further, it is possible to design the transport system such that a beam waist occurs at the location of the buncher gap. Therefore, I think whether one needs to worry about this time-dependent lens or not depends on the transport system around it.

REFERENCES

1. R. Perry, ANLAD-74, "Multiple-Harmonic Buncher for a Linear Accelerator", February 22, 1963.

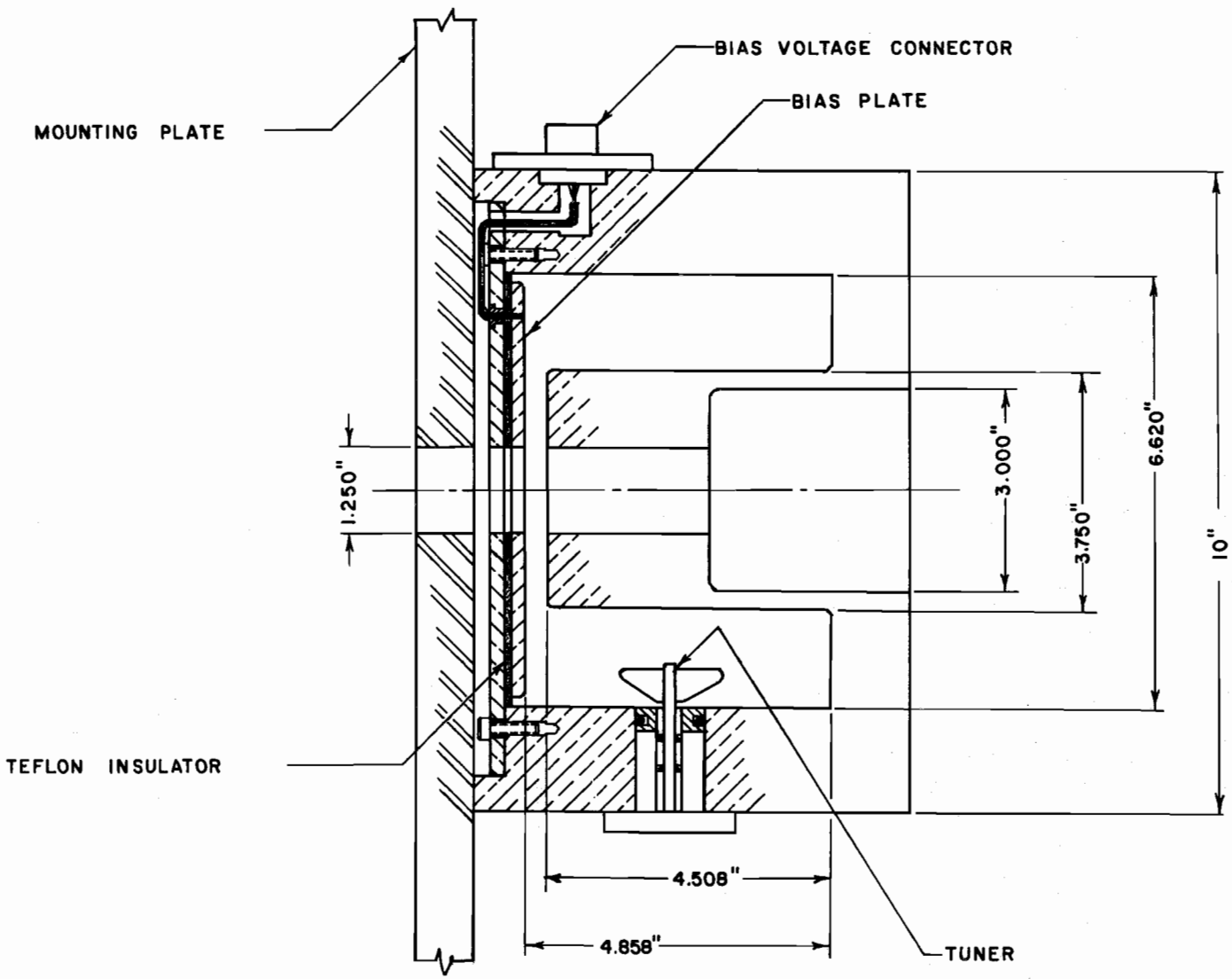

FIG. 7 SECOND HARMONIC BUNCHER CAVITY

A FAMILY OF IMPROVED LINAC BUNCHERS

R. Beringer and R. L. Gluckstern
Brookhaven National Laboratory and Yale University

Conventional bunchers use one or more gaps excited with fundamental frequency sinusoidal fields. They can be designed to inject about 2/3 of the dc beam into the admittance of a conventional drift-tube linac. However, the remainder of the particles (long tails) are not accelerated to the end of a long linac and will give rise to undesirable radiation and possible confusion in the beam-pickup instrumentation of a sophisticated multicavity linac.

Bunchers having several gaps with harmonically related sinusoidal fields[1,3] are somewhat better but still have long tails. They are approximations to the saw-tooth buncher[1,2,3,4] which has no tails and which can bunch all of the dc beam.

Unfortunately, no one seems to have a practical way of exciting a saw-tooth gap at frequencies as high as 200 Mc/s. Thus, other solutions are of interest.

The bunchers described here use an rf deflector to separate phase regions in space so that each phase region can be bunched independently with a sinusoidal field.

1. Isochronous Deflector

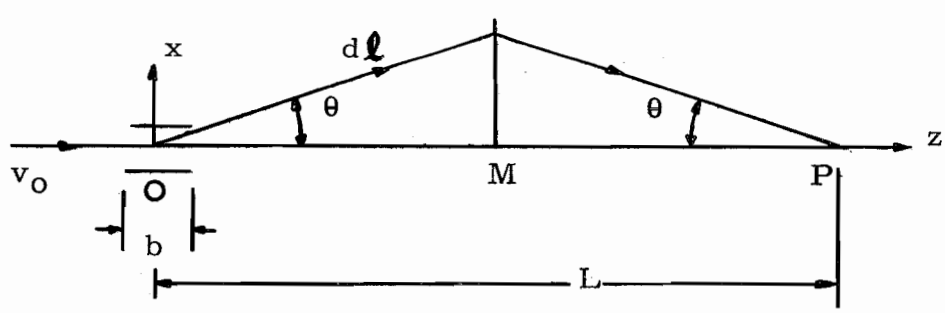

Consider an rf deflector at 0 with $E_x = E_o \sin \omega t$. The deflection angle is

$$\tan \theta = \frac{v_x}{v_o} = \frac{eE_o b}{mv_o^2} \sin \omega t ,$$

where dimension b includes a transit-time factor. M is a magnetic or electrostatic lens of unit magnification. If we approximate it as a thin lens, the elapsed time from 0 to P is

$$\frac{1}{v} \int_o^P d\ell = \frac{1}{\sqrt{v_o^2 + v_x^2}} \frac{L}{\cos \theta} = \frac{L}{v_o} .$$

Thus the system is isochronous.

2. Isochronous Deflector - Redeflector

The angles θ at P can be eliminated by a second deflector since the system is isochronous. The particle arrives at P at time $t + L/v_o$ with transverse velocity $v_x = -(eE_o b/mv_o) \sin \omega t$. If we excite an identical deflector with field $E_x = E_o \sin(\omega t - \omega L/v_o)$, then all axial

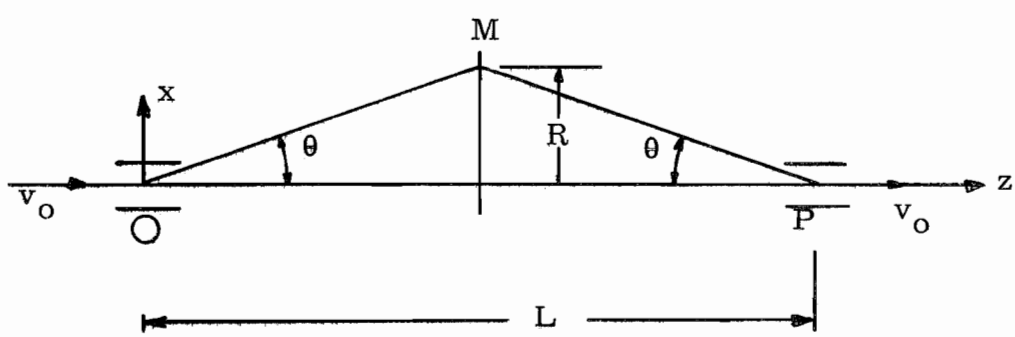

particles leave P with velocity v_o along z. This isochronous transport is also true for nonaxial particles incident at 0. Further, the field E_x need not be uniform over the aperture but only the same in the two deflectors provided that they are symmetrically placed with respect to M.

Phase errors $\Delta(\omega L/v_o) = -(\omega L/v_o)(\Delta v_o/v_o)$ arising from variations in v_o (dc preinjector voltage changes) give angular errors in the redeflected beam. These should be small compared to beam-emittance angles. The maximum angular error is

$$\frac{\Delta\theta_{max}}{\theta} = \frac{(\Delta v_x)_{max}}{v_o} = \frac{2\,\omega R}{v_o}\,\frac{\Delta v_o}{v_o} \quad .$$

It is independent of L for a given maximum deflection R. In a typical case the errors are about one milliradian.

3. <u>Deflector - Redeflector and a Bunching Gap</u>

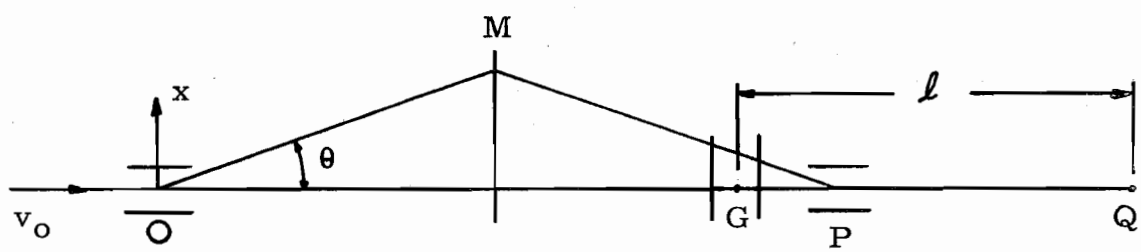

Near P, where the beam is still separated in space, we place a bunching gap with rf voltage

$$gE_z = -V_o \cos \omega t \; .$$

Particles leaving the gap have velocity

$$v = \sqrt{v_o^2\,(1 + \tan^2\theta) - \frac{2\,eV_o}{m}\cos \omega t} \quad .$$

Since $v_o^2 \gg eV_o/m$, the angles θ are not changed to first order by the bunching voltage. (In the formula V_o includes another transit-time factor.) The elapsed time G to Q is

$$t' = \frac{\ell}{v_o\sqrt{1 - \frac{2\,eV_o}{mv_o^2}\cos\omega t}}$$

$$\cong \frac{\ell}{v_o} + B\cos\omega t$$

with $B = (\ell/v_o)(eV_o/mv_o^2)$. This is the ordinary buncher equation. The arrival time at Q is $t' + t + L/v_o$. This is expressed as an arrival phase at Q defined as

$$\phi = \omega t' + \omega t + \frac{\omega\ell}{v_o} + \text{const.}$$

As is well known, it is not possible to make ϕ the same for all particles. For our choice of zero phase the "long tails" come from the region $\pi < \omega t < 2\pi$. Note, however, that this region corresponds to negative θ, and hence a beam stop for all (or some) negative θ <u>eliminates</u> the long tails.

Suppose we make ϕ the same for $\omega t = 0, \pi/2, \pi$. Then $B = \pi/2\omega$ and $\phi = \pi/2 + \text{const.}$ for these three particles. Figure 1 shows the arrival phases of all particles from $0 < \omega t < 7\pi/2$. The abscissa is ωt and the ordinate $\phi = \omega t' + \omega t - \omega\ell/v_o - \pi/2$. If we stop all $\theta < 0$ particles, then all remaining particles (half of the dc beam) arrive at Q within 37° wide phase bands centered at $0, 2\pi, 4\pi, \cdots$. As usual, a compromise between ℓ, V_o, and the energy stability of the dc pre-injector is necessary in order to match the admittance of a given linac.

4. Deflector - Redeflector and Two Biased Bunching Gaps

Instead of stopping the beam particles with $\theta < 0$, let us provide separate bunching gaps for the positive θ and negative θ beams.

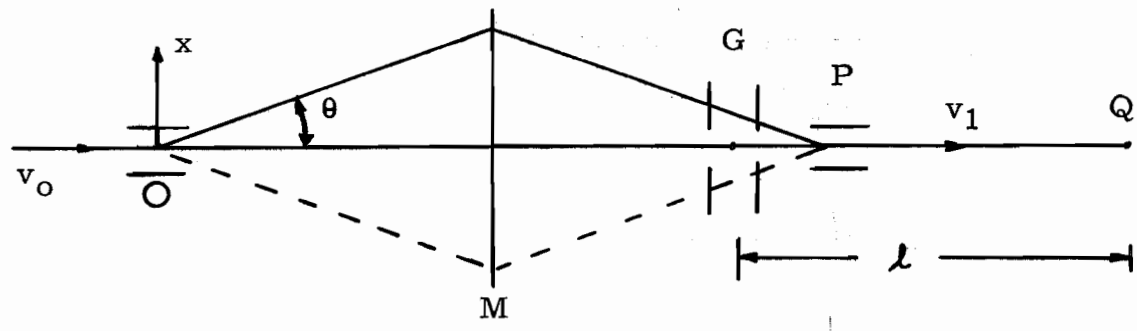

Let gap 1 have voltage $-V_o - V_o \cos \omega t$, for $\theta > 0$
and gap 2 have voltage $V_o + V_o \cos \omega t$, for $\theta < 0$.

The corresponding particle velocities in the drift space GQ are

$$v_1 = \sqrt{v_o^2 - \frac{2\,eV_o}{m}(1 + \cos \omega t)}\,, \quad \theta > 0$$

$$v_2 = \sqrt{v_o^2 + \frac{2\,eV_o}{m}(1 + \cos \omega t)}\,, \quad \theta < 0$$

and the elapsed times G to Q are

$$t_1' = \frac{\ell}{v_1} = \frac{\ell}{v_o\sqrt{1 - \frac{2\,eV_o}{mv_o^2}(1 + \cos \omega t)}}$$

$$t_1' \cong \frac{\ell}{v_o} + B\,(1 + \cos \omega t), \quad \text{for } \theta > 0, \text{ or } 2n\pi < \omega t < (2n+1)\pi\,, \quad n = 0, 1, 2 \cdots$$

and

$$t_2' \cong \frac{\ell}{v_o} - B\,(1 + \cos \omega t), \quad \text{for } \theta < 0, \text{ or } (2n+1)\pi < \omega t < (2n+2)\pi\,, \quad n = 0, 1, 2 \cdots$$

With the choice $B = (\ell/v_o)(eV_o/mv_o^2) = \pi/2\omega$ the arrival phases are the same for $\omega t = 0,\ \pi/2,\ \pi,\ 3\pi/2,\ 2\pi$. Figure 2 shows the arrival phases for all particles as a function of the input phase to the buncher.

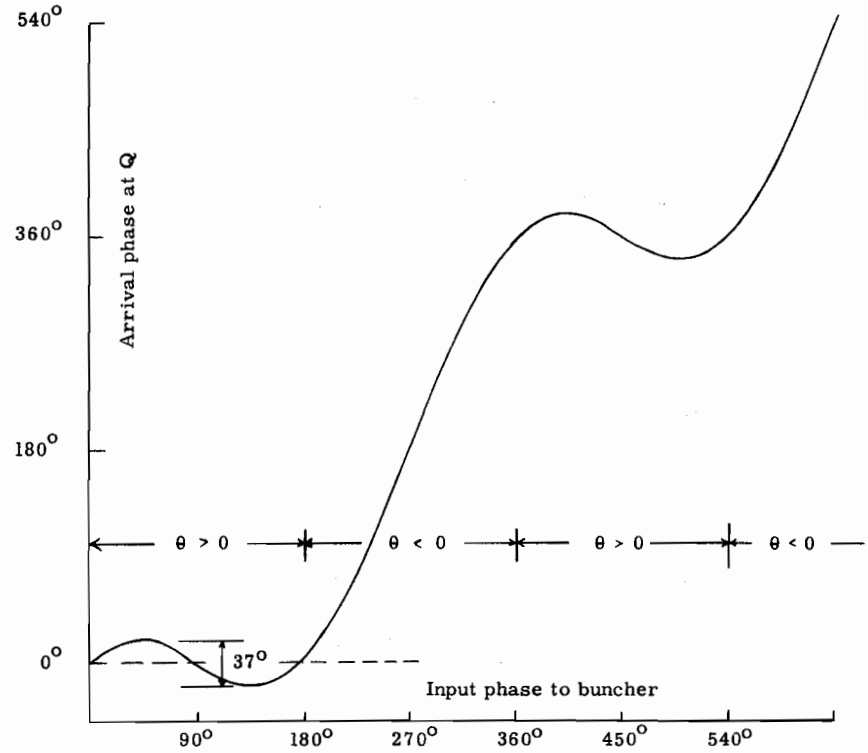

Fig. 1 - Phase of beam particles arriving at Q vs input phase to buncher for a single deflector and bunching gap.

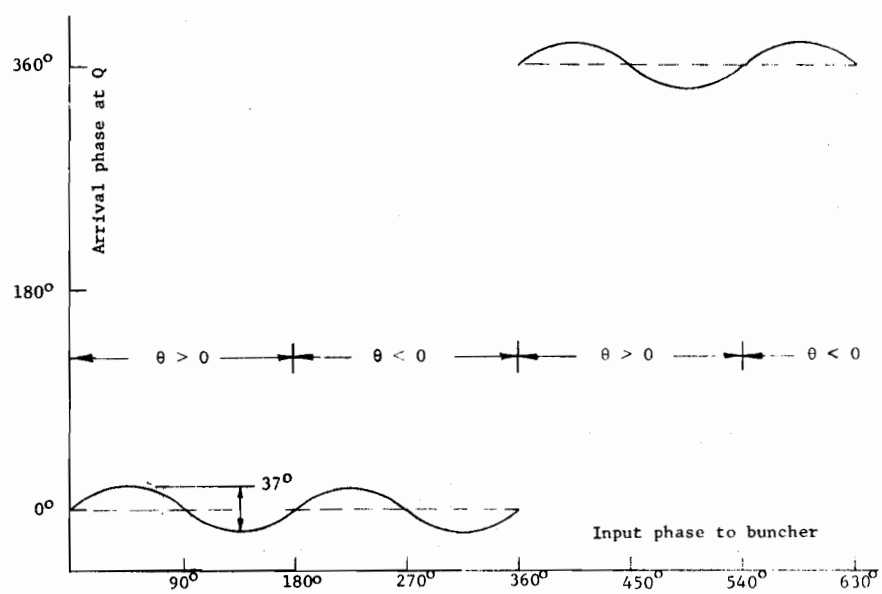

Fig. 2 - Phase of beam particles arriving at Q vs input phase for a two-gap fundamental frequency biased buncher.

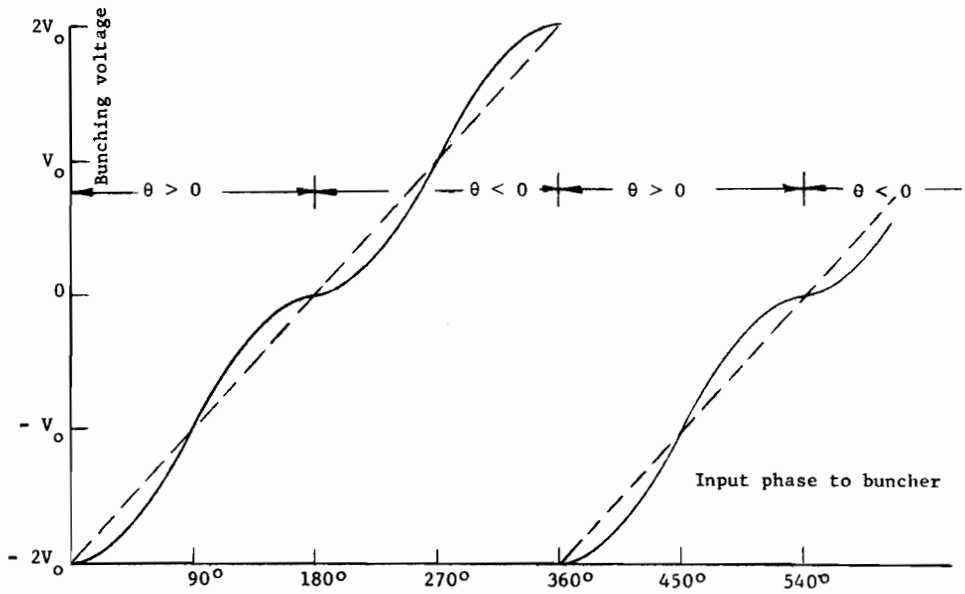

Fig. 3 - Bunching voltage waveshape for a two-gap fundamental frequency biased buncher.

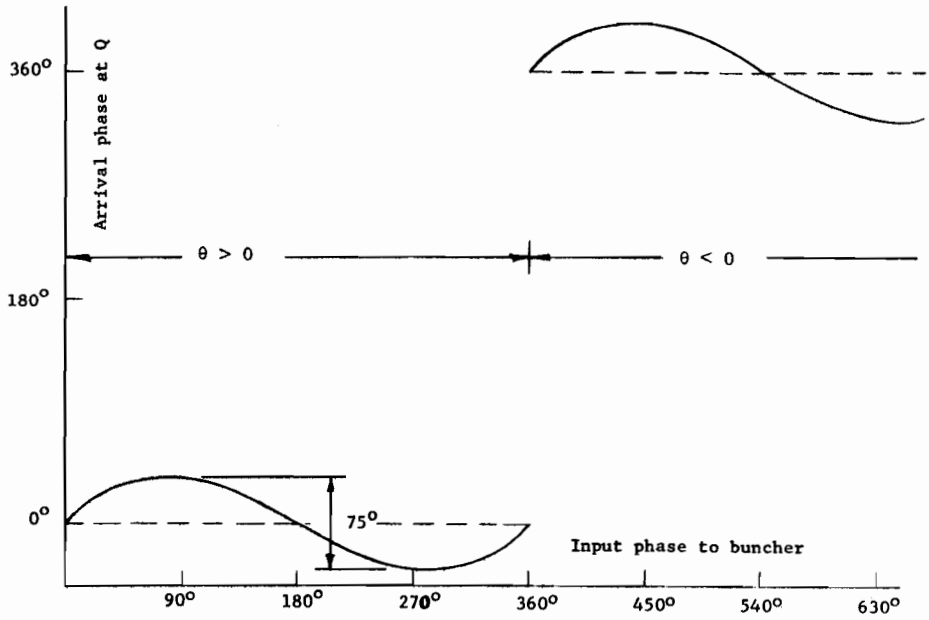

Fig. 4 - Phase of beam particles arriving at Q vs input phase for a two-gap second-subharmonic line-scan buncher.

The abscissa is ωt and the ordinate $\omega t' + \omega t - \frac{\ell\omega}{V_o} - \pi$. We see that all of the dc beam is bunched into 37° wide phase regions centered at 0, 2π, 4π, $\cdots$. The choice of V_o and ℓ is the same as for a conventional buncher.

The reason for the success of this buncher is easily seen if we plot the gap voltage vs input phase. This is shown in Fig. 3, and we see that we have provided nothing more than a good way of approximating a saw-tooth, but not, we note, by conventional Fourier analysis.

The buncher has one nontrivial complication. It requires a dc bias, either $\pm V_o$ for the two legs (or zero and $2 V_o$). These biases cannot be provided with electrostatic fields since the input beam is surrounded by an equipotential surface* (grounded beam pipe) and no arrangement of dc electrodes can accelerate or decelerate such a beam. However, an induction transformer can, in principle, provide a rectangular pulse of accelerating voltage. Since the linac is pulsed, this accelerating pulse should be of comparable duration (say 200 μsec). In a preliminary look, such a device appears feasible[5] for pulses of the order of 10 kV.

5. Subharmonic Deflector and Buncher

The need for dc bias can be eliminated if the alternate halves of input phase corresponding to $\pm\theta$ are bunched into separate linac buckets. This can be done with a subharmonic, $\omega/2$, deflector and buncher.

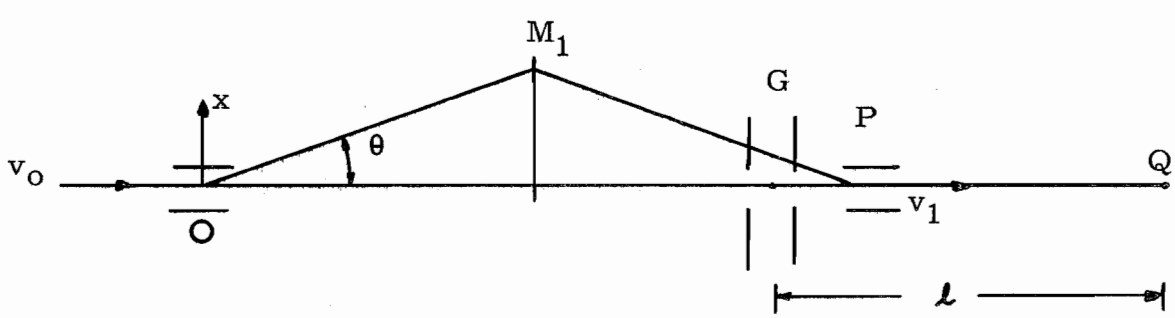

*This condition is imposed by the ion-source and accelerating column of the preinjector. However, one can conceive of devices in which the required dc bias can be provided in the incident beam. A klystron gun is such a device, and klystrons using these bunchers should have greatly improved efficiency.

Let gap 1 have voltage

$$- V_o \cos \frac{\omega}{2} t, \quad \theta > 0 \text{ or } 2n\pi < \frac{\omega}{2} t < (2n+1)\pi, \quad n = 0, 1, 2, \cdots$$

and gap 2 have voltage

$$V_o \cos \frac{\omega}{2} t, \quad \theta < 0 \text{ or } (2n+1)\pi < \frac{\omega}{2} t < (2n+2)\pi, \quad n = 0, 1, 2, \cdots.$$

At P we put a subharmonic redeflector. The elapsed times G to Q are

$$t_1' \cong \frac{\ell}{v_o} + B \cos \frac{\omega}{2} t, \quad \theta > 0$$

$$t_2' \cong \frac{\ell}{v_o} - B \cos \frac{\omega}{2} t, \quad \theta < 0$$

where $B = (\ell/v_o)(eV_o/mv_o^2)$. With the choice $B = \pi/\omega$ the arrival phases are the same for $\omega t = 0, \pi, 2\pi$. Figure 4 shows the arrival phases of all particles as a function of input phase to the buncher. The abscissa is ωt and the ordinate is $\phi = \omega t' + \omega t - \omega \ell / v_o - \pi$. Figure 5 shows the approximation to the saw-tooth for this case. Note that twice as large a bunching parameter B is required for this arrangement and that twice as large a phase spread (75°) is produced as compared with the biased two-gap buncher.

6. Conical-Scan Deflector and Buncher

The essential feature of all of these bunchers is the separation of phase regions in space and the application of appropriately phased sinusoidal bunching voltages to the separated beams. This can be accomplished in a more general way by a two rather than a one-dimensional deflection. In particular, conical-scan deflectors appear promising.

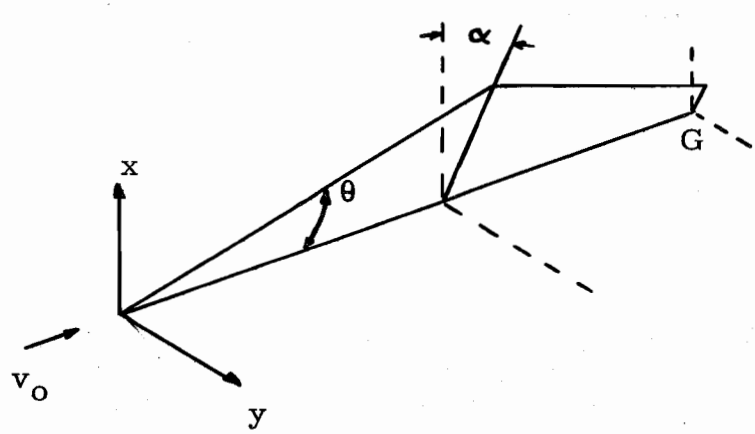

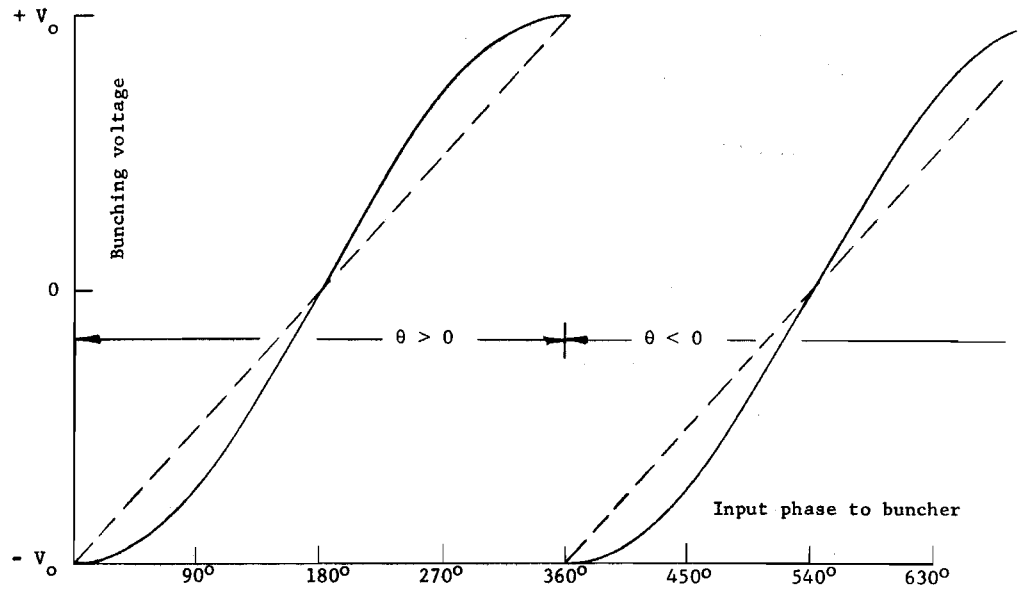

Fig. 5 - Bunching voltage waveshape for two-gap second-subharmonic line-scan buncher.

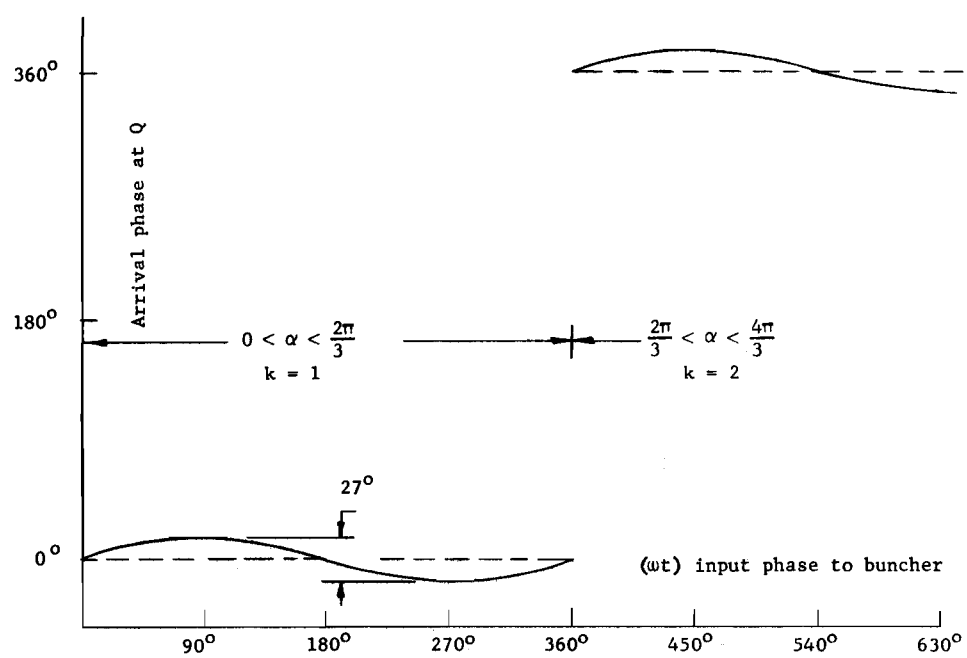

Fig. 6 - Arrival phase for a three-gap third-subharmonic conical-scan buncher.

Consider a deflector at 0 consisting of two perpendicular electric fields in quadrature extending a distance b along z.

$$E_x = E_o \cos \frac{\omega}{p} t$$

$$E_y = E_o \sin \frac{\omega}{p} t , \quad p = 2, 3, \cdots .$$

The deflection angle θ is constant,

$$\tan \theta = \frac{v_r}{v_o} = \frac{eE_o b}{mv_o^2} ,$$

where b includes a transit-time factor. The azimuth angle of the beam is $\alpha = \frac{\omega t}{p}$, where t is measured when the particle is at 0. The beam is scanned on a cone at uniform angular velocity. A plane parallel to xy at G is divided into p sectors in α, each sector containing a bunching gap with voltage

$$gE_z = - V_o \cos \left(\frac{\omega t}{p} - \frac{2 \pi k}{p} + \delta \right) .$$

The gaps are numbered with increasing α by k = 1, 2, $\cdots$ p. Note that after p cycles of the linac frequency ω the scan repeats exactly. The elapsed time G to Q is

$$t' \cong \frac{\ell}{v_o} + \frac{\ell}{v_o} \frac{eV_o}{mv_o^2} \cos \left(\frac{\omega t}{p} - \frac{2 \pi k}{p} + \delta \right) ,$$

and the arrival phase at Q is

$$\phi = \omega t + \omega t' + \text{const.} = \omega t + \omega B \cos \left(\frac{\omega t}{p} - \frac{2 \pi k}{p} + \delta \right) + C ,$$

with $B = (\ell/v_o)(eV_o/mv_o^2)$.

As in the previous case, the phase shift from gap to gap is so arranged that each 2π region of ωt is bunched into a separate linac bucket. The appropriate constants are

$$\delta = \frac{\pi}{p} + \frac{\pi}{2}, \quad C = -\pi , \quad \omega B = \pi / \sin (\pi/p) .$$

With this choice the arrival phase at Q is

$$\phi = \omega t - \pi + \frac{\pi}{\sin \frac{\pi}{p}} \cos \left[\frac{\omega t}{p} + \frac{(1 - 2k)\pi}{p} + \frac{\pi}{2} \right].$$

A large p yields a very close approximation to the saw-tooth since the sinusoidal voltage in the gap is being used only in the linear region where it changes sign. Figures 6, 7, 8, 9 show the arrival phase and bunching voltage vs ωt for p = 3 and p = 4. The p = 2 case is the same as for one-dimensional deflection.

7. Bunching Voltage and Drift Length

The conventional choice of bunching voltage and drift length should be re-examined for the very narrow bunches proposed here. For large bunching voltage and short drift length the phase shifts produced by dc voltage fluctuations of the preinjector are small but the velocity spread in the bunched beam is large. An optimum design is a compromise between these.

Assume that an optimum design is one which gives the best beam quality in longitudinal phase space at the input of the first linac tank. For a tank with uniform accelerating field and a bunch which occupies only a small part of the stable longitudinal phase region, the locus of a particle as it undergoes phase oscillations is the ellipse[6]

$$\left(\frac{w - w_s}{w_s}\right)^2 - \frac{2\, eE_o\, T}{m_o c^2 \beta_s} (\phi - \phi_s)^2 \sin \phi_s = \text{const.},$$

where $(w - w_s)$ is the energy deviation for the phase deviation $(\phi - \phi_s)$. The other symbols have the usual meanings. An optimum design fills a given ellipse along both axes and thereby achieves the smallest possible ellipse.

Consider a typical first tank for a proton linac.[7] At its input

$$\omega = 2\pi\ 200 \text{ Mc/s}, \quad \lambda = 1.5 \text{ m}, \quad \phi_s = -30^\circ, \quad E_o = 1.7 \text{ MV/m},$$

$$\beta_s = 0.04, \quad T = 0.9 .$$

For the four-gap buncher the maximum phase error is 7.5°. Suppose we choose an ellipse with semi-axis $\phi - \phi_s = 10.4^\circ = 0.18$ rad whose other semi-axis is $w - w_s = 19.0$ keV. This determines the bunching voltage, $V_o = \sqrt{2}\ 19.0 = 27$ kV, and the drift length from $\omega B = \sqrt{2}\ \pi = \ell \omega e V_o / m v_o^3$, $\ell = 2.36$ m. We now assume a dc

voltage stability for the preinjector which gives a phase error $10.4^{\circ} - 7.5^{\circ} = 2.9^{\circ}$ in the drift length 2.36 m. The relation is $\Delta\phi = (\omega \ell / v_o)(\Delta v_o / v_o) = 2.9^{\circ}$ giving $\Delta v_o / v_o = 0.204 \times 10^{-3}$ or $\Delta(1/2\, mv_o^2)/(1/2\, mv_o^2) = 0.41 \times 10^{-3}$ which is about the limit of stability of existing Cockcroft-Walton machines. As usual, the energy deviation $\Delta(1/2\, mv_o^2) = 0.31$ keV is a negligible addition to $w - w_s = 19$ keV. The design is an optimum filling of an ellipse of semi-axis 10.4° for the dc stability cited.

8. Second-Order Terms in the Bunch Width

Even an ideal saw-tooth buncher does not produce a bunch of zero phase width.[4] For very narrow widths it is necessary to examine this effect.

For the conical-scan buncher the arrival phase at Q, including second-order terms and for the choice of parameters which gives first-order zeros at $\omega t = 0, \pi, 2\pi$ is

$$\phi = \omega t - \pi + \frac{\pi}{\sin\frac{\pi}{p}} \cos\left(\frac{\omega t}{p} - \frac{2\pi k}{p} + \frac{\pi}{p} + \frac{\pi}{2}\right) + \frac{3 v_o}{2\omega\ell}\left[\frac{\pi}{\sin\frac{\pi}{p}} \cos\left(\frac{\omega t}{p} - \frac{2\pi k}{p} + \frac{\pi}{p} + \frac{\pi}{2}\right)\right]^2 .$$

The maximum errors in ϕ due to the first-order term occur near* $\omega t = \frac{\pi}{2}, \frac{3\pi}{2}$ and are

$$\Delta\phi_1 \cong \pm \pi\left(\frac{\sin(\pi/2p)}{\sin(\pi/p)} - \frac{1}{2}\right) .$$

Errors due to the second-order terms occur at $\omega t = 0,\ 2\pi$ and are

$$\Delta\phi_2 = \frac{3}{2}\frac{v_o}{\omega\ell}\pi^2 = \frac{3\pi\beta\lambda}{4\ell} .$$

For the four-gap case discussed above $\Delta\phi_1 = \pm 7.5^{\circ}$ and $\Delta\phi_2 = 3.4^{\circ}$. The distorted phase bunch for this case is shown in Fig. 10. There is no net increase in the 15° phase width but there is some distortion

*The maximum arrival phase errors occur at those ωt which are the solutions of $\cos(\omega t/p)\cot(\pi/p) + \sin(\omega t/p) = p/\pi$. For large p, $\omega t \cong 0.42\pi,\ 1.58\pi$. The errors themselves are almost the same as at $\pi/2,\ 3\pi/2$ for all values of p.

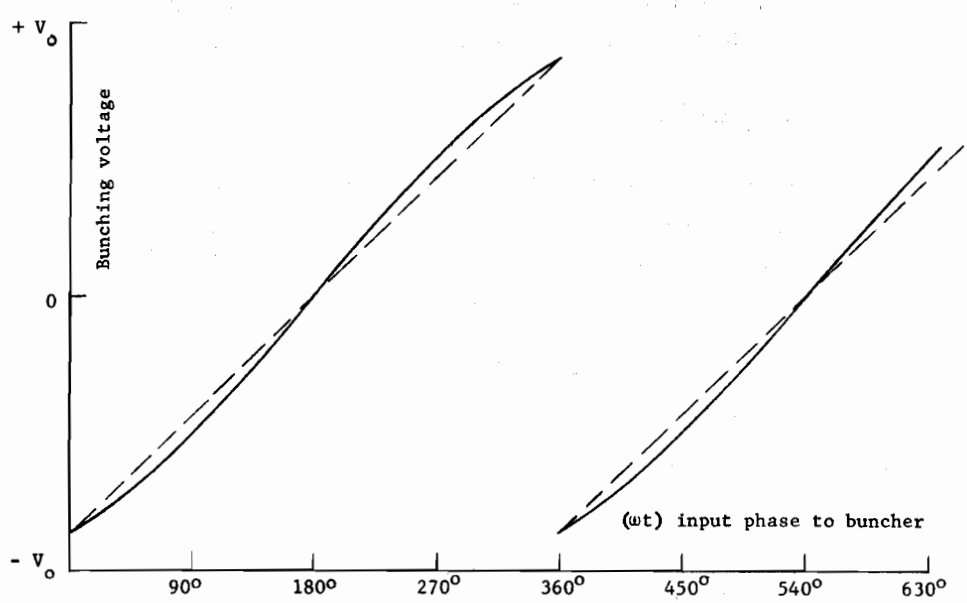

Fig. 7 - Bunching voltage waveshape for a three-gap third-subharmonic conical-scan buncher.

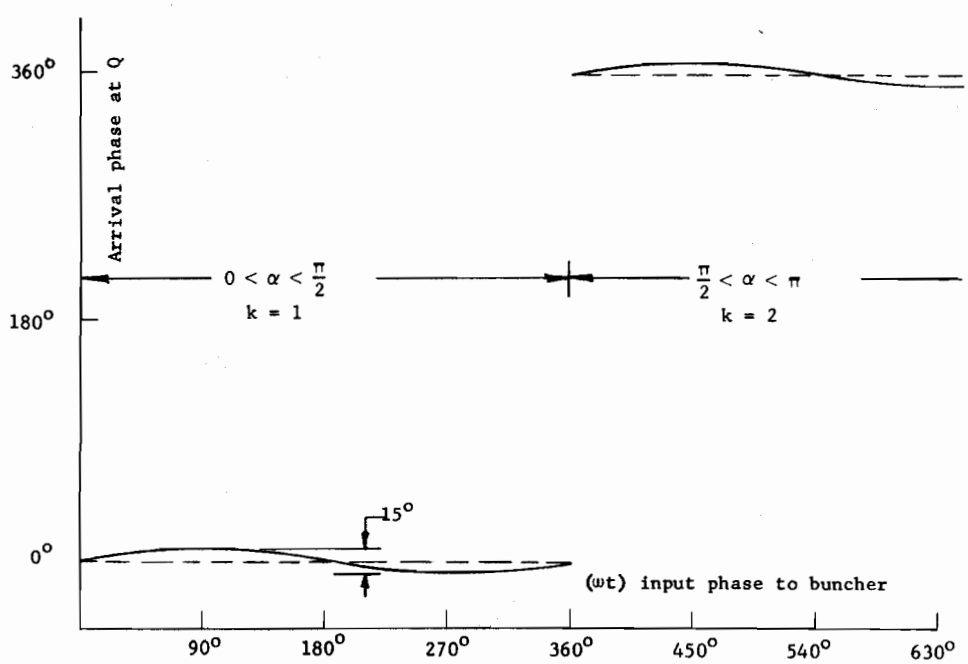

Fig. 8 - Arrival phase for a four-gap fourth-subharmonic conical-scan buncher.

around $\omega t = \pi$ which could be removed by a slightly different choice of the bunching phase and amplitude. In sum, the second-order terms are not negligible but do not seem to cause any trouble.

9. Parallel-Plate Deflector

It is clear that the deflection angles should be somewhat larger than the beam emittance angles at the deflector. Since the latter are, say, 0.5° for a 1 cm radius proton beam at 750 keV, the desired deflection angles are in the range 10° - 20°.

Consider a one-dimensional deflector consisting of a pair of parallel plates driven by rf voltages balanced to ground.

$$V_2 = -\frac{1}{2} E_o h \cos \frac{\omega t}{p}$$

$$V_4 = \frac{1}{2} E_o h \cos \frac{\omega t}{p} .$$

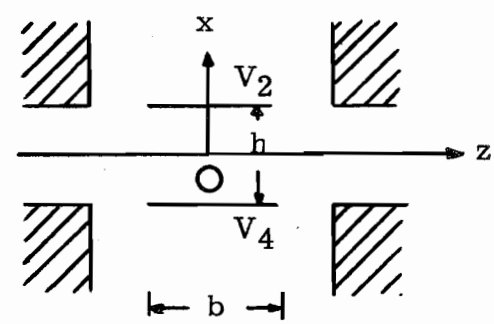

Ignore, for the present, the longitudinal fields in the end gaps, and consider only the deflection. Measure t_o when the particle reaches 0. The force equation is

$$m \frac{d^2x}{dt^2} = eE_o \cos \frac{\omega t}{p} .$$

The transverse velocity as the particle leaves the plates at $z = b/2$, $t = t_o + b/2\, v_o$ is

$$v_x = \frac{dx}{dt} = \frac{2\, eE_o p}{m\omega} \sin \frac{\omega b}{2\, p v_o} \cos \frac{\omega t_o}{p} .$$

Maximum deflection for a given E_o occurs for $\frac{\omega b}{p v_o} = \frac{2\pi\ b}{p\ \beta_o \lambda} = \pi$.

For this choice

$$v_x = \frac{dx}{dt} = \frac{2}{\pi} \frac{eE_o b}{mv_o} \cos \frac{\omega t_o}{p}$$

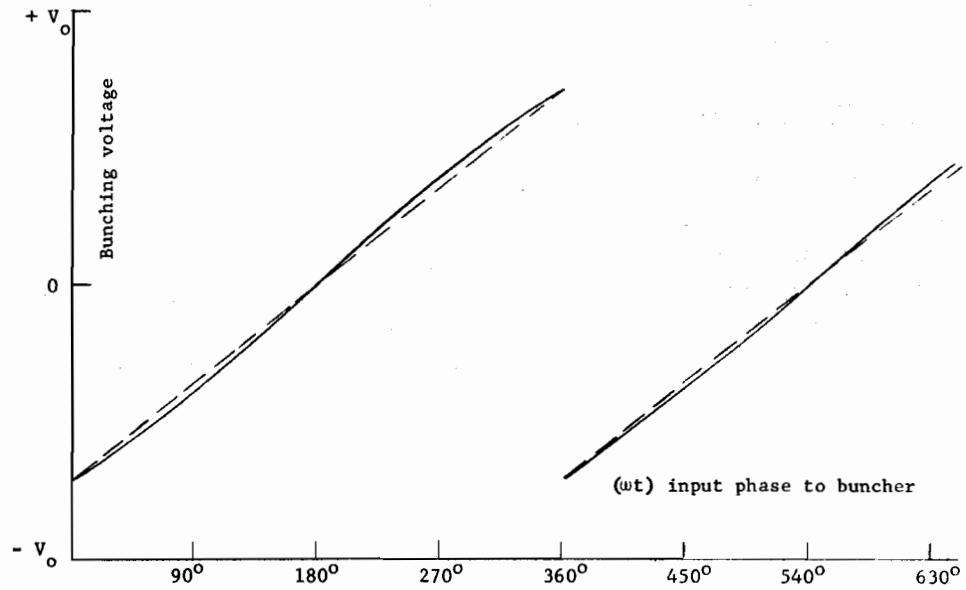

Fig. 9 - Bunching voltage waveshape for a four-gap fourth-subharmonic conical-scan buncher.

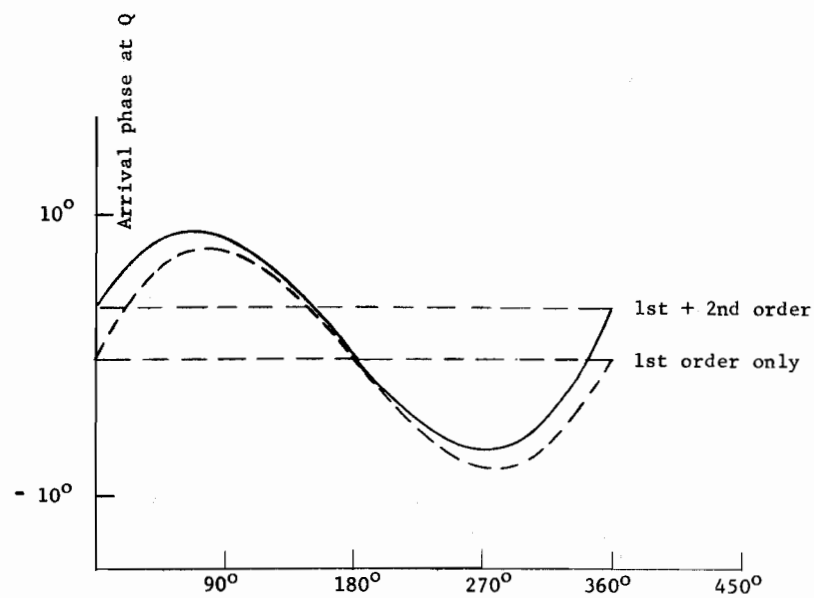

Fig. 10 - Effect of second order terms in a four-gap fourth-subharmonic conical-scan buncher.

For 10° maximum deflection with $p = 4$, $\lambda = 1.5$ m, $\beta_o = 0.04$, $E_o = 3.4$ MV/m and for 20°, $E_o = 7.1$ MV/m. These are high but probably attainable field strengths, but they would not be attainable for a fundamental frequency deflector ($p = 1$).

10. Crossed-Field Deflector

A conical scan deflector requires two mutually perpendicular sets of plates (or their equivalent). Consider two such plate sets, with each pair of plates balanced to ground. In general, the mere application of voltages in quadrature will not produce a uniform E field rotating at frequency ω/p, and the uniformity in space and time depends on the electrode shape. A typical case is four equal segments of a circular cylinder with voltages

$$V_1 = -V_3 = -E_o\, a \sin \frac{\omega t}{p}$$

$$V_2 = -V_4 = -E_o\, a \cos \frac{\omega t}{p} .$$

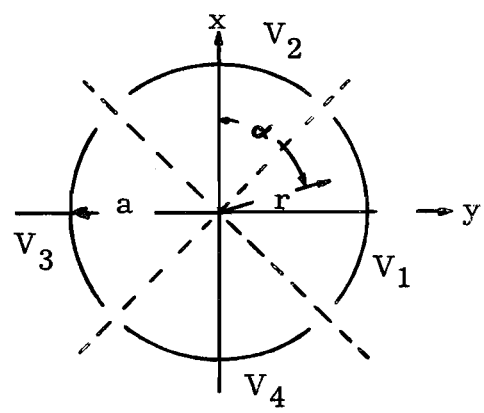

The electrostatic potential at $r = a$, $t = 0$ has the boundary value

$$V(\alpha) = \sum_{n=1,3,5\cdots} a_n \cos n\alpha$$

where

$$a_n = \frac{1}{\pi} \int_{-\pi}^{\pi} V(\alpha) \cos n\alpha \, d\alpha = -E_o\, a \frac{\sin (n\pi/4)}{(n\pi/4)} .$$

Thus, at $r = a$ and $t = t$ the boundary potential is

$$V(\alpha, t) = -E_o\, a \sum_{n=1,3,5\cdots} \frac{\sin (\frac{n\pi}{4})}{(\frac{n\pi}{4})} \left[\cos n\alpha \cos \frac{\omega t}{p} + \cos n(\alpha - \frac{\pi}{2}) \sin \frac{\omega t}{p}\right] .$$

The potential in the region of the axis can be expanded in terms of dipole, sextupole, etc. terms varying as $(r/a)^1$, $(r/a)^3$, etc. respectively. (Note that even n terms, e.g. quadrupole, are absent.) Thus the deflecting

fields near the axis are

$$E_r = -\frac{\partial V}{\partial r} = E_o \frac{2\sqrt{2}}{\pi} \Big[\cos\left(\alpha - \frac{\omega t}{p}\right) + \left(\frac{r}{a}\right)^2 \cos\left(3\alpha + \frac{\omega t}{p}\right)$$

$$- \left(\frac{r}{a}\right)^4 \cos\left(5\alpha - \frac{\omega t}{p}\right) - \left(\frac{r}{a}\right)^6 \cos\left(7\alpha + \frac{\omega t}{p}\right) + \cdots \Big] ,$$

$$E_\alpha = -\frac{1}{r}\frac{\partial V}{\partial \alpha} = E_o \frac{2\sqrt{2}}{\pi} \Big[-\sin\left(\alpha - \frac{\omega t}{p}\right) - \left(\frac{r}{a}\right)^2 \sin\left(3\alpha + \frac{\omega t}{p}\right)$$

$$+ \left(\frac{r}{a}\right)^4 \sin\left(5\alpha - \frac{\omega t}{p}\right) - \left(\frac{r}{a}\right)^6 \sin\left(7\alpha + \frac{\omega t}{p}\right) + \cdots \Big] ,$$

a series of vectors rotating at increasing rates, with alternate directions of rotation and alternate signs by pairs. The deflection is not truly conical but a scalloped cone depending on the initial radius of the beam particle. Since appreciable gaps in α must be provided to insulate adjacent electrodes, the higher multipoles will be somewhat larger than indicated. On the other hand, since the transit time is an appreciable fraction of a period, the rapid rotation of the higher multipoles will tend to average to zero and, more important, they are small near the axis.

The dynamics of deflection is more conveniently treated in (xy) where the fields are:

$$E_x = E_o \frac{2\sqrt{2}}{\pi} \Big\{\cos\frac{\omega t}{p} + \frac{1}{a^2}\Big[(x^2 - y^2)\cos\frac{\omega t}{p} - 2\,xy\sin\frac{\omega t}{p}\Big]$$

$$+ \frac{1}{a^4}\Big[(-x^4 - y^4 + 6\,x^2y^2)\cos\frac{\omega t}{p} + (4\,xy^3 - 4\,x^3y)\sin\frac{\omega t}{p}\Big] + \cdots\Big\}$$

$$E_y = E_o \frac{2\sqrt{2}}{\pi} \Big\{\sin\frac{\omega t}{p} + \frac{1}{a^2}\Big[(y^2 - x^2)\frac{\sin\omega t}{p} - 2\,xy\cos\frac{\omega t}{p}\Big]$$

$$+ \frac{1}{a^4}\Big[(-x^4 - y^4 + 6\,x^2y^2)\sin\frac{\omega t}{p} + (4\,x^3y - 4\,xy^3)\cos\frac{\omega t}{p}\Big] + \cdots\Big\}$$

The equations of motion

$$m\frac{d^2x}{dt^2} = e\,E_x$$

$$m\frac{d^2y}{dt^2} = e\,E_y$$

are coupled and too complicated for exact solution. An approximate solution is obtained by integrating twice for the pure dipole field, substituting these x, y into the sextupole term, and integrating this equation once to obtain the deflection angles. For the transit time $(\omega b/pv_o) = \pi$, the approximate (pure dipole) solutions are

$$m \frac{dx}{dt} = e E_o \frac{2\sqrt{2}}{\pi} \frac{p}{\omega} \left[\sin \frac{\omega t}{p} + \cos \frac{\omega t_o}{p}\right]$$

$$m \frac{dy}{dt} = e E_o \frac{2\sqrt{2}}{\pi} \frac{p}{\omega} \left[- \cos \frac{\omega t}{p} + \sin \frac{\omega t_o}{p}\right]$$

$$m x = e E_o \frac{2\sqrt{2}}{\pi} \frac{p^2}{\omega^2} \left[- \cos \frac{\omega t}{p} + \left(\frac{\omega t}{p} - \frac{\omega t_o}{p} + \frac{\pi}{2}\right) \cos \frac{\omega t_o}{p} + \sin \frac{\omega t_o}{p}\right]$$

$$m y = e E_o \frac{2\sqrt{2}}{\pi} \frac{p^2}{\omega^2} \left[- \sin \frac{\omega t}{p} + \left(\frac{\omega t}{p} - \frac{\omega t_o}{p} + \frac{\pi}{2}\right) \sin \frac{\omega t_o}{p} - \cos \frac{\omega t_o}{p}\right]$$

$$\tan \theta = \frac{e E_o 4\sqrt{2}\, p}{m v_o \pi \omega} = \frac{e E_o b\, 4\sqrt{2}}{m v_o^2 \pi^2}$$

where t_o is the time at which the particle reaches 0. The effect of the sextupole field is three scallops on the cone of trajectories. The amplitude of the scallops is approximately $\Delta\theta$ where

$$\frac{\Delta\theta}{\tan \theta} = \frac{\pi}{2 a^2} \left(\frac{e E_o 2\sqrt{2}\, p^2}{m \pi \omega^2}\right)^2$$

$$= \frac{1}{8\pi} \frac{b^2}{a^2} \tan^2 \theta .$$

For $\theta = 10^o$ and a maximum error $\Delta\theta/\tan \theta = 0.1$ the deflector radius must be greater than b/9, and if it is b/3, the error is 10 times less. The effect is not serious. In any case, a symmetrically placed re-deflector cancels the aberration.

11. Parallel Plates in Tandem

There is another solution to the conical scan deflector which uses smaller apertures for a given aberration and hence lower voltages for a given deflection. This consists of two independent sets of parallel plates mutually perpendicular and in tandem. Such a deflector cannot give a cone but it can produce a circular trace at the buncher. The analysis is not given here, being essentially the same as Section 9 above.

12. Twisted Parallel-Plate Deflector

Another conical-scan deflector which can be thought of as the limiting case of parallel-plate pairs in tandem is a pair of parallel plates, twisted with a uniform pitch, so that the field rotated uniformly with z. If the plate separation is small as compared with the pitch, the field is approximately uniform

$$E_x = E_o \cos kz \sin\left(\frac{\omega t}{p} + \phi\right)$$

$$E_y = E_o \sin kz \sin\left(\frac{\omega t}{p} + \phi\right).$$

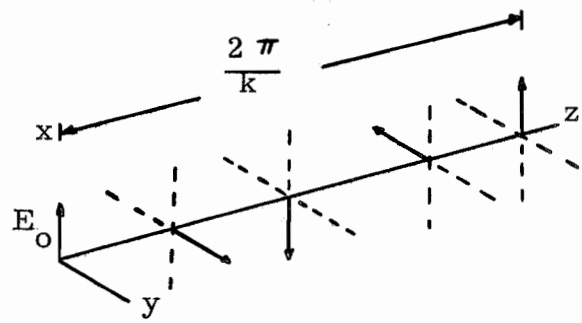

An axial particle of velocity v_o enters the deflector at $t = 0$, $z = 0$ and emerges at $t = T$, $z = b$. The radial velocities at emergence are

$$\dot{x} = \frac{eE_o}{2m}\left\{\left[\frac{1 - \cos\left(\frac{\omega T}{p} + kv_o T\right)}{\frac{\omega}{p} + kv_o} + \frac{1 - \cos\left(\frac{\omega T}{p} - kv_o T\right)}{\frac{\omega}{p} - kv_o}\right]\cos\phi + \left[\frac{\sin\left(\frac{\omega T}{p} + kv_o T\right)}{\frac{\omega}{p} + kv_o} + \frac{\sin\left(\frac{\omega T}{p} - kv_o T\right)}{\frac{\omega}{p} - kv_o}\right]\sin\phi\right\}$$

$$\dot{y} = \frac{eE_o}{2m}\left\{\left[\frac{1 - \cos\left(\frac{\omega T}{p} + kv_o T\right)}{\frac{\omega}{p} + kv_o} - \frac{1 - \cos\left(\frac{\omega T}{p} - kv_o T\right)}{\frac{\omega}{p} - kv_o}\right]\sin\phi - \left[\frac{\sin\left(\frac{\omega T}{p} + kv_o T\right)}{\frac{\omega}{p} + kv_o} - \frac{\sin\left(\frac{\omega T}{p} - kv_o T\right)}{\frac{\omega}{p} - kv_o}\right]\cos\phi\right\}.$$

For a conical scan $\dot{x}/\dot{y} = \pm \tan(\phi - \phi_o)$ which gives three types of solutions

a) $kv_o = \omega/p$ with $\omega T/p = \pi n$, $n = 1, 2, \cdots$

$$\dot{x} = \frac{eE_o}{2m} \pi n \frac{p}{\omega} \sin \phi$$

$$\dot{y} = \frac{eE_o}{2m} \pi n \frac{p}{\omega} \cos \phi \quad .$$

In this arrangement the velocities continue to grow with the length: the x and y impulses are in step with the particle everywhere, a sort of synchronous deflecting mode.

b) $\omega T/p - kv_o T = 2\pi n$, $n = 1, 2, \cdots$

$$\dot{x} = \frac{eE_o}{2m} \frac{1}{\frac{\omega}{p} + kv_o} \cos(\phi - \phi_o)$$

$$\dot{y} = \frac{eE_o}{2m} \frac{1}{\frac{\omega}{p} + kv_o} \sin(\phi - \phi_o)$$

$$\tan \phi_o = \frac{\sin\left(\frac{\omega T}{p} + kv_o T\right)}{1 - \cos\left(\frac{\omega T}{p} + kv_o T\right)} \quad .$$

c) $\omega T/p + kv_o T = 2\pi n$, $n = 1, 2, \cdots$

$$\dot{x} = \frac{eE_o}{2m} \frac{1}{\frac{\omega}{p} - kv_o} \cos(\phi - \phi_o)$$

$$\dot{y} = -\frac{eE_o}{2m} \frac{1}{\frac{\omega}{p} - kv_o} \sin(\phi - \phi_o)$$

$$\tan \phi_o = \frac{\sin\left(\frac{\omega T}{p} - kv_o T\right)}{1 - \cos\left(\frac{\omega T}{p} - kv_o T\right)} \quad .$$

For (b) and (c) the deflection does not grow with n. Solutions (a) give the largest deflections for a given E_o and b, and the deflection of

solutions (c) is the weakest. We also note that the twist is greatest for solutions (a), and the aberrations, which are related to the twist, are largest for (a). However, the synchronous mode (a) seems to be the most attractive for an actual design.

There are two kinds of aberrations produced by a twisted field. One is the lack of conical symmetry of the deflections (x_1, y_1) at emergence even though the velocities are without aberration; this is inherent in the twisted plates in lowest approximation. The second kind is a velocity aberration induced by the nonuniformity of the field across the aperture because of the twist. That is, a twisted uniform field cannot, in fact, be produced because it is not a solution of Laplace's equation. We consider the deflection aberration first.

For solutions (a) with $kv_o = \omega/p$ and $\omega T/p = \pi n$, the deflections at emergence for a uniform, twisted field, are

$$x_1 = \frac{eE_o}{2m} \frac{p^2}{2\omega^2} n\pi (\cos\phi + n\pi \sin\phi)$$

$$y_1 = \frac{eE_o}{2m} \frac{p^2}{2\omega^2} n\pi (\sin\phi + n\pi \cos\phi) .$$

The variation of $r_1 = (x_1^2 + y_1^2)^{1/2}$ with ϕ is an aberration. The magnitude of the aberration is

$$\frac{|\Delta r_1|_{max}}{(r_1)_{av.}} = \frac{n\pi}{1 + n^2\pi^2}$$

which is largest for $n = 1$ and varies approximately as $1/n$. Figure 11 shows the deflections for the worst ($n = 1$) case. We note, in particular, that a particle which enters when the field is a maximum ($\phi = \frac{\pi}{2}$) does not undergo a pure x deflection although its radial velocity at emergence is along x. For large n, this distortion disappears and r_1 becomes a circle.

While the effect is large in a relative sense for small n, it is not necessarily serious since the deflections (x_1, y_1) are usually small as compared with the deflections produced by drift with velocities (v_x, v_y) which are, in the uniform field approximation, without aberrations.

Now we consider the velocity aberrations. As we mentioned, a twisted uniform field is not a solution of Laplace's equation, but it can be the dominant term in a true solution. Write the potential as

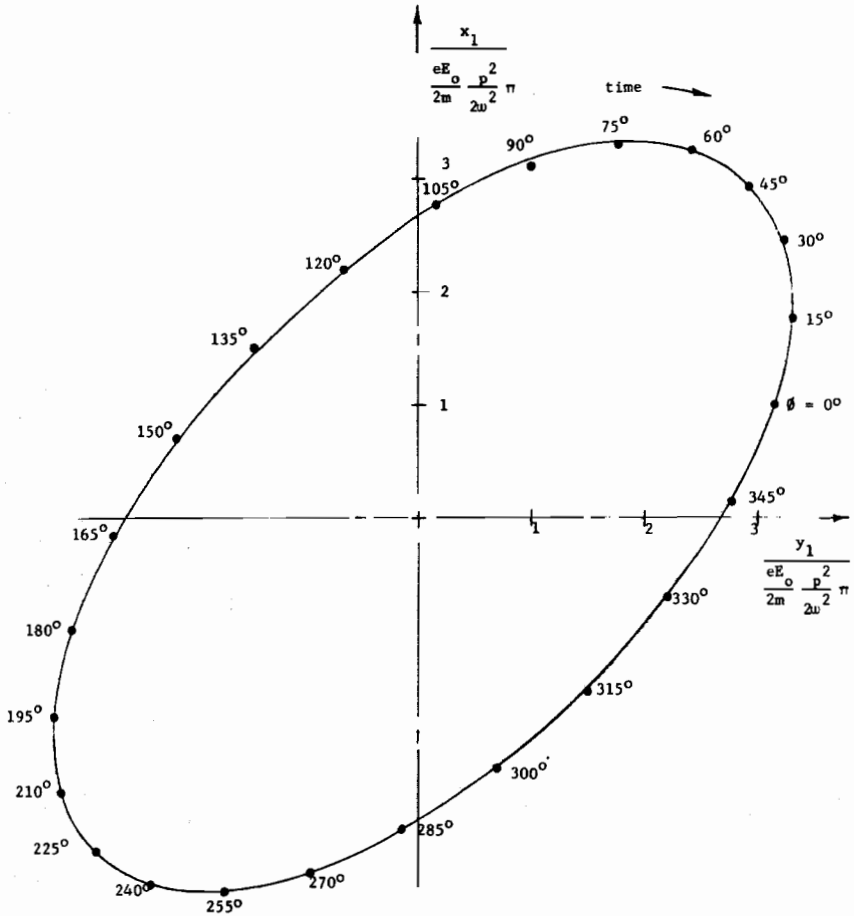

Fig. 11 - Deflections on emergence from twisted plate deflector for n = 1. Points labeled with entrance phase.

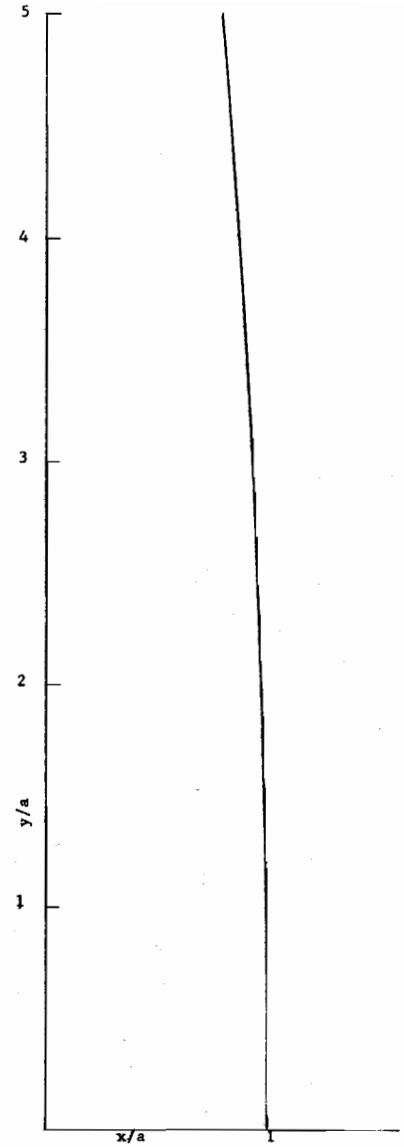

Fig. 12 - Plate shape for a pure $I_1(kr)$ field with ka = ½

$$V = -E_o f(r) \cos(\theta - kz) \sin\left(\frac{\omega t}{p} + \phi\right)$$

where $f(r) \to r$ as $r \to 0$. With this V, Laplace's equation in cylindrical coordinates is

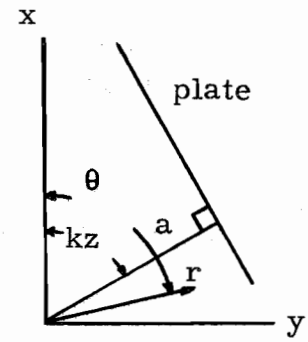

$$\frac{d^2 f}{dr^2} + \frac{1}{r}\frac{df}{dr} - \left(k^2 + \frac{1}{r^2}\right) f = 0 ,$$

the modified Bessel equation with solutions

$$f = S_1 I_1 (kr) .$$

Setting the plate potential at $-V_o$ for $\theta = kz$, $r = a$

$$V = -\frac{V_o}{I_1(ka)} I_1(kr) \cos(\theta - kz) \sin\left(\frac{\omega t}{p} + \phi\right) .$$

If $ka << 0$, $I_1(ka) \cong ka/2$ and

$$V \cong -V_o \frac{r}{a}\left\{1 + \frac{1}{8}k^2 r^2 + \frac{1}{192}k^4 r^4 + \cdots\right\} \cos(\theta - kz) \sin\left(\frac{\omega t}{p} + \phi\right) .$$

The plates must be shaped to give this solution, and the polar equation of the plates is obtained by setting $V = -V_o$. Figure 12 shows the plate shape for $2\pi/k = 24$ cm, $a = 3/\pi$ cm, i.e., $ka = 1/4$.

Assume that the plates are shaped to give a pure $I_1(kr)$ solution. We wish to know the aberration produced by the terms in r^3, r^5, etc. Keeping only the term in r^3

$$E_x = E_o \left\{\cos kz + \frac{1}{8}k^2 (3x^2 + y^2) \cos kz\right\} \sin\left(\frac{\omega t}{p} + \phi\right)$$

$$E_y = E_o \left\{\sin kz + \frac{1}{8}k^2 (3y^2 + x^2) \sin kz\right\} \sin\left(\frac{\omega t}{p} + \phi\right) .$$

The equations of motion can be solved, as before, by iteration. When this is done for a twist such that $kv_o = \omega/p$, we find that the emergence velocities are of the form

$$\dot{x} = \frac{eE_o}{m} \frac{p}{\omega} \left\{ \frac{1}{2} n\pi + \frac{1}{8} k^2 \left(\frac{eE_o}{2\,m} \right)^2 \frac{p^4}{\omega^4} F(\phi) \right\}$$

where $|F(\phi)| < 10$ for all ϕ. For a 10° deflection with $p = 4$, $n = 1$, the second term is about two thousandths of the first term. The conical aberrations due to the velocity are thus negligible.

Even so, the pure I_1 (kr) solution is not the best for small aberrations. Consider the general potential of a uniformly twisted field

$$V = - E_o f(r) \cos n (\theta - kz) \sin \left(\frac{\omega t}{p} + \phi\right)$$

which obeys

$$\frac{d^2 f}{dr^2} + \frac{1}{r} \frac{df}{dr} - \left(n^2 k^2 + \frac{n^2}{r^2}\right) f = 0$$

with solutions

$$f = S_n I_n (n\,kr) , \quad n = 1, 3, 5 \cdots .$$

The general solution is, therefore,

$$V = - \sum_{n=1,3\cdots} S_n I_n (n\,kr) \cos n (\theta - kz) \sin \left(\frac{\omega t}{p} + \phi\right)$$

with

$$\frac{V_o}{E_o} = S_1 I_1 (ka) + S_3 I_3 (3\,ka) + \cdots .$$

We can choose the constants S_n in various ways. We can eliminate the terms $r^n \cos (\theta - kz)$ for $n = 3, 5, \cdots$ by setting $S_3 = S_1/27$, $S_5 = S_1/125$, $\cdots$. The aberrations are then confined to terms of the type $r^n \cos^m (\theta - kz)$ with $n = 3, 5, \cdots$, $m = 3, 5, \cdots n$, with smaller coefficients than with the pure I_1 (kr) solution as well as smaller contributions by the integrals. An optimum choice requires detailed computations which we have not carried out.

13. Twisted Ribbon Deflector

As we shall see in Section 18, the twisted-plate deflector suffers from an asymmetric fringing field which causes unwanted bunching. This suggests a hybrid device which combines the best features of the twisted-plate and the segmented-cylinder deflectors. It would consist of p conducting ribbons wound helically on a cylinder and driven with the

usual push-pull voltages. The dominant deflecting field would be approximately uniform over the aperture and by rotating in both time and space it could give synchronous deflection.

Write for this dominant term

$$E_x = E_o \cos\left(\frac{\omega t}{p} + kz + \phi\right)$$

$$E_y = E_o \sin\left(\frac{\omega t}{p} + kz + \phi\right) .$$

As written, the expression gives clockwise rotation with t. If $k > 0$, the helix is clockwise also. The synchronous solution occurs for $kv_o = - w/p$. Then, since $z = v_o t$

$$\dot{x} = \frac{eE_o t}{m} \cos \phi$$

$$\dot{y} = \frac{eE_o t}{m} \sin \phi$$

$$x = \frac{eE_o t^2}{2\,m} \cos \phi$$

$$y = \frac{eE_o t^2}{2\,m} \sin \phi .$$

The device has unit transit time factor, can be cut to any length, and has E, r, and $\dot{r}$ in phase everywhere. The counter directions of rotation of E in t and z means that the particle sees a uniform E as it proceeds along z. The scan is purely conical.

The device also has other solutions, some of which may be very useful. It is possible to cancel $\dot{r}$ while preserving r and thus to scan conically without radial velocities. This removes the necessity for a lens. An obvious way to do this is to place two identical deflectors in tandem with the second one out of phase by π with the first. The second removes the $\dot{r}$ but allows r to grow to twice its value at the exit of the first deflector. At the transition between the two there is a natural bunching gap.

Another way to achieve zero $\dot{r}$ is to operate nonsynchronously. Let $kv_o = - f\,\omega/p$ where $0 < f < 1$. If we set $(1 - f)\,\omega T/p = 2\,\pi\,n$, where n is an integer and T is the emergence time, we find on emergence that

$$\dot{x}_1 = \dot{y}_1 = 0$$

$$x_1 = -\frac{eE_o}{m}\frac{T^2}{2\pi n}\sin\phi$$

$$y_1 = \frac{eE_o}{m}\frac{T^2}{2\pi n}\cos\phi \ .$$

The deflection is greatest for $n = 1$. The vector r_1 rotates in the same sense as E at emergence and is perpendicular to it, leading by $\pi/2$. If now we place in tandem an identical device, the second out of phase by π, (i.e. reversed voltages), the particles crossing the gap between them are bunched by the fringing fields between facing electrodes. The bunching is correct (early particles are decelerated) and, with some electrode shaping near the gap, this simple system may incorporate all of the desirable features of a conical scan subharmonic buncher. We have not yet studied any of the more complex features of such a system.

14. Rf Drive for Deflectors

The excitation of either the one-dimensional, four-plate conical scan or twisted-plate deflectors should be push-pull, balanced to ground. Since the voltages are high, the circuits should be resonant. In the region of 50 Mc/s where the $p = 4$ deflector operates, coaxial lines are convenient elements. A possible design can be derived from a half-wave line open at both eneds, with a plate attached to each end and the line folded to bring the plates together. The device is push-pull with respect to the outer conductor. For the four-plate deflector, two such circuits could be arranged to feed two pairs of push-pull plates in time quadrature. Because of the crossed polarization, the interaction will be small even though the E fields occupy the same space.

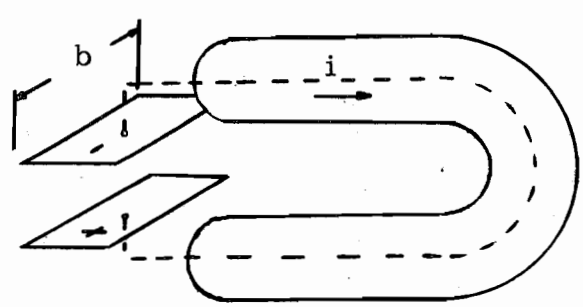

15. Lenses

For one-dimensional deflection the lens should be a true lens in the sense that it have the same focal length for all deflection angles. There are a variety of well-known electric and magnetic lenses which have this property for small angles and some which are quite good up to the maximum angles of interest here. In general, they will not be exactly isochonous if they focus exactly, and conversely. These aberrations should be examined in any serious design, but we have not done so.

We have considered in more detail lenses for the conical scan arrangement. Here, since the cone angle is almost constant, the lens may have large aberrations for angles other than the cone angle; the important property to preserve is isochronism as a function of the azimuth angle. Since lenses which are figures of revolution are automatically isochronous in this sense, we have considered two such types which show some promise: coaxial electrostatic systems and magnetic solenoids.

Consider a lens of two coaxial circular cylinders with potentials $\pm V$ of the correct magnitude to give a symmetrical path. The first integral of the equation of motion is

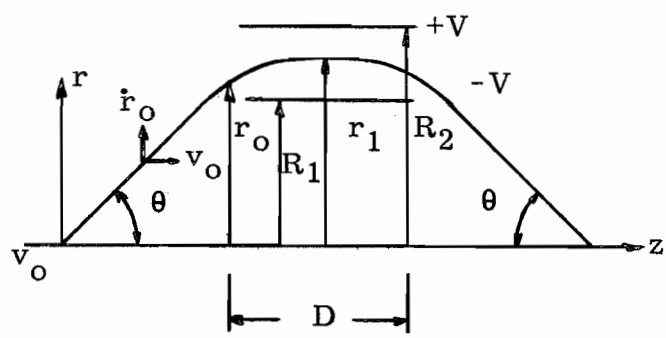

$$\dot{r}^2 - \dot{r}_o^{\,2} = - \frac{4\,eV}{m \ln \frac{R_2}{R_1}} \ln \frac{r}{r_o} ,$$

which determines the potential from

$$\frac{2\,eV}{\frac{1}{2} m v_o^2} = \tan^2 \theta \, \frac{\ln \frac{R_2}{R_1}}{\ln \frac{r_1}{r_o}} .$$

The second integral can be written

$$\frac{D}{v_o} \sqrt{\frac{eV}{\ln \frac{R_2}{R_1}}} = 2\, r_1 \int_o^{w_o} e^{-w^2}\, dw = r_1 \sqrt{\pi}\ \mathrm{Erf}\,(w_o)$$

which determines the length D, where $w^2 = \ln \frac{r_1}{r}$.

There are many other coaxial systems, all with rather similar properties. For the angles θ of interest here, the well-known concentric-sphere-segment lens is not attractive since it is too short and hence requires very large potentials. There is a large family of shapes intermediate between spheres and cylinders which consist of various arcs rotated around z. None of those examined have any important advantages over the cylinder lens.

All of these coaxial electrostatic systems have one serious technical difficulty - the support of the center electrode which lies completely inside the beam sheath. It could conceivably be cantilevered from a ground plane (perhaps part of the buncher) whose annular beam slot was not complete but rather segmented. This appears very unattractive, particularly if the electrode is at a large negative potential, which requires an insulated cable crossing the beam sheath.

Solenoids avoid this difficulty since the coil can be completely external. Consider a uniform axial field B. A particle deflected through angle θ describes a helix on a cylinder of radius R where

$$B = \frac{m v_o c \tan \theta}{eR}$$

and

$$L = \frac{2 \pi R}{\tan \theta} .$$

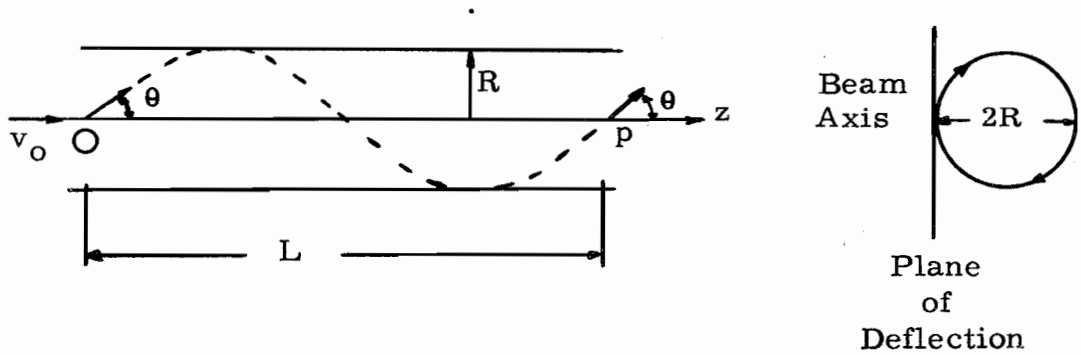

As the beam is scanned conically at frequency ω/p, the cylinder rotates in the same sense and at the same frequency, and the original beam cone is reconstructed at point P. The inside diameter of the solenoid coil must be at least 4 R. The plane of the bunching gaps can be anywhere between P and the 0 to P midpoint, and any radius of the bunching annulus from zero to 2 R can be arranged, depending on this position. For $\theta = 10^{o}$ and $\frac{v_o}{c} = 0.04$ a possible design choice is R = 10 cm, B = 2200 gauss, L = 360 cm. For an air solenoid the required current density in the winding would be about 2400 A/cm^2, which is feasible. Iron cladding could improve the efficiency, and there is no necessity for uniformity of B with either r or z so long as the field is axially symmetric.

As a lens, an ideal solenoid reconstructes the input transverse phase space. Thus it acts like a thin lens of unit magnification and focal length L/4.

Lenses which are not figures of revolution, such as electric or magnetic strong focusing triplets, may be sufficiently isochronous. They have one important property; for feasible fields they can have short focal lengths and so permit close spacing between the buncher and redeflector while preserving a large beam radius at the buncher. However, it is just this condition (large θ) which enhances the lack of isochronism. In a serious design these conflicting properties should be studied but we have not done so. As we shall see in the next section, the buncher - redeflector spacing is one of the most difficult problems in the whole scheme, and a successful design must minimize this spacing by a careful choice of the lens system and the transverse beam optics.

16. Redeflection Errors

One of the serious difficulties in the whole scheme is the angle errors introduced at the redeflector arising from the fact that the beam is partially bunched when it is redeflected. The errors are small for long drift lengths and short buncher - redeflector spacings but there are technical limits on both of these and near these limits the errors are not negligible.

Consider a conical scan beam converging to P from the bunching gap G. If the bunching is made correct at Q, the arrival phase at P is

$$\phi = t + \frac{z_o}{\ell} \frac{\pi}{\sin \frac{\pi}{p}} \cos \left(\frac{\omega t}{p} - \frac{2\pi k}{p} + \frac{\pi}{p} + \frac{\pi}{2} \right) + C \ .$$

At P the transverse velocities are

$$v_x = -v_o \tan\theta \sin\frac{\omega t}{p}$$

$$v_y = -v_o \tan\theta \cos\frac{\omega t}{p} \quad .$$

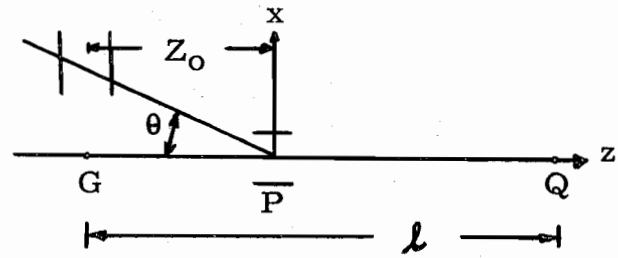

With the redeflector we add the velocities

$$v'_x = v_o \tan\theta' \sin\frac{\phi}{p}$$

$$v'_y = v_o \tan\theta' \cos\frac{\phi}{p} \quad .$$

If $z_o = 0$, $\tan\theta = \tan\theta'$, and $C = 0$, the beam is redeflected without errors. We find that no adjustment of phase (i.e., C) or amplitude (i.e., $\tan\theta'$) reduces the errors, so we remove this generality by setting $C = 0$, $\tan\theta = \tan\theta'$ and write for the angle errors,

$$\Delta\theta_x = \frac{v'_x + v_x}{v_o} = \tan\theta\left(\sin\frac{\phi}{p} - \sin\frac{\omega t}{p}\right)$$

$$\Delta\theta_y = \frac{v'_y + v_y}{v_o} = \tan\theta\left(\cos\frac{\phi}{p} - \cos\frac{\omega t}{p}\right) .$$

Figure 13 shows the angle errors for $p = 4$, $z_o/\ell = 0.1$ as a function of $\frac{\omega t}{p}$ for one complete scan. The points are labeled with $\omega t/p$ values to show the variation in time. The discontinuities in the errors make it essentially impossible to compensate them by changes in the voltage waveform. For the case of Fig. 13 the maximum angle error is $0.078 \tan\theta$ or 0.8^o for $\theta = 10^o$.

For angle errors up to a few degrees, the errors are linear in z_o/ℓ . Thus for $p = 4$, $z_o/\ell = 0.2$ the maximum error is $0.156 \tan\theta$.

These redeflection-angle errors add randomly to the beam emittance angles and hence the transverse phase space of the beam is degraded. This can be serious, depending on the design of the linac and the tolerances on its output beam quality.

Although complex voltage waveforms at the redeflector are not effective in reducing the errors, a second conical scan redeflector near the first linac gap is of some help. At the bunching point Q all of the particles on a single arc of Fig. 13 are essentially simultaneous. The addition of a small deflection voltage equal to the radius of the arc and

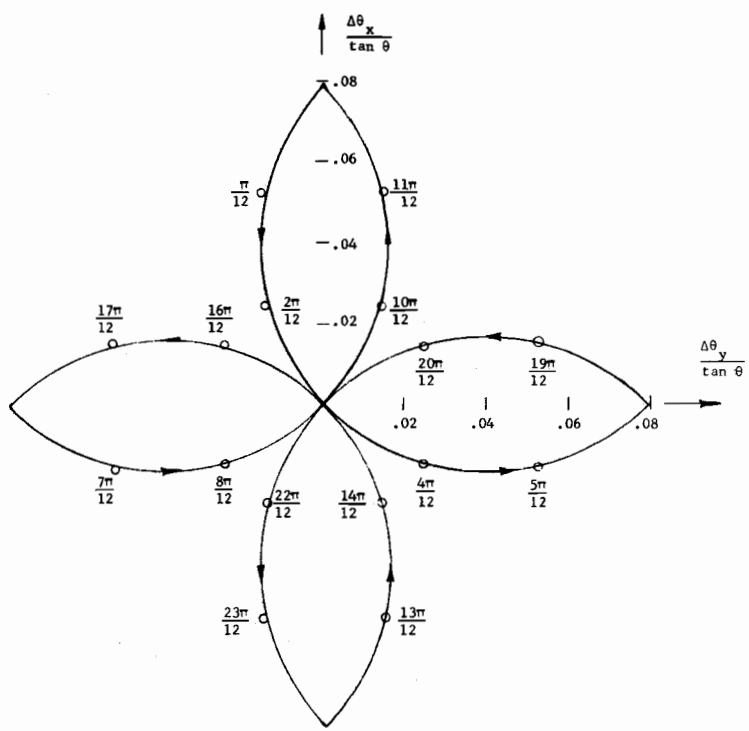

Fig. 13 - Redeflection-angle errors for a fourth-subharmonic conical-scan redeflector located at one-tenth of the drift length for bunching.

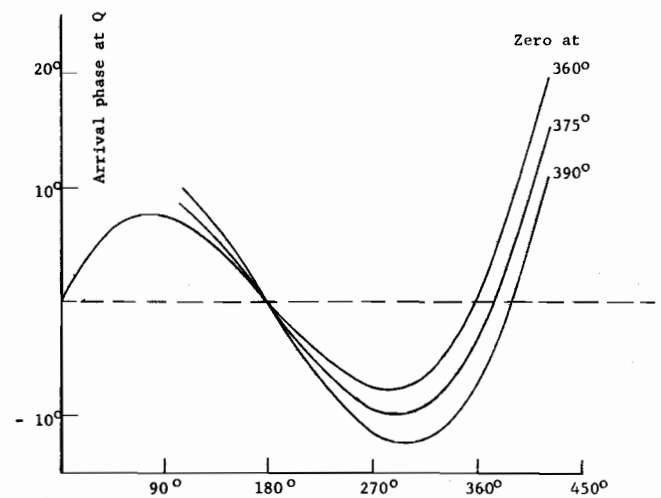

Fig. 14 - Arrival phase for a p = 4 buncher for several choices of the phase at the outer zeros.

of frequency $\omega t/p$ converts Fig. 13 into a circle of radius $0.078 \tan \theta/\sqrt{2}$ and thus reduces the errors by a factor $\sqrt{2}$.

17. The Buncher

For conical deflection the buncher is a set of p annular segments of mean radius R_B, each differing in phase from its neighbor by $2\pi/p$, where ω/p is the scanning and bunching frequency. The ratio of the arc length of a segment to the beam diameter should be large enough so that the beam does not spend too much time overlapping adjacent segments. It is not necessary to reduce this time to an extremely small value since the phase regions just outside the ideal boundaries are no worse than those just inside. For example, for p = 4 (see Fig. 8), the maximum arrival phase error (7.5°) which occurs at $\omega t = 285^\circ$ is not exceeded until ωt reaches 390°. If it is so arranged that at $\omega t = 360^\circ$ the beam center crosses to the next segment and at 390° the trailing edge crosses, then the diameter of the beam is equal to $\frac{\pi}{12} R_B$. If the beam diameter is 1 cm, then R_B must be at least 3.82 cm.

If it is desired to use larger beam diameters (or smaller buncher radii), the arrival phase error can be optimized by choosing a bunching voltage which gives a zero in arrival phase at an ωt somewhat greater than 360° with some sacrifice in the maximum arrival phase error. This is shown in Fig. 14. If, for the p = 4 case, we place the arrival phase zeros at -15°, 180°, 375°, the maximum arrival phase errors is $\pm 10^\circ$, which is not exceeded until ωt reaches 408°. Thus the usable phase overlap is increased from $390^\circ - 360^\circ = 30^\circ$ to $408^\circ - 360^\circ = 48^\circ$ with a corresponding increase in the allowable beam diameter.

For subharmonic bunchers the low frequency and the electrode complexity make drift tube bunchers attractive. For even p the electrodes at opposite ends of a bunching circle diameter are push-pull balanced to ground. Thus the buncher circuits can be the same half-wavelength folded coax that were suggested for the deflector. The two bunching gaps are separated by half a period of ω/p which is a length $\beta_0 \lambda\, p/2$. For p = 4, the maximum electrode-to-electrode voltage is $\sqrt{2}$ times the voltage to ground and gap g_2 must exceed g_1. For p = 6, these voltages are equal, and for larger p the electrode-to-electrode voltage continues to diminish. The region of the beam sheath deleted by the gaps g_2 can be used on the ground plane for radial straps to support its central disk. Because of the circuit balance, no current flows on these straps. The central annuli of the buncher electrodes require similar straps from the outside annuli; these radial grids will be needed anyhow for good beam dynamics. Such grids will carry current.

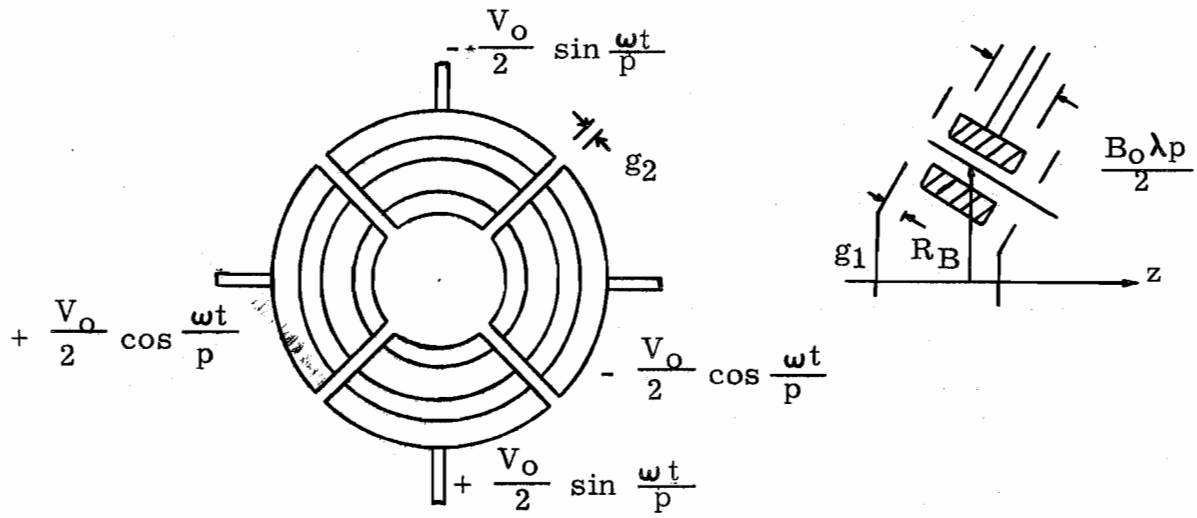

18. Bunching Due to End Effects in the Deflectors

When one attempts to formulate an actual design, it is found that the deflection fields are larger than typical bunching fields. This suggests that the ever present E_z at the ends of a deflector can give a large, and probably undesirable, bunching effect. If we neglect the beam diameter, these effects will occur only at the exit of the deflector and entrance of the redeflector for deflectors which are balanced to ground and hence have $E_z = 0$ on the z axis.

The segmented-cylinder deflector appears to be relatively free of such bunching effects. In the rotating dipole approximation the deflections at emergence (with $\omega b/pv_o = \pi$) are

$$x_1 = \frac{eE_o\, 2\sqrt{2}}{m\pi}\,\frac{p^2}{\omega^2}\; 2\left(\sin\frac{\omega t_o}{p} + \frac{\pi}{2}\cos\frac{\omega t_o}{p}\right)$$

$$y_1 = \frac{eE_o\, 2\sqrt{2}}{m\pi}\,\frac{p^2}{\omega^2}\; 2\left(-\cos\frac{\omega t_o}{p} + \frac{\pi}{2}\sin\frac{\omega t_o}{p}\right)$$

which is a constant radial deflection rotating around z with frequency ω/p and a constant phase delay relative to the deflecting field which it

encounters as it emerges. Hence each particle encounters the same fringing field relative to its path and the end effect is equivalent to a dc acceleration and of no importance. The higher multipoles do not behave in this cooperative manner. However, their size can be suppressed by a large aperture-to-deflection ratio and in addition they will fall off more rapidly with z than does the dipole field. We have not actually calculated their residual bunching effects.

The twisted plate deflector has a relatively large and undesirable bunching effect in lowest approximation. The fringing field does not rotate but merely oscillates in time and each ray on the emergent cone receives a different z impulse. Particles which emerge with maximum $\pm x$ deflection traverse the fringing field when it is a time maximum and are decelerated along z, whereas particles with maximum $\pm y$ deflection lie in the plane of zero E_z and also cross near the time zero. The deflector acts like a buncher of frequency $2\omega/p$.

If the z impulses were not too large, they could be compensated in a four-gap buncher by operating the two $\pm$ pairs at different voltages. However, the effect is large. It can be calculated if the fringing field shape is known. For parallel plates spaced by 2 a with potentials $\pm V_o$ the potential is given by a Schwartz-Christoffel transformation of a segmented plane, and can be written

$$\pi \frac{x}{a} = 1 + \ln \left[\frac{\pi (V/V_o - z/a)}{\sin \pi (V/V_o + 1)} \right] + \left[\frac{\pi (V/V_o - z/a)}{\sin \pi (V/V_o + 1)} \right] \cos \pi (V/V_o + 1)$$

where the origin of x, y is in the median plane in-line with the edge of the plates. Figure 15 shows some of the equipotentials and a typical exit trajectory. Since the latter crosses some of the equipotentials, there is a z impulse. For the example shown a numerical integration gives

$$mv_o \Delta v_z \cong -0.3\, eV_o$$

which is clearly intolerable since V_o is always larger than the peak voltage of the proposed bunchers. It is possible, but unlikely, that plate shaping or auxiliary electrodes in the fringing gap could lower substantially this z impulse. The same conclusions hold for simple one-dimensional deflection by parallel plates.

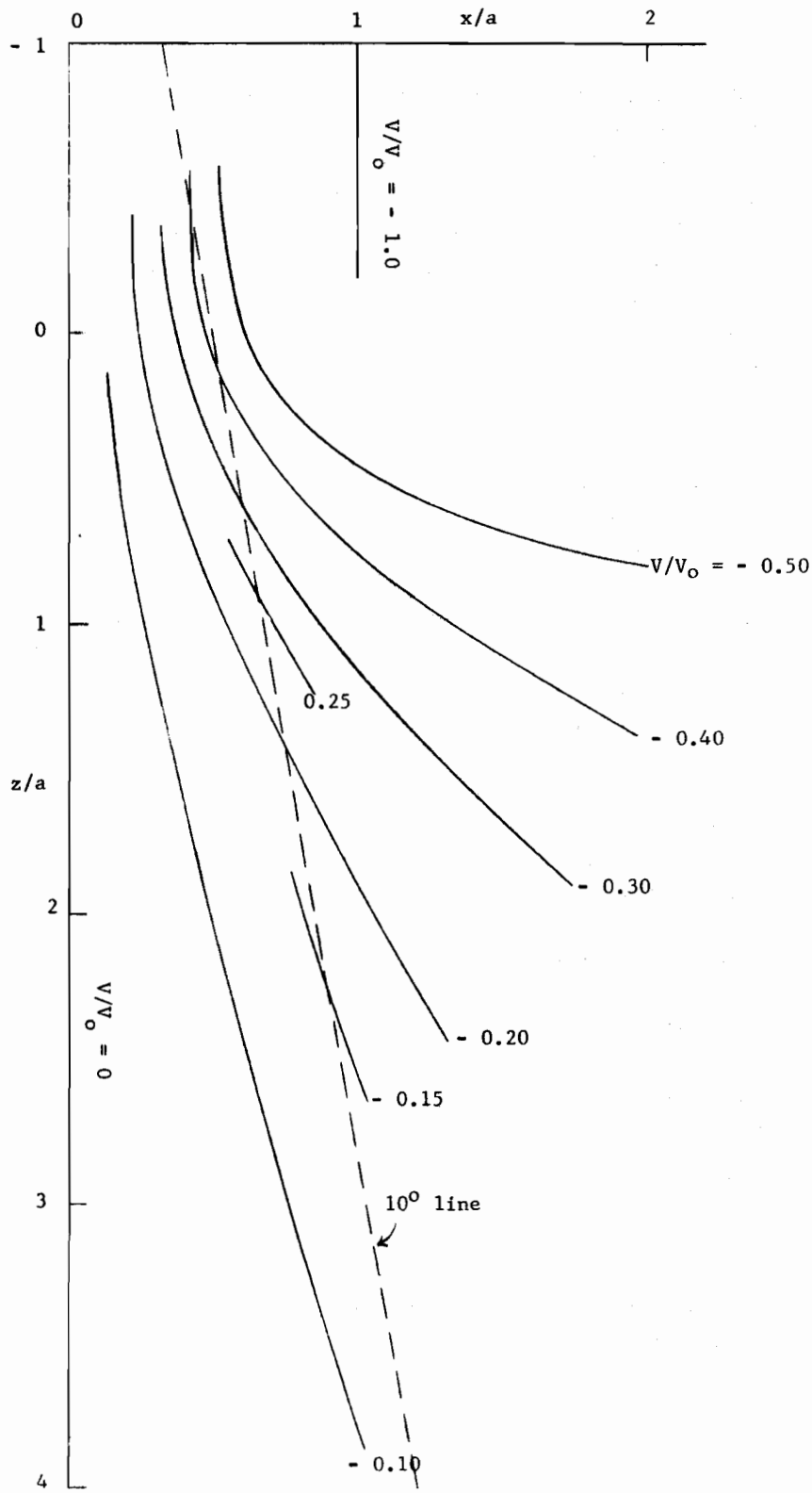
0
1
x/a
2
- 1
0
1
2
3
4
z/a
V/V$_o$ = - 1.0
V/V$_o$ = 0
V/V$_o$ = - 0.50
- 0.40
- 0.30
- 0.20
- 0.15
- 0.10
0.25
10° line

Fig. 15

19. Remarks

We have made some attempts to put together the various devices discussed into a system. These attempts have not been very successful because of the conflicting requirements and inadequacies of the components. Chief among these are (a) unwanted bunching by the deflection fields, (b) very high fields in the deflectors, and (c) redeflection errors. It is too early to be sure that these cannot be resolved and it is to be hoped that they can, for the general principle seems both sound and attractive. At this time the simple system of two nonsynchronous twisted ribbon deflectors seems to warrant careful study.

WHEELER: The engineering problems on this tailless buncher are formidable, but a good deal of thought has been given to them and it seems that reasonable solutions are at least possible.

MARTIN, J. H.: I do not want to deviate our discussion too far from linacs, but occasionally linacs are used to feed other machines, such as synchrotrons, and in ours, for example, we would like to be able to chop a beam or do something like this at something like 4 Mc. Now I have also heard of plasma oscillations occurring in ion sources in the few megacycles region and heard of people talking about bona fide chopping devices and so forth. Now I am wondering if anyone has ever tried to take advantage of plasma oscillations in an ion source in such a way that you actually chop the beam at the ion source at frequencies like 5 Mc?

WHEELER: Not that I have heard of.

VAN STEENBERGEN: I think at the AGS we have been most pronouncedly plagued in the past with those particular oscillations and we had a number of observations on them. It is not a single frequency, it is a whole pattern of frequencies and it is not predictable in the sense that one could use a particular frequency.

MARTIN: Well, if this kind of oscillation occurs as in certain kinds of electronic circuitry, you can encourage it to oscillate, usually at one single frequency, so I am proposing here essentially to drive an ion source at a frequency of your choosing and a phase of your choosing.

WHEELER: When are you going to try it?

MARTIN: Maybe we will get to it.

LAPOSTOLLE: Well, I will only comment to say that this (the tailless buncher) may be a difficult scheme to realize, but it is very similar to an rf separator, and rf separators are being built. I don't think it will be so much of a difficulty to built such a device.

WHEELER: I think its virtues are worth a good deal of effort.

REFERENCES

1. J. E. Leiss, Conference on Proton Linear Accelerators, Yale University October 21-25, 1963, p. 267.

2. S. Ohnuma, ibid., p. 273.

3. R. Perry, ibid., p. 279.

4. R. Beringer, Yale Design Study Technical Note RB-1, October 26, 1963.

5. M. Plotkin, private communication.

6. L. Smith, Handbuck der Physik, Vol. XLIV, p. 371.

7. Yale Study on High Intensity Proton Accelerators, Final Report, April 1964.

NIMROD INJECTOR

N. D. West
Rutherford High Energy Laboratory

(Presented by H. Wroe)

General Status

The Nimrod Injector is at present operating with a 600 keV proton beam current of 38 mA which, with the buncher, gives 18 mA at 15 MeV. The maximum 15 MeV beam current achieved has been 24 mA.

Emittance plots of the 600 keV and 15 MeV beams are shown in Fig. 1. An estimated 90% of the 600 keV beam current can be contained within an ellipse of area 7π cm-mrad, and 90% of the 15 MeV beam within an ellipse of area 3.3π cm-mrad.

The 600 keV beam is currently badly misaligned from the axis of the dc accelerating column, and this fact, together with the effect of aberrations, would explain the asymmetries of the 600 keV emittance. The accelerating column assembly, however, can be steered to align the beam on to the linac axis.

The mode of operation at present is to set up the injector to a standard beam condition. This means that all controls are set to predetermined levels. The 15 MeV beam current produced under these standard conditions is usually within 10% of the nominal, from week to week. The alignment of the beam as it leaves the linac is checked occasionally by means of a pair of four-jaw defining apertures. The results of the measurement are used to calculate the adjustments to a set of four steering magnets required to align the beam to the axis. The misalignments found are usually small, and the beam is only realigned infrequently.

Multipactor Experience

The occurrence of multipactoring in the Nimrod injector linac and the method of inhibiting it by coating the drift-tube faces with carbon black were reported at the Brookhaven Linear Accelerator Conference in 1962. Since then, it has been found possible to leave the faces of the first ten drift tubes uncoated, and to coat the remaining drift-tube faces only over four small areas, corresponding roughly to the positions of the quadrupole pole tips. This has considerably reduced the sparking problem. The effectiveness of the carbon black is demonstrated by the

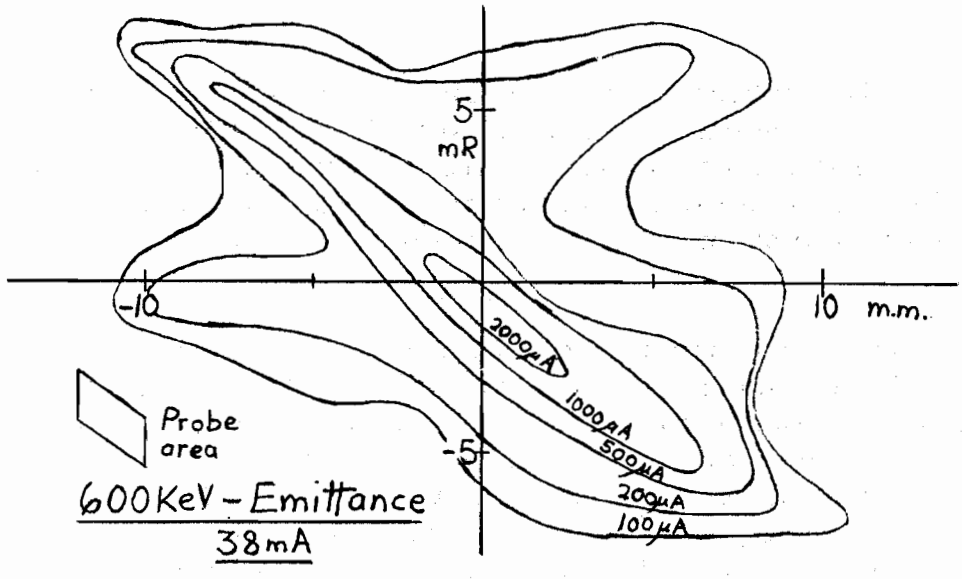

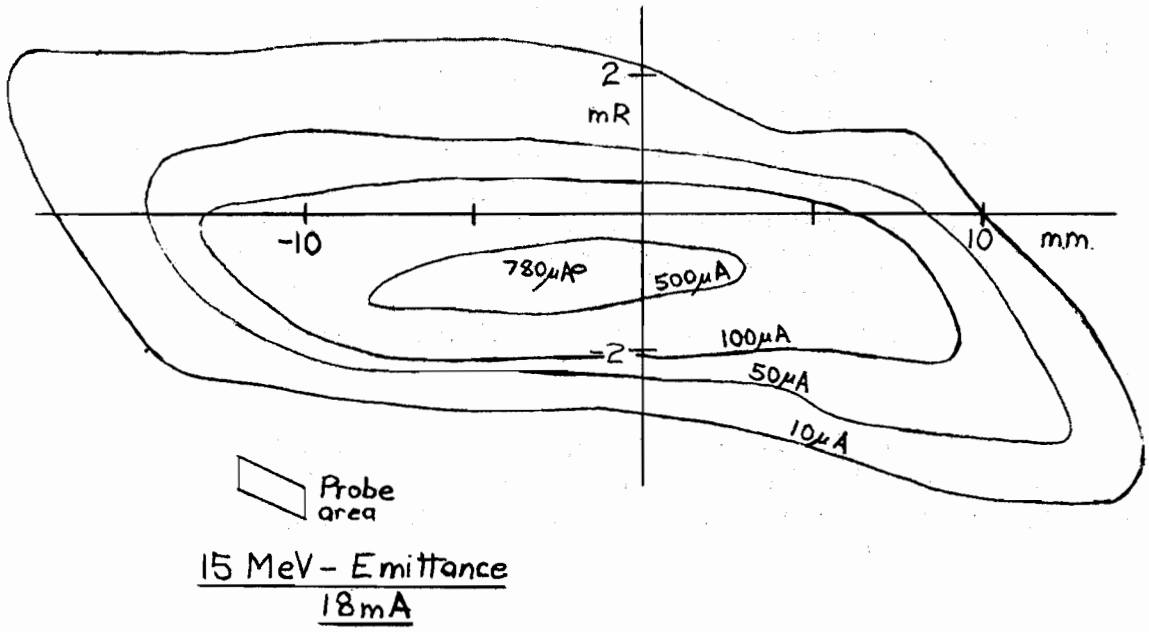

Fig. 1 Nimrod Injector

fact that the linac will still multipactor if the quadrupoles are switched off.

Similar multipactor trouble has been experienced with the buncher and debuncher cavities. It may be significant that the copper used in their construction was not oxygen free. Both of these single gap cavities were designed to allow a whole cavity end wall to be biased by a dc voltage of up to about 6 kV, but in neither case did the bias prevent multipactoring.

With the buncher cavity, a carbon black coating on the whole of each drift tube and end wall was found to be effective for a time, but eventually multipactoring occurred between the drift-tube faces. A gap splitter, capable of being biased, was then fitted. This consisted of a thin plate suspended at the center of the gap, parallel to the end walls, and of diameter equal to that of the drift tubes. For good measure, the gap splitter, as well as the other cavity surfaces, was carbon blacked. The cavity now operates without multipactoring even with no bias applied to the gap splitter.

In the case of the debuncher, carbon blacking the drift tubes and end walls failed to prevent multipactoring to the end walls. A gap splitter was then fitted, of diameter nearly equal to that of the cavity, and biasing it appeared to eliminate the multipactoring. Subsequently, it was discovered that the cavity was in fact operating at a high multipactor level and eventually operation became unstable. Inspection of the cavity showed that the multipactoring had occurred between the cavity end wall and the cylindrical wall, very close in the corner of the cavity, where there are low fields even at high gap voltages. Finally, all surfaces of the cavity were carbon blacked, including the cylindrical wall and the gap splitter, and since then multipactor-free operation has been possible.

The carbon black used is dispersed in alcohol and painted on the surfaces by brush. The presence of large carbon blacked surfaces does not appear to have any significant effect on the cavity Q factor or on the vacuum pressure.

BLEWETT: I have the greatest difficulty in understanding these remarkable experiences with multipactoring.

WHEELER: Some years ago at Yale, we built a single cavity proton linac operating at 50 Mc/sec. The resonator was a quarter wavelength coaxial

cavity, shorted at one end and capacitatively loaded at the other end where the acceleration took place. Therefore this resonator had radial electric fields except in the accelerating gap. The post loaded TM_{010} resonator that Wroe has mentioned also must have radial electric fields near the end walls. Now, in this coaxial resonator, the electric field between the post and the outer wall varies continuously from zero to the maximum gap field so that there will always be some point at which the voltage is correct for multipactoring. We tried every known scheme to suppress the multipactoring except carbon black. The method which finally worked was a high rate rise of the rf drive, which was accomplished by an oversized rf system.

BLEWETT: The only difference between this and other machines seems to be in the frequency. I can't believe that the 50 Mc drop in frequency could be responsible for all of these extraordinary effects.

DICKSON: On the last slide that you showed, there was scalloping on top of the drive pulse. Have you looked at the frequency of this scalloping in the same way as has been done on other linacs?

WROE: No. You will have to ask Nigil West about that.

WHEELER: That looks a little bit like an oscillation in the drive system.

INFORMAL DISCUSSION OF SPARKING PHENOMENA

SWENSON: We are fortunate to have a representative in this room of practically every proton linear accelerator in the world (Brookhaven, Argonne, CERN, Rutherford, Minnesota, New and Old Bevatron Injector, and the original Alvarez Linac). I have a short list of general questions which I would like to pose to a representative of each of these linacs. These questions were chosen to reveal the type of information which you as a group have and to stimulate a discussion on sparking phenomena. The questions that I have go something like this. Is sparking a problem in your linac? If so, where are the sparks? Why are they there rather than at other places?

HUBBARD: If we start talking about "why", we'll be here for a week.

SWENSON: I would also like to ask you if you have evidence that the sparking is beam dependent, dependent on the vacuum pressure, or dependent on surface contamination. Another question might be for what gradient would you build your next linac? And of course aside from answers to these questions, I would like to have any comments that you feel are pertinent.

Perhaps I should try to define the purpose of this session. The economics of linac design favors pushing the cavity excitation up to some level which is considered safe from the standpoint of sparking. There is very little reliable information on what the safe limit is. And there is no popular description of the nature of the sparking process which is observed in proton linacs. That is, there is no model of the process which explains why the sparks are where they are. Another important point is, how reliable must this linac be? That is, can we stand some sparking and can we allow some time for conditioning after the tank has been opened to air? I know there are some in this room who feel that the future linacs should be very conservative in their electric gradients and if this is the case, perhaps it is not necessary to understand the sparking phenomena.

VAN STEENBERGEN: That last comment I did not get. Why should future linacs be conservative in electric gradients?

HUBBARD: I will write three numbers on the board if you like. In 1948 the Lawrence Radiation Laboratory built a 200 Mc per second linac with a gradient of 0.9 MV/ft. In 1952 we built another with a gradient of 0.6 MV/ft, and in 1961 another linac with a gradient of 0.5 MV/ft.

LAMB: In 19-- something, it will probably be 0.4. It makes a great deal of difference what the application is. For an injector for a machine that costs x times the cost of any linac you are going to put on it, you can certainly afford to run it at half that gradient if you don't get spark one.

FEATHERSTONE: Do you worry about spark one?

LAMB: After it is baked in, you do, I think. You just don't want any sparks.

WHEELER: I think we tend to agree with that.

VAN STEENBERGEN: But isn't that demanding a bit too much. I mean, in all high voltage experiences, one normally expects some conditioning of a particular device under consideration, resulting in usually significant improved performance with regards to maximum electric fields, etc.

LIVDAHL: In January, we were open to air for one week. We did lots of things. Granted, we did not remove drift tubes, but after a week we pumped down late one afternoon. We came in the next morning, and in 30 minutes we had operating gradient. I do not think we had seen more than probably 200 sparks in that time and within an hour we were 10% over gradient, which is where we like to operate.

BLEWETT: Was the tank open to room air, dry nitrogen, or what?

LIVDAHL: It accidently got let up on kleenex and alcohol.

FEATHERSTONE: I think it is fair to say that often when a tank of the Minnesota linac has been down to air and has been pumped overnight, we can establish beam in half a day. It is another story, though, when we have gotten the drift tubes well coated with oil.

VAN STEENBERGEN: From that point of view, I feel again that the gradients could be made higher. It should be a rare occasion that one has to open the tank to air. In that case, conditioning periods of even a day or so would be acceptable.

HUBBARD: But if you are at a point where it requires a lot of conditioning, you are at a point where it will spark occasionally, even after you have done it.

SWENSON: Let me try the first question. Is sparking a problem in your linac?

BLEWETT: (On the BNL linac.) We have some color photographs of the first few drift tubes in our linac. Horrible as the drift tubes look, they still feel smooth to the touch.

VAN STEENBERGEN: Our experience is that in normal operation sparking is not a problem. These photographs look horrible, but we feel that this happens during the first half week after you have had the tank open.

BLEWETT: We feel it is important that the new injector operate at a 30-pulse per second repetition rate to speed up conditioning.

LIVDAHL: Our conditioning is done at 10 pulses per second which is higher than the current possiblities at Brookhaven and at Berkeley.

VAN STEENBERGEN: Let me make it clear that we do not see any deterioration of the sparking situation with time. We have never opened the linac to clean or treat the drift tube surfaces because of sparking.

LIVDAHL: (On the ANL linac.) I do not consider sparking a problem in the Argonne linac. I have seen no spark marks on any drift tube beyond the 20th gap.

BLEWETT: I think we can go even farther and say that we have seen no sparks beyond the 5th gap.

TAYLOR: (On the CERN linac.) I would say that sparking in our linac is a fault condition, that is, we open up the linac and find, for example, a faulty contact between the drift tube stem and the liner. When the linac is working properly, we just do not lose pulses because of sparking. We might have trouble for a day after being up to air for a week or so. The sparking damage that we see is concentrated on the first ten drift tubes.

DICKSON: (On the Harwell linac.) Sparking is not a problem now in the Harwell linac. A couple of years ago it used to be a problem in Tank one. We do not have direct evidence, but we think it was due to water vapor in the tank. I think I told some of you that we found some of the copper in the drift tubes to be porous to water. Since we have cured the porosity problem, we have a very short run-in time at 50 cps, at 1% duty cycle, and the linac seems to operate properly just for years with no problem. We see a few sparks on the first ten drift tubes but they do not bother us.

FEATHERSTONE: (On the Minnesota linac.) Sparking has never really been a problem on the Minnesota linac. The first cavity is a low gradient cavity, like the old Bevatron injector, and it just never sparks. We do

see evidence of sparks on the drift tubes of the second and third tanks. There is no apparent concentration of the sparks in any particular place along the length of the linac. They seem to appear at random.

SWENSON: I might say at this point in regard to the Minnesota linac that I calculated the fields in the vicinity of the drift tubes at three different places, that is, at both ends and at the middle, of their second and third tanks. There are some fairly small radii of curvature on the corners of the drift tubes at the high energy end of Tanks 2 and 3, and I got some electric fields on the metallic surfaces of 28 and 26 MV/m, respectively. I can present a table which compares some actual calculated quantities for the Minnesota linac with similar quantities in some of our latest linac designs.

	Units	Minnesota Linac	MURA Design Run 30547	MURA Design Run 30525
Energy	(MeV)	39	39	195
E_{ave} over cell	(MV/m)	3.0	2.8	2.3
E_{ave} over gap	(MV/m)	12.0	9.8	5.1
E_{max} on axis	(MV/m)	11.7	8.1	6.8
E_{max} on metallic surface	(MV/m)	28.3	15.1	13.4

By all the criteria listed in the left-hand column, the MURA designs are conservative in comparison to the Minnesota linac. However, it might be an error to assume that the critical criteria is listed in the table. Additional information is available on these calculations in a MURA Technical Note TN-467.

FEATHERSTONE: Incidentally, the location of the sparks that we do see does not coincide with the location of the peak fields on the drift tube surface. We tend to get a concentration near the bore radius.

REMARK: That is probably where the field is the highest.

CARNE: May I throw some wood on the fire at this point? It was mentioned in the PLA Progress Report for 1963* that we have done a redesign of our Tank 1, and we were quite concerned about breakdown. We have

*PLA Progress Report 1963, pp. 8-10, NIRL/R/60, January 1964.

done a whole series of electrolytic tank measurements to determine the electric field gradients across the drift tube surface. If you plot the field distribution along the drift tubes surface, you get a peak in the distribution where the outer radius of curvature meets the flat of the drift tube; you get a uniform distribution across the drift tube flat and another peak in the distribution near the radius of curvature of the bore hole. If we now plot surface fields against drift tube number (we have 41 + 2 half drift tubes in our machine) as in the sketch below, we find for the inner radius a surface electric field which goes from about 13 million volts per meter down to about 10. The field for the outer radius is initially less than for the inner radius, crossing over at about 6 or 7 MeV. So for the first 6 MeV it is the field near the inner radius of curvature that is critical. This may throw some light on the fact that the sparking seems to be concentrated in the first few MeV and that the sparks seem to be concentrated on the flat drift tube faces, or near the radius of curvature on the bore.

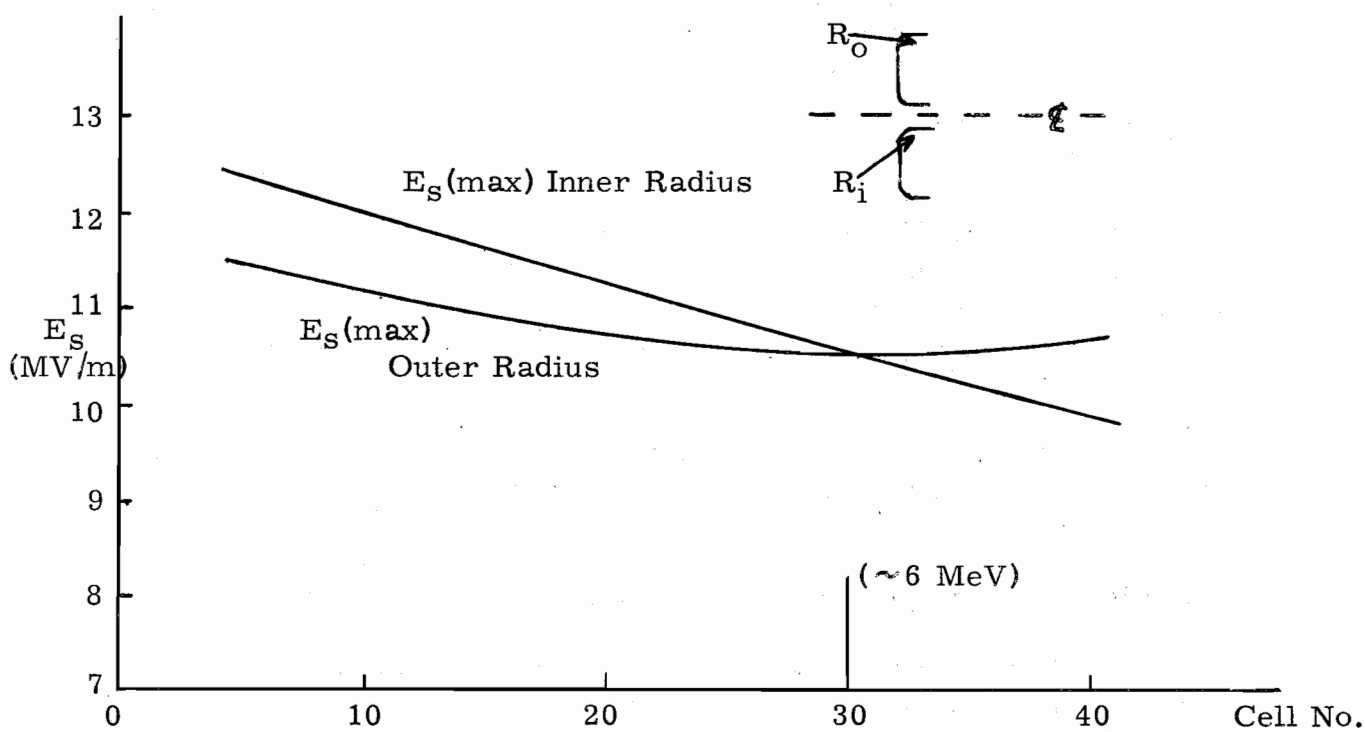

Plot of Maximum Surface E-Field Against Cell Number

HUBBARD: (On the new Bevatron injector.) It's not serious. I do not have any detailed information, but they do not lose any pulses in the machine. They do see evidence of sparks on the first few drift tubes but it does not interfere with the operation. They had trouble on the original Alvarez machine with sparking. Of course, this was with a poorly baffled oil pumping system. With regard to location of sparks, they were worse at the low energy end.

BLEWETT: I think what bothers everybody is that nobody seems to understand the mechanism.

SWENSON: That was my next question. Why are the sparks where they are rather than at some other place?

BLEWETT: Could I make some general comments? First of all, the story you get from the electrolytic tank is not the whole story. The rf magnetic fields are certainly playing a part in determining the electron trajectory. We found that whereas an electron may start off in the direction of the electric field, the magnetic field may very well turn it around. We know that electrons can get all the way across the gap. I want to propose, now that we have all the drift tube fields worked out on computers, that we ought to trace the trajectory of some ions and electrons across the gap and see what final energies and phases they have for a variety of starting phases.

HUBBARD: Are you going to insist that they get there in a half cycle?

BLEWETT: No, I think you should run the calculation for several cycles.

(At this point in the session about two-thirds of the people left to return to the regular afternoon session of the conference.)

CARNE: There is a theorem that says a nonuniform stationary rf field will have a dc force acting on any charge particle, directed toward the minimum in the field. We actually tried to use this force at one time to drive the electrons and ions towards the center of a resonant cavity. We were of course driving the electrons there much more easily and they were in fact sucking the ions in. If you look at the situation that you have across the face of the drift tube, you find, as I said earlier, a nonuniform distribution of field, with a minimum in the region of the face of the drift tube. So there can be this dc force acting on ions which will tend to drive the ions to the region of the flat face of the drift tube. If ions are indeed involved in the sparking process, this could explain the occurrence of sparks on the drift tube faces.

SWENSON: That would enhance the sparking on a flat face, would it not?

CARNE: Yes, certainly. Now the other point to observe is that as you go to higher energy drift tubes, the peak field near the bore radius decreases and the ions either tend to collect on the axis of the linac or tend to slide along the drift tube surface to the stem. If anyone has time to do the details of this calculation on a computer, I will certainly send him the details of the derivation.

PREIST: That is a very reasonable theory.

BLEWETT: It would be very interesting to take two cases, one at high energy and one at low energy and trace trajectories through the cell. The calculation ought to be run for several cycles, including both the electric and magnetic fields in the calculation.

FEATHERSTONE: I would like to point out another aspect of sparking, a question which has not been mentioned but may be significant in some cases. That is, when does sparking tend to clean up, as is usually observed, rather than produce progressive damage, as has been observed in a few notable accelerators? I have calculated that the energy stored in the Brookhaven tank is sufficient to vaporize several milligrams of copper, which is perhaps three orders of magnitude larger than any sparking damage that has been observed. So apparently only part of the energy in the cavity gets into the sparks.

BLEWETT: Yes, if you are watching the probes when the spark occurs, you can see the field drop to zero in the low energy end, and it is still there in the high energy end. With respect to the question made by Featherstone concerning the stored energy, there has been a criterion established by the beam separator people. They believe, if you store more than 50 joules in an electrostatic field, that the sparks will begin to be destructive.

HUBBARD: Yes, that is certainly a rough number, but the 50 joules is somewhere in the region where you might get damage from sparking.

BLEWETT: I think in the case of the Brookhaven linac, where we have about 100 joules, that the sparks detune the cavity and the power is dumped back into the amplifier.

PREIST: Have you come across this report by Little and Whitney at NRL?* People have suspected for years that what caused sparking to

*NRL Report #9544, dated 5/20/63, by R. P. Little and W. T. Whitney, entitled "Studies of the Inhibition of Electrical Breakdown in Vacuum." Astia Document #408298.

start in the dc case (that was all he was talking about) was the phenomenon of whiskers on the metallic surface. And he did a rather elegant experiment in which he saw the whiskers grow and actually measured them, and he computed the increase in the electric gradient that they caused and he found that they had a factor of 100 times the average gradient, and they found that no matter how well you polished the surfaces, that the whiskers were always there.

There is another paper, of which you might be aware, published in the Journal of Applied Physics in June of this year,* on gaps with dc fields in a vacuum. Their approach is to cover the cathode surface with a thin film of dielectric and they had remarkable success in two respects. One is that the ultimate breakdown voltage after conditioning is increased by a factor of two and the other is that (and they consider this most important) the pre-breakdown currents are decreased by three or four orders of magnitude, when you put this stuff on. They used some epoxies and fluorides and TiO_2. They point out you have to have a thin layer, and you have to have some electrical conduction. The whisker-growth idea may explain some of the area effects which were discussed in the main conference room. Of course, the bigger the area the more chance there is for whisker growth.

BLEWETT: This is probably quite true with dc, but I would be quite surprised at whisker growth in an rf field especially since the duty cycle is quite low.

CARNE: How large are the whiskers?

PREIST: I think they are typically a micron in diameter and some hundred microns long.

FEATHERSTONE: Is the presence of electric fields essential for the crystal growth or is it a chemical process?

BLEWETT: It must be an electrical process. I think the primary argument against this as an explanation of sparking in the rf case is that conditioning of the tank tends to get rid of sparking, whereas whisker growth should lend itself to a continuous process.

We have seen another funny effect. It was after a process of cleaning the drift tubes, in which we were using some sort of abrasive. We

---

*"Vacuum Insulation of High Voltages Utilizing Dielectric Coated Electrodes", by L. Jedynak, June 1964, JAP, p. 1727.

must have imbedded some sort of insulating particles in the drift tube walls. These did not result in any sort of disruptive breakdown, but if you peered into the cavity, you could see dozens of little stars on the drift tube faces at the lower energy end on every pulse.

SWENSON: Are there any other models which can help shed light on the sparking phenomena?

CARNE: Well, it seems that probably the rf pulse length is relevant. It would certainly be nice if someone would do some high power model studies (which I know you are going to do at MURA) at the actual pulse lengths for which you intend to run the machine.

HUBBARD: Isn't pulse length important because it affects the duty factor? Our experience suggests that you can convert from one duty factor to another just by taking the sparking rate proportional to the duty factor.

SWENSON: Have you seen any evidence for beam dependent sparking?

LIVDAHL: We have seen beam dependent sparking at Argonne but only in the case where the operator had steered the injected beam off to one side so that a majority of the beam piles into one drift tube, but in situations where the beam is properly steered into the tank, I can't say that anybody has ever seen it.

BLEWETT: We have not seen beam dependent sparking in our linac.

SWENSON: Lamb reported that he had seen beam dependent sparking, but I guess that was on the MTA.

HUBBARD: Yes, that is true, but they had very high currents, a quarter of an ampere at times.

PREIST: Now, I would like to mention one more thing. Something that has not been important yet on 200 Mc machines, but may become important on the machines you are talking about. The effect I speak of is multipactoring on dielectric surfaces. I hear people talking about a megawatt or so that has to be put through some kind of window. We've found, and we've done a lot of work on this, that we do get a single surface multipactor in a strong enough field, where the E field is parallel to the dielectric surface; you can work out the critical field for this process. You find a minimum field strength at which it can occur, of about 1 V/cm/Mc/sec. The mechanism is that the electron leaves the surface with some initial velocity. It will then be carried parallel to the surface by the electric field, and if there is a restoring force, it

will come back, and if it comes back in the right place and with enough energy, you will find that the process can continue. Well, this has been found to occur at three frequencies: about 600 Mc, about 3000 Mc, and 9000 Mc. It can be eliminated completely by suitable coatings applied to the dielectric surface.

SUMMARY OF INFORMAL SESSION ON MECHANICAL ENGINEERING ASPECTS

John E. O'Meara
Midwestern Universities Research Association

There were a number of topics we did not discuss, such as architectural and engineering problems, water-cooling problems, or other topics specific to any site. Also, we limited our discussion to the Alvarez type of structure rather than the waveguide portion of the linac. The general ground rule that we operated under was that a number of linacs of this type have been built and have performed satisfactorily from a mechanical engineering point of view. Obviously, the same tanks could be built in the future, therefore, any design change should yield some reduction in cost. We prepared a drawing of a different approach to tank construction, shown in Fig. 1. This controversial drawing started our discussion. The Argonne and Brookhaven tanks were constructed with a set of rails to hold the drift tube stems. Figure 1 illustrates a support structure which is independent of the tank, the objective being to eliminate precision machining on the large tank weldment as had been done previously. Figure 1 shows this continuous tank, perhaps as long as 85 feet. This would eliminate the multiplicity of flanges that we see in the present tanks. This, of course, would have to be traded off against additional cost in handling and perhaps more difficult machining because of the larger piece. Conventional ion pumps would be used on this tank and, while a ball tuner is shown, there is a question as to whether or not ball tuners are best. We at MURA object to this drawing in that this additional drift tube support structure adds to material cost, and further, any temperature cycling within this support structure would lead to misalignment of the drift tube inasmuch as they are firmly anchored to it rather than to the tank itself. The discussion led to the conclusion that the tank should be used to provide the drift tube support structure but eliminate the precision machining activity that had previously taken place on the tank itself. This could be done by attaching an adjustable set of rails, for instance.

The problem of holding straightness in a long tank as shown in Fig. 1 was raised. Worstell of LASL pointed out that cylinders of 100-foot lengths have been held to approximately 1/16-inch straightness.

The other topic that we spent a good deal of time discussing was drift tube construction. The MURA computer program results in a cylindrical drift tube. This leads to some economies in fabrication,

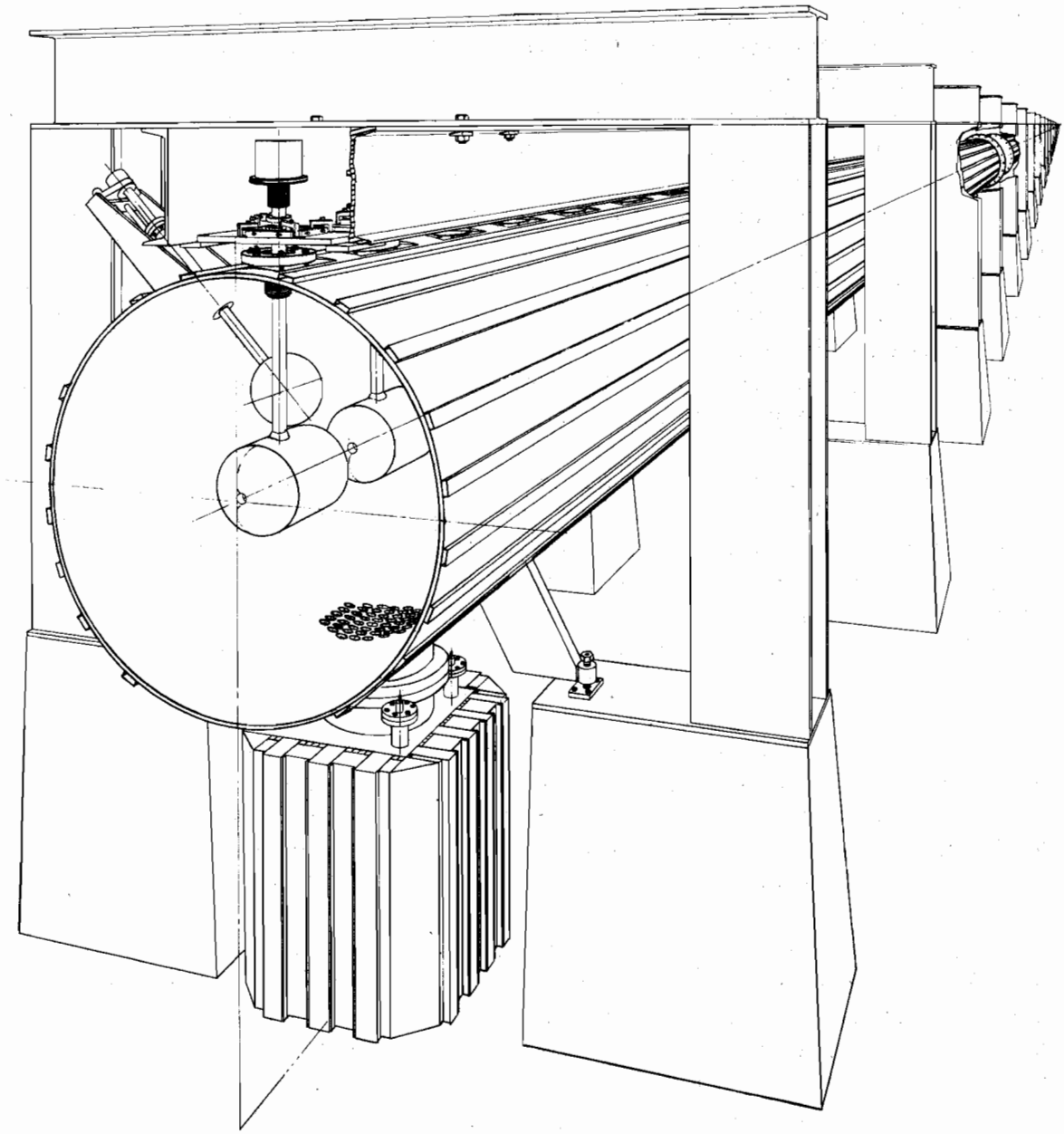

FIG 1 40 FOOT LINAC TANK WITH EXTERNAL DRIFT TUBE SUPPORT

especially when the drift tube diameter remains constant as it does from 50 MeV to the 200 MeV end of the linac. Figure 2 shows a proposed design of one of these drift tubes. Earlier designs required that the entire body be contoured. A cylindrical drift tube, of course, requires only contouring on the end and the center section can be fabricated from tubing. The drift tube in our Mark I tank in the MURA laboratory was fabricated from tubing with pressed end caps. The ends were made from flat sheet stock suggesting some savings over the previous method of construction. The quadrupole shown is constructed with laminations. Each lamination is split so that it may be stacked around a previously formed coil. Since the quadrupole cross section remains constant through a large number of drift tubes, it appears that a laminated magnet should be cheaper than a solid pole-piece magnet.

There was general agreement on tank construction that it should be of one-wall design rather than liner construction. There were some suggestions of alternate means of obtaining a copper surface on the inside. We also had some agreement on the total wall thickness. We feel that the tank could be constructed with a 1/2-inch total wall thickness with 1/8-inch copper. Hortonclad is available in any ratio of copper thickness to steel thickness so that it is possible to obtain this.

I think there is also a general agreement that ion pumps can be used on the tank proper, with some differences on what degree of rough vacuum is necessary and what type of pump should be used for roughing. While isolation valves over each pump may aid in starting, there is a difference of opinion on whether their cost is justified.

McGee of the AEC attended the mechanical engineering sessions and he is quite conscious of costs and the related topic of tolerances. One area of tight tolerances is the concentricity of the axis of the quadrupole magnetic fields with the geometric axis of the drift tube. In the past attempts have been made to hold the concentricity to within 2 mils. This puts rather stringent requirements on the fabrication of the quadrupole assembly plus the concentricity and fit of each piece as we build up the drift tube assembly. Rf resonance considerations require a tight tolerance on the over-all length of the drift tubes. An effort should be made to relax these tolerances or confirm that they are absolutely necessary.

Figure 2 also shows a stem illustrated which does not provide for any direct cooling of the stem proper; we all agreed that cooling must be done unless it can be demonstrated that elongation of the drift tube would not exceed a few tenths of a mil. In general, there are three

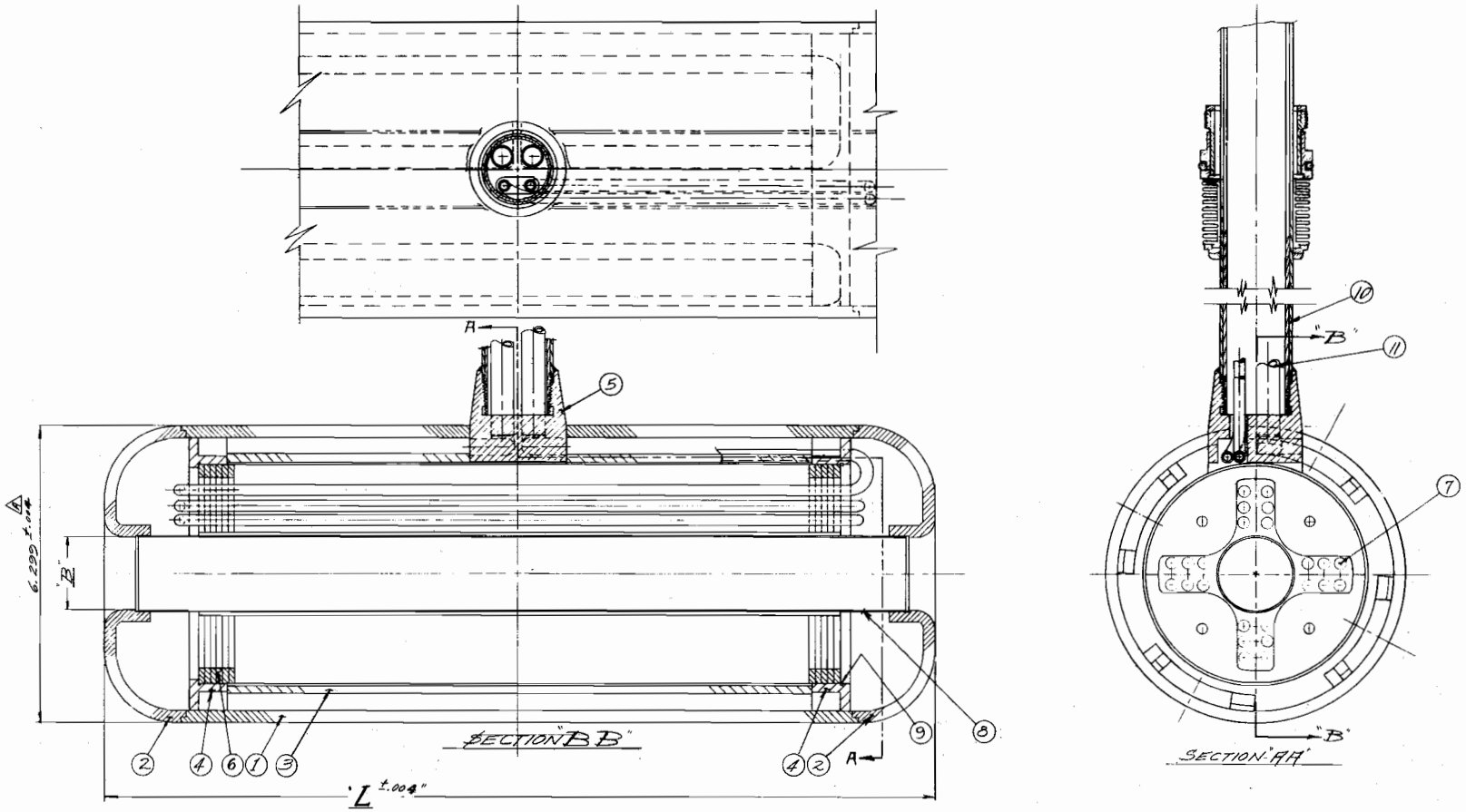

FIG 2 200 MeV DRIFT TUBE

methods of construction that could be used for drift tube stems. The stem in Fig. 2 is of stainless steel clad with copper. An alternate method of construction suggested by Grand would be to use solid copper rod and gun-drill the necessary holes for cooling and power leads. Another possibility would be to have a stainless steel tube surrounded by a still larger copper tube, the stainless steel tube furnishing the mechanical rigidity. All these methods are being considered by the major laboratories.

YOUNG: Can you describe the cooling used in the drift tube?

O'MEARA: Figure 2 shows two water tubes in the stem. These tubes are joined to a block at the drift tube. Water is distributed from this block to a liner cylinder on the inside of the drift tube body. This liner, along with the end caps, provides a labyrinth passage for the water. In connection with adjustment and alignment, we have three translational adjustments but only one rotary. We would like to have all six degrees of freedom. Brunk of Argonne National Laboratory is working on a design for such an alignment plate where each motion is completely decoupled from all other motions.

DICKSON: Do you feel that it is necessary to have some adjustment of the position of the quadrupole within the drift tube?

O'MEARA: It is our intention to locate the quadrupole in its proper position during assembly and hold it in that location. After the drift tube is completely sealed, our only reference to the position of the quadrupole is the body and bore of the drift tube.

Someone raised a question about rf joints. There was general agreement that a number of designs work well for static seals. Los Alamos representatives encountered difficulty with spring rings in adjustable rf seals. They also reported that they were able to overcome this problem by using a relatively coarsely pitched large diameter helix which had long travel without permanent set.

WHEELER: Have you given up the thought of evacuating the inside of the drift tube?

O'MEARA: No, we feel that we should be able to do this. In the Brookhaven-Argonne design, a roughing box provides a means of pulling rough vacuum in the interior of the stem and the cavity of the drift tube. In order to provide the same capability for the tank design in Fig. 1, two enclosures would be utilized on each stem.

(There was discussion questioning the necessity of providing this rough vacuum.)

Guilbaud of CSF described a copper electroforming process* that had been used for their 18-inch diameter by 1-inch wall waveguide. They are able to buy this at 50¢ per pound, which is less than we pay for copper sheet in the U.S.

HENDRICKS: What are the largest dimensions that they can fabricate?

O'MEARA: We understand that one meter in diameter by 8 meters in length is possible. This process could be an alternate means of fabricating tanks.

HENDRICKS: Can they form the water channels in the copper itself?

O'MEARA: Yes, the process is to plate on top of a wax-coated steel mandril. After the plating is completed, they are able to melt the wax and recover the mandril. Half-way through this process they stop and machine a number of cooling passages which are filled with wax. Resumption of the plating process results in a buried cooling channel.

GRAND: We would like to design a tank for better operation and make it less costly. My idea is to make an all-steel tank, machine and completely assemble it, and then copper-plate the interior. Some people do not agree with this idea, but I would like to pursue it and possibly build a short section.

O'MEARA: The German electroforming process was described after Pierre's suggestion was made. The electroformed copper has been reported to have high conductivity and high Q devices have been made using it. I think the earlier experience has shown that copper plating was porous, gassy, and had fairly high resistivity.

---

*Elmore's Metal Aktiengesellschaft, Schaladern/Sieg, West Germany.

SUMMARY OF EVENING SESSION ON BEAM LOADING EFFECTS

J. Leiss
National Bureau of Standards

On Wednesday evening a group gathered at the Ivy Inn to discuss informally beam loading effects in linacs. I am not sure anything was concluded at this session, but I can report that we did have a spirited discussion.

Beam loading in electron linacs is extremely important. There exist several machines that have reached large conversion values from the rf power in the wave guide to the beam (as high as 60 to 70%). There are many things that have been calculated and observed in the electron linacs. In proton linacs these beam loading effects have only recently become popular. In the proton linac beam loading effects are both more difficult to calculate and more important to understand. Rather than try to summarize what was discussed at this session, I would prefer to list various things that have a relation to beam loading. I personally believe that for the proton machines now being studied, many of these effects have not been studied to the extent that is really required.

1. Detuning

If you are running a tank as a self-resonant cavity and a beam passes through, does the cavity resonant frequency change or not? From the standpoint of doing a mathematical analysis of beam loading, this is an extremely important question because if detuning occurs, the problem becomes nonlinear and the analysis is extremely complicated. I believe that for the currents that are being considered, the detuning effect is not a serious problem and it can be ignored.

2. Transient Effect

There is a fairly clear indication, as indicated in some of the papers presented on Wednesday, that transient effects really do need to be considered in beam loading. The transient beam loading effect from the turn-on time, for a square wave beam, will occur for the same amount of time as the rf filling time of the tanks and this is an appreciable time. The data presented by Jameson[1] showed wiggles and oscillations in the rf transmission for amplitude step changes. Beam loading causes similar effects although their appearance will be different because in beam loading the source is spread throughout the tank. The time delay for transient

beam loading to be complete will be very important in designing phase and amplitude regulating systems to correct for beam loading effects.

3. Subharmonic Effects

Subharmonic effects were mentioned by Gluckstern[2] in the discussion on the resonant excitation of beam blow-up modes. There is additionally an effect in the fundamental mode. We have analyzed the subharmonic beam loading in electron linacs and for the particular case of our accelerating guide find, for injection of beam at the third to the fifth subharmonics, incorrect estimates of the magnitude of beam loading in the fundamental mode by as much as 15%. When this is done for the resonant cavity case, similar numbers will probably be obtained.

4. Tank Flatness

When a tank is flattened by making small tuning or local group velocity changes, one is partially compensating for a nondistributed excitation of the tank. However the beam loading is distributed by beam bunches moving at just the right speed, and there is reason to believe that the tanks would become nonflat. In particular, if you tune for one particular phase velocity which corresponds to the proton's velocity in the middle of the tank, the velocity of the source is too slow in one direction and a little too fast in the other direction. This will result in a tilt to the field in the tank. These effects can be evaluated by a detailed analysis.

5. Phase Shift Effects

For a proton linac one operates at a nonzero phase relative to the rf in the wave guide, say at 30° from the peak. The beam loading wave is just opposite to this, that is at 180° out of phase with the beam. Relative to the initial rf in the guide one can consider a component in phase with this normal unloaded cavity field, and a component 90° out of phase with the normal cavity field. The resultant field in the cavity will therefore be phase shifted. This will be changing during the transient period. For the beam currents now being considered, the phase shift will amount to 4 to 6 degrees in the total field and corrective measures will have to be taken. This is not a detuning effect. The beam loading would be the same if we had no external rf to use as a reference.

6. Beam Blow-Up (resonant and nonresonant)

We can say very little at this time about this phenomena. The first mixed mode that is experienced in most of the disc loaded guides for

electron linacs occurs approximately one and one-half times the frequency of the fundamental mode. The backward wave oscillator is for the excitation of this mode and is classified by Gluckstern[2] as the non-resonant effect. The resonant effect predicted for subharmonic injection is really the same thing and will undergo the same backward wave oscillator characteristic. The difference is that the coupling of the beam to this mode, due to the time dependent parts, is going to be greater for injection of beam at even subharmonics of the fundamental rf frequency because the beam pulse train just happens to have a high frequency component at this mode. If the structures that are chosen turn out to have this first mixed mode at approximately one and one-half times the fundamental frequency, there should be a worry about enhanced excitation of this deflecting mode. More calculations are needed, and experiments should be done on operating electron linacs by putting a first subharmonic buncher in front to see if a big beam blow-up occurs.

7. Space Harmonics

This topic considers beam excitation of the various possible modes in the pass band at the same frequency. These are generally considered to be sufficiently incoherent with the beam so that one does not have to worry about them. That is, they oscillate past the beam so fast that they have an average zero effect. We have done calculations which indicate that in the π mode (or more correctly, modes with zero group velocity) the cancellation of the effects of these spatial modes does not exist for beam excited rf waves and in fact these modes stay coherent with the beam as a steady-state affair. This is because the beam occurs as a series of discrete pulses and not a true sine wave as most theories assume. This can cause additional beam loading.

8. Beam Loading Limits

Techniques for the design of wave guides to reduce beam blow-up phenomena at any desired current are reasonably well known so that this need not be a limit unless the guide is already built. Other limits are economic, that is, how big to make the power supply or how large to make the tank. One will eventually reach a limit determined by true detuning of the tank.

9. Reaction Back on the Source

In traveling wave electron linacs the power from the klystron is sent down the wave guide to a terminating load and there is no reaction back on the power supply. The coupling is one way, just as if an isolator

were present. In proton linacs the coupling between the resonant tanks and the driver is tight. If the fields change due to beam loading, there will be a reaction back on the source. Beam loading calculations will have to include the interaction with the driving source.

MILLS: I would like to make several comments about beam-loading effects and instabilities. At the evening session, Leiss suggested a clever model for these effects. This was to treat the problem by simulating the electron beam by a dielectric rod. It may be possible to use this simple model to help anticipate the problems to be encountered in proton linacs. Since the beams are moving with high velocity, the "dielectric susceptibility" to be used differs by a factor of γ^2 between transverse and axial directions. Thus the fields excited by a given beam current would be expected to disturb primarily the transverse motion in an electron linac, as is the case so far. In these proton linacs, however, the value of γ is near unity, so fields excited by the same beam current may be expected to disturb the axial motion as well as the transverse motion. Then the studies made to date of "beam blowup" in electron linacs will be a guide to related phenomena in proton linacs but will probably not be the whole story.

The second comment concerns the relationship between instabilities presently observed in circular accelerators and those to be expected to occur in linacs. We see currently two instabilities, one in the direction of beam motion and one in a direction transverse to the beam motion, which are due to the phase shift of the beam-induced fields at the resistive walls of the "wave guide." Certainly we must expect to see similar phenomena in linear accelerators. It would certainly give us a good feeling to understand the relation between "beam blowup" and these instabilities.

LEISS: The dielectric rod may be a good way to help understand the difference between proton and electron linacs. On the second point, I believe we must be very careful in trying to extend results from circular to linear machines, since the same particle traverses a given locality many times in the circular machine. Further, the momentum compaction of circular accelerators can allow greater phase changes for a given field excitation than will occur in a linear machine.

GRAND: You mentioned that the major difference between the electron and proton machines is the running vs. standing wave. Other differences which may possibly be important are the separate couplings and the relatively long drift tubes. The beam fields might not have any effect around the coupling holes.

LEISS: It seems to me that you may reduce the group velocity by this means and thereby reduce the loading effects. On the other hand, this can be inferred immediately from the dispersion diagram.

GRAND: Another difference is that in the proton case, energy is being taken out during only a short phase interval, while in the electron case, the effect is spread out over the whole wave.

LEISS: I believe that questions like this can be handled only by detailed calculations. Keith Symon has told me of calculations they are making in which the real fields induced by a beam are allowed to modify the beam distribution. Such calculations give the complete answer and will be very valuable.

LAPOSTOLLE: In thinking about beam blowup, I wonder if anyone has any knowledge of the transverse modes in typical proton structures--even the Alvarez structure? Of course there is focusing in the Alvarez structure, but this will not reduce the blowup.

LEISS: Focusing helps a little in electron linacs, but not much.

WHEELER: The TE modes should not exist in the Alvarez structure, but we saw a few of them in the heavy ion machine at frequencies below that of the TM_{010}. They are very difficult to excite and we didn't work very hard at it.

LEISS: It certainly would be valuable for someone with a test cavity to do some measurements of these modes.

REFERENCES

1. R. A. Jameson, "RF Phase and Amplitude Control," page 505.

2. R. L. Gluckstern, "Transverse Beam Blow-Up in Standing Wave Linacs," page 186.